UNIVERSITY OF CAMBRIDGE

The Development of Divinyl-Heteroaryl Linkers for the Synthesis of Stable and Functional Antibody-Drug Conjugates

Stephen J. Walsh

Clare Hall

University of Cambridge

May 2019

Supervised by Professor David R. Spring

This dissertation is submitted for the degree of **Doctor of Philosophy**

Declaration

This dissertation is submitted in fulfilment of the requirements for the degree of Doctor of Philosophy. It describes work carried out in the Department of Chemistry, the Department of Biochemistry and the Cancer Research UK Cambridge Institute at the University of Cambridge between October 2015 and May 2019 under the supervision of Professor David Spring. This dissertation describes my own work and is not the product of collaboration, unless otherwise stated. The work presented has not been submitted for any other degree. It does not exceed the prescribed word count for the Physics and Chemistry Degree Committee.

Signed, Date:

_____ _____

Stephen J. Walsh

Clare Hall College, University of Cambridge

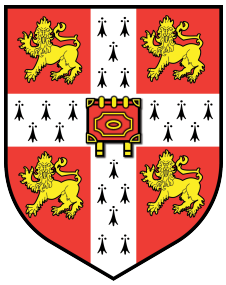

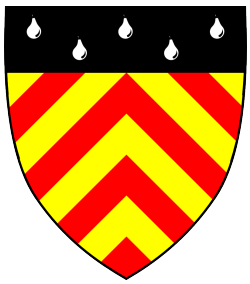

Abstract

Antibody-drug conjugates (ADCs) are a class of targeted therapeutics that utilise the exquisite selectivity of antibodies for membrane receptors to selectively deliver cytotoxic warheads to specific cell types, such as cancer cells. Much effort has been invested in recent years to deliver ADCs with improved pharmacokinetics, toxicology and overall pharmacological profiles over early generation ADCs. In particular, advances in linkage strategies through antibody engineering or enzymatic modification have yielded homogeneous ADC products with defined modification sites and stable linkages. Despite significant advances in this regard, these strategies are typically laborious and low-yielding, and the immunogenicity of these unnatural modifications is still unclear.

The primary aim of this work was to obtain a linker technology that yields homogeneous, stable and functional ADCs from native antibodies. To this end, cysteine bridging strategies, whereby a bis-reactive scaffold covalently cross-links the two cysteines of a reduced disulfide, were identified as a reported method to produce homogeneous and functional ADCs. However, a limited number of these reagents have been described in the literature and it was postulated that an expansion of the toolbox of these reagents would be beneficial to the ADC research community.

This report details the development of a novel set of divinylpyrimidine (DVP) cysteine bridging linkers. Early investigations into divinylpyridine reagents were initially conducted, but disappointingly, were deemed to have insufficient reactivity to enable efficient antibody disulfide rebridging. Alteration of the divinyl-heteroaryl scaffold by switching to a pyrimidine core was then explored. In the first instance, monovinylpyrimidine small molecule models demonstrated the improved reactivity of the scaffold, while maintaining the stability and chemoselectivity that was observed with the vinylpyridine reagents. DVP linkers including a dual-functional DVP were then readily prepared and were shown to efficiently rebridge the reduced disulfides of native antibodies, antibody fragments and other disulfide-containing proteins. Functionalisation of the protein substrates with biologically-relevant moieties (e.g. cytotoxins, fluorophores) could be achieved either before rebridging with a pre-functionalised linker or after rebridging through bioorthogonal chemistry. In addition, the receptor affinity and cellular selectivity of the antibodies were unaffected by rebridging and the antibody conjugates displayed exceptional stability in human plasma over two weeks. Critically, ADCs synthesised through DVP conjugation demonstrated highly potent and selective cytotoxicity in a series of *in vitro* cellular assays.

Acknowledgements

Firstly, I would like to thank Prof. David Spring for giving me the opportunity to work in his research group and for giving me the freedom to explore a truly fascinating area of research over the last four(ish) years. It has been a privilege and an honour to work in his group and I can never thank him enough for his support, advice and encouragement from start to finish. I would also like to thank Prof. Jason Carroll for allowing me to explore the wonders of biological research in his lab. It has been a truly inspirational experience to work alongside his group and I am eternally grateful for the opportunity and his guidance throughout. Thank you to Dr. Marko Hyvönen for letting me loose in his lab and for his help in teaching me of biochemical research. Thank you also to Dr. Jeremy Parker and Prof. Ian Paterson for helpful discussions and advice over the last few years. I would also like to acknowledge AstraZeneca, the Cambridge Trusts and Clare Hall College for financial support throughout.

Spring group near and far – where do I begin? It's been one hell of a ride! So many of you to thank for making the journey what is was. Terence, thank you for your supervision in the lab, for being an astounding friend and for mediating when Twigg and I had our lab 'fight'… Mike, remember that time Terence bought a Bentley? Thank you also for being my twin and for our sheer ridiculous antics, especially during our formative years. Thank you also to Joe for being my fried chicken and pizza partner; for this and countless other reasons, you are an inspiration! Twiggy, you're my boy blue! Thank you for putting up with me both in and out of the lab, for all of your help with chemistry and beyond and for our triumphant appearance on BBC Cricket as the faces of lab cricket!

I would also like to thank all Spring group members – past and present – for all of the wonderful times. I have learned so much from all of you and I am forever in your debt for your kindness and tolerability of my many quirks. I would especially like to thank Hannah S, Hannah S, Jonny, Súil, Niki, Gabri, Stephen, Tommy, Claudia and Warren for their advice and general chats on science, always having a listening ear, or partaking in a particular Christmas song in June over a pint of plain. Thank you to all in Team ADC for our thoroughly enjoyable discussions on the field and for listening to my mad ramblings. Thank you also to all those who have aided with suggestions and proof-reading of this thesis – Twigg, Sarah, Jessy, Gabri, Hannah and Jonny.

A special thanks must also go to my dear friends Sarah and Jessy. I am so glad that I have gotten to share the last four years with you both. I can't express how grateful I am for all of the

chats about science, life and everything in between. Your support and friendship in good times and bad has meant the world to me and I couldn't have made it without you. Most importantly, thank you for all the food and gin!

Sunny, my man, thank you for all you have taught me about cells and biology as a whole. It takes a brave soul to let a chemist anywhere near their precious cells. Mostly, thank you for always ensuring that somebody in the room has something more outrageous to say than me! To my other Carroll group peeps – Sankari, Rasmus, Rebecca, Eva, Silvia, Sanjeev, Al, Shalini, Igor, Joe, Danya and Emily, your enthusiasm and passion for science inspires me every day. Thank you for your patience and kindness in teaching me about your research. I'll hopefully do a chromatin fractionation one day! I always left the lab happier than when I arrived and for that more than anything, I thank you all.

To the Hyvönen group – Tom, Joe, Theo, Matt, Beata and Katharina, thank you for all you have taught me about cloning and proteins. A special thanks to Tom for all of his scientific wisdom, his outrageous shenanigans around the lab, an endless supply of frothies and being the OG fleece-wearing Coldham's Swoldier.

My Irish pals – Higgins, Jess, Sarah, Richie, Cormac and Catherina – thank you for sticking by exam Steve for all these years. I dearly miss the endless supply of tea! Thanks also to Jake and John for the many cups of coffee and random chats.

I reserve special thanks for my family. To Nicky, Katie and Eliza, thank you all for sharing the exact same horribly sarcastic sense of humour as me and for the constant stream of abuse that keeps me grounded. Thank you also to my mam and dad for sacrificing so much and working so hard to allow me to do anything I wanted. I would have never dreamed when you got me that chemistry kit all those years ago that it would lead me here. Mam – your unwavering love, support and belief in me has motivated more than anything to work hard and strive for my best. I can never thank you enough for all of it.

Finally, I owe a huge debt of gratitude to Elinor. You make every day better with your patience, understanding, encouragement and love. I could not have done this without you, and I will be forever indebted to you, particularly for the wine and pizza!

Abbreviations

°C	degrees centigrade
Å	Ångström(s)
aaRS	amino-acyl tRNA synthetase
ADC	antibody-drug conjugate
ADCC	antibody-dependent cell cytotoxicity
ADPN	arylene-dipropiolonitrile
AFC	antibody-fluorophore conjugate
ALCL	anaplastic large cell lymphoma
Alloc	allyloxycarbonyl
AML	acute myeloid leukemia
AKT	protein kinase B
ALL	acute lymphoblastic leukemia
aq.	aqueous
ASO	antisense oligonucleotide
ATCC	American Type Culture Collection
ATPase	adenosine triphosphatase
conc.	concentration
BBS	borate buffered saline
BCN	bicyclononyne
Boc	*tert*-butoxycarbonyl
bp	base pairs
CAR-T	chimeric antigen receptor T cell
Cas	CRISPR-associated protein
CDR	complementarity determining region
CRISPR	clustered regular interspaced short palindromic repeats
CRUK	Cancer Research UK
CuAAC	copper-catalysed azide-alkyne cycloaddition
δ	chemical shift
Da	Dalton
DAR	drug-antibody ratio
DBCO	aza-dibenzocyclooctyne
df-DVP	dual-functional divinylpyrimidine
DIPEA	*N,N,*-diisopropylethylamine
DLBCL	diffuse large B cell lymphoma

DM1	emtansine
DM4	ravtansine
DMAP	4-(dimethylamino)pyridine
DME	dimethoxyethane
DMEM	Dulbecco's Modified Eagle Medium
DMF	*N,N,*-dimethylformamide
DMP	Dess-Martin Periodinane
DMSO	dimethylsulfoxide
DNA	deoxyribonucleic acid
dppf	1,1'-bis(diphenylphosphino)ferrocene
DTT	dithiothreitol
DVP	divinylpyrimidine
ε	extinction coefficient
ECACC	European Collection of Authenticated Cell Cultures
E. coli	*Escherichia coli*
EDC	*N*-(3-dimethylaminopropyl)-*N'*-ethylcarbodiimide hydrochloride
EDTA	ethylenediaminetetraacetic acid
EEDQ	2-ethoxy-1-ethoxycarbonyl-1,2-dihydroquinoline
ELISA	enzyme-linked immunosorbent assay
EMA	European Medicines Agency
eq.	equivalents
ER	estrogen receptor
ESI	electrospray ionisation
Et	ethyl
et al.	and others
Fab	fragment, antigen-binding
FACS	fluorescence-activated cell sorting
FAR	fluorophore-antibody ratio
FBS	fetal bovine serum
Fc	fragment, crystallisable
FCC	flash column chromatography
FcγR	Fc receptor gamma
FDA	Food and Drug Administration
FGE	formylglycine-generating enzyme
Fmoc	9-fluorenylmethoxycarbonyl
g	gram(s)

GalNAz	*N*-azidogalactosamine
GlcNAc	*N*-acetylglucosamine
GF	gel filtration
GSH	*L*-glutathione
h	hour(s)
HATU	*N*-[(Dimethylamino)-1*H*-1,2,3-triazolo-[4,5-*b*]pyridine-1-ylmethylene]-*N*-methylmethanaminium hexafluorophosphate *N*-oxide
HBTU	*N,N,N',N'*-tetramethyl-*O*-(1*H*-benzotriazol-1-yl)uronium hexafluorophosphate
HC	heavy chain
HER2	human epidermal growth factor receptor 2
HIPS	hydrazine-*iso*-Pictet Spengler
HL	Hodgkin's lymphoma
HOBt·H_2O	1-hydroxybenzotriazole hydrate
HPLC	high performance liquid chromatography
HRMS	high resolution mass spectrometry
HSA	human serum albumin
IC_{50}	half-maximal inhibitory concentration
iEDDA	inverse electron demand Diels-Alder
IgG	immunoglobulin G
IPTG	isopropyl-β-thiogalactopyranoside
IR	infrared (spectroscopy)
k	kilo
k_2	second order rate constant
K_D	dissociation constant
L	litre(s)
λ_{max}	maximum absorption
LB	Luria-Bertani
LC	light chain
LCMS	liquid chromatography mass spectrometry
μ	micro
M	molar
m	milli
mAb	monoclonal antibody
MAPK	mitogen-activated protein kinase
MCC	4-(maleimidomethyl)cyclohexane-1-carboxylate
mc	maleimidocaproyl

MEC	minimum effective concentration
MES	4-morpholineethanesulfonic acid
Me	methyl
MGTase	microbial transglutaminase
MIDA	*N*-methyliminodiacetic acid
min	minute(s)
MMAE	monomethylauristatin E
MMAF	monomethylauristatin F
mol	mole(s)
m.p.	melting point
MS	mass spectrum
MTD	maximum tolerated dose
mTOR	mammalian target of rapamycin
MWCO	molecular weight cut-off
n	nano
NBD	nitrobenzofurazan
NGM	next generation maleimide
NHL	non-Hodgkin's lymphoma
NHS	*N*-hydroxysuccinimide
NIR	near-infrared
NMR	nuclear magnetic resonance
OD	optical density
p	pico
p	para
PABA	*para*-aminobenzylalcohol
PABC	*para*-aminobenzylcarbonyl
PBD	pyrrolobenzodiazepine
PBS	phosphate buffered saline
PCC	pyridinium chlorochromate
PCR	polymerase chain reaction
PE	petroleum ether
PEG	polyethylene glycol
Pf	*Pyrococcus furiosus*
PK	pharmacokinetics
PNGase F	peptide:*N*-glycosidase F
PNP	*para*-nitrophenyl
ppm	parts per million

py	pyridine
R	undefined chemical group
R_f	retention factor
RNA	ribonucleic acid
RP-HPLC	reverse phase high performance liquid chromatography
rt	room temperature
sat.	saturated
SDS-PAGE	sodium dodecyl sulfate polyacrylamide gel electrophoresis
scFv	single chain variable fragment
SEC	size exclusion chromatography
siRNA	short interfering ribonucleic acid
S_NAr	nucleophilic aromatic substitution
SPAAC	strain-promoted azide-alkyne cycloaddition
Su	succinimide
t / *tert*	tertiary
T3P	propylphosphonic anhydride
TBME	*tert*-butyl methyl ether
TBS	tris buffered saline
TCEP	tris(2-carboxyethyl)phosphine hydrochloride
TFA	trifluoroacetic acid
TI	therapeutic index
THF	tetrahydrofuran
THPTA	tris(3-hydroxypropyltriazolylmethyl)amine
TLC	thin layer chromatography
tRNA	transfer ribonucleic acid
UAA	unnatural amino acid
UDP	uridine diphosphate
UPLC	ultra performance liquid chromatography
UV-vis	ultraviolet-visible (spectroscopy)
v/v	volume concentration

Standard one and three letter codes are used for amino acids and nucleotide bases.

Table of Contents

Chapter 1

Introduction

1.1 Cancer Therapy

Cancer constitutes a serious risk to human health. The Cancer Research UK (CRUK) predicts that >50% of people currently under the age of 65 will be diagnosed with cancer in their life.[1] It can be characterised by a rapid and uncontrollable division of aberrant cells with mutations in their genetic material. The DNA mutations that result in oncogenesis can have multiple origins. Inherited faulty genes, environmental causes (e.g. diet, smoking, infection), random mutations or a combination of these can drive the activation of oncogenes or the inhibition of tumour suppressor genes.[2] Although more than 200 types of cancer have been identified, many forms of this disease are now curable but this is dependent on the aggressiveness of the cancer and the stage at which it is diagnosed, amongst other factors.[3]

Chemotherapy has been widely implemented since the 1940s as an effective method for the eradication of malignant cancer cells.[4,5] Most chemotherapeutics traditionally employ a small molecule to perturb a distinct mechanism that is crucial for cell survival or division, driving the cell toward apoptosis. For example, DNA cross-linkers such as the platinum-based alkylating agents (e.g. cisplatin, carboplatin, oxaliplatin) prevent DNA replication or DNA repair, and consequently block cell division (Figure 1.1).[6,7] Tubulin inhibitors such as paclitaxel or the Vinca alkaloids (e.g. vinblastine) prevent tubulin polymerisation or stabilise microtubules, thus inhibiting mitosis through metaphase arrest and induce apoptosis (Figure 1.1).[8,9] Although these mechanisms of action affect rapidly dividing cells such as cancer cells more than slowly replicating cells, they inevitably also cause the death of healthy tissue, resulting in dose-limiting toxicity.[10]

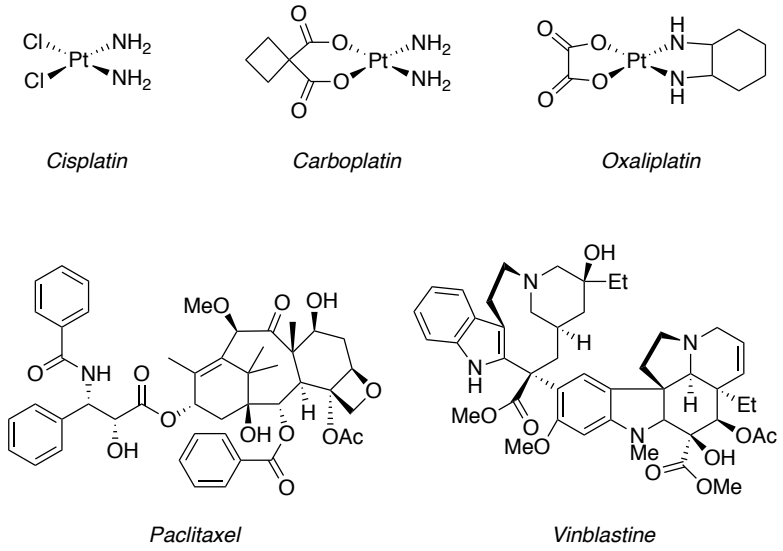

Figure 1.1: DNA cross-linkers such as cisplatin, carboplatin and oxaliplatin, and tubulin inhibitors such as paclitaxel and vinblastine are widely used chemotherapies.

Some small molecule therapies target cancer-specific mechanisms, thereby giving better selectivity profiles over standard chemotherapeutic regimens. For example, many breast cancers are driven by overexpression of the estrogen receptor (ER) transcription factor, which is activated by estrogen hormones.[11] ER inhibitors such as tamoxifen or fulvestrant can inhibit the growth of and eliminate such cancers (Figure 1.2).[12,13] However, many of these drugs still result in the death of healthy cells. Whilst small molecule drugs have undoubtedly had a hugely beneficial effect on cancer survival rates, the harmful side effects associated with these treatment strategies often cause a poor quality of life for the patient. Drug concentrations required to achieve *in vivo* efficacy cause severe side effects while lower concentrations that reduce the side effects limit the drugs effect.

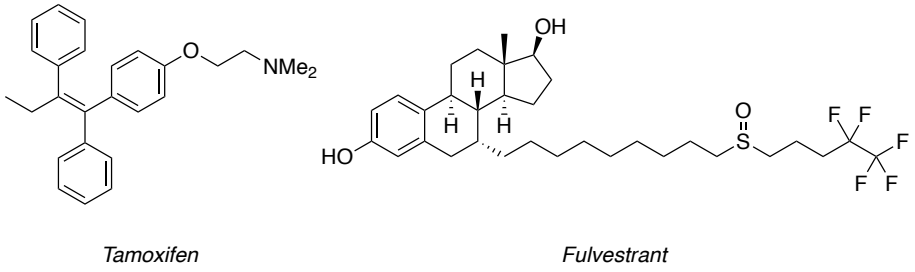

Figure 1.2: Estrogen receptor inhibitors tamoxifen and fulvestrant.

Many chemotherapeutic agents are administered as part of a combination therapy program, which can involve co-administration of multiple agents with distinct mechanisms of action or administration of chemotherapy alongside another treatment type, such as radiotherapy.[10]

Radiation therapy requires the use of radioactive particles to induce cancer cell apoptosis by damaging its DNA.[14] Although radiation therapy can be physically directed toward the malignant tissue, harmful side effects are typically associated with this approach and it can only be used to treat solid tumours.

Interest in biopharmaceuticals like small interfering RNA (siRNA) or antisense oligonucleotides (ASOs) as drug molecules has seen renewed growth in recent years.[15–17] Furthermore, complex biologics, including chimeric antigen receptor T cells (CAR-T) or genome editors such as clustered regularly interspaced short palindromic repeats (CRISPR)-Cas systems have witnessed a surge in the research landscape; these strategies have the potential to revolutionise the treatment of serious human disease through curative intervention with a single treatment.[18–20] However, many of these modalities are in early stages of development and have issues with cost, delivery or safety that must be overcome before widespread use for cancer treatment as well as other diseases can be implemented. Monoclonal antibody (mAb) therapies have proven to be the most developable biotherapeutic format. There are currently more than 80 mAbs approved for a range of diseases with approximately half of these used to treat an array of oncology indications.[21] The mechanism of action of mAb drugs can vary depending on the antibody, its cognate antigen and the cell type that it targets.

1.2 Antibody-Drug Conjugates

The concept of targeted drug delivery dates back to 1913 when Paul Ehrlich proposed the hypothesis of specifically delivering a ‘toxophore’ to a tumour using a ‘heptophore’.[22] By targeting a cytotoxic drug to a specific cell type, debilitating side-effects can be lowered, thus allowing the use of more potent toxins. The culmination of these events is that targeted therapeutics can decrease the minimum effective concentration (MEC) required to eradicate the cancer while concurrently increasing the maximum tolerated dose (MTD) of the drug, resulting in an overall increase in therapeutic index (TI) (Figure 1.3).

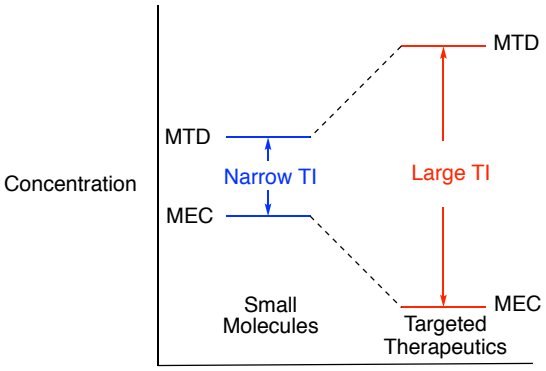

Figure 1.3: Targeted therapeutics have a larger TI than small molecule drugs.

The emergence of antibody-drug conjugates (ADCs) over the past 40 years lends promise to the realisation of Ehrlich's proposed 'magic bullet' therapy. An ADC is a ternary molecule comprised of a cytotoxic molecule that is covalently attached to a mAb via a chemical linker (Figure 1.4). Each of the three components has their own role within the ADC. However, each of the components also influences the function of the other and the construct design must be balanced to accommodate all three moieties.

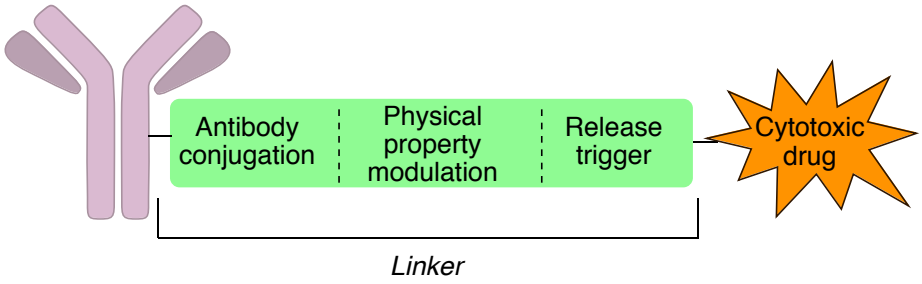

Figure 1.4: General structure of an ADC.

ADCs utilise the unique cell targeting ability of an antibody for its cognate antigen to discriminate between healthy and cancer tissue and selectively deliver a highly potent cytotoxin to the cancer cells. However, it is possible to use ADCs to target any cell type that expresses an appropriate antigen.[23] ADC binding of the cell surface antigen typically causes internalisation of the entire complex. Subsequent sub-cellular trafficking and processing in either the endosomes or lysosomes releases the cytotoxin which is then able to carry out its own mechanism of action to cause cell death (Figure 1.5).[24–26]

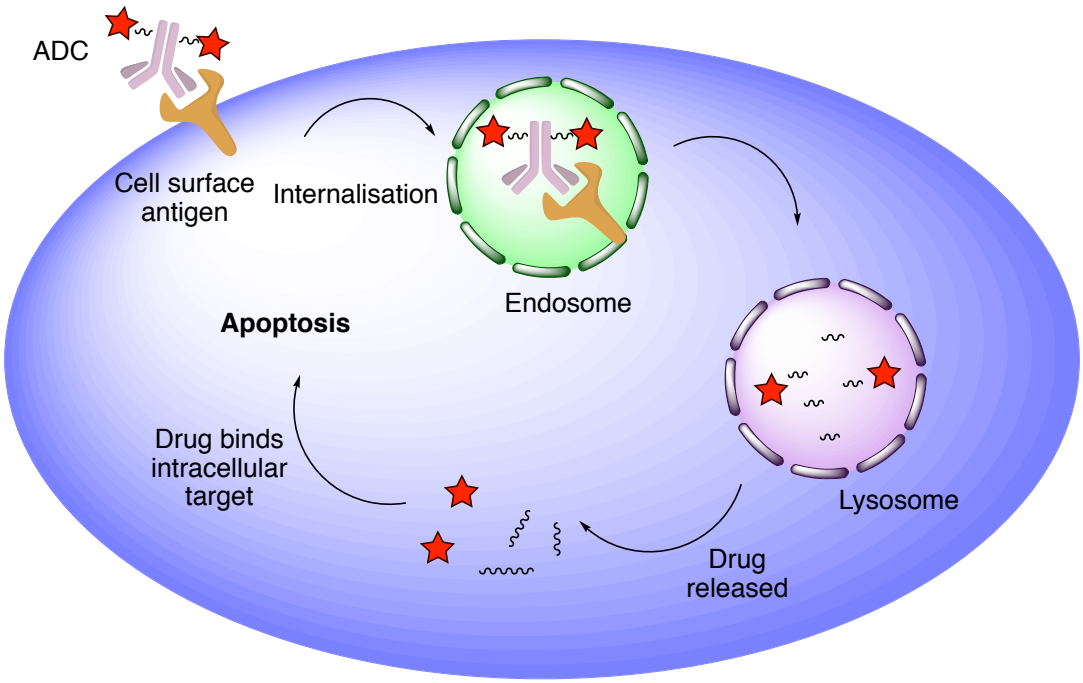

Figure 1.5: Internalisation, trafficking and processing of an ADC to release the active cytotoxin.

The first ADC was reported in 1958 by Mathé *et al.* who described the attachment of methotrexate to a leukemia cell-targeting antibody (Figure 1.6).[27,28] However, it wasn't until 2000 that the first ADC made it to market when gemtuzumab ozogamicin (Mylotarg®) gained Food and Drug Administration (FDA) approval for the treatment of acute myeloid leukemia (AML). A post-approval study demonstrated that Mylotarg® did not offer any patient benefit than standard chemotherapy and was voluntarily removed from the market by Pfizer in 2010.[29] Mylotarg® was re-introduced to the market in 2017 for patients CD33-positive AML, dependent on adverse risk factors.[30,31]

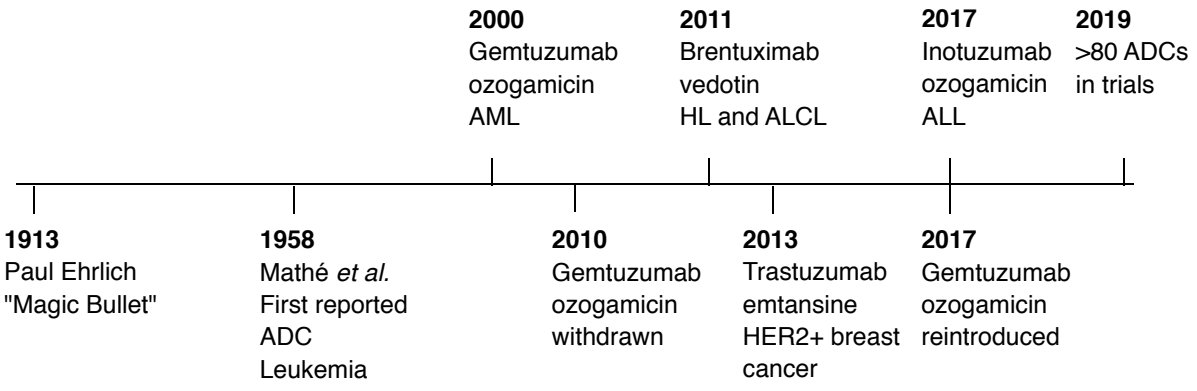

Figure 1.6: Historical timeline of ADC development.

The disappointment of Mylotarg's initial removal from the market in 2010 was quickly overcome with the approval of brentuximab vedotin (Adcetris®) in 2011 for the treatment of relapsed or refractory Hodgkin's Lymphoma (HL) and anaplastic large cell lymphoma (ALCL).[32–35] In 2013, trastuzumab emtansine (T-DM1, Kadcyla®) was approved for the treatment of HER2-positive metastatic breast cancer.[36,37] Apart from the re-introduction of Mylotarg®, 2017 also witnessed the approval of inotuzumab ozogamicin (Besponsa®) to treat relapsed or refractory B cell precursor acute lymphoblastic leukemia (ALL) via targeting of CD22.[38,39] There are currently over 80 other ADCs in the clinic, nine of which are in advanced trials. Sacituzumab govitecan has completed Phase III trials and is expected to be granted approval by the FDA and European Medicines Agency (EMA) in 2019 for the treatment of triple negative breast cancer.[21] In addition, polatuzumab vedotin is an anti-CD79b ADC that is under investigation for diffuse large B cell lymphoma (DLBCL) – a type of non-Hodgkin's lymphoma (NHL). Roche has submitted a request for accelerated approval of polatuzumab vedotin based on promising Phase II clinical data.[21,40,41]

1.3 Monoclonal Antibodies (mAbs)

Antibodies are Y-shaped glycoproteins comprised of four polypeptide chains – two identical light chains (LCs) and two identical heavy chains (HCs) (Figure 1.7). Together, these polypeptides form two Fab (fragment, antigen binding) arms and an Fc (fragment, crystallisable) stem. The Fc contains four constant domains – two on each HC (C_H2 and C_H3). Each Fab is comprised of two variable domains – one on the LC (V_L) and one on the HC (V_H) – and two constant domains – one on the LC (C_L) and one on the HC (C_H1). The constant regions of an antibody are highly conserved for a particular antibody subtype while the variable domains can have large degrees of sequence and structural variance. The C_H2 domains also contain a conserved glycosylation pattern at Asn297.[42,43] The most abundant antibody format in humans is immunoglobulin G (IgG).

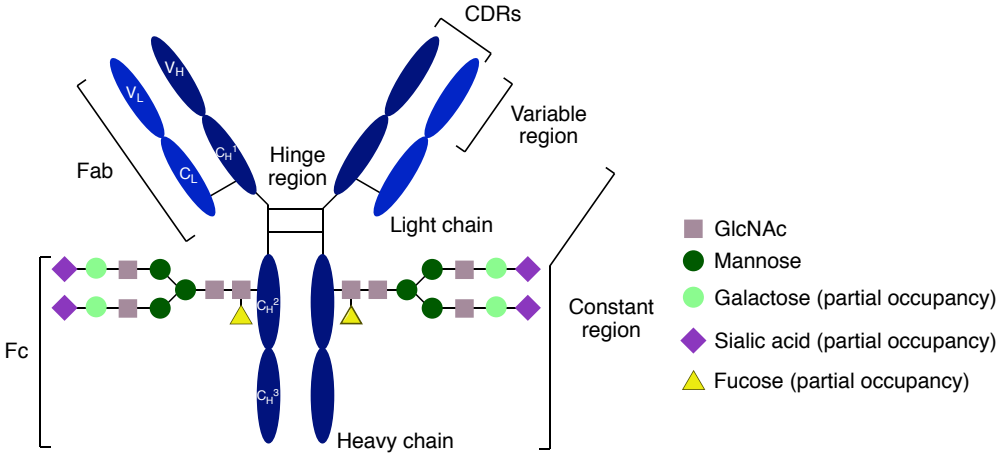

Figure 1.7: General structure of an IgG_1 antibody.

B lymphocytes comprise one half of the adaptive immune response. Upon detection of a foreign species through interaction of B cell receptors with surface receptors on the foreign pathogen, the B cell produces antibodies as part of the host defence against the infection. An antibody has two main functions. The first is to recognise and bind specific cell surface receptors called antigen. Antibodies recognise and bind to their target antigens via interactions at the hypervariable loops at the amino termini of the variable domains, called complementarity determining regions (CDRs).[44] Upon antigen recognition, the antibody then carries out its second function of recruiting effector immune cells to engulf and destroy the bound cell. The Fc region of the antibody is responsible for this identification and can cause pathogen removal through interaction with complement proteins or via antibody dependent cellular cytotoxicity (ADCC) by virtue of interaction of the Fc with Fc receptors (e.g. FcγR) on immune cells.[45,46]

In 1997, rituximab became the first stand-alone anti-tumour antibody to obtain FDA approval for the treatment of relapsed or refractory CD20+ B cell non-Hodgkin's lymphoma.[47] Despite the large number of mAb based therapies that have reached the market, many of them are insufficiently efficacious to eradicate the cancer on their own and require combination therapy strategies to cure the disease.[21] In contrast, highly toxic ADCs offer the opportunity to achieve the same selective cell killing offered with mAb therapies but with a decrease in the dose required to obtain that cancer eradication.

An ADC can only be used to selectively deliver cytotoxins to cancer cells if those cells express an antigen at higher levels than healthy cells. A range of targetable antigen have been identified that are overexpressed on a wide variety of cancer types.[48] A monoclonal antibody

(mAb) can then be matured to specifically bind that surface antigen. Advances in hybridoma and protein engineering mean that the production of therapeutic mAbs is now a relatively straightforward procedure.[49,50]

1.4 Cytotoxic Drugs

The cytotoxic drug (often referred to as the warhead or payload) is responsible for killing the target cancer cells. Early ADC research utilised existing chemotherapies such as methotrexate or doxorubicin (Figure 1.8).[27,51] However, early clinical investigations revealed much lower activity than predicted from preclinical evaluation. For example, the Lewis-Y targeted ADC BR96-doxorubicin demonstrated almost no clinical activity against metastatic breast cancer, having demonstrated selective toxicity preclinically.[52]

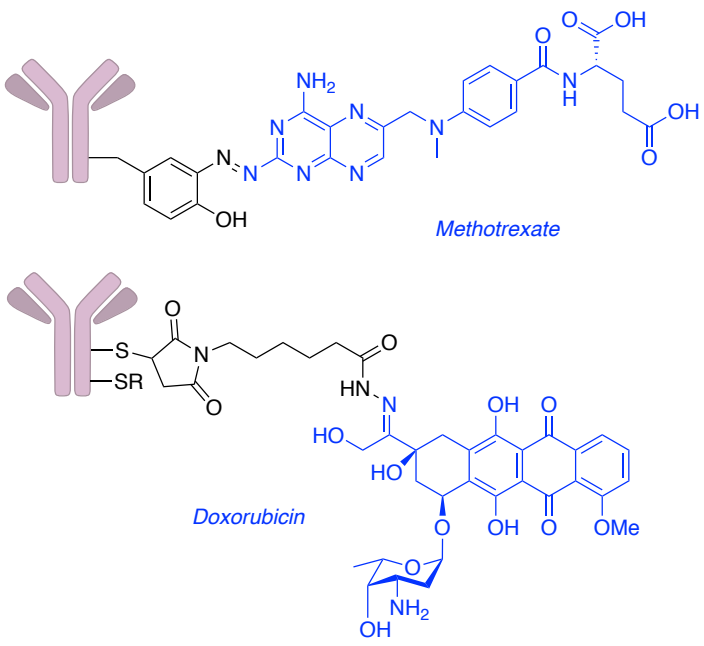

Figure 1.8: Early ADC research used existing chemotherapy agents such as methotrexate or doxorubicin as their payload. R indicates that modifications are on both cysteine residues. Cytotoxin highlighted in blue and linker in black.

There are a number of reasons that may explain the markedly lower clinical effect of these ADCs compared to the effect seen on preclinical evaluation. Due to the complex and variable route that an ADC molecule must undergo before an active drug molecule can be released inside a cancer cell, only a small amount of the administered dose will generate an active warhead in a cancer cell.[53] This means that payloads with exceptionally high toxicity (sub-nanomolar IC_{50}) are required. Early ADCs did not contain payloads in this potency range and

may go some way to explaining their failure.[54] In addition, a number of other criteria must be met for a cytotoxic drug to be used as an ADC warhead. Cytotoxic drugs tend to be lipophilic molecules and as such can have great influence on the pharmacokinetics of the ADC. Increased lipophilicity must be limited as this can cause antibody aggregation and increased clearance.[55] Furthermore, the drug must have some degree of aqueous solubility to enable conjugation to the antibody and it must be suitable for chemical modification with a linker.

After the failings of initial ADC trials using classic chemotherapy payloads, second generation ADCs explored more potent warheads. Investigations in this area focused on natural products and their derivatives that had been discovered and found to be too potent for use in chemotherapy. Combined, the calicheamicins, auristatins and maytansinoids account for all of the approved ADC payloads and the majority of those under clinical investigation. Calicheamicin is a potent anti-cancer natural product that causes site-specific double strand DNA breaks, initiating apoptosis (Figure 1.9a).[56] *N*-acetyl-γ-calicheamicin can be functionalised with a linker and is used as the cytotoxic payload in gemtuzumab ozogamicin and inotuzumab ozogamicin.

Dolastatin 10 is a highly potent cancer drug that causes cell death by binding to tubulin, thus preventing microtubule formation and subsequent mitosis. Monomethylauristatin E (MMAE) and monomethylauristatin F (MMAF) are synthetic derivatives of dolastatin 10 that have found widespread use in ADC research (Figure 1.9b).[57,58] Indeed, approved brentuximab vedotin contains an MMAE warhead, with many more ADCs in clinical development using either an MMAE or MMAF payload.[33]

Maytansinoids such as emtansine (DM1) and ravtansine (DM4) are another group of antimitotic agents based on the natural product maytansine, and are frequently used in ADC development (Figure 1.9c).[59] Indeed, trastuzumab emtansine has a DM1 payload.[37]

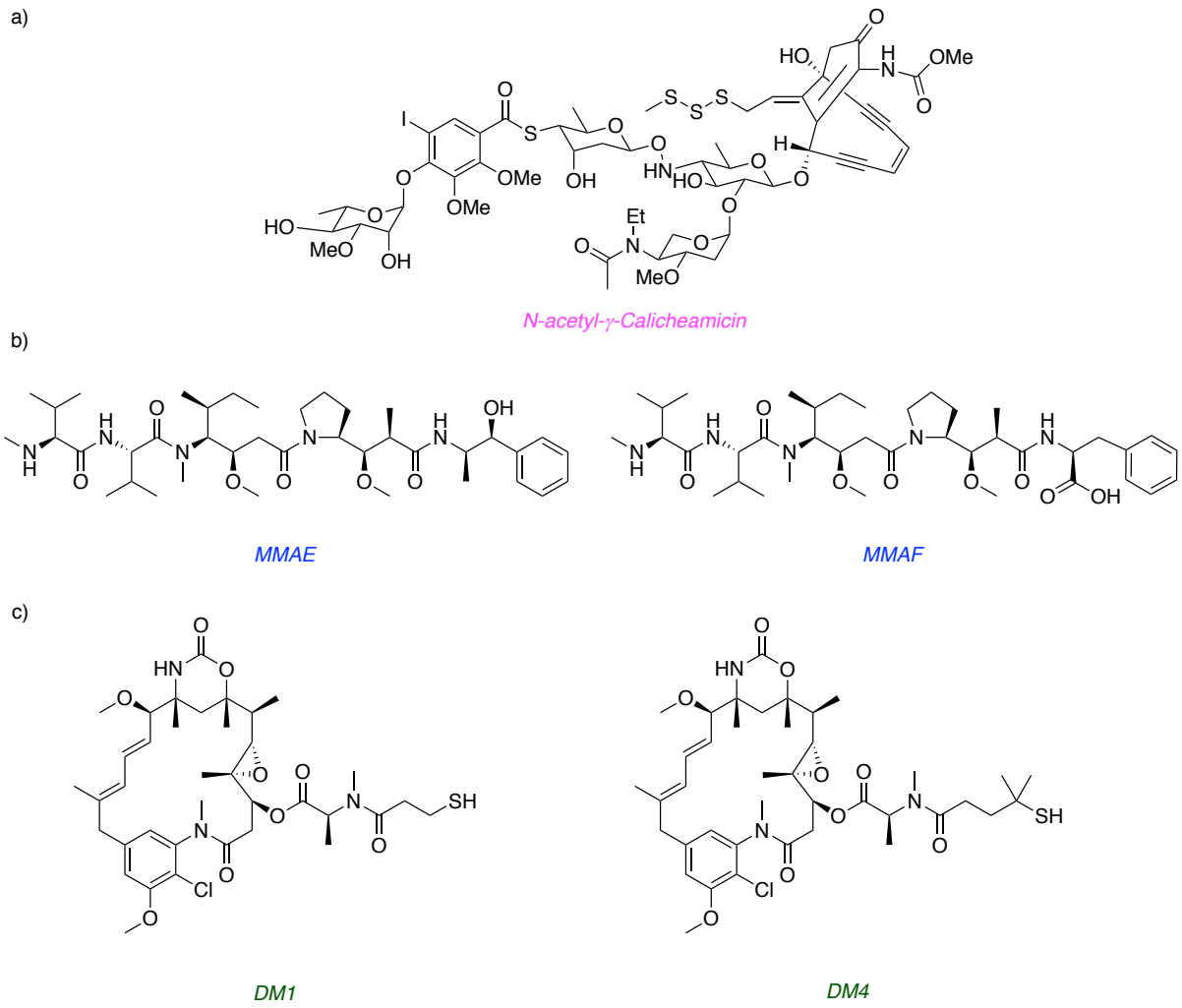

Figure 1.9: Widely used ADC payloads **a)** *N*-acetyl-γ-calicheamicin, **b)** auristatin payloads MMAE and MMAF, and **c)** maytansinoid payloads DM1 and DM4.

In recent years, the number of different ADC payloads under investigation has increased significantly. For instance, DNA alkylating agents such as the pyrrolobenzodiazepine (PBD) dimers and duocarmycins; antimitotic drugs including the tubulysins; and DNA topoisomerase I inhibitors such as the camptothecin analogues have all been studied as ADC payloads, with numerous examples of these payloads reaching the clinic (Figure 1.10).[60–67] All of these cytotoxins are exceptionally potent molecules with low or sub-nanomolar IC_{50} values.

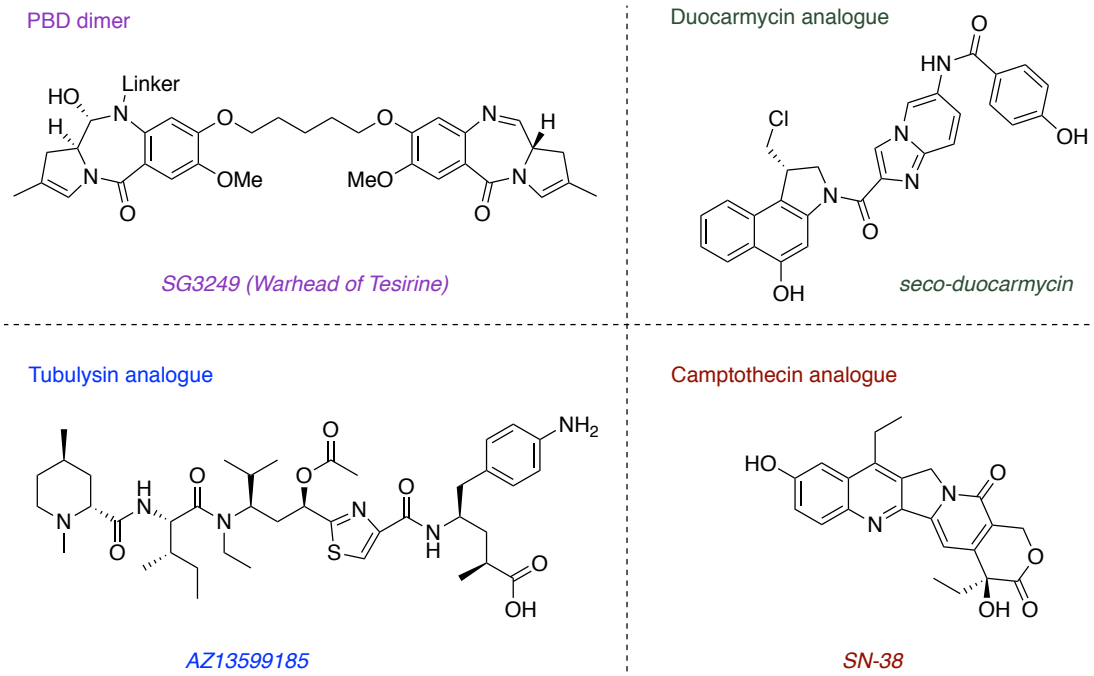

Figure 1.10: Natural product analogues currently under investigation as ADC payloads.

The choice of payload is dependent on the antibody, molecular characteristics of the cancer type and the desired release mechanism from the antibody.

1.5 Linkers

The ADC linker is responsible for connecting the cytotoxic warhead to the mAb. Linker reagents are hetero-bifunctional molecules with orthogonal functional groups to allow chemoselective reaction with the antibody and the payload. ADC linkers should adhere to a stringent set of prerequisites to ensure a safe and efficacious ADC is administered. First, the conjugate must remain intact while circulating the bloodstream as decomposition of the conjugate could cause systemic toxicity. The linker should then permit release of the cytotoxin from the antibody upon internalisation into target cells. It is crucial that the linker enables traceless release of an unmodified warhead or that the payload that is cleaved from the antibody is not inhibited by the attached linker.[68] Moreover, the conjugation chemistry should enable efficient and reproducible ADC synthesis. Aside from these absolute requirements, the linker can also be used to modulate the physical properties of the ADC.

1.5.1 Release Mechanism

ADC linkers can be classified in numerous ways. Oftentimes, they are categorised based on the method by which the payload is released from the antibody. In this sense, ADC linkers can be regarded as cleavable or non-cleavable.

1.5.1.1 Cleavable Linkers

Cleavable linkers utilise the distinct chemical or enzymatic intracellular conditions of the cell to release the payload from the antibody. Upon internalisation, the ADC-antigen complex is encapsulated in an endosome via receptor-mediated endocytosis. From here, the complex is trafficked to a lysosome, where proteins, including antibodies are digested into their constituent amino acids. Initial ADC linkers aimed to exploit the different intra- and extracellular chemical environments to release the drug molecule. Endosomes (pH 5.0 – 6.5) and lysosomes (pH 4.5 – 5.0) are more acidic than the bloodstream (pH 7.4).[69] This acidic environment can be exploited through the use of acid-labile groups to cause linker decay and subsequent drug release. Approved ADCs Mylotarg® and Besponsa® both utilise linkers that contain an acid-sensitive acyl-hydrazone, which upon exposure to endosomes or lysosomes triggers the release of calicheamicin from the antibody (Figure 1.11).[70]

Cytoplasmic concentrations of free thiols such as glutathione (GSH) are also much higher (1–10 mmol/L) than the extracellular environment (~5 μmol/L).[71,72] As such, disulfide linkers enable free thiol-mediated cleavage of the ADC to release the cytotoxic warhead (Figure 1.11). Maytansinoid payloads are commonly connected to the antibody via a disulfide linkage.[73] However, steric bulk around the disulfide is often required to ensure ADC stability in circulation. In spite of this, chemically-cleavable linkers containing disulfides or hydrazones tend to suffer from poor *in vivo* stability, lowering the MTD of these ADCs.[74,75]

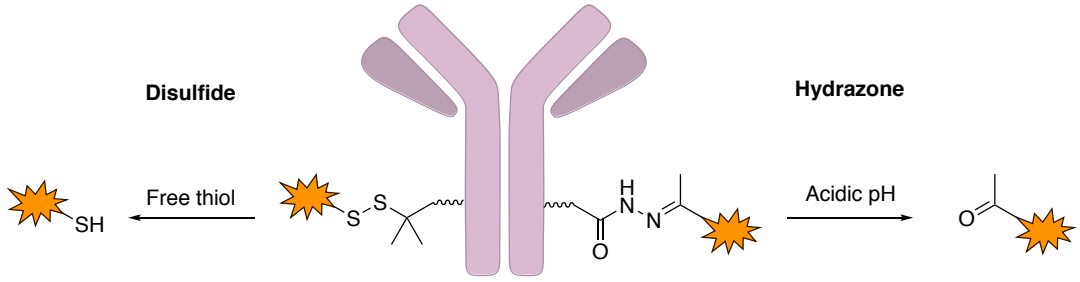

Figure 1.11: Chemically-cleavable disulfide and hydrazone ADC linkers. Disulfides can be cleaved in highly reducing conditions of the cytoplasm. Hydrazones can decay in the acidic endosomes or lysosomes to release the cytotoxic drugs.

Enzyme-cleavable linkers offer a more stable alternative than their chemically-sensitive counterparts. The cathepsins are a family of peptidases that recognise and cleave short peptide sequences in a sequence-specific manner. Cathepsin B is a member of this family that is overexpressed in many cancer types.[76,77] This enzyme catalyses the cleavage of the *C*-terminus amide of a number of short peptidic sequences. The valine-citrulline and valine-alanine dipeptides have been extensively used with auristatin and PBD payloads, respectively (Figure 1.12a). ADC payloads tend to be large, sterically-demanding molecules; a self-immolative *p*-aminobenzoylcarbonyl (PABC) spacer is typically used on the *C*-terminus of the linker to give the enzyme room to cleave the desired bond and to enable traceless release of the payload (Figure 1.12b).[78] Indeed, the approved ADC brentuximab vedotin contains a val-cit-PABC cleavable linker.[33] A number of other cathepsin B-sensitive motifs with enhanced enzyme selectivity or better physiochemical properties have also been developed, such as a simple lysine amino acid or a cyclobutane-containing linker (Figure 1.12a).[66,79,80]

β-glucuronidase has been shown to be overexpressed and present in high quantities in the lysosomes of cancer cells.[81] β-glucuronic acid-containing linkers have been developed and used in ADC research over the last decade to exploit this. In addition, the high polarity of a β-glucuronide moiety potentially masks the hydrophobicity of cytotoxic warheads, thus preventing antibody aggregation.[82] A PABC-type self-immolative spacer is also routinely used for these linkers. β-glucuronic acid linkers have been used to synthesise ADCs with various payloads including MMAE, MMAF, duocarmycin analogues and camptothecin analogues (Figure 1.12a).[83–86]

The development of pyrophosphate diester linkers has recently been described by researchers at Merck. Phosphodiesterases are known to be present at high levels in lysosomes.[87] In addition, phosphate diesters are charged, polar species. Combined, these

characteristics make such molecules attractive candidates as cleavable ADC linkers. ADCs containing glucocorticoid payloads have been described with phosphate diester linkers (Figure 1.12a). These ADCs were shown to be stable and efficacious in a series of *in vitro* investigations.[88–90]

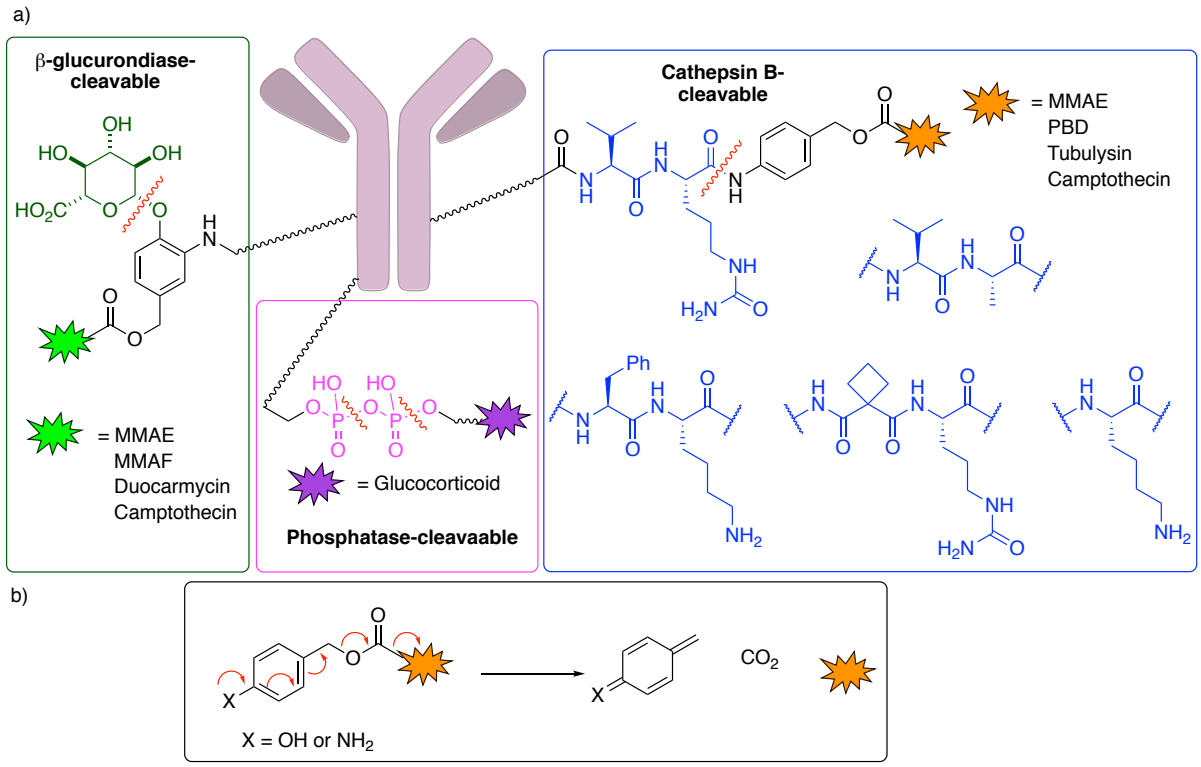

Figure 1.12: a) Enzyme-cleavable linkers used in ADC research include moieties that are sensitive to cathepsin B, β-glucuronidase and phosphatases. The cleaved bonds are indicated with a red line. **b)** A self-immolative PABC spacer is often incorporated in cathepsin B and β-glucuronidase linkers.

1.5.1.2 Non-Cleavable Linkers

An alternative strategy is to utilise the lysosomal degradation of the antibody into its constituent amino acids to release the warhead. Such linkers do not contain a specific release trigger and so the cytotoxic molecule is released with the linker and the amino acid on the antibody to which it was conjugated (Figure 1.13).[91] The success of so-called non-cleavable linkers is dependent on the mechanism of action of the warhead and the position on the warhead where the linker is attached. Ado-trastuzumab emtansine contains the non-cleavable linker 4-(maleimidylmethyl)cyclohexane-1-carboxylate (MCC). Conjugation of this linker to trastuzumab occurs via lysine modification and so the released maytansine contains a Lys-MCC auxiliary (Figure 1.13). This addition has been shown not to affect the potency of the maytansine payload.[37]

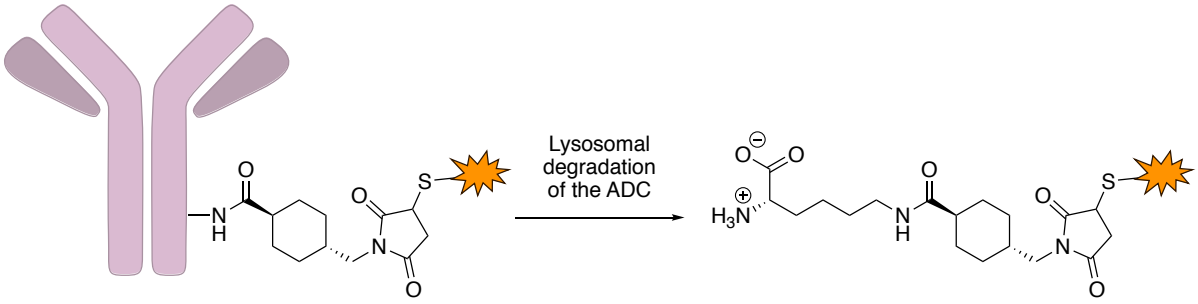

Figure 1.13: Non-cleavable ADC linkers such as the MCC linker shown here release the payload with the linker and conjugating amino acid attached.

The cleaved payload in non-cleavable linkers is zwitterionic. Therefore, it has poor membrane permeability and will not be able to diffuse out of the cell where it was released.[92] This can be seen as both beneficial or detrimental, depending on the cancer type that is being treated. In one sense, this can be advantageous as a highly potent cytotoxin cannot enter peripheral healthy tissue, causing harmful side-effects. However, the molecular characteristics of tumours can be highly heterogeneous; in certain cancers, large areas of the tumour may not express the target antigen of the ADC. The administered ADC will have little effect on these cells if a non-cleavable linker is employed. In contrast, the use of cleavable linkers will release an uncharged, unmodified payload that can permeate into neighbouring tumour cells, also killing these cells in a phenomenon known as the 'bystander effect'.[93,94]

1.5.2 Antibody Modification

The second main requirement for any linker molecule is to conjugate the drug to the antibody. The type of chemistry used to link the payload and subsequently the linker-drug to the antibody can greatly affect the performance of the ADC. Connecting the drug to the linker can typically be achieved with simple, robust chemistry. However, due to the large size (~150 kDa) and abundance of various functionalities on an antibody, reaction between the linker and the antibody can pose a formidable challenge. Reactions used in protein modification must meet a strict set of requirements to ensure efficient and robust conjugation; the reaction must work in aqueous conditions at low micromolar concentration, be selective for its target amino acid, and proceed with rapid reaction rates under mild conditions.[95,96] A large toolbox of protein modification reactions has been developed, enabling modification of many natural and genetically incorporated unnatural amino acids (UAAs).[97–100] The following sections will primarily focus on protein modification techniques that have been used for the modification of IgG antibodies, particularly for the synthesis of ADCs.

1.5.2.1 Drug-Antibody Ratio and Modification Site

An important consideration in ADC development is the number of drug molecules that are attached to each antibody molecule. A surface-expressed antigen can only internalise one ADC molecule and, depending on the target antigen, this internalisation can be limited. In order to maximise the cytotoxic potential of the internalised ADC, loading the antibody with many drug molecules to give a higher drug-antibody ratio (DAR) is desirable. However, this must be balanced with the physicochemical and toxicology properties of the antibody to ensure that the drug loading does not cause increased aggregation and clearance, or a poor safety profile. The site of attachment on the antibody can also affect its function by inhibiting antigen recognition and binding. The conjugation technique used to attach the payload can be used to modulate the DAR and location of conjugation. For example, synthetic procedures used to synthesise gemtuzumab ozogamicin generate a batch of ADC in which 50% of the antibody does not have any calicheamicin attached (i.e. DAR = 0).[101] Unconjugated antibodies will still bind the target antigen, inhibiting binding of ADC molecules and decreasing its potential efficacy. In contrast, overloaded antibodies with high DAR tend to have increased hydrophobicity and aggregation, resulting in higher clearance rates. ADCs with DARs ranging from two to eight have been widely investigated as drug loading to this degree offers a balance between reaching sufficient intracellular concentration of the payload without causing significant toxicity or pharmacokinetic (PK) issues. Even small alterations to the average DAR of the same ADC can result in dramatically different PK and toxicity profiles. A study has shown that *in vivo*, an anti-CD30 antibody conjugated with auristatin payloads with an average DAR of four demonstrated almost identical cytotoxicity as the same ADC with an average DAR of eight. The highly loaded DAR eight ADC was cleared from the body at a greater rate, suggesting that similarities in cytotoxicity were related to its poor PK profile.[102]

The site of payload conjugation on the antibody can also be critical to its resultant pharmacology. Attachment of the drug in the Fab region can affect antigen recognition by the antibody, with the potential to lower antibody-antigen binding and consequently the efficacy of the ADC. Additionally, the attachment position can also affect the stability of the linkage between the antibody and the linker.[103,104] Unstable conjugation resulting in premature cytotoxin release lowers the TI of the ADC by increasing off-target effects and decreasing efficacy.[105]

1.5.2.2 Heterogeneous Antibody Modification

Natural amino acids contain side chains with a range of functional groups. From a protein modification viewpoint, nucleophilic side chains such as the amino group of lysine residues or the thiol of cysteine represent the most attractive targets for conjugation sites via reaction with complementary electrophilic groups on a linker.

A) Lysine Modification

Early strategies for the covalent attachment of cytotoxic warheads onto mAbs targeted solvent-exposed lysine residues. Lysine amines can be readily functionalised via reaction with modified *N*-hydroxysuccinimide (NHS) esters (Figure 1.14). Indeed, Mylotarg®, Kadcyla® and Besponsa® are all synthesised via reaction of exposed lysines with NHS ester derivatives of their respective payloads. However, a standard IgG antibody has approximately 80 lysine residues, half of which are chemically modifiable. Therefore, synthesising an ADC with an exact DAR and control of the conjugation location is virtually impossible. ADCs synthesised via this stochastic lysine modification result in a mixture of ADC structures with varying DAR and with numerous regioisomers of ADCs with the same DAR. For example, Wang and co-workers demonstrated that modification of an IgG antibody with an NHS ester payload generated ADCs with DARs ranging from 0 to 6. In addition, the synthesised batch of ADC contained over 4.5 million different chemical species.[106] Each ADC will have its own unique pharmacokinetic, stability, toxicity and efficacy profile making it difficult to predict what the properties of the ADC mixture will be after administration.[43]

A number of other methods have also been described for the modification of IgG lysines including acyl fluorides, β-lactams, isothiocyanates and sulfonyl acrylates (Figure 1.14).[107,108] Although there are many surface lysine residues available for conjugation in a standard mAb, the microenvironment around these lysines is typically quite different and can alter the pKa values of lysine amines. Amines with decreased pKa will be less likely to be protonated at physiological pH and therefore have higher nucleophilicity than protonated lysines.[109] A number of studies using β-lactams and sulfonyl acrylate reagents have exploited this phenomenon to modify specific lysine residues in an antibody.[110–112] However, precise control with these methods and the generality of the approach is not yet clear.

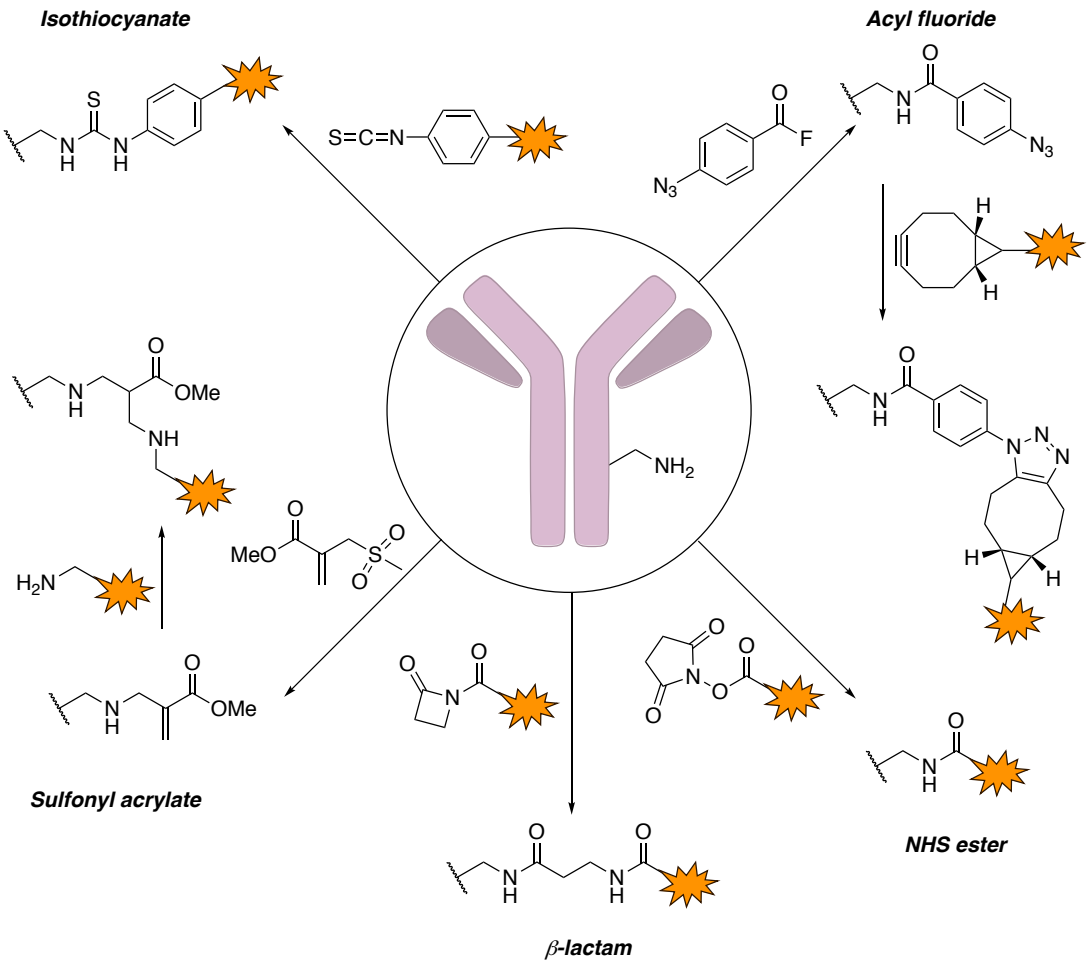

Figure 1.14: Methods used for the modification of antibody lysines.

B) Cysteine Modification

Cysteine modification has emerged as a popular modification site for synthesising ADCs. The unique reactivity of the cysteine side chain sulfhydryl enables selective modification with a catalogue of available reagents.[113,114] All IgG cysteines are present as disulfides, which must first be reduced to reveal the reactive thiol. Both intra- and interchain disulfides are found in IgG molecules. Favourably, reduction of accessible interchain disulfides is more facile than the buried intrachain disulfides. IgG_1 antibodies, which are most commonly used in ADC research contain four interchain disulfides that upon reduction yields eight free thiols available for reaction. Cysteine modification offers more control than lysine modification in terms of conjugation site as the interchain disulfides are all located either in or near the hinge region of the antibody, far from the CDR antigen-binding domains. Although cysteine conjugation also offers marginally better control of DAR than lysine modification with only eight available conjugation sites, heterogeneous mixtures of ADC are typically produced by modification of interchain cysteines. Alteration of the DAR via interchain cysteine conjugation is typically

controlled by a combination of partial reduction-reoxidation strategies and linker stoichiometry. This process is difficult to control and can lead to alterations in the antibody structure, potentially diminishing its biological function. Moreover, conjugation to these residues breaks the only covalent bonds that connect the heavy and light chains and may affect the stability and biological profile of the antibody.[115]

Maleimide reagents are routinely used for cysteine modification (Figure 1.15). Maleimides are easily functionalisable and react rapidly and efficiently with cysteine thiols under mild conditions. In the field of ADC research, maleimide linkers have been incorporated into a host of various linker-drug types, including chemically-cleavable, enzyme-cleavable and non-cleavable linker-drugs. Notably, Adcetris® is synthesised via maleimide-mediated payload attachment to interchain cysteine residues. Many other ADCs containing interchain cysteine-maleimide modifications are currently in clinical or preclinical development.[54] However, the generated thiosuccinimide linkage is inherently unstable and can undergo a retro-Michael addition to reform the unconjugated maleimide drug-linker and free thiol (Figure 1.15). In the absence of alternative thiols, the released drug-linker can simply react with the mAb again to reform the ADC. Unfortunately, thiol-containing molecules such as human serum albumin (HSA) are present in circulation, resulting in undesired maleimide exchange reactions. The payload is now no longer targeted to the desired cell type leading to undesired systemic toxicity and a decrease in efficacy.[116–118]

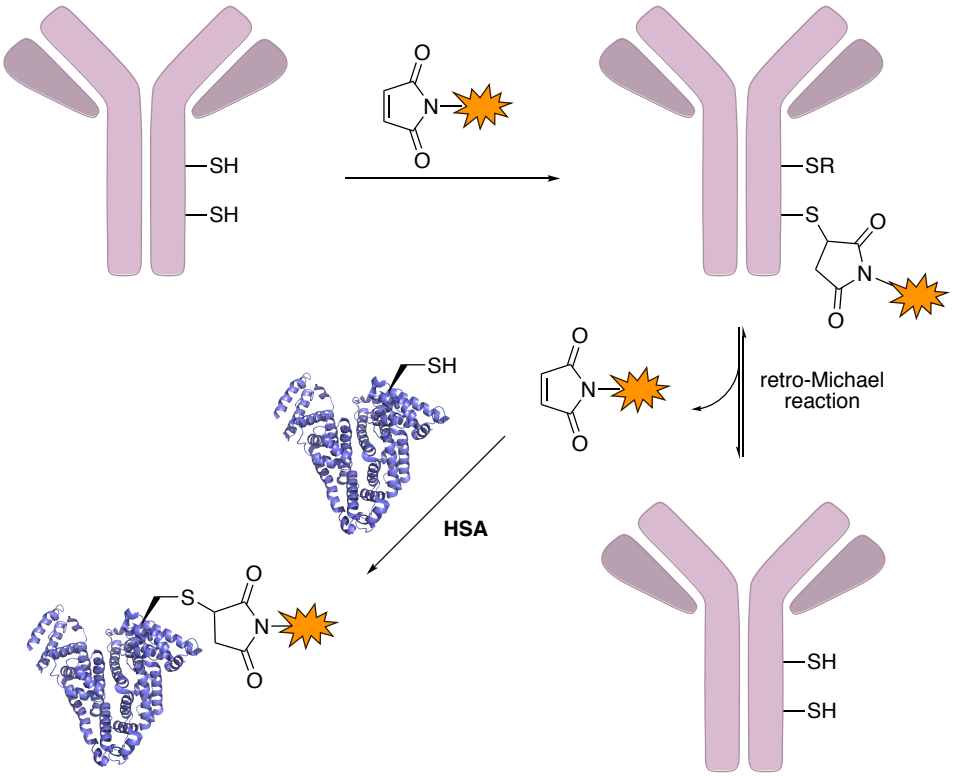

Figure 1.15: Maleimide linkers can be used to modify antibody cysteines. However, the thiosuccinimide product is unstable and can result in the release of the payload from the antibody and trapping of the reformed maleimide by serum thiols such as HSA. R indicates the same chemical modifications are present on both cysteine residues.

The stability of maleimide bioconjugates can be greatly increased by post-conjugation hydrolysis of the succinimide ring (Figure 1.16a).[119] A number of modified maleimide linkers and novel methods[120] have been developed that promote this hydrolysis (Figure 1.16b). The hydrolysis of *N*-alkyl maleimides takes days to proceed under physiological conditions. However, the rate of hydrolysis can be increased significantly via alteration of the *N*-substituent. Incorporation of a polyethylene glycol (PEG) group, a suitably placed primary amine, or a 1,3-dioxane (or dioxolane) between the maleimide and the payload results in rapid hydrolysis of the succinimide ring.[121–124] Additionally, *N*-aryl maleimides are also prone to rapid hydrolysis post-conjugation.[125,126]

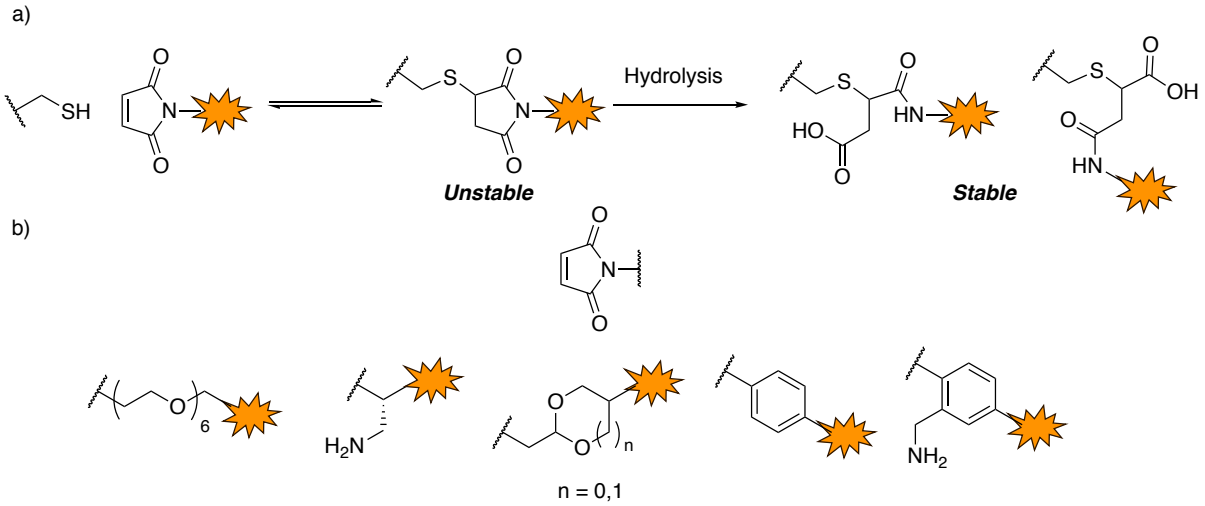

Figure 1.16: a) Hydrolysis of a maleimide-derived thiosuccinmide generates a mixture of stable isomers. **b)** A range of modified maleimide linkers that have been developed to promote thiosuccinimide hydrolysis post-conjugation.

Other methods that have been reported for the single modification of interchain cysteines include the use of α-halocarbonyl linkers or a palladium-mediated cysteine arylation (Figure 1.17).[117,127]

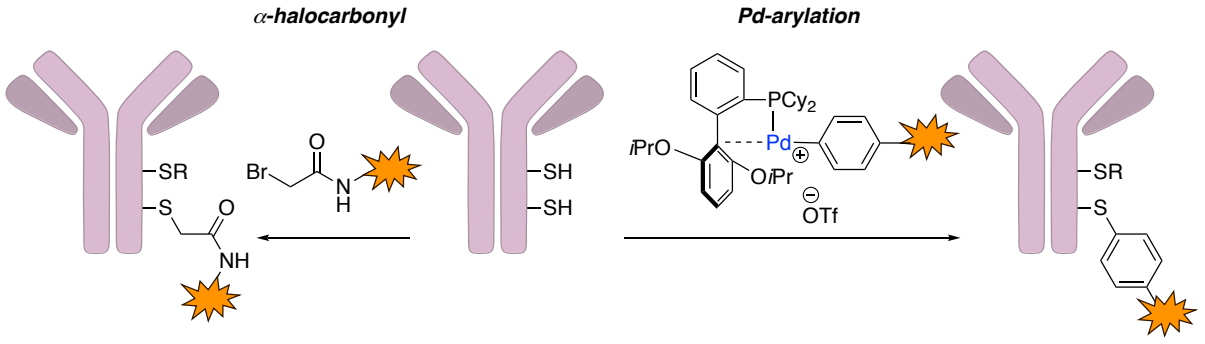

Figure 1.17: Interchain cysteine modification with α-halocarbonyl reagents and Pd-mediated arylation. R indicates the same chemical modifications are made on both cysteine residues.

1.5.2.3 Site-Selective Antibody Modification

Early generation ADCs relied on modification of native lysine and cysteine residues, which generated heterogeneous ADCs with variable pharmacokinetics, stability, toxicity and efficacy. More recent research into linker technologies has focused on strategies that enable the production of homogeneous ADCs with predictable and robust pharmacology. A variety of approaches have been taken to achieve this objective. These include the genetic incorporation

of additional natural or unnatural amino acids, enzymatic modification of amino acid side-chains or antibody glycans, or disulfide rebridging linkers.

A) Enzymatic Antibody Modification

Enzymes are renowned for their high levels of substrate and reaction specificity. Exploitation of these attributes for the generation of homogeneous ADCs via site-selective antibody modification is an attractive concept, which has been investigated in recent years.[128]

Microbial transglutaminase (MTGase) catalyses the formation of an amide bond between a glutamine side chain and an amino-alkyl substrate. It has high specificity for a sequence-specific glutamine residue but broad amino-alkyl substrate compatibility. The conserved Q295 in the C_H2 domain has been found to be an excellent substrate for MTGase if the conserved glycosylation at N297 is first removed by treatment with peptide:*N*-glycosidase F (PNGase F). PNGase F is an efficient and robust enzyme that completely deglycosylates mAbs. Homogeneous auristatin ADCs with DARs of two or four have been produced via MTGase-mediated modification of Q295 (Figure 1.18).[129,130]

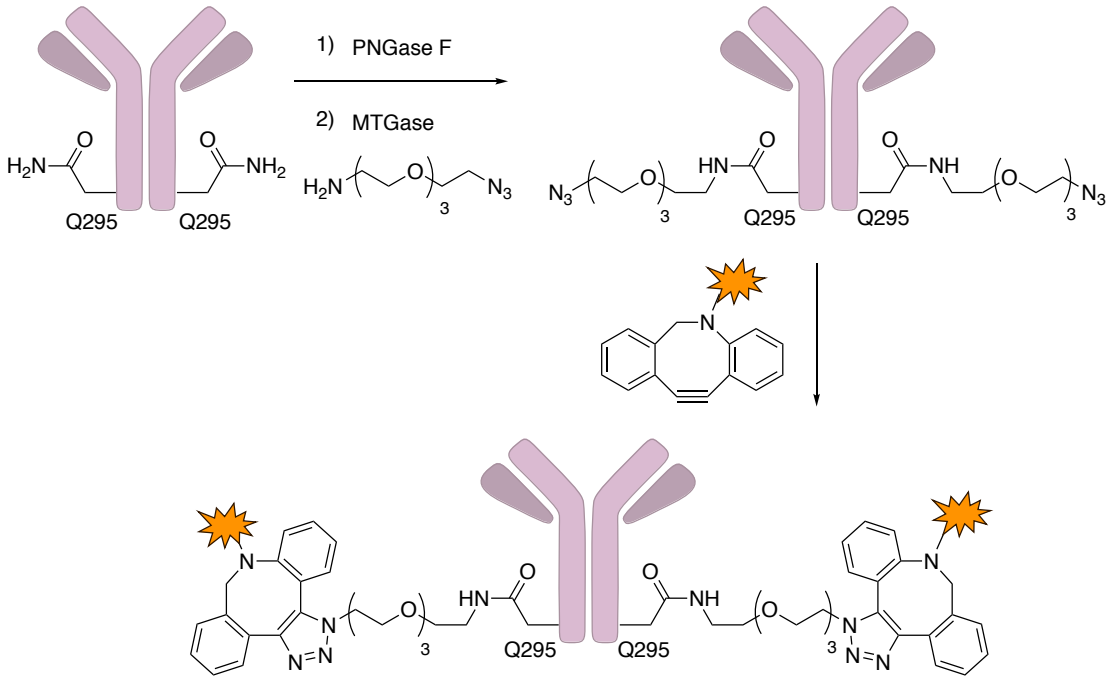

Figure 1.18: Synthesis of homogeneous ADCs via MTGase-catalysed modification of HC Q295.

Bacterial sortase is a transpeptidase that cleaves between threonine and glycine in the LPXTG sequence (X = any amino acid). The enzyme then enables the addition of a glycine-functionalised linker to the *C*-terminus of the threonine residue. Antibodies containing the LPXTG sequence at the *C*-termini of the HCs and LCs have been produced and used to synthesise homogeneous ADCs via sortase catalysis (Figure 1.19a).[131,132]

Similarly, formylglycine-generating enzyme (FGE) utilises a consensus sequence to modify the antibody structure. FGE catalyses the oxidation of cysteine in a CXPXR sequence (X = any amino acid) to a formylglycine amino acid. The CXPXR sequence must be genetically incorporated into the antibody sequence, most commonly at the *C*-termini of the HCs and LCs. This UAA can react to form oxime or hydrazine linkages via bioorthogonal chemistry. Furthermore, a hydrazine-*iso*-Pictet-Spengler (HIPS) reaction has been used to synthesise homogeneous ADCs via reaction of a hydrazine-functionalised indole with the generated formylglycine amino acid (Figure 1.19b).[133,134]

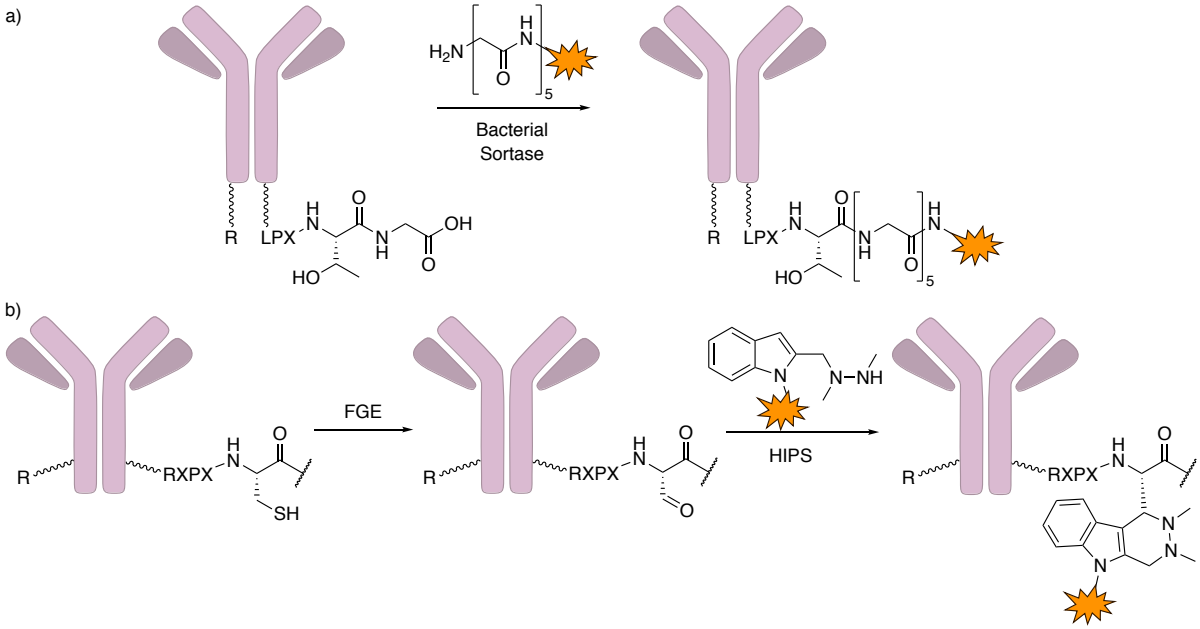

Figure 1.19: a) Sortase-mediated antibody modification and **b)** FGE conversion of cysteine to formylglycine followed by HIPS conjugation. R indicates that modifications are present on both HCs.

While the enzymes mentioned above catalyse modification of the amino acid residues of the antibody, it is also possible to use enzymes to modify the glycan moiety. As was discussed in Section 1.3, IgG antibodies contain conserved glycosylation at N297. However, this glycosylation pattern is heterogeneous across different IgGs. A consensus core

heptasaccharide comprised of *N*-acetylglucosamine (GlcNAc) and mannose can be modified with additional fucoses, galactoses and sialic acids.[135,136]

The most common method of modifying the antibody glycan is via the introduction of non-natural monosaccharides containing bioorthogonal reactive groups (Figure 1.20). For example, a mutant galactosyltransferase (β1,4Gal-T1-Y289L) has been developed that enables the incorporation of ketone-modified galactose (2-keto-Gal) or azide-containing *N*-azidoacetylgalactosamine (GalNAz).[137] The removal of any terminal galactose or mannose sugars from the glycan using β1,4-galactosidase is required before attachment of the modified monosaccharides. Homogeneous ADCs with DARs of two or four have been synthesised via glycan modification.[138,139]

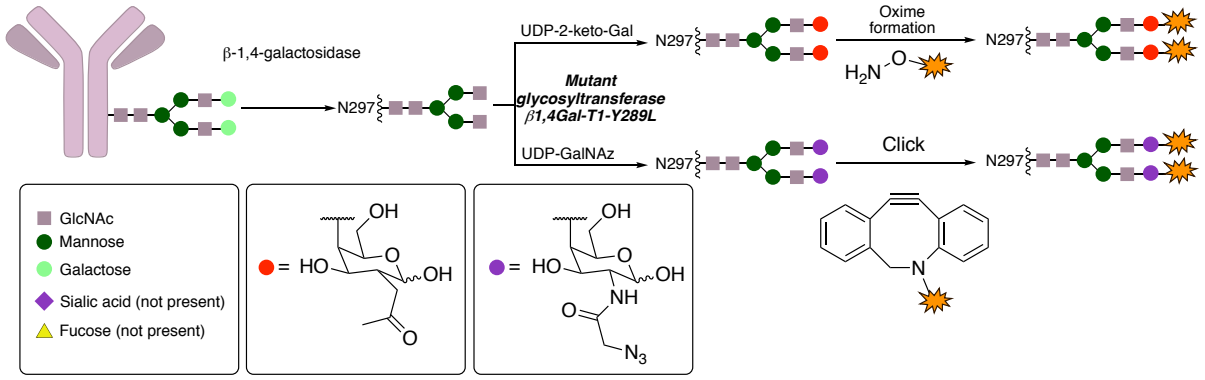

Figure 1.20: Mutant glycosyltransferases can be used to install non-natural monosaccharides containing bioorthogonal functional groups such as azides or ketones onto antibody glycans, enabling the synthesis of homogeneous ADCs. UDP = uridine diphosphate.

B) Genetic Engineering

The most widely employed method of achieving site-selective modification is through the alteration of the antibody gene sequence to enable the incorporation of additional reactive natural amino acids (e.g. cysteine) or UAAs with reactive bioorthogonal side chains.

i) Unnatural Amino Acid Incorporation

The incorporation of UAAs into a protein was pioneered by Schultz and co-workers in the 1980s.[140] In this method, a degenerate amber stop codon (TAG) representing the desired UAA is incorporated into the gene encoding the protein of interest. An orthogonal amino acyl-tRNA synthetase (aaRS)-tRNA pair that recognises this codon is used to install the UAA into the

protein sequence during ribosomal translation.[141] A range of UAAs with bioorthogonal side chains have been incorporated into antibodies using this technology to enable site-selective modification. Homogeneous ADCs have been generated by modification of genetically incorporated *p*-azidomethyl-phenylalanine, *p*-acetylphenylalanine, selenocysteine or azide and cyclopropene lysine derivatives, using established bioorthogonal reactions. (Figure 1.21).[142–146]

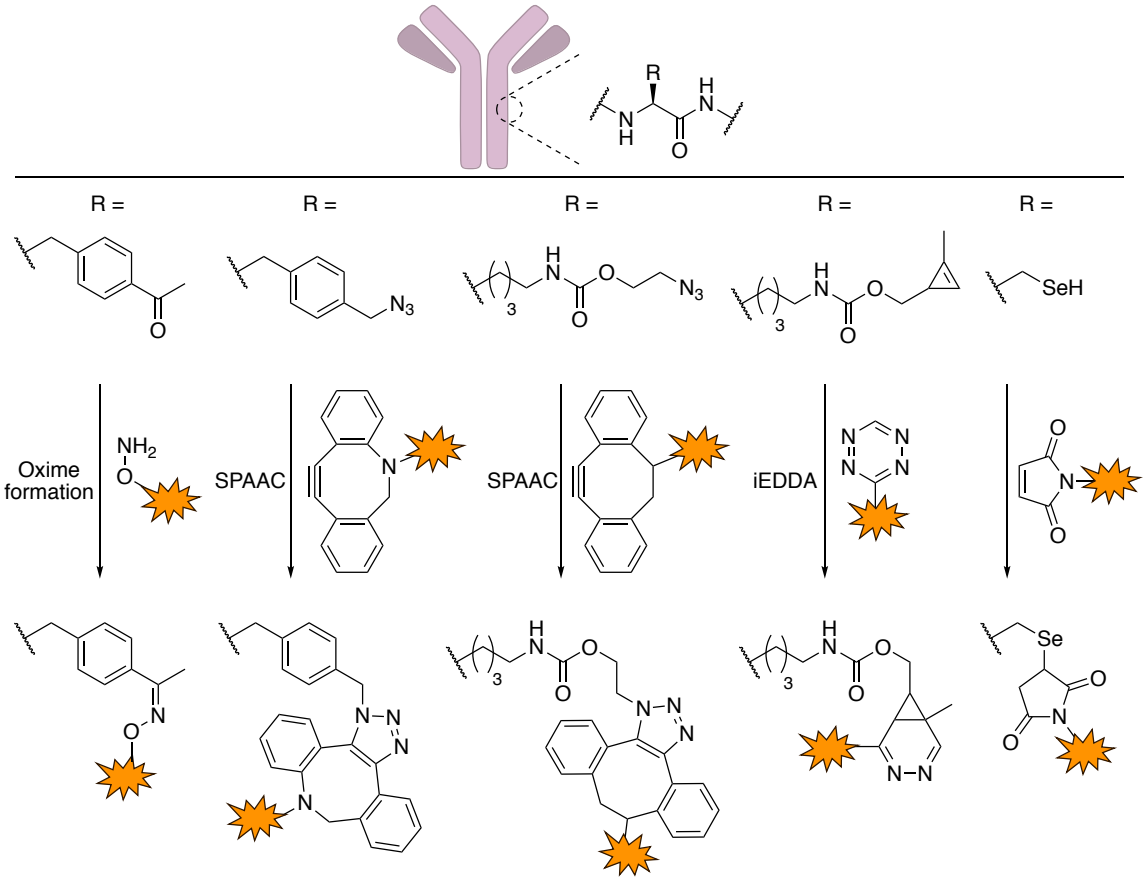

Figure 1.21: A range of UAAs including azide and ketone-modified phenylalanines, azide and cyclopropene-modified lysines and selenocysteine have been incorporated into antibodies, enabling the synthesis of homogeneous ADCs. SPAAC = strain-promoted azide-alkyne cycloaddition, iEDDA = inverse electron demand Diels-Alder.

ii) THIOMAB

One of the earliest investigated methods for site-selective conjugation was the mutation of selected cysteines from interchain disulfides to serine residues in the anti-CD30 antibody cAC10. This generated an antibody with two or four exposed cysteine thiols for conjugation. A highly homogeneous ADC could be produced compared to conjugation using the partially reduced endogenous antibody.[147] Engineered cysteine residues can also be introduced in

other locations on the light or heavy chains. In these so-called THIOMAB antibodies, carefully selected serine, threonine or more commonly alanine residues are mutated to cysteine residues via site-directed mutagenesis.[148–150] While THIOMAB ADCs have generally shown better efficacy and toxicology profiles than their corresponding heterogeneous ADC counterparts, it has become clear that the site of mutation is crucial to the stability, safety and efficacy of the ADC.[42] Moreover, many THIOMAB ADCs are produced with maleimide linkers, which have safety concerns of their own (*vide supra*). A small number of THIOMAB ADCs have been reported that use alternate cysteine modification reagents such as bromomaleimides, carbonylacrylates, quaternised vinylpyridines and disulfide reagents (Figure 1.22).[151–154]

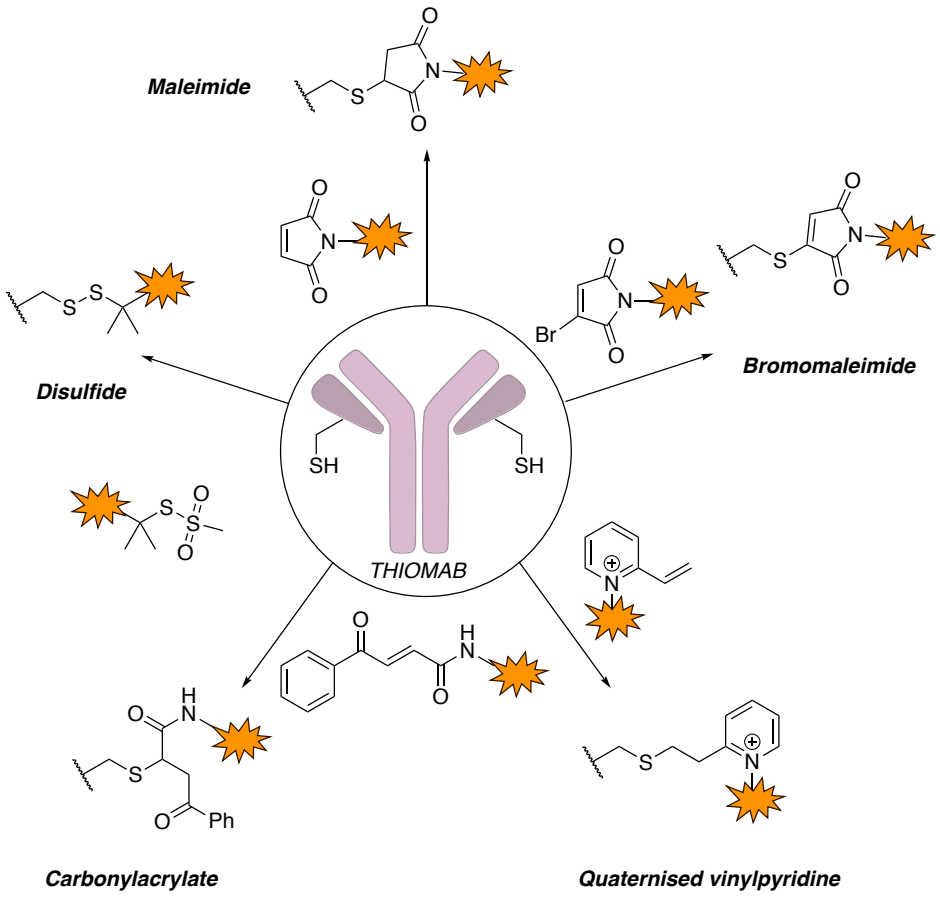

Figure 1.22: Overview of the linkers used to synthesise THIOMAB ADCs. Maleimide, bromomaleimide, quaternised vinylpyridines, carbonylacrylates and disulfides have been reported.

Complementary to the THIOMAB antibodies, researchers at MIT have reported two methods for sequence-specific cysteine modification. Both methods involve fusion of a short cysteine-containing peptide to the *C*-terminus of the HCs. In one approach, a perfluoroaryl reagent reacts selectively with cysteine in a FCPF tetrapeptide sequence, referred to as a π-clamp

(Figure 1.23a).[155] In the second method, an aza-dibenzocyclooctyne (DBCO) reagent reacts selectively with the cysteine in a seven-residue LCYPWVY tag (Figure 1.23b).[156] In both cases, homogeneous ADCs were synthesised and no reactivity was observed with reduced interchain disulfides of a trastuzumab antibody.

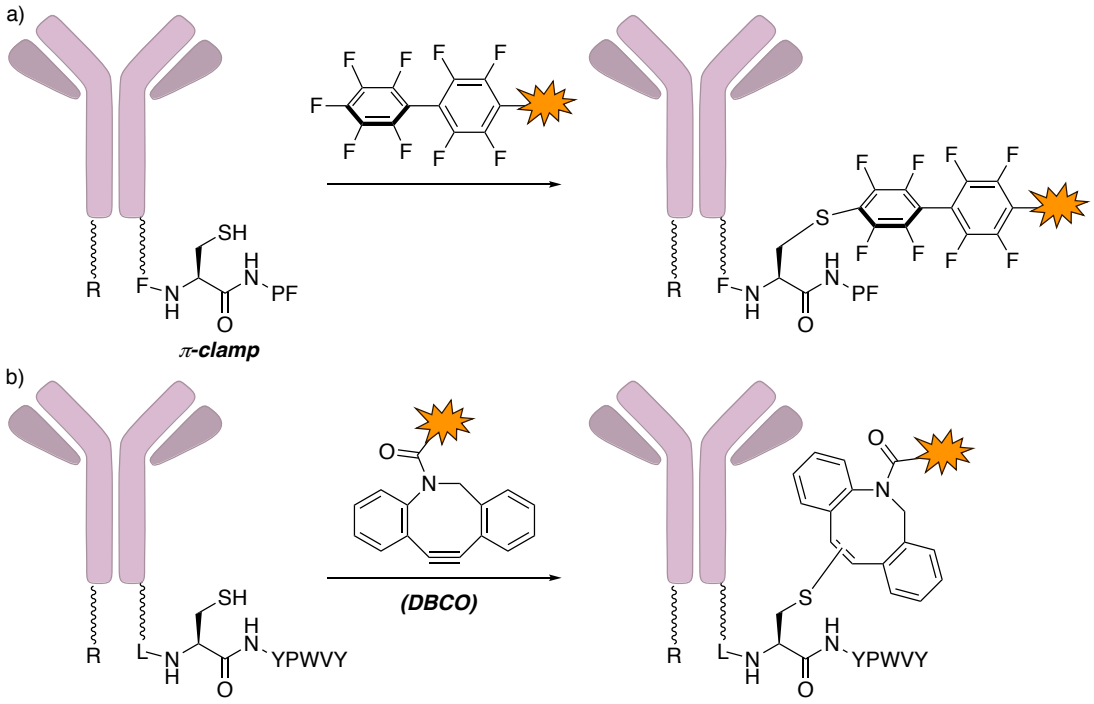

Figure 1.23: Sequence-specific cysteine modification via **a)** perfluoroaryl-mediated modification of a so-called π-clamp tetrapeptide sequence and **b)** DBCO-mediated modification via a LCYPWVY heptapeptide sequence. R indicates the same peptide tags and chemical modifications are present on both HCs.

Numerous strategies have been discussed so far that have enabled the production of homogeneous ADCs via site-selective antibody modification. While the ADCs synthesised via these methods typically had improved efficacy, pharmacokinetics and safety data compared to heterogeneous ADCs, all of these methods have drawbacks. Genetic engineering to install UAAs, synthesise THIOMABS or install affinity tags requires extensive optimisation for every mAb and the immunogenic or antibody mechanistic effects of installing UAAs or modifying the antibody sequence is still unclear. Additionally, the effects of glycan alteration on mAb biology is also unknown and requires further investigation.

C) Disulfide Rebridging

Disulfide rebridging linkers have emerged as an attractive reagent choice to achieve site-selective, homogeneous ADC production from non-engineered antibodies without the need for enzymatic amino acid or glycan modification. In this technique, interchain disulfides are reduced to reveal eight free thiols (for an IgG_1). A bis-reactive linker subsequently rebridges the cysteine residues by cross-linking of the thiols. In this way, a covalent bond is reformed between the polypeptide chains, the DAR of the ADC can be controlled (DAR of four) and the site of modification is consistent, away from any antibody-antigen recognition sites.[157] A limited number of rebridging reagents have been described for the synthesis of ADCs.

The groups of Caddick, Baker and Chudasama have conducted seminal work in this area through the development of next-generation maleimide (NGM) and pyridazinedione linkers, which have been shown to produce homogeneous and stable ADCs with precise control of the DAR (Figure 1.24). The NGM platform encompasses both dibromomaleimides and dithiophenolmaleimides. Initial work with NGM linkers demonstrated their ability to selectively rebridge reduced mAb disulfides.[158–160] However, NGM bioconjugates may also suffer from the same instability issues observed with classic maleimide linkers. To circumvent this, optimisation of this platform to afford rapid post-conjugation hydrolysis of the maleimide ring has recently been demonstrated for NGM reagents.[161] ADCs generated from NGM linkers have shown high levels of serum stability post-hydrolysis and good efficacy *in vivo*.[162] Similarly, a number of studies have shown the utility of pyridazinedione linkers to generate homogeneous (DAR two or four) and stable ADCs with excellent *in vivo* activity.[163–169] Of note, these reagents enable the attachment of multiple different payloads onto the antibody via compatible bioorthogonal chemistry.

While the NGM and pyridazinedione reagents have witnessed the most significant developments in the field, a number of other linkers in this class have been recently reported for the synthesis of ADCs. Bissulfone reagents have been used to synthesise ADCs with DARs ranging from one to four (Figure 1.24). ADCs synthesised via this method were shown to be stable and highly potent through *in vivo* investigations.[170–172] In a different approach, the C-Lock™ platform developed by Concortis Biosystems involves the use of dibromomethyl heteroaryls, particularly dibromomethyl quinoxalines to synthesise ADCs via disulfide rebridging (Figure 1.24).[173] A C-Lock™ ADC is currently undergoing Phase I clinical evaluation.[157] Similarly, arylene-dipropiolonitrile (ADPN) reagents have also been reported for

the synthesis of a trastuzumab ADC, which was shown to be highly potent *in vitro* (Figure 1.24).[174] Finally, a Novartis patent illustrates the use of dichloroacetone reagents for two-step synthesis of ADCs via initial installation of a ketone functionality on the mAb, followed by oxime formation upon treatment with a cytotoxin-functionalised amino-oxy linker (Figure 1.24).[175]

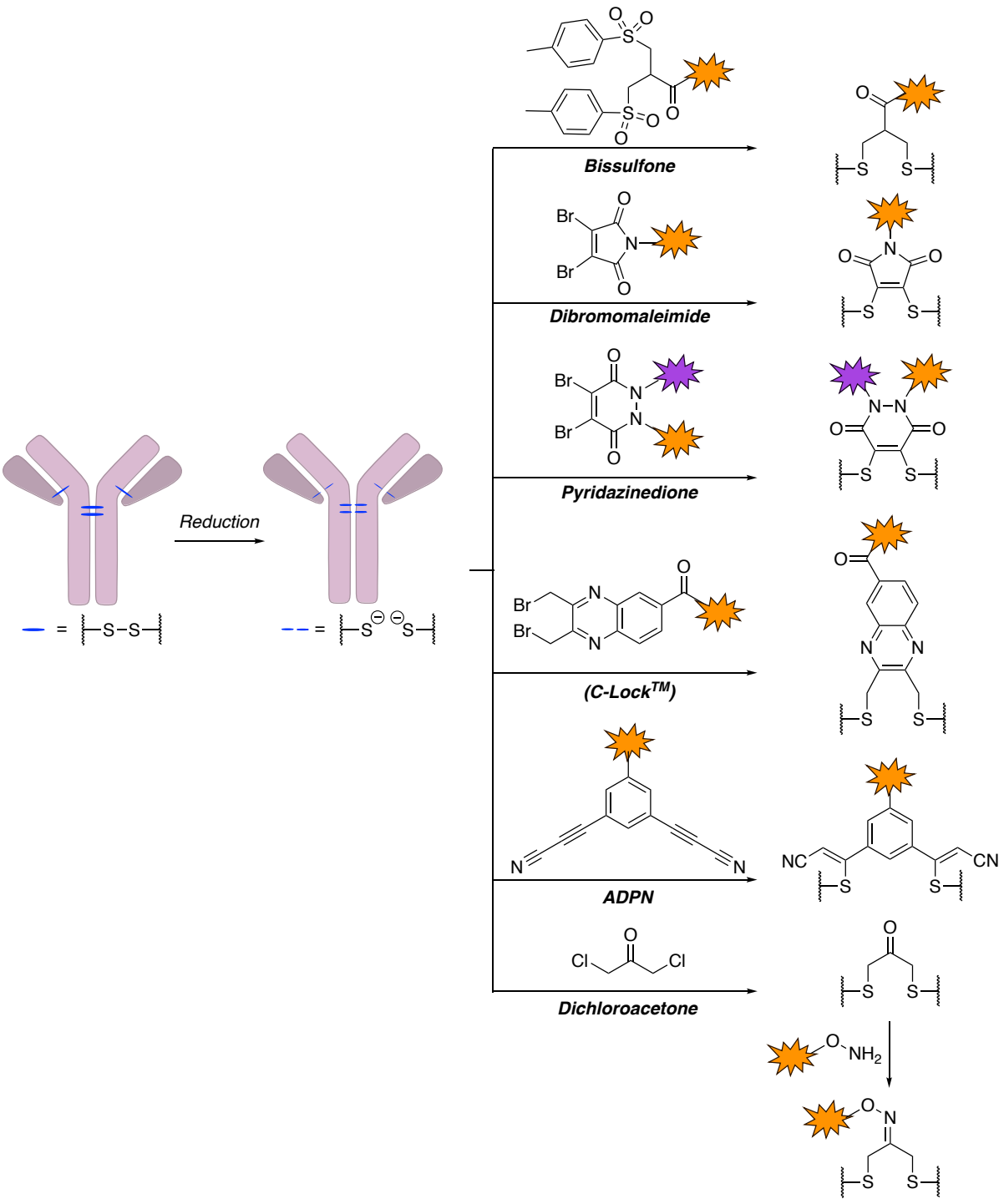

Figure 1.24: Disulfide bridging linkers used for the synthesis of homogeneous ADCs include bissulfones, dibromomaleimides, pyridaziniediones, dibromomethyl-quinoxalines (C-Lock™), arylene dipropiolonitriles (ADPN) and dichloroacetone reagents.

Chapter 2

Project Overview and Aims

The primary aim of this project is to develop a novel methodology for the synthesis of stable and homogeneous ADCs using native antibodies. The technique should be suitable to any antibody without extensive case-by-case optimisation requirements. At the time that this work commenced, the only disulfide rebridging strategies that had been reported were the NGM, pyridazinedione and bissulfone strategies. With such a small toolbox of rebridging linkers available, the effects of using a different linker for rebridging were unknown. Expansion of this toolbox with a new methodology may unlock further information about the widespread applicability of disulfide rebridging for the synthesis of ADCs. Early ADC linkers suffered from the heterogeneity and poor stability of the synthesised bioconjugates. It was thought that a rebridging strategy would potentially alleviate issues of heterogeneity. For that reason, the primary objective of this work was to develop a rebridging linker that generated an exceptionally stable linkage between the antibody and the payload.

The linkers developed in this work will be required to satisfy a number of criteria:

- Synthesis of the desired rebridging reagent should use simple chemistry and require minimal reaction steps (<5).
- The reagents should be stable and soluble in aqueous media.
- The rebridging reaction should be fast, efficient and proceed with high conversion.
- Rebridging should not affect the structure or biological activity of the mAb.
- The bioconjugates should be stable in human plasma for at least one week.
- Functionalisation of the linker with a variety of payloads should be synthetically facile and involve robust, efficient chemistry.
- The linker should not affect the activity of the attached payload.

The work described in this thesis can be divided into three distinct sections.

In Chapter 3, investigations centred around divinylpyridine linkers as a novel method of functional disulfide rebridging. A series of reactivity and stability analyses were initially carried out on a small molecule system. Upon completion, cysteine rebridging was then optimised on

a model protein, which was cloned and expressed to contain spatially adjacent cysteine residues. Finally, evaluation of the divinylpyridine linkers as antibody rebridging reagents was conducted. This scaffold was found to have insufficient chemical reactivity to enable efficient antibody modification and ADC synthesis.

In Chapter 4, the divinyl-heteroaryl motif was investigated further. Improvement in scaffold reactivity was achieved through use of a divinylpyrimidine core. Small molecule studies demonstrated the improved reactivity of the scaffold, and that doing so did not compromise conjugate stability. Subsequently, modification of an IgG mAb, a Fab and a non-antibody protein then highlighted the ability of the divinylpyrimidine linkers to efficiently modify a range of protein substrates with various functional payloads (multiple cytotoxins and a fluorescent tag). Finally, biological evaluation of the modified antibodies demonstrated their exquisite stability, binding affinity and cell-selective cytotoxicity.

In Chapter 5, synthesis of and payload attachment to a dual-functional divinylpyrimidine linker is described. Preliminary conjugation studies were then conducted on this linker, which enables the attachment of two different payloads via orthogonal chemical reactions.

Chapter 3

Divinylpyridine Cysteine Rebridging Linkers

3.1 Introduction

Vinylpyridine reagents have been used for many decades for the modification of cysteines in proteins. Most commonly, they have been documented as a method for quantifying the number of thiols present in biological fluids or on proteins (Scheme 3.1a).[176–181] Vinylpyridines have also been described as robust and stable thiol protecting groups, with removal only possible after quaternisation of the pyridine nitrogen.[182,183] Iksuda Therapeutics (formerly Glythera) have utilised the exceptionally high stability of vinylpyridine-derived bioconjugates to synthesise ADCs via interchain or THIOMAB cysteine modification (Scheme 3.1b). ADCs synthesised via this so-called PermaLink™ technology have been shown to have much higher stability and better *in vivo* efficacy and safety than maleimide-derived ADCs.[184,185]

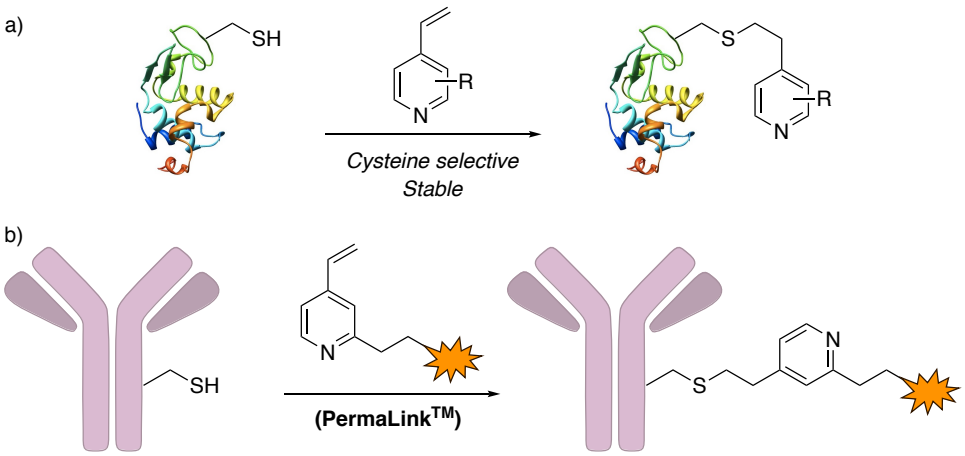

Scheme 3.1: a) Vinylpyridines have been used for the cysteine-selective modification of proteins, generating highly stable bioconjugates and **b)** cytotoxin-functionalised vinylpyridines (PermaLink™) have been developed by Iksuda Therapeutics to synthesise stable, safe and efficacious ADCs.

Building upon previous reports of successful monovinylpyridine reagents for protein modification, it was envisaged that incorporation of a second reactive vinyl group within such scaffolds could generate novel divinylpyridine linkers (Figure 3.1). The primary aim of the work described in this chapter was to investigate the use of divinylpyridine linkers for the synthesis of stable, homogeneous and functional ADCs. As was set out in Chapter 2, these linkers required a set of desirable attributes for ADC production such as fast, efficient disulfide

rebridging, generation of a stable bioconjugate, easy functionalisation and having little effect on the attached payload.

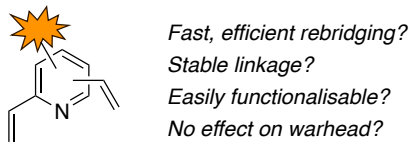

Figure 3.1: The initial focus of this work will be to investigate the properties of divinylpyridine linkers for the functional rebridging of mAbs.

Upon starting investigations, we first identified a potential obstacle presented by the different reactivity of the three accessible vinylpyridine regioisomers. Due to their previous use in protein modification, and their demonstrated applicability as reactive cysteine handles, efforts focused on the 2- and 4-vinylpyridines. Moreover, the applicability of these moieties has been demonstrated through their incorporation within PermaLink™. Since both 2,4- and 2,6-divinylpyridine isomers could potentially be used as rebridging reagents, focus was placed on investigating the reactivity differences between the 2- and 4-vinylpyridine species (Figure 3.2). It was also necessary to determine a suitable reactive handle to enable successful payload attachment (*vide infra*).

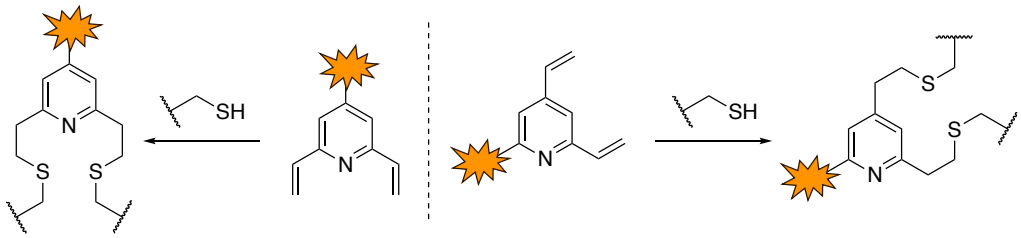

Figure 3.2: Potential use of 2,4-divinylpyridine or 2,6-divinylpyridine linkers for disulfide rebridging.

3.2 Reactivity of 2-vinylpyridine and 4-vinylpyridine

In order to determine the difference in reactivity between the 2- and 4-vinylpyridine scaffolds, two model substrates were chosen to mimic the final linker and reaction conditions. Since reactivity studies will be carried out in aqueous conditions, inclusion of an amino moiety on the pyridine was deemed necessary, with the potential deactivation of the system toward conjugate addition counterbalanced by the necessity for water solubility. Accordingly, Suzuki

coupling from 2- and 4-bromopyridines affected the corresponding vinylpyridine products **1** and **2** in good yields (Scheme 3.2).[186,187]

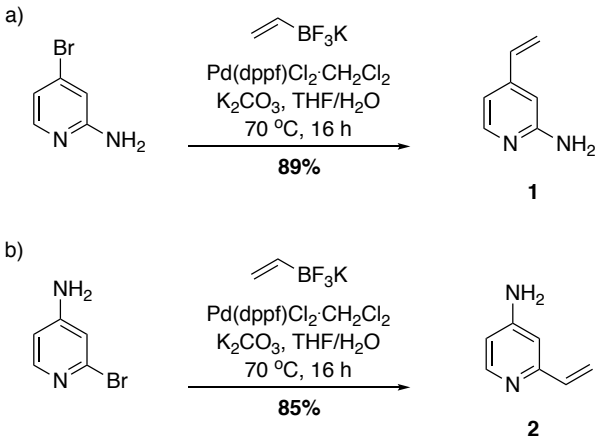

Scheme 3.2: Suzuki cross-coupling **a)** from 2-amino-4-bromopyridine to 2-amino-4-vinylpyridine **1** and **b)** from 4-amino-2-bromopyridine to 4-amino-2-vinylpyridine **2**.

With vinylpyridines **1** and **2** in hand, determination of the reactivity of these linkers toward conjugate addition with cysteine was subsequently conducted. In these studies, *N*-Boc-Cys-OMe was utilised as a model surrogate for an antibody cysteine and therefore used as the limiting reagent, whilst the stoichiometry of the vinylpyridine substrates was varied to determine the effects of relative linker concentration on reactivity. Accordingly, **1** and **2** were reacted with *N*-Boc-Cys-OMe in a mixture of sodium phosphate buffer (NaPi, pH 8) and acetonitrile at 37 °C (Table 3.1). Aliquots were removed from the reactions at 15-minute intervals and analysed by TLC for consumption of *N*-Boc-Cys-OMe. For both vinylpyridine isomers, *N*-Boc-Cys-OMe remained after four hours when using one or two molar equivalents of **1** and **2** (Table 3.1, entries 1, 2, 6 and 7). Small differences in reactivity were seen between the linkers at five and ten molar equivalents of linker (Table 3.1, entries 3, 4, 8 and 9). Interestingly, when the substrate was exposed to 20 molar equivalents of **1** or **2**, in both cases, full consumption of *N*-Boc-Cys-OMe and conversion to conjugates **3** and **4**, respectively, was observed after only 30 minutes by TLC analysis (Table 3.1, entries 5 and 10). This result suggested only marginal reactivity differences between the 2- and 4-vinylpyridine isomers and thus the 2,4- or the 2,6-divinylpyridine isomer could be utilised depending on synthetic tractability.

Table 3.1: Evaluation of the reactivity of *N*-Boc-Cys-OMe with **a)** vinylpyridine **1** to form conjugate **3** and **b)** vinylpyridine **2** to form conjugate **4**.

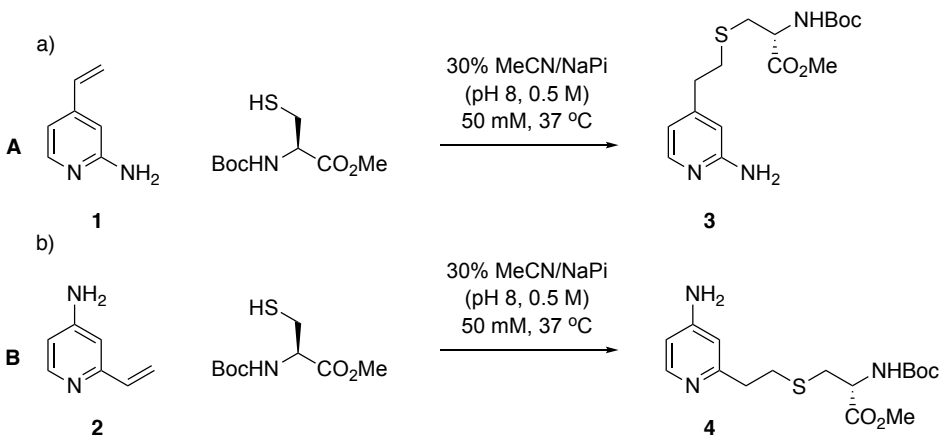

Entry	Reaction	Eq. Cys	Eq. 1 or 2	Consumption of Cys (min)
1	A	1	1	>240
2	A	1	2	>240
3	A	1	5	180
4	A	1	10	60
5	A	1	20	30
6	B	1	1	>240
7	B	1	2	>240
8	B	1	5	240
9	B	1	10	90
10	B	1	20	30

3.2 Divinylpyridine Synthesis and Functionalisation

It was envisaged that a divinylpyridine featuring a carboxylic acid or alkyne handle could be convenient points for payload attachment. Thus, having ascertained that 2-vinylpyridines exhibit similar reactivity to 4-vinylpyridines, and due to the increased synthetic tractability, the 2,6-divinylpyridine scaffold was initially explored (Figure 3.3). It was hypothesised that introduction of a modifiable chemical handle at the 4-position of such a species would be beneficial for two reasons; 1) this scaffold would generate the least steric hindrance to incoming thiols, and 2) the symmetric nature of the scaffold would prevent the formation of

regioisomeric products. In line with this and previous reactivity studies, a carboxylic acid-functionalised pyridine served as an attractive candidate for several reasons; 1) it would activate the ring further to conjugate addition chemistry, 2) it would have increased aqueous solubility through the potential presence of a carboxylate anion, and 3) it would enable facile modification of the linker through amide formation.

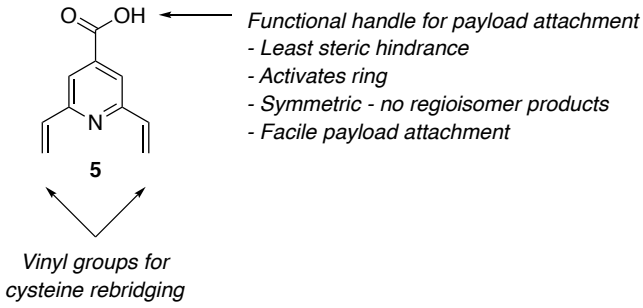

Figure 3.3: Proposed divinylpyridine linker **5**.

To this end, reaction of commercially available 2,6-dibromopyridine-4-carboxylic acid under Suzuki cross-coupling conditions produced 2,6-divinylpyridine-carboxylic acid **5** in good yield (Scheme 3.3). To ensure that further functionalisation would be possible, carboxylic acid **5** was then reacted with 4-amino-1-butyne hydrochloride under *N*-[(Dimethylamino)-1*H*-1,2,3-triazolo-[4,5-*b*]pyridine-1-ylmethylene]-*N*-methylmethanaminium hexafluorophosphate *N*-oxide (HATU)-mediated amide coupling conditions to yield alkyne **6** in moderate yield (Scheme 3.3). In addition to demonstrating the functionalisation capability of the carboxylic acid, another linker was generated that would be amenable to copper-catalysed azide-alkyne cycloaddition (CuAAC) to later modify the linker with desired payloads. Indeed, the CuAAC has been widely used as a bioorthogonal method of functionalising proteins and a wide range of azide-functionalised payloads are commercially available or can be routinely synthesised.[188,189]

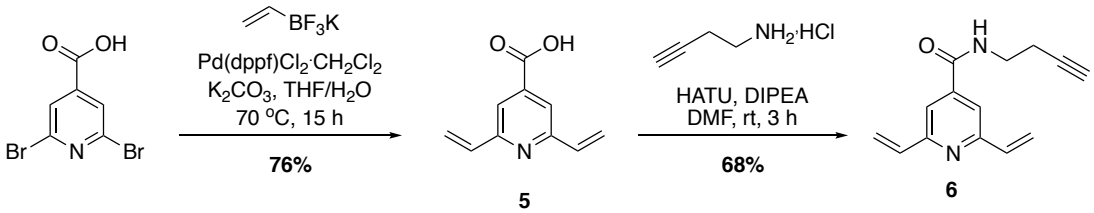

Scheme 3.3: Synthesis of divinylpyridine linker **5** through Suzuki cross-coupling and subsequent modification of this reagent through amide bond formation to produce alkyne **6**.

3.3 Divinylpyridine Stability

With a viable route to access functionalisable divinylpyridine linkers in hand, the next challenge involved investigating the stability of divinylpyridine-derived conjugates. The high stability of bioconjugates derived from vinylpyridine reagents is well known,[176,184] but whilst it could be inferred that divinylpyridine conjugates should also display a high degree of stability, this has not been previously reported. Consequently, to evaluate the stability of the conjugates produced by cysteine alkylation with divinylpyridine reagents, a small molecule stability assay was envisaged. First, divinylpyridine **5** was reacted with *N*-Boc-Cys-OMe in a mixture of NaPi and acetonitrile, generating **7** in good yield (Scheme 3.4).

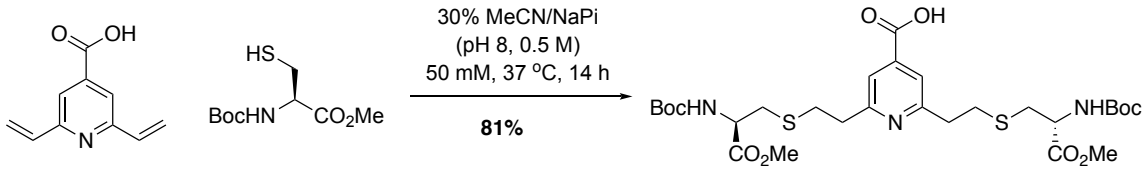

Scheme 3.4: Synthesis of conjugate **7** through reaction of divinylpyridine **5** and *N*-Boc-Cys-OMe.

To test the stability of the linkage formed from divinylpyridine conjugation to two cysteine residues, **7** was incubated with an excess of reduced *L*-glutathione (GSH) in a mixture of deuterated aqueous buffer (NaPi, 50 mM, pH 7.4) – representative of physiological pH – and deuterated methanol (Figure 3.4a). The use of deuterated solvents was chosen to allow reaction monitoring by ^{1}H NMR. After 200 hours incubation under these conditions, no evidence of the GSH addition product or of released vinylpyridine could be observed (Figure 3.4b). These results suggest that conjugates produced through divinylpyridine conjugation would be stable under physiological conditions containing an excess of other free thiols, and therefore would be viable substrates for the production of ADCs.

a)

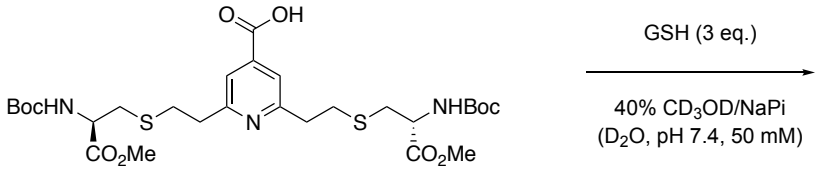

b) **7**

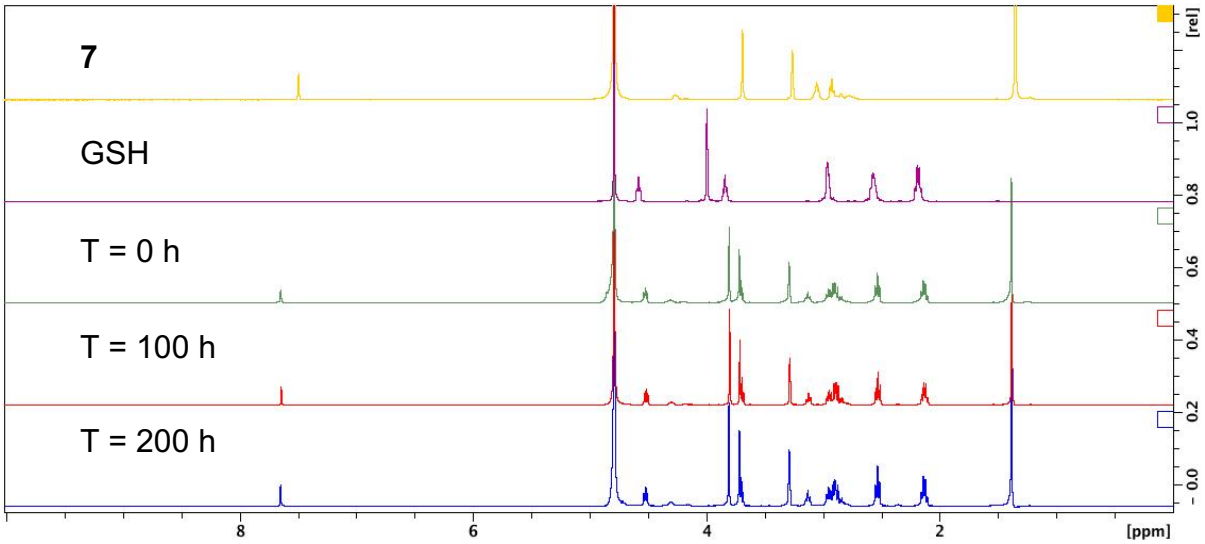

Figure 3.4: a) Incubation of conjugate **7** with GSH under physiological relevant model conditions and **b)** ^{1}H NMR analysis over 200 hours.

3.4 *Pf*RadA-dCys Modification

Having evaluated the reactivity, stability and synthetic tractability of functionalisable divinylpyridine reagents, investigations commenced into the feasibility of protein modification with the divinylpyridine linkers. It was postulated that a model protein containing a single cysteine bridging site (i.e. two cysteine residues) would serve as an excellent initial substrate, enabling facile optimisation and analysis of the reaction without incurring the complications of working immediately on a full antibody with multiple polypeptide chains and multiple target disulfides for rebridging.

3.4.1 *Pf*RadA-dCys Cloning and Expression

This work was conducted under the supervision of Dr. Marko Hyvönen, Department of Biochemistry. *Pf*RadA is a DNA recombinase enzyme from *Pyrococcus furiosus*.[190] Its *C*-terminal ATPase domain (residues 108 – 349) has previously been expressed in bacterial cell cultures and has proven a viable substrate for mutagenesis.[191,192] Importantly in the context of this work, the amino acid sequence of the wild type ATPase domain of *Pf*RadA does not

contain any cysteine residues. Therefore, it was proposed that a construct could be generated via mutation of two neighbouring surface residues to cysteines to facilitate divinylpyridine cross-linking. To select suitable amino acids for mutation, the crystal structure of the ATPase domain of *Pf*RadA was examined using PyMol. Two residues (N188 and E344) were identified as good sites for mutation due to their close proximity in the tertiary structure and the exposure of their side chains to solvent (Figure 3.5).

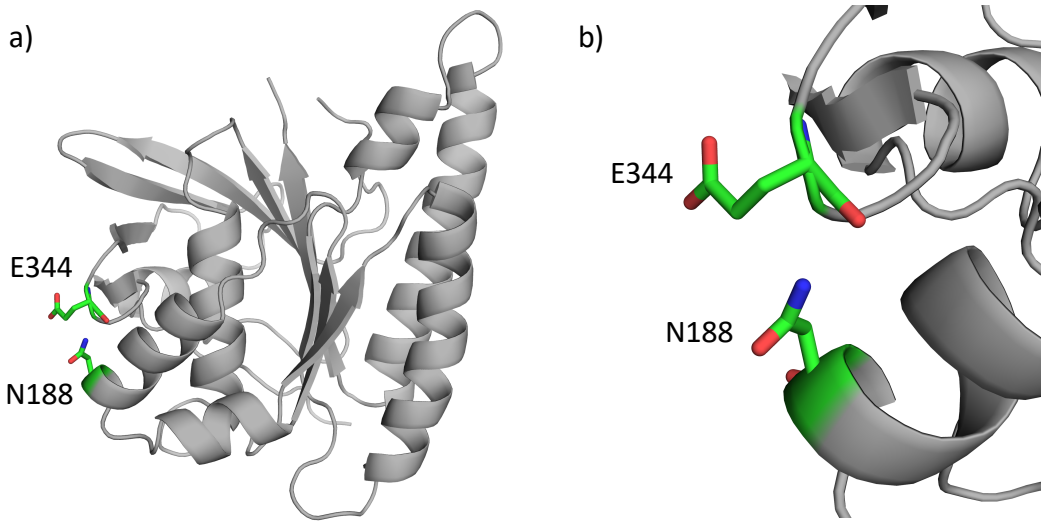

Figure 3.5: a) Crystal structure of ATPase domain of *Pf*RadA showing mutation sites of N188 and E344 and **b)** close-up view of mutation sites.

To begin production of the designed protein, it was hoped that the desired mutations could be inserted into the *Pf*RadA gene sequence through molecular cloning using the well-described technique of site-directed mutagenesis via overlap extension polymerase chain reaction (PCR) (Figure 3.6). Briefly, incorporation of the desired mutation into forward and reverse primers enables the mutant gene to be synthesised in two halves via PCR. In turn, purification of each gene fragment and further PCR with the 5' and 3' primers of the gene facilitates complete synthesis of the entire, mutated gene.

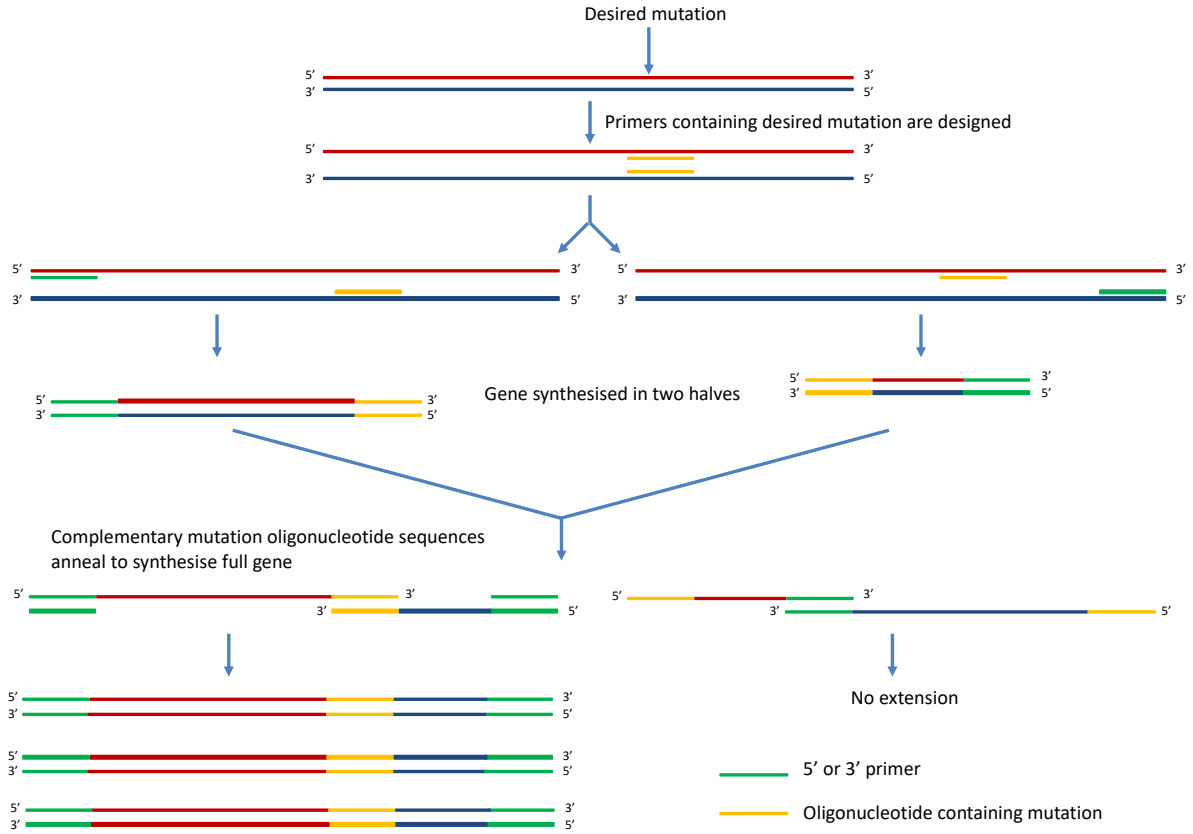

Figure 3.6: Overview of site-directed mutagenesis via overlap extension PCR. Upon identification of the point mutation, complementary forward and reverse primers (oligonucleotides) are designed that contain the desired mutated codon. The gene is then synthesised in two fragments with termination occurring at the forward and reverse primer sequences. The gene segments are purified and are recombined for further PCR cycles. After melting, the complementary forward and reverse primers anneal and the full gene can be synthesised using forward (5') and reverse (3') primers for the native gene. Note that half of the original fragment gene DNA does not elongate as the 5' and 3' primers are in the opposite direction.

Thus, forward and reverse primers containing the desired codon mutations were designed and purchased (Sigma) (Table 3.2). Importantly, due to the close proximity of the E344C mutation to the 3'-end of the gene, this mutation was inserted in the reverse primer for the full gene and used in place of the reverse primer for the wild type protein when combining the two gene fragments.

Table 3.2: Forward and reverse primers were designed for site-directed mutagenesis. Mutated codons are underlined.

Name	Mutation	Primer	Primer sequence
*Pf*RadA-dCys	N188C & E344C	*Pf*RadA101	5' GAAATTGCCCAGTGTAGAGGGTTG 3'
		*Pf*RadA102	5' CAACCCTCTACACTGGGCAATTTC 3'
		*Pf*RadA103	5' ATATACTCGAGTTAATCCTCTATCCC TTTACAAGTTATTG 3'

This method of two-step overlap extension PCR proved successful, enabling the desired gene sequence to be synthesised with ease. Agarose-gel analysis of the resulting two segments of the construct containing the desired mutations revealed DNA of appropriate base pair (bp) lengths (~500 and ~300 bp) (Figure 3.7a). In the second step, the complementary forward and reverse primers annealed and subsequent cycles of PCR amplified the complete *Pf*RadA-dCys gene (~700 bp) (Figure 3.7b).

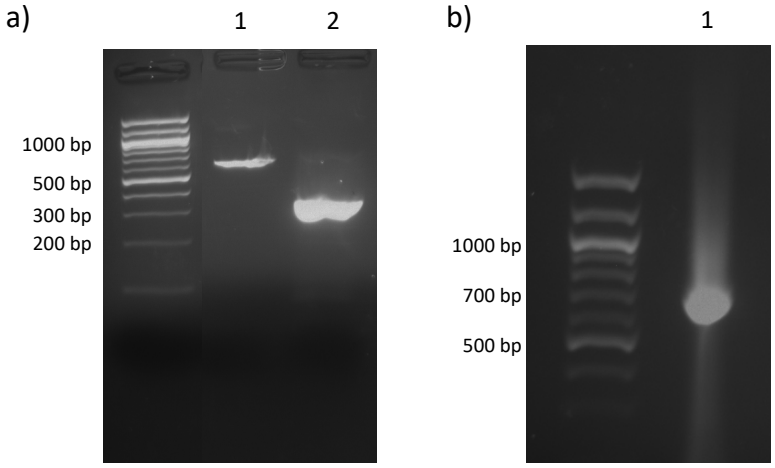

Figure 3.7: Agarose gel analysis of the synthesis of the mutant *Pf*RadA-dCys gene via overlap extension PCR. **a)** in the first step, the mutant gene is synthesised in two segments and **b)** the two segments are combined in the second step to synthesise the full gene.

In order to achieve *Pf*RadA-dCys expression in *Escherichia coli*, the mutated gene was inserted within a pBAT4 vector.[193] This plasmid contains a T7*lac* promoter with expression conducted by T7 RNA polymerase and which is induced by isopropyl-β-thiogalactopyranoside (IPTG). The pBAT4 vector was chosen as it contains *NcoI HF* (restriction site: 5' CCATGG 3')

and *XhoI* (restriction site: 5' CTCGAG 3') restriction sites, enabling precise insertion of the gene. Furthermore, protein expression using this vector generates an untagged protein.

Upon restriction digestion of the synthetic gene and pBAT4 vector with *NcoI HF* and *XhoI* (Figure 3.8a), the gene was ligated into the plasmid and transformed into DH5α strain *Escherichia coli*., a high-quality strain commonly used in DNA cloning. Transformants were then selected, sub-cultured and the DNA extracted from the cells for restriction analysis. Isolated DNA was digested with *NcoI HF* and *XhoI* restriction enzymes. If the cells have taken up the plasmid containing the desired insert, a gene of the appropriate size will be observed by agarose gel analysis. A band at approximately 700 bp was observed in all cultures (Figure 3.8b). The sequence of the genes from appropriate colonies were confirmed by DNA sequencing (Department of Biochemistry DNA Sequencing Department – Appendix D).

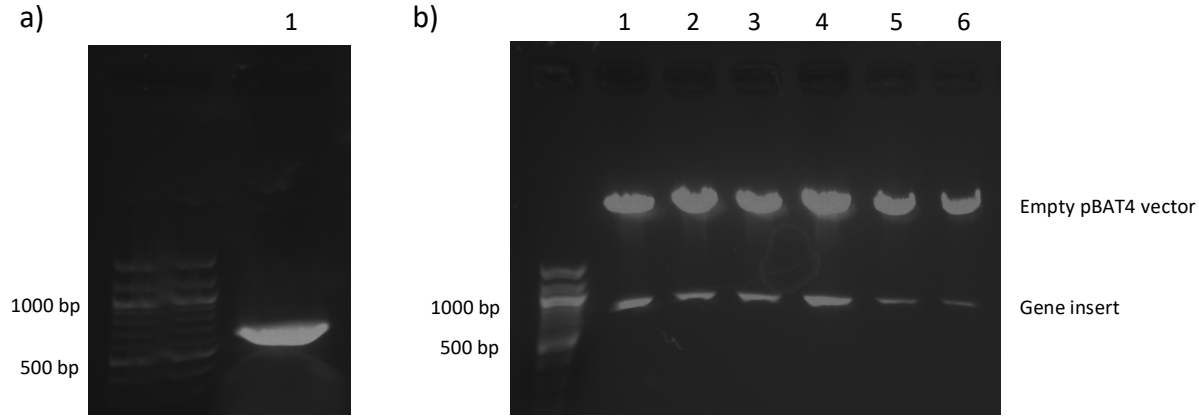

Figure 3.8: a) *Pf*RadA-dCys gene was digested with *NcoI HF* and *XhoI* restriction enzymes and purified from agarose gel. **b)** Restriction analysis of DH5α colonies.

With a protocol in place to obtain a plasmid containing the desired mutation, a small-scale expression test was carried out to find optimal conditions for protein expression in BL21 (DE3) strain of *E. coli*. Analysis of the expression tests via sodium dodecyl sulfate polyacrylamide gel electrophoresis (SDS-PAGE) revealed that *Pf*RadA-dCys (~25 kDa) was present in high quantities in the soluble cellular fraction and that many of the other proteins could be removed by heat treatment at 65 °C (Figure 3.9, Lanes 1-4).

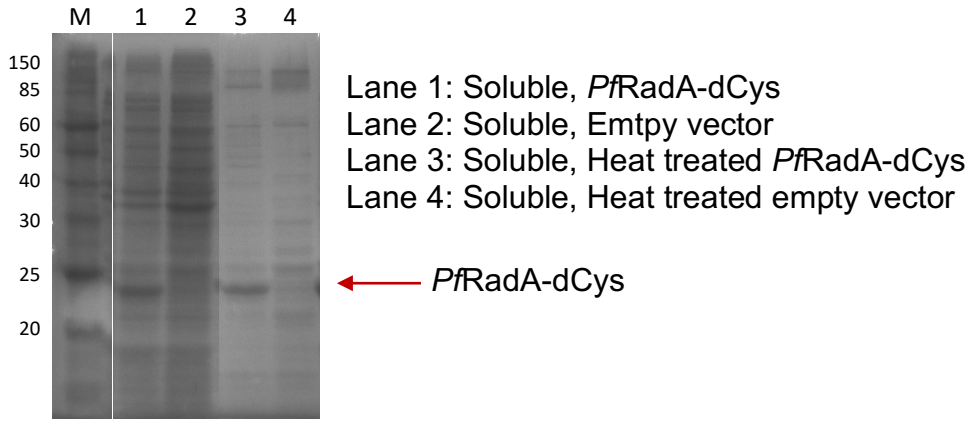

Figure 3.9: SDS-PAGE analysis of *Pf*RadA-dCys expression test. The desired protein was found in the soluble fractions and appeared thermostable. The empty vector does not contain the *Pf*RadA-dCys gene and so no band appears in the gels at ~25 kDa.

Having obtained a viable system for protein expression, scale-up commenced to produce larger quantities of protein to enable conjugation investigations. In this case, after heat treatment, the protein was further purified by ion exchange chromatography (Figure 3.10a) and finally using gel filtration (Figure 3.10b). LCMS analysis of the protein also confirmed its identity and demonstrated excellent sample purity (Figure 3.10c and d).

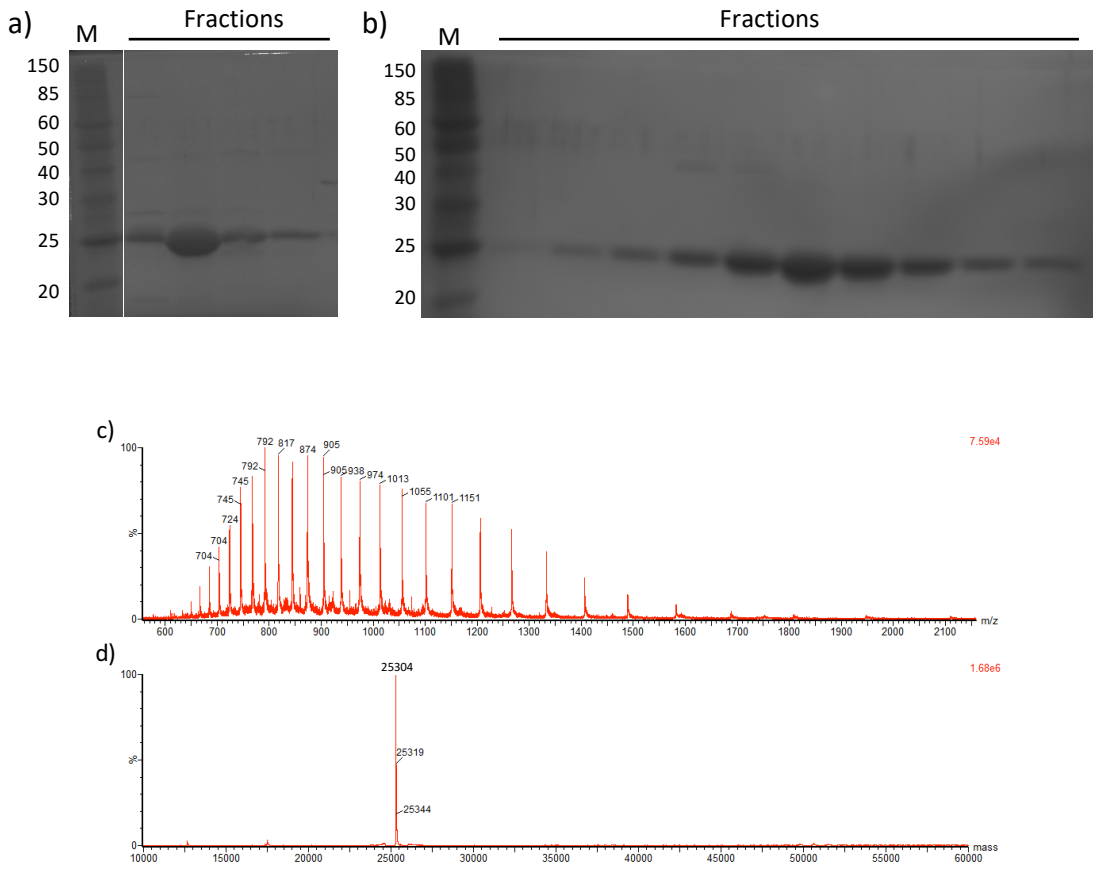

Figure 3.10: Protein fractions after **a)** ion exchange chromatography and **b**) gel filtration, **c)** mass spectrum of *Pf*RadA-dCys and **d)** deconvoluted mass spectrum of *Pf*RadA-dCys. Expected mass of 25,305 Da with *N*-terminus methionine cleavage.

3.4.2 *Pf*RadA-dCys Bioconjugation

With bis-cysteine containing protein, *Pf*RadA-dCys in hand, site-selective cysteine rebridging of this protein using the divinylpyridine linkers was then investigated. Reducing agents such as dithiothreitol (DTT) or tris(2-carboxyethyl)phosphine hydrochloride (TCEP) are widely used disulfide reducing agents in chemical biology. *Pf*RadA-dCys was firstly treated with TCEP for one hour at 37 °C to reduce any potential intra- or intermolecular disulfide bonds. The reduced protein was subsequently treated with linker **5** (10 molar equivalents) in 5% DMSO in a Tris buffer (50 mM Tris HCl pH 8, 150 mM NaCl) (Table 3.3, entry 1). Aliquots were removed from the reaction after 1-, 2-, 4- and 24-hour incubation and analysed by LCMS. Disappointingly, only minimal conversion to the desired bioconjugate **8** was observed, even after 24-hour incubation. In subsequent attempts to increase the conversion to the modified protein, numerous conditions were screened. First, linker stoichiometry was varied using 10, 20, 50 or 100 molar equivalents of **5** (Table 3.3, entries 2-4). Encouragingly, it was found that when

treating the protein with 50 and 100 equivalents of **5**, significantly higher consumption of the unmodified protein was observed. However, undesired bis-alkylated *Pf*RadA-dCys bioconjugate **9** was also observed as a major side product at these higher linker stoichiometries. To overcome this issue, the reaction concentration was lowered from 3 mg/mL to 1 and 2 mg/mL. Again, the same relative concentrations of **5** were tested in these systems (Table 3.3, entries 5-12). However, no improvement in conversion to the bridged derivative **8** was observed by LCMS analysis.

Table 3.3: Optimisation of the reaction of *Pf*RadA-dCys with **5**. Buffer conditions – pH 8 (50 mM Tris HCl pH 8, 150 mM NaCl), pH 7 (50 mM NaPi pH 7, 100 mM NaCl).

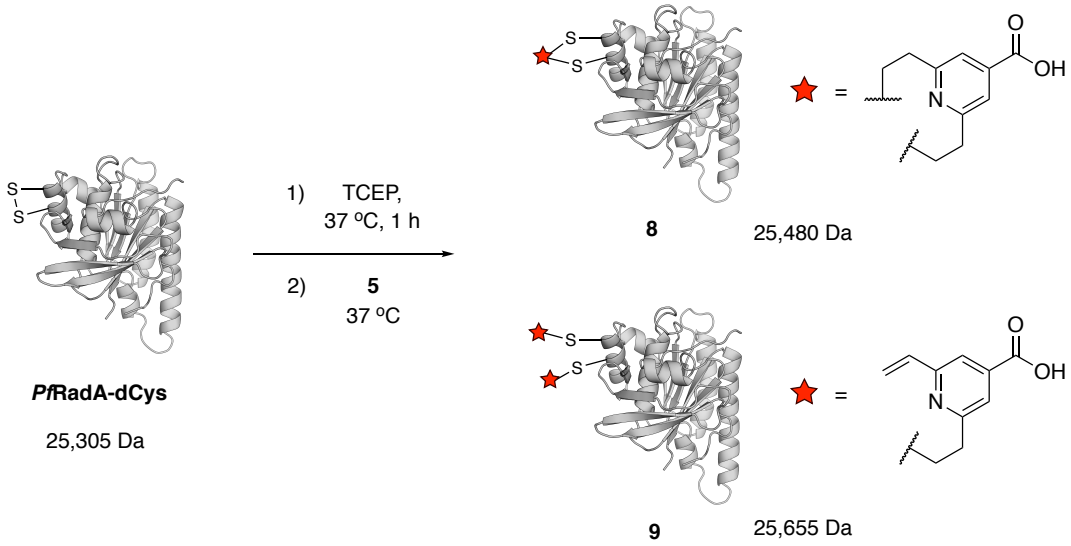

Entry	Conc. (mg/mL)	5 Eq.	TCEP Eq.	pH	SM (%)*	8 (%)*	9 (%)*
1	3	10	5	8	90	10	0
2	3	20	5	8	60	40	0
3	3	50	5	8	20	75	5
4	3	100	5	8	20	70	10
5	2	10	5	8	70	30	0
6	2	20	5	8	70	30	0
7	2	50	5	8	40	60	0
8	2	100	5	8	40	60	10
9	1	10	5	8	95	5	0
10	1	20	5	8	90	10	0
11	1	50	5	8	45	65	0
12	1	100	5	8	40	50	10
13	2	15 (x2)	5	8	95	5	0
14	2	20	10	8	95	5	0
15	2	50	10	8	90	10	0
16	2	10	5	7	95	5	0
17	2	20	5	7	95	5	0
18	2	50	5	7	80	20	0
19	2	100	5	7	75	25	0
20	5	20	5	8	10	80	10
21	5	35	5	8	5	85	10
22	5	50	5	8	5	85	10
23	7	20	5	8	20	60	20
24	7	35	5	8	5	85	10
25	7	50	5	8	5	75	20

* conversion measured by LCMS after 4 hours reaction time

In light of these findings, attempts to add the linker batch-wise (Table 3.3, entry 13), use higher equivalents of TCEP (Table 3.3, entries 14 and 15) or alteration of the reaction pH (Table 3.3, entries 16-19) were trialled. In all cases, minimal effects on conversion were observed and large amounts of unreacted *Pf*RadA-dCys remained. Finally, it was thought that increasing the

reaction concentration to 5 and 7 mg/mL and using lower linker equivalents may generate desirable conversion to **8** (Table 3.3, entries 20-25). Encouragingly, at 5 mg/mL and using 35 equivalents of **5**, good conversion to **8** was observed with only a relatively small amount (~10%) of bis-alkylated protein observed. Moreover, these conditions also resulted in the most successful conversion to the desired bridged conjugate **8** (85%) leaving only 5% unreacted *Pf*RadA-dCys remaining. Examples of the typical deconvoluted LCMS traces are shown in Figure 3.11.

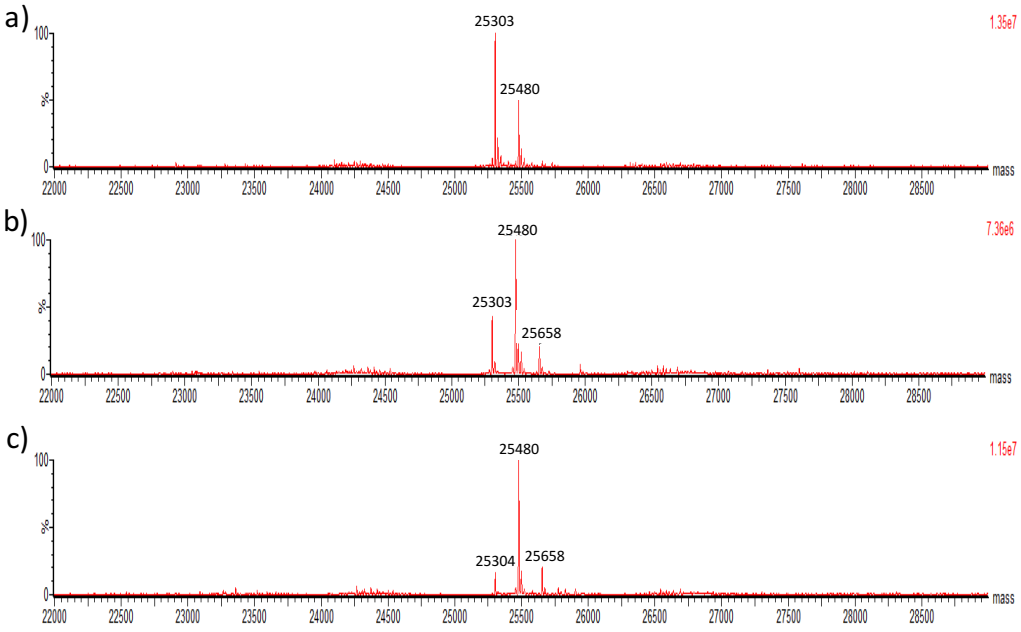

Figure 3.11: Examples of the deconvoluted mass spectrums obtained in the optimisation of the reaction of *Pf*RadA-dCys and divinylpyridine **5**; **a)** Entry 5 – poor reactivity with unmodified *Pf*RadA-dCys (expected mass 25,305 Da) as the major product and some bridged bioconjugate **8** (expected mass 25,480 Da), **b)** Entry 4 – mixture of unmodified protein, **8** and bis-alkylated protein **9** (expected mass 25,655 Da), and **c)** Entry 21 – major product is desired **8** with small amounts of unreacted protein and **9** present.

Given the comprehensive screen of conditions explored, it was concluded that achieving complete modification of *Pf*RadA-dCys to bridged bioconjugate **8** would not be possible without forming any unbridged, bis-alkylated bioconjugate **9**. It was proposed that incomplete conversion to the cysteine rebridged protein may have been due to the orientation of the engineered cysteine residues. Specifically, the cysteines incorporated into *Pf*RadA-dCys may not have been present in a favourable tertiary conformation to allow facile rebridging.[194]

3.5 Antibody Modification

Given the intrinsic difficulty in engineering a simple, monomeric protein model substrate bearing only one disulfide bridge, we decided to move onto a full antibody. Despite the aforementioned issues with multiple cysteine bonds and polypeptide chains, we envisioned that this would be a more feasible way to test our linker strategy on a relevant substrate. Furthermore, it was hypothesised that the right orientation of the disulfide bridges would be the most important factor in determining the feasibility of our strategy.

3.5.1 Trastuzumab and HER2

The human epidermal growth factor receptor 2 (HER2, ErbB2, neu) is a receptor tyrosine kinase that has been found to be overexpressed in 20-30% of invasive breast carcinomas and typically correlates with poor prognosis.[195–198] It is a transmembrane receptor comprised of an extracellular binding domain and an intracellular tyrosine kinase domain. Tyrosine kinase activity can be induced by receptor hetero- or homo-dimerisation, or ligand binding. Upon induction, a resulting signalling cascade is initiated which promotes cell proliferation through the RAS-MAPK pathway and inhibits cell death through AKT-mTOR signalling (Figure 3.12a).[199]

Trastuzumab is a monoclonal antibody against the HER2 receptor. It was developed by Genentech/Roche and gained its first FDA approval in 1998 for HER2-positive metastatic breast cancer.[200] Trastuzumab is a humanised murine IgG_1 antibody that is now used in multiple cancer types that overexpress HER2.[201] It has been proposed that trastuzumab can act via several mechanisms of action and that is it is likely that synergistic effects between many of these contribute to the tyrosine kinase inhibition, inducing cell death. For example, trastuzumab inhibits receptor dimerisation and shedding of the extracellular domain, whilst increasing HER2 endocytosis. Ultimately, all of these actions prevent tyrosine kinase activity of the HER2 intracellular domain and lead to cell death. Furthermore, trastuzumab has been shown to initiate immune activation at the tumour site through Fc-mediated recruitment of effector cells and subsequent antibody-dependent cell-mediated cytotoxicity (ADCC) (Figure 3.12c-f).[202,203]

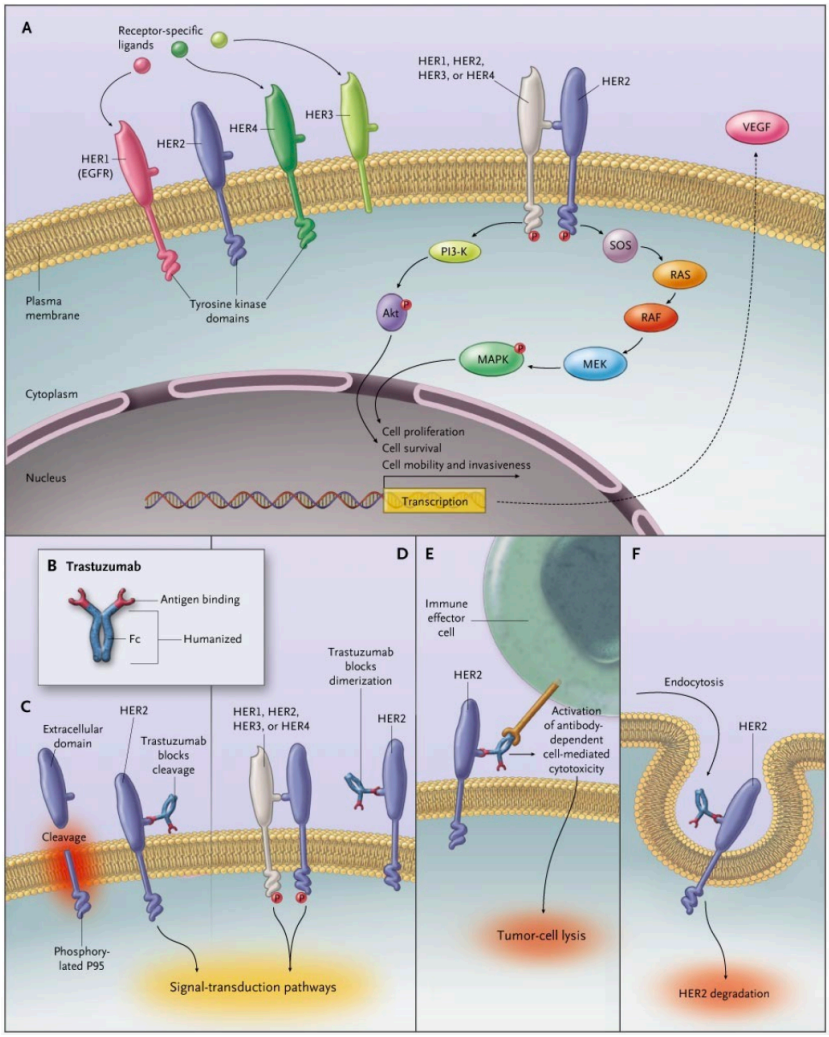

Figure 3.12: a) Mechanism of HER2 signalling through the tyrosine kinase induction and **b)** mechanisms for trastuzumab activity via **c)** inhibition of receptor shedding, **d)** inhibition of receptor dimerisation, **e)** immune recruitment and subsequent antibody-dependent cell-mediated cytotoxicity (ADCC) and **f)** receptor endocytosis. Reproduced with permission from Hudis, copyright Massachusetts Medical Society.[202]

3.5.2 Trastuzumab Modification

IgG_1 antibodies such as trastuzumab contain four interchain disulfides that can be chemically reduced to reveal nucleophilic free thiols. Before commencing a conjugation study, identification of suitable conditions to afford complete reduction of the trastuzumab interchain disulfides was required. Following a literature procedure developed by Schumacher *et al.*,[159] treatment of trastuzumab in borate buffered saline (BBS) buffer (25 mM sodium borate pH 8, 25 mM NaCl, 0.5 mM EDTA pH 8) with 10 molar equivalents of TCEP for one hour at 37 °C yielded full reduction of the interchain disulfides, as evidenced by SDS-PAGE (Figure 3.13a and b). Quantification of the number of free thiols present was also conducted using an

Ellman's assay which utilises 5,5'-dithiobis(2-nitrobenzoic acid) (DTNB or Ellman's reagent). Using this method, free thiols react with Ellman's reagent, producing a characteristic UV-vis absorbance that is then used to calculate the number of free thiols present in solution. This analysis revealed the presence of 8.15 free thiols, confirming that all of the trastuzumab interchain disulfide bonds had been reduced (Figure 3.13c and d).

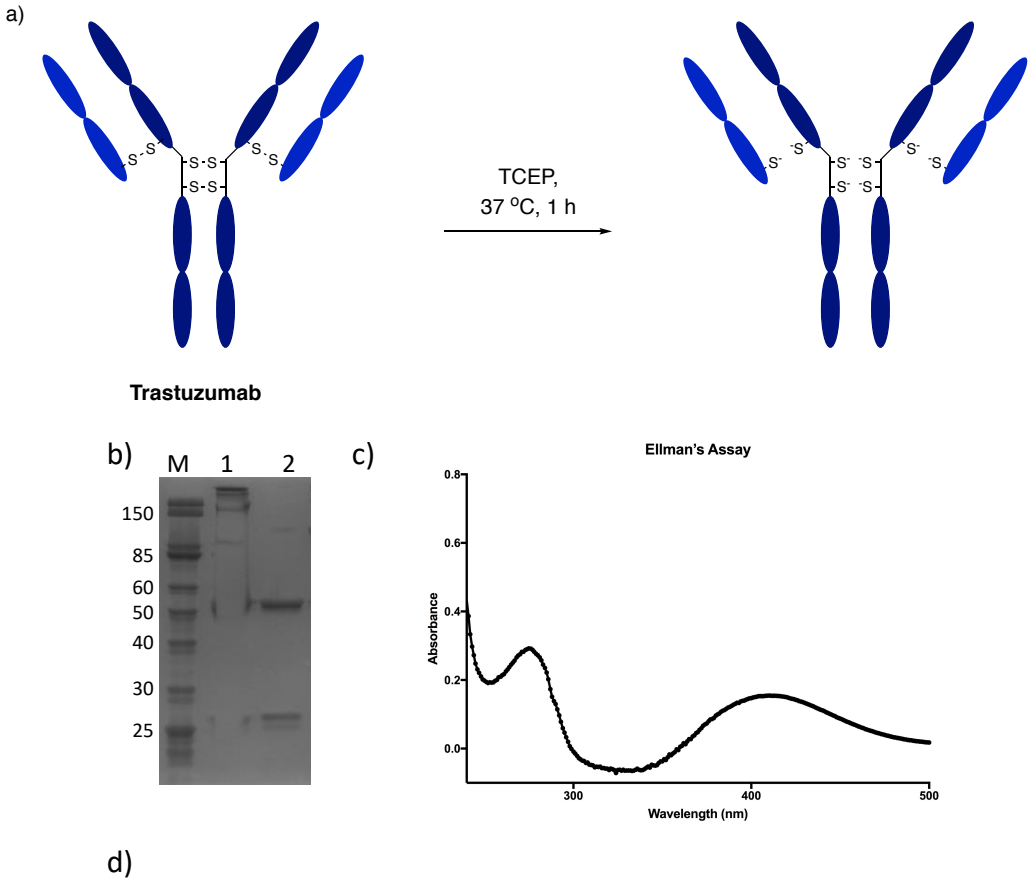

d)

$$No.\,of\ free\ thiols = \frac{Abs_{412}/\varepsilon_{412}}{Abs_{280}/\varepsilon_{280}}$$

ε_{412} = 14,150 M^{-1} cm^{-1} $\quad Abs_{412}$ = 0.15

ε_{280} = 215,380 M^{-1} cm^{-1} $\quad Abs_{280}$ = 0.28

Figure 3.13: a) Reduction of trastuzumab with TCEP as evidenced by **b)** SDS-PAGE. Lanes; M) molecular weight marker, 1) unreduced trastuzumab, 2) reduced trastuzumab, and **c)** Ellman's assay, **d)** formula used in Ellman's assay to calculate the number of free thiols present. Buffer conditions – BBS; sodium borate pH 8 (25 mM), NaCl (25 mM), EDTA pH 8 (0.5 mM).

With conditions in hand to afford interchain disulfide reduction, modification of trastuzumab with divinylpyridine linkers was subsequently investigated. To this end, conjugation with simple divinylpyridine **5** was attempted under a range of reaction conditions (Table 3.4, entries 1-15).

SDS-PAGE and LCMS were used to monitor reaction progression, with aliquots removed from the reactions after 2-, 4- and 8-hour incubation for analysis. Attempted reaction optimisation included varying the stoichiometry of **5** (40, 60 100, 200 and 500 molar equivalents), reaction concentration (2.5, 5 and 7.5 mg/mL) and reaction buffer (Tris-buffer saline [TBS] or BBS).

Table 3.4: Conditions screened in the reaction of trastuzumab with **5**. Buffer conditions – TBS; Tris HCl pH 8 (25 mM), NaCl (25 mM), EDTA pH 8 (0.5 mM). BBS; sodium borate pH 8 (25 mM), NaCl (25 mM), EDTA pH 8 (0.5 mM). Conversion determined from SDS-PAGE analysis.

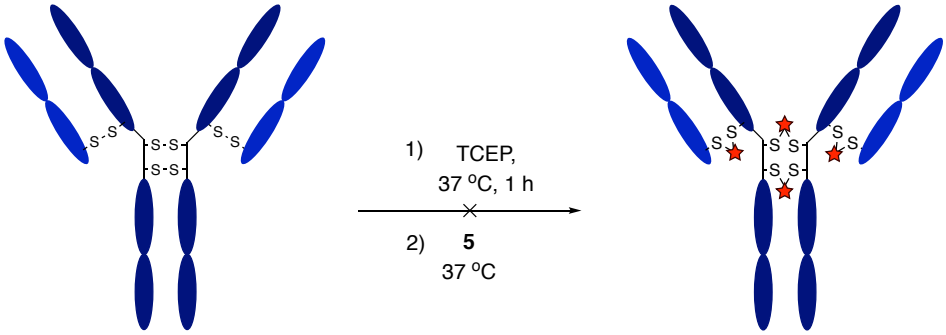

Trastuzumab **10**

Entry	Conc. (mg/mL)	5 Eq.	Buffer	pH	Time (h)	Conversion
1	2.5	40	TBS	8	2, 4, 8	Moderate
2	2.5	60	TBS	8	2, 4, 8	Moderate
3	2.5	100	TBS	8	2, 4, 8	Moderate
4	2.5	200	TBS	8	2, 4, 8	Moderate
5	2.5	500	TBS	8	2, 4, 8	Moderate
6	5	100	TBS	8	2, 4, 8	Moderate
7	5	200	TBS	8	2, 4, 8	Moderate
8	7.5	100	TBS	8	2, 4, 8	Moderate
9	7.5	200	TBS	8	2, 4, 8	Moderate
10	2.5	100	BBS	8	2, 4, 8	Moderate
11	2.5	200	BBS	8	2, 4, 8	Moderate
12	5	100	BBS	8	2, 4, 8	Moderate
13	5	200	BBS	8	2, 4, 8	Moderate
14	7.5	100	BBS	8	2, 4, 8	Moderate
15	7.5	200	BBS	8	2, 4, 8	Moderate

In all investigations, analysis by SDS-PAGE suggested conversion from unmodified light and heavy chain to the desired rebridged antibody **10** improved over time. Examples of the typical gels obtained are shown in Figure 3.14a. However, a number of other species were also observed in the reaction mixture, such as the half antibody conjugate formed from correct rebridging of the light and heavy chains but intrachain misbridging of the cysteine residues in the heavy chain hinge region (Figure 3.14b). The heavy-heavy-light and heavy-heavy partially rebridged species were also identified in the gel. Unfortunately, large quantities of unreacted light and heavy chain were also observed, ostensibly showing poor reactivity of divinylpyridine **5** (Figure 3.14). Alteration of the linker concentration, reaction concentration or buffer had little effect on the conversion. Unmodified light and heavy chains and the half-antibody conjugate could also be identified and characterised by LCMS analysis (Appendix C). Formation of the half antibody conjugate as the dominant product of the reaction can be attributed to the close proximity of the heavy chain hinge region cysteines. These residues are separated by just two proline residues, enabling an intramolecular cysteine cross-linking reaction to occur upon conjugation of the first vinyl group of **5** to one cysteine. Indeed, formation of half-antibody trastuzumab bioconjugates has been observed with other cysteine rebridging reagents such as the isobutylene reagents reported by Sun *et al.* and the ADPN reagents developed by Koniev *et al*.[174,204]

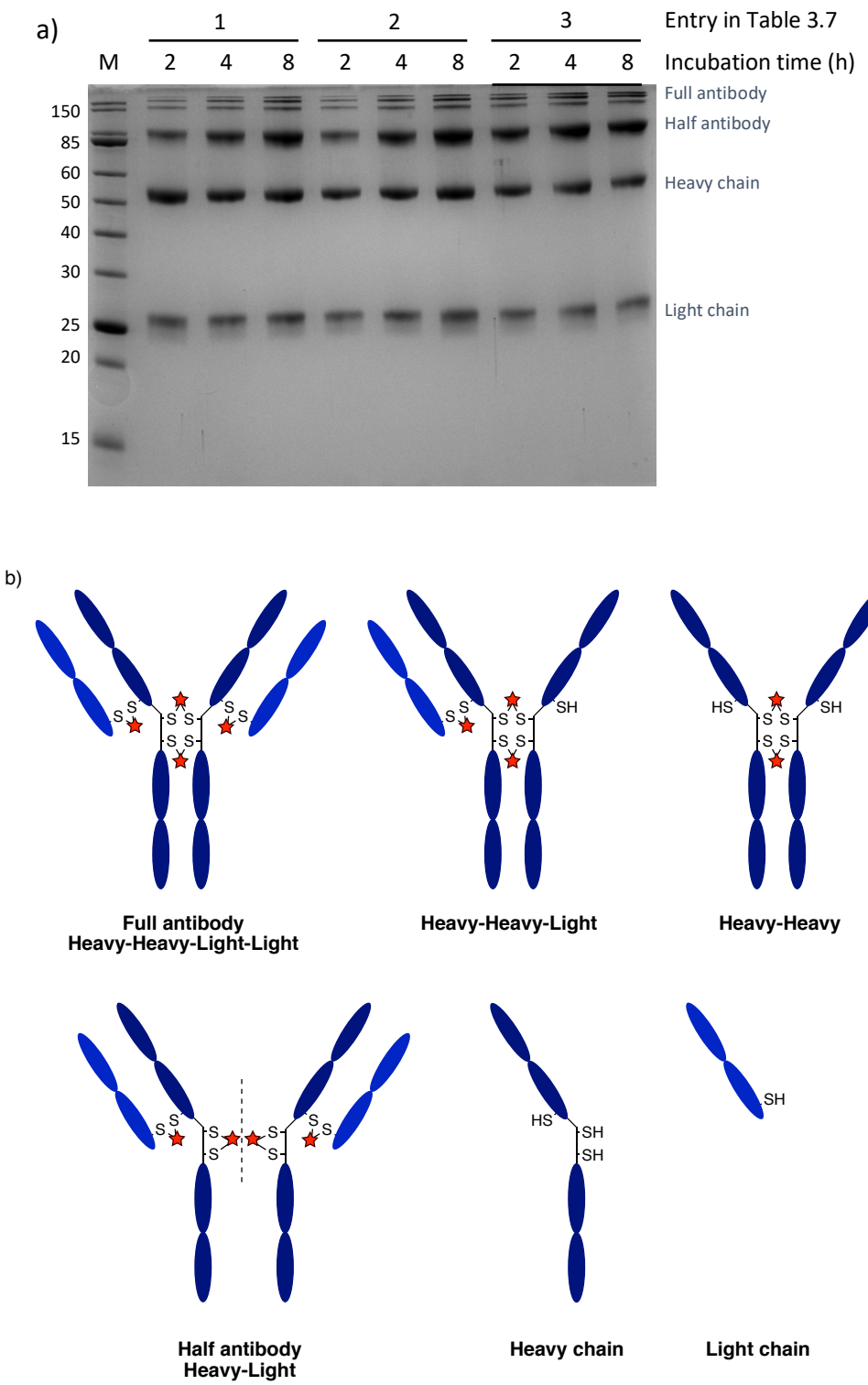

Figure 3.14: Analysis of the reaction between reduced trastuzumab and **5** by **a)** SDS-PAGE. The gel shown here is typical for all of the gels run in this analysis. Numbers above lanes represent entry number in Table 3.7 (1, 2, 3) and hours incubation (2, 4, 8). **b)** The various species observed in the reaction.

3.6 Conclusions

Investigation of a divinylpyridine linker system for bridging of protein cysteine residues was described in this chapter. The reactivity of the scaffold was firstly detailed, followed by the synthesis of divinylpyridine reagents with reactive handles for further derivatisation with biologically-relevant payloads. Divinylpyridine conjugates were shown to be exceptionally stable in the presence of other free thiols in a small molecule model assay. Subsequently, genetic engineering and expression of a *Pf*RadA-dCys protein containing two non-native cysteine residues was carried out followed by optimisation of the conjugation reaction of a divinylpyridine linker with *Pf*RadA-dCys. Finally, an extensive screen of conditions was attempted to modify a trastuzumab antibody with a divinylpyridine linker. Disappointingly, the divinylpyridine linker was insufficiently reactive to enable efficient modification of trastuzumab. Although the trastuzumab modification results were disappointing, the work undertaken in this chapter did suggest the potential utility of a divinyl-heteroaryl motif for the synthesis of ADCs upon improvement to the scaffold reactivity.

Chapter 4

Divinylpyrimidine Cysteine Rebridging Linkers

4.1 Introduction

Initial investigations with divinylpyridine linkers suggested that the vinyl-heteroaryl scaffold had the potential to fulfil the primary objectives of this work to generate highly stable bioconjugates. However, the poor reaction profile observed in antibody conjugation experiments demonstrated that in order to generate a robust bioconjugation platform, the reaction rate needed to be improved. It was also important to ensure that any modifications to the scaffold would not compromise the stability of the conjugates. Guided by these observations, it was hypothesised that increasing the electron deficiency of the ring would lead to an improved conjugate addition rate. This could be achieved by decorating the pyridine ring with electron withdrawing groups (e.g. NO_2, CF_3) or by replacement of the pyridine ring with a more electron deficient ring (e.g. a pyrimidine) (Figure 4.1). The pyrimidine core was chosen as a starting point for reactivity improvement due to the availability of starting reagents and the anticipated synthetic tractability of potential linkers.

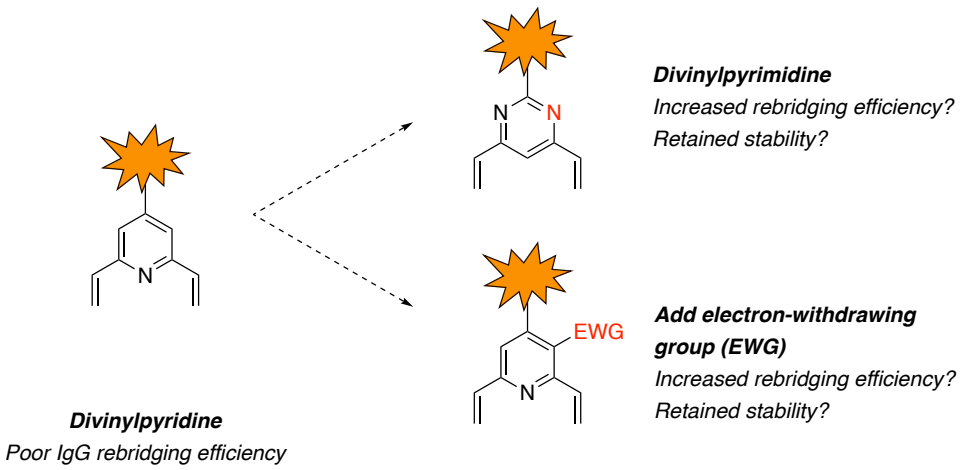

Figure 4.1: Potential strategies to increase the reactivity of the vinyl-heteroaryl motif.

4.2 Reactivity of 4-vinylpyrimidine

To begin investigations into the vinylpyrimidine scaffold, it was crucial to ascertain the rate of cysteine addition into a vinylpyrimidine. Thus, monovinylpyrimidine **11** was initially synthesised

from commercially available 2-amino-4-chloropyrimidine via a Suzuki reaction in good yield (Scheme 4.1).

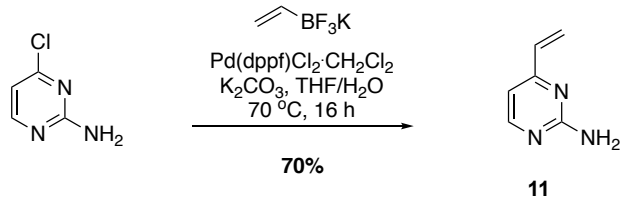

Scheme 4.1: Synthesis of vinylpyrimidine **11** via Suzuki cross-coupling.

Monovinylpyrimidine **11** (50 mM) was subsequently reacted with *N*-Boc-Cys-OMe (50 mM) in a mixture of acetonitrile and NaPi (50mM, pH 8) at 37 °C (Scheme 4.2). Monitoring of the reaction by TLC suggested that both starting materials had been consumed after just 15 minutes. In comparison, analogous vinylpyridines **1** and **2**, showed incomplete conversion after 240 minutes under the same conditions (Table 3.1, entries 1 and 6).

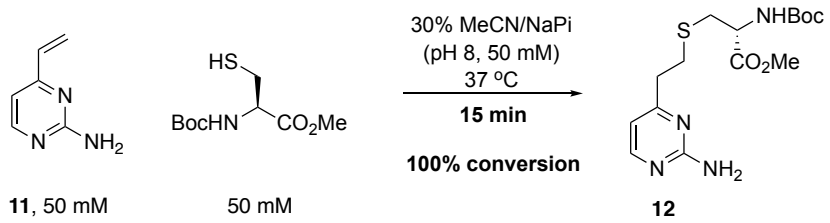

Scheme 4.2: Reaction of vinylpyrimidine **11** with *N*-Boc-Cys-OMe to generate **12**.

Commonly used bioorthogonal reactions have second-order rate constants ranging from 10^{-4} M^{-1} s^{-1} to 10^{3} M^{-1} s^{-1}.[205] Inspired by the encouraging initial result, the rate constant for the reaction between cysteine and vinylpyrimidine **11** was measured to compare to other widely used bioconjugation methods. ^{1}H NMR was determined to be an appropriate method for measuring the rate constant as the characteristic signals from the vinyl protons would be lost upon reaction. To this end, vinylpyrimidine **11** (10 mM) was treated with an excess of *N*-Boc-Cys-OMe (50 mM, 100 mM or 150 mM) and the reaction monitored by ^{1}H NMR with scans recorded at 10-second intervals (Scheme 4.3).

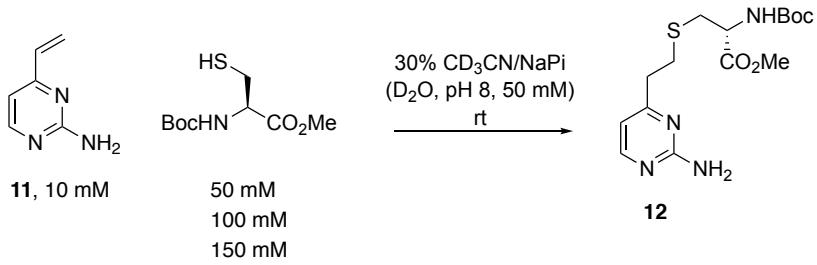

Scheme 4.3: Reaction rate studies between **11** with *N*-Boc-Cys-OMe.

Disappearance of the vinyl proton signals could indeed be observed over time and could be used to quantify consumption of **11** (Figure 4.2a-d).

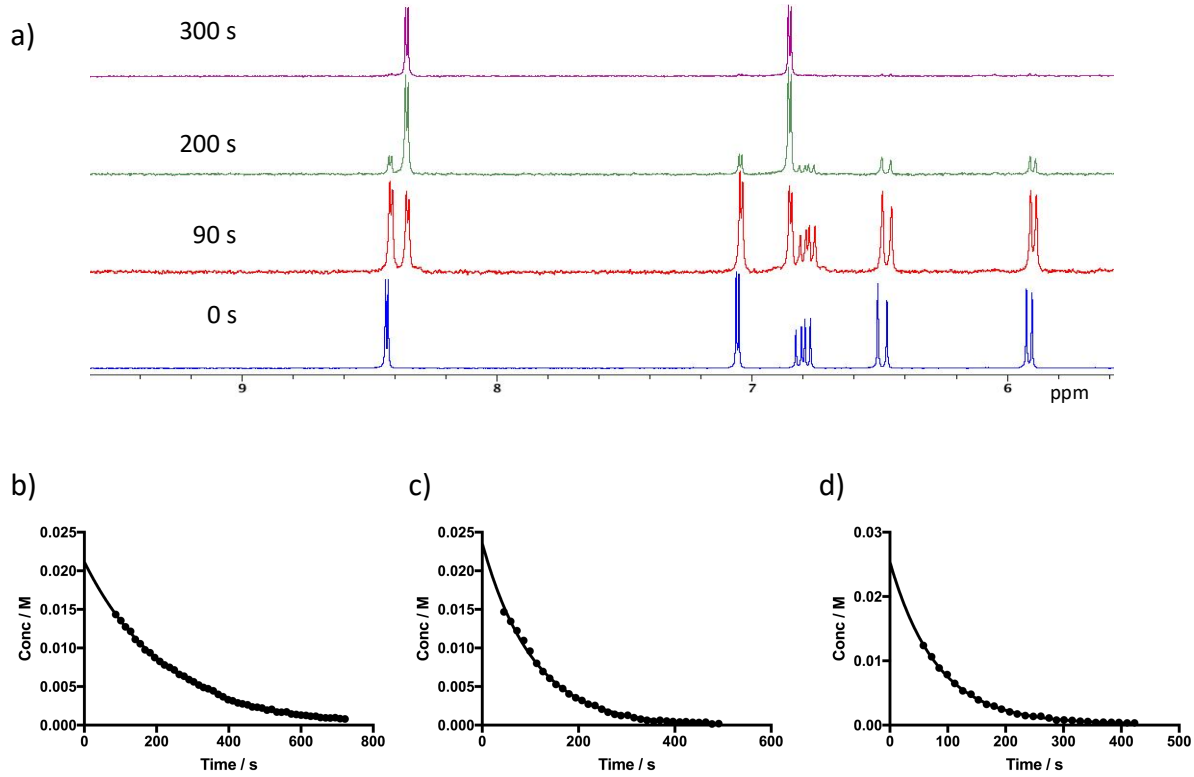

Figure 4.2: a) Typical ^{1}H NMR spectra obtained over time of reaction, with disappearing vinyl signals, and graphs of consumption of vinylpyrimidine **11** over time with **b)** 5 **c)** 10 and **d)** 15 molar equivalents of *N*-Boc-Cys-OMe.

Utilising these NMR results from the treatment of vinylpyrimidine **11** with an excess of *N*-Boc-Cys-OMe enabled determination of pseudo-first order rate constants for the consumption of **11** (Table 4.1).

Table 4.1: Pseudo-first order reaction rates of **11** with increasing concentration of *N*-Boc-Cys-OMe.

Entry	[Cys] / mM	k_1 / s^{-1}	Error / s^{-1}	R^2
1	50	4.396×10^{-3}	6.673×10^{-5}	0.999
2	100	9.475×10^{-3}	2.239×10^{-4}	0.997
3	150	1.241×10^{-2}	2.648×10^{-4}	0.999

The pseudo-first order rate constants could then be used to calculate a second order rate constant (k_2) for the reaction of vinylpyrimidine **11** with *N*-Boc-Cys-OMe by plotting these calculated rate constants against the concentration of cysteine used (Figure 4.3). The second order rate constant was determined to be ~10^{-1} M^{-1} s^{-1}.

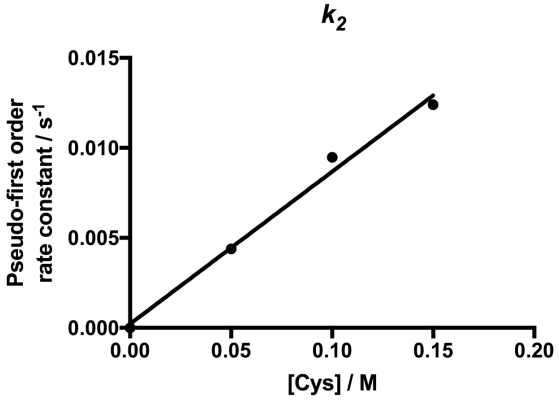

$k_2 = 8.462\times10^{-2} \pm 6.11\times10^{-3}$ M^{-1} s^{-1}

$R^2 = 0.990$

Figure 4.3: Calculation of second order rate constant for the reaction of *N*-Boc-Cys-OMe with **11** from experimental pseudo-first order rate constants.

Although the rate constant for the reaction of vinylpyrimidine **11** with cysteine was on the lower end of the scale of typical bioconjugation rate constants, it is in a similar range to that of the ruthenium catalysed cross metathesis reaction or the strain-promoted azide-alkyne cycloaddition (SPAAC), both of which have been used extensively in bioorthogonal protein modification.[206–209] It was also proposed that the relatively low rate constant for this reaction compared to other bioconjugation reaction may be beneficial as it could potentially offer a balance between efficient antibody conjugation and high levels of conjugate stability.

4.3 Monovinylpyrimidine Stability

In light of these promising reactivity results, it was hoped that the increase in reactivity of vinylpyrimidine **11** compared to the vinylpyridine reagents would not negatively affect the stability profile of this scaffold. To determine the stability of vinylpyrimidine conjugates, **12** was prepared from vinylpyrimidine **11** and *N*-Boc-Cys-OMe under the conditions described in Scheme 4.2 (Scheme 4.4). In order to compare the stability of cysteine conjugate **12** to a widely used cysteine modifying reagent, maleimide conjugate **13** was prepared in excellent yield by reaction of *N*-benzyl maleimide with *N*-Boc-Cys-OMe (Scheme 4.4).

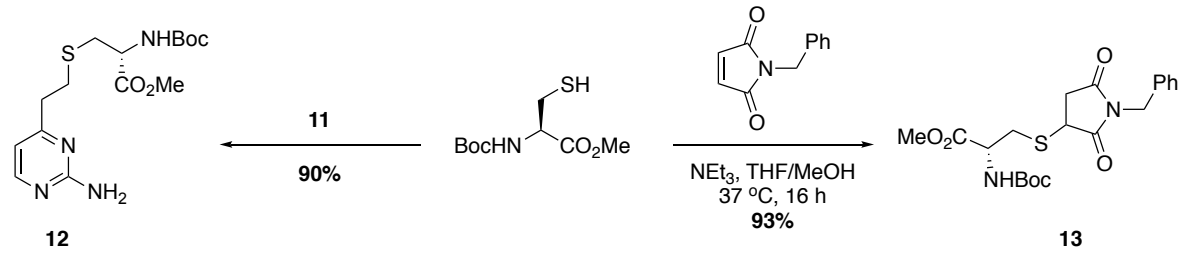

Scheme 4.4: Synthesis of vinylpyrimidine derivative **12** and maleimide derivative **13**.

Vinylpyrimidine-derived **12** and maleimide-derived **13** were subsequently incubated in a mixture of deuterated methanol and deuterated NaPi (50 mM, pH 7.4) in the presence of an excess (3 equivalents) of GSH (Scheme 4.5).

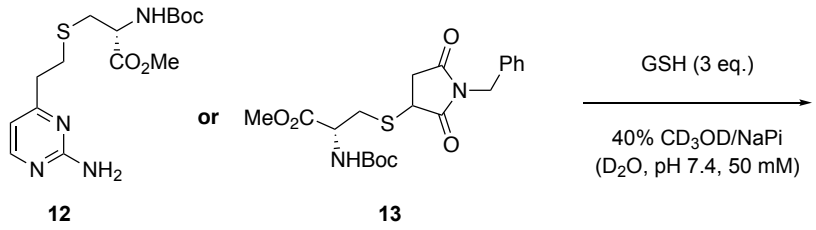

Scheme 4.5: Stability analysis of conjugates **12** and **13** in the presence of GSH.

The stability was monitored over two weeks by ^{1}H NMR, with spectra obtained at 24-hour intervals (Appendix A). Encouragingly, **12** displayed >95% stability over this time course with only minimal degradation observed (Figure 4.4). In comparison, under the same conditions <50% of the maleimide-derived conjugate **13** remained intact over two weeks. This analysis suggested that circumvention of the reactivity issues observed with the vinylpyridine linkers by switching to a vinylpyrimidine core had not affected the stability of the cysteine conjugates under the conditions tested.

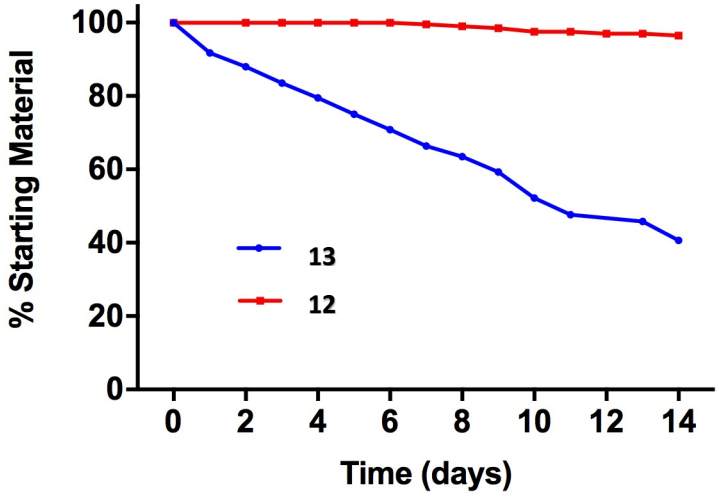

Figure 4.4: The degradation of **12** and **13** after two weeks incubation with GSH, as determined by ^{1}H NMR; see Appendix A.

4.4 Monovinylpyrimidine Chemoselectivity

As was discussed in Chapter 3, vinylpyridine reagents selectively react with cysteine residues over other amino acids, even at basic pH. However, it was unknown if this was also the case for vinylpyrimidine reagents. In particular, it could be envisaged that vinylpyrimidines could also react with the nucleophilic amine of solvent-exposed lysine residues. To investigate the selectivity of the reagent for cysteine residues over lysine residues, a competition experiment was conducted. Vinylpyrimidine **12** was incubated with *N*-Boc-Cys-OMe and *N*-Boc-Lys-OMe under the previously used conjugation conditions of 30% MeCN in NaPi (50 mM, pH 8) at 37 °C (Figure 4.5a). Analysis of the reaction after two hours by HPLC suggested that conversion to the cysteine adduct was the sole reaction product. Pleasingly, no evidence of the lysine conjugate was observed, even with a large excess of **11** present in the reaction (Figure 4.5b-d).

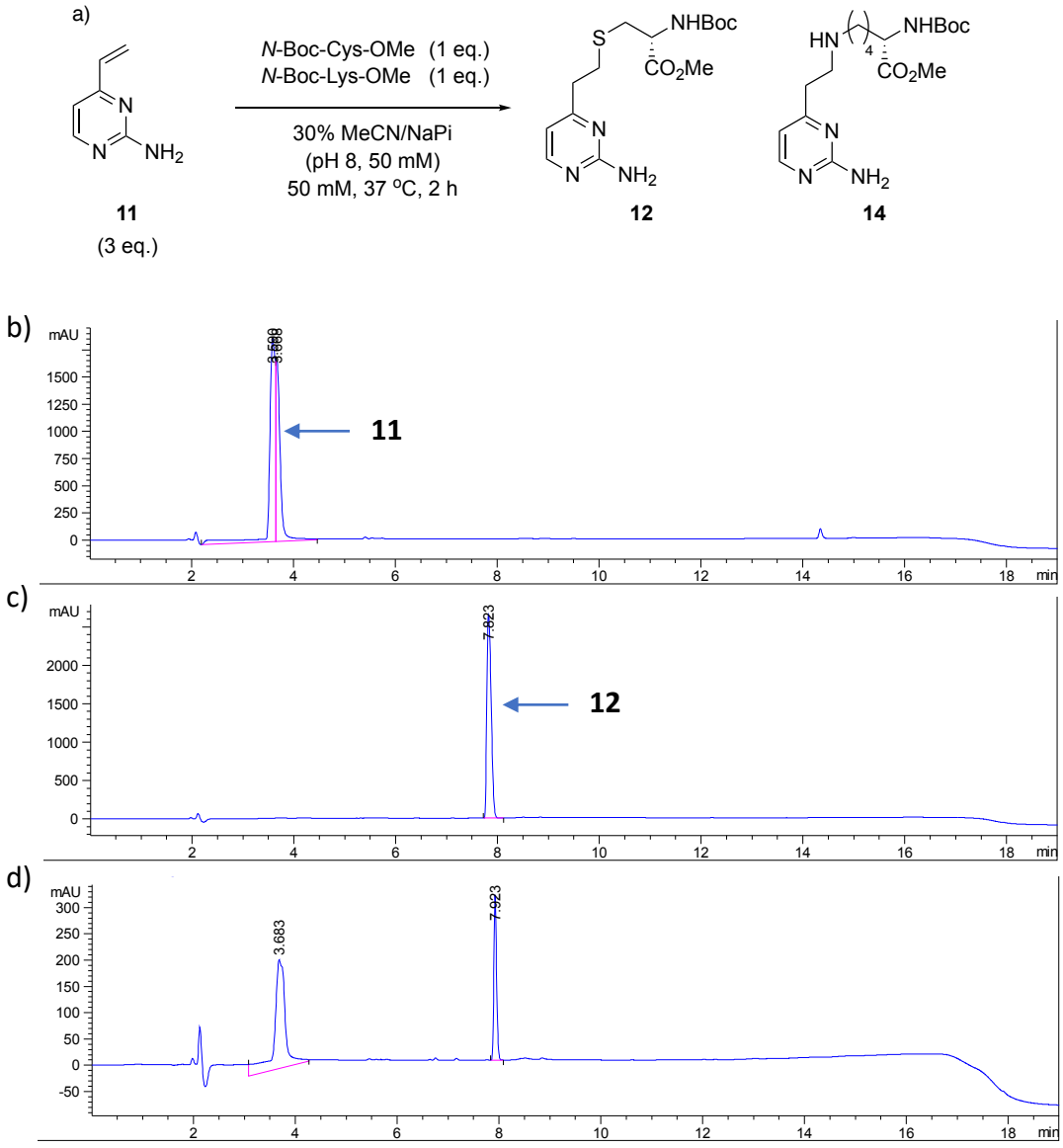

Figure 4.5: a) Chemoselectivity competition experiment by reaction of **11** with *N*-Boc-Cys-OMe and *N*-Boc-Lys-OMe. HPLC analysis of **b) 11**, **c) 12** and **d)** the reaction after 2 hours.

These promising reactivity, stability and chemoselectivity results inspired confidence that the vinylpyrimidine scaffold could be explored further and developed into a divinylpyrimidine motif for investigations into cysteine rebridging of antibodies.

4.5 Divinylpyrimidine Synthesis

In Section 3.3, the rationale for investigating symmetrical divinylpyridine linkers was explained. Similarly, it was decided that a symmetrical divinylpyrimidine (DVP) scaffold would be beneficial due to the potential synthetic tractability and the prevention of regioisomeric product formation. Thus, 4,6-divinylpyrimidines with a third synthetic vector for payload attachment

were chosen as the starting point for investigations. Accordingly, commercially available building block 2-amino-4,6-dichloropyrimidine was subjected to Suzuki reaction conditions to synthesise divinylpyrimidine **15** in good yield (Scheme 4.6).

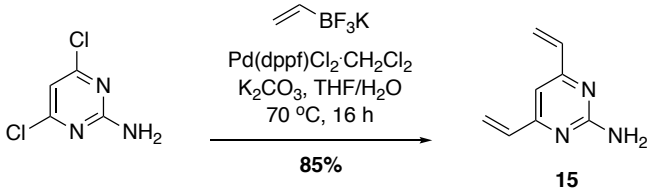

Scheme 4.6: Synthesis of DVP **15** via Suzuki cross-coupling.

With a viable synthetic route to **15** in hand, synthetic efforts then moved toward modifying the amino group with other functionalities that would be amenable to payload attachment. A series of alkylation and amidation reactions were attempted in this endeavour (Table 4.2). First, amide coupling of **15** with 4-pentynoic acid was attempted under *N,N,N',N'*-tetramethyl-*O*-(1*H*-benzotriazol-1-yl)uronium hexafluorophosphate (HBTU), *N*-(3-dimethylaminopropyl)-*N'*-ethylcarbodiimide hydrochloride (EDC) and propylphosphonic anhydride (T3P) conditions (Table 4.2, entries 1-4). Disappointingly, no evidence of the desired product was evident in the crude reaction mixtures via LCMS or TLC analysis with only unreacted starting material observed in all cases. To increase the reactivity of the acylating reagent, 4-pentynoic acid was converted into its corresponding acyl chloride and used immediately. Several bases (NEt_3, NaH, DMAP) were screened in these investigations, yet no desired product was observed again after LCMS or TLC analysis of the reaction mixtures (Table 4.2, entries 5-9). Having tested a number of conditions in an attempt to acylate **15**, it was proposed that its primary amine may be more amenable to alkylation. To this end, **15** was initially treated with propargyl bromide in the presence of a strong base (NaH) (Table 4.2, entry 10). Under these reaction conditions, double alkylation of the amine was observed in the reaction mixture via LCMS and ^{1}H NMR analysis. Although encouraging, mono-alkylation of the amine was desired and so a less reactive alkyl halide was explored. However, treatment of **15** with 6-chloro-1-hexyne and NaH yielded no observable product on analysis via LCMS (Table 4.2, entry 11). Gratifyingly, replacement of the alkyl chloride with its corresponding alkyl iodide generated the desired product **18** in 15% yield (Table 4.2, entry 12). Attempts to improve the conversion by varying the concentration of 6-iodo-1-hexyne and NaH garnered an increase in yield to 36% (Table 4.2, entries 5-9). Indeed, increasing the scale of the reaction under the optimised conditions resulted in isolation of the desired alkynyl DVP **18** in 52% yield. However, further attempts to alkylate **15** to introduce other functional handles other than an alkyne under the optimised conditions were unsuccessful (Table 4.2, entries 16-18).

Table 4.2: Conditions attempted for the acylation or alkylation of DVP **15**.

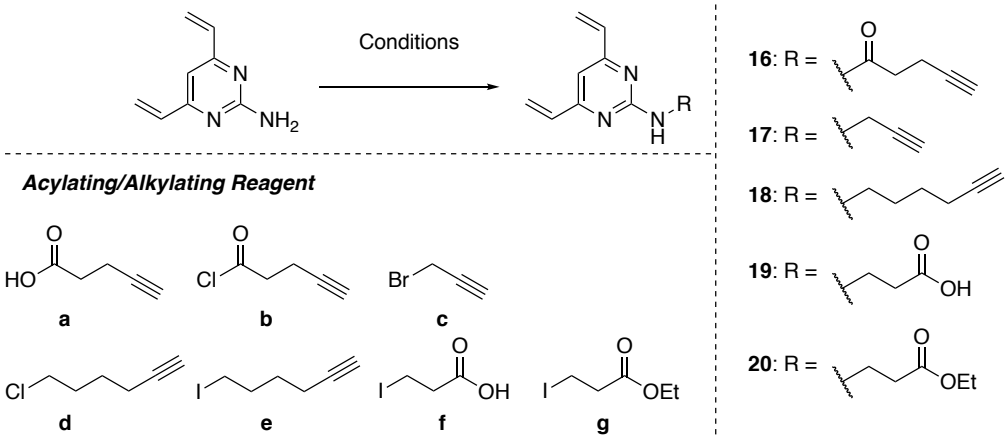

Entry	Reagent (eq.)	Additives (eq.)	Base (eq.)	Solvent	Time (h)	Temp. (°C)	Product (%)
1	**a** (10)	HBTU (10)	DIPEA (10)	DMF	16	rt	**16** (0)
2	**a** (20)	HBTU (20)	DIPEA (20)	DMF	3	rt	**16** (0)
3	**a** (10)	T3P (10)	DIPEA (10)	DMF	16	rt	**16** (0)
4	**a** (10)	EDC (10)	DMAP (10)	DMSO	16	rt	**16** (0)
5	**b** (10)	-	NEt_3 (2)	CH_2Cl_2	16	rt	**16** (0)
6	**b** (50)	-	NEt_3 (10)	CH_2Cl_2	16	rt	**16** (0)
7	**b** (10)	-	DMAP (10)	THF	16	rt	**16** (0)
8	**b** (50)	-	NaH (10)	DMF	16	rt	**16** (0)
9	**b** (50)	-	NaH (10)	DMF	16	80	**16** (0)
10	**c** (6.2)	-	NaH (6.2)	DMF	6	rt	**17** (0)
11	**d** (2)	-	NaH (2)	DMF	16	rt	**18** (0)
12	**e** (1.2)	-	NaH (1.2)	DMF	6	rt	**18** (15)
13	**e** (5)	-	NaH (5)	DMF	6	rt	**18** (36)[a]
14	**e** (5)	-	NaH (10)	DMF	16	rt	**18** (15)
15	**e** (10)	-	NaH (5)	DMF	16	rt	**18** (34)
16	**f** (5)	-	NaH (5)	DMF	16	rt	**19** (0)
17	**f** (10)	-	NaH (10)	DMF	16	rt	**19** (0)
18	**g** (5)	-	NaH (5)	DMF	16	rt	**20** (0)

[a] yield increased to 52% on 50 mg scale

In light of the difficulties observed with the attempted derivatisations of **15**, it was proposed that another synthetic route may provide easier access to a range of functionalised divinylpyrimidines. Nucleophilic aromatic substitution (S_NAr) is typically considered to be a robust and reliable method for the substitution of electrophilic aromatic halides with nucleophilic reagents. Research within the Spring group (Dr. Masao Yoshida, unpublished work) has demonstrated that S_NAr chemistry can be used to substitute a single chlorine in hetero-aryl substrates containing multiple chloride groups. Thus, it was suggested that a trichloropyrimidine could firstly undergo S_NAr with an appropriate nucleophile, followed by Suzuki cross-coupling to install the vinyl groups. To achieve this, 2,4,6-trichloropyrimidine was first treated with sarcosine ethyl ester hydrochloride in the presence of triethylamine for two hours at 0 °C (Figure 4.6). Analysis of the reaction mixture by LCMS and TLC suggested the formation of regioisomers from substitution at both the 2- and 4-position on the pyrimidine. Both regioisomers were isolated after FCC and subsequent identification by ^{13}C NMR spectroscopy revealed that the 4-substituted isomer **22** was formed as the major product (50%) while the desired 2-substituted isomer **21** was generated as the minor product in just 22% isolated yield.

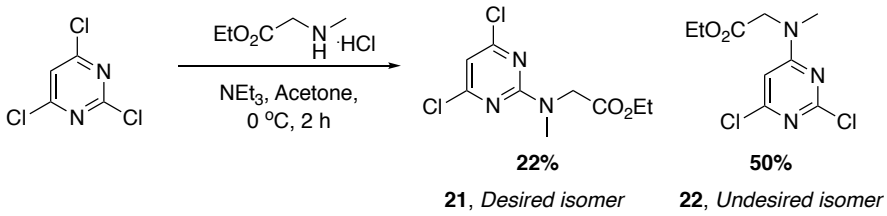

Figure 4.6: Nucleophilic aromatic substitution reaction between 2,4,6-trichloropyrimdine and sarcosine ethyl ester produces a mixture of isomers through substitution at the 2- and 4-positions.

Dichloropyrimidine **21** was subsequently subjected to Suzuki reaction conditions to obtain DVP **23** in excellent yield. To complete the synthesis, hydrolysis of the ethyl ester of **23** was achieved using lithium hydroxide monohydrate, producing the desired DVP **24** in good yield (Scheme 4.7).

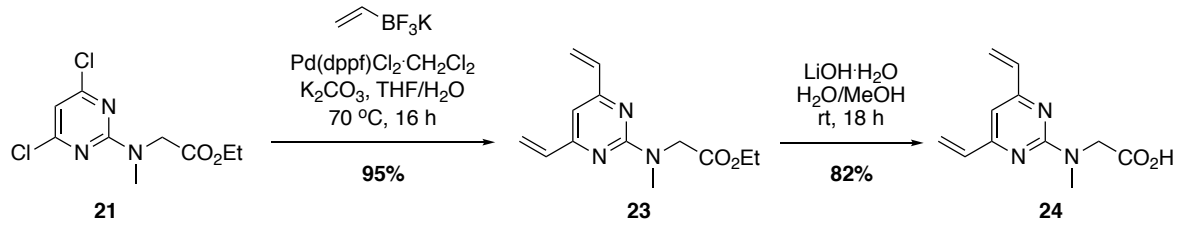

Scheme 4.7: Synthesis of **23** via Suzuki cross-coupling and subsequent ester hydrolysis to provide DVP reagent **24**.

Whilst the yield for the S_NAr reaction was disappointing, it was thought that the short synthetic route and inexpensive starting materials would enable the use of this synthetic sequence to access functionalised DVP reagents. As a result of this work, two short synthetic routes were now available to generate divinylpyrimidine scaffolds with suitable reactive handles for attachment of biologically-relevant modalities.

4.6 Divinylpyrimidine Stability

In Section 4.3, the stability of monovinylpyrimidine-derived conjugate **12** in the presence of another free thiol (GSH) was assessed, demonstrating that this conjugate was highly stable under the conditions tested. Before proceeding further in DVP development, it was important to confirm that the DVP scaffold also demonstrated the same high levels of conjugate stability. Accordingly, DVP linkers **15**, **18** and **24** were reacted with *N*-Boc-Cys-OMe in 30% MeCN in NaPi (50 mM, pH 8) at 37 °C to yield cysteine conjugates **25**, **26** and **27** in moderate to excellent yields (Scheme 4.8).

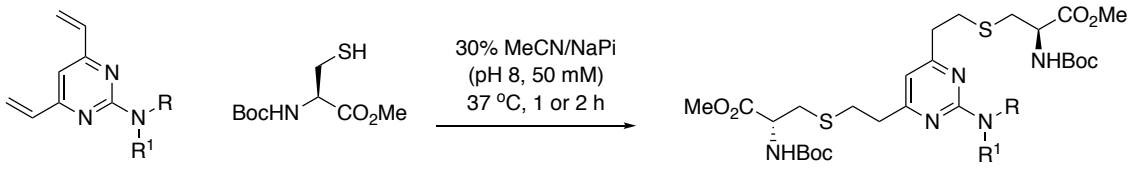

15; R = H, R^1 = H
18: R = $(CH_2)_4CCH$, R^1 = H
24; R = CH_2CO_2H, R^1 = CH_3

25; R = H, R^1 = H, **55%**
26: R = $(CH_2)_4CCH$, R^1 = H, **91%**
27; R = CH_2CO_2H, R^1 = CH_3, **55%**

Scheme 4.8: Synthesis of **25**, **26** and **27** through reaction of DVP linkers **15**, **18** and **24** with *N*-Boc-Cys-OMe.

Cysteine conjugates **25** and **27** were subsequently incubated with an excess of GSH in 40% CD_3OD in deuterated NaPi (50 mM, pH 7.4) (Scheme 4.9).

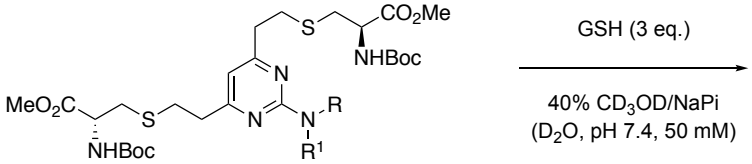

25; R = H, R^1 = H
27; R = CH_2CO_2H, R^1 = CH_3

Scheme 4.9: Incubation of **25** and **27** with GSH in 40% CD_3OD in deuterated NaPi.

The stability of the conjugates was monitored by ^{1}H NMR over two weeks, with spectra obtained every 24 hours (Appendix A). Pleasingly, both **25** and **27** displayed >95% stability under the conditions investigated (Figure 4.7). Attempts to monitor the stability of cysteine conjugate **26** under the same conditions were unsuccessful due to its poor aqueous solubility.

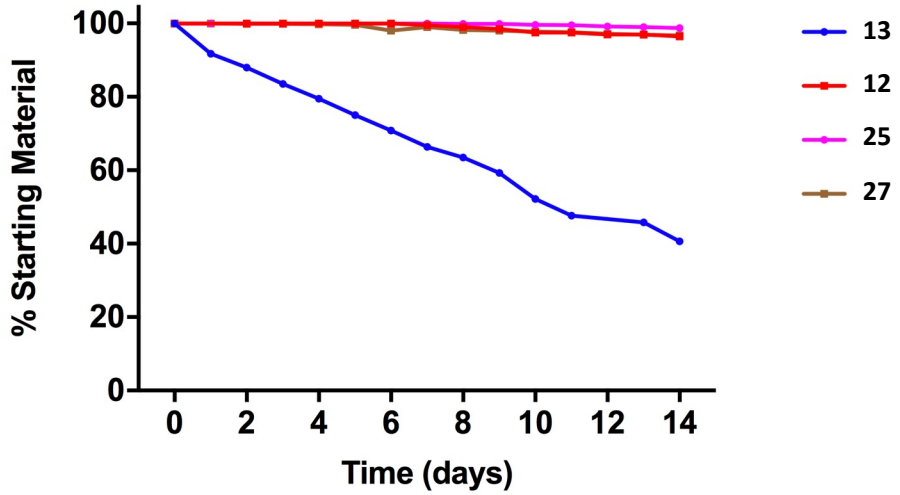

Figure 4.7: Graph representing the degradation of **25** and **27** after two weeks incubation with GSH and comparison with **12** and **13** as detailed in Section 4.3.

4.7 Divinylpyrimidine Chemoselectivity

In Section 4.4, the chemoselectivity of monovinylpyrimidine **11** for cysteine residues was determined via a competition experiment. Studies to ensure that the DVP linkers maintained that chemoselectivity for cysteine over lysine residues were then undertaken. In this assay, DVP reagents **15**, **18** and **24** were treated with *N*-Boc-Cys-OMe and *N*-Boc-Lys-OMe in 30% MeCN in NaPi (50 mM, pH 8) at 37 °C. As each linker had two reactive vinyl groups, the excess of DVP in the reaction would potentially result in the formation of a mixture of mono- and bis-conjugated products. The reactions were monitored over four hours by HPLC and LCMS. In all cases, the mono-conjugated cysteine products (**28**, **29** and **30**) were observed as the major product, with some evidence of the bis-conjugated cysteine products (Scheme 4.10 and Appendix B). No evidence of the lysine-modified reagents was observed, confirming that this scaffold was chemoselective for cysteine residues over lysines.

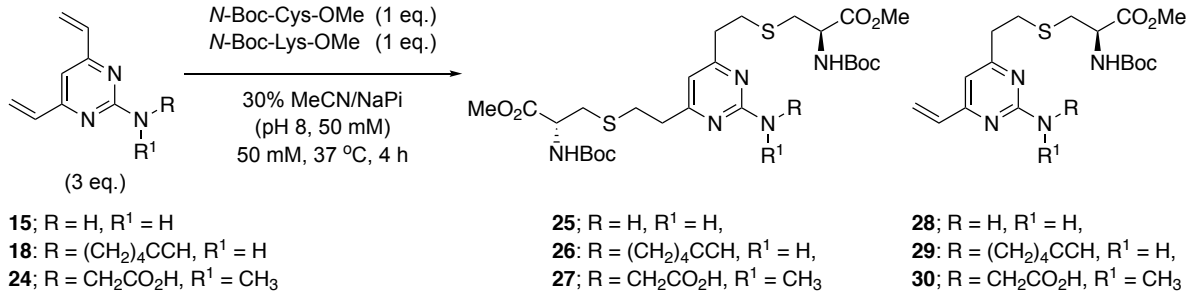

15; R = H, R^1 = H
18: R = $(CH_2)_4CCH$, R^1 = H
24; R = CH_2CO_2H, R^1 = CH_3

25; R = H, R^1 = H,
26: R = $(CH_2)_4CCH$, R^1 = H,
27; R = CH_2CO_2H, R^1 = CH_3

28; R = H, R^1 = H,
29: R = $(CH_2)_4CCH$, R^1 = H,
30; R = CH_2CO_2H, R^1 = CH_3

Scheme 4.10: Chemoselectivity competition experiment of **15**, **18**, and **19** with *N*-Boc-Cys-OMe and *N*-Boc-Lys-OMe. Only the cysteine conjugates were observed on analysis by HPLC and MS.

4.8 Protein Chemistry

Having investigated the potential of a DVP linker platform on a series of small molecule model systems, efforts now shifted toward the use of the synthesised DVPs for the modification of protein susbtrates. Initial protein investigations on the divinylpyridine reagents focused on the modification of *Pf*RadA-dCys as a model protein with genetically incorporated cysteine residues (Section 3.4). This was chosen on the basis of using a simpler protein for initial reactivity investigations. However, it was thought that a more reflective model protein might be found in the use of an antibody fragment, such as an antibody Fab. Antibody fragments have experienced widespread interest in recent years as potential therapeutic agents and as potential delivery vehicles for cytotoxic warheads.[210–212] Antibody fragments such as a Fab, a single chain variable region fragment (scFv), or diabodies are attractive molecules for targeted therapy development as they typically maintain the receptor affinity and selectivity that is seen with full antibodies, but their smaller size can allow better tissue penetration, faster clearance, and eliminates Fc-mediated antibody biology, which can result in non-cell-specific antibody internalisation.[213–215] A Fab fragment is comprised of two polypeptide chains that are covalently linked by a single disulfide. One of the polypeptide chains is the light chain of an antibody (V_L and C_L domains) and the other is comprised of the V_H and $C_H{}^1$ domains of the antibody heavy chain (Figure 4.8). Indeed, there are currently three antibody Fabs that have gained FDA approval for different diseases.[216] It was envisaged that the small size (~50 kDa) and single native disulfide of an antibody Fab would make it an ideal candidate for initial studies on the DVP linkers. In addition, modification of Fab molecules may also generate useful therapeutic agents for evaluation.

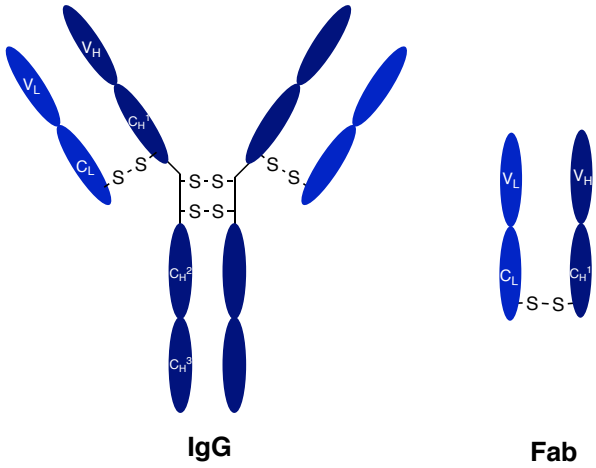

Figure 4.8: Comparison of the structures of an IgG antibody and an antibody Fab.

4.9 Trastuzumab Fab Synthesis

The simplest method for generating antibody Fabs is through enzymatic digestion of an IgG molecule. Papain digestion of an IgG typically segments the antibody into two Fab fragments and an Fc fragment. Selis *et al.* have reported the digestion of trastuzumab using this method to produce a pure supply of trastuzumab Fab.[217] In contrast, Castañeda *et al.* reported that direct cleavage of trastuzumab with papain generates a mixture of products.[218] Instead, they implemented a two-step procedure. First, treatment of trastuzumab with pepsin generated the $F(ab')_2$ fragment, which subsequently underwent papain digestion to generate pure trastuzumab Fab (Figure 4.9).

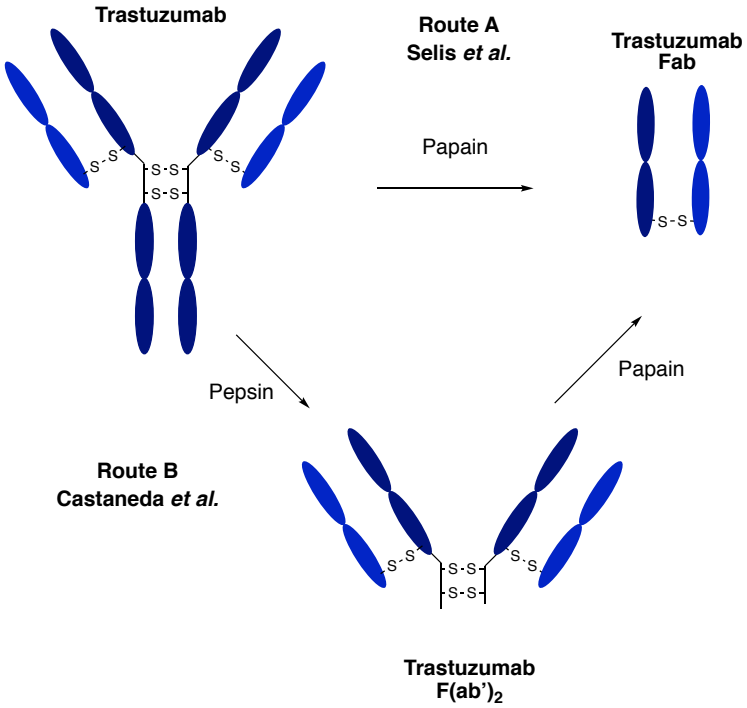

Figure 4.9: Methods for the digestion of trastuzumab to produce trastuzumab Fab.

With the hope of simplifying the synthesis of the Fab, it was decided to investigate the one-step procedure via direct papain digestion first. As such, trastuzumab was digested with immobilised papain from a Pierce™ Fab preparation kit. Attempts to purify via protein A affinity chromatography were unsuccessful as the Fab appeared to also bind the protein A column. However, pure trastuzumab Fab was obtained after gel filtration and analysis by SDS-PAGE and LCMS (Figure 4.10).

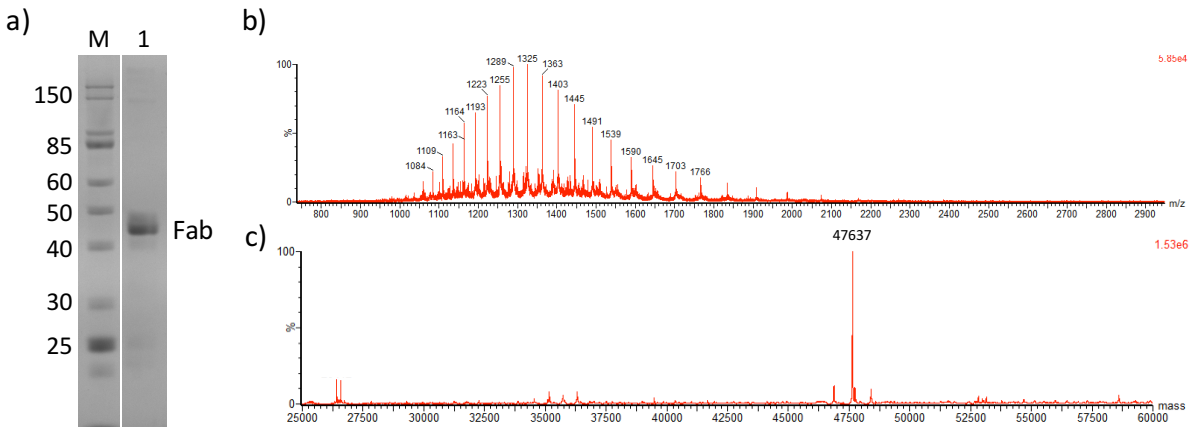

Figure 4.10: Analysis of trastuzumab Fab via **a)** SDS-PAGE, Lanes: M) molecular weight marker, 1) trastuzumab Fab, and **b)** non-deconvoluted MS and **c)** deconvoluted MS.

4.10 Trastuzumab Fab Modification

With trastuzumab Fab in hand, investigations then commenced into the rebridging potential of DVP linkers on this protein substrate. The single interchain disulfide of trastuzumab Fab was reduced by treatment with five equivalents of TCEP at 37 °C for one hour. Subsequently, the reduced Fab was treated with a range of DVP linkers (**15**, **18** or **24**) in 5% DMSO in BBS (pH 8) at 37 °C (Figure 4.11a). A small excess (10 molar equivalents) of linker enabled efficient rebridging of the Fab polypeptide chains in just one hour for all of the linkers, generating rebridged Fab conjugates **31**, **32** and **33** (Figure 4.11b-g). Gratifyingly, TCEP removal was not required before addition of the linkers, suggesting that it did not interfere significantly in the conjugation reaction.

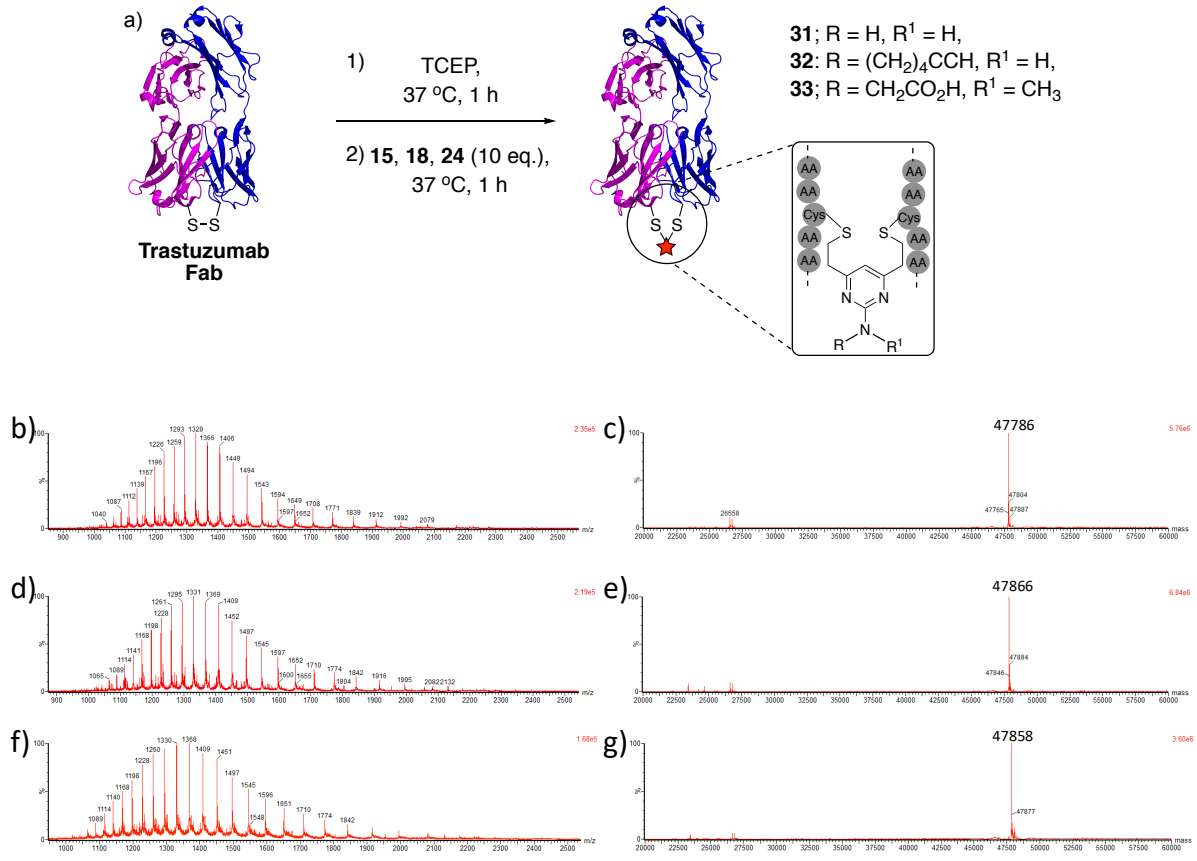

Figure 4.11: a) DVP rebridging of trastuzumab Fab with DVPs **15**, **18** and **24** and analysis by LCMS, Buffer conditions – BBS; sodium borate pH 8 (25 mM), NaCl (25 mM), EDTA pH 8 (0.5 mM), **b)** non-deconvoluted MS of **31**, **c)** deconvoluted MS of **31**, expected mass 47,784 Da, **d)** non-deconvoluted MS of **32**, **e)** deconvoluted MS of **32**, expected mass 47,864 Da, **f)** non-deconvoluted MS of **33**, and **g)** deconvoluted MS of **34**, expected mass 47,856 Da.

These promising studies suggested that Fab rebridging was complete after one hour using DVP linkers **15**, **18** and **24**. However, it is possible that the reactions were complete on a much

faster timescale. In order to understand the rate of rebridging of the Fab light and heavy chains, trastuzumab Fab was first reduced and then treated with 10 or 20 molar equivalents of **18** (Figure 4.12a). At intervals of 5, 10, 15, 20, 30, 40 and 60 minutes, an aliquot was removed from each reaction, quenched with 100-fold molar excess of cysteine and conversion to the rebridged species quantified by LCMS. This analysis suggested that at both 10 and 20 equivalents of **18**, >90% rebridging had occurred after only 15 minutes, representative of an exceptionally fast rebridging reaction (Figure 4.12b).

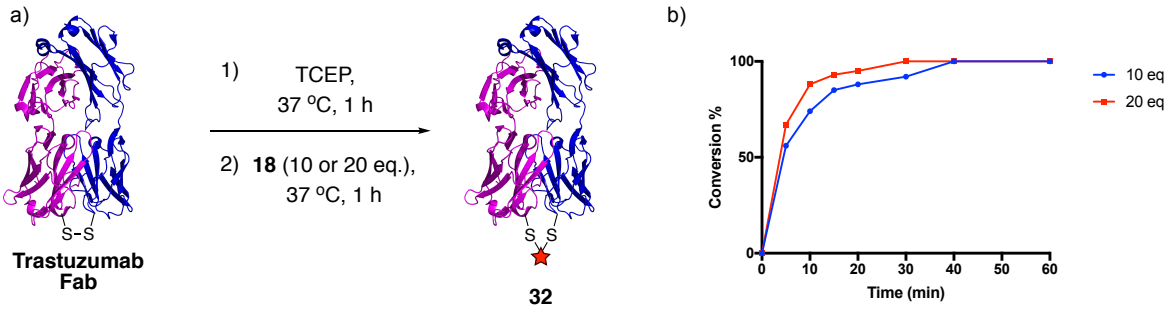

Figure 4.12: a) Studies on the rate of trastuzumab Fab rebridging after treatment with **18**. Buffer conditions – BBS; sodium borate pH 8 (25 mM), NaCl (25 mM), EDTA pH 8 (0.5 mM), and **b)** graph of conversion to the rebridged Fab with varying equivalents of **18** with respect to time.

With good conditions in hand for the rebridging of trastuzumab Fab, the chemoselectivity of the reaction was assessed on a protein system. Unreduced Fab contains no free thiols and so any modification of this protein without disulfide reduction would indicate modification of other amino acid residues. Unreduced trastuzumab Fab was treated with 10 equivalents of DVP **18** in 5% DMSO in BBS (pH 8) for two hours at 37 °C (Figure 4.13a). LCMS analysis of the reaction mixture revealed no modification of the protein, confirming the chemoselectivity of the DVP scaffold for cysteine residues (Figure 4.13b and c).

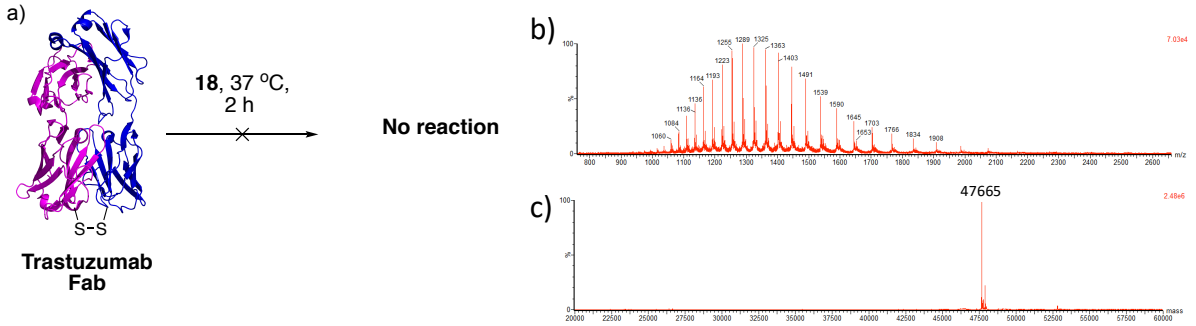

Figure 4.13: a) Treatment of unreduced trastuzumab Fab with **18** and analysis by LCMS, Buffer conditions – BBS; sodium borate pH 8 (25 mM), NaCl (25 mM), EDTA pH 8 (0.5 mM), **b)** non-deconvoluted MS of reaction between unreduced Fab and **18** and **c)** deconvoluted MS, mass of unmodified Fab 47,655 Da. Small peak at higher mass than Fab is 47,910 Da and was present in the starting material of the reaction.

4.11 Trastuzumab Modification

The DVP linkers were shown to effectively rebridge an antibody Fab fragment, only requiring a small excess of rebridging linker to achieve full conversion in less than one hour. Investigations then commenced into DVP rebridging of an IgG molecule. As was discussed in Section 3.5.2, the four interchain disulfides in trastuzumab could be reduced upon treatment with 10 equivalents of TCEP for one hour at 37 °C. In an initial study, reduced trastuzumab was treated with 40 molar equivalents of simple DVP **15** in 10% DMSO in a TBS buffer (25 mM Tris HCl pH 8, 25 mM NaCl, 0.5 mM EDTA pH 8) at 37 °C for two hours (Figure 4.14a). Analysis of the conjugation reactions by LCMS and reducing SDS-PAGE suggested good consumption of the light and heavy chains. This marked a radical improvement over divinylpyridine rebridging of reduced trastuzumab, which had significant quantities of unreacted light and heavy chain remaining after eight hours incubation and with much higher relative linker concentrations (Section 3.5.2). However, LCMS analysis suggested that the major product of the reaction was the half antibody conjugate (72,886 kDa) (Figure 4.14c and d). SDS-PAGE confirmed its presence, but also showed the presence of the correctly bridged full antibody conjugate (Figure 4.14b). It is interesting that the full antibody was only barely visible in the LCMS trace. This can potentially be attributed to the better ionisation ability of the smaller half antibody conjugate or to the ionisation parameters used in the LCMS method. Furthermore, the $[M+2H]^{2+}$ ion of the correctly rebridged antibody would have the same mass-to-charge ratio (m/z) as the $[M+H]^{+}$ ion of the half antibody conjugate. Nevertheless, the combination of SDS-PAGE and LCMS analysis was found to give definitive evidence of good conversion from the unmodified light and heavy chains to a mixture of the full and half antibody conjugates.

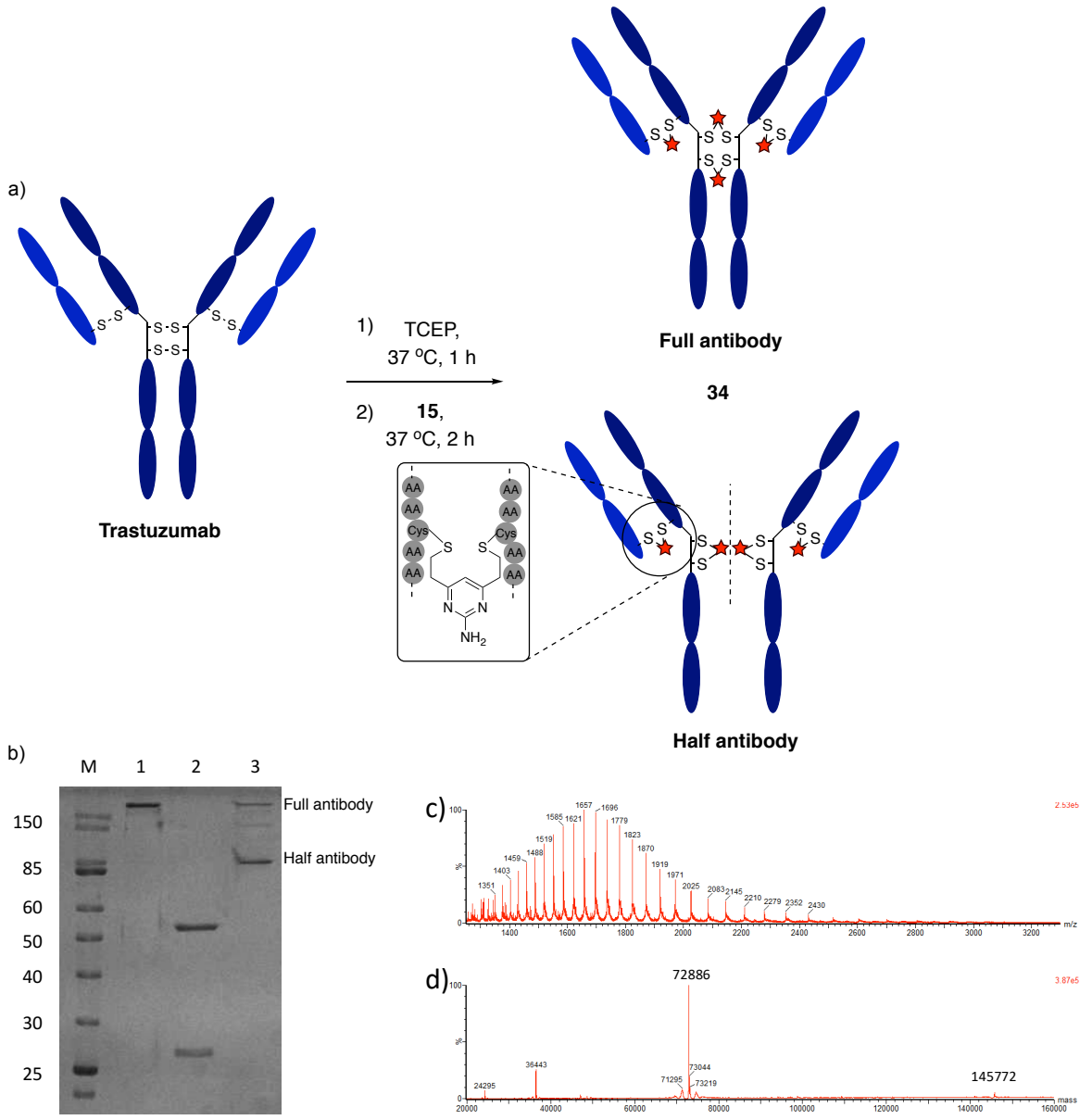

Figure 4.14: a) Synthesis of trastuzumab bioconjugate **34** as a mixture of full and half antibody via DVP rebrdging of reduced trastuzumab with **15**, Buffer conditions – TBS; Tris HCl pH 8 (25 mM), NaCl (25 mM), EDTA pH 8 (0.5 mM), **b)** SDS-PAGE analysis, Lanes: M) molecular weight marker, 1) trastuzumab, 2) reduced trastuzumab, 3) **34**, Lane 1 is non-reduced, lanes 2 and 3 are reduced, **c)** non-deconvoluted MS of **34**, and **d)** deconvoluted MS of **34**, expected mass 72,880 and 145,760 Da.

In an attempt to overcome this potential issue of half antibody formation, a large number of reaction conditions were explored (Table 4.3). Unfortunately, modifications to reaction concentration, linker stoichiometry, organic co-solvent, co-solvent percentage and temperature had little effect on the ratio of half to full antibody conjugates formed in the reaction, as evidenced by SDS-PAGE and LCMS analysis. Morais *et al.* and Bahou *et al.* have recently reported optimised conditions to prevent half antibody formation with dibromomaleimide and dibromopyridazinedione reagents, respectively.[161,166] In these cases, a so-called *in situ* protocol was employed whereby the cross-linking reagent is first incubated

with the antibody before TCEP addition to afford disulfide reduction. The same approach was also attempted with the DVP linkers, but without improvement to the ratio of half antibody formation (Table 4.3, entries 20-22).

Table 4.3: Attempted conditions to prevent half antibody conjugate formation in the reaction of trastuzumab and **15**. In all cases, no change in the ratio of half antibody to full antibody was observed. Conversion determined from SDS-PAGE analysis and reported as conversion after one hour.

Entry	Conc. (mg/mL)	Temp. (°C)	Co-solvent (%)	Linker (15) Eq.	Time (h)	Conversion
1	2.5	37	DMSO (10)	10	1,2,4,8,24	Excellent
2	2.5	37	DMSO (10)	20	1,2,4,8,24	Excellent
3	2.5	37	DMSO (10)	40	1,2,4,8,24	Excellent
4	2.5	37	DMSO (10)	60	1,2,4,8,24	Excellent
5	2.5	37	DMSO (10)	100	1,2,4,8,24	Excellent
6	2.5	37	DMSO (10)	200	1,2,4,8,24	Excellent
7	2.5	37	DMSO (10)	500	1,2,4,8,24	Excellent
8	1	37	DMSO (10)	40	1,2,4	Excellent
9	5	37	DMSO (10)	40	1,2,4	Excellent
10	7.5	37	DMSO (10)	40	1,2,4	Excellent
11	2.5	37	DMSO (1)	40	1,2,4	Excellent
12	2.5	37	DMSO (5)	40	1,2,4	Excellent
13	2.5	37	DMSO (12)	40	1,2,4	Excellent
14	2.5	37	DMSO (15)	40	1,2,4	Excellent
15	2.5	25	DMSO (10)	40	1,2,4	Excellent
16	2.5	4	DMSO (10)	40	1,2,4	Excellent
17	2.5	37	DMF (10)	40	1,2,4	Excellent
18	2.5	37	MeCN (10)	40	1,2,4	Excellent
19	2.5	37	MeOH (10)	40	1,2,4	Excellent
20[a]	2.5	37	DMSO (10)	40	1,2,4	Excellent
21[a]	2.5	25	DMSO (10)	40	1,2,4	Excellent
22[a]	2.5	4	DMSO (10)	40	1,2,4	Excellent

[a] Linker (**15**) was added to trastuzumab and incubated for 10 minutes before the addition of TCEP (10 molar eq.).

The screen of conditions tested did highlight the efficiency of the DVP rebridging reaction. Conversion from unmodified light and heavy chain to the half and full antibody conjugates was found to occur at very low linker stoichiometry (10 molar equivalents), at low antibody concentration (~5 μM), at low percentages of organic co-solvent, and at lower temperature. In addition, under all reaction conditions tested, the reaction appeared to be complete after just one hour.

To further exemplify this approach, determination of the rebridging ability of alternative DVP reagents was also required. Accordingly, reduction of trastuzumab with TCEP and subsequent incubation with DVPs **18** and **24** in 10% DMSO in TBS at 37 °C for two hours resulted in good conversion to conjugates **35** and **36** (Figure 4.15a). Formation of both half and full antibody conjugates was again observed in both reactions by SDS-PAGE and LCMS analysis (Figure 4.15b-f).

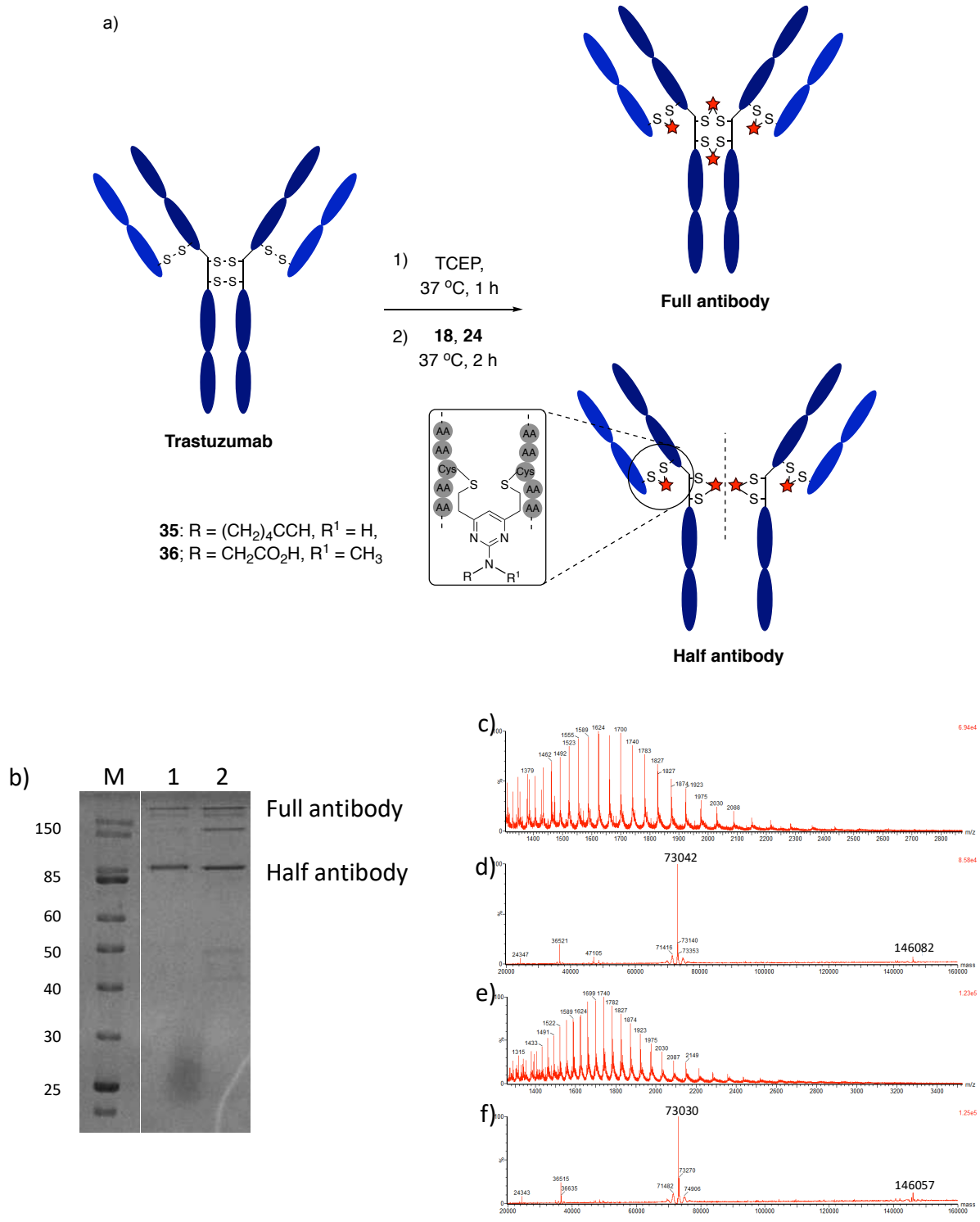

Figure 4.15: a) Synthesis of **35** and **36** from the reaction of trastuzumab with **18** and **24**. Buffer conditions – TBS; Tris HCl pH 8 (25 mM), NaCl (25 mM), EDTA pH 8 (0.5 mM). **b)** Reducing SDS-PAGE analysis, Lanes: M) molecular weight marker, 1) **35** 2) **36**, **c)** non-deconvoluted MS of **35**, **d)** deconvoluted MS of **35**, expected mass 73,040 and 146,080 Da, **e)** non-deconvoluted MS of **36**, **f)** deconvoluted MS of **36**, expected mass 73,024 and 146,048 Da.

LCMS and SDS-PAGE analysis suggested conversion from the reduced antibody to the full and half antibody bioconjugates was occurring upon reaction with the DVP linkers. However,

to quantify this conversion and analyse the effects of rebridging on the antibody structure, trastuzumab conjugate **35** was analysed by reverse phase HPLC (RP-HPLC) and size exclusion chromatography (SEC) at Spirogen (a biotechnology company specialising in ADC therapeutics, London). RP-HPLC analysis confirmed ~90% consumption of the unmodified light and heavy chains to both the full and half antibody conjugates in approximately a 40:50 ratio, respectively (Figure 4.16).

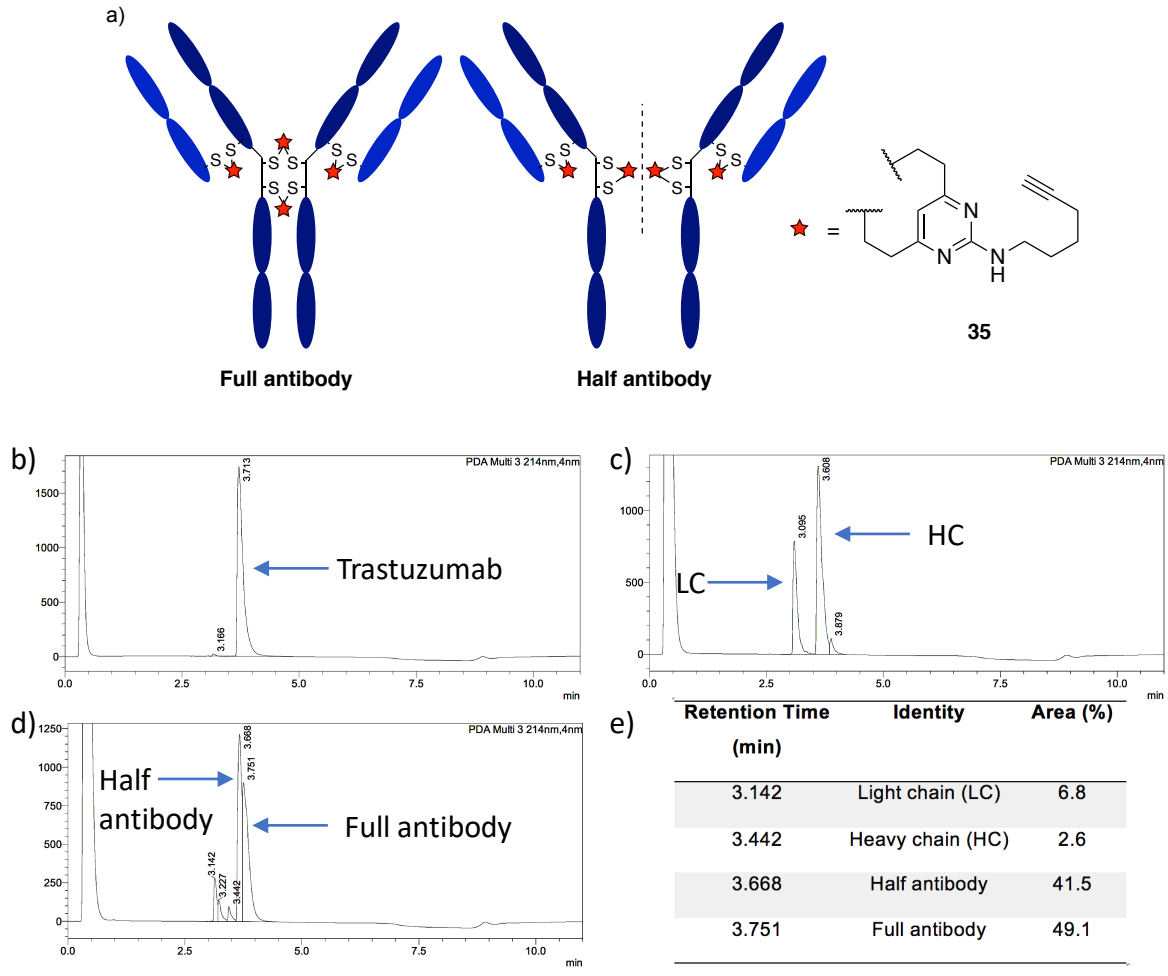

e)

Retention Time (min)	Identity	Area (%)
3.142	Light chain (LC)	6.8
3.442	Heavy chain (HC)	2.6
3.668	Half antibody	41.5
3.751	Full antibody	49.1

Figure 4.16: a) Analysis of the full and half antibody mixture of bridged trastuzumab **35** via RP-HPLC. **b)** RP-HPLC of trastuzumab, **c)** reduced trastuzumab and **d**) reduced **35**. **e)** Percentage of the constituents of **35**. This analysis was conducted at Spirogen.

It is important to note that although undesirable, the half antibody conjugate remains highly useful, even as a mixture with the full antibody conjugate. Indeed, Lyon *et al.* have reported that ADCs with no interchain linkages have demonstrated exquisite *in vivo* activity.[219] Critically, with DVP antibody conjugates, the light and heavy chains are covalently attached through rebridging of the Fab disulfide, ensuring that the region of the antibody that confers its receptor affinity and selectivity is rebridged. Although the covalent linkage between the two heavy

chains has been lost, other non-covalent attractions such as hydrogen bonds, salt bridges and hydrophobic interactions will likely still hold the entire antibody together. This is evidenced by non-reducing and non-boiled SDS-PAGE analysis and SEC. A non-reduced SDS-PAGE analysis of conjugate **35** showed a single band in the gel at the same mass as unmodified trastuzumab (Figure 4.17a). Similarly, **35** eluted as a single peak from a SEC column at an identical retention time to trastuzumab (Figure 4.17b).

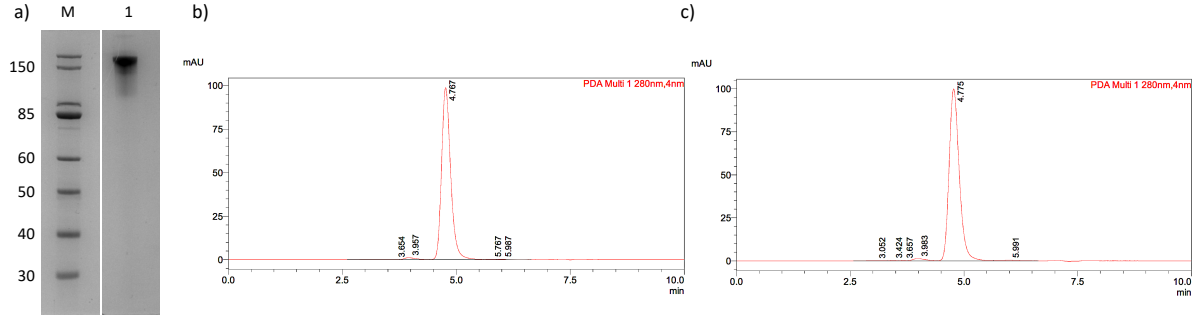

Figure 4.17: a) Non-reducing SDS-PAGE analysis of **35**, Lanes: M) molecular weight marker, 1) non-reduced **35**, **b)** SEC of trastuzumab and **c)** SEC of **35**.

4.12 Functional Antibody Modification

The functionalisation of antibodies with biologically useful modalities (e.g. cytotoxic warheads, fluorophores, affinity tags) can provide extremely important tools in the study or perturbation of biological systems. The simple DVP reagents described thus far do not contain any functional payloads, the physical characteristics of which can vary greatly. For example, MMAE is a stable molecule that can be easily derivatised to attach to a bioconjugation linker. In contrast, routinely used imaging agents such as near-infrared (NIR) dyes are generally unstable, difficult to synthesise, and can only be purchased in low quantities (<1 mg). On this scale, chemical modification with a linker is challenging. However, if conjugation of the payload can be conducted directly on the protein of interest, low or sub-milligram quantities of reagent are more than sufficient. With this in mind, it was envisaged that functional modification of the antibody could take on two possible formats. In one approach, a pre-functionalised linker could be used to attach stable, modifiable payloads to the antibody. In another format, the DVP linkers could be used to install a bioorthogonal handle on the antibody which could be subsequently reacted with a complementary functional group on a more sensitive payload.

4.12.1 Post-Rebridging Functionalisation

A library of bioorthogonal reactions has now been developed that enables chemo- and site-selective modification of proteins.[43,99] One of the most commonly employed bioorthogonal reactions is the copper-catalysed azide-alkyne cycloaddition (CuAAC) "Click" reaction (*vide supra*). It was proposed that DVP reagents could be used to decorate an antibody with an alkyne or an azide handle, which would then be amenable to the attachment of the desired payload via CuAAC chemistry. This was seen as an attractive strategy for a number of reasons: 1) the CuAAC reaction has been shown to be a robust method of modifying a range of proteins and other biomacromolecules including DNA/RNA and polysaccharides;[188,189] and 2) a catalogue of potential payloads containing azide or alkyne groups are commercially available.

4.12.1.1 Doxorubicin ADC

Doxorubicin is a DNA intercalating agent that has seen significant use as a small molecule therapeutic and as a cytotoxic warhead in ADC development. Indeed, numerous ADCs armed with doxorubicin payloads have undergone clinical evaluation.[220,221] It has been demonstrated that while this cytotoxin is not amenable to many chemical reactions, attachment of an azide-containing moiety to doxorubicin through mild amide coupling conditions is tolerable.[222] To this end, modification of its daunosamine sugar with a pendant azide group via HBTU-mediated amide coupling generated azide **37** in good yield (Scheme 4.11).

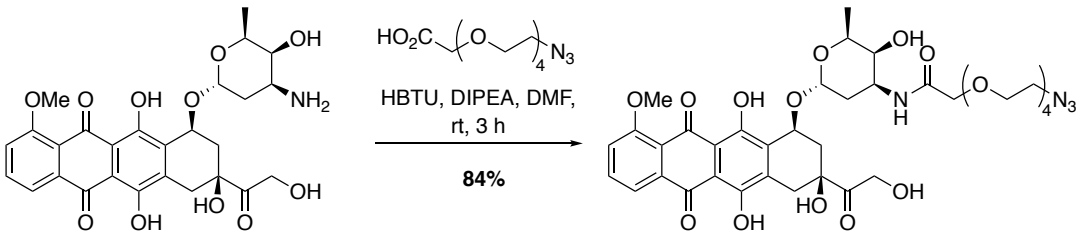

Scheme 4.11: Synthesis of azide **37**.

With alkyne-functionalised trastuzumab **35** and azide **37** now in hand, post-rebridging investigations were able to commence. Accordingly, bioconjugate **35** was reacted with azide **37** in PBS in the presence of $CuSO_4 \cdot H_2O$, tris(3-hydroxypropyltriazolylmethyl)amine (THPTA) and sodium ascorbate to yield ADC **38** (Figure 4.18a). UV-vis and LCMS analysis of this ADC

was performed and showed excellent conversion to the desired ADC **38** with a measured DAR of 4.0. (Figure 4.18b-e).

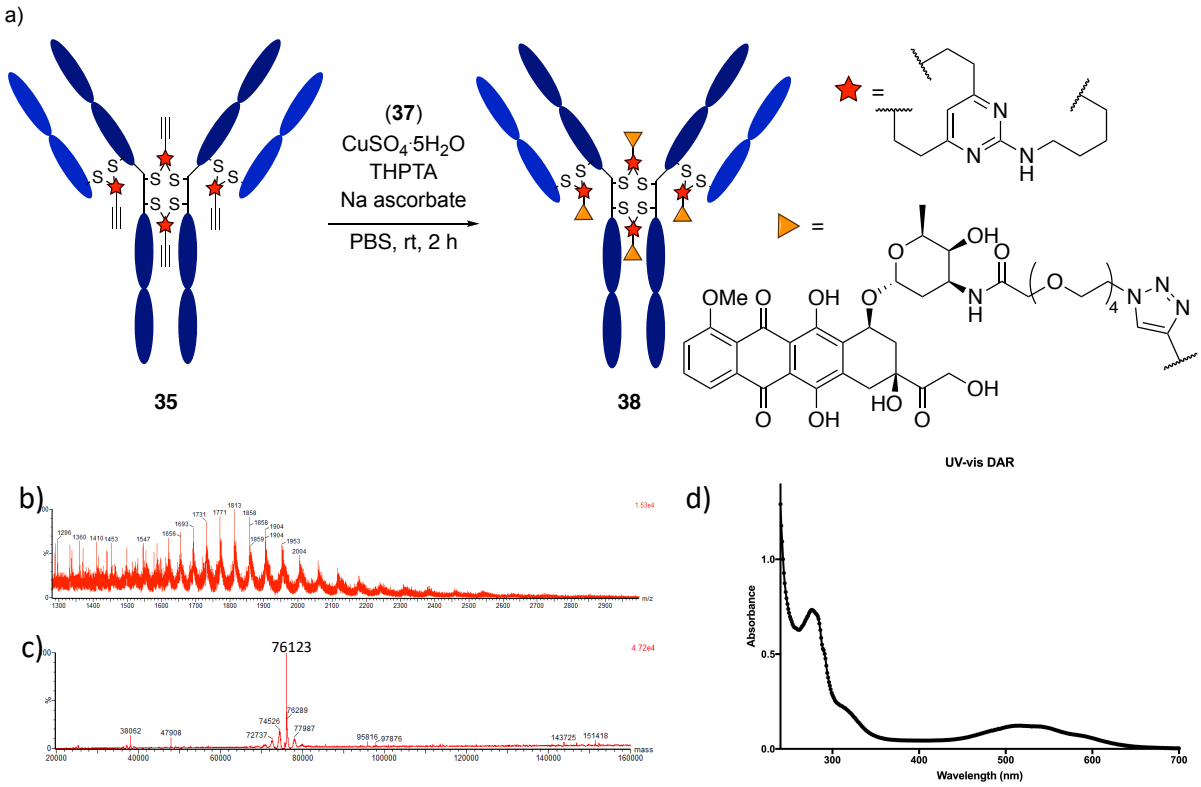

e)

$$DAR = \frac{Abs_{495}/\varepsilon_{495}}{(Abs_{280} - 0.724 \times Abs_{495})/\varepsilon_{280}}$$

ε_{495} = 8,030 M^{-1} cm^{-1}

ε_{280} = 215,380 M^{-1} cm^{-1}

Correction factor = 0.724

Figure 4.18: a) Post-conjugation CuAAC reaction between alkyne-modified trastuzumab **35** and azide **37**. **b)** Non-deconvoluted MS and **c)** deconvoluted MS of **38,** expected mass 76,119 Da. **d)** UV-vis spectrum of **38**, and **e)** calculation used to measure the DAR of **38** from the UV-vis data. A correction factor of 0.724 was required to account for doxorubicin absorbance at 280 nm.

4.12.1.2 AlexaFluor™ 488 Antibody-Fluorophore Conjugate

Antibody-based imaging agents have seen a surge in interest in recent years in diagnostics due to the highly specific cellular imaging that can be achieved with antibody strategies.[223,224] With the aim of creating a potentially valuable imaging agent, alkyne-modified trastuzumab **35** was reacted with commercially available AlexaFluor™ 488 azide in PBS in the presence of $CuSO_4 \cdot H_2O$, THPTA and sodium ascorbate to yield the antibody-fluorophore conjugate (AFC) **39** (Figure 4.19a). SDS-PAGE followed by in-gel fluorescence analysis suggested formation of the AFC (Figure 4.19b). Further analysis by UV-vis spectrophotometry confirmed excellent

conversion to the desired conjugate with a measured fluorophore-antibody ratio (FAR) of 3.9 (Figure 4.19c and d).

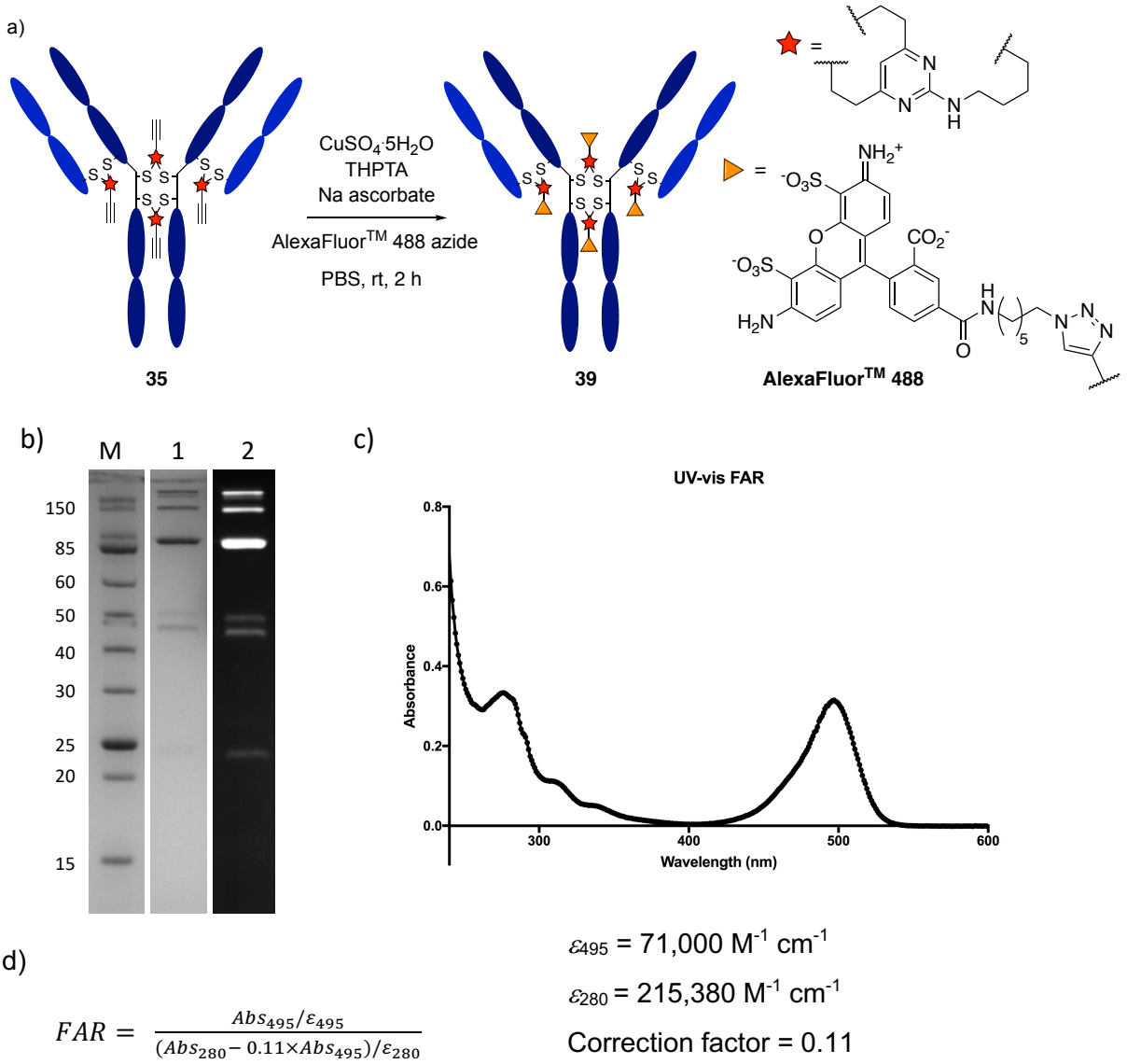

Figure 4.19: a) Post-conjugation CuAAC reaction between alkyne-modified trastuzumab **35** and AlexaFluor™ 488 azide. **b)** SDS-PAGE analysis of **39**, Lanes: M) molecular weight marker, 1) Coomassie stain of **39**, 2) in-gel fluorescent image of **39**. **c)** UV-vis spectrum of **39**, and **d)** calculation used to measure the FAR of **39** from the UV-vis data. A correction factor of 0.11 was used to account for AlexaFluor™ 488 absorbance at 280 nm.

The synthesis of a potentially useful therapeutic ADC and diagnostic AFC via post-rebridging CuAAC chemistry shows that DVP reagents can serve as a powerful tool for affecting tandem cysteine modification and bioorthogonal functionalisation (*vide infra*).

4.12.2 Pre-Rebridging Functionalisation with MMAE

MMAE is a highly potent cytotoxin that inhibits tubulin polymerisation, thus preventing microtubule formation and subsequent cell division.[57] It has been widely employed in ADC research, and is the payload used in many ADCs currently in clinical development and in the FDA-approved brentuximab vedotin (Adcetris®).[33] Typically, MMAE is combined with a cleavable linker such as the cathepsin B-cleavable Val-Cit linker to release the free warhead from the antibody upon cellular internalisation. It was proposed to synthesise both cleavable and non-cleavable MMAE-containing ADCs, for comparison. Numerous examples of MMAE functionalisation with a variety of linkers have been reported, suggesting that synthesis of a DVP-MMAE linker-drug would be achievable prior to antibody conjugation.[10,54,57] MMAE is an exceptionally potent cytotoxin and so extreme care should be taken during its use. Please see Chapter 7, General Experimental for full details on use of this chemical.

4.12.2.1 Non-Cleavable MMAE ADC

The design of any linker-drug molecule is crucial to ensure that one component does not disrupt the function of the other. This is particularly important for non-cleavable linkers as the two moieties will remain attached throughout the lifetime of the molecule *in vivo*, and it is important that the linker will not impede the biological mechanism of action of the warhead. It was hoped that a short polyethylene glycol (PEG) spacer would be sufficient to prevent negative interaction. Thus, modification of the MMAE *N*-terminus with a PEG spacer was achieved through an amide coupling with N_3-PEG_4-COOH in the presence of HBTU and DIPEA, providing azide-modified MMAE **40** in excellent yield (Scheme 4.12). Azide **40** was subsequently reacted with DVP **18** under CuAAC conditions to produce DVP-MMAE linker-drug **41**.

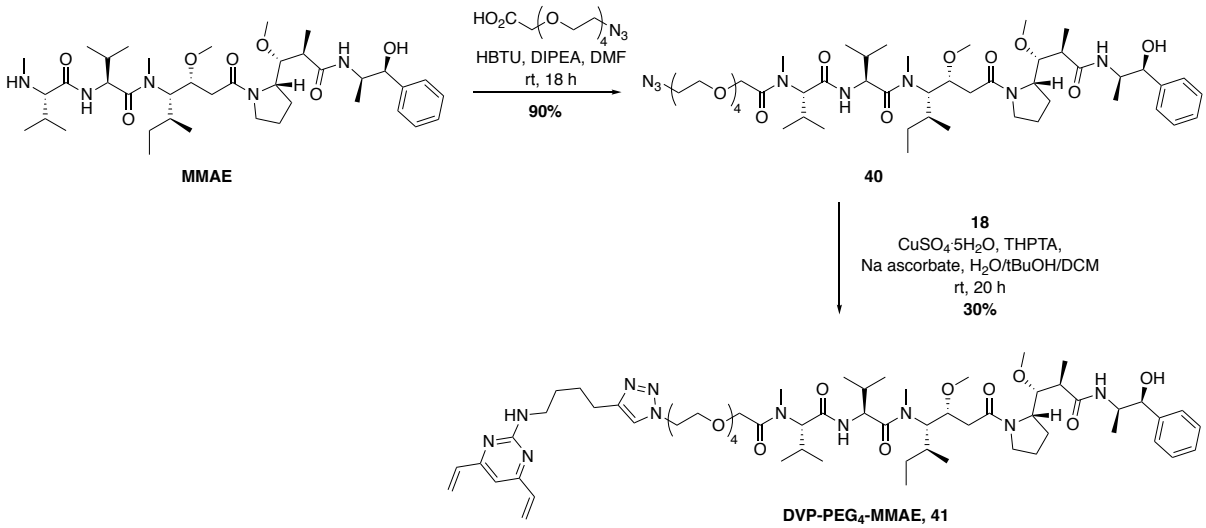

Scheme 4.12: Synthesis of DVP-PEG$_4$-MMAE (**41**).

Subsequently, reduction of trastuzumab was followed by treatment with linker-drug **41** (40 equivalents) in 10% DMSO in TBS at 37 °C for two hours (Figure 4.20a). Excellent conversion to the rebridged non-cleavable MMAE ADC **42** was observed by LCMS and SDS-PAGE (Figure 4.20b-d). A mixture of the half and full antibody conjugates was again present in similar ratios to those observed with the unfunctionalised linkers (See Section 4.11).

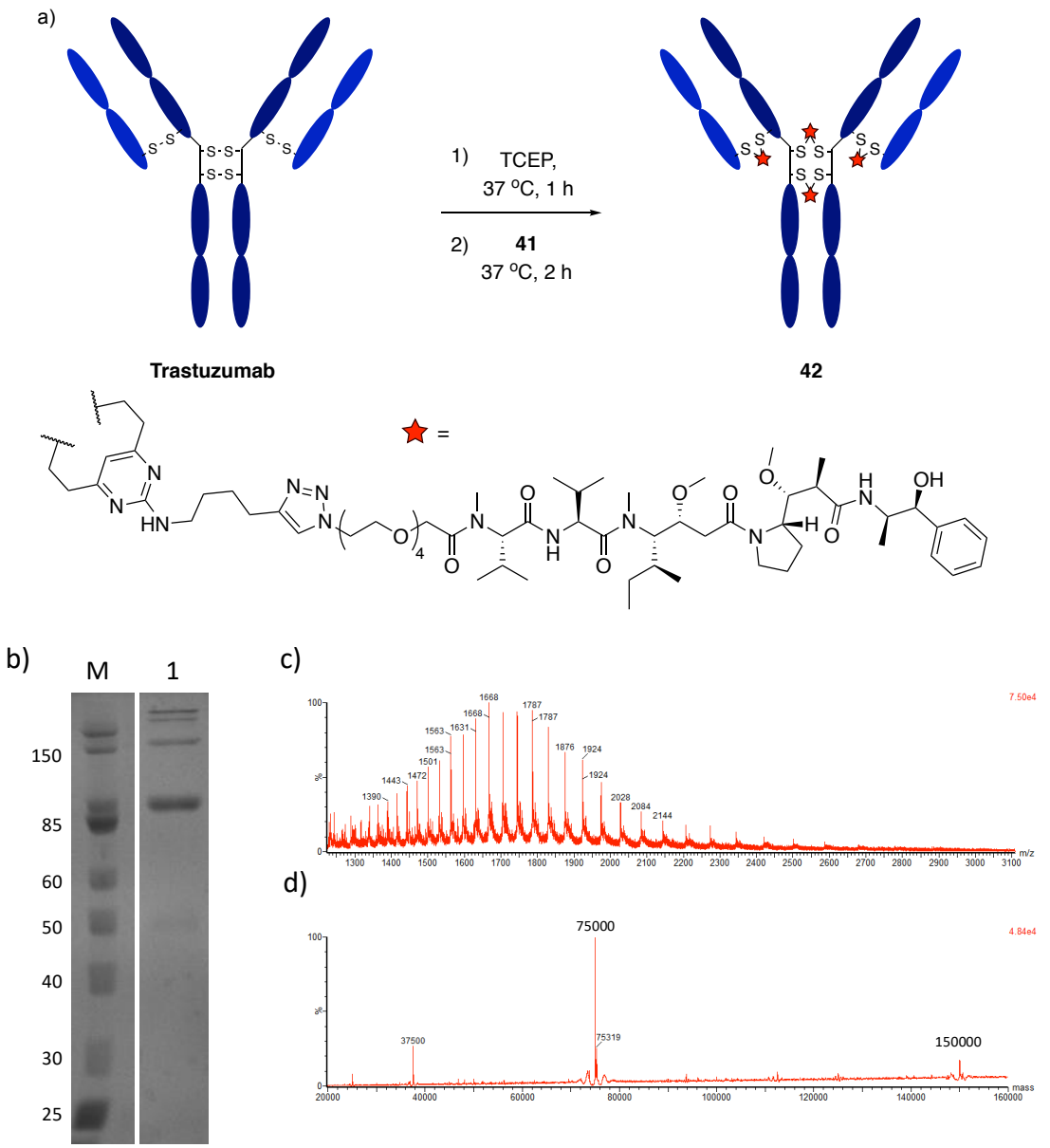

Figure 4.20: a) Synthesis of ADC **42**. Buffer conditions – TBS; Tris HCl pH 8 (25 mM), NaCl (25 mM), EDTA pH 8 (0.5 mM). **b)** SDS-PAGE analysis, Lanes: M) molecular weight marker, 1) reduced **42**. **c)** Non-deconvoluted MS and **d)** deconvoluted MS of **42**, expected mass 74,994 and 149,988 Da.

4.12.2.2 Cleavable MMAE ADC

A range of cleavable linkers have been successfully employed in ADC research, as described in Section 1.5.1. The most commonly used drug release mechanism is the cathepsin B-mediated cleavage of valine-citrulline and valine-alanine dipeptide motifs to release an unmodified cytotoxic warhead (*vide supra*). Synthetic routes to Val-Cit and Val-Ala MMAE linker-drugs are well described.[225,226] In addition, Alloc-protected valine-alanine-4-aminobenzyl alcohol (Alloc-Val-Ala-PABA, **43**) was readily available from AstraZeneca and so was chosen as a starting cleavable motif. Accordingly, **43** was treated with bis(4-nitrophenyl)

carbonate in the presence of diisopropylethylamine (DIPEA) (Scheme 4.13). This activated carbonate intermediate was subsequently reacted with MMAE in the presence of 1-hydroxybenzotriazole hydrate (HOBt·H_2O) and pyridine, providing access to **44** in 88% yield over two steps. Removal of the Alloc protecting group proceeded smoothly under $Pd(PPh_3)_4$ catalysis in the presence of pyrrolidine as an allyl scavenger.[227] Amide coupling of the unprotected amine with the carboxylic acid of DVP **24** was achieved with HBTU, HOBt·H_2O and DIPEA to yield cleavable DVP-MMAE linker-drug **45** in excellent yield over two steps (Scheme 4.13).

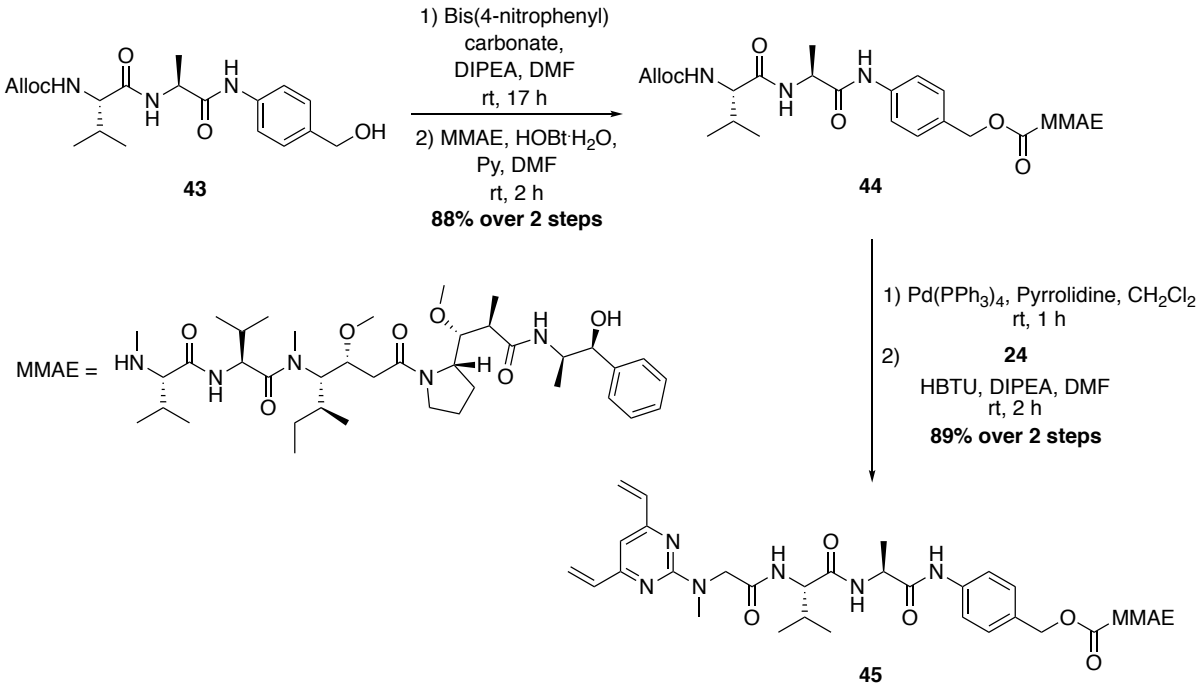

Scheme 4.13: Synthesis of cleavable linker-drug **45**.

With **45** in hand, conjugation of this linker-drug to reduced trastuzumab was attempted using 40 equivalents of **45** in 10% DMSO in TBS at 37 °C (Figure 4.21a). Disappointingly, no conjugation was observed by LCMS or SDS-PAGE analysis (Figure 4.21b).

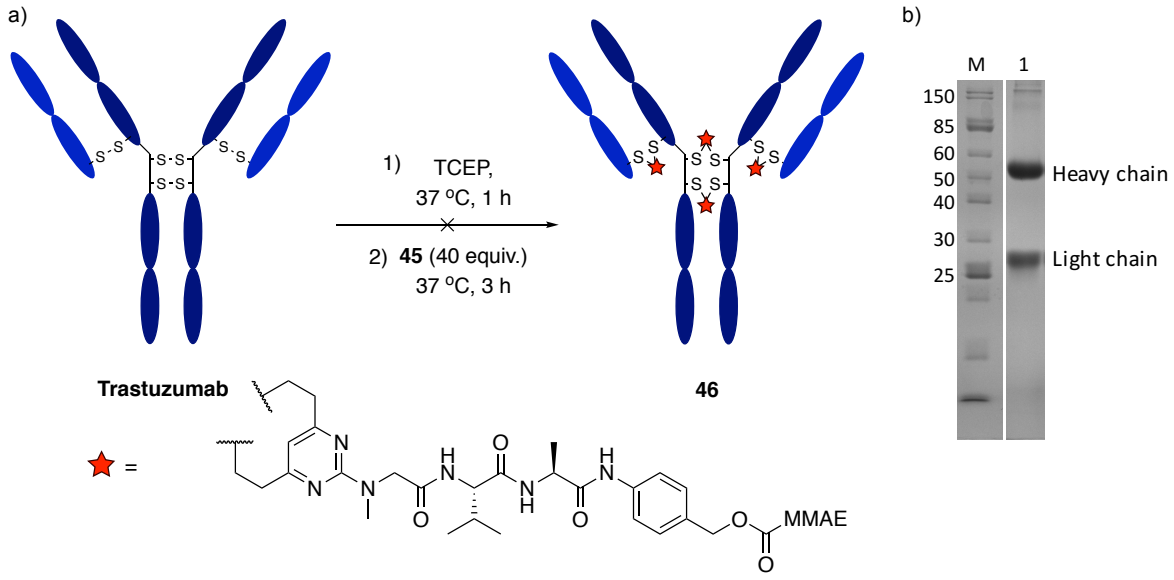

Figure 4.21: a) Attempted modification of trastuzumab with **45** and **b)** example reducing SDS-PAGE analysis of the reaction showing only unreacted light and heavy chains. Lanes; M) molecular weight marker, 1) reaction of trastuzumab with 40 eq. of drug-linker **45**. Buffer conditions – TBS; Tris HCl pH 8 (25 mM), NaCl (25 mM), EDTA pH 8 (0.5 mM).

It was noted that on addition of the linker-drug solution in DMSO into the solution of reduced trastuzumab in TBS, a white precipitate immediately formed, suggesting that **45** was insoluble in this solvent system. A small screen of conditions was performed, varying the organic solvent (DMSO, DMF, MeCN and MeOH) and the final percentage of organic co-solvent in the reaction (10 and 15%) (Table 4.4). In all cases, the concentration of the drug-linker stock solution was adjusted so that the final percentage of organic solvent would be present immediately on addition. However, a white precipitate was formed in all cases and no conversion to the rebridged half or full antibody conjugates was observed in any of the reactions by LCMS and SDS-PAGE analysis.

Table 4.4: Attempted modification of trastuzumab with linker-drug **45**. Conversion determined from SDS-PAGE analysis.

Entry	Co-solvent	Co-solvent % (v/v)	Conversion
1	DMSO	10	None
2	DMF	10	None
3	MeCN	10	None
4	MeOH	10	None
5	DMSO	15	None
6	DMF	15	None
7	MeCN	15	None
8	MeOH	15	None

This result was somewhat surprising as the structurally similar maleimide linker-drug, mc-Val-Cit-PABC-MMAE (Figure 4.22b) is a widely used linker-drug for synthesising cleavable MMAE ADCs. It was proposed that the short spacer between the DVP linker and the valine residue may be affecting the solubility and thus the reactivity of the linker, as the mc-Val-Cit-PABC-MMAE has a longer alkyl chain between the maleimide and the valine. Drug-linkers **47** and **48** were proposed as a potential solution to these solubility and reactivity issues (Figure 4.22c and d).

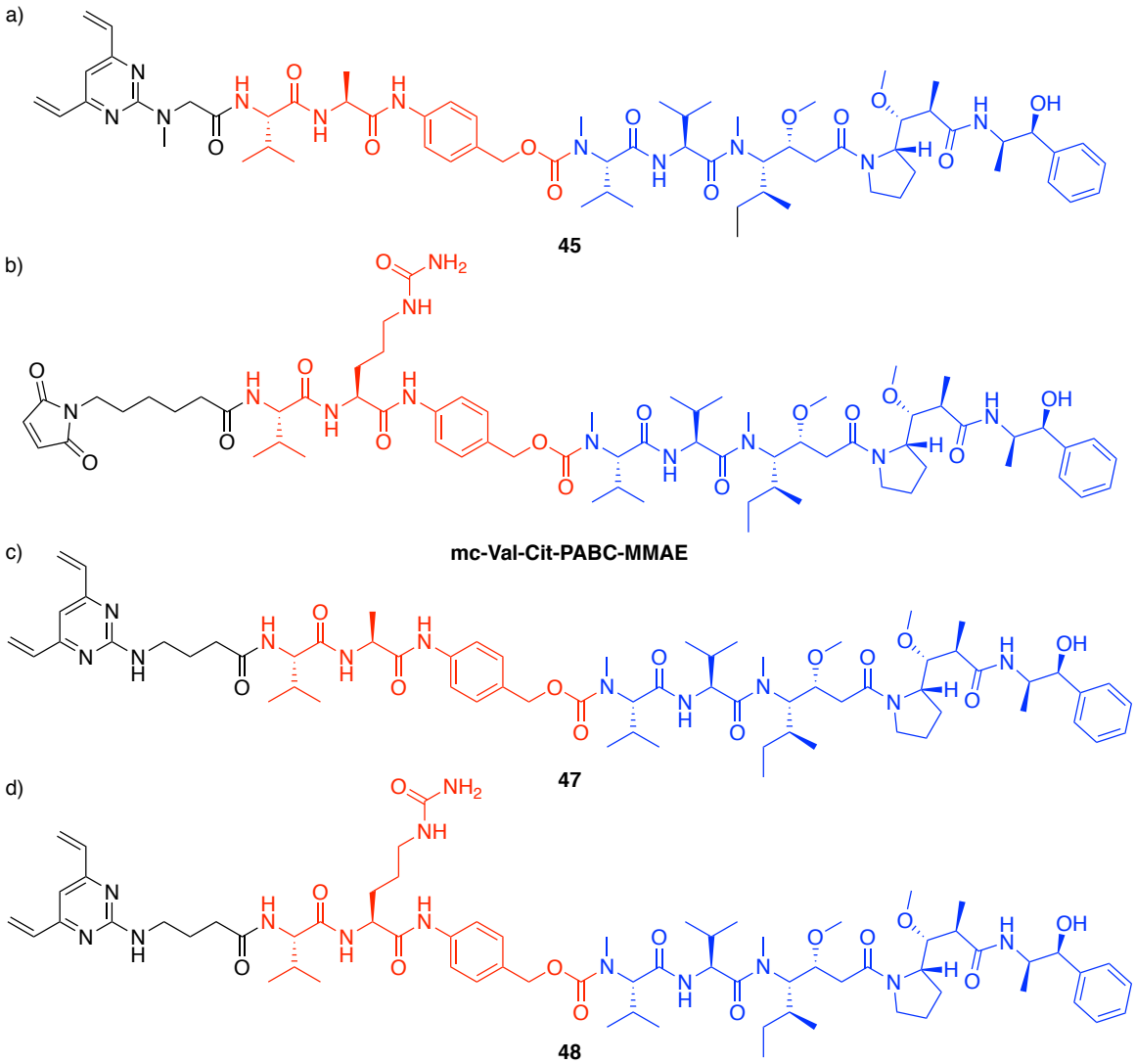

Figure 4.22: a) Linker-drug **45** failed to show any reactivity with trastuzumab, **b)** commonly used maleimide reagent mc-Val-Cit-PABC-MMAE, and proposed DVP reagents **c) 47** and **d) 48** that are similar in structure to mc-Val-Cit-PABC-MMAE. MMAE highlighted in blue, cleavable motif in red and linker in black.

Synthesis of the Val-Cit-PABC-MMAE fragment of proposed linker-drug **48** commenced from succinimide-activated amino acid Fmoc-Val-OSu, which was treated with *L*-citrulline to produce the Fmoc-protected Val-Cit dipeptide **49** in near quantitative yield (Scheme 4.14). Attachment of the self-immolative PABC spacer was subsequently achieved by treatment of the protected dipeptide **49** with 4-aminobenzyl alcohol in the presence of 2-ethoxy-1-ethoxycarbonyl-1,2-dihydroquinoline (EEDQ) coupling agent, to produce **50** in moderate yield. Activation of the benzyl alcohol was then achieved as previously described for the Val-Ala dipeptide by treatment with bis(4-nitrophenyl) carbonate in the presence of DIPEA. Conversion of the active carbonate to the desired carbamate proceeded smoothly upon reaction with MMAE, HOBt·H_2O and pyridine, producing **51** in 39% yield over two steps. Finally, Fmoc removal under piperidine conditions was followed by amide coupling of the free

amine with DVP **52** (see Section 7.2.1 for synthetic details) in the presence of HBTU, HOBt·H_2O and DIPEA, to generate the desired linker-drug **48** in 20% yield over two steps. Although the final deprotection and amide coupling sequence produced **48** in a relatively low yield, sufficient material was produced to conduct conjugation studies.

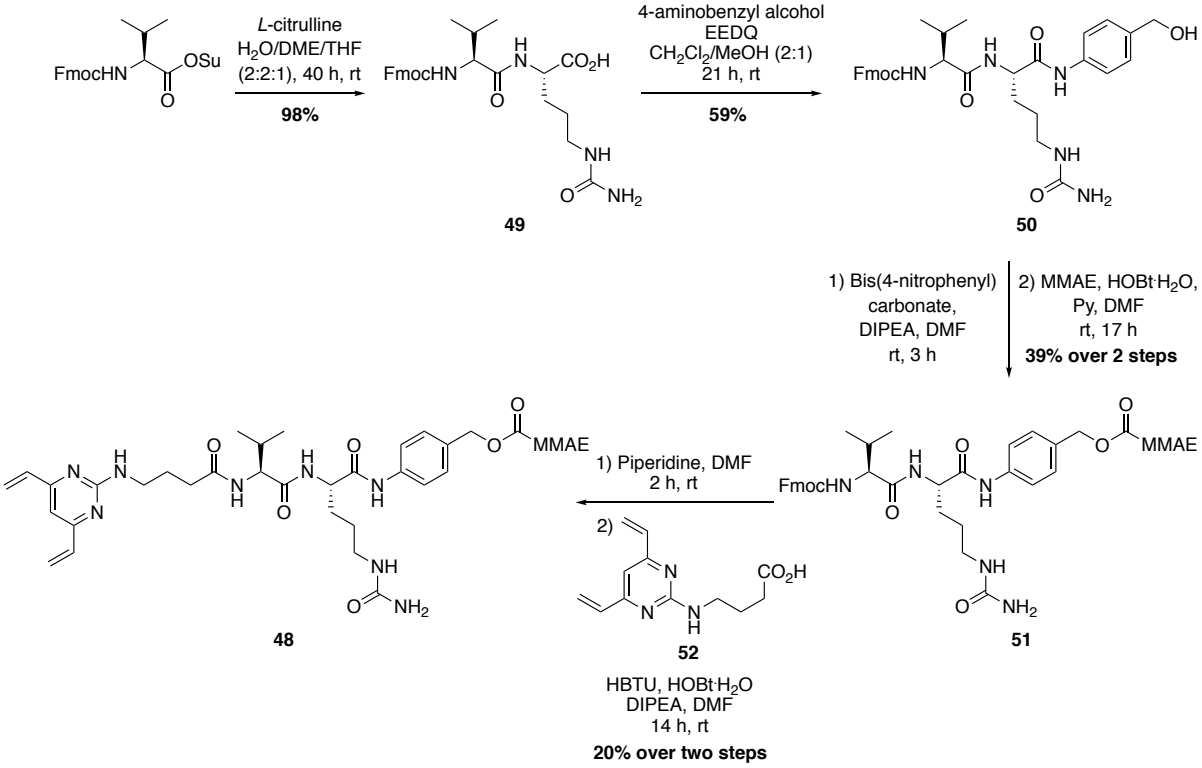

Scheme 4.14: Synthesis of linker-drug **48**.

In order to compare the conjugation abilities of Val-Cit- and Val-Ala-containing linker-drugs, the analogous Val-Ala cleavable linker-drug **47** was also synthesised in two steps from the previously synthesised Alloc-Val-Ala-PABC-MMAE **44**. Alloc deprotection via $Pd(PPh_3)_4$ catalysis was followed by amide coupling of the free amine and DVP **52** in the presence of HBTU and DIPEA, to yield Val-Ala linker-drug **47** (Scheme 4.15).

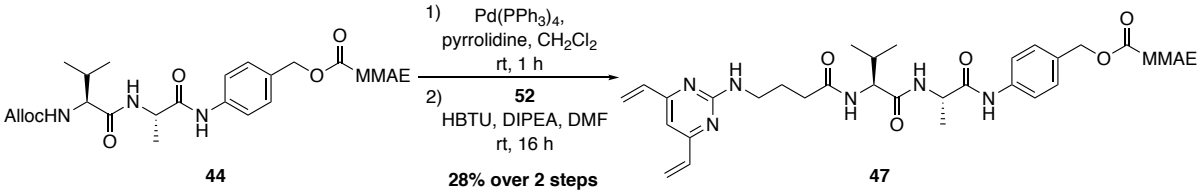

Scheme 4.15: Synthesis of linker-drug **47**.

The conjugation capabilities of linker-drugs **47** and **48** to trastuzumab were then investigated. The linker-drug conjugates were again added to reduced trastuzumab in four different organic co-solvents (DMSO, DMF, MeCN and MeOH), with each reaction containing 10% v/v organic solvent (Figure 4.23a). Disappointingly, no conversion to the desired bridged conjugates **53** or **54** could be observed by SDS-PAGE and LCMS analysis under any of the reaction conditions tested (Figure 4.23b). In a similar fashion to the conjugation studies conducted with **45**, a white precipitate was formed in all reactions with **53** and **54** upon addition into the TBS buffer.

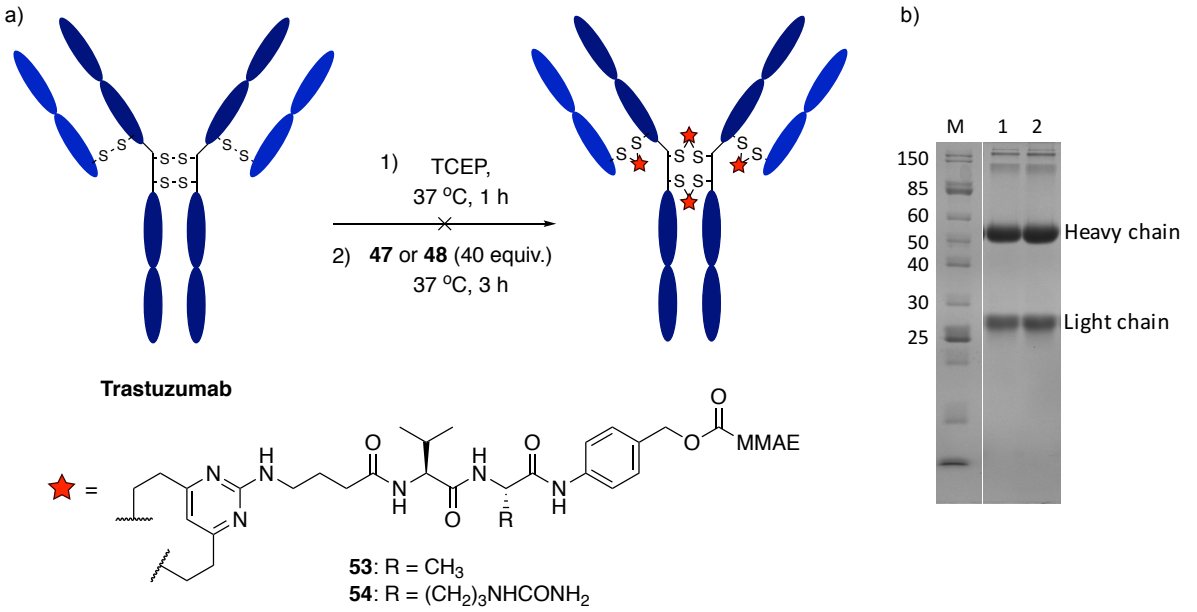

Figure 4.23: a) Attempted modification of trastuzumab with **47** and **48**. **b)** Example reducing SDS-PAGE analysis of the reactions showing only unreacted light and heavy chains. Lanes, M) molecular weight marker, 1) example reaction of trastuzumab with Val-Cit linker-drug **48**, 2) example reaction of trastuzumab with Val-Ala linker-drug **47**. Buffer conditions – TBS; Tris HCl pH 8 (25 mM), NaCl (25 mM), EDTA pH 8 (0.5 mM).

Given the apparent solubility issues with the initial cleavable linkers, it was postulated that PEGylation of the linker-drug conjugate would potentially increase the aqueous solubility of the constructs. Based on this hypothesis, two linker-drug constructs were synthesised using commercially available hetero-bifunctional PEGylation reagents. Linker-drug conjugates containing four and nine PEG units were synthesised in three and five steps, respectively, from a common Alloc-Val-Ala-PABC-MMAE intermediate **44** (Scheme 4.16). Synthesis of DVP-PEG$_4$-Val-Ala-PABC-MMAE **57** commenced with Alloc deprotection of dipeptide **44** under standard Pd(PPh$_3$)$_4$ catalysis followed by HBTU-mediated amide coupling with N$_3$-PEG$_4$-CO$_2$H to give azide **56** in 70% yield over two steps. Subsequent reaction of azide **56** with alkynyl DVP **18** under CuAAC conditions produced DVP-PEG$_4$-Val-Ala-PABC-MMAE **57** in moderate yield.

Similarly, synthesis of DVP-PEG$_9$-Val-Ala-PABC-MMAE **60** commenced by Alloc deprotection followed by amide coupling with FmocHN-PEG$_5$-CO$_2$H, producing PEGylated dipeptide **58** in moderate yield. Fmoc removal with piperidine was followed by another amide coupling with N$_3$-PEG$_4$-CO$_2$H generated azide **59**. The synthesis of the desired linker-drug was completed via a CuAAC reaction between azide **59** and alkyne **18** to give DVP-PEG$_9$-Val-Ala-PABC-MMAE **60** in 59% yield.

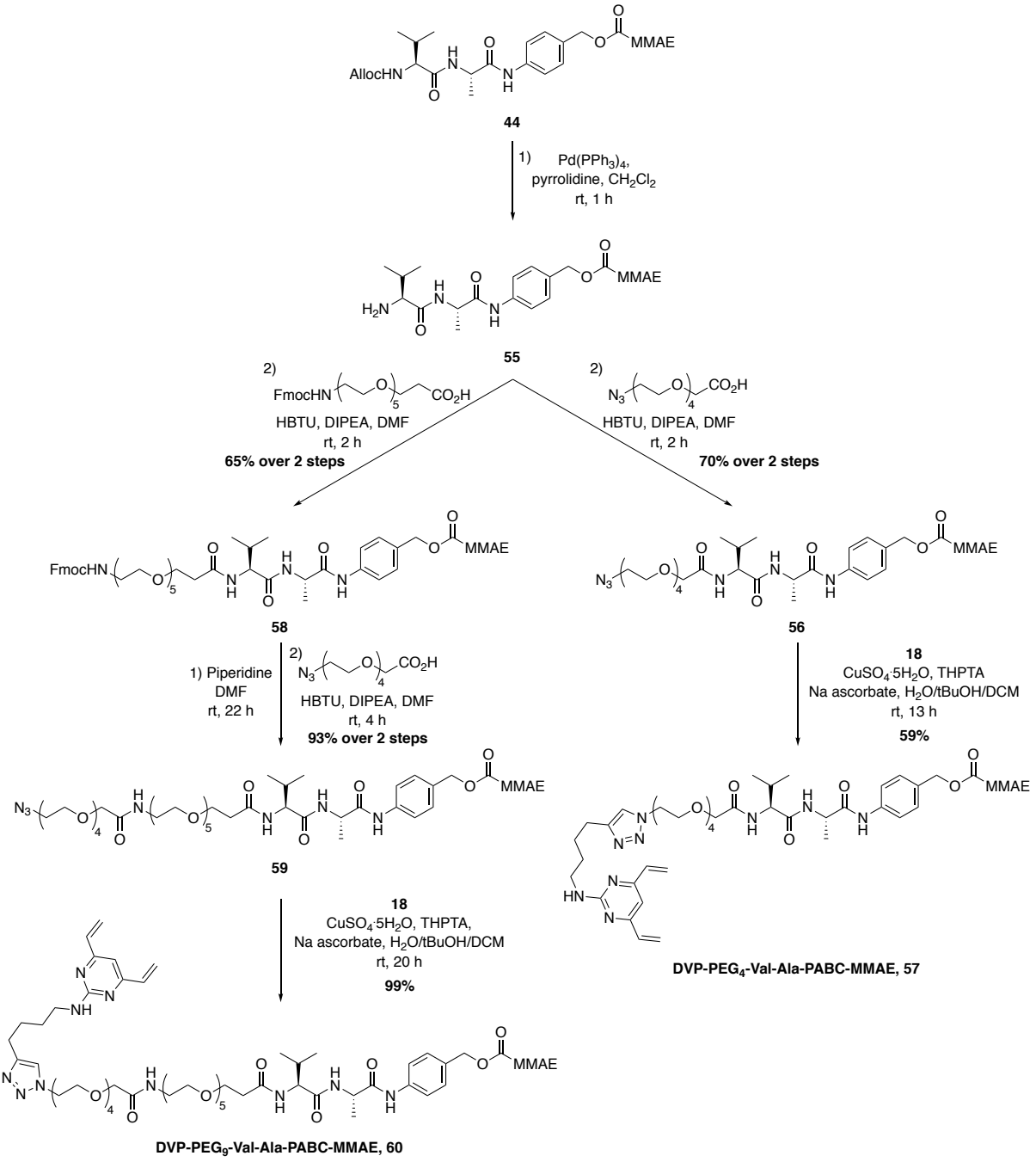

Scheme 4.16: Synthesis of PEGylated linker-drugs **57** and **60**.

Initial antibody conjugation investigations focused on DVP-PEG_9-Val-Ala-PABC-MMAE **60** due to its potentially better aqueous solubility and thus better probability of reactivity. A number of conditions were screened, varying the organic co-solvent, organic co-solvent percentage, linker equivalents and reaction concentration (Table 4.5).

Table 4.5: a) Attempted conjugation of trastuzumab with linker-drug **60** and **b)** typical reducing SDS-PAGE analysis. Lanes; M) molecular weight marker, 1) entry 16 reaction. Buffer conditions – TBS; Tris HCl pH 8 (25 mM), NaCl (25 mM), EDTA pH 8 (0.5 mM). Conversion determined from SDS-PAGE analysis.

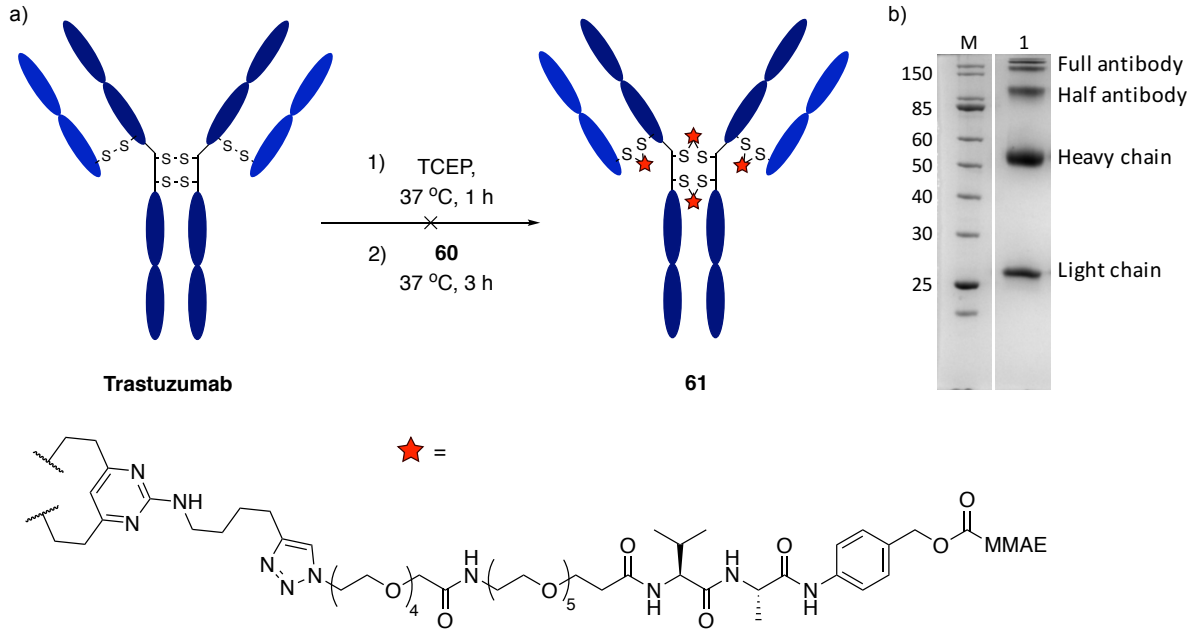

Entry	Co-solvent	Co-solvent % (v/v)	60 Eq.	Conc. (mg/mL)	Conversion
1	DMF	10	40	2.5	None
2	DMSO	10	40	2.5	None
3	MeCN	10	40	2.5	None
4	MeOH	10	40	2.5	None
5	DMF	15	40	2.5	None
6	DMSO	15	40	2.5	None
7	MeCN	15	40	2.5	None
8	MeOH	15	40	2.5	None
9	DMSO	20	60	2.5	Moderate
10	DMSO	20	80	2.5	Moderate
11	DMSO	20	100	2.5	Moderate
12	DMSO	20	120	2.5	Moderate
13	DMSO	20	60	5	Moderate
14	DMSO	20	80	5	Moderate
15	DMSO	20	100	5	Moderate
16	DMSO	20	120	5	Moderate

Varying the organic co-solvent to either DMSO, DMF, MeCN or MeOH at 10% v/v yielded no reaction to the desired conjugate by LCMS and SDS-PAGE analysis (Table 4.5, entries 1-4). Similarly, increasing the organic solvent percentage in the reaction to 15% v/v had little effect on reactivity (Table 4.5, entries 5-8). Disappointed by these results, an exceptionally high organic solvent make-up (20% v/v) was investigated. Moderate reactivity was observed with this high organic solvent ratio upon increasing the linker stoichiometry from 40 to 120 molar equivalents (Table 4.5, entries 9-12). An increase in the reaction concentration from 2.5 mg/mL to 5 mg/mL also yielded slight improvements in reactivity (Table 4.5, entries 13-16). However, even under these forcing conditions, large amounts of unreacted heavy and light chain could still be observed by SDS-PAGE analysis and the harsh conditions required to observe any reactivity suggested that this linker-drug could not be used to produce an ADC with a cleavable payload.

The shorter PEGylated cleavable linker-drug **57** was then examined for its antibody conjugation properties (Table 4.6).

Table 4.6: Optimisation of trastuzumab conjugation with PEGylated linker-drug **57**. Buffer conditions – TBS; Tris HCl pH 8 (25 mM), NaCl (25 mM), EDTA pH 8 (0.5 mM). Conversion determined from SDS-PAGE analysis.

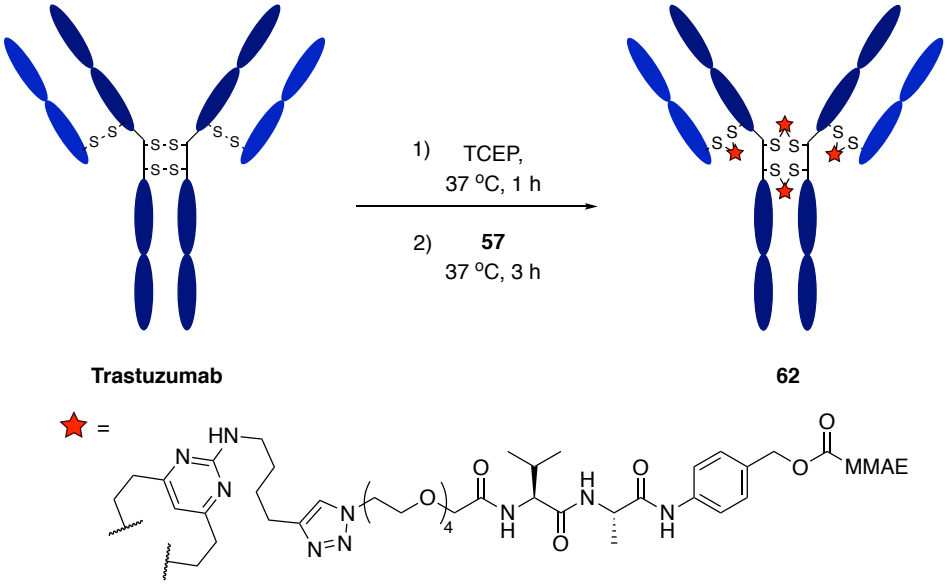

Entry	Co-solvent	Co-solvent % (v/v)	57 Eq.	Conc. (mg/mL)	Conversion
1	DMF	10	40	2.5	Moderate
2	DMSO	10	40	2.5	Moderate
3	MeCN	10	40	2.5	Moderate
4	MeOH	10	40	2.5	Moderate
5	DMF	15	40	2.5	Good
6	DMSO	15	40	2.5	Moderate
7	MeCN	15	40	2.5	Good
8	MeOH	15	40	2.5	Moderate
9	MeCN	15	60	2.5	Good
10	MeCN	15	80	2.5	Good
11	DMF	15	80	2.5	Excellent

The same initial screen of conditions was tested for DVP-PEG$_4$-Val-Ala-PABC-MMAE **57** as was previously attempted with linker-drug **60** by varying the organic co-solvent (DMSO, DMF, MeCN or MeOH) and co-solvent percentage (10 or 15% v/v) (Table 4.6, entries 1-8). Pleasingly, at 15% (v/v) MeCN and DMF and using 40 molar equivalents of linker-drug **57** (Table 4.6, entries 5 and 7), good reactivity was observed and the predominant species in both reactions was identified as the half and full antibodies, indicative of good reactivity. Increasing the equivalents of linker in MeCN did little to affect the conjugation efficiency of the

reaction (Table 4.6, entries 9 and 10). However, an increase in linker stoichiometry in DMF from 40 to 80 molar equivalents produced high levels of conversion from the reduced antibody to the rebridged bioconjugate **62**. This was confirmed by LCMS and SDS-PAGE (Figure 4.24a-c).

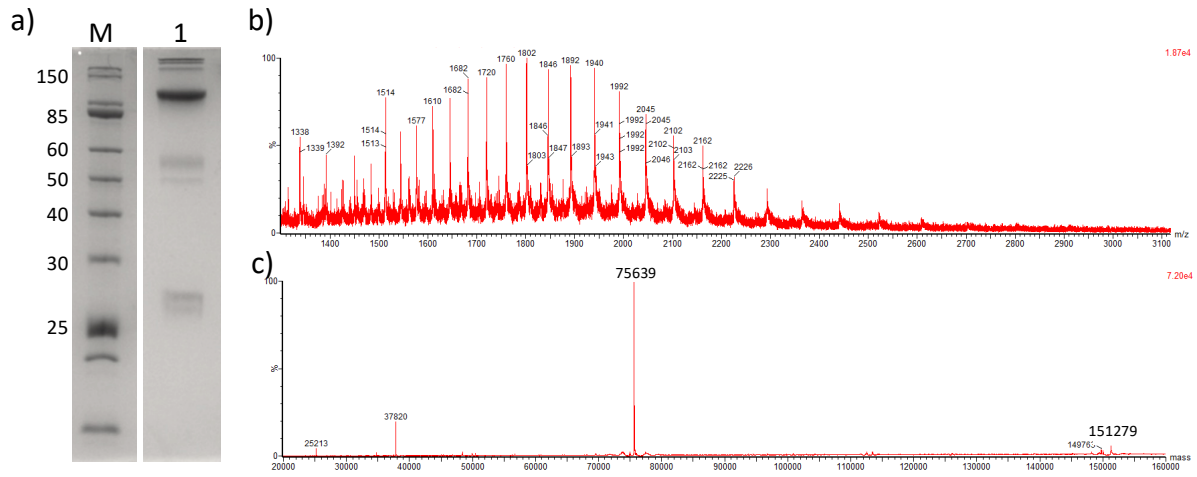

Figure 4.24: Analysis of cleavable ADC **62** by **a)** SDS-PAGE, Lanes: M) molecular weight marker, 1) reduced **62**. **b)** Non-deconvoluted MS and **c)** deconvoluted MS of **62**, expected mass 75,636 and 151,272 Da.

With some modification and optimisation to the linker-drug design and bioconjugation reaction conditions, the DVP linkers were shown to efficiently modify trastuzumab to produce both cleavable and non-cleavable ADCs. Initial difficulties in synthesising an ADC with a cleavable linker were overcome by the introduction of a short PEG chain (PEG_4) between the cleavable dipeptide motif and the DVP moiety.

4.13 Biological Evaluation

Having demonstrated the capability of a series of DVP linkers to rebridge disulfide bonds in antibodies with functional payloads (both cytotoxins and a fluorescent imaging agent), it was now important to understand the effects of modification on the biological properties of the synthesised conjugates. When developing any method for synthesising ADCs, a number of factors must be considered when evaluating the effects of conjugation on the antibody. For example, it is critical that the linkage formed is highly stable in circulation to ensure that the cytotoxic warhead is only released upon endocytosis. The effects of modification on receptor affinity and selectivity must also be considered. Ultimately, the conjugation methodology must create a functionally active ADC with the desired potency and selectivity. This section details

a series of assays that were designed and developed to enable this analysis and give a comprehensive understanding of the characteristics of DVP-modified antibody conjugates.

4.13.1 Stability

The first priority was to ascertain the stability of the DVP linkage to the antibody. Small molecule studies described in Sections 4.3 and 4.6 indicated that the thioether linkage was stable at physiological pH and in the presence of other thiols such as GSH. While useful, a more robust and potentially biologically-relevant assay would be required to gain a clear understanding of the stability of the linkage under physiological conditions. It was proposed that analysis of the stability in plasma would generate data reflective of the potential circulatory stability of the conjugates. Human plasma contains a large number of proteins, the most abundant of which is human serum albumin (HSA). HSA constitutes approximately 50% of all serum proteins and its main functions involve the transport of hormones, fatty acids, and other nutrients throughout the body.[228] Approximately 70% of HSA contains one free thiol (Cys34) that could potentially react with any free linker if a retro-conjugate addition occurred to release the linker-drug. Indeed, the free thiol of Cys34 has been exploited in many instances to generate albumin-drug conjugates or other biotherapeutics.[229,230]

A stability assay was designed that would enable analysis by SDS-PAGE, which would be able to separate the complex mixture of proteins present in human plasma including HSA (~66 kDa) from the full antibody (~150 kDa) or half antibody (~75 kDa) conjugates. Fluorescent antibody conjugate **39** was deemed to be ideally suited for this analysis. Using this AFC, SDS-PAGE analysis of human plasma containing **39** could be monitored by in-gel fluorescence imaging and compared to Coomassie staining of the gel. This comparison would reveal if the linker-fluorophore had been released or transferred to HSA. In contrast, if an unfunctionalised DVP linker conjugate or even an ADC was analysed, it would not be possible to observe if the linker had been released from the antibody via this analytical method. To this end, AFC **39** was incubated in human plasma at 37 °C for two weeks (Figure 4.25a). Aliquots were removed on days 0, 1, 3, 5, 7, 9, 11 and 14, and analysed by SDS-PAGE (Figure 4.25b and c). Gratifyingly, in-gel fluorescent imaging followed by Coomassie staining demonstrated almost no transfer of the fluorescent linker-drug conjugate to HSA or any of the other plasma proteins after two weeks of incubation.

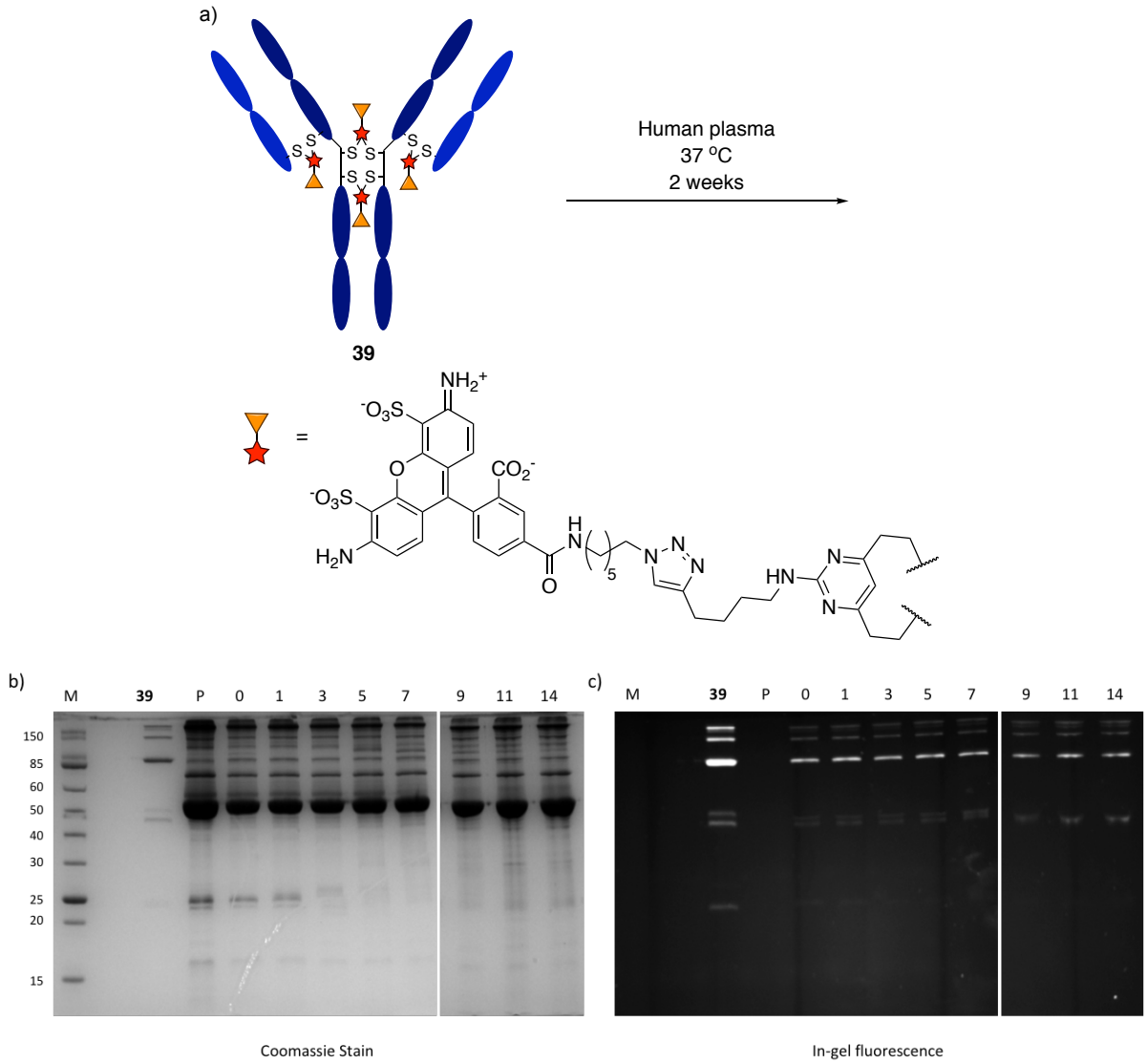

Figure 4.25: Stability evaluation of DVP bioconjugates by **a)** incubation of fluorescent trastuzumab bioconjugate **39** in human plasma for two weeks and analysis by SDS-PAGE. **b)** Coomassie stained SDS-PAGE analysis, **c)** in-gel fluorescence analysis, Lanes: M) molecular weight marker, 39) AFC **39**, P) human plasma. Numbers above the remaining lanes indicate the day of incubation when aliquot was removed from the reaction.

This analysis confirmed the exquisite stability profile of the DVP linker system and enabled further investigation into the biological profile of the antibody conjugates.

4.13.2 Binding Affinity

The effect of DVP rebridging on the binding affinity of trastuzumab for its native HER2 receptor was then investigated. DVP rebridging introduces a seven-atom linkage between the disulfide-derived thiols. It is possible to envisage that this bridge would change the tertiary structure of the antibody sufficiently to alter its receptor recognition. However, it is also possible that

rebridging could improve the binding affinity of the antibody for its receptor. Recent work by Martínez-Saez *et al.* demonstrated that a disulfide rebridged trastuzumab using a dibromo-oxetane reagent had a lower dissociation constant (K_D) for HER2 than its native, disulfide-containing counterpart.[231] To determine the binding affinity of the modified antibodies in comparison to the unmodified antibody, an enzyme-linked immunosorbent assay (ELISA) was devised. Accordingly, the binding affinity of trastuzumab DVP bioconjugates **34**, **35** and **36** to the HER2 receptor were analysed by ELISA. Encouragingly, no significant difference was observed between any of the trastuzumab conjugates and unmodified trastuzumab (Figure 4.26). The binding affinity results are suggestive that rebridging with DVP reagents does not have any effect on the affinity of modified trastuzumab antibodies for the HER2 receptor.

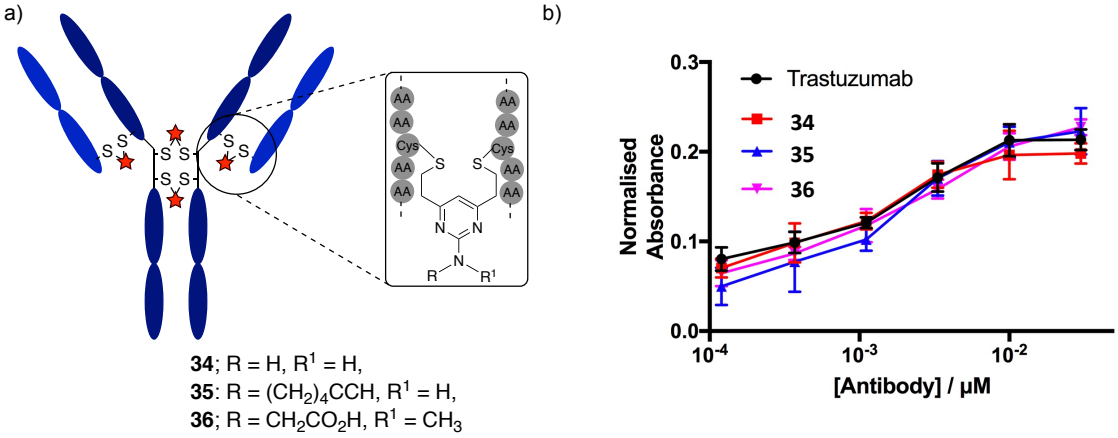

Figure 4.26: a) DVP-modified trastuzumab bioconjugates analysed for HER2 binding affinity by ELISA. **b)** Comparison of binding affinity of trastuzumab, **34**, **35** and **36**. Error bars represent the standard deviation of technical quadruplicates.

4.13.3 Cellular Selectivity

Pleased by the retained binding affinity of our modified ADCs for HER2, we then moved on to determine if selectivity was also retained. There is a huge number of receptors present on the cell surface making it virtually impossible to carry out ELISA analysis on all of these and compare binding affinities. However, flow cytometry could be used to determine the cellular selectivity of fluorescent antibody conjugates. Upon treatment with AFC **39**, comparison of the labelling of HER2-positive cell lines with labelling of HER2-negative cell lines could be used to elucidate the receptor selectivity of the DVP bioconjugate. To this end, two HER2-positive cell lines (SKBR3 and BT474) and two HER2-negative cell lines (MCF7 and T47D) were incubated with AFC **39** (50 nM) for one hour at 37 °C. The cells were collected, washed and analysed by fluorescence-activated cell sorting (FACS) (Figure 4.27a-d). Pleasingly, this analysis revealed exceptionally high levels of antibody labelling in both the SKBR3 and BT474

cell lines. In contrast, the MCF7 and T47D lines showed almost no fluorescent signal on any cells (Figure 4.27e). Cellular images obtained from the flow cytometry investigations also confirmed the high levels of selectivity observed for the HER2-positive cell lines (Figure 4.27f).

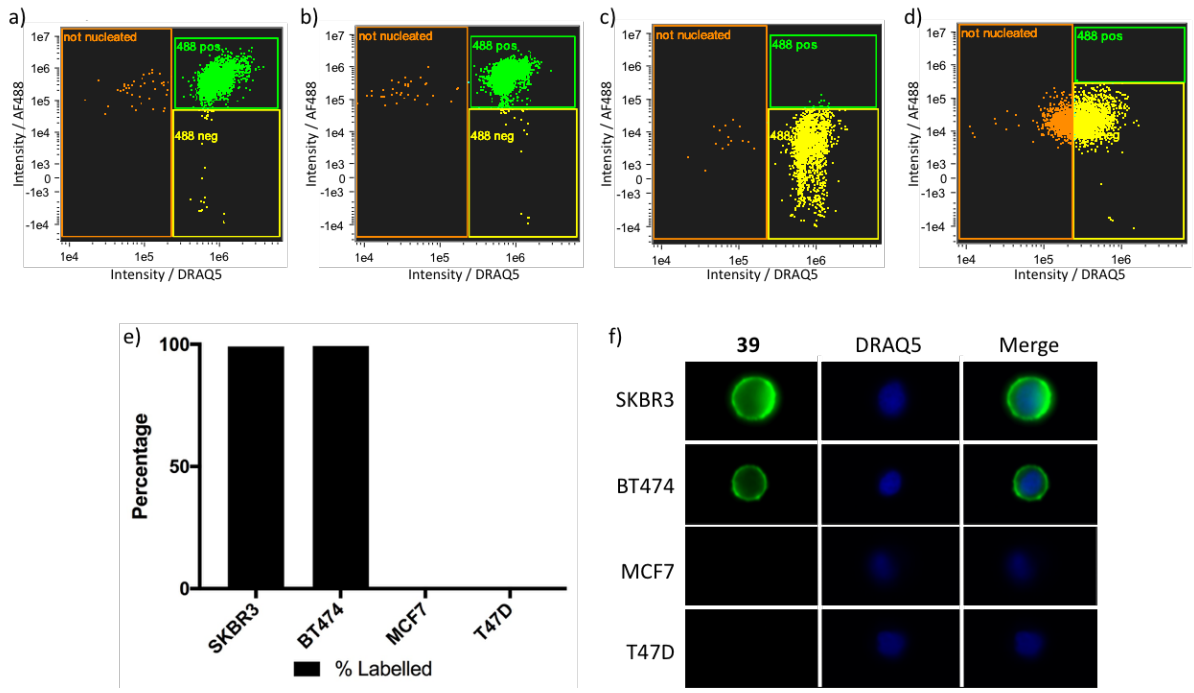

Figure 4.27: FACS analysis of **39** labelling of **a)** SKBR3 cells, **b)** BT474 cells, **c)** MCF7 cells and **d)** T47D cells. **e)** Percentage of cells labelled in the four cell lines after incubation with **39**, and **f)** imaging of the four cell lines shows **39** labelling of HER2-positive cells (SKBR3 and BT474), with no observed labelling of HER2-negative cell lines (MCF7 and T47D). DRAQ5 is a nuclear stain.

4.13.4 Cytotoxicity

The stability, receptor affinity and cellular selectivity data obtained inspired confidence that the DVP ADCs could be evaluated for their cytotoxic potential. First, appraisal of non-cleavable DVP ADC **42** to selectively kill HER2-positive cells was undertaken. SKBR3, BT474, MCF7 and T47D cell lines were treated with varying concentrations of **42**, trastuzumab and MMAE. After 96 hours incubation, a CellTiter-Glo® assay was used to measure the number of viable cells present for each concentration of the different compounds tested. Pleasingly, ADC **42** demonstrated exquisite potency against both SKBR3 and BT474 cell lines, whilst displaying no activity against MCF7 or T47D lines at the concentrations tested (Figure 4.28a). The ADC had IC_{50} values of ~62 pM and ~275 pM against SKBR3 and BT474 cell lines, respectively. In contrast, MMAE was exceptionally potent against all four cell lines, regardless of HER2 expression (Figure 4.28b), while trastuzumab alone displayed almost no activity against any of the cell lines (Figure 4.28c).

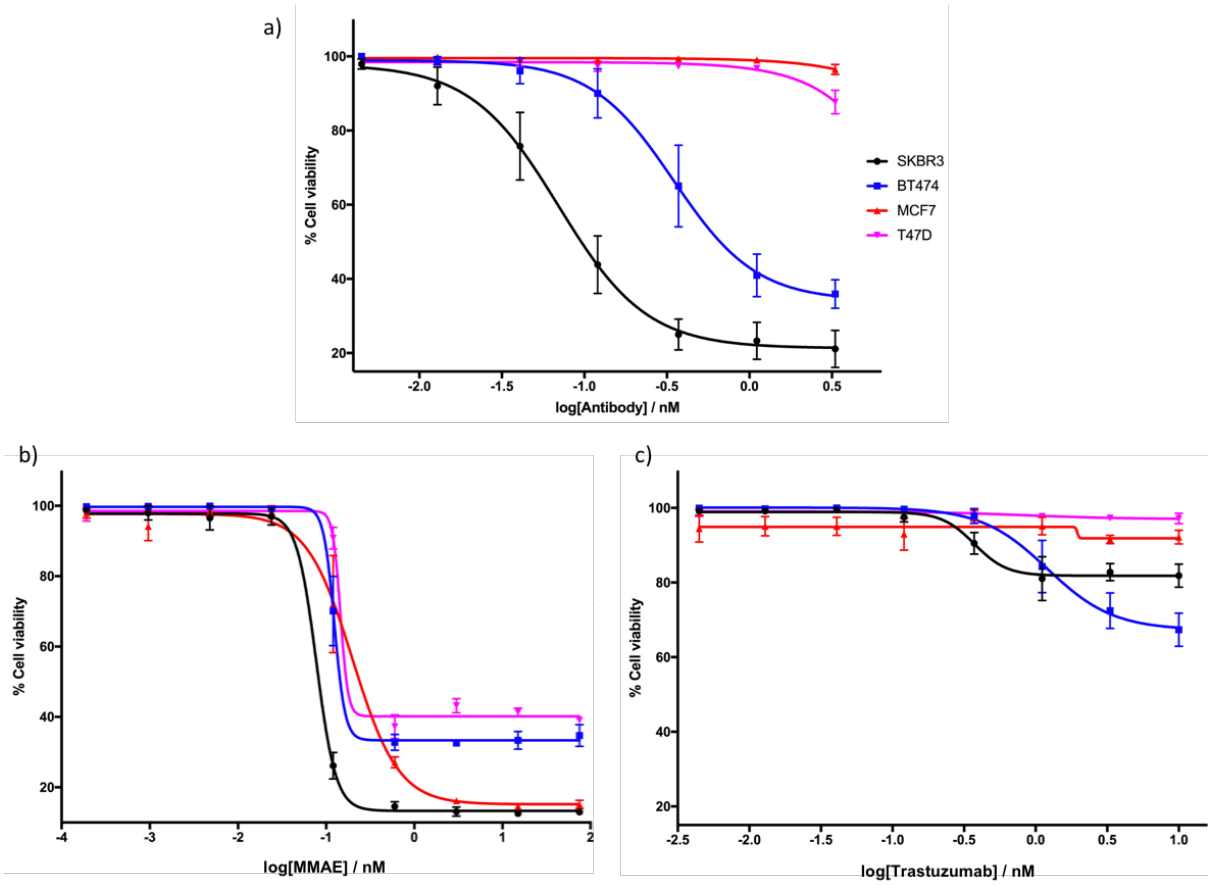

Figure 4.28: Cell viability of HER2-positive (SKBR3 and BT474) and HER2-negative cell lines after 96-hour treatment with **a) 42**, **b)** MMAE and **c**) trastuzumab. Each treatment had three technical replicates with the results represented as the average of three biological replicates from independent passages of each cell line. Data reported as the mean of the three biological replicates and error bars represent s.e.m.

To confirm the potency and selectivity observed with the 96-hour cell viability assay, cell growth was monitored for six days after treatment of all four cell lines with ADC **42**. Confirming the CellTiter-Glo® assay results, the ADC displayed a high degree of potency against both SKBR3 and BT474 cell lines, whilst no significant activity was observed against the HER2-negative MCF7 and T47D cell lines (Figure 4.29a-d).

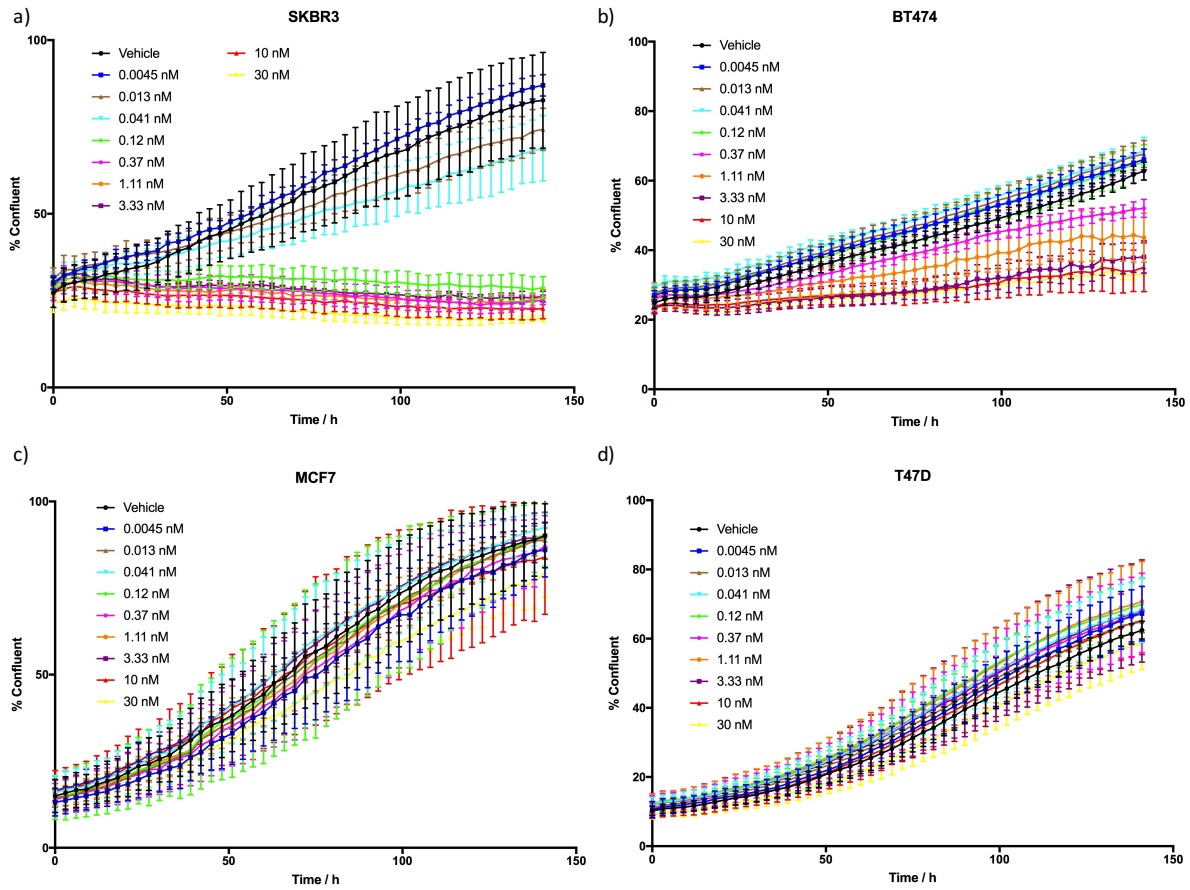

Figure 4.29: Cell growth curves after incubation with ADC **42** for six days in **a)** SKBR3, **b)** BT474, **c)** MCF7 and **d)** T47D cell lines.

Finally, the potency of cathepsin-cleavable ADC **62** was evaluated in a HER2-positive and HER2-negative cell line. Treatment of SKBR3 and MCF7 cell lines with **62** was followed by CellTiter-Glo® cell viability determination after 96 hours incubation. ADC **62** showed exceptional potency against SKBR3 cells, with little cytotoxicity observed in MCF7 cells at the concentrations tested (Figure 4.30a). The ADC had a calculated IC_{50} of ~15 pM against the SKBR3 cell line. Growth of the cells was also monitored over four days and similarly showed high levels of activity in SKBR3 cells with no significant activity observed in MCF7 cells (Figure 4.30b and c).

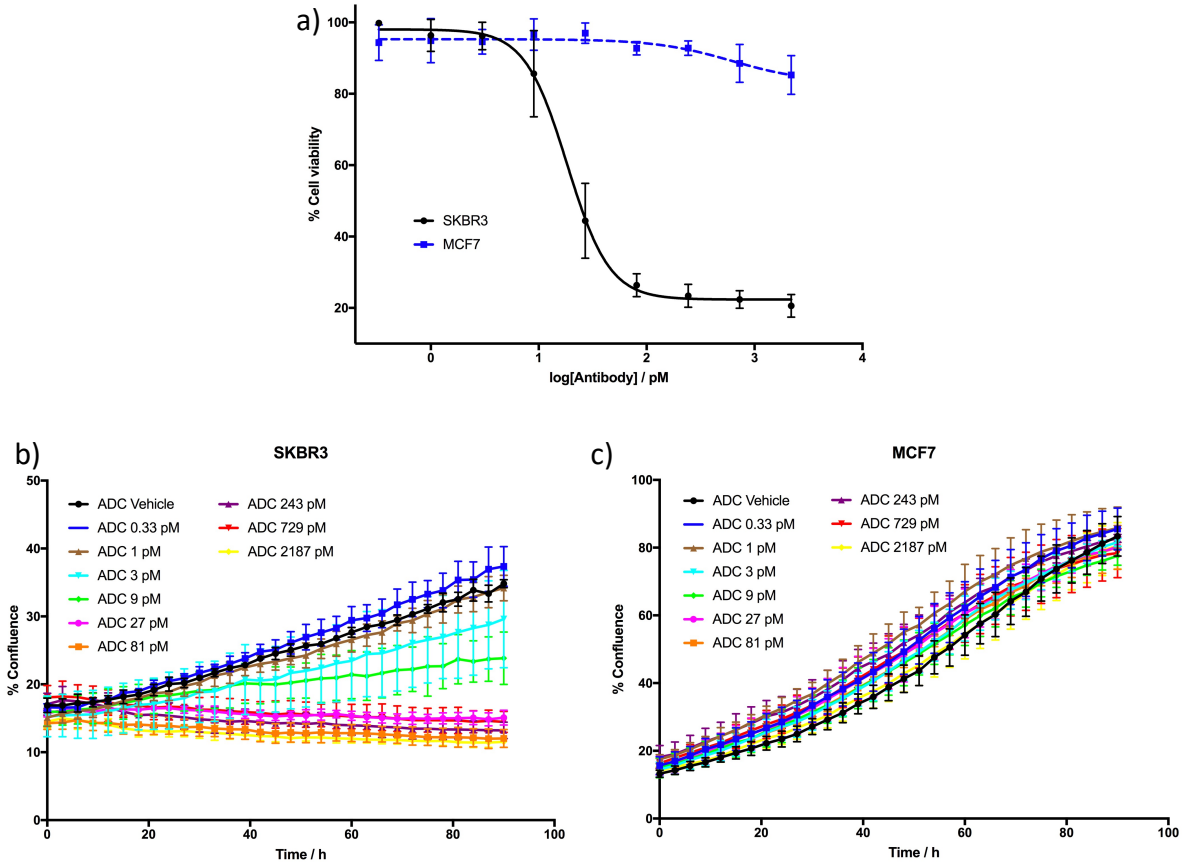

Figure 4.30: a) Cell viability of SKBR3 and MCF7 cells after 96-hour treatment with **62** and four-day cell growth analysis of **62** in **b)** SKBR3 cells and **c)** MCF7 cells. Viability data reported as the mean of three biological replicates from independent passages of each cell line and error bars represent s.e.m.

4.14 Modification of *Pf*RadA-dCys

The synthesis of ADCs via DVP cysteine rebridging was shown to proceed in a site-selective and efficient manner. Functionalised antibodies demonstrated an excellent biological profile with outstanding stability, receptor affinity and selectivity, and highly potent and selective cytotoxicity. It was also hoped that DVP reagents could be used to modify non-antibody proteins. To this end, *Pf*RadA-dCys was treated with a slight excess (15 molar equivalents) of unfunctionalised DVP linkers **15**, **18** and **24** for one hour at 37 °C (Figure 4.31a). Subsequent analysis by LCMS revealed full conversion to the desired bioconjugates **63**, **64** and **65** (Figure 4.31b-g).

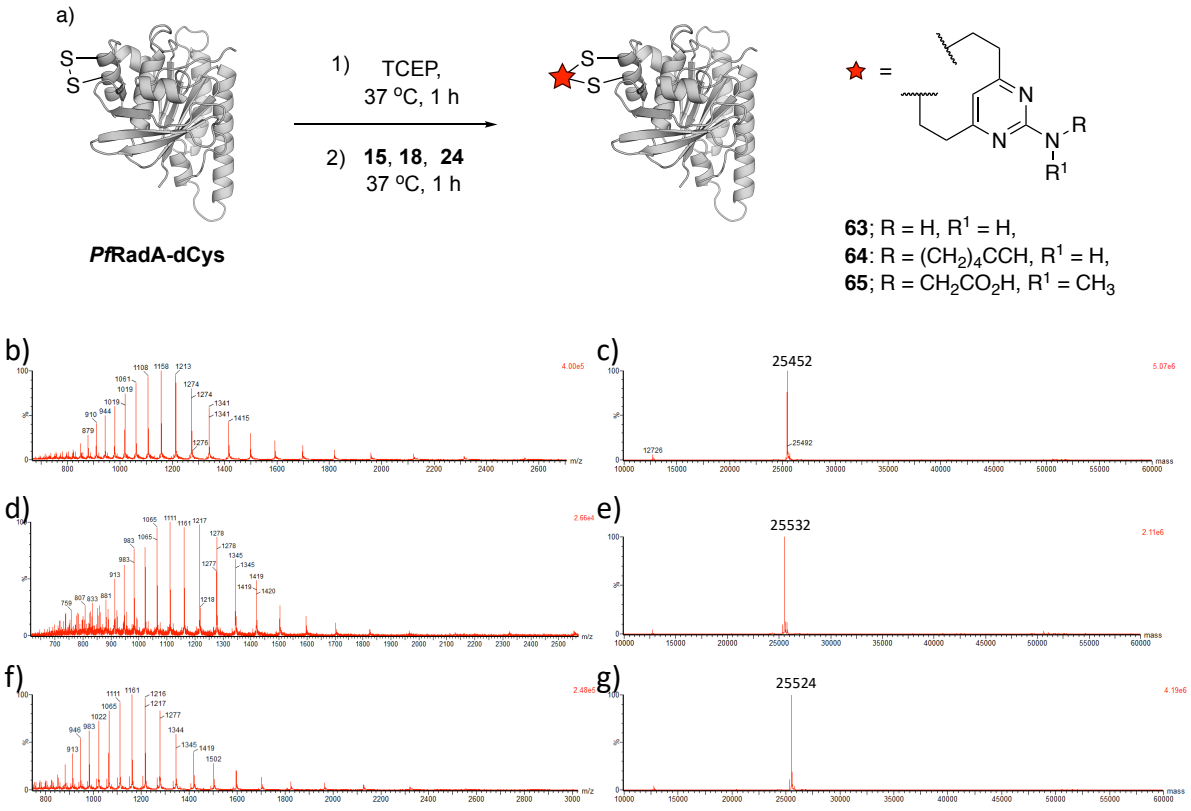

Figure 4.31: a) Modification of *Pf*RadA-dCys with **15**, **18** and **24**. LCMS analysis of the resulting bioconjugates **63**, **64**, and **65**; **b)** non-deconvoluted MS of **63**, **c)** deconvoluted MS of **63**, expected mass 25,451 Da, **d)** non-deconvoluted MS and **e)** deconvoluted MS of **64**, expected mass 25,531 Da; **f)** non-deconvoluted MS and **g)** deconvoluted MS of **65**, expected mass 25,523 Da. Buffer conditions – TBS; Tris HCl pH 8 (25 mM), NaCl (25 mM), EDTA pH 8 (0.5 mM), guanidine hydrochloride (3 M).

In contrast to the divinylpyridine modification of *Pf*RadA-dCys described in Section 3.4, no evidence of double alkylation was observed when treated with higher equivalents of **18** and left for an extended reaction time. This result indicated that the increased rebridging efficiency was due to the higher reactivity of the DVP reagents over the divinylpyridine reagents (Figure 4.32).

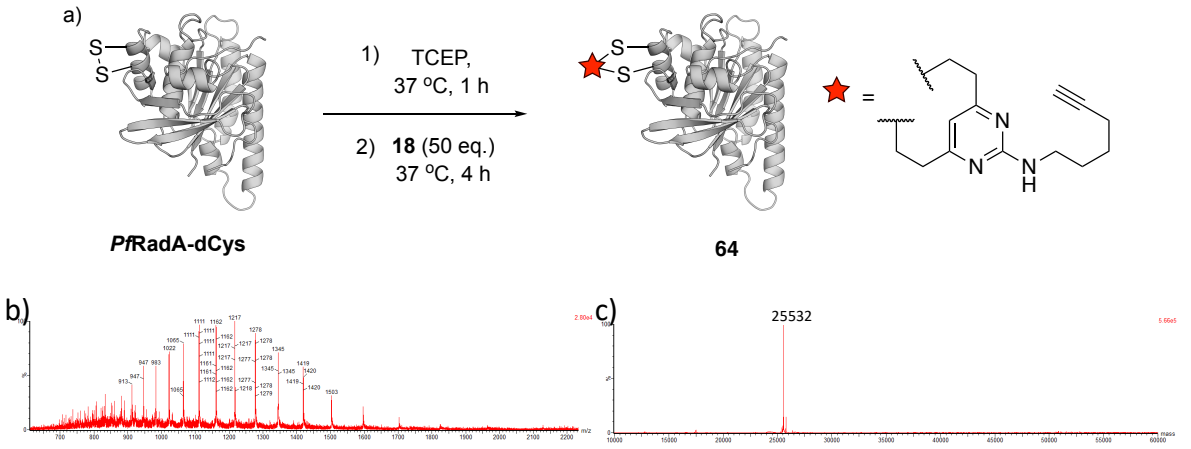

Figure 4.32: a) Modification of *Pf*RadA-dCys with high molar equivalents of **18** and LCMS analysis of the reaction; **b)** non-deconvoluted MS and **c)** deconvoluted MS of the reaction mixture, expected mass 25,531 Da. No evidence of double alkylation, expected mass, 25,758 Da. Buffer conditions – TBS; Tris HCl pH 8 (25 mM), NaCl (25 mM), EDTA pH 8 (0.5 mM), guanidine hydrochloride (3 M).

4.15 Conclusions

In this chapter, the development of a divinylpyrimidine (DVP) linker system was described. In the first instance, assessment of the reactivity, chemoselectivity and stability of the thioether conjugates was undertaken on the vinylpyrimidine scaffold in a series of small molecule model systems. Having completed analysis on the monovinylpyrimidine system, synthetic procedures for the production of a series of DVP reagents were then developed.

Initial protein chemistry studies utilising simple, unfunctionalised DVP linkers demonstrated their excellent rebridging efficiency in the modification a trastuzumab Fab. Modification of a trastuzumab antibody was then extensively investigated. DVP reagents were shown to rebridge the reduced interchain disulfides in trastuzumab with an excellent reactivity profile and only a small excess of linker required. It was discovered that a mixture of half and full antibody conjugates was formed due to intrachain misbridging of the heavy chain cysteine residues. Although undesired, further analysis showed that the non-covalent interactions were likely to keep the antibody intact as a single entity. Furthermore, receptor binding data and cellular selectivity analysis confirmed that rebridging with DVP reagents did not affect receptor recognition of the trastuzumab conjugates for their native HER2 receptor. Crucially, assessment of the stability of a fluorescent antibody imaging agent revealed that the bioconjugates had near-perfect stability in human plasma over multiple weeks. In addition, both cleavable and non-cleavable ADCs synthesised via DVP conjugation displayed highly potent and selective cell cytotoxicity in multiple *in vitro* assays.

Finally, the DVP linkers were also used to cross-link cysteine residues in *Pf*Rad-dCys. This collective data highlights the utility of the DVP platform to generate highly stable and functional protein bioconjugates via cysteine bridging chemistry.[232]

Chapter 5

Dual-Functional Divinylpyrimidine Linkers

5.1 Introduction

In classic ADC or AFC synthesis, one linker molecule is used to attach one molecule of drug or fluorescent dye. In contrast, generic protein modification often involves the functionalisation of a protein with multiple payloads, either via a dual-functional linker or via modification of orthogonal protein sites.[233] Only a handful of strategies for the bis-modification of antibodies have been reported. In one example, Levengood *et al.* described the use of an orthogonal cysteine protecting group strategy to synthesise a high DAR ADC with eight MMAE payloads and eight MMAF payloads in an aim to overcome auristatin resistance mechanisms (Figure 5.1a).[234] In another approach, Xiao *et al.* have reported the synthesis of a theranostic ADC via conjugation of an AlexaFluor™ 488 fluorescent tag and an MMAF cytotoxin. In this strategy, the unnatural amino acid *p*-acetylphenylalanine and an azido-lysine amino acid were incorporated into the heavy and light chains of an antibody via genetic engineering. Subsequent oxime formation via reaction of the ketone-containing amino acid with an amino-oxy tagged MMAF (nAF) followed by a SPAAC reaction with an AlexaFluor™ 488 cyclooctyne derivative yielded the fluorescent ADC (Figure 5.1b).[144]

Similarly, Maruani *et al.* have described the use of the pyridazinedione reagents to modify both Fabs and IgG molecules with cytotoxic warheads, fluorescent tags and PEG chains. In this method, the complementarity of the CuAAC and SPAAC reactions has been exploited to first modify an antibody with an azide modified payload via a SPAAC reaction. A subsequent CuAAC reaction was then used to decorate the antibody with an alternate payload, generating fluorescent ADCs or Fab-drug/fluorophore conjugates with extended half-lives due to PEGylation (Figure 5.1c).[165] The pyridazinedione reagents were also used to synthesise a different type of theranostic agent, which combines photodynamic therapy with *in vivo* imaging capabilities.[235] Finally, an approach developed by Puthenveetil and co-workers details a solid phase method, whereby a THIOMAB antibody was firstly immobilised on a Protein A-modified bead. Subsequent deglycosylation of the antibody with PNGase F was followed by the attachment of a strained bicyclononyne (BCN) to the exposed glutamine 295 residue in the antibody heavy chains. A maleimide-modified BODIPY reagent could then be used to modify the engineered cysteine residues on the light chains and an azide-modified Cy5.5 dye reacted

with the BCN alkyne in a SPAAC reaction to generate the bis-fluorophore modified antibody (Figure 5.1d).[236] This strategy was also used to synthesise a theranostic Fab-drug conjugate.

Dual-modification of an antibody or antibody fragment in this way could potentially be used to attach a number of useful payloads. Incorporation of two different cytotoxins with alternate mechanisms of action would potentially decrease the occurrence of resistance; attachment of a cytotoxin and an imaging agent would generate a fluorescent ADC; or modification with a cytotoxin and a PEG group would enable modulation of the physicochemical properties of the ADC or other biotherapeutic.

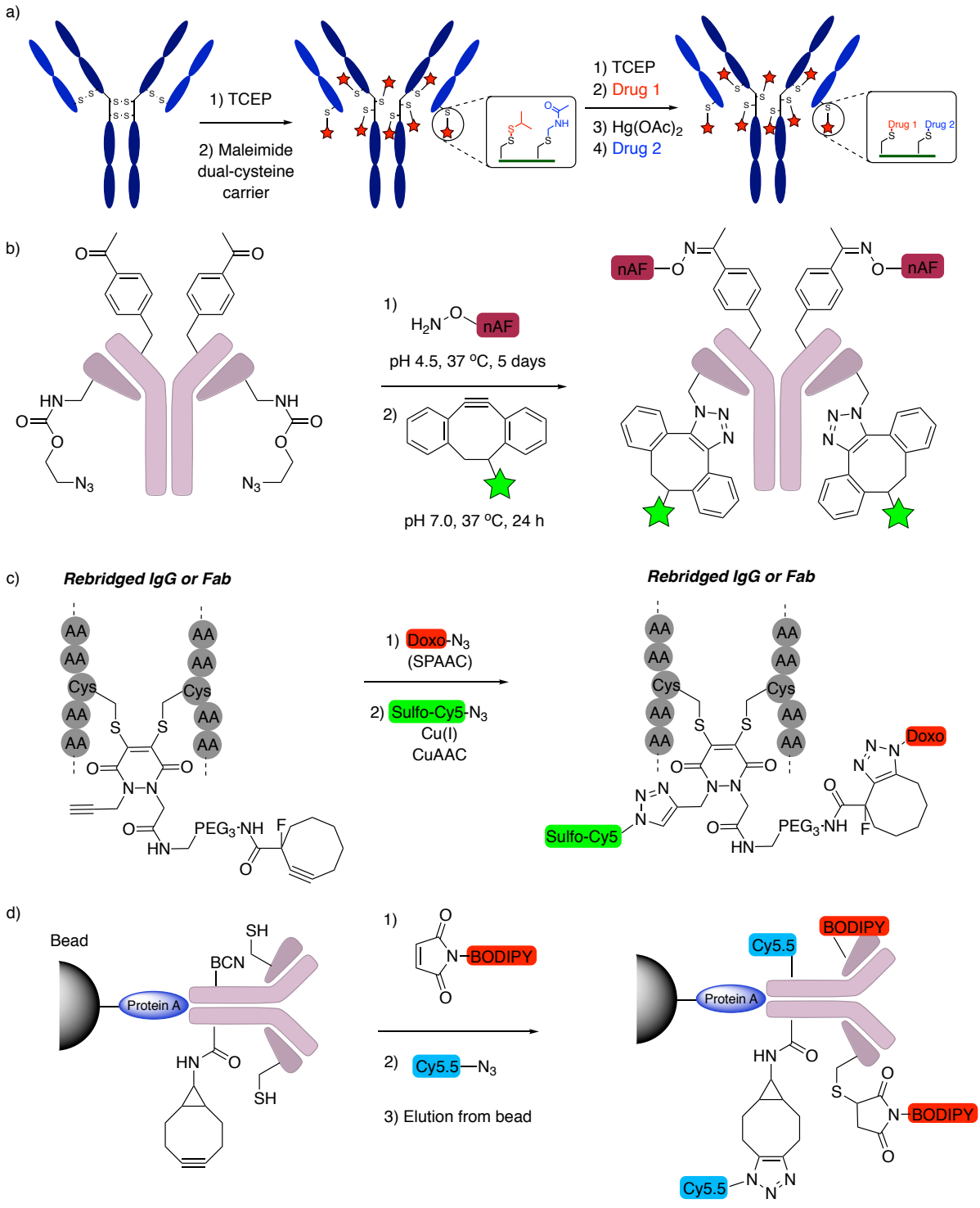

Figure 5.1: a) Orthogonal cysteine protection enables attachment of two different payloads with the same maleimide linker, **b)** genetic engineering of unnatural amino acids with bioorthogonally reactive azide and acetyl groups. Modified from Xiao *et al.*,[144] **c)** pyridazinedione reagents containing strained and unstrained alkynes can react in orthogonal SPAAC and CuAAC reactions, respectively and **d)** combination of THIOMAB with glycan remodelling enables attachment of different fluorescent dyes.

It was hypothesised that the DVP linkers could be used to synthesise valuable bis-functionalised antibodies (Figure 5.2a).

We proposed that the synthetic routes used to synthesise original DVPs could also be used to synthesise dual-functional divinylpyrimidine (df-DVP) reagents. The S_NAr reaction developed in Section 4.5 to attach desired functional groups was shown to work well with both primary and secondary amine nucleophiles. With this knowledge at hand, it was postulated that a secondary amine would give two synthetic vectors to incorporate the desired orthogonal functionalities to achieve dual-modification of an antibody (Figure 5.2b).

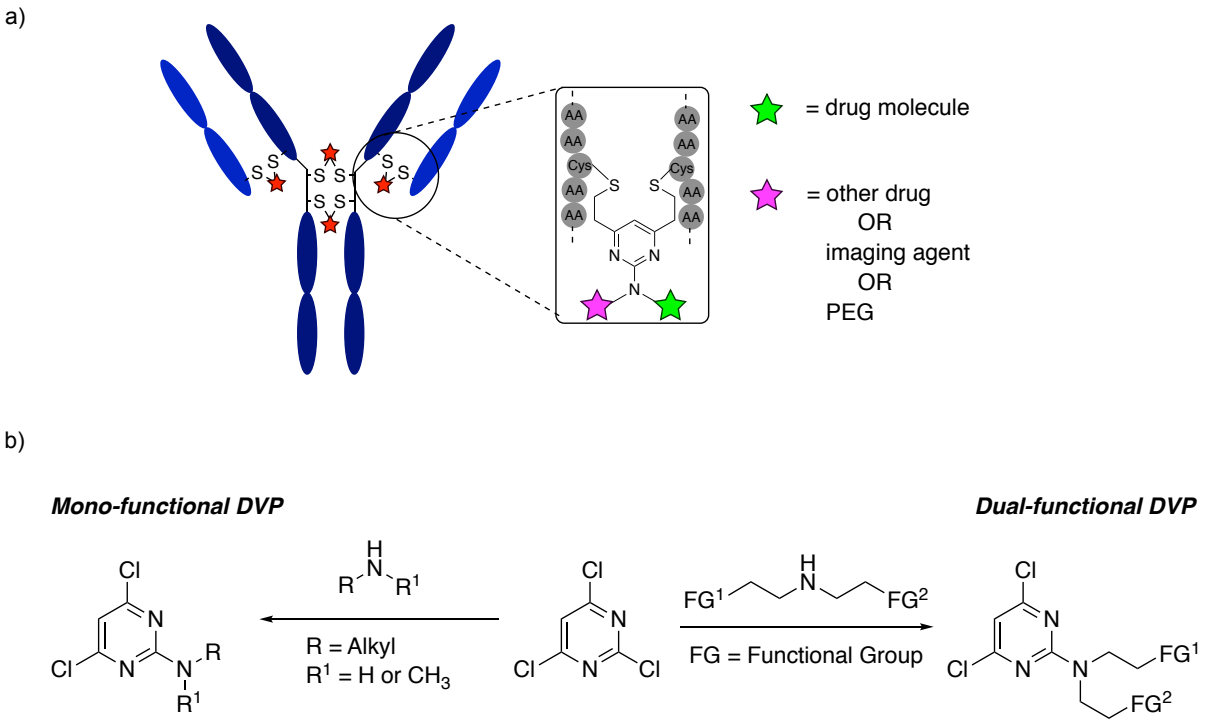

Figure 5.2: a) potential modified antibodies that could be synthesised with dual-functional DVP linkers and **b)** synthetic route used in Section 4.5 to synthesise mono-functional DVP reagents and the proposed chemistry that would enable the synthesis of dual-functional DVP reagents.

5.2 Synthesis of a df-DVP Linker

In order to implement the proposed synthetic strategy, a secondary amine containing two orthogonal functional groups was required. In Chapter 4, both carboxylic acid and alkyne functional groups were shown to be compatible with the attachment of multiple different payloads. In addition, the alkynyl DVP **18** demonstrated excellent post-rebridging reactivity in a series of on-antibody CuAAC modifications. Combination of an alkyne with a carboxylic acid on the same DVP linker would enable hetero-bifunctional modification of a protein through both pre- and post-rebridging functionalisation. Exploration of commercially available secondary amines did not yield any promising candidates. However, it was thought that the desired secondary amine could be synthesised from simple primary amines. A reductive

amination approach with a primary amine and an appropriately functionalised aldehyde was deemed to be an attractive strategy. No useful alkynyl aldehydes were found to be commercially available. However, oxidation of an alkynyl alcohol and subsequent reductive amination with an appropriate amino acid could be conducted to yield the desired secondary amine. To this end, 5-hexyn-1-ol was treated with pyridinium chlorochromate (PCC) in CH_2Cl_2 following a known literature procedure (Table 5.1, entry 1).[237] However, TLC analysis of the reaction suggested a number of products had been formed in the reaction. Dess-Martin periodinane (DMP) oxidation of the same substrate had also been previously reported and was attempted accordingly (Table 5.1, entry 2).[238] Again, TLC analysis of the crude reaction mixture also suggested that multiple products had been formed. Undeterred, a Parikh-Doering reaction using a sulfur trioxide complex with pyridine (SO_3·Py), pyridine (Py), DMSO and DIPEA was attempted on the alcohol (Table 5.1, entry 3).[239] Pleasingly, a single spot was observed on TLC analysis of the reaction mixture which was confirmed to be the desired oxidation product via ^{1}H NMR of the crude reaction mixture. Acidic work-up conditions provided the desired aldehyde **68** which was immediately subjected to reductive amination conditions.

Table 5.1: Optimisation of the oxidation of 5-hexyn-1-ol to aldehyde **68**.

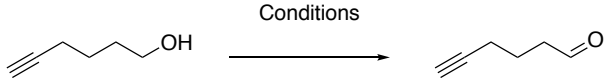

68

Entry	Reagents	Solvent	Temp.	Time (h)
1	PCC	CH_2Cl_2	0 °C to rt	17 h[a]
2	DMP	CH_2Cl_2	0 °C to rt	2 h
3	SO_3·Py, Py, DIPEA, DMSO	CH_2Cl_2	–40 to –20 °C	4 h

[a] monitored by TLC after 2, 4, 6, 8 and 17 hours.

Ethyl 4-aminobutyrate was selected as the amino acid to condense with the aldehyde. A small screen of conditions for the reductive amination between this substrate and aldehyde **68** and was carried out (Table 5.2). First, attempts to form the imine by pre-mixing crude aldehyde **68** and the amine before the addition of sodium borohydride yielded the desired secondary amine **69** in just 8% yield, over two steps (Table 5.2, entry 1). Use of milder reductants, such as $NaBH(OAc)_3$ or $NaBH_3CN$, enabled immediate addition of the reductant and gave much cleaner conversion to the desired amine **69** without the need to pre-form the imine (Table 5.2,

entries 2 and 3). Use of $NaBH(OAc)_3$ gave the cleanest conversion to secondary amine **69** with an isolated yield of 40% over two steps.

Table 5.2: Optimisation of the reductive amination reaction between aldehyde **68** and ethyl 4-aminobutyrate hydrochloride to yield amine **69**.

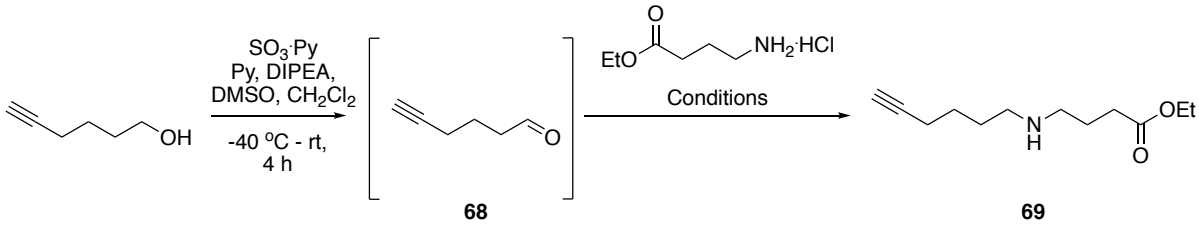

Entry	Reductant	Pre-stir	4 Å MS	Solvent	Base	Yield[a]
1	$NaBH_4$	16 h	No	MeOH	NEt_3	8%
2	$NaBH(OAc)_3$	2 min	Yes	CH_2Cl_2/MeOH	NEt_3	40%
3	$NaBH_3CN$	2 min	Yes	CH_2Cl_2/MeOH	NEt_3	31%

[a] over two steps

Synthesis of the df-DVP reagent could now proceed using the same synthetic strategy previously described in Section 4.5. First, S_NAr reaction of 2,4,6-trichloropyrimidine with amine **69** proceeded smoothly in the presence of NEt_3 to produce **70** in 35% yield (Scheme 5.1). Subsequent installation of the vinyl groups was achieved via Suzuki chemistry to yield DVP **71** in moderate yield. Finally, hydrolysis of ethyl ester **71** with $LiOH{\cdot}H_2O$ generated the desired df-DVP **72** in good yield.

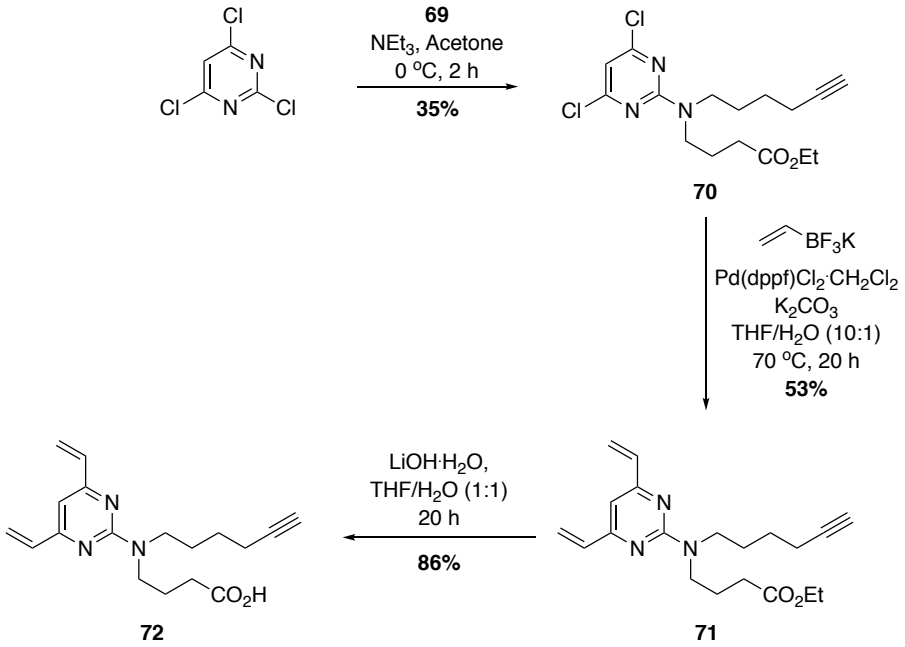

Scheme 5.1: Synthetic route used to produce df-DVP **72**.

To ensure that the addition of extra functionality around the DVP core did not affect the conjugation performance of the scaffold, df-DVP **72** was reacted with reduced trastuzumab in 10% DMSO in TBS for two hours at 37 °C (Figure 5.3a). Pleasingly, excellent conversion to the desired antibody conjugate **73** was observed by LCMS and SDS-PAGE analysis (Figure 5.3b-d).

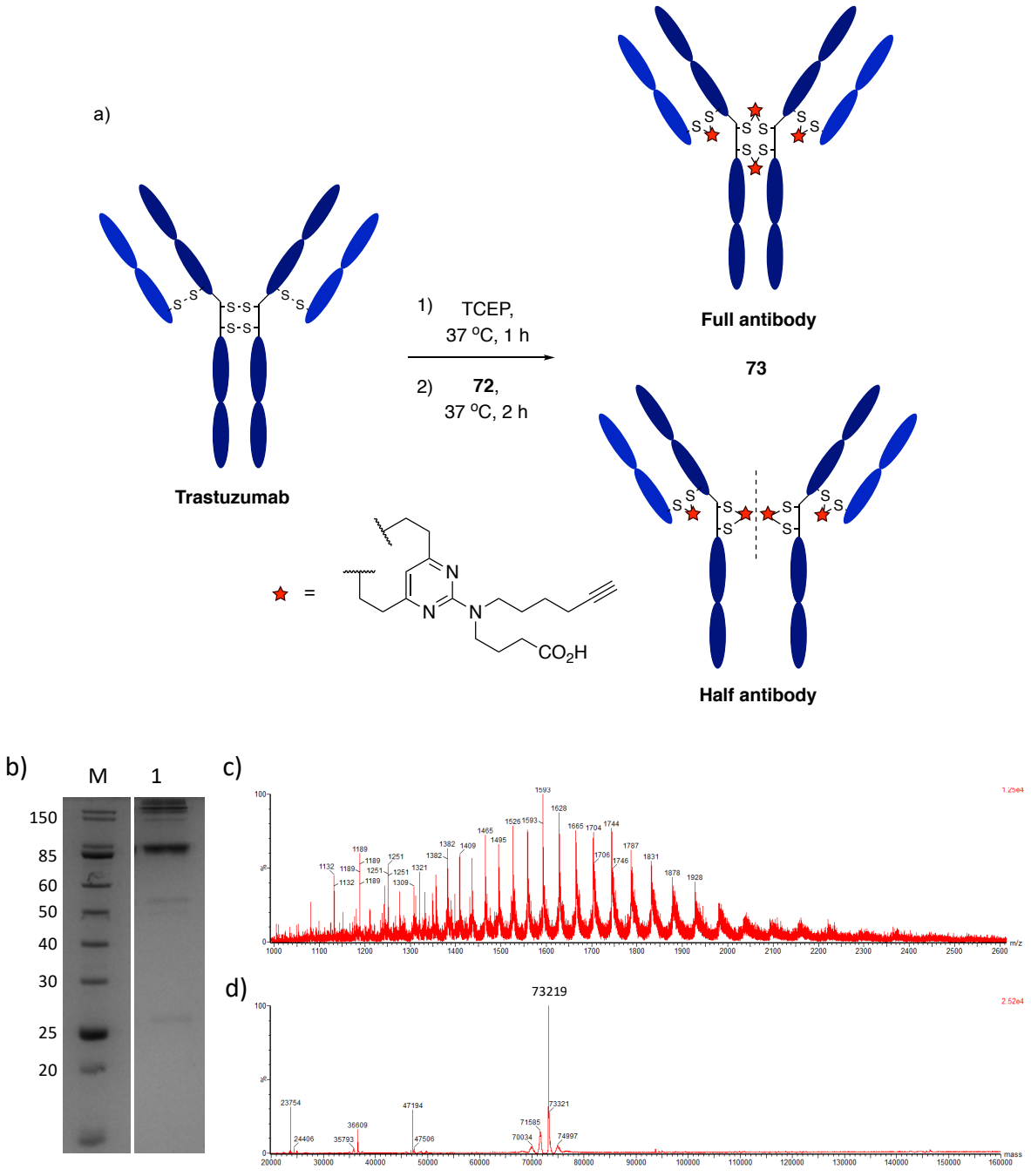

Figure 5.3: a) Reaction between trastuzumab and df-DVP **72** to produce bioconjugate **73** as a mixture of full and half antibody. **b)** SDS-PAGE analysis, Lanes; M) molecular weight marker, 1) reduced bioconjugate **73**, showing both full and half antibody conjugates. **c)** Non-deconvoluted MS and **d)** deconvoluted MS of **73**, expected mass 73,214 Da. Buffer conditions – TBS; Tris HCl pH 8 (25 mM), NaCl (25 mM), EDTA pH 8 (0.5 mM).

5.3 MMAE-Functionalised df-DVP

Theranostic agents are so-called due to their ability to treat and diagnose disease states simultaneously.[240] Small molecule theranostic conjugates have witnessed more widespread

development and use than antibody based theranostics, potentially due to the complexity of synthesising these agents.[241–247]

Having completed the synthesis and analysed the antibody conjugation capabilities of a simple, unfunctionalised df-DVP, efforts then moved toward synthesis of biologically-functional hetero-bis-modified antibodies. As an initial proof-of-concept study, it was aimed to firstly synthesise a theranostic ADC by attachment of a cytotoxin such as MMAE and an imaging agent such as AlexaFluor™ 488. It was envisaged that MMAE could be attached via the carboxylic acid moiety of **72** before antibody conjugation and subsequent post-rebridging attachment of the dye via a CuAAC reaction.

Functionalisation of df-DVP **72** with an MMAE payload was firstly undertaken. It was thought that a cleavable trigger would be required to release free MMAE upon internalisation as the sterically bulky linker and imaging agent may impede its mechanism of action if a non-cleavable linker was used. To this end, previously synthesised Fmoc-protected linker-drug **58** was deprotected with piperidine and reacted with df-DVP **72** in the presence of HBTU, HOBt·H_2O and DIPEA to yield df-DVP-MMAE linker-drug **74** in 40% yield over two steps (Scheme 5.2).

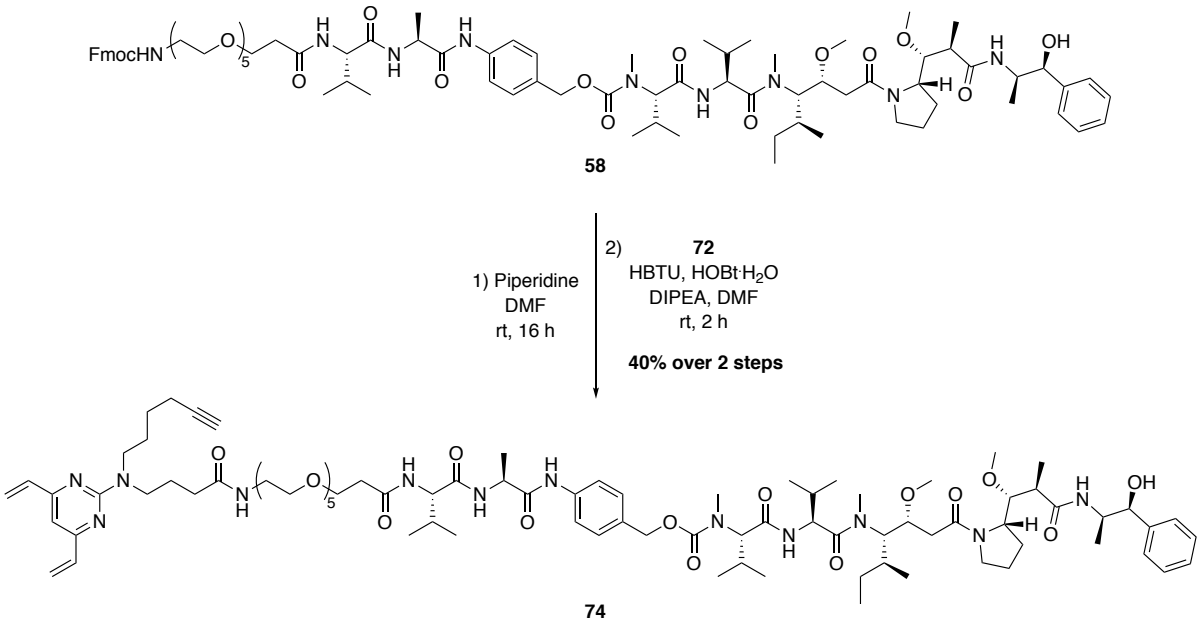

Scheme 5.2: Synthesis of linker-drug **74** from protected compound **58** via Fmoc deprotection and subsequent amide coupling.

With a viable route to linker-drug **74** in hand, conjugation of this compound to trastuzumab was then investigated (Table 5.3a). Initial conditions involved varying the organic co-solvent (DMSO, DMF or MeCN) and co-solvent percentage (10-25%) (Table 5.3, entries 1-9). In all cases, no evidence of the desired conjugate **75** was observed by LCMS and SDS-PAGE analysis, with the linker-drug **74** appearing to have poor aqueous solubility under all of the conditions tested (Table 5.3b). Attempts to aid the solubility of the linker-drug by decreasing the reaction concentration (1 mg/mL) were also unsuccessful (Table 5.3, entries 10-12).

Table 5.3: a) Conditions tested in the attempted reaction between trastuzumab and **74**. **b)** Typical reducing SDS-PAGE analysis of the reactions showing primarily unmodified light and heavy chains. Lanes: M) molecular weight marker, 1) entry 1, 2) entry 2, 3) entry 3. Buffer conditions – TBS; Tris HCl pH 8 (25 mM), NaCl (25 mM), EDTA pH 8 (0.5 mM). Conversion determined from SDS-PAGE analysis.

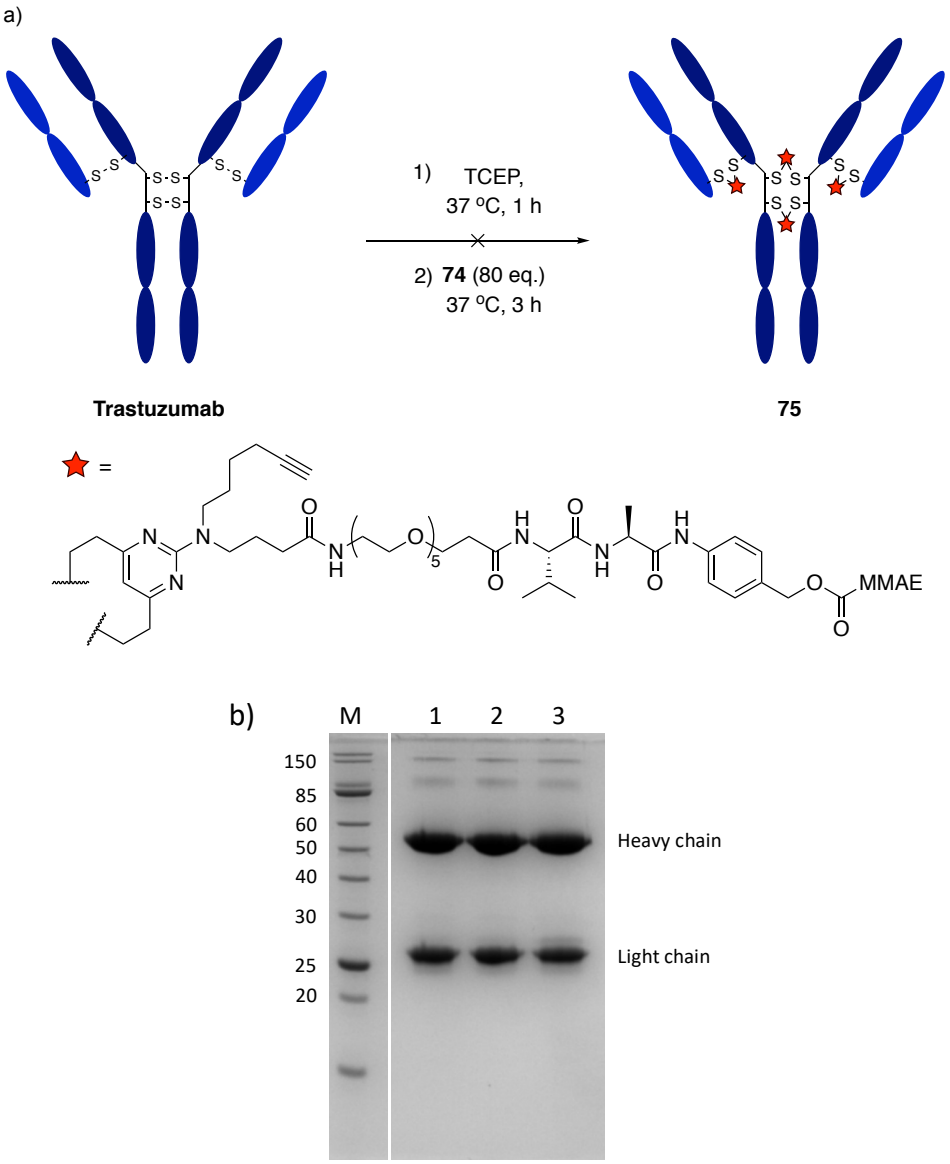

Entry	Co-solvent	Co-solvent % (v/v)	Conc. (mg/mL)	Conversion
1	DMF	10	2.5	None
2	DMF	12	2.5	None
3	DMF	15	2.5	None
4	DMSO	10	2.5	None
5	DMSO	12	2.5	None
6	DMSO	15	2.5	None
7	MeCN	15	2.5	None
8	MeCN	20	2.5	None
9	MeCN	25	2.5	None
10	DMF	15	1.0	None
11	DMSO	15	1.0	None
12	MeCN	15	1.0	None

It was proposed that an alternate synthetic strategy to allow more facile modification of the solubility profile of the linker-drug would potentially be beneficial. It was envisaged that df-DVP **72** could still be used in these investigations. A CuAAC reaction between an azide-modified MMAE fragment and df-DVP **72** could be used to install the cytotoxic component. Subsequently, amide bond formation with a tuneable amino alkyne could be used to install the desired bioorthogonal handle for post-rebridging modification. Accordingly, cleavable MMAE fragment **56** was subjected to a CuAAC reaction with df-DVP **72** to provide carboxylic acid **76** in moderate yield. Finally, amide formation was carried out by reaction of carboxylic acid **76** with 3-butynylamine hydrochloride in the presence of HBTU, HOBt·H_2O and DIPEA, generating the desired linker-dug **77** in 53% yield (Scheme 5.3).

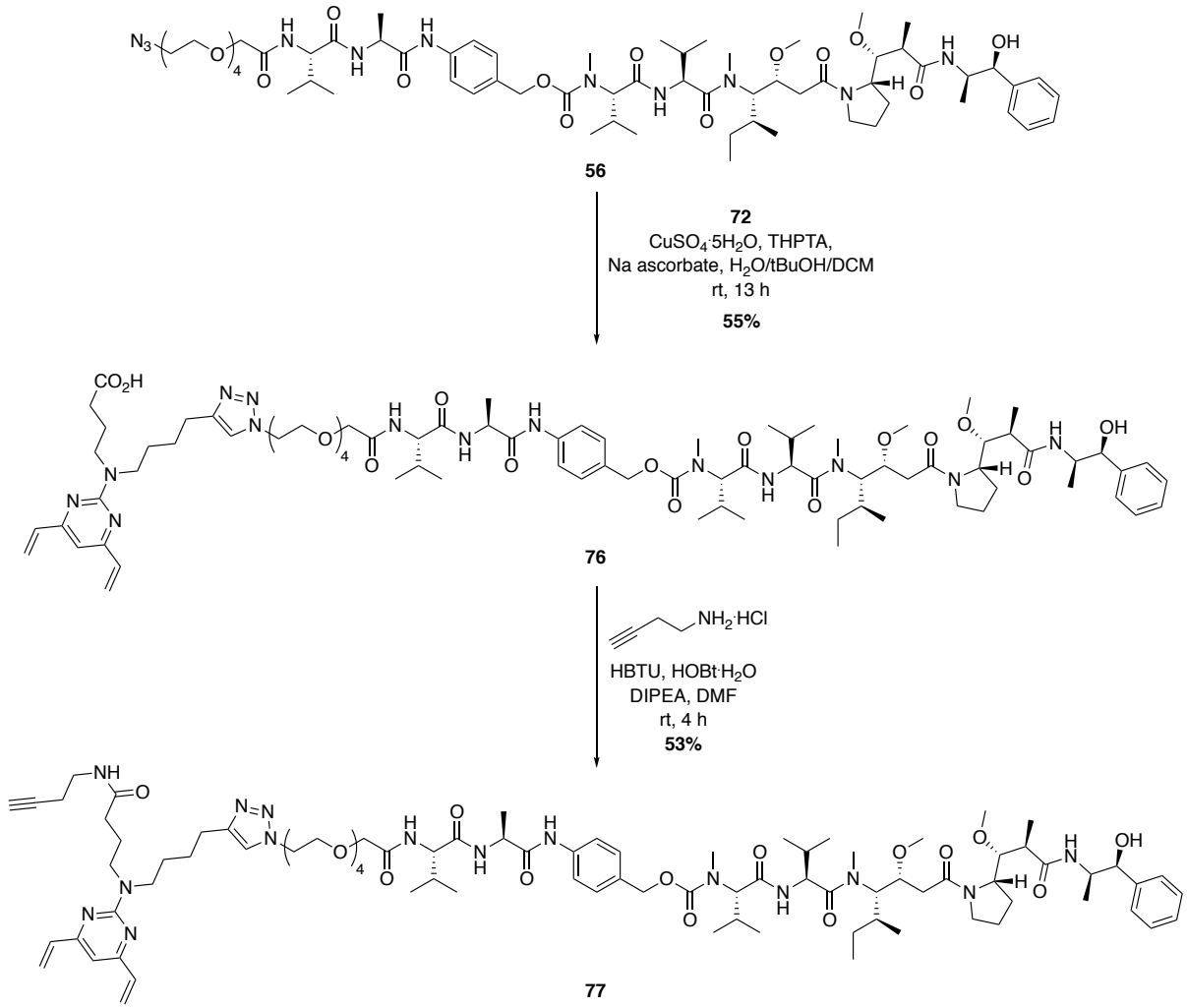

Scheme 5.3: Synthetic sequence used for the synthesis of df-DVP **77**.

Having successfully synthesised linker-drug **77**, conjugation to trastuzumab was investigated. Disappointingly, despite extensive screening of reaction conditions, including organic co-solvent, co-solvent percentage, and reaction concentration, no significant rebridging of the reduced trastuzumab light and heavy chains was observed by LCMS and SDS-PAGE analysis (Table 5.4).

Table 5.4: a) Conditions tested in the attempted reaction between trastuzumab and **77**. **b)** Typical reducing SDS-PAGE analysis of the reactions showing primarily unmodified light and heavy chains. Lanes: M) molecular weight marker, 1) entry 1, 2) entry 2, 3) entry 3. Buffer conditions – TBS; Tris HCl pH 8 (25 mM), NaCl (25 mM), EDTA pH 8 (0.5 mM). Conversion determined from SDS-PAGE analysis.

a)

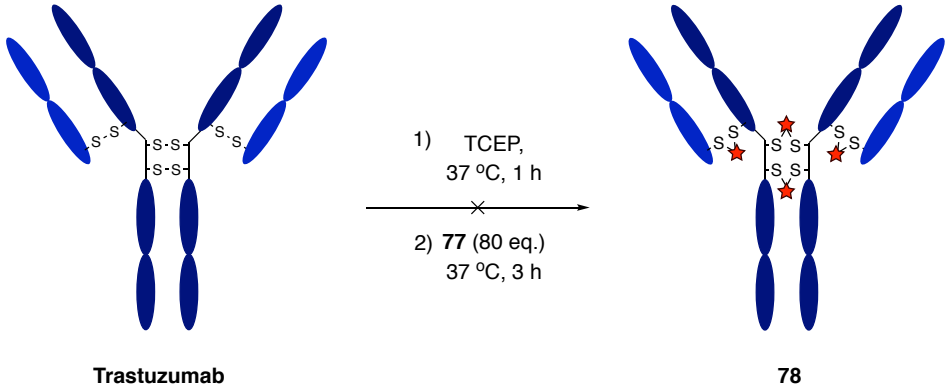

Trastuzumab **78**

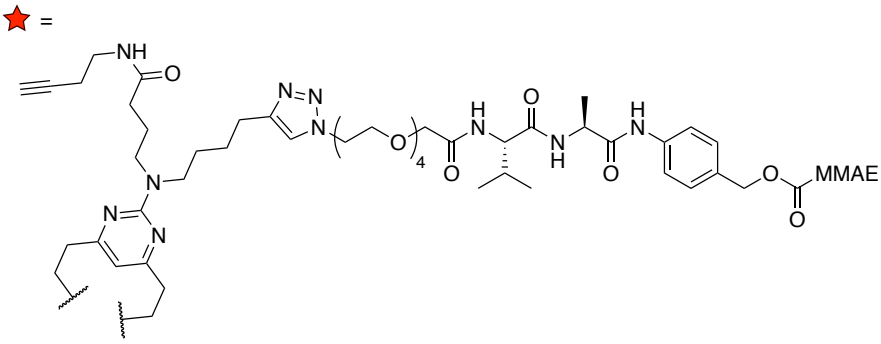

b)

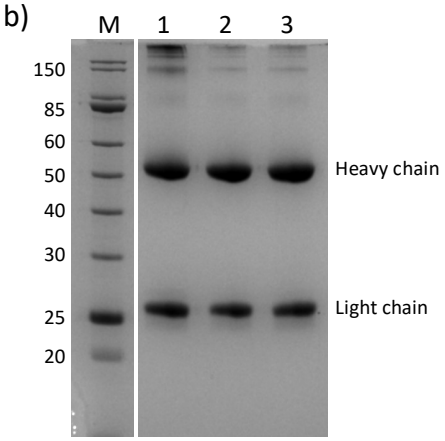

Entry	Co-solvent	Co-solvent % (v/v)	Conc. (mg/mL)	Conversion
1	DMF	10	2.5	None
2	DMF	12	2.5	None
3	DMF	15	2.5	None
4	DMF	20	2.5	None
5	DMF	15	1.0	None
6	DMF	15	5.0	None
7	DMSO	15	1.0	None
8	DMSO	15	2.5	None
9	DMSO	15	5.0	None
10	MeCN	15	1.0	None
11	MeCN	15	2.5	None
12	MeCN	15	5.0	None

5.4 Conclusions

The synthesis of a DVP linker with orthogonally reactive functional groups was described in this chapter. The simple dual-functional linker **72** displayed similar reactivity with trastuzumab as previously described DVP linkers. This suggested that the extra functionality and additional steric bulk around the DVP core did not affect the conjugation capabilities of the DVP scaffold. A number of cytotoxin-modified reagents were then synthesised. While disappointing results were obtained in terms of reactivity of these compounds with reduced trastuzumab, the evidence we gathered pointed toward a solubility issue of the highly lipophilic Val-Ala-PABC-MMAE construct, rather than to a fundamental reactivity problem inherent in the nature of our molecules. It is thus envisioned that slight modification of the synthetic strategy would yield more favourable results (*vide infra*).

Chapter 6

Conclusions and Future Work

6.1 Conclusions

An outstanding problem in the field of ADC research is the lack of easily transferrable methodologies that enable the synthesis of homogeneous and stable ADCs. The large amount of resources that have been invested in developing such techniques have undoubtedly had success. However, the strategies developed typically require extensive engineering or alteration of the native antibody structure to achieve the desired attributes. As such, methods that are capable of modifying native antibodies to generate stable and homogeneous ADCs are desirable. Disulfide rebridging reagents have emerged as an attractive technique to achieve this objective; reagents in this class have shown promise for generating homogeneous ADCs from non-engineered antibodies. However, only a limited number of such reagents have been described and the effects of using rebridging linkers with different scaffolds is not yet known.

This thesis describes the development of a novel cysteine bridging method for the production of ADCs. At the outset, the primary objectives were to deliver a methodology that; 1) enabled the construction of homogeneous ADCs with robust pharmacology, 2) generated ADCs with high levels of plasma stability to prevent premature payload release during circulation and 3) could be used to modify native antibodies to mitigate the requirement of unnatural amino acid incorporation or glycan modification.

Preliminary studies in this area, described in Chapter 3, focused on a divinylpyridine scaffold. Several reports have described the use of monovinylpyridine linkers to selectively modify proteinogenic cysteine residues to generate highly stable bioconjugates. In the first instance, small molecule model systems demonstrated that divinylpyridine reagents were synthetically tractable, and that the conjugates formed from reaction with cysteines were highly stable. Subsequent evaluation of divinylpyridine cysteine cross-linking on a non-antibody protein (*Pf*RadA-dCys) surrogate system suggested that protein modification with these reagents would be possible, as evidenced by cross-linking of two engineered cysteines. However, attempts to effectively rebridge the reduced disulfides of a mAb with these linkers were found to be generally inefficient, with only modest conversion to the rebridged antibody observed.

To overcome this issue, it was hypothesised that improvement of the conjugation reaction rate of this scaffold may generate a rebridging reagent that would enable the efficient synthesis of ADCs. It was postulated that increasing the electron deficiency of the divinyl-heteroaryl motif by switching from a pyridine to a pyrimidine core would increase the conjugation rate sufficiently to accomplish this, which is detailed in Chapter 4. As such, small molecule model investigations demonstrated the significantly enhanced reactivity of divinylpyrimidine reagents over divinylpyridine linkers. Critically, vinylpyrimidine conjugates displayed high levels of stability, analogous to those observed with vinylpyridine conjugates. Subsequently, the ability of a series of DVP linkers to rebridge reduced disulfides in antibodies and antibody fragments was then assessed, which revealed that these reagents efficiently (90–95%) rebridged the free cysteines in these proteins under a range of conditions. Functional modification of a trastuzumab antibody with relevant payloads such as cytotoxic warheads or fluorescent imaging agents was also achieved. These functionalities could be introduced by pre-functionalisation of the DVP linker or in a post-rebridging bioorthogonal CuAAC after DVP-mediated installation of an alkyne handle on the antibody. Biological evaluation of the DVP bioconjugates was then conducted. Studies toward investigating the stability of the antibody conjugates demonstrated that DVP reagents generated a linkage that was highly stable for at least two weeks in human plasma. Furthermore, the bioconjugates demonstrated almost identical affinity for the HER2 receptor compared to unmodified trastuzumab, high levels cellular selectivity and exquisite potency against HER2-positive cell lines. Moreover, the DVP reagents were also shown to be compatible with the modification of non-antibody protein scaffolds, as evidenced by the efficient cross-linking of two cysteine residues in a monomeric RadA protein.

Finally, as an extension of these studies, a dual-functional DVP reagent was synthesised. Synthetic investigations revealed that modification of either alkyne or carboxylic acid handles with functional payloads could be achieved orthogonally to one another and to the vinyl groups. Preliminary antibody conjugation studies were unsuccessful; however, this was potentially due to the poor aqueous solubility of the linker-drug molecules. Nevertheless, the df-DVP will potentially be a valuable tool, facilitating the synthesis of bis-functionalised biomolecules.

Overall, this work describes the development of a novel linker platform that enables the site-selective modification of native antibodies, to generate highly stable and functional ADCs. Efficient modification of *Pf*RadA-dCys also highlighted the potential use of these reagents for other purposes aside from ADC synthesis.

6.2 Future Work

6.2.1 *In vivo* Evaluation of ADCs

This thesis describes the evaluation of DVP-synthesised ADCs in a series of *in vitro* assays, demonstrating their stability, selectivity and potency. However, *in vivo* evaluation of these ADCs is required to fully understand their biological profile. In order to achieve this, appropriate HER2-positive mouse xenograft models (cell lines and patient-derived) could be used to investigate the efficacy, tolerability and pharmacokinetics of cleavable and non-cleavable DVP ADCs.

6.2.2 Preventing Half Antibody Formation

The primary obstacle encountered with DVP-mediated antibody modification was the formation of the half antibody conjugate as the major product of the disulfide rebridging reaction. As discussed in detail in Chapter 4, whilst not detrimental to their application, it would be preferable to have a single molecular species formed in the reaction by sole conversion to the full antibody conjugate. In order to overcome this issue, a number of avenues could be explored.

6.2.2.1 Increasing Rate of Conjugation

A remarkable increase in antibody rebridging efficiency was achieved when moving from a vinylpyridine to a vinylpyrimidine scaffold due to an increase in scaffold reactivity. Similarly, it might be expected that increasing the reactivity of the scaffold further could lead to increased rebridging efficiency. It is postulated that an increase in reaction rate may potentially also favour full antibody formation.[248] To this end, a more electron deficient scaffold such as a divinyltriazine could be explored. As such, it is envisaged that divinyltriazine reagents such as **79** could be evaluated for their antibody rebridging capabilities (Figure 6.1).

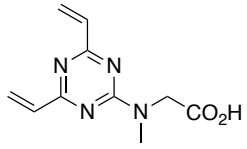

79

Figure 6.1: Potential divinyltriazine reagent **79**.

6.2.2.2 Varying Cross-Linking Reagent Length

DVP linkers generate a conjugate with seven atoms between cysteine sulfur atoms. It is possible that alteration of the distance between the sulfur atoms could be utilised to favour either half or full antibody formation. Accordingly, bis-monovinylpyrimidines of the general structure A (Figure 6.2) would give conjugates with greater distance between sulfur atoms. Conversely, an alkynylpyrimidine of general structure B (Figure 6.2) could be used to generate bioconjugates with only a one-atom bridge between sulfur atoms. In this case, a double addition mechanism into the terminal alkyne carbon would produce the rebridged bioconjugate. In both cases, triazine variants could also be explored.

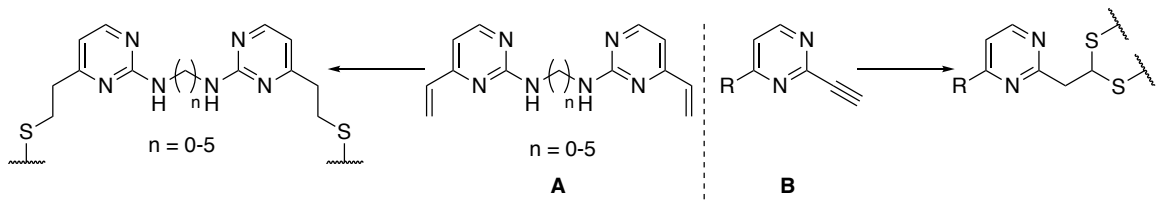

Figure 6.2: Bis-monovinylpyrimidines **A** and alkynylpyrimdines **B** would potentially favour full antibody formation.

6.2.3 Metal-Free Post-Rebridging Conjugation

In this thesis, combining CuAAC chemistry with DVP rebridging was shown to be highly effective at modifying trastuzumab with functional payloads. However, there are disadvantages to using transition metal-catalysed reactions for the production of biotherapeutics, such as potential residual metal contaminants, metal-catalysed oxidation of the protein and poor synthetic yields. To circumvent these issues, modification of the protein through DVP rebridging with bioorthogonal functional groups such as strained alkynes/alkenes or tetrazines could enable metal-free functionalisation of the antibody (Figure 6.3). Tetrazines have been widely used in the bioorthogonal modification of biomacromolecules via an inverse electron demand Diels-Alder reaction (iEDDA) with a small set of compatible reagents (e.g.

cyclopropenes, trans-cyclooctenes).[249–251] Combining this chemistry with the DVP technology, linkers such as tetrazine **80** or strained alkyne **81** could be explored.

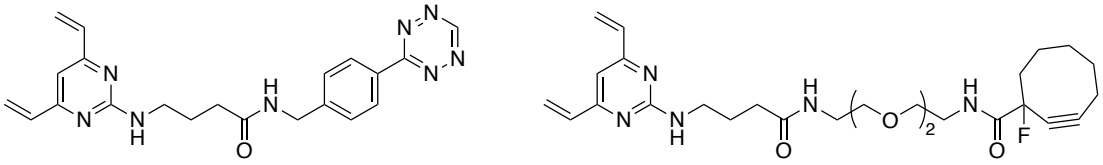

80 **81**

Figure 6.3: Potential metal-free bioconjugation linkers such as tetrazine-functionalised DVP **80** and strained alkyne-functionalised DVP **81**.

6.2.4 Dual-Functional DVPs

A number of possible strategies could be investigated to overcome the poor reactivity of the df-DVP linkers described in Chapter 5. First, modification of the linker to include two compatible bioorthogonal groups would enable rebridging with a potentially more soluble df-DVP reagent, followed by bioorthogonal chemistry to attach the desired payloads. An alkyne- and tetrazine-modified DVP such as **82** would be amenable to this sequence (Figure 6.4a). Alternatively, a reversal of the conjugation order by attachment of an imaging agent to the linker before rebridging followed by bioorthogonal attachment of the cytotoxin post-conjugation could potentially mitigate these issues. Indeed, small, polar fluorescent dyes such as nitrobenzofurazans (NBD) have been used in the generation of AFCs and as such could aid the reactivity of the described df-DVP linkers (Figure 6.4b).[151,252]

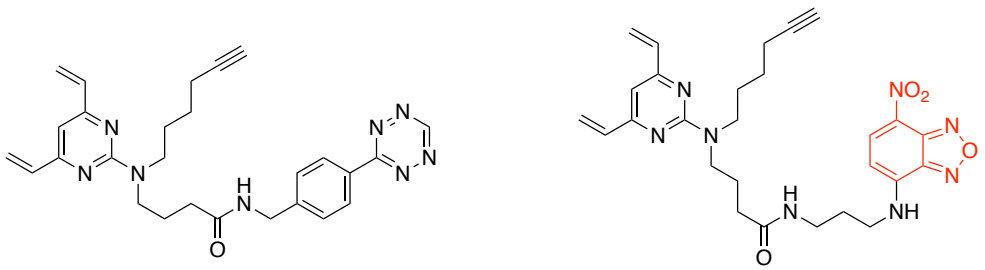

82 **83**

Alkyne and tetrazine df-DVP *Alkyne and NDB df-DVP*

Figure 6.4: Potential strategies to overcome the poor reactivity of the df-DVP drug-linkers by using a df-DVP containing two bioorthogonal handles such as **82** or small polar imaging agents such as an NBD fluorophore as the pre-conjugation payload (**83**). NBD tag highlighted in red.

6.2.5 Peptide Stapling

Protein-protein interactions (PPIs) govern many cellular processes. However, they have classically been deemed undruggable due to their large and shallow binding interfaces, making it difficult to design small molecule inhibitors.[253] Peptide molecules have proven to be attractive candidates for the interrogation and perturbation of these interfaces. However, linear peptides typically suffer from poor physiological properties such as poor membrane permeability and low levels of circulatory stability.[254] A process known as peptide stapling, whereby two amino acids in the peptide sequence are covalently linked has been extensively used to improve these characteristics and thus the overall pharmacological profile of the peptide. Many of the most commonly used macrocyclisation techniques utilise bioorthogonal chemistry to link unnatural amino acids containing complementary reactive groups.[255,256] Stapling of cysteine residues enables peptide macrocyclisation without the need to synthesise or purchase unnatural amino acids.[257–259] In this context, DVP linkers could potentially serve as valuable tools in the development of peptide therapeutics (Figure 6.5). Functionalisation of the peptide with cell-penetrating peptides, fluorescent tags or additional drug molecules would also be possible in a facile manner, as demonstrated in this work in the synthesis of ADCs.

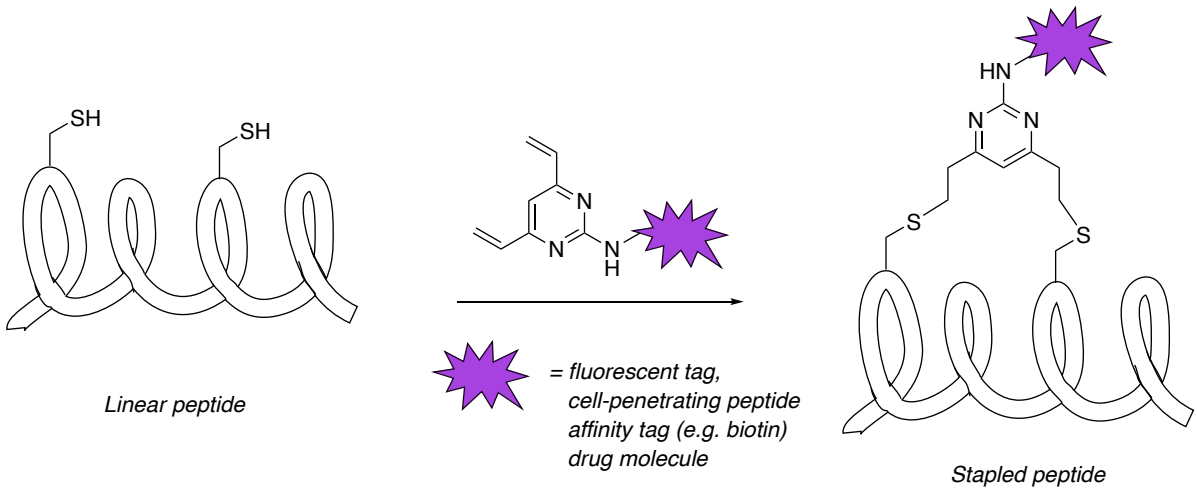

Figure 6.5: Peptide stapling of linear peptides with DVP reagents.

Chapter 7

Experimental

General Experimental

All solvents and reagents were used as received unless otherwise stated. Ethyl acetate, methanol, dichloromethane, acetonitrile and toluene were distilled from calcium hydride. Diethyl ether was distilled from a mixture of lithium aluminium hydride and calcium hydride. Petroleum ether refers to the fraction between 40 – 60 °C upon distillation. Tetrahydrofuran was dried using Na wire and distilled from a mixture of lithium aluminium hydride and calcium hydride with triphenylmethane as indicator.

Non-aqueous reactions were conducted under a stream of dry nitrogen using oven-dried glassware. All temperatures below 0 °C were maintained using an acetone-dry ice bath. Temperatures of 0 °C were maintained using an ice-water bath. Room temperature (rt) refers to ambient temperature.

Yields refer to spectroscopically and chromatographically pure compounds unless otherwise stated. Reactions were monitored by thin layer chromatography (TLC) or liquid chromatography mass spectrometry (LCMS). TLC was performed using glass plates pre-coated with Merck silica gel 60 F_{254} and visualised by quenching of UV fluorescence (λ_{max} = 254 nm) or by staining with potassium permanganate. Retention factors (R_f) are quoted to 0.01. LCMS was carried out using a Waters ACQUITY H-Class UPLC with an ESCi Multi-Mode Ionisation Waters SQ Detector 2 spectrometer using MassLynx 4.1 software; ESI refers to the electrospray ionisation technique; LC system: solvent A: 2 mM NH_4OAc in H_2O/MeCN (95:5); solvent B: MeCN; solvent C: 2% formic acid; column: ACQUITY UPLC® CSH C18 (2.1 mm × 50 mm, 1.7 µm, 130 Å) at 40 °C; gradient: 5 – 95 % B with constant 5 % C over 1 min at flow rate of 0.6 mL/min; detector: PDA eλ Detector 220 – 800 nm, interval 1.2 nm.

Flash column chromatography (FCC) was carried out using slurry-packed Merck 9385 Kieselgel 60 SiO_2 (230-400 mesh) under a positive pressure of nitrogen.

Analytical high performance liquid chromatography (HPLC) was performed on Agilent 1260 Infinity machine, using a Supelcosil™ ABZ+PLUS column (150 mm × 4.6 mm, 3 μm) with a linear gradient system (solvent A: 0.05% (v/v) TFA in H_2O; solvent B: 0.05% (v/v) TFA in MeCN) over 15 min at a flow rate of 1 mL/min, and UV detection (λ_{max} = 220 – 254 nm).

Preparative HPLC was performed on Agilent 1260 Infinity machine, using a Supelcosil™ ABZ+PLUS column (250 mm × 21.2 mm, 5 μm) with a linear gradient system (solvent A: 0.1% (v/v) TFA in H_2O; solvent B: 0.05% (v/v) TFA in MeCN) over 20 min at a flow rate of 20 mL/min, and UV detection (λ_{max} = 220 – 254 nm).

Melting points (m.p.) were obtained using a Büchi Melting Point B-545 melting point apparatus and are uncorrected.

Infrared (IR) spectra were recorded neat on a Perkin-Elmer Spectrum One spectrometer with internal referencing. Selected absorption maxima (ν_{max}) are reported in wavenumbers (cm^{-1}).

Proton and carbon nuclear magnetic resonance (NMR) were recorded using an internal deuterium lock on Bruker DPX-400 (400 MHz, 101 MHz), Bruker Avance 400 QNP (400 MHz, 101 MHz) and Bruker Avance 500 Cryo Ultrashield (500 MHz, 126 MHz). In proton NMR, chemical shifts (δ_H) are reported in parts per million (ppm), to the nearest 0.01 ppm and are referenced to the residual non-deuterated solvent peak ($CDCl_3$: 7.26, DMSO-d_6: 2.50, CD_3OD: 3.31, D_2O: 4.79). Coupling constants (*J*) are reported in Hertz (Hz) to the nearest 0.1 Hz. Data are reported as follows: chemical shift, multiplicity (s = singlet; d = doublet; t = triplet; q = quartet; qn = quintet; sx = sextet; sep = septet; m = multiplet; or as a combination of these, e.g. dd, dt etc.), integration, coupling constant(s) and assignment. Proton assignments are reported in reference to alphabetical labelling of protons in the structures. In carbon NMR, chemical shifts (δ_C) are quoted in ppm, to the nearest 0.1 ppm, and are referenced to the residual non-deuterated solvent peak ($CDCl_3$: 77.16, DMSO-d_6, 39.52, CD_3OD: 49.00). Carbon assignments are reported in reference to alphabetical labelling of carbons in the structures. ^1H NMR and ^{13}C NMR spectra assignments are supported by DEPT-135 editing, COSY (2D, ^1H-^1H correlations), HSQC (2D, one bond ^1H-^{13}C correlations), HMBC (2D, multi-bonds ^1H-^{13}C correlations), or by analogy to fully interpreted spectra of related compounds.

High resolution mass spectrometry (HRMS) measurements were recorded with a Micromass Q-TOF mass spectrometer or a Waters LCT Premier Time of Flight mass spectrometer. Mass

values are reported within the error limits of ±5 ppm mass units. ESI refers to the electrospray ionisation technique.

Protein LCMS was performed on a Xevo G2-S TOF mass spectrometer coupled to an Acquity UPLC system using an Acquity UPLC BEH300 C4 column (1.7 µm, 2.1 × 50 mm). H_2O with 0.1% formic acid (solvent A) and 95% MeCN and 5% water with 0.1% formic acid (solvent B), were used as the mobile phase at a flow rate of 0.2 mL/min. The gradient was programmed as follows: 95% A for 0.93 min, then a gradient to 100% B over 4.28 min, then 100% B for 1.04 minutes, then a gradient to 95% A over 1.04 min. The electrospray source was operated with a capillary voltage of 2.0 kV and a cone voltage of 40 V. Nitrogen was used as the desolvation gas at a total flow of 850 L/h. Total mass spectra were reconstructed from the ion series using the MaxEnt algorithm preinstalled on MassLynx software (v4.1 from Waters) according to the manufacturer's instructions. Trastuzumab samples were deglycosylated with PNGase F (New England Biolabs) prior to LCMS analysis unless otherwise stated.

Extreme care was taken when conducting any reactions containing MMAE or its derivatives. All handling was conducted in a fumehood while wearing full personal protective equipment (safety glasses, labcoat and nitrile gloves). Reactions were conducted on small scale with <75 µmol MMAE used in all instances. Safety notices should be placed on the front of the fumehood during operation. All aqueous waste should be treated with sodium hypochlorite for a minimum of 24 hours before disposal. All organic waste should be disposed of immediately in the appropriate waste containers. Any spillages should be cleaned up immediately. Tissue waste should be double bagged and cable-tied before disposal as 'Toxic Waste'. A competent person should be made aware of the intended use before beginning any experiments.

7.1 Chapter 3: Divinylpyridine Linkers

7.1.1 Synthetic Procedures

2-amino-4-vinylpyridine (1)

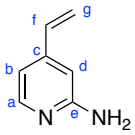

2-amino-4-bromopyridine (250 mg, 1.45 mmol), potassium vinyltrifluoroborate (290 mg, 2.17 mmol), $Pd(dppf)Cl_2{\cdot}CH_2Cl_2$ (118 mg, 0.145 mmol) and potassium carbonate (599 mg, 4.34 mmol) in THF/H_2O (10:1, 5.5 mL) were heated to 70 °C for 16 h. Upon completion, the reaction mixture was filtered through Celite® and the solvent removed *in vacuo*. The resulting residue was purified by flash column chromatography (FCC) (5% $MeOH/CH_2Cl_2$ with 0.5% Et_3N) to yield 2-amino-4-vinylpyridine **1** (155 mg, 1.29 mmol, 89%) as a brown solid.

R_f 0.19 (SiO_2; 5% $MeOH/CH_2Cl_2$ with 1% Et_3N); **m.p.** 53-55 °C; **ν_{max}** (neat/cm^{-1}) 3436, 1630, 1603, 1543, 1494; **δ_H** (400 MHz, CD_3OD) 7.82 (d, 1H, *J* = 5.6 Hz, Ha), 6.70 (dd, 1H, *J* = 5.6, 1.4 Hz, Hb), 6.60 (dd, 1H, *J* = 17.6, 10.9 Hz, Hf), 6.56 (s, 1H, Hd), 5.94 (dd, 1H, *J* = 17.6, 0.8 Hz, Hg^t), 5.42 (dd, 1H, *J* = 10.9, 0.8 Hz, Hg^c); **δ_C** (101 MHz, CD_3OD) 161.4 (Ce), 148.5 (Cc), 147.9 (Ca), 136.5 (Cf), 118.5 (Cg), 111.1 (Cb), 107.7 (Cd); **HRMS** (ESI) *m/z* found $[M+H]^+$ 121.0760, $C_7H_9N_2^+$ required 121.0760.

4-amino-2-vinylpyridine (2)

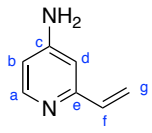

4-amino-2-bromopyridine (250 mg, 1.45 mmol), potassium vinyltrifluoroborate (290 mg, 2.17 mmol), $Pd(dppf)Cl_2{\cdot}CH_2Cl_2$ (118 mg, 0.145 mmol) and potassium carbonate (599 mg, 4.34 mmol) in THF/H_2O (10:1, 5.5 mL) were heated to 70 °C for 16 h. Upon completion, the reaction mixture was filtered through Celite® and the solvent removed *in vacuo*. The resulting residue was purified by FCC (5% $MeOH/CH_2Cl_2$ with 0.5% Et_3N) to yield 4-amino-2-vinylpyridine **2** (148 mg, 1.23 mmol, 85%) as a brown oil.

R_f 0.26 (SiO_2; 5% $MeOH/CH_2Cl_2$ with 1% Et_3N); **ν_{max}** (neat/cm^{-1}) 3329, 3208, 1636, 1595, 1560, 1487; **δ_H** (400 MHz, CD_3OD) 7.92 (d, 1H, *J* = 5.8 Hz, Ha), 6.70 (d, 1H, *J* = 2.4 Hz, Hd), 6.63 (dd, 1H, *J* = 17.6, 11.0 Hz, Hf), 6.47 (dd, 1H, *J* = 5.8, 2.4 Hz, Hb), 6.00 (dd, 1H, *J* = 17.6, 1.1 Hz, Hg^t), 5.40 (dd, 1H, *J* = 11.0, 1.1 Hz, Hg^c); **δ_C** (101 MHz, CD_3OD) 157.6 (Cc), 156.5 (Ce), 149.1 (Ca), 137.6 (Cf), 118.1 (Cg), 109.3 (Cb), 107.3 (Cd); **HRMS** (ESI) *m/z* found $[M+H]^+$ 121.0759, $C_7H_9N_2^+$ required 121.0760.

Methyl *S*-(2-(2-aminopyridin-4-yl)ethyl)-*N*-(*tert*-butoxycarbonyl)-*L*-cysteinate (3)

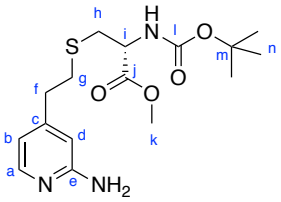

To a solution of *N*-*tert*-butoxycarbonyl-*L*-cysteine methyl ester (48.9 mg, 0.208 mmol) in sodium phosphate buffer (0.5 M, pH 8, 2.91 mL) was added a solution of amine **1** (125 mg, 1.04 mmol) in MeCN (1.25 mL). The mixture was heated to 37 °C for 180 min. Upon completion, the reaction mixture was diluted with H_2O (5 mL) and the product extracted with EtOAc (4 × 10 mL). The combined organic fractions were dried ($MgSO_4$) and the crude purified by FCC (5% $MeOH/CH_2Cl_2$) to yield yield methyl *S*-(2-(2-aminopyridin-4-yl)ethyl)-*N*-(*tert*-butoxycarbonyl)-*L*-cysteinate **3** (69.5 mg, 0.196 mmol, 94%) as a pale yellow oil.

R_f 0.20 (SiO_2; 5% MeOH/CH_2Cl_2); **ν_{max}** (neat/cm^{-1}) 3324, 1703, 1665, 1624, 1514; **δ_H** (400 MHz, CD_3OD) 7.78 (d, 1H, *J* = 5.4 Hz, Ha), 6.52 (dd, 1H, *J* = 5.4, 1.2 Hz, Hb), 6.47 (s, 1H, Hd), 4.36-4.32 (m, 1H, Hi), 3.73 (s, 3H, Hk), 2.97 (dd, 1H, *J* = 13.9, 5.3 Hz, Hh) 2.85-2.74 (m, 5H, Hf, Hg, Hh) 1.44 (s, 9H, Hn); **δ_C** (101 MHz, CD_3OD) 173.2 (Cj), 160.9 (Cc), 153.2 (Ce), 147.8 (Cl), 147.5 (Ca), 114.7 (Cb), 110.0 (Cd) 80.8 (Cm), 55.2 (Ci), 52.8 (Ck) 36.4 (Ch), 34.7 (Cg), 33.3 (Cf), 28.7 (Cn); **HRMS** (ESI) *m/z* found $[M+H]^+$ 356.1636, $C_{16}H_{26}N_3O_4{}^{32}S_1{}^+$ required 356.1639.

Methyl *S*-(2-(4-aminopyridin-2-yl)ethyl)-*N*-(*tert*-butoxycarbonyl)-*L*-cysteinate (4)

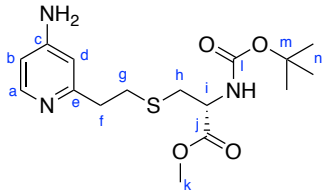

To a solution of *N*-*tert*-butoxycarbonyl-*L*-cysteine methyl ester (12.9 mg, 54.8 µmol) in sodium phosphate buffer (0.5 M, pH 8, 770 µL) was added a solution of amine **2** (32.9 mg, 274 µmol) in MeCN (330 µL). The mixture was heated to 37 °C for 4 h. Upon completion, the reaction mixture was diluted with H_2O (5 mL) and the product extracted with EtOAc (4 × 10 mL). The combined organic fractions were dried ($MgSO_4$) and the crude purified by FCC (5-10% MeOH/CH_2Cl_2) to yield methyl *S*-(2-(4-aminopyridin-2-yl)ethyl)-*N*-(*tert*-butoxycarbonyl)-*L*-cysteinate **4** (18.6 mg, 52.3 µmol, 96%) as a pale yellow oil.

R_f 0.20 (SiO_2; 10% MeOH/CH_2Cl_2); **ν_{max}** (neat/cm^{-1}) 3359, 2980, 1740, 1695, 1632, 1606, 1515; **δ_H** (400 MHz, $CDCl_3$) 8.04 (d, 1H, *J* = 5.6 Hz, Ha), 6.55-6.53 (m, 2H, Hb and Hd), 5.58 (d, 1H, *J* = 7.8 Hz, NH), 4.51-4.50 (m, 1H, Hi), 3.74 (s, 3H, Hk), 2.98-2.91 (m, 6H, Hf, Hg and Hh), 1.43 (s, 9H, Hn); **δ_C** (101 MHz, $CDCl_3$) 171.7 (Cj), 157.7 (Cc), 155.5 (Ce or Cl), 155.4 (Ce or Cl), 146.6 (Ca), 108.9 (Cb or Cd) 108.1 (Cb or Cd), 80.3 (Cm), 53.6 (Ci), 52.7 (Ck), 36.7 (Cf or Cg or Ch), 34.7 (Cf or Cg or Ch), 32.0 (Cf or Cg or Ch), 28.5 (Cn); **HRMS** (ESI) *m/z* found $[M+H]^+$ 356.1629, $C_{16}H_{26}N_3O_4{}^{32}S_1{}^+$ required 356.1639.

2,6-divinylpridine-4-carboxylic acid (5)

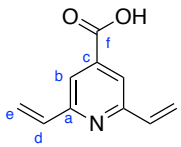

2,6-dibromopyridine-4-carboxylic acid (300 mg, 1.07 mmol), potassium vinyltrifluoroborate (430 mg, 3.21 mmol), Pd(dppf)Cl_2·CH_2Cl_2 (188 mg, 0.230 mmol) and potassium carbonate (887 mg, 6.42 mmol) in THF/H_2O (10:1, 6.6 mL) were heated to 70 °C for 15 h. Upon completion, the reaction mixture was filtered through Celite® and the solvent removed *in vacuo*. The resulting residue was purified by FCC (10% MeOH/CH_2Cl_2 with 1% AcOH) to yield 2,6-divinylpridine-4-carboxylic acid **5** (180 mg, 1.03 mmol, 96%) as a brown solid.

R_f 0.41 (SiO_2; 10% MeOH/CH_2Cl_2); **m.p.** 121-123 °C; **ν_{max}** (neat/cm^{-1}) 2927, 1715, 1592, 1556, 1424; **δ_H** (400 MHz, CD_3OD) 7.84 (s, 2H, Hb), 6.90 (dd, 2H, *J* = 17.5, 10.9 Hz, Hd), 6.30 (dd, 2H, *J* = 17.5, 1.0 Hz, He^t), 5.56 (dd, 2H, *J* = 10.9, 1.0 Hz, He^c); **δ_C** (101 MHz, CD_3OD) 168.0 (Cf), 157.7 (Ca), 141.4 (Cc), 137.5 (Cd), 120.3 (Cb), 120.0 (Ce); **HRMS** (ESI) *m/z* found $[M+H]^+$ 176.0698, $C_{10}H_{10}N_1O_2^+$ required 176.0706.

N-(but-3-yn-1-yl)-2,6-divinylisonicotinamide (6)

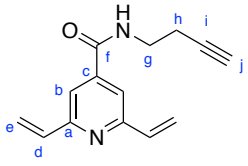

To a solution of carboxylic acid **5** (30.0 mg, 0.171 mmol) in DMF (2.00 mL) was added DIPEA (0.147 mL, 0.855 mmol) followed by HBTU (78.0 mg, 0.206 mmol). The mixture was stirred at rt for 5 min. But-3-ynylamine hydrochloride (90.0 mg, 0.855 mmol) was added and the mixture stirred for 3 h. Upon completion, the reaction mixture was diluted with H_2O (10 mL) and the product extracted in CH_2Cl_2 (4 × 10 mL) and dried ($MgSO_4$). The organic fractions were concentrated and the crude residue purified by FCC (20% EtOAc/PE) to yield *N*-(but-3-yn-1-yl)-2,6-divinylisonicotinamide **6** (26.3 mg, 0.116 mmol, 68%) as a clear oil.

R_f 0.27 (SiO_2; 40% EtOAc/PE); **ν_{max}** (neat/cm^{-1}) 3297, 1647, 1544, 1425; **δ_H** (400 MHz, $CDCl_3$) 7.49 (s, 2H, Hb), 6.86 (dd, 2H, *J* = 17.4, 10.7 Hz, Hd), 6.33 (dd, 2H, *J* = 17.4, 1.2 Hz, He^t), 5.56 (dd, 2H, *J* = 10.7, 1.2 Hz, He^c), 3.63 (q, 2H, *J* = 6.2 Hz, Hg), 2.54 (td, 2H, *J* = 9.6, 2.7 Hz, Hh), 2.07 (t, 1H, *J* = 2.7 Hz, Hj); **δ_C** (101 MHz, $CDCl_3$) 166.0 (Cf), 156.3 (Ca), 142.8 (Cc), 136.3 (Cd), 119.7 (Ce), 117.1 (Cb), 81.2 (Ci), 70.5 (Cj), 38.5 (Cg), 19.3 (Ch); **HRMS** (ESI) *m/z* found $[M+H]^+$ 227.1180, $C_{14}H_{15}N_2O_1^+$ required 227.1184.

2,6-bis(2-(((*R*)-2-((*tert*-butoxycarbonyl)amino)-3-methoxy-3-oxopropyl)-thio)ethyl)isonicotinic acid (7)

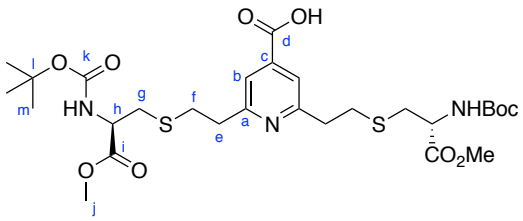

A mixture of 2,6-divinylpyridine-4-carboxylic acid **5** (8.97 mg, 51.2 µmol) and *N-tert*-butoxycarbonyl-*L*-cysteine methyl ester (26.5 mg, 113 µmol) in 30% MeCN/sodium phosphate buffer (0.5 M, pH 8, 1.02 mL) was heated to 37 °C for 14 h. Upon completion, the mixture was diluted with H_2O (5 mL) and the product extracted with CH_2Cl_2 (4 × 10 mL). The combined organic fractions were dried ($MgSO_4$) and the crude purified by FCC (5-10% MeOH/CH_2Cl_2) to yield 2,6-bis(2-(((*R*)-2-((*tert*-butoxycarbonyl)amino)-3-methoxy-3-oxopropyl)-thio)ethyl)isonicotinic acid **7** (26.8 mg, 41.5 µmol, 81%) as a clear oil.

R_f 0.26 (SiO_2; 10% MeOH/CH_2Cl_2); **ν_{max}** (neat/cm^{-1}) 3363, 1742, 1694, 1555, 1505; **δ_H** (400 MHz, CD_3OD) 7.64 (s, 2H, Hb), 4.34-4.23 (m, 2H, Hh), 3.72 (s, 6H, Hj), 3.11-3.08 (m, 4H, He), 2.97-2.92 (m, 6H, Hf and Hg), 2.86-2.82 (m, 2H, Hg), 1.43 (s, 18H, Hm); **δ_C** (101 MHz, CD_3OD) 173.2 (Ci), 170.5 (Cd), 161.6 (Ca), 157.8 (Ck) 144.0 (Cc), 122.0 (Cb), 80.8 (Cl), 55.2 (Ch), 52.8 (Cj), 38.9 (Ce), 34.7 (Cg), 33.1 (Cf), 28.7 (Cm); **HRMS** (ESI) *m/z* found $[M+H]^+$ 646.2437, $C_{28}H_{44}N_3O_{10}{}^{32}S_2^+$ required 646.2463.

7.1.2 Monovinylpyridine Rate Studies

2-amino-4-vinylpyridine (1)

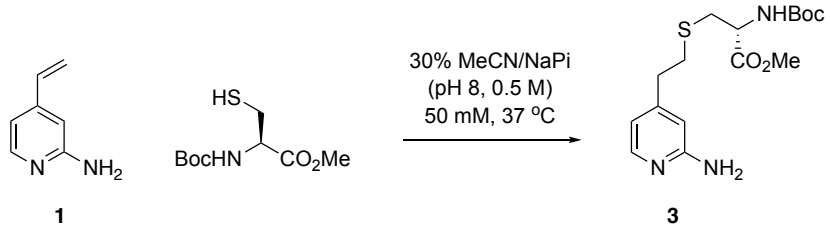

1 **3**

To a solution of *N*-Boc-Cys-OMe (5.00 mg, 21.2 μmol) in MeCN (127 μL) and NaPi (297 μL, 0.5 M, pH 8) was added amine **1** (21.2 μmol, 42.4 μmol, 106 μmol, 212 μmol or 424 μmol) and the reaction mixture stirred at 37 °C. Aliquots were removed from the reaction at 15 min intervals up to 2 h, then at 30 min intervals up to 4 h. Reaction progress was monitored by TLC.

4-amino-2-vinylpyridine (2)

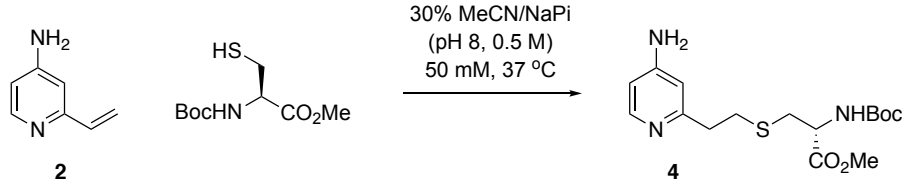

2 **4**

To a solution of *N*-Boc-Cys-OMe (3.50 mg, 14.9 μmol) in MeCN (89.0 μL) and NaPi (209 μL, 0.5 M, pH 8) was added amine **2** (14.9 μmol, 29.8 μmol, 74.5 μmol, 149 μmol or 298 μmol) and the reaction mixture stirred at 37 °C. Aliquots were removed from the reaction at 15 min intervals up to 2 h, then at 30 min intervals up to 4 h. Reaction progress was monitored by TLC.

7.1.3 Divinylpyridine Stability Studies

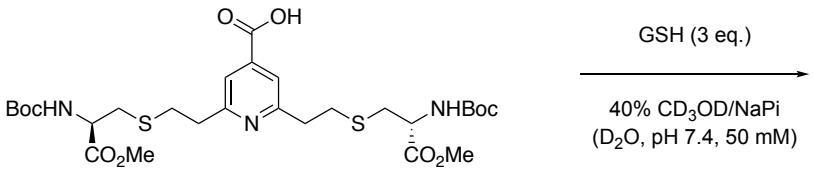

7

To a solution of carboxylic acid **7** (4.30 mg, 6.70 µmol) in CD_3OD (280 µL) and deuterated NaPi (420 µL, 50 mM, pH 7.4) was added reduced *L*-glutathione (6.20 mg, 20.1 µmol). The mixture was incubated at rt and analysed by ^1H NMR after 24, 100 and 200 h.

7.2 Chapter 4: Divinylpyrimidine Linkers

7.2.1 Synthetic Procedures

2-amino-4-vinylpyrimidine (11)

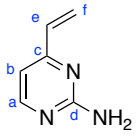

A solution of 2-amino-4-chloropyrimidine (300 mg, 2.32 mmol), potassium vinyltrifluoroborate (931 mg, 6.95 mmol), $Pd(dppf)Cl_2{\cdot}CH_2Cl_2$ (189 mg, 0.232 mmol) and potassium carbonate (1.92 g, 13.9 mmol) in THF/H_2O (10:1, 7.7 mL) was heated to 70 °C for 16 h. Upon completion, the reaction mixture was filtered through Celite® and the solvent removed *in vacuo*. The resulting residue was purified by FCC (40% EtOAc/PE) to yield 2-amino-4-vinylpyrimidine **11** (195 mg, 1.61 mmol, 70%) as an off-white solid.

R_f 0.12 (SiO_2; 40% EtOAc/PE); **m.p.** 83-86 °C; **ν_{max}** (neat/cm^{-1}) 3318, 1648, 1546, 1466, 1403; **δ_H** (400 MHz, $CDCl_3$) 8.26 (d, 1H, *J* = 5.2 Hz, Ha), 6.65 (d, 1H, *J* = 5.2 Hz, Hb), 6.58 (dd, 1H, *J* = 17.4, 10.6 Hz, He), 6.37 (dd, 1H, *J* = 17.4, 1.3 Hz, Hf^t), 5.64 (dd, 1H, *J* = 10.6, 1.3 Hz, Hf^c), 5.20 (s, 2H, NH_2); **δ_C** (101 MHz, $CDCl_3$) 163.9 (Cc), 162.7 (Cd), 158.4 (Ca), 135.4 (Ce), 123.0 (Cf), 108.9 (Cb); **HRMS** (ESI) *m/z* found $[M+H]^+$ 122.0715, $C_6H_8N_3^+$ required 122.0713.

Methyl *S*-(2-(2-aminopyrimidin-4-yl)ethyl)-*N*-*tert*-butoxycarbonyl)-*L*-cysteinate (12)

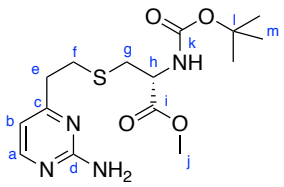

A solution of amine **11** (15.0 mg, 124 µmol), *N*-(*tert*-butoxycarbonyl)-*L*-cysteine methyl ester (29.2 mg, 124 µmol) in 30% MeCN/sodium phosphate buffer (pH 8, 50 mM, 2.48 mL) was stirred at 37 °C for 15 min. Upon completion, the mixture was diluted with H_2O (10 mL), extracted with EtOAc (4 × 10 mL), dried ($MgSO_4$) and concentrated *in vacuo*. The crude residue was purified by FCC (50-100% EtOAc/PE) to yield methyl *S*-(2-(2-aminopyrimidin-4-yl)ethyl)-*N*-*tert*-butoxycarbonyl)-*L*-cysteinate **12** (39.6 mg, 111 µmol, 90%) as a clear oil.

R_f 0.10 (SiO_2; 50% EtOAc/PE); **ν_{max}** (neat/cm^{-1}) 3334, 2977, 1741, 1704, 1616, 1562, 1457; **δ_H** (400 MHz, $CDCl_3$) 8.17 (d, 1H, *J* = 5.3 Hz, Ha), 6.49 (d, 1H, *J* = 5.3 Hz, Hb), 5.70 (d, 1H, *J* = 7.5 Hz, NH), 5.13 (s, 2H, NH_2), 4.60-4.56 (m, 1H, Hh), 3.74 (s, 3H, Hj), 3.03-2.96 (m, 2H, Hg), 2.95-2.81 (m, 4H, He, Hf), 1.44 (s, 9H, Hm); **δ_C** (101 MHz, $CDCl_3$) 171.9 (Ci), 169.3 (Cc), 163.1 (Cd), 158.3 (Ca), 155.4 (Ck), 111.0 (Cb), 80.4 (Cl), 53.7 (Ch), 52.7 (Cj), 37.5 (Ce), 34.7 (Cg), 30.8 (Cf), 28.5 (Cm); **HRMS** (ESI) *m/z* found $[M+H]^+$ 357.1606, $C_{15}H_{25}N_4O_4{}^{32}S_1{}^+$ required 357.1597.

Methyl *S*-(1-benzyl-2,5-dioxopyrrolidin-3-yl)-*N*-(*tert*-butoxycarbonyl)-*L*-cysteinate (13)

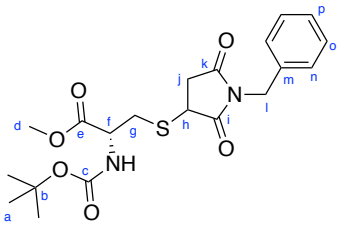

A solution of *N*-benzylmaleimide (100 mg, 0.534 mmol), *N*-(*tert*-butoxycarbonyl)-*L*-cysteine methyl ester (151 mg, 0.641 mmol) and triethylamine (74.0 µL, 0.534 mmol) was stirred at 37 °C for 16 h. Upon completion, the reaction mixture was concentrated *in vacuo* and the crude

residue purified by FCC (35% EtOAc/PE) to yield methyl *S*-(1-benzyl-2,5-dioxopyrrolidin-3-yl)-*N*-(*tert*-butoxycarbonyl)-*L*-cysteinate **13** (210 mg, 0.497 mmol, 93%) as a white solid.

R_f 0.16 (SiO_2; 35% EtOAc/PE); **m.p.** 73-77 °C; **ν_{max}** (neat/cm^{-1}) 2982, 1744, 1700, 1498, 1434; **δ_H** (400 MHz, $CDCl_3$) 7.37-7.28 (m, 10H, Hn, Ho and Hp), 5.54 (d, 1H, *J* = 7.6 Hz, NH), 5.32 (d, 1H, *J* = 7.6 Hz, NH), 4.70-4.56 (m, 6H, Hf and Hl), 3.94-3.91 (m, 1H, Hh), 3.84-3.81 (m, 1H, Hh), 3.77-3.76 (m, 6H, Hd), 3.57-3.53 (m, 1H, Hg), 3.41-3.36 (m, 1H, Hg), 3.17-3.07 (m, 3H, Hg and Hj), 2.98-2.92 (m, 1H, Hg), 2.52-2.42 (m, 2H, Hj), 1.44 (s, 18H, Ha); **δ_C** (101 MHz, $CDCl_3$) 176.4, 176.3 (Ci or Ck), 174.2, 174.0 (Ci or Ck), 171.4 (Ce), 155.4, 155.3 (Cc), 2 × 135.4 (Cm), 128.9, 128.8, 2 × 128.2 (Cn, Co, Cp), 80.5 (Cb), 53.7, 52.9 (Cd), 52.9, 52.7 (Cf), 2 × 42.8 (Cl), 39.3, 38.6 (Ch), 36.1, 35.8 (Cj), 34.7, 34.3 (Cg), 2 × 28.4 (Ca); **HRMS** (ESI) *m/z* found $[M+H]^+$ 423.1576, $C_{20}H_{27}N_2O_6{}^{32}S_1{}^+$ required 423.1584.

2-amino-4,6-divinylpyrimidine (15)

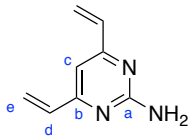

A solution of 2-amino-4,6-dichloropyrimidine (200 mg, 1.22 mmol), potassium vinyltrifluoroborate (490 mg, 3.66 mmol), $Pd(dppf)Cl_2{\cdot}CH_2Cl_2$ (100 mg, 0.122 mmol) and potassium carbonate (1.01 g, 7.32 mmol) in THF/H_2O (10:1, 3.3 mL) was heated to 70 °C for 18 h. Upon completion, the reaction mixture was filtered through Celite® and the solvent removed *in vacuo*. The resulting residue was purified by FCC (20-40% EtOAc/PE) to yield 2-amino-4,6-divinylpyrimidine **15** (152 mg, 1.03 mmol, 85%) as an off-white solid.

R_f 0.29 (SiO_2; 50% EtOAc/PE); **m.p.** 81-83 °C; **ν_{max}** (neat/cm^{-1}) 3213, 1567, 1536, 1415; **δ_H** (500 MHz, DMSO-d_6) 6.81 (s, 1H, Hc), 6.57 (dd, 2H, *J* = 17.4, 10.7 Hz, Hd), 6.54 (s, 2H, NH_2), 6.32 (dd, 2H, *J* = 17.4, 1.5 Hz, He^t), 5.58 (dd, 2H, *J* = 10.7, 1.5 Hz, He^c); **δ_C** (126 MHz, DMSO-d_6) 163.6 (Cb), 163.4 (Ca), 136.1 (Ce), 121.5 (Cd), 104.7 (Cc); **HRMS** (ESI) *m/z* found $[M+H]^+$ 148.0871, $C_8H_{10}N_3{}^+$ required 148.0869.

N-(hex-5-yn-1-yl)-4,6-divinylpyrimidin-2-amine (18)

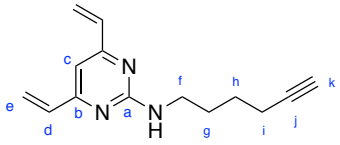

To a solution of amine **15** (50.0 mg, 0.340 mmol) in DMF (1.5 mL) was added 6-iodo-1-hexyne (223 µL, 1.69 mmol) followed by the slow addition of sodium hydride (60% in mineral oil, 68.0 mg, 1.69 mmol). The reaction mixture was stirred at rt for 15 h, then diluted with H_2O (15 mL) and extracted with CH_2Cl_2 (3 × 15 mL). The combined organic fractions were washed with brine, dried ($MgSO_4$) and concentrated *in vacuo*. The crude residue was purified by FCC (20% EtOAc/PE) to yield *N*-(hex-5-yn-1-yl)-4,6-divinylpyrimidin-2-amine **18** (40.0 mg, 0.176 mmol, 52%) as a clear oil.

R_f 0.36 (SiO_2; 25% EtOAc/PE); **ν_{max}** (neat/cm^{-1}) 3298, 2936, 1635, 1539, 1458, 1420; **δ_H** (500 MHz, $CDCl_3$) 6.58 (dd, 2H, *J* = 17.4, 10.6 Hz, Hd), 6.53 (s, 1H, Hc), 6.38 (d, 2H, *J* = 17.4 Hz, He^t), 5.58 (dd, 2H, *J* = 10.6, 1.4 Hz, He^c), 5.29 (s, 1H, NH), 3.51 (q, 2H, *J* = 6.6 Hz, Hf), 2.25 (td, 2H, *J* = 10.5, 2.7 Hz, Hi), 1.95 (t, 1H, *J* = 2.7 Hz, Hk), 1.78-1.72 (m, 2H, Hg), 1.67-1.61 (m, 2H, Hh); **δ_C** (126 MHz, $CDCl_3$) 163.7 (Cb), 162.4 (Ca), 135.8 (Cd), 121.9 (Ce), 105.7 (Cc), 84.4 (Cj), 68.7 (Ck), 41.0 (Cf), 28.9 (Cg), 25.9 (Ch), 18.3 (Ci); **HRMS** (ESI) *m/z* found $[M+H]^+$ 228.1497, $C_{14}H_{18}N_3^+$ required 228.1495.

Ethyl *N*-(4,6-dichloropyrimidin-2-yl)-*N*-methylglycinate (21)

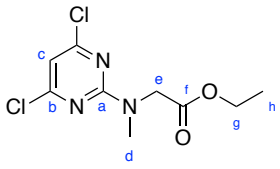

To a solution of 2,4,6-trichloropyrimidine (1.00 g, 5.45 mmol) in acetone (6 mL) at 0 °C was added sarcosine ethyl ester hydrochloride (1.01 g, 6.54 mmol) followed by the slow addition of triethylamine (1.90 mL, 13.6 mmol) and the reaction mixture stirred at 0 °C for 90 min. Upon completion, the solvent was removed *in vacuo* then redissolved in H_2O (20 mL) and extracted with CH_2Cl_2 (4 × 20 mL). The combined organic fractions were dried ($MgSO_4$), concentrated

in vacuo and the crude residue purified by FCC (2-20% EtOAc/PE) to yield ethyl *N*-(4,6-dichloropyrimidin-2-yl)-*N*-methylglycinate **21** (266 mg, 1.01 mmol, 19%) as a white solid.

R_f 0.34 (SiO_2; 10% EtOAc/PE); **m.p.** 40-42 °C; **ν_{max}** (neat/cm^{-1}) 1747, 1567, 1511, 1413, 1198; **δ_H** (400 MHz, $CDCl_3$) 6.59 (s, 1H, Hc), 4.33 (s, 2H, He), 4.21 (q, 2H, *J* = 7.2 Hz, Hg), 3.23 (s, 3H, Hd), 1.28 (t, 3H, *J* = 7.2 Hz, Hh); **δ_C** (101 MHz, $CDCl_3$) 169.5 (Cf), 2 × 161.4 (Ca and Cb), 108.8 (Cc), 61.4 (Cg), 51.4 (Ce), 36.8 (Cd), 14.4 (Ch); **HRMS** (ESI) *m/z* found $[M+H]^+$ 264.0299, $C_9H_{12}{}^{35}Cl_2N_3O_2^+$ required 264.0301.

Ethyl *N*-(4,6-divinylpyrimidin-2-yl)-*N*-methylglycinate (23)

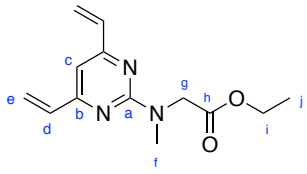

Dichloropyrimidine **21** (204 mg, 0.722 mmol), potassium vinyltrifluoroborate (517 mg, 3.86 mmol), $Pd(dppf)Cl_2{\cdot}CH_2Cl_2$ (94.6 mg, 0.116 mmol) and potassium carbonate (641 mg, 4.63 mmol) in THF/H_2O (10:1, 5.5 mL) were heated to 70 °C for 16 h. Upon completion, the reaction mixture was filtered through Celite® and the solvent removed *in vacuo*. The resulting residue was purified by FCC (0-4% EtOAc/PE) to yield ethyl *N*-(4,6-divinylpyrimidin-2-yl)-*N*-methylglycinate **23** (182 mg, 0.736 mmol, 95%) as a pale yellow oil.

R_f 0.30 (SiO_2; 10% Et OAc/PE); **ν_{max}** (neat/cm^{-1}); 1747, 1560, 1540, 1508, 1401, 1196; **δ_H** (400 MHz, $CDCl_3$) 6.59 (dd, 2H, *J* = 17.2, 10.5 Hz, Hd), 6.49 (s, 1H, Hc), 6.38 (d, 2H, *J* = 17.2 Hz, He^t), 5.53 (dd, 2H, *J* = 10.5, 1.0 Hz, He^c), 4.36 (s, 2H, Hg), 4.18 (q, 2H, *J* = 7.2 Hz, Hi), 3.32 (s, 3H, Hf), 1.23 (t, 3H, *J* = 7.2 Hz, Hj); **δ_C** (101 MHz, $CDCl_3$) 171.1 (Ch), 2 × 162.2 (Ca and Cb), 136.2 (Cd), 121.3 (Ce), 105.7 (Cc), 60.8 (Ci), 51.8 (Cg), 36.6 (Cf), 14.4 (Cj); **HRMS** (ESI) *m/z* found $[M+H]^+$ 248.1397, $C_{13}H_{18}N_3O_2^+$ required 248.1399.

N-(4,6-divinylpyrimidin-2-yl)-*N*-methylglycine (24)

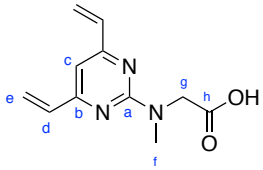

To a solution of ester **23** (40.0 mg, 0.162 mmol) in THF/H_2O (1:1, 2 mL) was added LiOH·H_2O (14.9 mg, 0.178 mmol) and the reaction mixture stirred at rt for 18 h. Upon completion, the mixture was diluted with H_2O (10 mL) and washed with Et_2O (10 mL). The aqueous phase was neutralised with 1M HCl and extracted with CH_2Cl_2 (4 × 20 mL). The combined organic fractions were dried ($MgSO_4$) and concentrated *in vacuo*. The crude residue was triturated with PE to yield *N*-(4,6-divinylpyrimidin-2-yl)-*N*-methylglycine **24** (29.0 mg, 0.132 mmol, 82%) as a pale yellow solid.

m.p. 92-95 °C; ν_{max} (neat/cm^{-1}) 2935, 1705, 1630, 1536, 1395, 1243, 1220; δ_H (400 MHz, CD_3OD) 6.67-6.60 (m, 3H, Hc and Hd), 6.40 (dd, 2H, *J* = 17.4, 1.5 Hz, He^t), 5.55 (dd, 2H, *J* = 10.6, 1.5 Hz, He^c), 4.36 (s, 2H, Hg), 3.28 (s, 3H, Hf); δ_C (101 MHz, CD_3OD) 174.6 (Ch), 164.8 (Cb), 163.4 (Ca), 137.2 (Cd), 121.8 (Ce), 106.1 (Cc), 52.1 (Cg), 36.7 (Cf); **HRMS** (ESI) *m/z* found $[M+H]^+$ 220.1087, $C_{11}H_{14}N_3O_2^+$ required 220.1086.

Dimethyl 3,3'-(((2-aminopyrimidine-4,6-diyl)bis(ethane-2,1-diyl))bis(sulfanediyl))(2*S*,2'*S*)bis(2-((*tert*-butoxycarbonyl)amino)propanoate) (25)

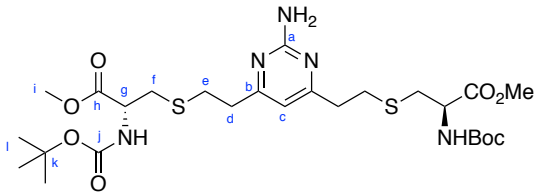

A solution of DVP **15** (10.0 mg, 68.0 µmol), *N*-(*tert*-butoxycarbonyl)-*L*-cysteine methyl ester (40.0 mg, 170 µmol) in 30% MeCN/sodium phosphate buffer (pH 8, 50 mM, 1.36 mL) was stirred at 37 °C for 2 h. Upon completion, the mixture was diluted with H_2O (10 mL), extracted with EtOAc (4 × 10 mL), dried ($MgSO_4$) and concentrated *in vacuo*. The crude residue was

purified by FCC (70% EtOAc/PE) to yield dimethyl 3,3'-(((2-aminopyrimidine-4,6-diyl)bis(ethane-2,1-diyl))bis(sulfanediyl))(2*S*,2'*S*)bis(2-((*tert*-butoxycarbonyl)amino)propanoate) **25** (23.0 mg, 37.0 µmol, 55%) as a clear oil.

R_f 0.33 (SiO_2; 70% EtOAc/PE); **ν_{max}** (neat/cm^{-1}) 3359, 2977, 1742,1703, 1615, 1579, 1560, 1503, 1437; **δ_H** (400 MHz, CD_3OD) 6.54 (s, 1H, Hc), 4.37-4.34 (m, 2H, Hg), 3.73 (s, 6H, Hi), 2.99-2.79 (m, 12H, Hd, He, Hf) 1.44 (s, 18H, Hl); **δ_C** (101 MHz, CD_3OD) 173.2 (Ch), 171.1 (Cb), 164.7 (Ca), 157.8 (Cj), 110.5 (Cc), 80.8 (Ck), 55.1 (Cg), 52.9 (Ci), 38.5 (Cd), 34.6 (Cf), 31.6 (Ce), 28.7 (Cl); **HRMS** (ESI) *m/z* found $[M+H]^+$ 640.2469, $C_{26}H_{43}N_5O_8{}^{32}S_2{}^{23}Na_1{}^+$ required 640.2451.

Dimethyl 3,3'-(((2-(hex-5-yn-1-ylamino)pyrimidine-4,6-diyl)bis(ethane-2,1-diyl))bis(sulfanediyl))(2*R*,2'*R*)-bis(2-((*tert*-butoxycarbonyl)amino)propanoate) (26)

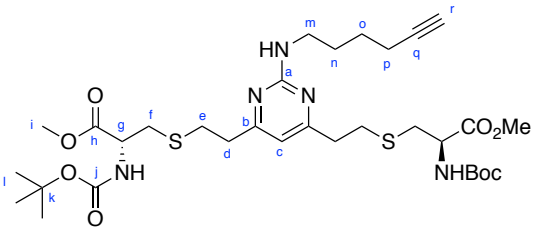

A solution of DVP **18** (10.0 mg, 44.0 µmol), *N*-(*tert*-butoxycarbonyl)-*L*-cysteine methyl ester (25.9 mg, 110 µmol) in 30% MeCN/sodium phosphate buffer (pH 8, 50 mM, 880 µL) was stirred at 37 °C for 1 h. Upon completion, the mixture was diluted with H_2O (10 mL), extracted with CH_2Cl_2 (4 × 10 mL), dried ($MgSO_4$) and concentrated *in vacuo*. The crude residue was purified by FCC (EtOAc) to yield dimethyl 3,3'-(((2-(hex-5-yn-1-ylamino)pyrimidine-4,6-diyl)bis(ethane-2,1-diyl))bis(sulfanediyl))(2*R*,2'*R*)-bis(2-((*tert*-butoxycarbonyl)amino)-propanoate) **26** (28.0 mg, 40.0 µmol, 91%) as a clear oil.

R_f 0.07 (SiO_2; 70% EtOAc/PE); **ν_{max}** (neat/cm^{-1}) 2976, 2344, 1744, 1711, 1642, 1565; **δ_H** (500 MHz, $CDCl_3$) 6.25 (s, 1H, Hc), 5.54-5.41 (m, 2H, 2 × NH), 5.14 (s, 1H, NH), 4.61-4.54 (m, 2H, Hg), 3.74 (s, 6H, Hi), 3.45-3.41 (m, 2H, Hm), 2.98 (d, 4H, *J* = 5.1 Hz, Hf), 2.91-2.86 (m, 4H, Hd), 2.78-2.75 (m, 4H, He), 2.23 (td, 2H, *J* = 10.5, 2.5 Hz, Hp), 1.95 (t, 1H, *J* = 2.5 Hz, Hr), 1.73-1.72 (m, 2H, Hn), 1.65-1.59 (m, 2H, Ho), 1.44 (s, 18H, Hl); **δ_C** (126 MHz, $CDCl_3$) 171.7 (Ch), 168.8 (Cb), 162.7 (Ca), 155.3 (Cj), 108.9 (Cc), 84.4 (Cq), 80.3 (Ck), 68.7 (Cr), 53.5 (Cg),

52.7 (Ci), 40.9 (Cm), 37.7 (Cd), 34.8 (Cf), 31.0 (Ce), 2 × 28.4 (Cn and Cl), 25.9 (Co), 18.3 (Cp); **HRMS** (ESI) *m/z* found $[M+H]^+$ 698.3243, $C_{32}H_{52}N_5O_8{}^{32}S_2{}^+$ required 698.3252.

N-(4,6-bis(2-(((*R*)-2-((*tert*-butoxycarbonyl)amino)-3-methoxy-3-oxopropyl)thio)ethyl)pyrimidin-2-yl)-*N*-methylglycine (27)

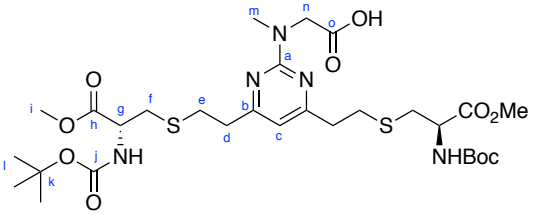

A solution of DVP **24** (5.00 mg, 22.8 µmol), *N*-(*tert*-butoxycarbonyl)-*L*-cysteine methyl ester (13.4 mg, 57.0 µmol) in 30% MeCN/sodium phosphate buffer (pH 8, 50 mM, 456 µL) was stirred at 37 °C for 1 h. Upon completion, the mixture was diluted with H_2O (10 mL), extracted with CH_2Cl_2 (4 × 10 mL), dried ($MgSO_4$) and concentrated *in vacuo*. The crude residue was purified by FCC (70-100% EtOAc/PE then 1% AcOH/EtOAc) to yield *N*-(4,6-bis(2-(((*R*)-2-((*tert*-butoxycarbonyl)amino)-3-methoxy-3-oxopropyl)-thio)ethyl)pyrimidin-2-yl)-*N*-methylglycine **27** (8.60 mg, 12.5 µmol, 55%) as a clear oil.

R_f 0.17 (SiO_2; 70% EtOAc/PE); **ν_{max}** (neat/cm^{-1}) 2974, 1704, 1561, 1509; **δ_H** (500 MHz, CD_3OD) 6.46 (s, 1H, Hc), 4.34-4.32 (m, 4H, Hg and Hn), 3.72 (s, 6H, Hi), 3.24 (s, 3H, Hm), 2.97-2.91 (m, 6H, Hd and Hf), 2.85-2.81 (m, 6H, Hd and He), 1.44 (s, 18H, Hl); **δ_C** (126 MHz, CD_3OD) 174.7 (Co), 173.3 (Ch), 170.1 (Cb), 163.5 (Ca), 157.8 (Cj), 109.6 (Cc), 80.8 (Ck), 55.2 (Cg), 52.8 (Cn), 52.2 (Ci), 38.7 (Cd), 36.7 (Cm), 34.7 (Cf), 31.6 (Ce), 28.7 (Cl); **HRMS** (ESI) *m/z* found $[M+H]^+$ 690.2831, $C_{29}H_{48}N_5O_{10}{}^{32}S_2{}^+$ required 690.2837.

Dox-PEG$_4$-N$_3$ (37)

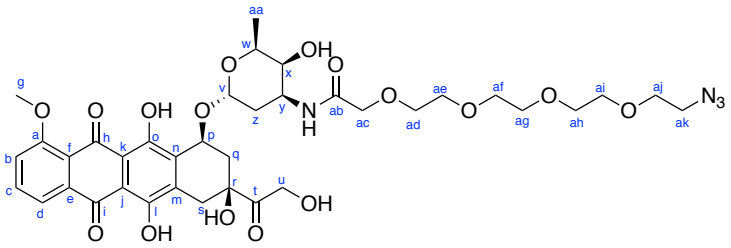

To a solution of doxorubicin hydrochloride (10.9 mg, 20.0 μmol) in DMF (1.10 mL) was added DIPEA (7.00 μL, 40.0 μmol) followed by HBTU (9.10 mg, 24.0 μmol). The mixture was stirred at rt for 5 min. 14-azido-3,6,9,12-tetraoxatetradecanoic acid (N_3-PEG_4-COOH, 0.5 M in TBME, 44.5 μL, 20.0 mmol) was added and the mixture stirred for 3 h. Upon completion, the reaction mixture was diluted with H_2O (10 mL) and the product extracted in CH_2Cl_2 (4 × 10 mL) and dried ($MgSO_4$). The organic fractions were concentrated and the crude residue purified by FCC (5-10% MeOH/EtOAc) to yield Dox-PEG$_4$-N$_3$ **37** (13.5 mg, 16.8 μmol, 84%) as an orange solid.

R_f 0.22 (SiO_2; 10% MeOH/CH_2Cl_2); **ν_{max}** (neat/cm^{-1}) 2922, 2106, 1724, 1654, 1619, 1578, 1535, 1411; **δ_H** (500 MHz, $CDCl_3$) 8.04 (d, 1H, *J* = 7.9 Hz, Hd), 7.78 (t, 1H, *J* = 7.9 Hz, Hc), 7.39 (d, 1H, *J* = 7.9 Hz, Hb), 5.51 (d, 1H, *J* = 3.8 Hz, Hv), 5.30-5.29 (m, 1H, Hp), 4.77 (d, 2H, *J* = 3.1 Hz, Hu), 4.61 (s, 1H, OH), 4.22-4.16 (m, 1H, Hy), 4.13 (q, 1H, *J* = 6.5 Hz, Hw), 4.08 (s, 3H, Hg), 3.93 (m, 2H, 1 × CH_2 of ac-aj), 3.72-3.63 (m, 15H, x and 7 × CH_2 of ac-aj), 3.40 (t, 2H, *J* = 5.0 Hz, ak), 3.28 (dd, 1H, *J* = 18.8, 1.7 Hz, Hs), 3.04 (s, 1H, Hs), 2.37 (d, 1H, *J* = 14.7 Hz, Hq), 2.16 (dd, 1H, *J* = 14.7, 4.0 Hz, Hq), 1.93 (td, 1H, *J* = 19.8, 5.0 Hz, Hz), 1.80 (dd, 1H, *J* = 13.4, 5.0 Hz, Hz), 1.29 (d, 3H, *J* = 6.5 Hz, aa); **δ_C** (126 MHz, $CDCl_3$) 214.1 (Ct), 187.3 (Ch), 186.9 (Ci), 169.4 (Cab), 161.2 (Ca), 156.4 (Co), 155.9 (Cl), 135.9 (Ce), 135.7 (Cc), 133.8 (Cm), 133.8 (Cn), 121.1 (Cf), 120.0 (Cd), 118.6 (Cb), 111.7 (Ck or Cj), 111.5 (Ck or Cj), 101.1 (Cv), 76.8 (under $CDCl_3$ peak, Cr), 71.1, 70.9, 70.7, 70.6, 70.6, 70.4, 70.2, 70.2 (8 × CH_2 of ac-aj), 69.8 (Cp), 69.3 (Cx), 67.6 (Cw), 65.7 (Cu), 56.8 (Cg), 50.8 (Cak), 45.0 (Cy), 35.8 (Cq), 34.1 (Cs), 29.8 (Cz), 17.1 (Caa); **HRMS** (ESI) *m/z* found $[M+H]^+$ 803.2968, $C_{37}H_{47}N_4O_{16}^+$ required 803.2982.

N_3-PEG_4-MMAE (40)

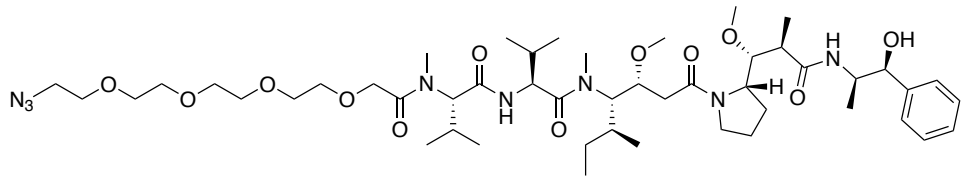

A solution of N_3-PEG_4-COOH (50.0 µL, 25.1 µmol, 0.5 M in TBME, 90%), HBTU (12.7 mg, 33.4 µmol) and DIPEA (17.5 µL, 100 µmol) in DMF (0.5 mL) was stirred at rt for 15 min. To this was added a solution of MMAE (12.0 mg, 16.7 µmol) in DMF (0.5 mL) and the reaction mixture stirred at rt for 18 h. Upon completion, the solvent was removed under a stream of N_2 and the crude residue was purified by FCC (0-5% MeOH/CH_2Cl_2) to yield N_3-PEG_4-MMAE **40** (14.6 mg, 14.9 µmol, 90%) as a clear oil.

R_f 0.48 (SiO_2; 10% MeOH/CH_2Cl_2); **ν_{max}** (neat/cm^{-1}) 3423, 2926, 2109, 1629, 1454, 1098; **δ_H** (500 MHz, $CDCl_3$) 7.77-7.75 (m, 1H), 7.70-7.68 (m, 1H), 7.40-7.37 (m, 2H), 7.31-7.27 (m, 2H), 4.90 (s, 1H), 4.71-4.53 (m, 3H), 4.38-4.20 (m, 3H), 4.16-4.08 (m, 2H), 3.89-3.86 (m, 1H), 3.75-3.63 (m, 13H), 3.52-3.43 (m, 5H), 3.37 (s, 3H), 3.25-3.23 (m, 2H), 3.05-3.00 (m, 2H), 2.94-2.89 (m, 2H), 2.55-2.38 (m, 2H), 2.34-2.20 (m, 2H), 2.11-1.97 (m, 4H), 1.88 (s, 2H), 1.72 (s, 1H), 1.47 (t, 2H, *J* = 6.4 Hz), 1.38 (d, 2H, *J* = 6.5 Hz), 1.25-1.22 (m, 5H), 1.00 (d, 3H, *J* = 7.5 Hz), 0.94-0.71 (m, 18H); **δ_C** (126 MHz, $CDCl_3$) 174.2, 173.3, 171.1, 169.5, 140.3, 128.5, 128.3, 126.7, 126.5, 117.0, 111.6, 82.2, 76.1, 70.2, 69.9, 69.6, 66.8, 61.3, 60.3, 57.8, 54.9, 50.9, 50.5, 50.4, 48.3, 48.1, 46.9, 45.3, 37.4, 32.1, 31.0, 29.9, 26.3, 25.8, 25.2, 23.6, 22.8, 19.4, 19.1, 18.7, 17.5, 17.2, 16.0, 14.9, 10.8, 10.0; **HPLC** (5-95% MeCN/H_2O over 20 min) retention time 11.097 min; **HRMS** (ESI) *m/z* found $[M+Na]^+$ 999.6100, $C_{49}H_{84}N_8O_{12}{}^{23}Na_1{}^+$ required 999.6101.

DVP-PEG$_4$-MMAE (41)

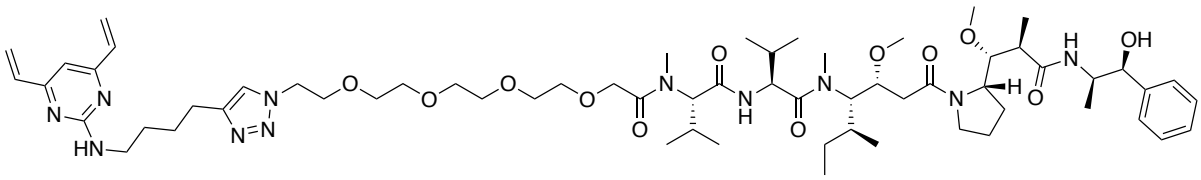

To a degassed solution of azide **40** (4.90 mg, 5.00 μmol) and alkyne **18** (2.30 mg, 10.0 μmol) in CH_2Cl_2 (0.25 mL) was added a degassed solution of $CuSO_4{\cdot}5H_2O$ (1.50 mg, 6.00 μmol), THPTA (4.40 mg, 10.0 μmol) and sodium ascorbate (5.00 mg, 25.0 μmol) in H_2O/tBuOH (0.5 mL, 1:1) and the reaction mixture stirred at rt for 2 h. Upon completion, the reaction was diluted with H_2O (15 mL) and extracted with CH_2Cl_2 (5 × 15 mL). The combined organic fractions were dried ($MgSO_4$), concentrated *in vacuo* and the crude residue purified by FCC (0-10% MeOH/CH_2Cl_2) to yield DVP-PEG$_4$-MMAE **41** (1.80 mg, 1.50 μmol, 30%) as a clear oil.

R_f 0.28 (SiO_2; 7.5% MeOH/CH_2Cl_2); **ν_{max}** (neat/cm^{-1}) 3301, 2926, 1632, 1544, 1452, 1098; **δ_H** (500 MHz, $CDCl_3$) 7.45-7.38 (m, 1H), 7.38-7.37 (m, 2H), 7.34-7.31 (m, 3H), 6.57 (dd, 2H, *J* = 17.2, 10.7 Hz), 6.52 (s, 1H), 6.34 (dd, 2H, *J* = 17.2, 1.4 Hz), 5.55 (dd, 2H, *J* = 10.7, 1.4 Hz), 5.16 (s, 1H), 4.95-4.95 (m, 1H), 4.75-4.71 (m, 1H), 4.69-4.63 (m, 1H), 4.57-4.47 (m, 3H), 4.26-4.23 (m, 2H), 4.18-4.15 (m, 3H), 4.08-4.03 (m, 1H), 3.86-3.83 (m, 3H), 3.76-3.73 (m, 1H), 3.68-3.65 (m, 3H), 3.62-3.58 (m, 9H), 3.52-3.48 (m, 3H), 3.41-3.37 (m, 4H), 3.33-3.33 (m, 1H), 3.30 (s, 3H), 3.14-3.11 (m, 1H), 3.01-2.99 (m, 2H), 2.87-2.85 (m, 2H), 2.77-2.74 (m, 2H), 2.48-2.30 (m, 4H), 2.27-2.21 (m, 2H), 2.11-1.93 (m, 5H), 1.85-1.81 (m, 2H), 1.80-1.75 (m, 2H), 1.72-1.66 (m, 3H), 1.39-1.33 (m, 1H), 1.02 (d, 3H, *J* = 6.7 Hz), 0.96 (d, 3H, *J* = 6.8), 0.91-0.88 (m, 6H), 0.84-0.80 (m, 9H); **δ_C** (126 MHz, $CDCl_3$) 174.7, 170.7, 170.4, 169.7, 169.0, 163.8, 162.8, 148.0, 141.3, 136.1, 128.4, 128.2, 127.4, 126.5, 122.0, 121.5, 105.6, 85.7, 82.1, 75.9, 70.6, 70.2, 69.8, 66.2, 62.6, 61.0, 60.3, 58.1, 54.0, 51.8, 50.2, 47.9, 45.0, 41.2, 37.9, 33.6, 32.0, 31.1, 29.8, 29.4, 27.1, 26.0, 25.6, 25.1, 23.4, 22.8, 19.4, 18.7, 18.0, 16.1, 14.6; **HPLC** (5-95% MeCN/H_2O over 20 min) retention time 10.309 min; **HRMS** (ESI) *m/z* found $[M+Na]^+$ 1226.7502, $C_{63}H_{101}N_{11}O_{12}{}^{23}Na_1{}^+$ required 1226.7523.

Alloc-Val-Ala-PABA-PNP (65)

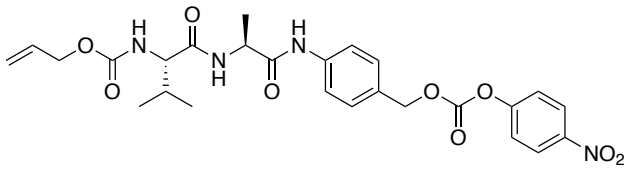

A solution of Alloc-Val-Ala-PABA **43** (100 mg, 0.265 mmol), bis(4-nitrophenyl) carbonate (121 mg, 0.397 mmol) and DIPEA (231 µL, 1.33 mmol) was stirred at rt for 13 h. Upon completion, the mixture was concentrated under a stream of N_2. The crude residue was redissolved in CH_2Cl_2 (20 mL) and saturated aqueous $NaHCO_3$ (25 mL), the layers separated and the aqueous phase extracted with further CH_2Cl_2 (3 × 20 mL). The combined organic fractions were dried ($MgSO_4$) and concentrated to yield Alloc-Val-Ala-PABA-PNP **65** as a pale yellow solid, which was carried forward without further purification.

δ_H (400 MHz, $CDCl_3$) 8.81 (s, 1H), 8.30-8.26 (m, 2H), 7.62 (d, 2H, *J* = 8.3 Hz), 7.40-7.37 (m, 4H), 6.95 (d, 1H, *J* = 7.0 Hz), 5.97-5.88 (m, 1H), 5.46 (d, 1H, *J* = 7.7 Hz), 4.71 (qn, 1H, *J* = 7.1 Hz), 4.65-4.56 (m, 2H), 4.11 (t, 1H, *J* = 6.7 Hz), 2.98 (DMF), 2.91 (DMF), 2.18 (sx, 2H, *J* = 2.2 Hz), 1.49 (d, 3H, *J* = 7.0 Hz), 1.00 (d, 3H, *J* = 7.0 Hz), 0.96 (d, 3H, *J* = 7.0 Hz).

Alloc-Val-Ala-PABC-MMAE (44)

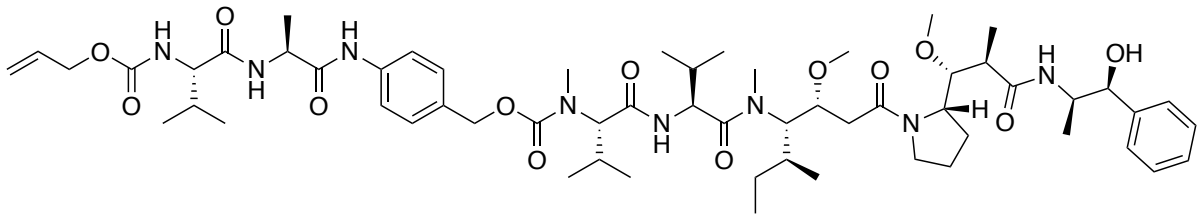

A solution of MMAE (40.0 mg, 74.0 μmol), Alloc-Val-Ala-PAB-PNP **65** (36.0 mg, 50.1 μmol), 1-hydroxybenzotriazole hydrate (HOBt·H_2O, 16.6 mg, 123 μmol) and pyridine (50.0 μL, 614 μmol) in DMF (0.5 mL) was stirred at rt for 2 h. Upon completion, the reaction mixture was concentrated under a stream of N_2 and the crude residue purified by FCC (0-6% MeOH/CH_2Cl_2) to yield Alloc-Val-Ala-PABC-MMAE **44** (49.5 mg, 44.1 μmol, 88%) as a white solid.

HPLC (5-95% MeCN/H_2O over 20 min) retention time 12.237 min; **HRMS** (ESI) *m/z* found $[M+H]^+$ 1121.6819, $C_{59}H_{93}N_8O_{13}^+$ required 1121.6857.

DVP(1C)-Val-Ala-PABC-MMAE (45)

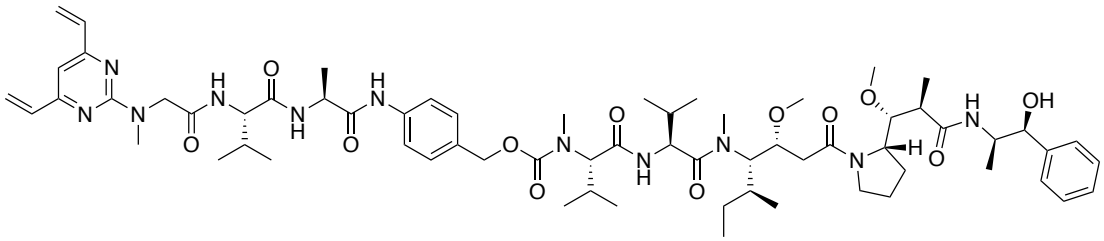

A solution of Alloc-Val-Ala-PABC-MMAE **44** (37.0 mg, 33.0 μmol), $Pd(PPh_3)_4$ (2.00 mg, 1.65 μmol) and pyrrolidine (5.50 μL, 66.0 μmol) in CH_2Cl_2 (0.6 mL) was stirred at rt for 1 h. Upon completion, the reaction mixture was diluted with CH_2Cl_2 (15 mL) and $NaHCO_3$ (sat. aq., 15 mL). The layers were separated and the aqueous phase was extracted with further CH_2Cl_2 (3 × 20 mL). The combined organic fractions were dried ($MgSO_4$), concentrated *in vacuo* and the crude amine **55** carried through without further purification.

HPLC (5-95% MeCN/H_2O over 20 min) retention time 11.795 min. **HRMS** (ESI) *m/z* found $[M+H]^+$ 1037.6610, $C_{55}H_{89}N_8O_{11}^+$ required 1037.6645.

A solution of the deprotected amine **55** (7.50 mg, 7.23 µmol), DVP **24** (4.00 mg, 18.1 µmol), HBTU (5.50 mg, 14.5 µmol), HOBt·H_2O (2.00 mg, 14.5 µmol) and DIPEA (6.30 µL, 36.2 µmol) in DMF (0.5 mL) was stirred at rt for 2 h. Upon completion, the solvent was removed under a stream of N_2 and the crude residue was purified by FCC (0-8% MeOH/CH_2Cl_2) to yield DVP(1C)-Val-Ala-PABC-MMAE **45** (8.00 mg, 6.46 µmol, 89%) as a clear oil.

HPLC (5-95% MeCN/H_2O over 20 min) retention time 12.237 min; **HRMS** (ESI) *m/z* found $[M+H]^+$ 1238.7537, $C_{66}H_{100}N_{11}O_{12}^+$ required 1238.7547.

Ethyl 4-((4,6-dichloropyrimidin-2-yl)amino)butanoate (66)

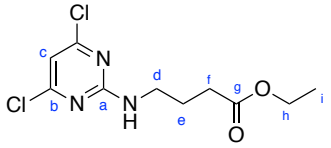

A solution of 2,4,6-trichloropyrimidine (1.00 g, 5.45 mmol), ethyl 4-aminobutyrate hydrochloride (1.10 g, 6.54 mmol) and triethylamine (1.90 mL, 13.6 mmol) in acetone (20 mL) was stirred at 0 °C for 2 h. Upon completion, the reaction was concentrated *in vacuo* and the residue redissolved in H_2O (20 mL) and CH_2Cl_2 (20 mL). The layers were separated and the aqueous phase was extracted with further CH_2Cl_2 (3 × 20 mL). The combined organic fractions were dried ($MgSO_4$), concentrated *in vacuo* and the crude residue purified by FCC (5-30% EtOAc/PE) to yield ethyl 4-((4,6-dichloropyrimidin-2-yl)amino)butanoate **66** (420 mg, 1.51 mmol, 28%) as a white solid.

R_f 0.33 (SiO_2; 20% EtOAc/PE); **ν_{max}** (neat/cm^{-1}) 2981, 1735, 1569, 1513, 1450; **δ_H** (400 MHz, CD_3OD) 6.65 (s, 1H, Hc), 4.12 (q, 2H, *J* = 7.2 Hz, Hh), 3.40 (t, 2H, *J* = 7.0 Hz, Hd), 2.38 (t, 2H, *J* = 7.0 Hz, Hf), 1.89 (t, 2H, *J* = 7.0 Hz, He), 1.24 (t, 3H, *J* = 7.2 Hz, Hi); **δ_C** (101 MHz, CD_3OD) 175.1 (Cg), 163.4 (Ca and Cb), 108.8 (Cc), 61.6 (Ch), 41.6 (Cd), 32.3 (Cf), 25.5 (Ce), 14.5 (Ci); **HRMS** (ESI) *m/z* found $[M+H]^+$ 278.0448, $C_{10}H_{14}{}^{35}Cl_2N_3O_2^+$ required 278.0458.

Ethyl 4-((4,6-divinylpyrimidin-2-yl)amino)butanoate (67)

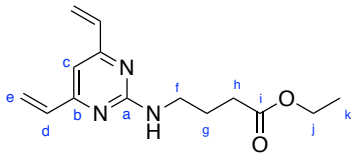

A solution of dichloropyrimidine **66** (200 mg, 0.719 mmol), potassium vinyltrifluoroborate (482 mg, 3.60 mmol), $Pd(dppf)Cl_2 \cdot CH_2Cl_2$ (88.1 mg, 0.108 mmol) and potassium carbonate (596 mg, 4.31 mmol) in THF/H_2O (10:1, 5.5 mL) was heated to 70 °C for 15 h. Upon completion, the reaction mixture was filtered through Celite® and the solvent removed *in vacuo*. The resulting residue was purified by FCC (20% EtOAc/PE) to yield ethyl 4-((4,6-divinylpyrimidin-2-yl)amino)butanoate **67** (181 mg, 0.693 mmol, 96%) as a pale yellow oil.

R_f 0.18 (SiO_2; 20% EtOAc/PE); **ν_{max}** (neat/cm^{-1}) 2971, 1734, 1636, 1543, 1418, 1371; **δ_H** (400 MHz, CD_3OD) 6.69 (s, 1H, Hc), 6.61 (dd, 2H, *J* = 17.4, 10.7 Hz, Hd), 6.37 (d, 2H, *J* = 17.4 Hz, He^t), 5.57 (dd, 2H, *J* = 10.7, 1.5 Hz, He^c), 4.10 (q, 2H, *J* = 7.2 Hz, Hj), 3.48 (t, 2H, *J* = 7.1 Hz, Hf), 2.40 (t, 2H, *J* = 7.1 Hz, Hh), 1.92 (qn, 2H, *J* = 7.1 Hz, Hg), 1.22 (t, 3H, *J* = 7.2 Hz, Hk); **δ_C** (101 MHz, CD_3OD) 175.4 (Ci), 165.3 (Cb), 164.1 (Ca), 137.1 (Cd), 122.0 (Ce), 105.8 (Cc), 61.5 (Cj), 41.5 (Cf), 32.6 (Ch), 26.1 (Cg), 14.5 (Ck); **HRMS** (ESI) *m/z* found $[M+H]^+$ 262.1541, $C_{14}H_{20}N_3O_2^+$ required 262.1550.

4-((4,6-divinylpyrimidin-2-yl)amino)butanoic acid (52)

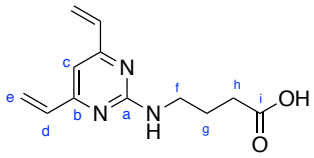

A solution of ester **67** (160 mg, 0.612 mmol) and $LiOH \cdot H_2O$ (56.6 mg, 1.35 mmol) in THF/H_2O (6 mL, 1:1) was stirred at rt for 20 h. Upon completion, the reaction was diluted with H_2O (10 mL) and washed with Et_2O (15 mL) and concentrated *in vacuo*. The residue was suspended in MeOH, filtered and the filtrate concentrated *in vacuo* to yield 4-((4,6-divinylpyrimidin-2-yl)amino)butanoic acid **52** (138 mg, 0.592 mmol, 97%) as a pale yellow solid.

ν_{max} (neat/cm^{-1}) 3311, 2935, 1711, 1636, 1542, 1418, 1348, 1320; δ_H (400 MHz, D_2O) 6.84 (s, 1H, Hc), 6.63 (dd, 2H, *J* = 17.5, 10.9 Hz, Hd), 6.31 (d, 2H, *J* = 17.5 Hz, He^t), 5.71 (d, 2H, *J* = 10.9 Hz, He^c), 3.40 (t, 2H, *J* = 7.3 Hz, Hf), 2.29 (t, 2H, *J* = 7.3 Hz, Hh), 1.88 (qn, 2H, *J* = 7.3 Hz, Hg); δ_C (101 MHz, D_2O) 183.1 (Ci), 164.7 (Cb), 162.3 (Ca), 134.8 (Cd), 123.2 (Ce), 104.7 (Cc), 40.9 (Cf), 35.0 (Ch), 25.8 (Cg); **HRMS** (ESI) *m/z* found $[M+H]^+$ 234.1225, $C_{12}H_{16}N_3O_2^+$ required 234.1237.

DVP(3C)-Val-Ala-PABC-MMAE (47)

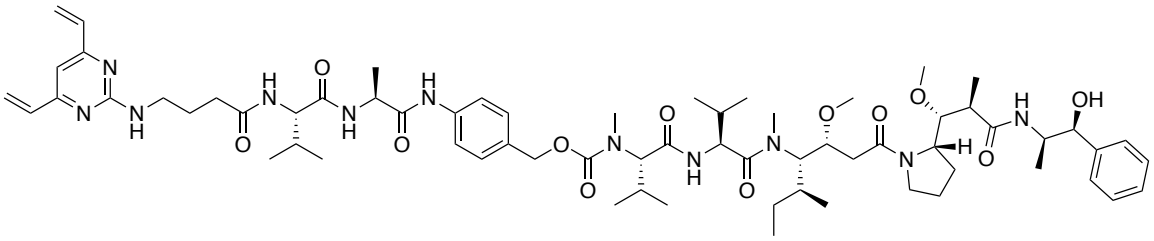

A solution of crude amine **55** (12.0 mg, 11.6 µmol), DVP **52** (6.80 mg, 29.0 µmol), HBTU (8.80 mg, 23.2 µmol), HOBt·H_2O (3.10 mg, 23.2 µmol) and DIPEA (13.6 µL, 58.0 µmol) in DMF (1 mL) was stirred at rt for 16 h. Upon completion, the reaction was concentrated under a stream of N_2 and the crude residue purified by FCC (0-8% MeOH/CH_2Cl_2) to yield DVP(3C)-Val-Ala-PABC-MMAE **47** (4.10 mg, 3.27 µmol, 28%) as a clear oil.

HPLC (5-95% MeCN/H_2O over 20 min) retention time 10.764 min; **HRMS** (ESI) *m/z* found $[M+H]^+$ 1252.7711, $C_{67}H_{102}N_{11}O_{12}^+$ required 1252.7704.

Fmoc-Val-Cit-OH (49)

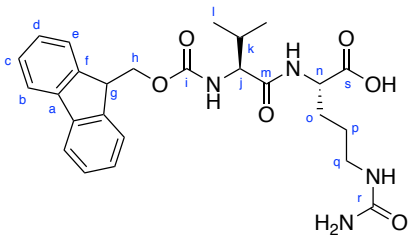

To a solution of Fmoc-Val-OSu (1.00 g, 2.29 mmol) and $NaHCO_3$ (260 mg, 3.09 mmol) in H_2O (7.5 mL) at 0 °C was added a solution of *L*-citrulline (501 mg, 2.87 mmol) in DME (7.5 mL).

THF (4 mL) was added, the reaction warmed to rt and stirred for 28 h. Upon completion, the reaction was adjusted to pH 10 with saturated aqueous K_2CO_3 and washed with EtOAc (2 × 50 mL). The aqueous layer was acidified to pH 4 with 15% aqueous citric acid and the formed gelatinous mixture was filtered. The wet cake was redissolved in THF/MeOH (50 mL), TBME (100 mL) was added and the mixture was stirred at rt for 16 h. The mixture was filtered and the filtrate concentrated *in vacuo* to yield Fmoc-Val-Cit-OH **49** (1.12 g, 2.25 mmol, 98%) as an off-white solid.

$\boldsymbol{\nu_{max}}$ (neat/cm^{-1}) 3385, 2935, 1691, 1641, 1536, 1446, 1342; $\boldsymbol{\delta_H}$ (400 MHz, DMSO-d_6) 7.89 (d, 2H, *J* = 7.7 Hz, Hb), 7.75 (t, 2H, *J* = 7.3 Hz, He), 7.41 (t, 2H, *J* = 7.7 Hz, Hc), 7.34-7.30 (m, 2H, Hd), 5.36 (s, 1H, NH), 4.31-4.19 (m, 3H, Hg and Hh), 4.17-4.13 (m, 1H, Hn), 3.94-3.87 (m, 1H, Hj), 2.97-2.92 (m, 2H, Hq), 1.98 (app sx, 1H, *J* = 6.8 Hz, Hk), 1.74-1.65 (m, 1H, Ho), 1.61-1.52 (m, 1H, Ho), 1.46-1.34 (m, 2H, Hp), 0.89 (d, 3H, *J* = 6.8 Hz, Hl), 0.86 (d, 3H, *J* = 6.8 Hz, Hl); $\boldsymbol{\delta_C}$ (101 MHz, DMSO-d_6) 173.5 (Cs), 171.3 (Cm), 158.8 (Cr), 156.1 (Ci), 144.0 (Ca), 140.7 (Cf), 127.7 (Cc), 127.1 (Cd), 125.4 (Ce), 120.1 (Cb), 65.7 (Ch), 59.9 (Cj), 51.9 (Cn), 46.7 (Cg), 38.8 (Cq), 30.6 (Ck), 28.4 (Co), 26.7 (Cp), 19.2 (Cl), 18.3 (Cl); **HRMS** (ESI) *m/z* found $[M+H]^+$ 497.2394, $C_{26}H_{33}N_4O_6^+$ required 497.2395.

Fmoc-Val-Cit-PABA (50)

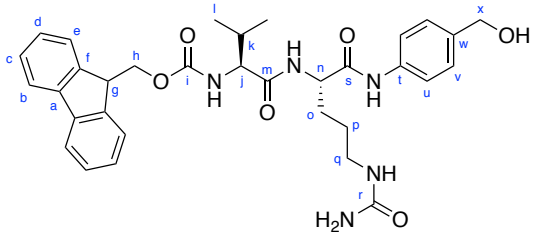

A solution of dipeptide **49** (600 mg, 1.21 mmol), 4-aminobenzyl alcohol (PABA, 298 mg, 2.42 mmol) and 2-ethoxy-1-ethoxycarbonyl-1,2-dihydroquinoline (EEDQ, 598 mg, 2.42 mmol) in CH_2Cl_2/MeOH (12.6 mL, 2:1) was stirred at rt for 21 h. Upon completion, the mixture was diluted with Et_2O (30 mL), sonicaated briefly, filtered and washed with Et_2O to yield Fmoc-Val-Cit-PABA **50** (428 mg, 0.710 mmol, 59%) as an off-white solid.

$\boldsymbol{\nu_{max}}$ (neat/cm^{-1}) 3258, 1691, 1642, 1590, 1538, 1448; $\boldsymbol{\delta_H}$ (400 MHz, DMSO-d_6) 9.98 (s, 1H, NH), 8.12 (d, 1H, *J* = 7.5 Hz, NH), 7.89 (d, 2H, *J* = 7.6 Hz, Hb), 7.74 (t, 2H, *J* = 8.1 Hz, He), 7.54 (d, 2H, *J* = 8.4 Hz, Hu), 7.46-7.39 (m, 3H, Hc and NH), 7.34-7.30 (m, 2H, Hd), 7.23 (d,

2H, *J* = 8.4 Hz, Hv), 6.00 (t, 1H, *J* = 5.8 Hz, NH), 5.41 (s, 2H, NH_2), 5.09 (t, 1H, *J* = 5.5 Hz, OH), 4.43-4.39 (m, 3H, Hn and Hx), 4.33-4.20 (m, 3H, Hg and Hh), 3.95-3.91 (m, 1H, Hj), 3.06-2.89 (m, 2H, Hq), 2.04-1.95 (m, 1H, Hk), 1.74-1.55 (m, 2H, Ho), 1.50-1.32 (m, 2H, Hp), 0.89-0.84 (m, 6H, Hl); **δ_C** (101 MHz, DMSO-d_6) 171.3 (Cm), 170.4 (Cs), 158.9 (Cr), 156.1 (Ci), 143.9, (Ca or Cf), 140.7 (Ca or Cf), 137.5 (Ct or Cw), 137.4 (Ct or Cw), 127.7 (Cc), 127.1 (Cd), 126.9 (Cv), 125.4 (Ce), 120.1 (Cb), 118.9 (Cu), 65.7 (Ch), 62.6 (Cx), 60.1 (Cj), 53.1 (Cn), 46.7 (Cg), 38.6 (Cq), 30.5 (Ck), 29.5 (Co), 26.8 (Cp), 19.2 (Cl), 18.3 (Cl); **HRMS** (ESI) *m/z* found $[M+H]^+$ 602.2968, $C_{33}H_{40}N_5O_6^+$ required 602.2973.

Fmoc-Val-Cit-PABC-MMAE (51)

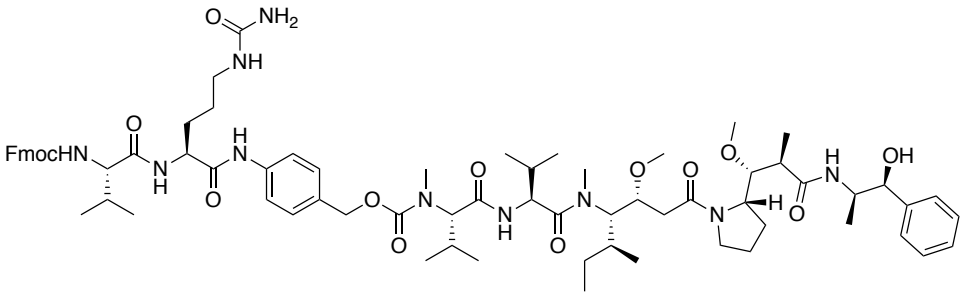

A solution of Fmoc-Val-Cit-PABA **50** (200 mg, 0.332 mmol), bis(4-nitrophenyl) carbonate (202 mg, 0.665 mmol) and DIPEA (86.8 µL, 0.498 mmol) was stirred at rt for 3 h. Upon completion, the mixture was concentrated under a stream of N_2. The crude residue was precipitated with EtOAc (3 mL) and Et_2O (30 mL), allowed to stand for 30 min and then filtered to yield Fmoc-Val-Cit-PAB-PNP as a light brown solid, which was carried through without further purification.

A solution of MMAE (25.0 mg, 34.8 µmol), Fmoc-Val-Cit-PAB-PNP (53.4 mg, 69.6 µmol), HOBt·H_2O (9.40 mg, 69.6 µmol) and pyridine (28.2 µL, 348 µmol) in DMF (1.5 mL) was stirred at rt for 17 h. Upon completion, the reaction mixture was concentrated under a stream of N_2. The crude residue was dissolved in CH_2Cl_2/MeOH (30 mL, 3:2), filtered and the filtrate purified by FCC (0-10% MeOH/CH_2Cl_2) to yield Fmoc-Val-Cit-PABC-MMAE **51** (22.0 mg, 16.4 µmol, 47%) as a white solid.

HPLC (5-95% MeCN/H_2O over 20 min) retention time 13.281 min; **HRMS** (ESI) *m/z* found $[M+H]^+$ 1345.7795, $C_{73}H_{105}N_{10}O_{14}^+$ required 1345.7806.

DVP(3C)-Val-Cit-PABC-MMAE (48)

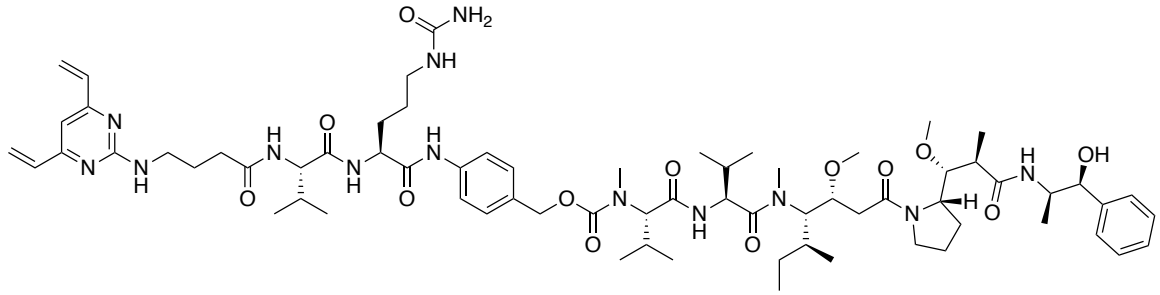

A solution of Fmoc-Val-Cit-PABC-MMAE **51** (20.0 mg, 14.9 μmol) and piperidine (7.40 μL, 74.3 μmol) in DMF (1 mL) was stirred at rt for 2 h. Upon completion, the reaction mixture was concentrated under a stream of N_2 and carried forward without further purification.

A solution of H-Val-Cit-PABC-MMAE (5.00 mg, 4.45 μmol), DVP **52** (2.60 mg, 11.1 μmol), HBTU (3.40 mg, 8.90 μmol), HOBt·H_2O (1.20 mg, 8.90 μmol) and DIPEA (3.90 μL, 22.3 μmol) in DMF (1 mL) was stirred at rt for 14 h. Upon completion, the reaction was concentrated under a stream of N_2 and the crude residue purified by preparative HPLC to yield DVP(3C)-Val-Cit-PABC-MMAE **48** (1.20 mg, 0.896 μmol, 20%) as a white solid.

HPLC (5-95% MeCN/H_2O over 20 min) retention time 10.156 min; **HRMS** (ESI) *m/z* found $[M+H]^+$ 1338.8167, $C_{70}H_{108}N_{13}O_{13}^+$ required 1338.8184.

Fmoc-PEG$_5$-Val-Ala-PABC-MMAE (58)

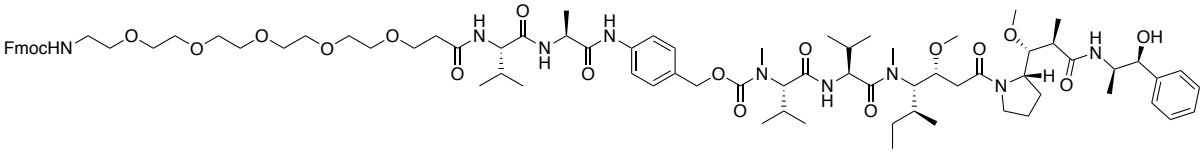

A solution of crude amine **55** (8.00 mg, 7.70 μmol), Fmoc-18-amino-4,7,10,13,16-pentaoxaoctadecanoic (FmocHN-PEG$_5$-COOH, 5.00 mg, 9.30 μmol), HBTU (5.90 mg, 15.4 μmol) and DIPEA (2.70 μL, 15.4 μmol) in DMF (0.5 mL) was stirred at rt for 2 h. Upon completion, the reaction was diluted with H_2O (15 mL) and extracted with CH_2Cl_2 (5 × 10 mL). The combined organic fractions were dried ($MgSO_4$), concentrated *in vacuo* and the crude

residue purified by FCC (0-9% MeOH/CH_2Cl_2) to yield Fmoc-PEG_5-Val-Ala-PABC-MMAE **58** (7.70 mg, 4.97 µmol, 65%) as a clear oil.

HPLC (5-95% MeCN/H_2O over 20 min) retention time 13.203 min; **HRMS** (ESI) *m/z* found $[M+Na]^+$ 1572.8883, $C_{83}H_{123}N_9O_{19}{}^{23}Na_1{}^+$ required 1572.8827.

N_3-PEG_9-Val-Ala-PABC-MMAE (59)

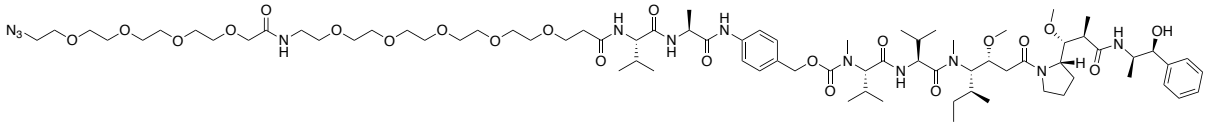

To a solution of protected amine **58** (6.50 mg, 4.20 µmol) in DMF (0.5 mL) was added piperidine (2.10 µL, 21.0 µmol) and the reaction mixture stirred for 22 h at rt. Upon completion, the reaction mixture was concentrated under a stream of N_2 and the crude amine carried forward without further purification.

A solution of the deprotected amine, N_3-PEG_4-COOH (16.8 µL, 8.40 µmol, 0.5 M in TBME, 90%), HBTU (3.20 mg, 8.40 µmol) and DIPEA (1.50 µL, 8.40 µmol) and the reaction mixture stirred at rt for 4 h. Upon completion, the solvent was removed under a stream of N_2 and the crude residue was purified by FCC (0-9% MeOH/CH_2Cl_2) to yield N_3-PEG_9-Val-Ala-PABC-MMAE **59** (6.20 mg, 3.90 µmol, 93%) as a clear oil.

HPLC (5-95% MeCN/H_2O over 20 min) retention time 11.252 min; **HRMS** (ESI) *m/z* found $[M+Na]^+$ 1609.9317, $C_{78}H_{130}N_{12}O_{22}{}^{23}Na_1{}^+$ required 1609.9315.

DVP-PEG$_9$-Val-Ala-PABC-MMAE (60)

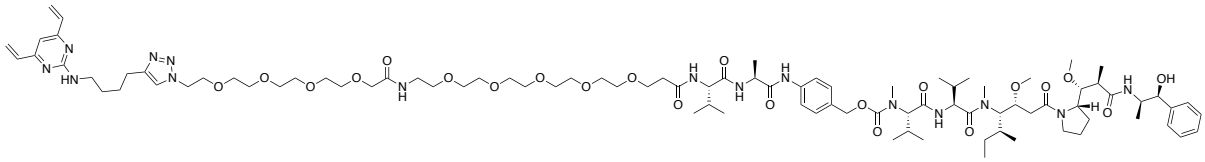

To a degassed solution of azide **59** (5.50 mg, 3.50 µmol) and alkyne **18** (1.60 mg, 7.00 µmol) in CH_2Cl_2 (0.25 mL) was added a degassed solution of $CuSO_4 \cdot 5H_2O$ (1.00 mg, 4.20 µmol), THPTA (3.00 mg, 7.00 µmol) and sodium ascorbate (3.50 mg, 17.5 µmol) in H_2O/tBuOH (0.5 mL, 1:1) and the reaction mixture stirred at rt for 20 h. Upon completion, the reaction was diluted with H_2O (15 mL) and extracted with CH_2Cl_2 (5 × 15 mL). The combined organic fractions were dried ($MgSO_4$), concentrated *in vacuo* and the crude residue purified by FCC (0-10% MeOH/CH_2Cl_2) to yield DVP-PEG$_9$-Val-Ala-PABC-MMAE **60** (6.30 mg, 3.47 µmol, 99%) as a clear oil.

HPLC (5-95% MeCN/H_2O over 20 min) retention time 10.599 min; **HRMS** (ESI) *m/z* found $[M+Na]^+$ 1837.0746, $C_{92}H_{147}N_{15}O_{22}{}^{23}Na^+$ required 1837.0737.

N$_3$-PEG$_4$-Val-Ala-PABC-MMAE (56)

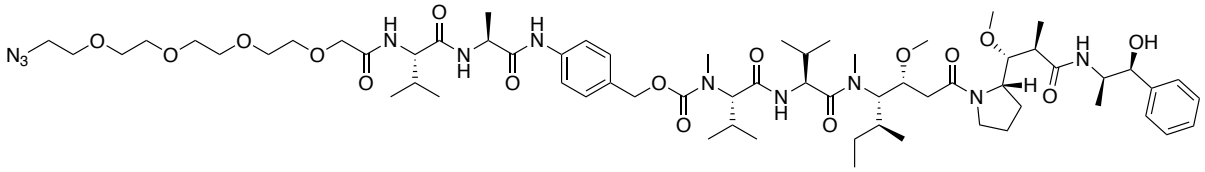

A solution of crude amine **55** (10.5 mg, 10.1 µmol), N$_3$-PEG$_4$-COOH (40.4 µL, 20.2 µmol, 0.5 M in TBME, 90%), HBTU (7.70 mg, 20.2 µmol) and DIPEA (3.50 µL, 20.2 µmol) in DMF (0.5 mL) was stirred at rt for 2 h. Upon completion, the solvent was removed under a stream of N_2 and the crude residue was purified by FCC (0-8% MeOH/CH_2Cl_2) to yield N$_3$-PEG$_4$-Val-Ala-PABC-MMAE **56** (9.10 mg, 7.02 µmol, 70%) as a white solid.

HPLC (5-95% MeCN/H_2O over 20 min) retention time 11.921 min; **HRMS** (ESI) *m/z* found $[M+H]^+$ 1296.7771, $C_{65}H_{106}N_{11}O_{16}{}^+$ required 1296.7814.

DVP-PEG$_4$-Val-Ala-PABC-MMAE (57)

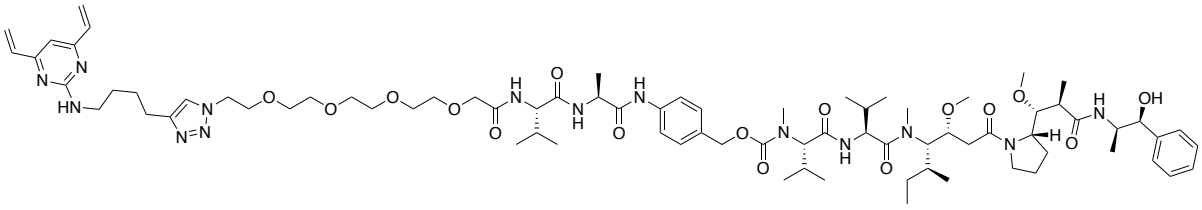

To a degassed solution of azide **56** (8.00 mg, 6.20 μmol) and alkyne **18** (2.80 mg, 12.4 μmol) in CH_2Cl_2 (0.5 mL) was added a degassed solution of $CuSO_4{\cdot}5H_2O$ (1.90 mg, 7.40 μmol), THPTA (5.40 mg, 12.4 μmol) and sodium ascorbate (6.10 mg, 31.0 μmol) in H_2O/tBuOH (1 mL, 1:1) and the reaction mixture stirred at rt for 13 h. Upon completion, the reaction was diluted with H_2O (15 mL) and extracted with CH_2Cl_2 (5 × 15 mL). The combined organic fractions were dried ($MgSO_4$), concentrated *in vacuo* and the crude residue purified by FCC (0-8% MeOH/CH_2Cl_2) to yield DVP-PEG$_4$-Val-Ala-PABC-MMAE **57** (5.60 mg, 3.67 μmol, 59%) as a clear oil.

HPLC (5-95% MeCN/H_2O over 20 min) retention time 10.966 min; **HRMS** (ESI) *m/z* found $[M+H]^+$ 1523.9174, $C_{79}H_{123}N_{14}O_{16}^+$ required 1523.9236.

7.2.2 Monovinylpyrimidine Rate Studies

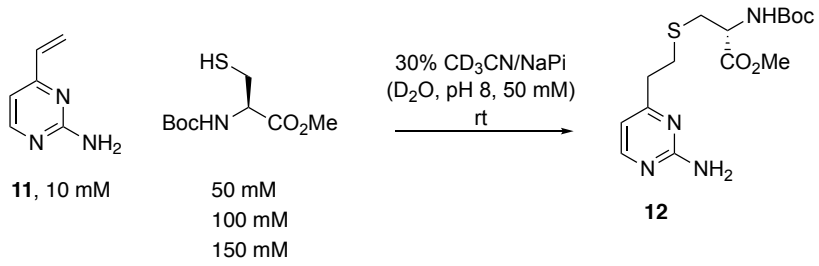

To a solution of amine **11** in 30% CD_3CN/deuterated NaPi (700 μL of a 20 mM stock solution) in an NMR tube was added a solution of *N*-Boc-Cys-OMe in 30% CD_3CN/deuterated NaPi (700 μL of a 100 mM, 200 mM or 300 mM stock solution). A timer was started as the mixture was shaken vigorously and rapidly inserted in a 500 MHz Bruker NMR machine. Scans were recorded every 10 s for up to 700 s.

7.2.3 Monovinylpyrimidine Stability Studies

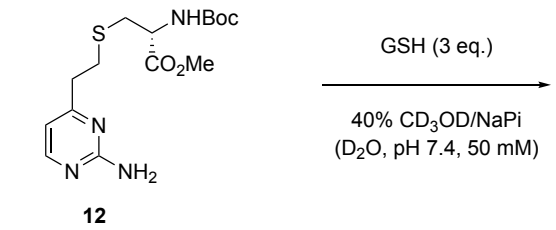

12

To a solution of amine **12** (5.20 mg, 14.6 µmol) in CD_3CN (389 µL) and deuterated NaPi (584 µL, 50 mM, pH 7.4) was added reduced *L*-glutathione (13.4 mg, 43.7 µmol). The mixture was incubated at rt and analysed by ^1H NMR at 24 h intervals for 14 days.

7.2.4 Maleimide Stability Studies

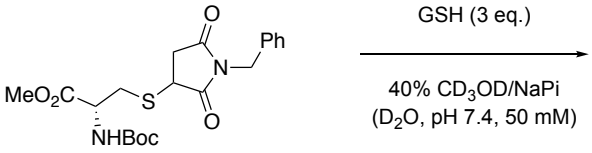

13

To a solution of succinimide **13** (5.90 mg, 14.0 µmol) in CD_3CN (400 µL) and deuterated NaPi (600 µL, 50 mM, pH 7.4) was added reduced *L*-glutathione (12.9 mg, 42.0 µmol). The mixture was incubated at rt and analysed by ^1H NMR at 24 h intervals for 14 days.

7.2.5 Monovinylpyrimidine Chemoselectivity Studies

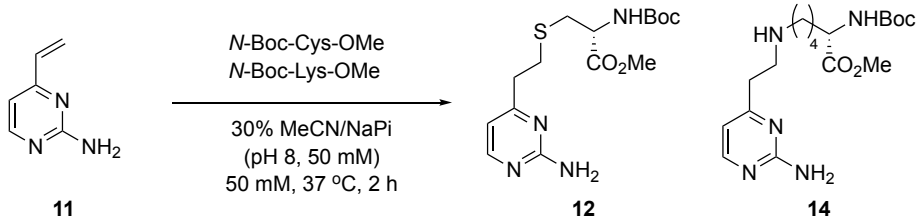

11 **12** **14**

A solution of amine **11** (12.0 mg, 99.0 µmol), *N*-Boc-Cys-OMe (7.80 mg, 33.0 µmol) and *N*-Boc-Lys-OMe·HCl (9.70 mg, 33.0 µmol) in 30% MeCN/NaPi (1.98 mL, 50 mM, pH 8) was stirred at 37 °C for 2 h. Aliquots were removed from the reaction at 0 and 2 h and analysed by HPLC.

7.2.6 Divinylpyrimidine Stability

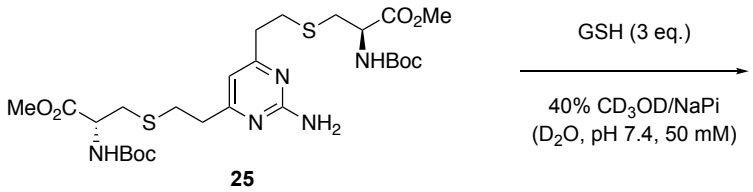

25

To a solution of amine **25** (4.70 mg, 7.61 μmol) in CD_3CN (280 μL) and deuterated NaPi (420 μL, 50 mM, pH 7.4) was added reduced *L*-glutathione (7.00 mg, 22.8 μmol). The mixture was incubated at rt and analysed by ^1H NMR at 24 h intervals for 14 days.

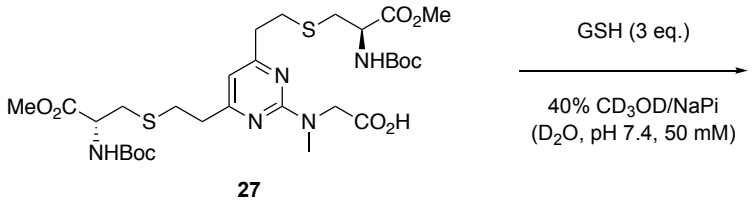

27

To a solution of carboxylic acid **27** (4.00 mg, 5.80 μmol) in CD_3OD (309 μL) and deuterated NaPi (464 μL, 50 mM, pH 7.4) was added reduced *L*-glutathione (5.40 mg, 17.4 μmol). The mixture was incubated at rt and analysed by ^1H NMR at 24 h intervals for 14 days.

7.2.7 Divinylpyrimidine Chemoselectivity Studies

2-amino-4,6-divinylpyrimidine (15)

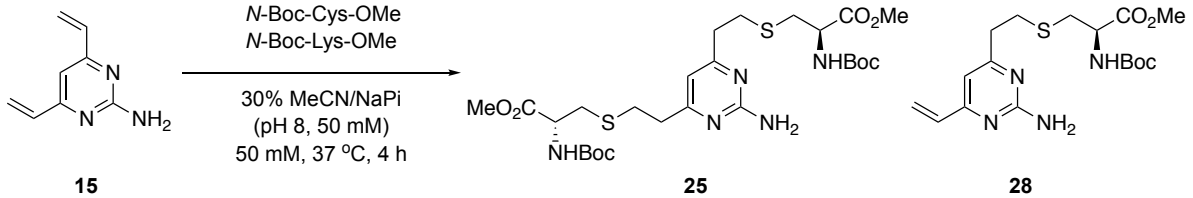

15 **25** **28**

A solution of amine **15** (4.00 mg, 27.0 μmol), *N*-Boc-Cys-OMe (2.10 mg, 9.10 μmol) and *N*-Boc-Lys-OMe·HCl (2.70 mg, 9.10 μmol) in 30% MeCN/NaPi (540 μL, 50 mM, pH 8) was stirred at 37 °C for 4 h. Aliquots were removed from the reaction at 0, 2 and 4 h and analysed by HPLC and LCMS.

N-(hex-5-yn-1-yl)-4,6-divinylpyrimidin-2-amine (18)

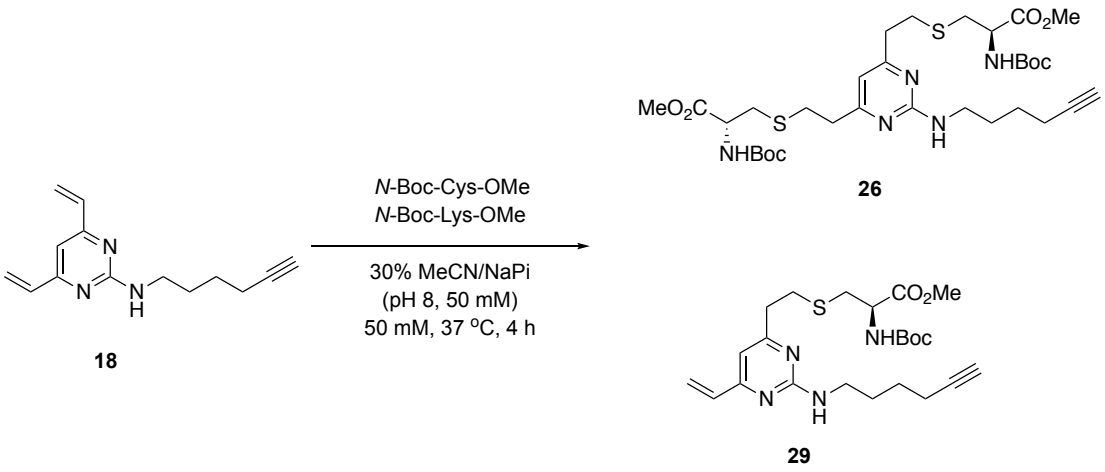

A solution of alkyne **18** (2.70 mg, 11.9 μmol), *N*-Boc-Cys-OMe (1.00 mg, 4.00 μmol) and *N*-Boc-Lys-OMe·HCl (1.20 mg, 4.00 μmol) in 30% MeCN/NaPi (238 μL, 50 mM, pH 8) was stirred at 37 °C for 4 h. Aliquots were removed from the reaction at 0, 2 and 4 h and analysed by HPLC and LCMS.

N-(4,6-divinylpyrimidin-2-yl)-*N*-methylglycine (24)

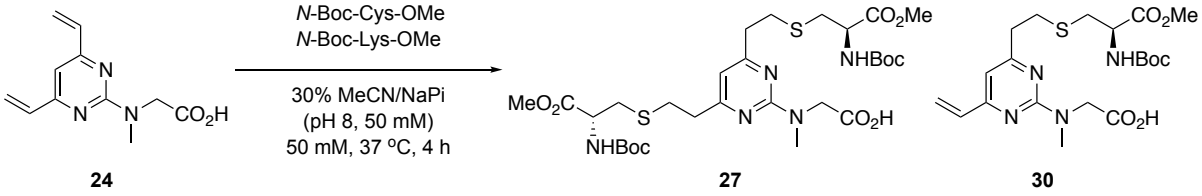

A solution of carboxylic acid **24** (4.00 mg, 18.2 μmol), *N*-Boc-Cys-OMe (1.50 mg, 6.10 μmol) and *N*-Boc-Lys-OMe·HCl (1.80 mg, 6.10 μmol) in 30% MeCN/NaPi (364 μL, 50 mM, pH 8) was stirred at 37 °C for 4 h. Aliquots were removed from the reaction at 0, 2 and 4 h and analysed by HPLC and LCMS.

7.3 Chapter 5: Dual-functional Divinylpyrimidine

7.3.1 Synthetic Procedures

Ethyl 4-(hex-5-yn-1-ylamino)butanoate (69)

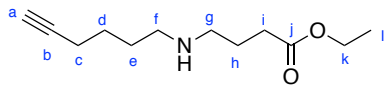

A solution of sulfur trioxide pyridine complex (2.44 g, 15.3 mmol) and pyridine (1.24 mL, 15.3 mmol) in CH_2Cl_2 (5 mL) was stirred at rt for 5 min. To this solution was added DIPEA (2.67 mL, 15.3 mmol) and DMSO (3.62 mL, 51.0 mmol) and stirred at rt for 5 min. The mixture was cooled to –40 °C and to this was added 5-heyn-1-ol (500 mg, 5.10 mmol). The reaction was stirred for 2 h warming slowly to –20 °C. Upon completion, the reaction was acidified to pH 3 with 1 M HCl and diluted with CH_2Cl_2 (10 mL). The layers were separated and the aqueous phase was extracted with further CH_2Cl_2 (2 × 20 mL). The combined organic fractions were washed with brine (2 × 50 mL), dried ($MgSO_4$) and concentrated *in vacuo*. The crude oil was immediately redissolved in MeOH (4 mL). A separate solution of ethyl 4-aminobutyrate hydrochloride (1.28 g, 7.65 mmol), triethylamine (1.07 mL, 7.65 mmol) and 4 Å molecular sieves in CH_2Cl_2 (12 mL) was stirred at rt for 5 min. To this solution was added the aldehyde (**68**) solution, followed by $NaBH(OAc)_3$ (3.24 g, 15.3 mmol) and the reaction mixture stirred at room temperature for 3 h. Upon completion, the reaction mixture was filtered, diluted with $NaHCO_3$ (sat. aq., 15 mL) and extracted with CH_2Cl_2 (3 × 25 mL). The combined organic layers were washer with brine (50 mL), dried ($MgSO_4$) and concentrated *in vacuo*. The crude residue was purified by FCC (0-12% MeOH/CH_2Cl_2) to yield ethyl 4-(hex-5-yn-1-ylamino)butanoate **69** (430 mg, 2.04 mmol, 40%) as a clear oil.

R_f 0.16 (SiO_2; 10% MeOH/CH_2Cl_2); **ν_{max}** (neat/cm^{-1}) 3455, 2931, 2148, 1730, 1660; **δ_H** (400 MHz, CD_3OD) 4.12 (q, 2H, *J* = 7.1 Hz, Hk), 2.64-2.59 (m, 4H, Hf and Hg), 2.36 (t, 2H, *J* = 7.5 Hz, Hi), 2.23-2.19 (m, 3H, Ha and Hc), 1.81 (qn, 2H, *J* = 7.5 Hz, Hh), 1.68-1.51 (m, 4H, Hd and He), 1.25 (t, 3H, *J* = 7.1 Hz, Hl); **δ_H** (101 MHz, CD_3OD) 175.1 (Cj), 84.7 (Cb), 69.7 (Ca), 61.5 (Ck), 50.0 (Cf or Cg), 49.8 (Cf or Cg), 32.8 (Ci), 29.3 (Cd or Ce), 27.4 (Cd or Ce), 25.5 (Ch), 18.9 (Cc), 14.5 (Cl); **HRMS** (ESI) *m/z* found $[M+H]^+$ 212.1647, $C_{12}H_{22}N_1O_2^+$ required 212.1645.

Ethyl 4-((4,6-dichloropyrimidin-2-yl)(hex-5-yn-1-yl)amino)butanoate (70)

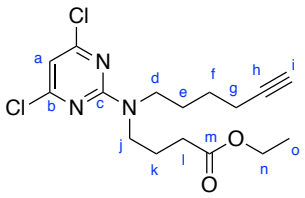

A solution of 2,4,6-trichloropyrimidine (327 µL, 2.84 mmol), amine **69** (720 mg, 3.41 mmol) and triethylamine (792 µL, 5.68 mmol) in acetone (10 mL) was stirred at 0 °C for 2 h. Upon completion, the reaction was concentrated *in vacuo* and the residue redissolved in H_2O (10 mL), $NaHCO_3$ (sat. aq., 10 mL) and CH_2Cl_2 (20 mL). The layers were separated and the aqueous phase was extracted with further CH_2Cl_2 (3 × 20 mL). The combined organic fractions were dried ($MgSO_4$), concentrated *in vacuo* and the crude residue purified by FCC (0-40% EtOAc/PE) to yield ethyl 4-((4,6-dichloropyrimidin-2-yl)(hex-5-yn-1-yl)amino)butanoate **70** (353 mg, 0.985 mmol, 35%) as a white solid.

R_f 0.44 (SiO_2; 20% EtOAc/PE); **ν_{max}** (neat/cm^{-1}) 3302, 2945, 2175, 1729, 1571, 1529; **δ_H** (400 MHz, CD_3OD) 6.64 (s, 1H, Ha), 4.11 (q, 2H, *J* = 7.1 Hz, Hn), 3.60 (qn, 4H, *J* = 7.2 Hz, Hd and Hj), 2.35 (t, 2H, *J* = 7.2 Hz, Hl), 2.26-2.20 (m, 3H, Hg and Hi), 1.93 (qn, 2H, *J* = 7.2 Hz, Hk), 1.78-1.70 (m, 2H, He), 1.52 (qn, 2H, *J* = 7.2 Hz, Hf), 1.24 (t, 3H, *J* = 7.1 Hz, Ho); **δ_H** (101 MHz, CD_3OD) 174.9 (Cm), 162.8 (Cb or Cc), 162.3 (Cb or Cc), 108.2 (Ca), 84.7 (Ch), 69.8 (Ci), 61.6 (Cn), 48.3 (Cd or Cj), 48.0 (Cd or Cj), 32.2 (Cl), 27.5 (Ce), 26.8 (Cf), 23.8 (Ck), 18.8 (Cg), 14.5 (Co); **HRMS** (ESI) *m/z* found $[M+H]^+$ 358.1086, $C_{16}H_{22}{}^{35}Cl_2N_3O_2^+$ required 358.1084.

Ethyl 4-((4,6-divinylpyrimidin-2-yl)(hex-5-yn-1-yl)amino)butanoate (71)

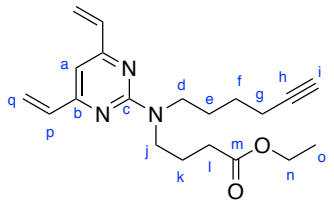

A solution of dichloropyrimidine **70** (23.0 mg, 64.2 µmol), potassium vinyltrifluoroborate (43.0 mg, 321 µmol), $Pd(dppf)Cl_2{\cdot}CH_2Cl_2$ (8.00 mg, 9.63 µmol) and potassium carbonate (53.0 mg, 385 µmol) in THF/H_2O (10:1, 1.1 mL) was heated to 70 °C for 20 h. Upon completion, the reaction mixture was filtered through Celite® and the solvent removed *in vacuo*. The resulting residue was purified by FCC (5% EtOAc/PE) to yield ethyl 4-((4,6-divinylpyrimidin-2-yl)(hex-5-yn-1-yl)amino)butanoate **71** (11.5 mg, 33.7 µmol, 53%) as a pale yellow oil.

R_f 0.51 (SiO_2; 15% EtOAc/PE); **ν_{max}** (neat/cm^{-1}) 2935, 2194, 1736, 1543; **δ_H** (400 MHz, CD_3OD) 6.62 (dd, 2H, *J* = 17.3, 10.5 Hz, Hp), 6.56 (s, 1H, Ha), 6.39 (dd, 2H, *J* = 17.3, 1.8 Hz, Hq^t), 5.52 (dd, 2H, *J* = 10.5, 1.8 Hz, Hq^c), 4.09 (q, 2H, *J* = 7.2 Hz, Hn), 3.70-3.63 (m, 4H, Hd and Hj), 2.36-2.33 (m, 2H, Hl), 2.26-2.21 (m, 2H, Hg), 2.18 (t, 1H, *J* = 2.7 Hz, Hi), 2.01-1.93 (m, 2H, Hk), 1.80-1.64 (m, 2H, He), 1.58-1.50 (m, 2H, Hf), 1.21 (t, 3H, *J* = 7.2 Hz, Ho); ; **δ_C** (101 MHz, CD_3OD) 175.3 (Cm), 164.8 (Cb), 163.1 (Cc), 137.5 (Cp), 121.3 (Cq), 105.5 (Ca), 84.9 (Ch), 69.6 (Ci), 61.5 (Cn), 48.0 (Cd or Cj), 47.7 (Cd or Cj), 32.5 (Cl), 27.9 (Ce), 27.1 (Cf), 24.3 (Ck), 18.9 (Cg), 14.5 (Co); **HRMS** (ESI) *m/z* found $[M+H]^+$ 342.2189, $C_{20}H_{28}N_3O_2^+$ required 342.2182.

4-((4,6-divinylpyrimidin-2-yl)(hex-5-yn-1-yl)amino)butanoic acid (72)

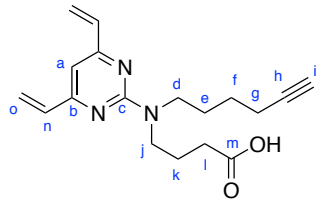

A solution of ester **71** (8.00 mg, 23.4 μmol) and $LiOH{\cdot}H_2O$ (4.00 mg, 93.8 μmol) in THF/H_2O (0.5 mL, 1:1) was stirred at rt for 21 h. Upon completion, the reaction was diluted with H_2O (10 mL) and washed with Et_2O (10 mL). The aqueous phase was neutralised with 1M HCl and extracted with CH_2Cl_2 (4 × 20 mL). The combined organic fractions were dried ($MgSO_4$) and concentrated *in vacuo* to yield 4-((4,6-divinylpyrimidin-2-yl)(hex-5-yn-1-yl)amino)butanoic acid **72** (6.30 mg, 20.1 μmol, 86%) as a pale yellow oil.

$\boldsymbol{\nu_{max}}$ (neat/cm^{-1}) 2927, 2117, 1705, 1539; $\boldsymbol{\delta_H}$ (400 MHz, CD_3OD) 6.62 (dd, 2H, *J* = 17.3, 10.6 Hz, Hn), 6.56 (s, 1H, Ha), 6.40 (dd, 2H, *J* = 17.3, 1.8 Hz, Ho^t), 5.52 (dd, 2H, *J* = 10.6, 1.8 Hz, Ho^c), 3.68 (q, 4H, *J* = 7.2 Hz, Hd and Hj), 2.33 (t, 2H, *J* = 7.2 Hz, Hl), 2.23 (td, 2H, *J* = 10.5, 2.6 Hz, Hg), 2.18 (t, 1H, *J* = 2.6 Hz, Hi), 1.95 (qn, 2H, *J* = 7.2 Hz, Hk), 1.81-1.74 (m, 2H, He), 1.55 (qn, 2H, *J* = 7.2 Hz, Hf); $\boldsymbol{\delta_H}$ (101 MHz, CD_3OD) 178.2 (Cm), 164.8 (Cb), 163.1 (Cc), 137.5 (Cn), 121.3 (Co), 105.4 (Ca), 84.9 (Ch), 69.6 (Ci), 48.1 (Cd or Cj), 47.9 (Cd or Cj), 32.3 (Cl), 28.0 (Ce), 27.1 (Cf), 24.4 (Ck), 18.9 (Cg); **HRMS** (ESI) *m/z* found $[M+H]^+$ 314.1873, $C_{18}H_{24}N_3O_2^+$ required 314.1869.

df-DVP-alkyne-PEG$_5$-Val-Ala-PABC-MMAE (74)

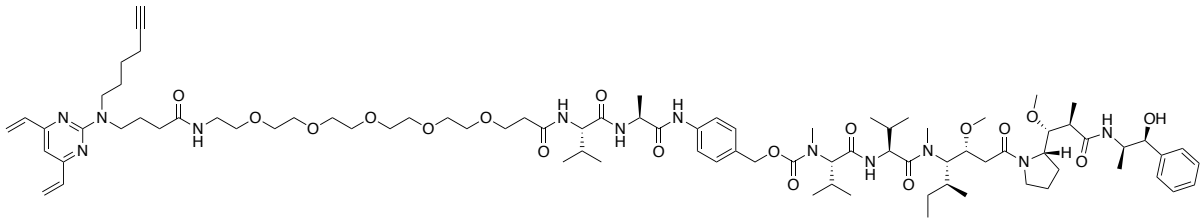

To a solution of protected amine **58** (9.30 mg, 6.00 μmol) in DMF (0.5 mL) was added piperidine (2.10 μL, 21.0 μmol) and the reaction mixture stirred for 22 h at rt. Upon completion, the reaction mixture was concentrated under a stream of N_2 and the crude amine carried forward without further purification.

A solution of crude amine, df-DVP **72** (3.80 mg, 12.0 μmol), HBTU (4.60 mg, 12.0 μmol), HOBt·H_2O (2.00 mg, 12.0 μmol) and DIPEA (2.10 μL, 12.0 μmol) was stirred at rt for 2 h. Upon completion, the reaction was diluted with H_2O (15 mL) and extracted with CH_2Cl_2 (5 × 15 mL). The combined organic fractions were washed with brine, dried ($MgSO_4$), concentrated *in vacuo* and the crude residue purified by FCC (0-8% MeOH/CH_2Cl_2) to yield df-DVP-alkyne-PEG$_5$-Val-Ala-PABC-MMAE **74** (3.90 mg, 2.40 μmol, 40%) as a clear oil.

HPLC (5-95% MeCN/H_2O over 20 min) retention time 12.056 min; **HRMS** (ESI) *m/z* found $[M+H]^+$ 1623.9996, $C_{86}H_{135}N_{12}O_{18}^+$ required 1624.0012.

df-DVP-acid-PEG$_4$-Val-Ala-PABC-MMAE (76)

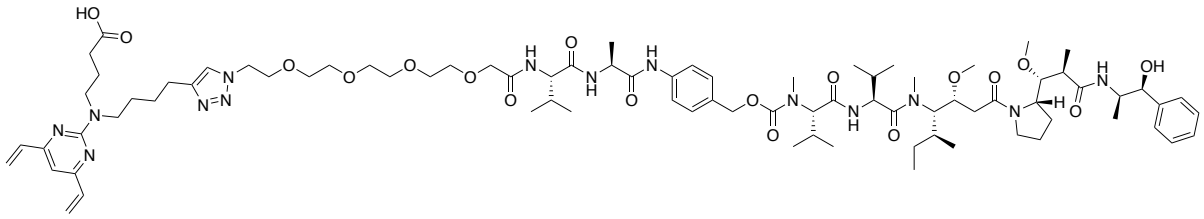

To a degassed solution of azide **56** (25.0 mg, 19.3 μmol) and alkyne **72** (12.1 mg, 38.6 μmol) in CH_2Cl_2 (1 mL) was added a degassed solution of $CuSO_4·5H_2O$ (5.80 mg, 23.2 μmol), THPTA (16.8 mg, 38.6 μmol) and sodium ascorbate (19.2 mg, 96.5 μmol) in H_2O/^{t}BuOH (2 mL, 1:1) and the reaction mixture stirred at rt for 16 h. Upon completion, the solvent was

removed under a stream of N_2 and the crude residue purified by FCC (0-10% MeOH/CH_2Cl_2) to yield df-DVP-acid-PEG_4-Val-Ala-PABC-MMAE **76** (17.1 mg, 10.6 µmol, 55%) as a clear oil.

HPLC (5-95% MeCN/H_2O over 20 min) retention time 11.320 min; **HRMS** (ESI) *m/z* found $[M+H]^+$ 1609.9619, $C_{83}H_{129}N_{14}O_{18}^+$ required 1609.9604.

df-DVP-amide-alkyne-PEG_4-Val-Ala-PABC-MMAE (77)

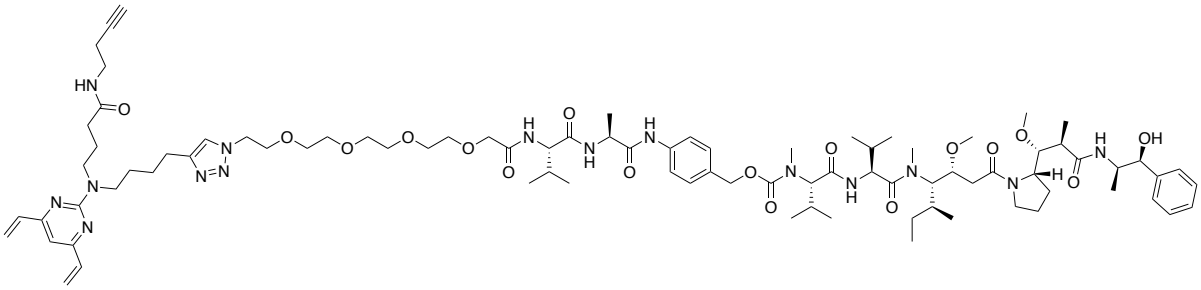

A solution of carboxylic acid **76** (6.30 mg, 3.90 µmol), but-3-ynylamine hydrochloride (0.800 mg, 7.80 µmol), HBTU (3.00 mg, 7.80 µmol), HOBt·H_2O (1.30 mg, 7.80 µmol) and DIPEA (1.40 µL, 7.80 µmol) was stirred at rt for 4 h. Upon completion, the reaction was diluted with H_2O (15 mL) and extracted with CH_2Cl_2 (5 × 20 mL). The combined organic fractions were dried ($MgSO_4$), concentrated *in vacuo* and the crude residue purified by FCC (0-8% MeOH/CH_2Cl_2) to yield df-DVP-amide-alkyne-PEG_4-Val-Ala-PABC-MMAE **77** (3.40 mg, 2.05 µmol, 53%) as a clear oil.

HPLC (5-95% MeCN/H_2O over 20 min) retention time 11.154 min; **HRMS** (ESI) *m/z* found $[M+H]^+$ 1661.0027, $C_{87}H_{134}N_{15}O_{17}^+$ required 1661.0077.

7.4 Protein Chemistry

7.4.1 Chapter 3: Divinylpyridine

*Pf*RadA-dCys Preparation

Synthetic DNA Production

The synthetic gene of the *Pf*RadA *C*-terminal ATPase domain containing the desired cysteine mutations was constructed from DNA oligos using overlap-extension PCR. Oligos of approximately 25 bases (Sigma) were designed to include the cysteine mutations. Primers were present in the polymerase chain reaction (PCR) at a concentration of 1 µg/µL. PCR was conducted with Phusion polymerase (Thermo Scientific), and products were purified from agarose gel using a Gel Extraction kit (Qiagen). PCR products and pBAT4 vector were digested using *NcoI* and *XhoI* (New England Biolabs) for at least two hours at 37 °C, dephosphorylated with Shrimp alkaline phosphatase (SAP) (Agilent Technologies) and gel purified. The gene insert was ligated into the plasmid using a Quick Ligase Kit (New England Biolabs). The construct was then transformed into DH5α strain *E. coli* by heat shock at 42 °C. Transformants were selected using 100 µg/mL ampicillin in Luria-Bertani (LB) medium. Plasmid was extracted from 2 mL overnight cell cultures using a Miniprep Spin kit (Qiagen). The insert was verified by restriction digest analysis and DNA sequencing.

Expression and Purification

The plasmids containing the desired insert were transformed into the BL21(DE3)-pUBS520 strain of *E. coli* and soluble expression of mutated proteins was confirmed in a small scale expression test. For large scale expression, cells were streaked from previously stored glycerol stocks on ampicillin- and kanamycin-supplemented LB agar plates. Colonies were grown overnight at 37 °C and used to inoculate 1 L cultures of LB media with ampicillin (100 µg/mL) and kanamycin (25 µg/mL). After 4.5 hours incubation at 37 °C (OD_{600} = 0.7 – 1.0), cells were induced with IPTG (400 mM). Further incubation at 37 °C was carried out for 3 hours, followed by centrifugation of the cultures. The cell pellet was resuspended in 20 mM MES pH 6.0. Cells were lysed using EmulsiFlex C5 homogeniser (Avestin). The cell lysate was heated to 65 °C for 10 minutes followed by centrifugation. The clarified supernatant was loaded onto a 5 mL HiTrap SP-Sepharose HP column using an ÄKTA purifier 10

chromatography system (GE Healthcare). The protein was eluted using ion exchange elution buffer (20 mM MES pH 6.0, 0.5 mM EDTA, 1 M NaCl) gradient of 0 – 0.5 M NaCl. Appropriate fractions were concentrated to 2 mL using an Amicon-Ultra centrifugal filter (10000 MWCO, Merck Millipore). To the concentrated sample was added TCEP (~180 µL, 10% v/v) which was subsequently loaded onto a Superdex 75 16/60 gel filtration (GF) column equilibrated with GF buffer (20 mM MES pH 6.0, 1 mM EDTA, 100 mM NaCl, 0.1 mM TCEP) using an ÄKTA purifier 10 chromatography system. The protein was eluted using GF buffer. Fractions containing purified *Pf*RadA-dCys were concentrated to 2 mL using an Amicon-Ultra centrifugal filter (10000 MWCO, Merck Millipore) and protein purity analysed by 15% SDS-PAGE.

*Pf*RadA-dCys 5 modification

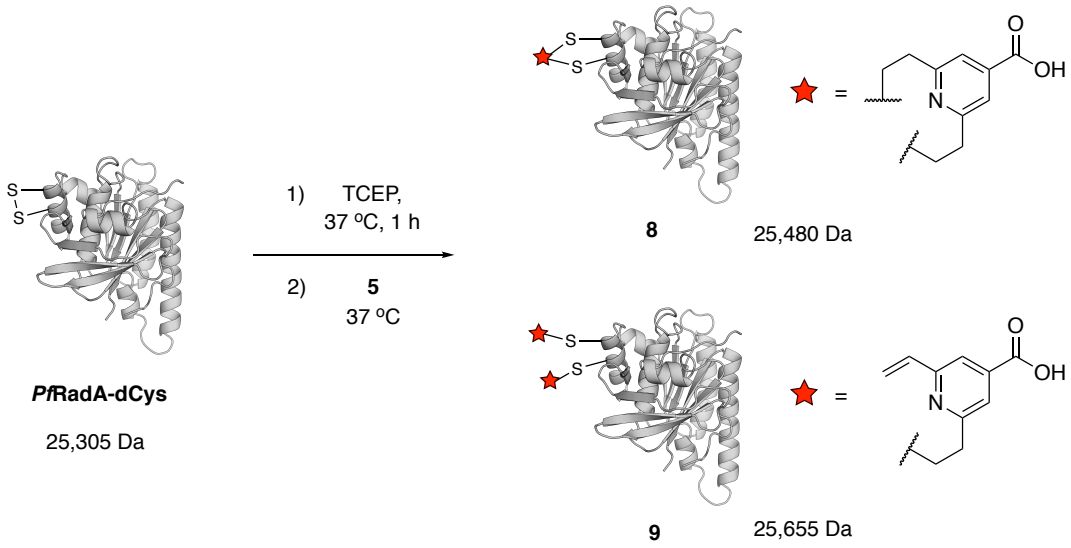

To a solution of *Pf*RadA-dCys (15 µL, 2.94 mg/mL) in TBS (50 mM Tris HCl pH 8, 100 mM NaCl) was added TCEP (5 eq.). The mixture was vortexed and incubated at 37 °C for 1 h. A solution of **5** (10 mM in DMSO) was added (35 eq.), the reaction adjusted to 5% DMSO (v/v) and the reaction mixture incubated at 37 °C for 4 h. An aliquot was removed from the reaction, diluted with PBS and analysed by LCMS.

Trastuzumab modification

Ellman's Assay

To a solution of trastuzumab (5 µL, 36.4 µM, 5.41 mg/mL) in TBS (25 mM Tris HCl pH 8, 25 mM NaCl, 0.5 mM EDTA) was added TCEP (10 eq.). The mixture was vortexed and incubated at 37 °C for 1 h. Excess TCEP was removed by repeated diafiltration into fresh TBS buffer using an Amicon-Ultra centrifugal filter (10000 MWCO, Merck Millipore) and concentrated to 1.35 µM (100 µL). To this solution was added 5,5'-dithiobis(2-nitrobenzoic acid) (DTNB) in 10% DMSO/TBS buffer (final concentration of 54 µM, 40 eq.) and the mixture incubated at room temperature for 10 min. UV-visible spectrometry revealed an absorption of 0.28 at 280 nm and 0.15 at 412 nm. The number of free thiols was calculated to be 8.15 using the following formula:[160]

$$No.\ of\ free\ sulfhydryls = \frac{Abs_{412}/\varepsilon_{412}}{Abs_{280}/\varepsilon_{280}}$$

where;

ε_{412} = 14,150 M^{-1} cm^{-1}

ε_{280} = 215,389 M^{-1} cm^{-1}

Trastuzumab 5 General Procedure

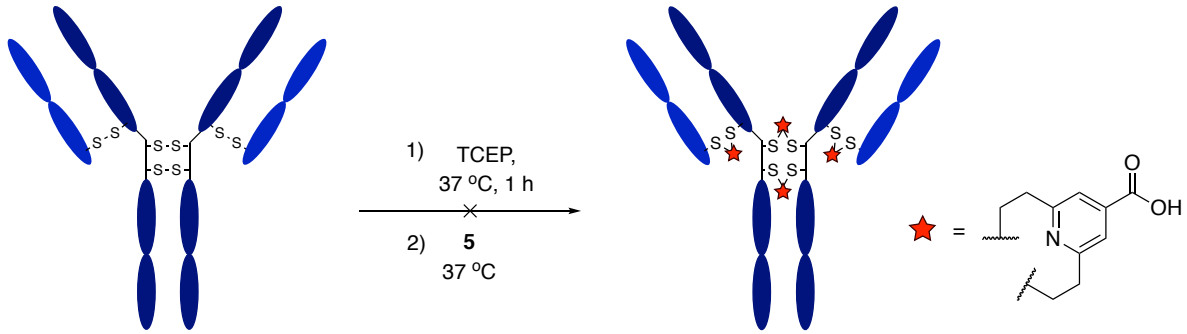

Trastuzumab **10**

To a solution of trastuzumab (2.50, 5.00 or 7.50 mg/mL) in TBS (25 mM Tris HCl pH 8, 25 mM NaCl, 0.5 mM EDTA) or BBS (25 mM sodium borate pH 8, 25 mM NaCl, 0.5 mM EDTA) was added TCEP (10 eq.). The mixture was vortexed and incubated at 37 °C for 1 h. A solution of **5** (10 mM in DMSO) was added (40, 60, 100, 200 or 500 molar eq.) and the reaction mixture incubated at 37 °C for 8 h. An aliquot was removed from the reaction after 2, 4 and 8 hours, diluted with PBS and analysed by LCMS and SDS-PAGE.

SDS-PAGE

Non-reducing Tris-Glycine SDS-PAGE with 12% acrylamide (15% for *Pf*RadA-dCys) with 4% stacking gel was performed as standard. Broad range molecular weight marker (10-200 kDa, New England BioLabs) was run in all gels. Samples (10 µL of 0.4 mg/mL) were prepared with reducing loading dye (10 µL, containing β-mercaptoethanol) and heated to 95 °C for 5 min. Gels were run at constant voltage (200 V) for 48 min in 1 × Laemmli running buffer (LRB). All gels were stained with Coomassie dye or $ZnCl_2$/imidazole staining and imaged on a Syngene gel imaging system.

7.4.2 Chapter 4: Divinylpyrimidine

Trastuzumab Fab Preparation

Trastuzumab Fab was prepared using the Pierce™ Fab Preparation Kit (ThermoFisher). Briefly, 0.25 mL of immobilised papain was washed with Digestion Buffer containing cysteine·HCl to activate the enzyme. Trastuzumab (500 µL, 2.95 mg/mL) in Digestion Buffer was added to the immobilised papain and incubated with gentle mixing at 37 °C for 16 h. The digest was isolated from the papain and the Fab purified using a Nab Protein A Plus Spin Column followed by preparative size-exclusion chromatography (25 mM sodium borate pH 8, 100 mM NaCl, 0.5 mM EDTA). The isolated Fab was aliquoted and stored at -20 °C until use.

Trastuzumab Fab General Modification Procedure

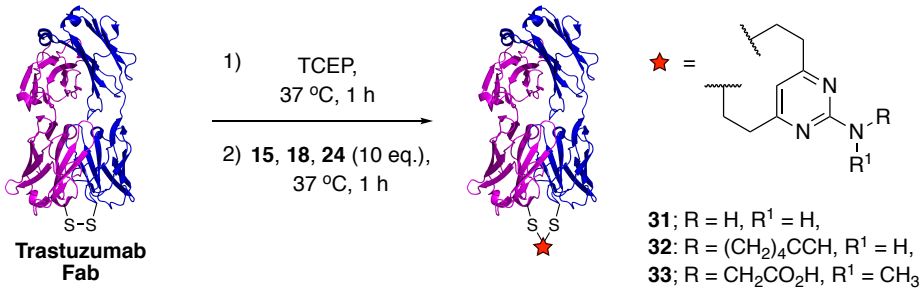

To a solution of trastuzumab Fab (10 µL, 27 µM, 1.28 mg/mL) in BBS (25 mM sodium borate pH 8, 25 mM NaCl, 0.5 mM EDTA) was added TCEP (5 eq.). The mixture was vortexed and incubated at 37 °C for 1 h. A solution of **15**, **18** or **24** (10 mM in DMSO) was added (final concentration of 270 µM, 10 eq.) and the reaction mixture incubated at 37 °C for 1 h. The excess reagents were removed by repeated diafiltration into fresh BBS using an Amicon-Ultra centrifugal filter (10000 MWCO, Merck Millipore). Samples were either stored at 4 °C or flash frozen and stored at -20 °C until analysis.

Trastuzumab Fab Reduction Control

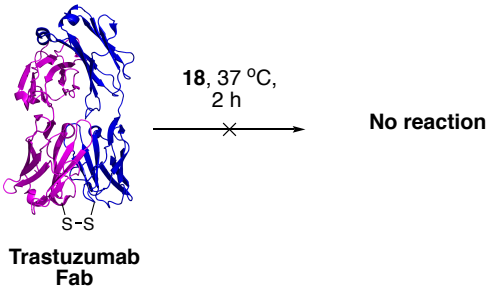

To a solution of trastuzumab Fab (5 µL, 29.6 µM, 1.41 mg/mL) in BBS (25 mM sodium borate pH 8, 25 mM NaCl, 0.5 mM EDTA) was added solution of DVP **18** (10 mM in DMSO, final concentration of 296 µM, 10 eq.). The reaction mixture was vortexed and incubated at 37 °C for 2 h. LCMS analysis revealed that no reaction had occurred.

Trastuzumab Fab Rate Studies

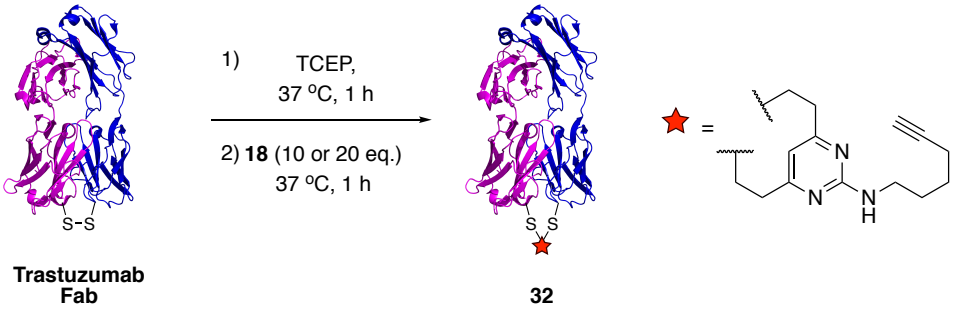

To a solution of trastuzumab Fab (5 µL, 51 µM, 2.39 mg/mL) in BBS (25 mM sodium borate pH 8, 25 mM NaCl, 0.5 mM EDTA) was added TCEP (5 eq.). The mixture was vortexed and incubated at 37 °C for 1 h. A solution of DVP **18** (10 mM in DMSO) was added (final concentration equal to 10 or 20 equivalents) and the reaction mixture incubated at 37 °C. At t = 0, 5, 10, 15, 20, 30, 40 and 60 min, 0.5 µL was removed from each reaction, diluted with MilliQ water (9 µL) and quenched with 100 eq. of cysteine (5 mM in DMSO). LCMS analysis was then used to quantify conversion.

Trastuzumab General Modification Procedure

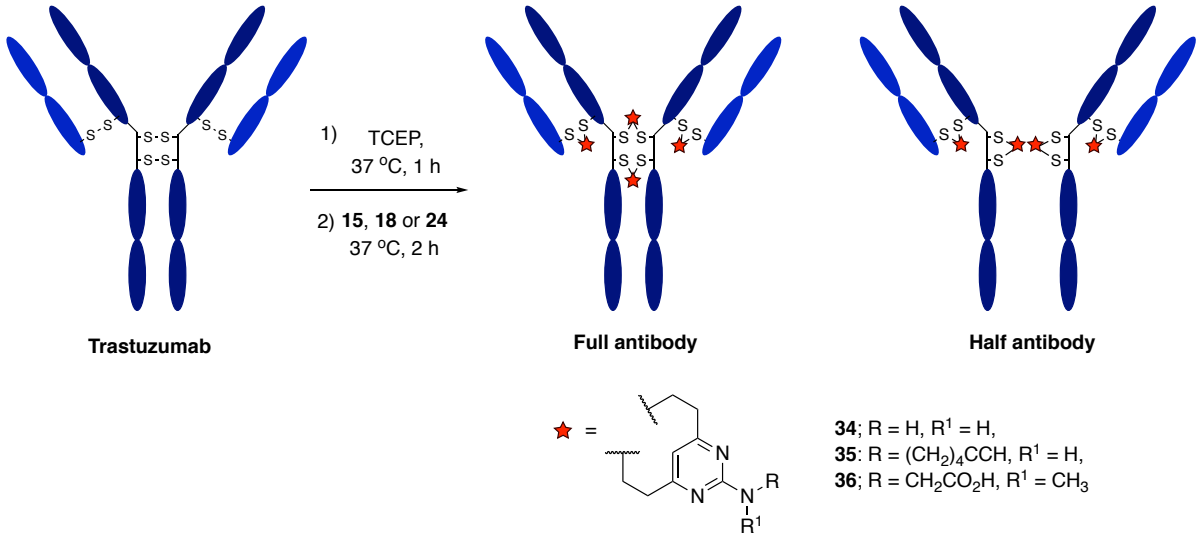

To a solution of trastuzumab (10 µL, 17 µM, 2.5 mg/mL) in TBS (25 mM Tris HCl pH 8, 25 mM NaCl, 0.5 mM EDTA) was added TCEP (10 eq.). The mixture was vortexed and incubated at 37 °C for 1 h. A solution of **15**, **18** or **24** (10 mM in DMSO) was added (final concentration of 680 µM, 40 eq.) and the reaction mixture incubated at 37 °C for 2 h. The excess reagents were removed by repeated diafiltration into PBS using an Amicon-Ultra centrifugal filter (10000 MWCO, Merck Millipore). Samples were either stored at 4 °C or flash frozen and stored at -20 °C until analysis.

Trastuzumab-DVP (35) Dox-PEG$_4$-N$_3$ (37) CuAAC

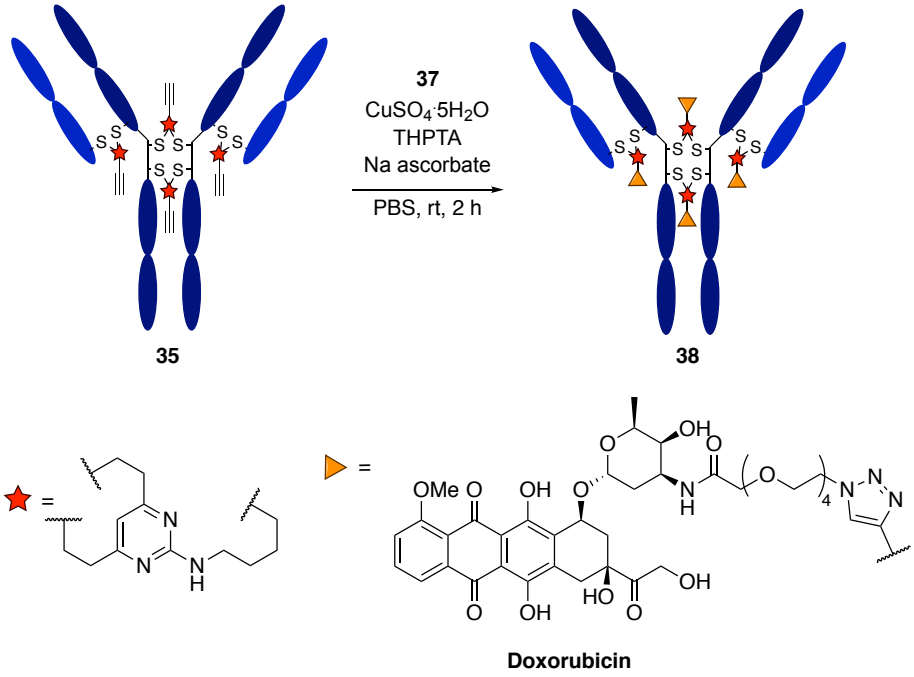

To a solution of trastuzumab-DVP **35** (70 µL, 12.5 µM, 1.86 mg/mL) in PBS was added Dox-PEG$_4$-N$_3$ **37** (5 mM in DMSO, final concentration of 150 µM), $CuSO_4 \cdot 5H_2O$ (final concentration of 250 µM), THPTA (final concentration of 1.25 mM) and sodium ascorbate (final concentration of 1.88 mM). The mixture was vortexed and incubated at 37 °C for 2 h. The excess reagents were removed by repeated diafiltration into PBS using an Amicon-Ultra centrifugal filter (10000 MWCO, Merck Millipore). Sample was either stored at 4 °C or flash frozen and stored at -20 °C until analysis.

Trastuzumab-DVP (35) AlexaFluor™ 488 CuAAC

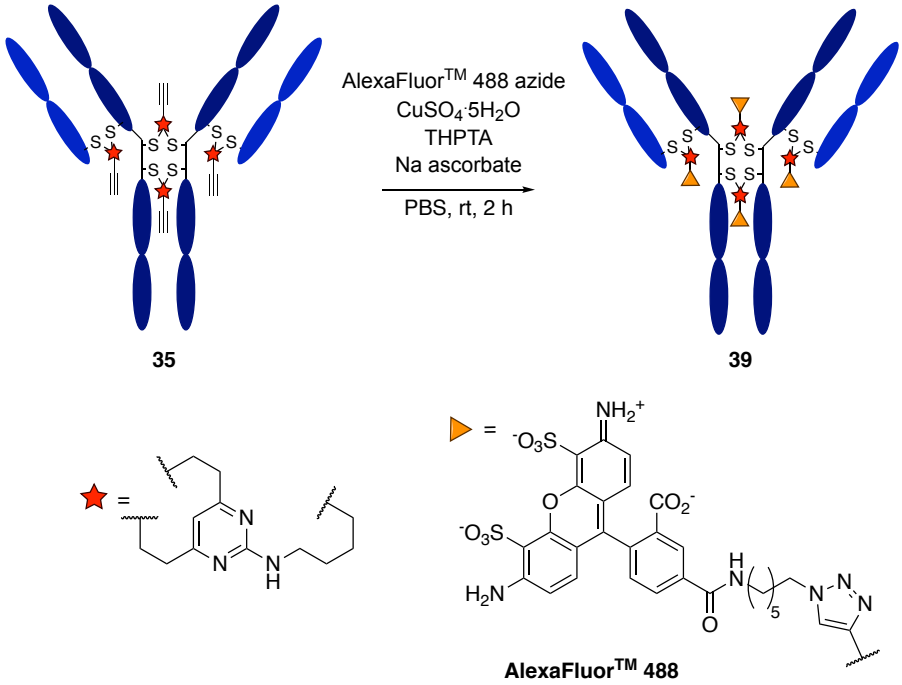

To a solution of trastuzumab-DVP **35** (55 µL, 13.7 µM, 2.05 mg/mL) in PBS was added AlexaFluor™ 488 Azide (ThermoFisher) (5 mM in DMSO, final concentration of 164.4 µM), $CuSO_4 \cdot 5H_2O$ (final concentration of 274 µM), THPTA (final concentration of 1.37 mM) and sodium ascorbate (final concentration of 2.06 mM). The mixture was vortexed and incubated at 37 °C for 4 h. The excess reagents were removed by repeated diafiltration into PBS using an Amicon-Ultra centrifugal filter (10000 MWCO, Merck Millipore). Sample was either stored at 4 °C or flash frozen and stored at -20 °C until analysis.

Trastuzumab 41 Modification

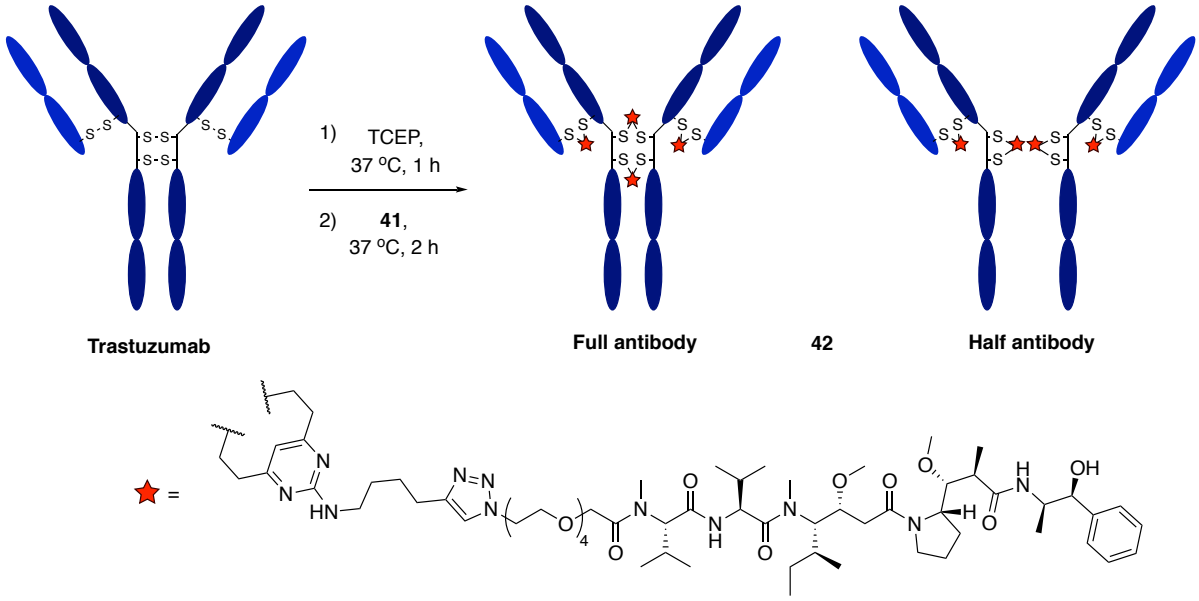

To a solution of trastuzumab (30 µL, 25.5 µM, 3.81 mg/mL) in TBS (25 mM Tris HCl pH 8, 25 mM NaCl, 0.5 mM EDTA) was added TCEP (10 eq.). The mixture was vortexed and incubated at 37 °C for 1 h. A solution of linker-drug **41** (10 mM in DMSO) was added (final concentration of 1.02 mM, 40 eq.) and the reaction mixture incubated at 37 °C for 2 h. The excess reagents were removed by repeated diafiltration into PBS using an Amicon-Ultra centrifugal filter (10000 MWCO, Merck Millipore). Sample was either stored at 4 °C or flash frozen and stored at -20 °C until analysis.

Trastuzumab 57 Modification

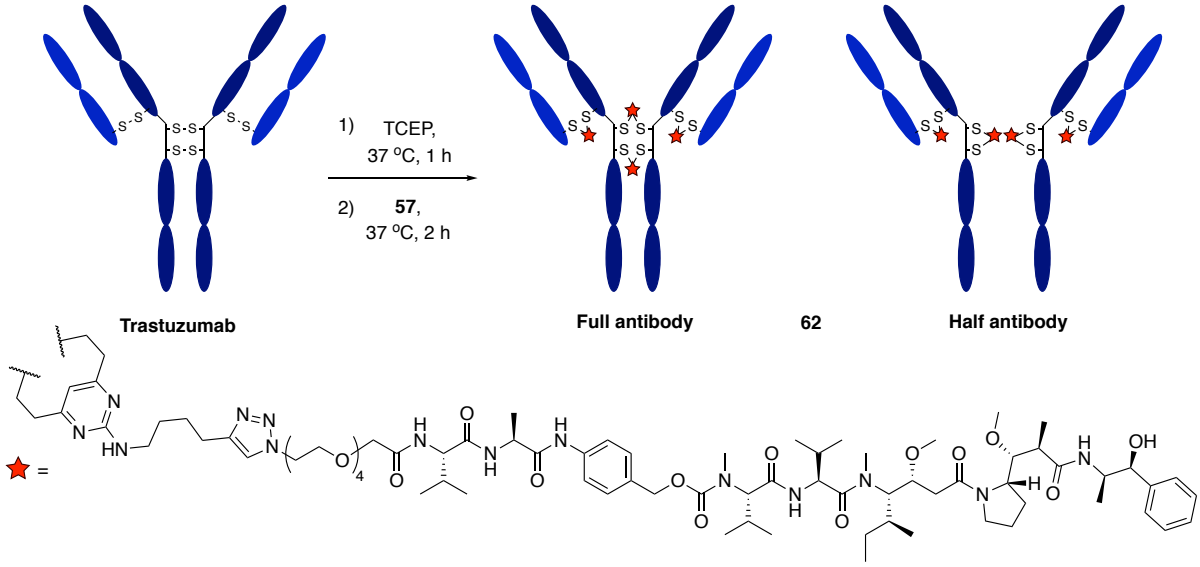

To a solution of trastuzumab (100 µL, 27.0 µM, 2.5 mg/mL) in TBS (25 mM Tris HCl pH 8, 25 mM NaCl, 0.5 mM EDTA) was added TCEP (10 eq.). The mixture was vortexed and incubated at 37 °C for 1 h. A solution of linker-drug **57** (10 mM in DMSO) was added (final concentration of 2.04 mM, 80 eq.) and the reaction mixture incubated at 37 °C for 2 h. The excess reagents were removed by repeated diafiltration into PBS using an Amicon-Ultra centrifugal filter (10000 MWCO, Merck Millipore). Sample was either stored at 4 °C or flash frozen and stored at -20 °C until analysis.

DVP-Antibody Ratio and Antibody Concentration Calculations

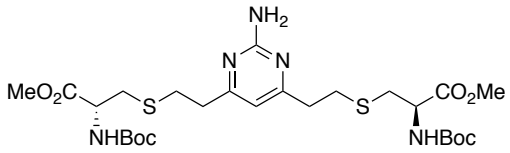

25

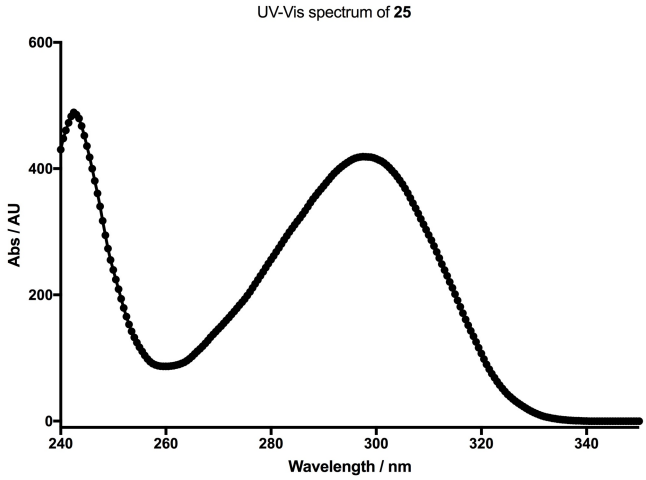

MMAE does not display significant absorbance at 280 nm, thus the DAR and antibody concentration can be calculated using the following formulas. DVP conjugate **25** has an absorption maximum at 298 nm; a correction factor of 0.61 is used to account for DVP absorbance at 280 nm[260], and a correction factor of 0.1 is used to account for trastuzumab absorbance at 298 nm.

$$DAR = \frac{Abs_{298}/\varepsilon_{298}}{(Abs_{280} - [0.61 \times Abs_{298}] + [0.1 \times Abs_{280}])/\varepsilon_{280}}$$

$$ADC\ (mg/mL) = \frac{Abs_{280} - (0.61 \times A_{298}) + (0.1 \times Abs_{280})}{1.46}$$

ε_{280} = 215,380 M^{-1} cm^{-1}

ε_{298} = 4,160 M^{-1} cm^{-1}

*Pf*RadA-dCys Modification

*Pf*RadA-dCys General Modification Procedure

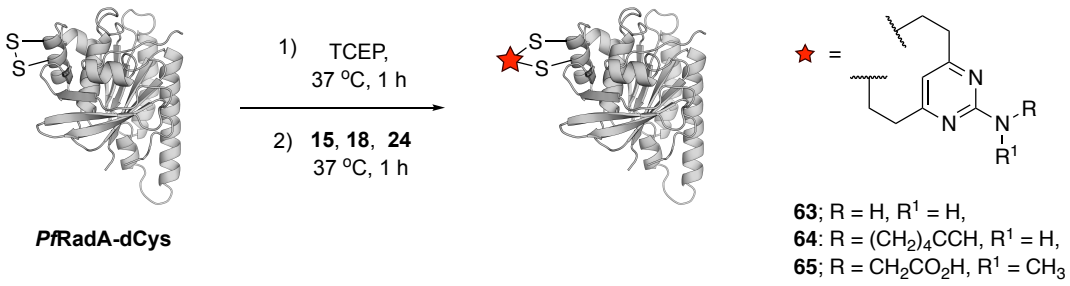

***Pf*RadA-dCys**

63; R = H, R^1 = H,
64: R = $(CH_2)_4CCH$, R^1 = H,
65; R = CH_2CO_2H, R^1 = CH_3

To a solution of *Pf*RadA-dCys (10 µL, 2.94 mg/mL) in TBS (25 mM Tris HCl pH 8, 25 mM NaCl, 0.5 mM EDTA, 3 M guanidine hydrochloride) was added TCEP (5 eq.). The mixture was vortexed and incubated at 37 °C for 1 h. A solution of DVPs **15**, **18** or **24** (10 mM in DMSO) was added (15 eq.) and the reaction mixture incubated at 37 °C for 1 h. The excess reagents were removed by repeated diafiltration into PBS using an Amicon-Ultra centrifugal filter (10000 MWCO, Merck Millipore). Samples were either stored at 4 °C or flash frozen and stored at -20 °C until analysis.

7.4.3 Chapter 5: Dual-functional Divinylpyrimidine

Trastuzumab 72 Modification

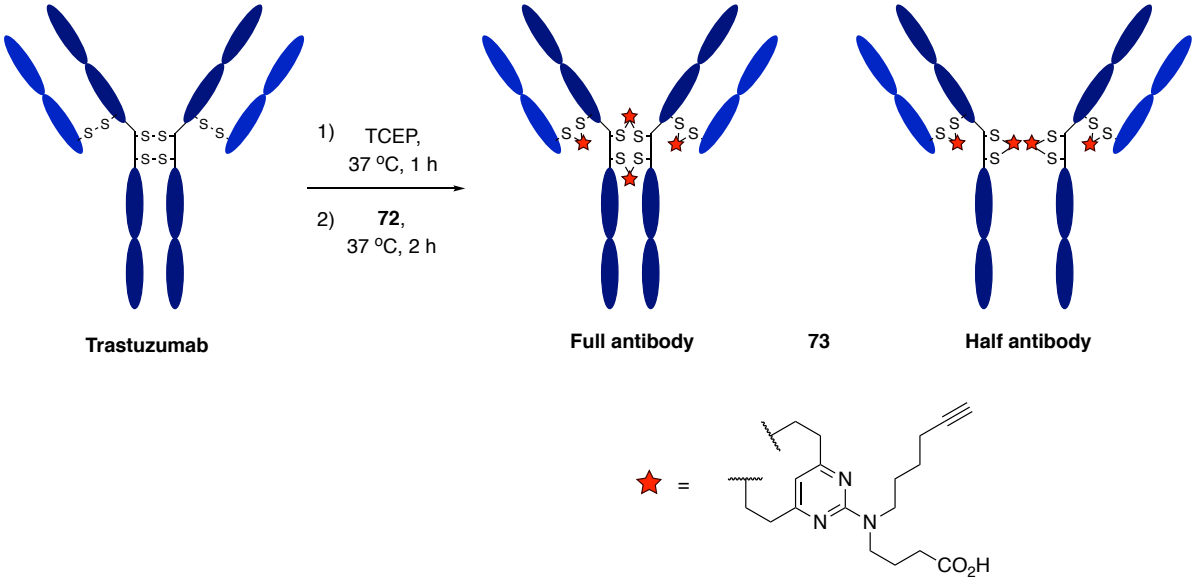

To a solution of trastuzumab (10 µL, 27.0 µM, 2.5 mg/mL) in TBS (25 mM Tris HCl pH 8, 25 mM NaCl, 0.5 mM EDTA) was added TCEP (10 eq.). The mixture was vortexed and incubated at 37 °C for 1 h. A solution of df-DVP **72** (10 mM in DMSO) was added (final concentration of 1.08 mM, 40 eq.) and the reaction mixture incubated at 37 °C for 2 h. The excess reagents were removed by repeated diafiltration into PBS using an Amicon-Ultra centrifugal filter (10000 MWCO, Merck Millipore). Sample was either stored at 4 °C or flash frozen and stored at -20 °C until analysis.

7.5 Biological Evaluation

7.5.1 Plasma Stability

A solution of trastuzumab-AlexaFluor™ 488, **39** (70 µL, 2.10 µM) in PBS was diluted with 15 µL of reconstituted human plasma (Sigma) and 70 µL of PBS. To this solution was added reduced L-glutathione (final concentration of 1 µM) and mixture incubated at 37 °C for 14 days. Aliquots were removed after 0, 1, 3, 5, 7, 9, 11 and 14 days, flash frozen and stored at -20 °C until analysis. SDS-PAGE was followed by in-gel fluorescence and Coomassie brilliant blue staining.

7.5.2 Enzyme-Linked Immunosorbent Assay (ELISA)

A 96-well plate was coated with 100 µL of a 0.25 µg/mL solution of HER2 (Sino Biological, His-tagged) overnight at 4 °C. Coating solutions were removed and each well washed with PBS (2 × 200 µL). Each well was then blocked with 1% BSA in PBS (200 µL) for 1 h at room temperature. The blocking solution was then removed and each well washed with PBS (3 × 200 µL). Wells were treated with a serial dilution of trastuzumab and trastuzumab-DVP conjugates **34**, **35** and **36** in PBS (100 µL of 30 nM, 10 nM, 3.33 nM, 1.11 nM, 0.37 nM, 0.12 nM, 0 nM) and incubated at room temperature for 2 h. The conjugate solutions were removed and each well was washed with 0.1% Tween 20 in PBS (2 × 200 µL) followed by PBS (3 × 200 µL). Next, 100 µL of detection antibody (1:1000 dilution of a mouse anti-human IgG-HRP, ThermoFisher) in PBS was added to each well and incubated at room temperature for 1 h. Each well was washed with 0.1% Tween 20 in PBS (2 × 200 µL) followed by PBS (3 × 200 µL). Finally, an OPD solution [100 µL of a solution prepared by dissolving 1 capsule in 9 mL H_2O and 1 mL stable peroxide substrate buffer (10×), ThermoFisher] was added to each well. After 10-15 minutes, 4M $HCl_{(aq)}$ (50 µL) was added to each well to quench the reaction. Absorbance was measured at 490 nm and 590 nm. Measurements were performed in quadruplicate and three independent repeats were performed.[165]

7.5.3 Cells Lines

HER2-positive SKBR3 and BT474 cells were obtained from the American Type Culture Collection (ATCC) and HER2-negative MCF7 and T47D cells were obtained from the European Collection of Authenticated Cell Cultures (ECACC) and ATCC, respectively. SKBR3

cells were maintained in high glucose McCoy's 5A medium, supplemented with 10% heat-inactivated foetal-bovine serum (FBS), 50 U/mL penicillin and 50 µg/mL streptomycin. MCF7 cells were maintained in Dulbecco's Modified Eagle Medium (DMEM) supplemented with 10% heat-inactivated FBS, 2 mM L-glutamine, 50 U/mL penicillin and 50 µg/mL streptomycin. BT474 and T47D cell lines were maintained in RPMI1640 medium supplemented with 10% heat-inactivated FBS, 2 mM L-glutamine, 50 U/mL penicillin and 50 µg/mL streptomycin. All cell lines were incubated at 37 °C with 5% CO_2.

7.5.4 Live Cell Labelling by Fluorescence-Activated Cell Sorting (FACS)

SKBR3, BT474, MCF7 and T47D cell lines were seeded in 6-well plates at 10^6 cells/well and allowed to adhere for 24 h at 37 °C with 5% CO_2. Cells were treated with 50 nM **39**, AlexaFluor™488 azide or PBS in complete growth medium for 1 h at 37 °C. Next, growth medium was removed, the cells were washed with PBS to remove unbound antibodies and the cells were detached with Accutase® cell dissociation reagent (StemPro), washed with PBS, pelleted and resuspended in PBS (100 µL). Analysis was conducted on an Amnis® ImageStream® imaging flow cytometer (Merck Millipore). DRAQ5™ (ThermoFisher) was used as a nuclear stain.

7.5.5 Cell Viability

Cells were seeded in 96-well plates for 24 h at 37 °C with 5% CO_2. SKBR3 cells were seeded at 15,000 cells/well, BT474 cells were seeded at 20,000 cells/well, MCF7 cells were seeded at 7,500 cells/well and T47D cells were seeded at 10,000 cells/well. Serial dilutions of ADCs **42** or **62**, trastuzumab and MMAE were added to the cells in complete growth medium and incubated at 37 °C with 5% CO_2 for 96 h. Cell viability was measured using CellTiter-Glo viability assay (Promega) according to the manufacturer's instructions. Cell viability was plotted as a percentage of untreated cells. Each measurement was taken in triplicate and three independent repeats were performed from different cell passages.

7.5.6 Cell Growth Assay

Cells were seeded in 96-well plates for 24 h at 37 °C with 5% CO_2. SKBR3 cells were seeded at 15,000 cells/well, BT474 cells were seeded at 20,000 cells/well, MCF7 cells were seeded at 7,500 cells/well and T47D cells were seeded at 10,000 cells/well. Serial dilutions of **42** or

62 were added to the cells in complete growth medium and incubated at 37 °C with 5% CO_2 for four or six days in an IncuCyte®. Cell growth was measured every four hours and is given as percentage confluence. Each concentration was measured in triplicate and error bars indicate standard deviation.

References

1 A. S. Ahmad, N. Ormiston-Smith and P. D. Sasieni, *Br. J. Cancer*, 2015, **112**, 943–947.

2 H. P. Rang, M. M. Dale, J. M. Ritter and P. K. Moore, in *Pharmacology*, Elsevier, 5th edn., 2003, pp. 693–696.

3 A. Urruticoechea, R. Alemany, J. Balart, A. Villanueva, F. Viñals and G. Capellá, *Curr. Pharm. Des.*, 2010, **16**, 3–10.

4 B. A. Chabner and T. G. Roberts, *Nat. Rev. Cancer*, 2005, **5**, 65–72.

5 V. T. DeVita and E. Chu, *Cancer Res.*, 2008, **68**, 8643–8653.

6 S. Dasari and P. Bernard Tchounwou, *Eur. J. Pharmacol.*, 2014, **740**, 364–378.

7 K. Barabas, R. Milner, D. Lurie and C. Adin, *Vet. Comp. Oncol.*, 2008, **6**, 1–18.

8 C. M. Spencer and D. Faulds, *Drugs*, 1994, **48**, 794–847.

9 M. Moudi, R. Go, C. Y. S. Yien and M. Nazre, *Int. J. Prev. Med.*, 2013, **4**, 1231–1235.

10 R. V. J. Chari, M. L. Miller and W. C. Widdison, *Angew. Chemie - Int. Ed.*, 2014, **53**, 3796–3827.

11 C. S. Ross-Innes, R. Stark, A. E. Teschendorff, K. A. Holmes, H. R. Ali, M. J. Dunning, G. D. Brown, O. Gojis, I. O. Ellis, A. R. Green, S. Ali, S. F. Chin, C. Palmieri, C. Caldas and J. S. Carroll, *Nature*, 2012, **481**, 389–393.

12 S. J. Johnston and J. S. Carroll, *Biochim. Biophys. Acta - Rev. Cancer*, 2015, **1855**, 183–192.

13 V. C. Jordan, *Nat. Rev. Drug Discov.*, 2003, **2**, 205–213.

14 R. Baskar, K. A. Lee, R. Yeo and K. W. Yeoh, *Int. J. Med. Sci.*, 2012, **9**, 193–199.

15 D. Adams, A. Gonzalez-Duarte, W. D. O'Riordan, C.-C. Yang, M. Ueda, A. V. Kristen, I. Tournev, H. H. Schmidt, T. Coelho, J. L. Berk, K.-P. Lin, G. Vita, S. Attarian, V. Planté-Bordeneuve, M. M. Mezei, J. M. Campistol, J. Buades, T. H. Brannagan, B. J. Kim, J. Oh, Y. Parman, Y. Sekijima, P. N. Hawkins, S. D. Solomon, M. Polydefkis, P. J. Dyck, P. J. Gandhi, S. Goyal, J. Chen, A. L. Strahs, S. V. Nochur, M. T. Sweetser, P. P. Garg, A. K. Vaishnaw, J. A. Gollob and O. B. Suhr, *N. Engl. J. Med.*, 2018, **379**, 11–21.

16 C. Chakraborty, A. R. Sharma, G. Sharma, C. G. P. Doss and S. S. Lee, *Mol. Ther. - Nucleic Acids*, 2017, **8**, 132–143.

17 X. Shen and D. R. Corey, *Nucleic Acids Res.*, 2018, **46**, 1584–1600.

18 V. Prasad, *Nat. Rev. Clin. Oncol.*, 2018, **15**, 11–12.

19 C. Fellmann, B. G. Gowen, P. C. Lin, J. A. Doudna and J. E. Corn, *Nat. Rev. Drug Discov.*, 2017, **16**, 89–100.

20 A. C. Komor, A. H. Badran and D. R. Liu, *Cell*, 2017, **168**, 20–36.

21 H. Kaplon and J. M. Reichert, *MAbs*, 2019, **11**, 219–238.

22 P. Ehrlich, *BMJ*, 1913, **2**, 353–359.

23 S. M. Lehar, T. Pillow, M. Xu, L. Staben, K. K. Kajihara, R. Vandlen, L. DePalatis, H. Raab, W. L. Hazenbos, J. Hiroshi Morisaki, J. Kim, S. Park, M. Darwish, B. C. Lee, H. Hernandez, K. M. Loyet, P. Lupardus, R. Fong, D. Yan, C. Chalouni, E. Luis, Y. Khalfin, E. Plise, J. Cheong, J. P. Lyssikatos, M. Strandh, K. Koefoed, P. S. Andersen, J. A. Flygare, M. Wah Tan, E. J. Brown and S. Mariathasan, *Nature*, 2015, **527**, 323–328.

24 H. Bouchard, C. Viskov and C. Garcia-Echeverria, *Bioorganic Med. Chem. Lett.*, 2014, **24**, 5357–5363.

25 S. Xu, *Pharm. Res.*, 2015, **32**, 3577–3583.

26 M. Ritchie, L. Tchistiakova and N. Scott, *MAbs*, 2013, **5**, 13–21.

27 K. C. Nicolaou and S. Rigol, *Angew. Chemie - Int. Ed.*, , DOI:10.1002/anie.201903498.

28 H. L. Perez, P. M. Cardarelli, S. Deshpande, S. Gangwar, G. M. Schroeder, G. D. Vite and R. M. Borzilleri, *Drug Discov. Today*, 2014, **19**, 869–881.

29 A. Beck, J.-F. Haeuw, T. Wurch, L. Goetsch, C. Bailly and N. Corvaïa, *Discov. Med.*, 2010, **10**, 329–339.

30 F. R. Appelbaum and I. D. Bernstein, *Blood*, 2017, **130**, 2373–2376.

31 V. Chudasama, *Drug Discov. Today Technol.*, 2018, **30**, 1–2.

32 J. Katz, J. E. Janik and A. Younes, *Clin. Cancer Res.*, 2011, **17**, 6428–6436.

33 P. D. Senter and E. L. Sievers, *Nat. Biotechnol.*, 2012, **30**, 631–637.

34 S. M. Ansell, *Blood*, 2014, **124**, 3197–3200.

35 A. Younes, N. L. Bartlett, J. P. Leonard, D. A. Kennedy, C. M. Lynch, E. L. Sievers and A. Forero-Torres, *N. Engl. J. Med.*, 2010, **363**, 1812–1821.

36 S. Verma, D. Miles, L. Gianni, I. E. Krop, M. Welslau, J. Baselga, M. Pegram, D.-Y. Oh, V. Diéras, E. Guardino, L. Fang, M. W. Lu, S. Olsen, K. Blackwell and EMILIA

Study Group, *N. Engl. J. Med.*, 2012, **367**, 1783–1791.

37 J. M. Lambert and R. V. J. Chari, *J. Med. Chem.*, 2014, **57**, 6949–6964.

38 Y. N. Lamb, *Drugs*, 2017, **77**, 1603–1610.

39 B. Shor, H. P. Gerber and P. Sapra, *Mol. Immunol.*, 2015, **67**, 107–116.

40 R. Lyon, *Drug Discov. Today Technol.*, 2018, **30**, 105–109.

41 A. G. Poison, J. Calemine-Fenaux, P. Chan, W. Chang, E. Christensen, S. Clark, F. J. De Sauvage, D. Eaton, K. Elkins, J. Michael Elliott, G. Frantz, R. N. Fuji, A. Gray, K. Harden, G. S. Ingle, N. M. Kljavin, H. Koeppen, C. Nelson, S. Prabhu, H. Raab, S. Ross, J. P. Stephan, S. J. Scales, S. D. Spencer, R. Vandlen, B. Wranik, S. F. Yu, B. Zheng and A. Ebens, *Cancer Res.*, 2009, **69**, 2358–2364.

42 V. Chudasama, A. Maruani and S. Caddick, *Nat. Chem.*, 2016, **8**, 114–119.

43 P. Agarwal and C. R. Bertozzi, *Bioconjug. Chem.*, 2015, **26**, 176–192.

44 I. Sela-Culang, V. Kunik and Y. Ofran, *Front. Immunol.*, 2013, **4**, 302.

45 J. M. Woof and D. R. Burton, *Nat. Rev. Immunol.*, 2004, **4**, 89–99.

46 Y. Cao, J. Y. Axup, J. S. Y. Ma, R. E. Wang, S. Choi, V. Tardif, R. K. V. Lim, H. M. Pugh, B. R. Lawson, G. Welzel, S. A. Kazane, Y. Sun, F. Tian, S. Srinagesh, T. Javahishvili, P. G. Schultz and C. H. Kim, *Angew. Chemie - Int. Ed.*, 2015, **54**, 7022–7027.

47 D. G. Maloney, *Blood*, 1997, **90**, 2188–2195.

48 R. G. Panchal, *Biochem. Pharmacol.*, 1998, **55**, 247–252.

49 G. Köhler and C. Milstein, *Nature*, 1975, **256**, 495–497.

50 M. Kamionka, *Curr. Pharm. Biotechnol.*, 2011, **12**, 268–274.

51 P. A. Trail, D. Willner, S. J. Lasch, A. J. Henderson, S. Hofstead, A. M. Casazza, R. A. Firestone, I. Hellström and K. E. Hellström, *Science*, 1993, **261**, 212–215.

52 A. W. Tolcher, S. Sugarman, K. A. Gelmon, R. Cohen, M. Saleh, C. Isaacs, L. Young, D. Healey, N. Onetto and W. Slichenmyer, *J. Clin. Oncol.*, 1999, **17**, 478–484.

53 A. A. Epenetos, D. Snook, H. Durbin, J. Taylor-Papadimitriou and P. M. Johnson, *Cancer Res.*, 1986, **46**, 3183–3191.

54 A. Beck, L. Goetsch, C. Dumontet and N. Corvaïa, *Nat. Rev. Drug Discov.*, 2017, **16**, 315–337.

55 A. Beck, T. Wurch, C. Bailly and N. Corvaïa, *Nat. Rev. Immunol.*, 2010, **10**, 345–352.

56 M. D. Lee, T. S. Dunne, M. M. Siegel, G. O. Morton, D. B. Borders and C. C. Chang, *J. Am. Chem. Soc.*, 1987, **109**, 3464–3466.

57 S. O. Doronina, B. E. Toki, M. Y. Torgov, B. A. Mendelsohn, C. G. Cerveny, D. F. Chace, R. L. DeBlanc, R. P. Gearing, T. D. Bovee, C. B. Siegall, J. A. Francisco, A. F. Wahl, D. L. Meyer and P. D. Senter, *Nat. Biotechnol.*, 2003, **21**, 778–784.

58 U. Vaishampayan, M. Glode, W. Du, A. Kraft, G. Hudes, J. Wright and M. Hussain, *Clin. Cancer Res.*, 2000, **6**, 4205–4208.

59 S. M. Kupchan, Y. Komoda, W. A. Court, G. J. Thomas, R. M. Smith, A. Karim, C. J. Gilmore, R. C. Haitiwanger and R. F. Bryan, *J. Am. Chem. Soc.*, 1972, **94**, 1354–1356.

60 J. Mantaj, P. J. M. Jackson, K. M. Rahman and D. E. Thurston, *Angew. Chemie - Int. Ed.*, 2017, **56**, 462–488.

61 A. C. Tiberghien, J. N. Levy, L. A. Masterson, N. V. Patel, L. R. Adams, S. Corbett, D. G. Williams, J. A. Hartley and P. W. Howard, *ACS Med. Chem. Lett.*, 2016, **7**, 983–987.

62 E. M. Stein, R. B. Walter, H. P. Erba, A. T. Fathi, A. S. Advani, J. E. Lancet, F. Ravandi, T. Kovacsovics, D. J. DeAngelo, D. Bixby, S. Faderl, A. P. Jillella, P. A. Ho, M. M. O'Meara, B. Zhao, C. Biddle-Snead and A. S. Stein, *Blood*, 2018, **131**, 387–396.

63 R. C. Elgersma, R. G. E. Coumans, T. Huijbregts, W. M. P. B. Menge, J. A. F. Joosten, H. J. Spijker, F. M. H. De Groot, M. M. C. Van Der Lee, R. Ubink, D. J. Van Den Dobbelsteen, D. F. Egging, W. H. A. Dokter, G. F. M. Verheijden, J. M. Lemmens, C. M. Timmers and P. H. Beusker, *Mol. Pharm.*, 2015, **12**, 1813–1835.

64 R. M. Sharkey, W. J. McBride, T. M. Cardillo, S. V. Govindan, Y. Wang, E. A. Rossi, C. H. Chang and D. M. Goldenberg, *Clin. Cancer Res.*, 2015, **21**, 5131–5138.

65 L. N. Tumey, C. A. Leverett, B. Vetelino, F. Li, B. Rago, X. Han, F. Loganzo, S. Musto, G. Bai, S. C. K. Sukuru, E. I. Graziani, S. Puthenveetil, J. Casavant, A. Ratnayake, K. Marquette, S. Hudson, V. R. Doppalapudi, J. Stock, L. Tchistiakova, A. J. Bessire, T. Clark, J. Lucas, C. Hosselet, C. J. O'Donnell and C. Subramanyam, *ACS Med. Chem. Lett.*, 2016, **7**, 977–982.

66 J. S. Parker, M. McCormick, D. W. Anderson, B. A. Maltman, L. Gingipalli and D. Toader, *Org. Process Res. Dev.*, 2017, **21**, 1602–1609.

67 J. Y. Li, S. R. Perry, V. Muniz-Medina, X. Wang, L. K. Wetzel, M. C. Rebelatto, M. J. M. Hinrichs, B. Z. Bezabeh, R. L. Fleming, N. Dimasi, H. Feng, D. Toader, A. Q.

Yuan, L. Xu, J. Lin, C. Gao, H. Wu, R. Dixit, J. K. Osbourn and S. R. Coats, *Cancer Cell*, 2016, **29**, 117–129.

68 L. Ducry and B. Stump, *Bioconjug. Chem.*, 2010, **21**, 5–13.

69 K. Tsuchikama and Z. An, *Protein Cell*, 2018, **9**, 33–46.

70 A. D. Ricart, *Clin. Cancer Res.*, 2011, **17**, 6417–6427.

71 B. J. Mills and C. A. Lang, *Biochem. Pharmacol.*, 1996, **52**, 401–406.

72 G. Wu, Y.-Z. Fang, S. Yang, J. R. Lupton and N. D. Turner, *J. Nutr.*, 2004, **134**, 489–492.

73 W. Widdison, S. Wilhelm, K. Veale, J. Costoplus, G. Jones, C. Audette, B. Leece, L. Bartle, Y. Kovtun and R. Chari, *Mol. Pharm.*, 2015, **12**, 1762–1773.

74 M. N. Saleh, S. Sugarman, J. Murray, J. B. Ostroff, D. Healey, D. Jones, C. R. Daniel, D. LeBherz, H. Brewer, N. Onetto and A. F. LoBuglio, *J. Clin. Oncol.*, 2000, **18**, 2282–2292.

75 H. Xie, *J. Pharmacol. Exp. Ther.*, 2004, **308**, 1073–1082.

76 C. S. Gondi and J. S. Rao, *Expert Opin. Ther. Targets*, 2013, **17**, 281–291.

77 J. E. Koblinski, M. Ahram and B. F. Sloane, *Clin. Chim. Acta*, 2000, **291**, 113–135.

78 G. M. Dubowchik, R. A. Firestone, L. Padilla, D. Willner, S. J. Hofstead, K. Mosure, J. O. Knipe, S. J. Lasch and P. A. Trail, *Bioconjug. Chem.*, 2002, **13**, 855–869.

79 B. Wei, J. Gunzner-Toste, H. Yao, T. Wang, J. Wang, Z. Xu, J. Chen, J. Wai, J. Nonomiya, S. P. Tsai, J. Chuh, K. R. Kozak, Y. Liu, S. F. Yu, J. Lau, G. Li, G. D. Phillips, D. Leipold, A. Kamath, D. Su, K. Xu, C. Eigenbrot, S. Steinbacher, R. Ohri, H. Raab, L. R. Staben, G. Zhao, J. A. Flygare, T. H. Pillow, V. Verma, L. A. Masterson, P. W. Howard and B. Safina, *J. Med. Chem.*, 2018, **61**, 989–1000.

80 N. Jain, S. W. Smith, S. Ghone and B. Tomczuk, *Pharm. Res.*, 2015, **32**, 3526–3540.

81 N. Albin, L. Massaad, C. Toussaint, M. C. Mathieu, J. Morizet, O. Parise, A. Gouyette and G. G. Chabot, *Cancer Res.*, 1993, **53**, 3541–3546.

82 S. C. Jeffrey, J. B. Andreyka, S. X. Bernhardt, K. M. Kissler, T. Kline, J. S. Lenox, R. F. Moser, M. T. Nguyen, N. M. Okeley, I. J. Stone, X. Zhang and P. D. Senter, *Bioconjug. Chem.*, 2006, **17**, 831–840.

83 S. C. Jeffrey, M. T. Nguyen, R. F. Moser, D. L. Meyer, J. B. Miyamoto and P. D. Senter, *Bioorganic Med. Chem. Lett.*, 2007, **17**, 2278–2280.

84 P. J. Burke, P. D. Senter, D. W. Meyer, J. B. Miyamoto, M. Anderson, B. E. Toki, G.

Manikumar, M. C. Wani, D. J. Kroll and S. C. Jeffrey, *Bioconjug. Chem.*, 2009, **20**, 1242–1250.

85 S. C. Jeffrey, J. De Brabander, J. Miyamoto and P. D. Senter, *ACS Med. Chem. Lett.*, 2010, **1**, 277–280.

86 R. V. Kolakowski, K. T. Haelsig, K. K. Emmerton, C. I. Leiske, J. B. Miyamoto, J. H. Cochran, R. P. Lyon, P. D. Senter and S. C. Jeffrey, *Angew. Chemie - Int. Ed.*, 2016, **55**, 7948–7951.

87 B. A. Schröder, C. Wrocklage, A. Hasilik and P. Saftig, *Proteomics*, 2010, **10**, 4053–4076.

88 J. C. Kern, M. Cancilla, D. Dooney, K. Kwasnjuk, R. Zhang, M. Beaumont, I. Figueroa, S. C. Hsieh, L. Liang, D. Tomazela, J. Zhang, P. E. Brandish, A. Palmieri, P. Stivers, M. Cheng, G. Feng, P. Geda, S. Shah, A. Beck, D. Bresson, J. Firdos, D. Gately, N. Knudsen, A. Manibusan, P. G. Schultz, Y. Sun and R. M. Garbaccio, *J. Am. Chem. Soc.*, 2016, **138**, 1430–1445.

89 P. E. Brandish, A. Palmieri, S. Antonenko, M. Beaumont, L. Benso, M. Cancilla, M. Cheng, L. Fayadat-Dilman, G. Feng, I. Figueroa, J. Firdos, R. Garbaccio, L. Garvin-Queen, D. Gately, P. Geda, C. Haines, S. Hseih, D. Hodges, J. Kern, N. Knudsen, K. Kwasnjuk, L. Liang, H. Ma, A. Manibusan, P. L. Miller, L. Y. Moy, Y. Qu, S. Shah, J. S. Shin, P. Stivers, Y. Sun, D. Tomazela, H. C. Woo, D. Zaller, S. Zhang, Y. Zhang and M. Zielstorff, *Bioconjug. Chem.*, 2018, **29**, 2357–2369.

90 J. C. Kern, D. Dooney, R. Zhang, L. Liang, P. E. Brandish, M. Cheng, G. Feng, A. Beck, D. Bresson, J. Firdos, D. Gately, N. Knudsen, A. Manibusan, Y. Sun and R. M. Garbaccio, *Bioconjug. Chem.*, 2016, **27**, 2081–2088.

91 H. K. Erickson, P. U. Park, W. C. Widdison, Y. V. Kovtun, L. M. Garrett, K. Hoffman, R. J. Lutz, V. S. Goldmacher and W. A. Blättler, *Cancer Res.*, 2006, **66**, 4426–4433.

92 A. H. Staudacher and M. P. Brown, *Br. J. Cancer*, 2017, **117**, 1736–1742.

93 S. Golfier, C. Kopitz, A. Kahnert, I. Heisler, C. A. Schatz, B. Stelte-Ludwig, A. Mayer-Bartschmid, K. Unterschemmann, S. Bruder, L. Linden, A. Harrenga, P. Hauff, F.-D. Scholle, B. Muller-Tiemann, B. Kreft and K. Ziegelbauer, *Mol. Cancer Ther.*, 2014, **13**, 1537–1548.

94 Y. V. Kovtun, C. A. Audette, Y. Ye, H. Xie, M. F. Ruberti, S. J. Phinney, B. A. Leece, T. Chittenden, W. A. Blättler and V. S. Goldmacher, *Cancer Res.*, 2006, **66**, 3214–3221.

95 M. T. Taylor, J. E. Nelson, M. G. Suero and M. J. Gaunt, *Nature*, 2018, **562**, 563–568.

96 C. D. Spicer and B. G. Davis, *Nat. Commun.*, 2014, **5**, 4740.

97 E. A. Hoyt, P. M. S. D. Cal, B. L. Oliveira and G. J. L. Bernardes, *Nat. Rev. Chem.*, 2019, **3**, 147–171.

98 T. Tamura and I. Hamachi, *J. Am. Chem. Soc.*, 2019, **141**, 2782–2799.

99 E. M. Sletten and C. R. Bertozzi, *Angew. Chemie - Int. Ed.*, 2009, **48**, 6974–6998.

100 N. Krall, F. P. Da Cruz, O. Boutureira and G. J. L. Bernardes, *Nat. Chem.*, 2016, **8**, 103–113.

101 A. Wakankar, Y. Chen, Y. Gokarn and F. S. Jacobson, *MAbs*, 2011, **3**, 164–175.

102 K. J. Hamblett, P. D. Senter, D. F. Chace, M. M. C. Sun, J. Lenox, C. G. Cerveny, K. M. Kissler, S. X. Bernhardt, A. K. Kopcha, R. F. Zabinski, D. L. Meyer and J. A. Francisco, *Clin. Cancer Res.*, 2004, **10**, 7063–7070.

103 T. H. Pillow, J. D. Sadowsky, D. Zhang, S. F. Yu, G. Del Rosario, K. Xu, J. He, S. Bhakta, R. Ohri, K. R. Kozak, E. Ha, J. R. Junutula and J. A. Flygare, *Chem. Sci.*, 2016, **8**, 366–370.

104 B. Q. Shen, K. Xu, L. Liu, H. Raab, S. Bhakta, M. Kenrick, K. L. Parsons-Reponte, J. Tien, S. F. Yu, E. Mai, D. Li, J. Tibbitts, J. Baudys, O. M. Saad, S. J. Scales, P. J. McDonald, P. E. Hass, C. Eigenbrot, T. Nguyen, W. A. Solis, R. N. Fuji, K. M. Flagella, D. Patel, S. D. Spencer, L. A. Khawli, A. Ebens, W. L. Wong, R. Vandlen, S. Kaur, M. X. Sliwkowski, R. H. Scheller, P. Polakis and J. R. Junutula, *Nat. Biotechnol.*, 2012, **30**, 184–189.

105 P. Strop, S.-H. Liu, M. Dorywalska, K. Delaria, R. G. Dushin, T.-T. Tran, W.-H. Ho, S. Farias, M. G. Casas, Y. Abdiche, D. Zhou, R. Chandrasekaran, C. Samain, C. Loo, A. Rossi, M. Rickert, S. Krimm, T. Wong, S. M. Chin, J. Yu, J. Dilley, J. Chaparro-Riggers, G. F. Filzen, C. J. O'Donnell, F. Wang, J. S. Myers, J. Pons, D. L. Shelton and A. Rajpal, *Chem. Biol.*, 2013, **20**, 161–167.

106 L. Wang, G. Amphlett, W. A. Blättler, J. M. Lambert and W. Zhang, *Protein Sci.*, 2005, **14**, 2436–2446.

107 D. S. Wilbur, M. K. Chyan, H. Nakamae, Y. Chen, D. K. Hamlin, E. B. Santos, B. T. Kornblit and B. M. Sandmaier, *Bioconjug. Chem.*, 2012, **23**, 409–420.

108 I. Dovgan, S. Ursuegui, S. Erb, C. Michel, S. Kolodych, S. Cianférani and A. Wagner, *Bioconjug. Chem.*, 2017, **28**, 1452–1457.

109 G. Chaubet, F. Thoreau and A. Wagner, *Drug Discov. Today Technol.*, 2018, **30**, 21–26.

110 M. J. Matos, B. L. Oliveira, N. Martínez-Sáez, A. Guerreiro, P. M. S. D. Cal, J. Bertoldo, M. Maneiro, E. Perkins, J. Howard, M. J. Deery, J. M. Chalker, F. Corzana, G. Jiménez-Osés and G. J. L. Bernardes, *J. Am. Chem. Soc.*, 2018, **140**, 4004–4017.

111 M. Hayakawa, N. Toda, N. Carrillo, N. J. Thornburg, J. E. Crowe and C. F. Barbas, *ChemBioChem*, 2012, **13**, 2191–2195.

112 A. R. Nanna, X. Li, E. Walseng, L. Pedzisa, R. S. Goydel, D. Hymel, T. R. Burke, W. R. Roush and C. Rader, *Nat. Commun.*, 2017, **8**, 1112.

113 J. M. Chalker, G. J. L. Bernardes, Y. A. Lin and B. G. Davis, *Chem. - An Asian J.*, 2009, **4**, 630–640.

114 P. Trail, *Antibodies*, 2013, **2**, 113–129.

115 P. A. Szijj, C. Bahou and V. Chudasama, *Drug Discov. Today Technol.*, 2018, 30, 27–34.

116 A. D. Baldwin and K. L. Kiick, *Bioconjug. Chem.*, 2011, **22**, 1946–1953.

117 S. C. Alley, D. R. Benjamin, S. C. Jeffrey, N. M. Okeley, D. L. Meyer, R. J. Sanderson and P. D. Senter, *Bioconjug. Chem.*, 2008, **19**, 759–765.

118 J. F. Ponte, X. Sun, N. C. Yoder, N. Fishkin, R. Laleau, J. Coccia, L. Lanieri, M. Bogalhas, L. Wang, S. Wilhelm, W. Widdison, J. Pinkas, T. A. Keating, R. Chari, H. K. Erickson and J. M. Lambert, *Bioconjug. Chem.*, 2016, **27**, 1588–1598.

119 J. D. Gregory, *J. Am. Chem. Soc.*, 1955, **77**, 3922–3923.

120 W. Huang, X. Wu, X. Gao, Y. Yu, H. Lei, Z. Zhu, Y. Shi, Y. Chen, M. Qin, W. Wang and Y. Cao, *Nat. Chem.*, 2019, **11**, 310–319.

121 R. P. Lyon, J. R. Setter, T. D. Bovee, S. O. Doronina, J. H. Hunter, M. E. Anderson, C. L. Balasubramanian, S. M. Duniho, C. I. Leiske, F. Li and P. D. Senter, *Nat. Biotechnol.*, 2014, **32**, 1059–1062.

122 L. N. Tumey, M. Charati, T. He, E. Sousa, D. Ma, X. Han, T. Clark, J. Casavant, F. Loganzo, F. Barletta, J. Lucas and E. I. Graziani, *Bioconjug. Chem.*, 2014, **25**, 1871–1880.

123 I. Dovgan, S. Kolodych, O. Koniev and A. Wagner, *Sci. Rep.*, 2016, **6**, 30835.

124 E. Tobaldi, I. Dovgan, M. Mosser, J. M. Becht and A. Wagner, *Org. Biomol. Chem.*, 2017, **15**, 9305–9310.

125 R. J. Christie, R. Fleming, B. Bezabeh, R. Woods, S. Mao, J. Harper, A. Joseph, Q. Wang, Z. Q. Xu, H. Wu, C. Gao and N. Dimasi, *J. Control. Release*, 2015, **220**, 660–670.

126 D. Kalia, S. P. Pawar and J. S. Thopate, *Angew. Chemie - Int. Ed.*, 2017, **56**, 1885–1889.

127 E. V. Vinogradova, C. Zhang, A. M. Spokoyny, B. L. Pentelute and S. L. Buchwald, *Nature*, 2015, **526**, 687–691.

128 S. S. van Berkel and F. L. van Delft, *Drug Discov. Today Technol.*, 2018, **30**, 3–10.

129 S. Jeger, K. Zimmermann, A. Blanc, J. Grünberg, M. Honer, P. Hunziker, H. Struthers and R. Schibli, *Angew. Chemie - Int. Ed.*, 2010, **49**, 9995–9997.

130 P. Dennler, A. Chiotellis, E. Fischer, D. Brégeon, C. Belmant, L. Gauthier, F. Lhospice, F. Romagne and R. Schibli, *Bioconjug. Chem.*, 2014, **25**, 569–578.

131 R. R. Beerli, T. Hell, A. S. Merkel and U. Grawunder, *PLoS One*, 2015, **10**, e0131177.

132 N. Stefan, R. Gébleux, L. Waldmeier, T. Hell, M. Escher, F. I. Wolter, U. Grawunder and R. R. Beerli, *Mol. Cancer Ther.*, 2017, **16**, 879–892.

133 P. Agarwal, R. Kudirka, A. E. Albers, R. M. Barfield, G. W. De Hart, P. M. Drake, L. C. Jones and D. Rabuka, *Bioconjug. Chem.*, 2013, **24**, 846–851.

134 P. M. Drake, A. E. Albers, J. Baker, S. Banas, R. M. Barfield, A. S. Bhat, G. W. De Hart, A. W. Garofalo, P. Holder, L. C. Jones, R. Kudirka, J. McFarland, W. Zmolek and D. Rabuka, *Bioconjug. Chem.*, 2014, **25**, 1331–1341.

135 L. Liu, *J. Pharm. Sci.*, 2015, **104**, 1866–1884.

136 T. B. Parsons, W. B. Struwe, J. Gault, K. Yamamoto, T. A. Taylor, R. Raj, K. Wals, S. Mohammed, C. V. Robinson, J. L. P. Benesch and B. G. Davis, *Angew. Chemie - Int. Ed.*, 2016, **55**, 2361–2367.

137 B. Ramakrishnan and P. K. Qasba, *J. Biol. Chem.*, 2002, **277**, 20833–20839.

138 Z. Zhu, B. Ramakrishnan, J. Li, Y. Wang, Y. Feng, P. Prabakaran, S. Colantonio, M. A. Dyba, P. K. Qasba and D. S. Dimitrov, *MAbs*, 2014, **6**, 1190–1200.

139 B. M. Zeglis, C. B. Davis, R. Aggeler, H. C. Kang, A. Chen, B. J. Agnew and J. S. Lewis, *Bioconjug. Chem.*, 2013, **24**, 1057–1067.

140 C. J. Noren, S. J. Anthony-Cahill, M. C. Griffith and P. G. Schultz, *Science*, 1989, **244**, 182–188.

141 J. W. Chin, *Nature*, 2017, **550**, 53–60.

142 J. Y. Axup, K. M. Bajjuri, M. Ritland, B. M. Hutchins, C. H. Kim, S. A. Kazane, R. Halder, J. S. Forsyth, A. F. Santidrian, K. Stafin, Y. Lu, H. Tran, A. J. Seller, S. L. Biroc, A. Szydlik, J. K. Pinkstaff, F. Tian, S. C. Sinha, B. Felding-Habermann, V. V

Smider and P. G. Schultz, *Proc. Natl. Acad. Sci. U. S. A.*, 2012, **109**, 16101–16106.

143 E. S. Zimmerman, T. H. Heibeck, A. Gill, X. Li, C. J. Murray, M. R. Madlansacay, C. Tran, N. T. Uter, G. Yin, P. J. Rivers, A. Y. Yam, W. D. Wang, A. R. Steiner, S. U. Bajad, K. Penta, W. Yang, T. J. Hallam, C. D. Thanos and A. K. Sato, *Bioconjug. Chem.*, 2014, **25**, 351–361.

144 H. Xiao, A. Chatterjee, S. H. Choi, K. M. Bajjuri, S. C. Sinha and P. G. Schultz, *Angew. Chemie - Int. Ed.*, 2013, **52**, 14080–14083.

145 B. Oller-Salvia, G. Kym and J. W. Chin, *Angew. Chemie - Int. Ed.*, 2018, **57**, 2831–2834.

146 T. Hofer, L. R. Skeffington, C. M. Chapman and C. Rader, *Biochemistry*, 2009, **48**, 12047–12057.

147 C. F. McDonagh, E. Turcott, L. Westendorf, J. B. Webster, S. C. Alley, K. Kim, J. Andreyka, I. Stone, K. J. Hamblett, J. A. Francisco and P. Carter, *Protein Eng. Des. Sel.*, 2006, **19**, 299–307.

148 J. R. Junutula, S. Bhakta, H. Raab, K. E. Ervin, C. Eigenbrot, R. Vandlen, R. H. Scheller and H. B. Lowman, *J. Immunol. Methods*, 2008, **332**, 41–52.

149 J. R. Junutula, H. Raab, S. Clark, S. Bhakta, D. D. Leipold, S. Weir, Y. Chen, M. Simpson, S. P. Tsai, M. S. Dennis, Y. Lu, Y. G. Meng, C. Ng, J. Yang, C. C. Lee, E. Duenas, J. Gorrell, V. Katta, A. Kim, K. McDorman, K. Flagella, R. Venook, S. Ross, S. D. Spencer, W. Lee Wong, H. B. Lowman, R. Vandlen, M. X. Sliwkowski, R. H. Scheller, P. Polakis and W. Mallet, *Nat. Biotechnol.*, 2008, **26**, 925–932.

150 J. R. Junutula, K. M. Flagella, R. A. Graham, K. L. Parsons, E. Ha, H. Raab, S. Bhakta, T. Nguyen, D. L. Dugger, G. Li, E. Mai, G. D. L. Phillips, H. Hiraragi, R. N. Fuji, J. Tibbitts, R. Vandlen, S. D. Spencer, R. H. Scheller, P. Polakis and M. X. Sliwkowski, *Clin. Cancer Res.*, 2010, **16**, 4769–4778.

151 B. Bernardim, P. M. S. D. Cal, M. J. Matos, B. L. Oliveira, N. Martínez-Saéz, I. S. Albuquerque, E. Perkins, F. Corzana, A. C. B. Burtoloso, G. Jiménez-Osés and G. J. L. Bernardes, *Nat. Commun.*, 2016, **7**, 13128.

152 M. J. Matos, C. D. Navo, T. Hakala, X. Ferhati, A. Guerreiro, D. Hartmann, B. Bernardim, K. L. Saar, I. Compañón, F. Corzana, T. P. J. Knowles, G. Jiménez-Osés and G. J. L. Bernardes, *Angew. Chemie - Int. Ed.*, , DOI:10.1002/anie.201901405.

153 J. P. M. Nunes, V. Vassileva, E. Robinson, M. Morais, M. E. B. Smith, R. B. Pedley, S. Caddick, J. R. Baker and V. Chudasama, *RSC Adv.*, 2017, **7**, 24828–24832.

154 J. D. Sadowsky, T. H. Pillow, J. Chen, F. Fan, C. He, Y. Wang, G. Yan, H. Yao, Z. Xu, S. Martin, D. Zhang, P. Chu, J. Dela Cruz-Chuh, A. O'Donohue, G. Li, G. Del Rosario, J. He, L. Liu, C. Ng, D. Su, G. D. Lewis Phillips, K. R. Kozak, S. F. Yu, K. Xu, D. Leipold and J. Wai, *Bioconjug. Chem.*, 2017, **28**, 2086–2098.

155 C. Zhang, M. Welborn, T. Zhu, N. J. Yang, M. S. Santos, T. Van Voorhis and B. L. Pentelute, *Nat. Chem.*, 2016, **8**, 120–128.

156 C. Zhang, P. Dai, A. A. Vinogradov, Z. P. Gates and B. L. Pentelute, *Angew. Chemie - Int. Ed.*, 2018, **57**, 6459–6463.

157 N. Forte, V. Chudasama and J. R. Baker, *Drug Discov. Today Technol.*, 2018, **30**, 11–20.

158 M. E. B. Smith, F. F. Schumacher, C. P. Ryan, L. M. Tedaldi, D. Papaioannou, G. Waksman, S. Caddick and J. R. Baker, *J. Am. Chem. Soc.*, 2010, **132**, 1960–1965.

159 F. F. Schumacher, J. P. M. Nunes, A. Maruani, V. Chudasama, M. E. B. Smith, K. A. Chester, J. R. Baker and S. Caddick, *Org. Biomol. Chem.*, 2014, **12**, 7261–7269.

160 J. P. M. Nunes, M. Morais, V. Vassileva, E. Robinson, V. S. Rajkumar, M. E. B. Smith, R. B. Pedley, S. Caddick, J. R. Baker and V. Chudasama, *Chem. Commun.*, 2015, **51**, 10624–10627.

161 M. Morais, J. P. M. Nunes, K. Karu, N. Forte, I. Benni, M. E. B. Smith, S. Caddick, V. Chudasama and J. R. Baker, *Org. Biomol. Chem.*, 2017, **15**, 2947–2952.

162 C. R. Behrens, E. H. Ha, L. L. Chinn, S. Bowers, G. Probst, M. Fitch-Bruhns, J. Monteon, A. Valdiosera, A. Bermudez, S. Liao-Chan, T. Wong, J. Melnick, J. W. Theunissen, M. R. Flory, D. Houser, K. Venstrom, Z. Levashova, P. Sauer, T. S. Migone, E. H. Van Der Horst, R. L. Halcomb and D. Y. Jackson, *Mol. Pharm.*, 2015, **12**, 3986–3998.

163 V. Chudasama, M. E. B. Smith, F. F. Schumacher, D. Papaioannou, G. Waksman, J. R. Baker and S. Caddick, *Chem. Commun.*, 2011, **47**, 8781–8783.

164 E. Robinson, J. P. M. Nunes, V. Vassileva, A. Maruani, J. C. F. Nogueira, M. E. B. Smith, R. B. Pedley, S. Caddick, J. R. Baker and V. Chudasama, *RSC Adv.*, 2017, **7**, 9073–9077.

165 A. Maruani, M. E. B. Smith, E. Miranda, K. A. Chester, V. Chudasama and S. Caddick, *Nat. Commun.*, 2015, **6**, 6645.

166 C. Bahou, D. A. Richards, A. Maruani, E. A. Love, F. Javaid, S. Caddick, J. R. Baker and V. Chudasama, *Org. Biomol. Chem.*, 2018, **16**, 1359–1366.

167 S. Shao, M. H. Tsai, J. Lu, T. Yu, J. Jin, D. Xiao, H. Jiang, M. Han, M. Wang and J. Wang, *Bioorganic Med. Chem. Lett.*, 2018, **28**, 1363–1370.

168 M. T. W. Lee, A. Maruani, J. R. Baker, S. Caddick and V. Chudasama, *Chem. Sci.*, 2016, **7**, 799–802.

169 M. T. W. Lee, A. Maruani, D. A. Richards, J. R. Baker, S. Caddick and V. Chudasama, *Chem. Sci.*, 2017, **8**, 2056–2060.

170 P. Bryant, M. Pabst, G. Badescu, M. Bird, W. McDowell, E. Jamieson, J. Swierkosz, K. Jurlewicz, R. Tommasi, K. Henseleit, X. Sheng, N. Camper, A. Manin, K. Kozakowska, K. Peciak, E. Laurine, R. Grygorash, A. Kyle, D. Morris, V. Parekh, A. Abhilash, J. W. Choi, J. Edwards, M. Frigerio, M. P. Baker and A. Godwin, *Mol. Pharm.*, 2015, **12**, 1872–1879.

171 G. Badescu, P. Bryant, M. Bird, K. Henseleit, J. Swierkosz, V. Parekh, R. Tommasi, E. Pawlisz, K. Jurlewicz, M. Farys, N. Camper, X. Sheng, M. Fisher, R. Grygorash, A. Kyle, A. Abhilash, M. Frigerio, J. Edwards and A. Godwin, *Bioconjug. Chem.*, 2014, **25**, 1124–1136.

172 M. Pabst, W. McDowell, A. Manin, A. Kyle, N. Camper, E. De Juan, V. Parekh, F. Rudge, H. Makwana, T. Kantner, H. Parekh, A. Michelet, X. B. Sheng, G. Popa, C. Tucker, F. Khayrzad, D. Pollard, K. Kozakowska, R. Resende, A. Jenkins, F. Simoes, D. Morris, P. Williams, G. Badescu, M. P. Baker, M. Bird, M. Frigerio and A. Godwin, *J. Control. Release*, 2017, **253**, 160–164.

173 Z. Miao, Y. Hong, T. Zhu and A. W. Chucholowski, *WO/2013/173391*, 2013.

174 O. Koniev, I. Dovgan, B. Renoux, A. Ehkirch, J. Eberova, S. Cianférani, S. Kolodych, S. Papot and A. Wagner, *Med. Chem. Commun.*, 2018, **9**, 827–830.

175 Q.-Y. Hu and H. Imase, *WO/2014/083505*, 2014.

176 M. Friedman, L. H. Krull and J. F. Cavins, *J. Biol. Chem.*, 1970, **245**, 3868–3871.

177 R. Sebastiano, A. Citterio, M. Lapadula and P. G. Righetti, *Rapid Commun. Mass Spectrom.*, 2003, **17**, 2380–2386.

178 J. R. Winther and C. Thorpe, *Biochim. Biophys. Acta - Gen. Subj.*, 2014, **1840**, 838–846.

179 J. Heukeshoven, *Anal. Biochem.*, 1980, **109**, 421–425.

180 G. Gorin, P. A. Martic and G. Doughty, *Arch. Biochem. Biophys.*, 1966, **115**, 593–597.

181 K. Lindorff-Larsen and J. R. Winther, *Anal. Biochem.*, 2000, **286**, 308–310.

182 A. R. Katritzky, G. R. Khan and O. A. Schwarz, *Tetrahedron Lett.*, 1984, **25**, 1223–

1226.

183 A. R. Katritzky, I. Takahashi and C. M. Marson, *J. Org. Chem.*, 1986, **51**, 4914–4920.

184 A. G. Watts, T. Kantner and A. B. Mackensie, *WO/2010/070300*, 2010.

185 A. D. Baxter, C. M. Birchall, D. J. Mansell, J. H. Mysliwy and J. Thirlway, *WO/2016/067021*, 2016.

186 M. S. Frei, M. K. Bilyard, T. A. Alanine, W. R. J. D. Galloway, J. E. Stokes and D. R. Spring, *Bioorganic Med. Chem.*, 2015, **23**, 2666–2679.

187 D. G. Twigg, N. Kondo, S. L. Mitchell, W. R. J. D. Galloway, H. F. Sore, A. Madin and D. R. Spring, *Angew. Chemie - Int. Ed.*, 2016, **55**, 12479–12483.

188 Q. Wang, T. R. Chan, R. Hilgraf, V. V. Fokin, K. B. Sharpless and M. G. Finn, *J. Am. Chem. Soc.*, 2003, **125**, 3192–3193.

189 C. S. McKay and M. G. Finn, *Chem. Biol.*, 2014, **21**, 1075–1101.

190 D. E. Scott, M. T. Ehebauer, T. Pukala, M. Marsh, T. L. Blundell, A. R. Venkitaraman, C. Abell and M. Hyvönen, *ChemBioChem*, 2013, **14**, 332–342.

191 M. Rossmann, S. J. Greive, T. Moschetti, M. Dinan and M. Hyvönen, *Protein Eng. Des. Sel.*, 2017, **30**, 419–430.

192 T. Moschetti, T. Sharpe, G. Fischer, M. E. Marsh, H. K. Ng, M. Morgan, D. E. Scott, T. L. Blundell, A. R. Venkitaraman, J. Skidmore, C. Abell and M. Hyvönen, *J. Mol. Biol.*, 2016, **428**, 4589–4607.

193 J. Peränen, M. Rikkonen, M. Hyvönen and L. Kääriäinen, *Anal. Biochem.*, 1996, **236**, 371–373.

194 T. Liu, Y. Wang, X. Luo, J. Li, S. A. Reed, H. Xiao, T. S. Young and P. G. Schultz, *Proc. Natl. Acad. Sci.*, 2016, **113**, 5910–5915.

195 A. L. Schechter, D. F. Stern, L. Vaidyanathan, S. J. Decker, J. A. Drebin, M. I. Greene and R. A. Weinberg, *Nature*, 1984, **312**, 513–516.

196 D. Slamon, G. Clark, S. Wong, W. Levin, A. Ullrich and W. McGuire, *Science*, 1987, **235**, 177–182.

197 I. L. Andrulis, S. B. Bull, M. E. Blackstein, D. Sutherland, C. Mak, S. Sidlofsky, K. P. H. Pritzker, R. W. Hartwick, W. Hanna, L. Lickley, R. Wilkinson, A. Qizilbash, U. Ambus, M. Lipa, H. Weizel, A. Katz, M. Baida, S. Mariz, G. Stoik, P. Dacamara, D. Strongitharm, W. Geddie and D. McCready, *J. Clin. Oncol.*, 1998, **16**, 1340–1349.

198 B. A. Gusterson, R. D. Gelber, A. Goldhirsch, K. N. Price, J. Säve-Söderborgh, R.

Anbazhagan, J. Styles, C. M. Rudenstam, R. Golouh and R. Reed, *J. Clin. Oncol.*, 2017, **10**, 1049–1056.

199 Y. Yarden and M. X. Sliwkowski, *Nat. Rev. Mol. Cell Biol.*, 2001, **2**, 127–137.

200 D. J. Slamon, B. Leyland-Jones, S. Shak, H. Fuchs, V. Paton, A. Bajamonde, T. Fleming, W. Eiermann, J. Wolter, M. Pegram, J. Baselga and L. Norton, *N. Engl. J. Med.*, 2001, **344**, 783–792.

201 K. S. Gunturu, Y. Woo, N. Beaubier, H. E. Remotti and M. W. Saif, *Ther. Adv. Med. Oncol.*, 2013, **5**, 143–151.

202 C. A. Hudis, *N. Engl. J. Med.*, 2007, **357**, 39–51.

203 G. Valabrega, F. Montemurro and M. Aglietta, *Ann. Oncol.*, 2007, **18**, 977–984.

204 S. Sun, P. Akkapeddi, M. C. Marques, N. Martínez-Sáez, V. M. Torres, C. Cordeiro, O. Boutureira and G. J. L. Bernardes, *Org. Biomol. Chem.*, 2019, **17**, 2005–2012.

205 K. Lang and J. W. Chin, *ACS Chem. Biol.*, 2014, **9**, 16–20.

206 Y. A. Lin, J. M. Chalker, N. Floyd, G. J. L. Bernardes and B. G. Davis, *J. Am. Chem. Soc.*, 2008, **130**, 9642–9643.

207 Y. A. Lin, J. M. Chalker and B. G. Davis, *J. Am. Chem. Soc.*, 2010, **132**, 16805–16811.

208 N. J. Agard, J. A. Prescher and C. R. Bertozzi, *J. Am. Chem. Soc.*, 2004, **126**, 15046–15047.

209 X. Ning, J. Guo, M. A. Wolfert and G. J. Boons, *Angew. Chemie - Int. Ed.*, 2008, **47**, 2253–2255.

210 P. Holliger, T. Prospero and G. Winter, *Proc. Natl. Acad. Sci. U. S. A.*, 1993, **90**, 6444–6448.

211 P. Holliger and P. J. Hudson, *Nat. Biotechnol.*, 2005, **23**, 1126–1136.

212 M. P. Deonarain, G. Yahioglu, I. Stamati and J. Marklew, *Expert Opin. Drug Discov.*, 2015, **10**, 463–481.

213 D. Litvak-Greenfeld and I. Benhar, *Adv. Drug Deliv. Rev.*, 2012, **64**, 1782–1799.

214 C. Wu, H. Ying, C. Grinnell, S. Bryant, R. Miller, A. Clabbers, S. Bose, D. McCarthy, R. R. Zhu, L. Santora, R. Davis-Taber, Y. Kunes, E. Fung, A. Schwartz, P. Sakorafas, J. Gu, E. Tarcsa, A. Murtaza and T. Ghayur, *Nat. Biotechnol.*, 2007, **25**, 1290–1297.

215 N. A. Goebl, C. M. Babbey, A. Datta-Mannan, D. R. Witcher, V. J. Wroblewski and K. W. Dunn, *Mol. Biol. Cell*, 2008, **19**, 5490–5505.

216 A. L. Nelson and J. M. Reichert, *Nat. Biotechnol.*, 2009, **27**, 331–337.

217 F. Selis, G. Focà, A. Sandomenico, C. Marra, C. Di Mauro, G. S. Jotti, S. Scaramuzza, A. Politano, R. Sanna, M. Ruvo and G. Tonon, *Int. J. Mol. Sci.*, 2016, **17**, 1–15.

218 L. Castañeda, A. Maruani, F. F. Schumacher, E. Miranda, V. Chudasama, K. A. Chester, J. R. Baker, M. E. B. Smith and S. Caddick, *Chem. Commun.*, 2013, **49**, 8187–8189.

219 R. P. Lyon, T. D. Bovee, S. O. Doronina, P. J. Burke, J. H. Hunter, H. D. Neff-Laford, M. Jonas, M. E. Anderson, J. R. Setter and P. D. Senter, *Nat. Biotechnol.*, 2015, **33**, 733–735.

220 S. V. Govindan, T. M. Cardillo, R. M. Sharkey, F. Tat, D. V. Gold and D. M. Goldenberg, *Mol. Cancer Ther.*, 2013, **12**, 968–978.

221 H. J. Ross, L. L. Hart, P. M. Swanson, M. U. Rarick, R. A. Figlin, A. D. Jacobs, D. E. McCune, A. H. Rosenberg, A. D. Baron, L. E. Grove, M. D. Thorn, D. M. Miller, J. G. Drachman and C. M. Rudin, *Lung Cancer*, 2006, **54**, 69–77.

222 J. H. Beijnen, G. Wiese and W. J. Underberg, *Pharm. Weekbl. Sci.*, 1985, **7**, 109–116.

223 G. A. Pietersz, J. Kanellos, M. J. Smyth, J. Zalcberg and I. F. C. McKenzie, *Immunol. Cell Biol.*, 1987, **65**, 111–125.

224 S. Knutson, E. Raja, R. Bomgarden, M. Nlend, A. Chen, R. Kalyanasundaram and S. Desai, *PLoS One*, 2016, **11**, e0157762.

225 H. Bouchard, M.-P. Brun and P. Hubert, *WO/2018/206635*, 2018.

226 A. Dal Corso and D. Neri, *J. Control. Release*, 2017, **246**, 39–45.

227 F. Garro-Helion, A. Merzouk and F. Guibé, *J. Org. Chem.*, 1993, **58**, 6109–6113.

228 F. Kratz, *J. Control. Release*, 2008, **132**, 171–183.

229 J. Drevs, I. Hofmann, D. Marmé, C. Unger and F. Kratz, *Drug Deliv. J. Deliv. Target. Ther. Agents*, 1999, **6**, 89–95.

230 M. T. Larsen, M. Kuhlmann, M. L. Hvam and K. A. Howard, *Mol. Cell. Ther.*, 2016, **4**, 3.

231 N. Martínez-Sáez, S. Sun, D. Oldrini, P. Sormanni, O. Boutureira, F. Carboni, I. Compañón, M. J. Deery, M. Vendruscolo, F. Corzana, R. Adamo and G. J. L. Bernardes, *Angew. Chemie - Int. Ed.*, 2017, **56**, 14963–14967.

232 S. J. Walsh, S. Omarjee, W. R. J. D. Galloway, T. T.-L. Kwan, H. F. Sore, J. S.

Parker, M. Hyvönen, J. S. Carroll and D. R. Spring, *Chem. Sci.*, 2019, **10**, 694–700.

233 D. M. Patterson and J. A. Prescher, *Curr. Opin. Chem. Biol.*, 2015, **28**, 141–149.

234 M. R. Levengood, X. Zhang, J. H. Hunter, K. K. Emmerton, J. B. Miyamoto, T. S. Lewis and P. D. Senter, *Angew. Chemie - Int. Ed.*, 2017, **56**, 733–737.

235 H. Pye, M. A. Butt, H. W. Reinert, A. Maruani, J. P. M. Nunes, J. S. Marklew, M. Qurashi, L. Funnell, A. May, I. Stamati, R. Hamoudi, J. R. Baker, M. E. B. Smith, S. Caddick, M. P. Deonarain, G. Yahioglu, V. Chudasama and L. B. Lovat, *Photochem. Photobiol. Sci.*, 2016, **15**, 1227–1238.

236 S. Puthenveetil, S. Musto, F. Loganzo, L. N. Tumey, C. J. O'Donnell and E. Graziani, *Bioconjug. Chem.*, 2016, **27**, 1030–1039.

237 L. S. Kocsis, E. Benedetti and K. M. Brummond, *Org. Lett.*, 2012, **14**, 4430–4433.

238 L. W. K. Moodie and D. S. Larsen, *European J. Org. Chem.*, 2014, 1684–1694.

239 J. R. Parikh and W. von E. Doering, *J. Am. Chem. Soc.*, 1967, **89**, 5505–5507.

240 S. S. Kelkar and T. M. Reineke, *Bioconjug. Chem.*, 2011, **22**, 1879–1903.

241 A. Kumar, T. Mastren, B. Wang, J. T. Hsieh, G. Hao and X. Sun, *Bioconjug. Chem.*, 2016, **27**, 1681–1689.

242 X. Wu, X. Sun, Z. Guo, J. Tang, Y. Shen, T. D. James, H. Tian and W. Zhu, *J. Am. Chem. Soc.*, 2014, **136**, 3579–3588.

243 J. B. Wu, T. P. Lin, J. D. Gallagher, S. Kushal, L. W. K. Chung, H. E. Zhau, B. Z. Olenyuk and J. C. Shih, *J. Am. Chem. Soc.*, 2015, **137**, 2366–2374.

244 S. A. Kularatne, K. Wang, H. K. R. Santhapuram and P. S. Low, *Mol. Pharm.*, 2009, **6**, 780–789.

245 S. Santra, C. Kaittanis, O. J. Santiesteban and J. M. Perez, *J. Am. Chem. Soc.*, 2011, **133**, 16680–16688.

246 A. Moss, J. Gudas, T. Albertson, N. Whiting and C.-L. Law, *Cancer Res.*, 2015, **74**, 104.

247 K. L. Moek, D. Giesen, I. C. Kok, D. J. A. de Groot, M. Jalving, R. S. N. Fehrmann, M. N. Lub-de Hooge, A. H. Brouwers and E. G. E. de Vries, *J. Nucl. Med.*, 2017, **58**, 83S–90S.

248 C. Bahou, E. A. Love, S. Leonard, R. J. Spears, A. Maruani, K. Armour, J. R. Baker and V. Chudasama, *Bioconjug. Chem.*, 2019, **30**, 1048–1054.

249 K. Lang, L. Davis, S. Wallace, M. Mahesh, D. J. Cox, M. L. Blackman, J. M. Fox and

J. W. Chin, *J. Am. Chem. Soc.*, 2012, **134**, 10317–10320.

250 B. L. Oliveira, Z. Guo and G. J. L. Bernardes, *Chem. Soc. Rev.*, 2017, **46**, 4895–4950.

251 I. Nikič, T. Plass, O. Schraidt, J. Szymański, J. A. G. Briggs, C. Schultz and E. A. Lemke, *Angew. Chemie - Int. Ed.*, 2014, **53**, 2245–2249.

252 P. M. S. D. Cal, R. F. M. Frade, V. Chudasama, C. Cordeiro, S. Caddick and P. M. P. Gois, *Chem. Commun.*, 2014, **50**, 5261–5263.

253 J. Iegre, J. S. Gaynord, N. S. Robertson, H. F. Sore, M. Hyvönen and D. R. Spring, *Adv. Ther.*, 2018, **1**, 1800052.

254 T. Uhlig, T. Kyprianou, F. G. Martinelli, C. A. Oppici, D. Heiligers, D. Hills, X. R. Calvo and P. Verhaert, *EuPA Open Proteomics*, 2014, **4**, 58–69.

255 Y. H. Lau, P. De Andrade, S. T. Quah, M. Rossmann, L. Laraia, N. Sköld, T. J. Sum, P. J. E. Rowling, T. L. Joseph, C. Verma, M. Hyvönen, L. S. Itzhaki, A. R. Venkitaraman, C. J. Brown, D. P. Lane and D. R. Spring, *Chem. Sci.*, 2014, **5**, 1804–1809.

256 C. E. Schafmeister, J. Po and G. L. Verdine, *J. Am. Chem. Soc.*, 2000, **122**, 5891–5892.

257 A. J. Rojas, C. Zhang, E. V. Vinogradova, N. H. Buchwald, J. Reilly, B. L. Pentelute and S. L. Buchwald, *Chem. Sci.*, 2017, **8**, 4257–4263.

258 C. M. Grison, G. M. Burslem, J. A. Miles, L. K. A. Pilsl, D. J. Yeo, Z. Imani, S. L. Warriner, M. E. Webb and A. J. Wilson, *Chem. Sci.*, 2017, **8**, 5166–5171.

259 Z. Li, R. Huang, H. Xu, J. Chen, Y. Zhan, X. Zhou, H. Chen and B. Jiang, *Org. Lett.*, 2017, **19**, 4972–4975.

260 D. Willner, P. A. Trail, S. J. Hofstead, S. J. Lasch, G. R. Braslawsky, S. J. Lasch, R. S. Greenfield, G. R. Braslawsky, T. Kaneko, R. S. Greenfield and T. Kaneko, *Bioconjug. Chem.*, 1993, **4**, 521–527.

Appendix A – NMR

2-amino-4-vinylpyridine (1)

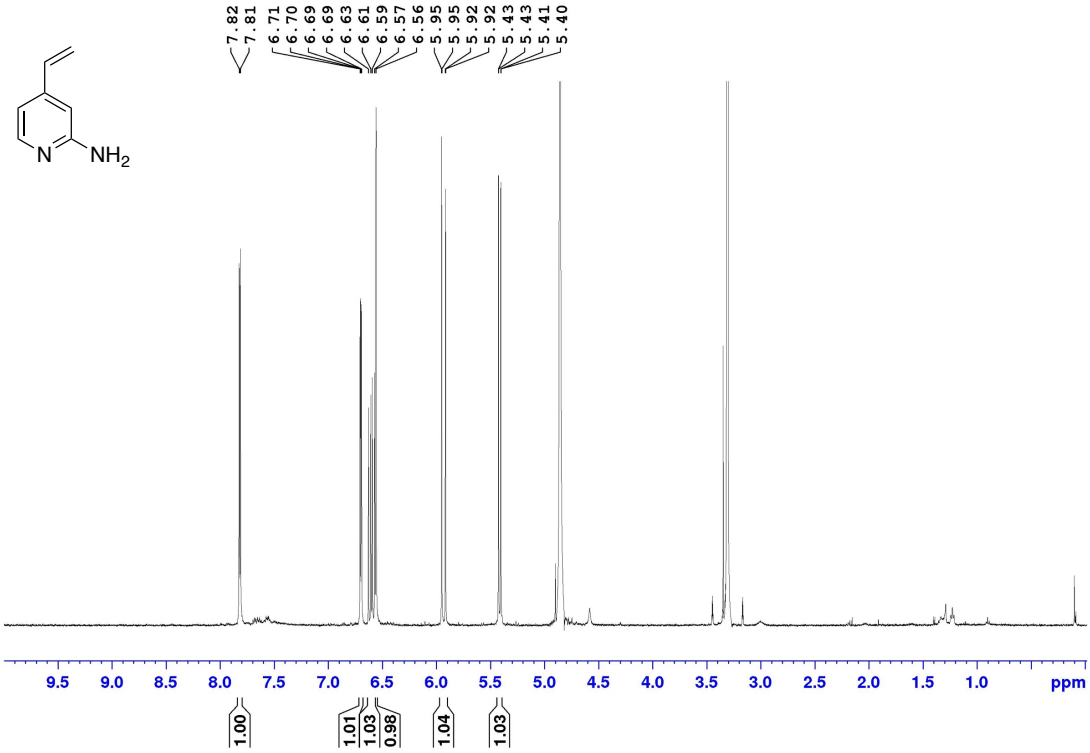

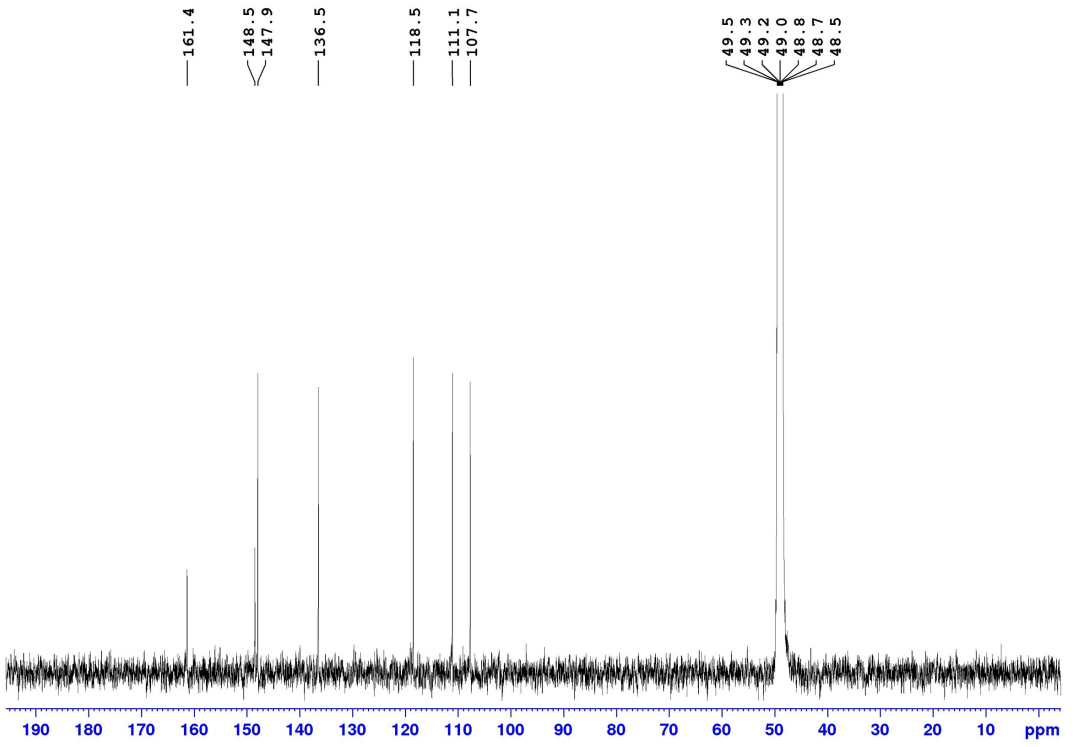

4-amino-2-vinylpyridine (2)

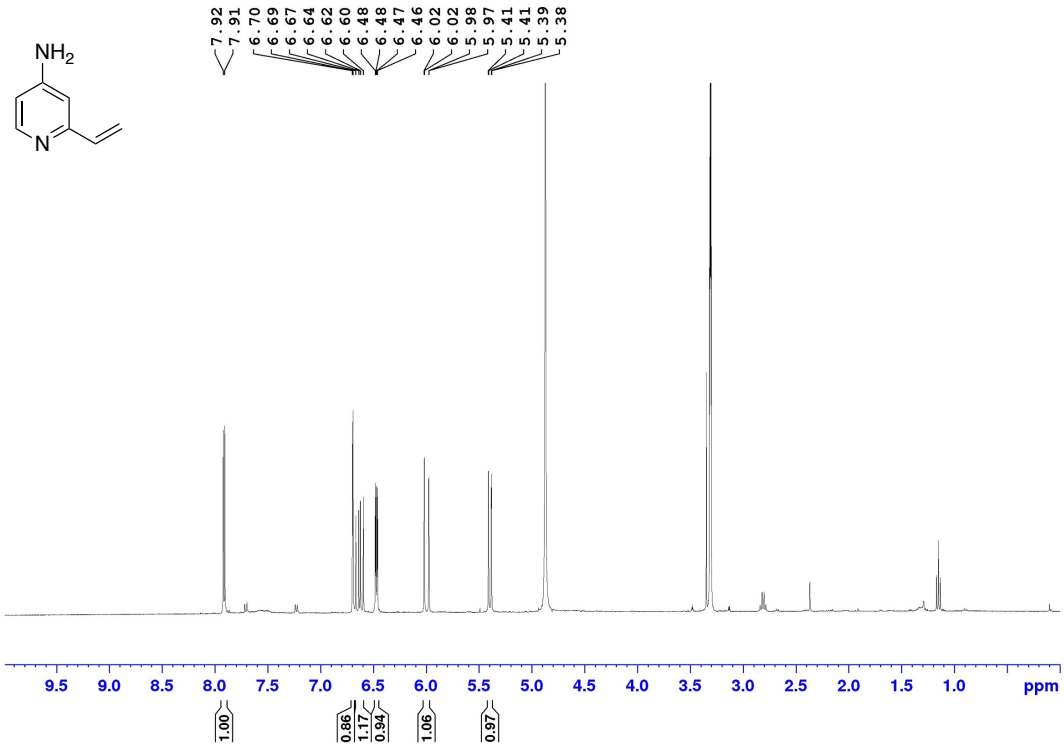

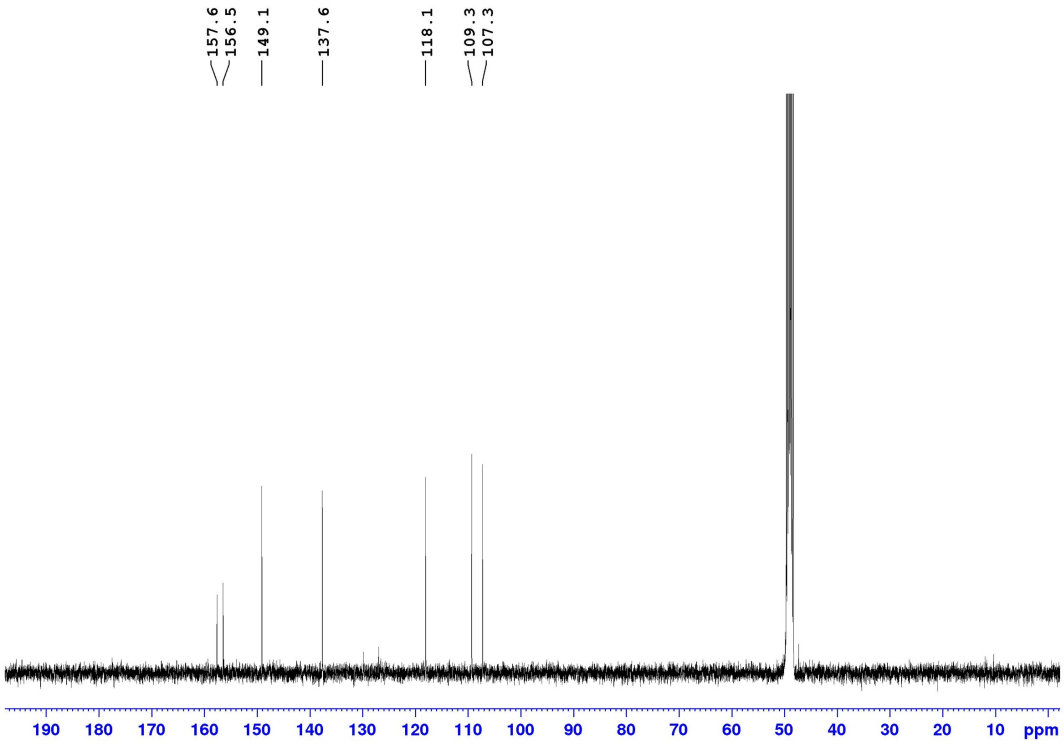

Methyl *S*-(2-(2-aminopyridin-4-yl)ethyl)-*N*-(*tert*-butoxycarbonyl)-*L*-cysteinate (3)

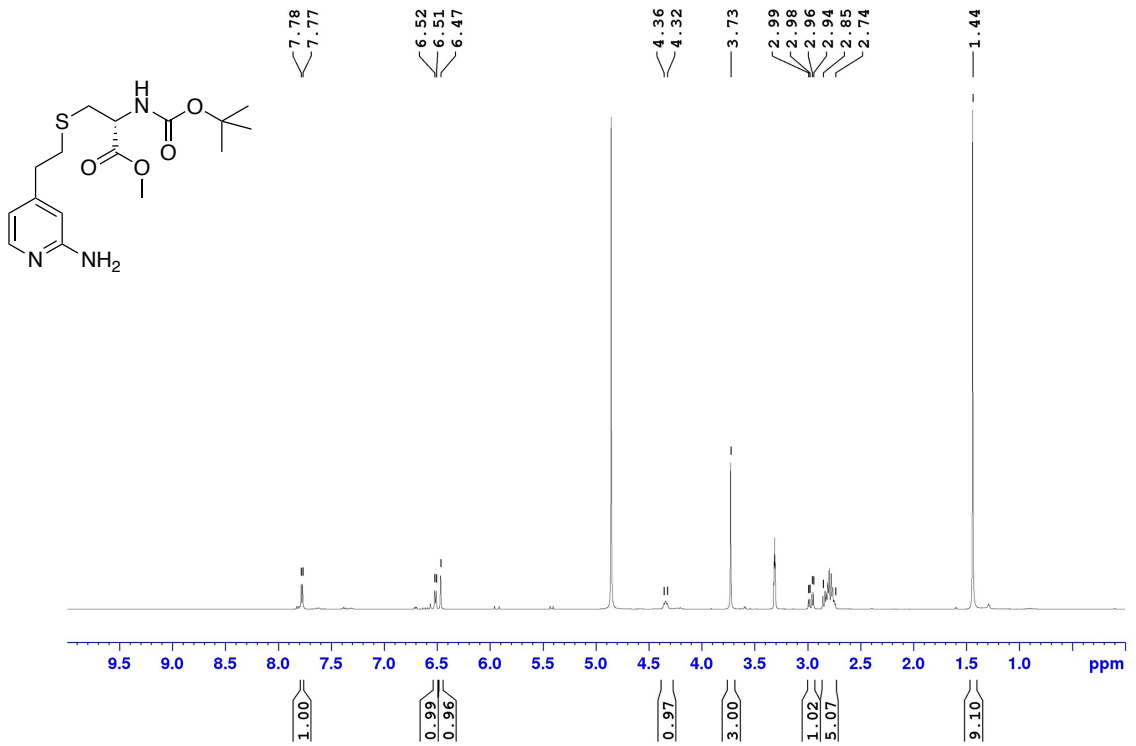

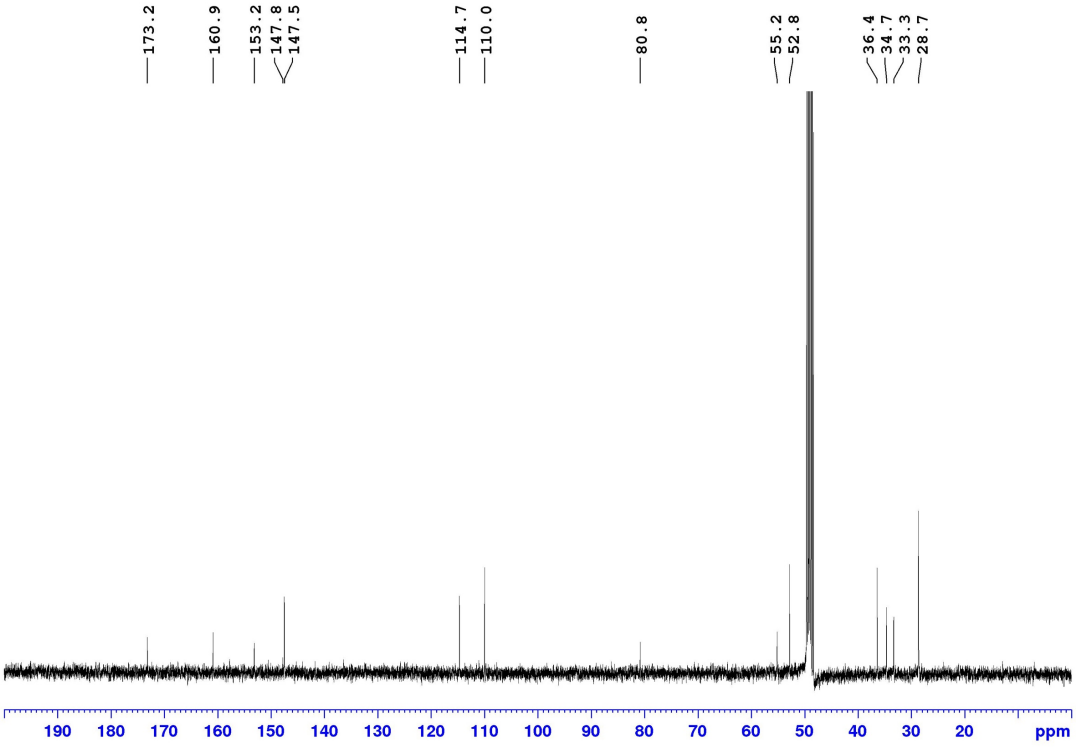

Methyl *S*-(2-(4-aminopyridin-2-yl)ethyl)-*N*-(*tert*-butoxycarbonyl)-*L*-cysteinate (4)

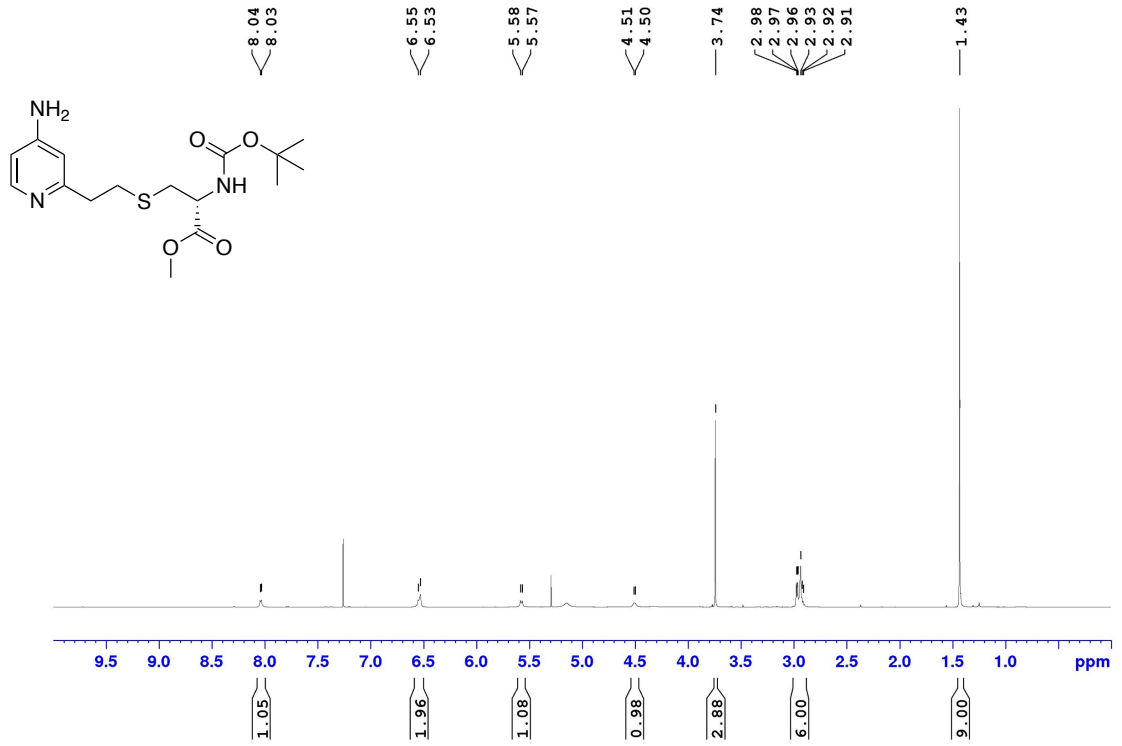

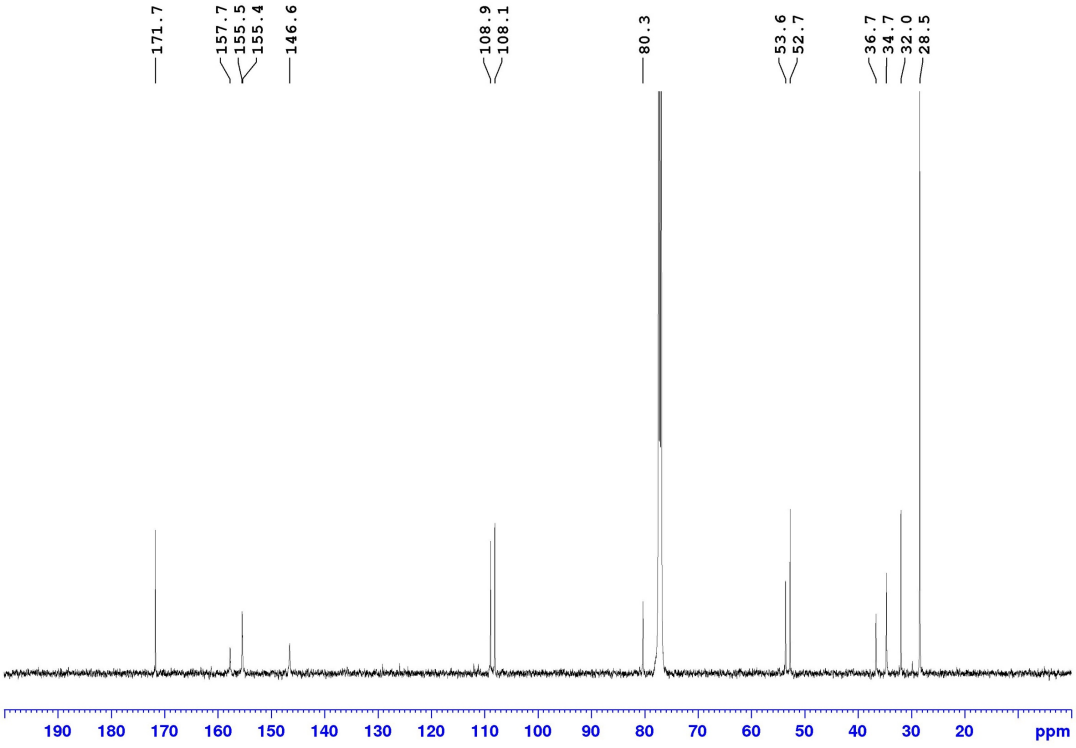

2,6-divinylpridine-4-carboxylic acid (5)

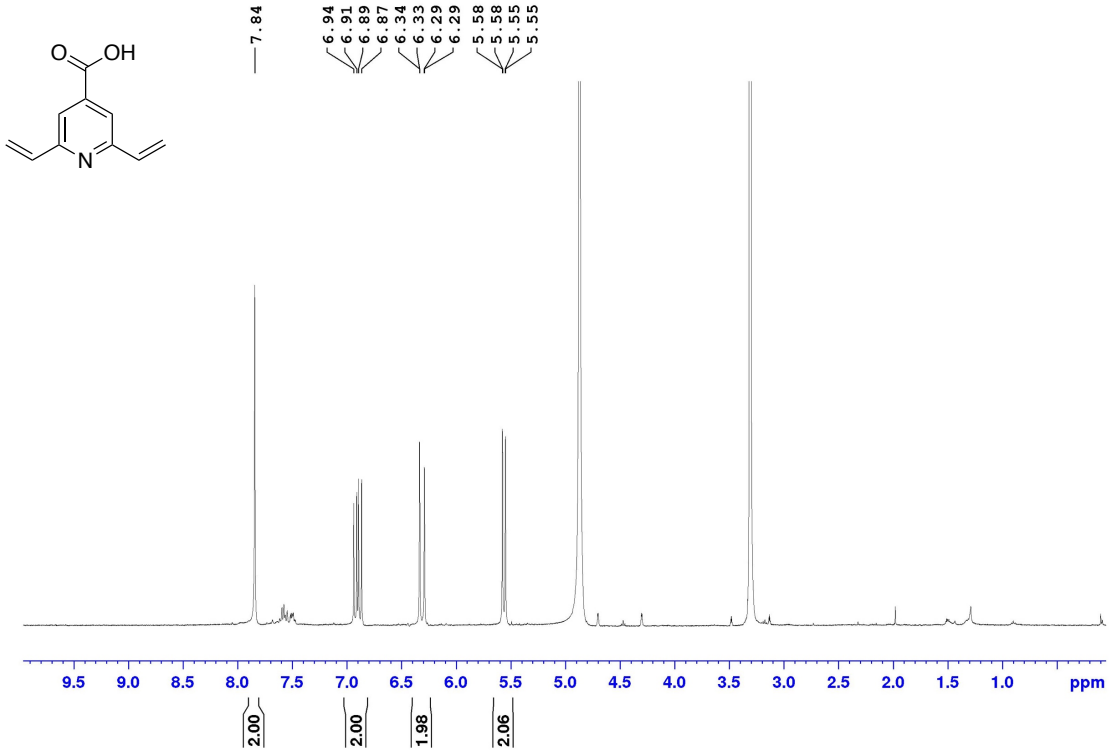

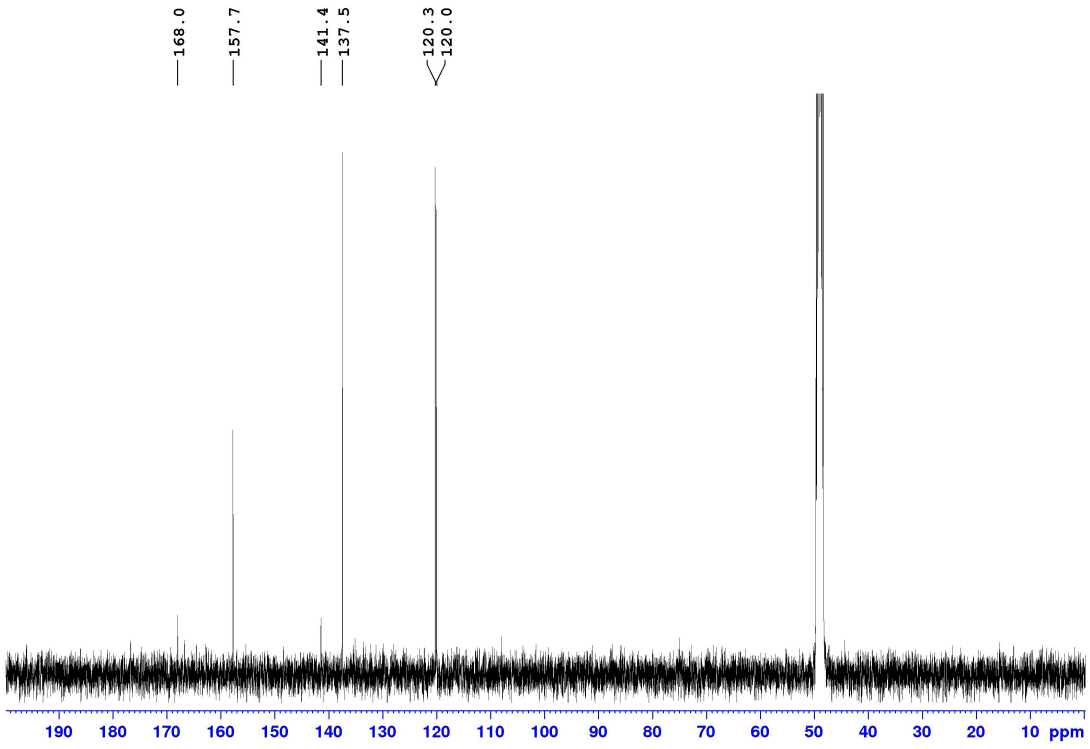

N-(but-3-yn-1-yl)-2,6-divinylisonicotinamide (6)

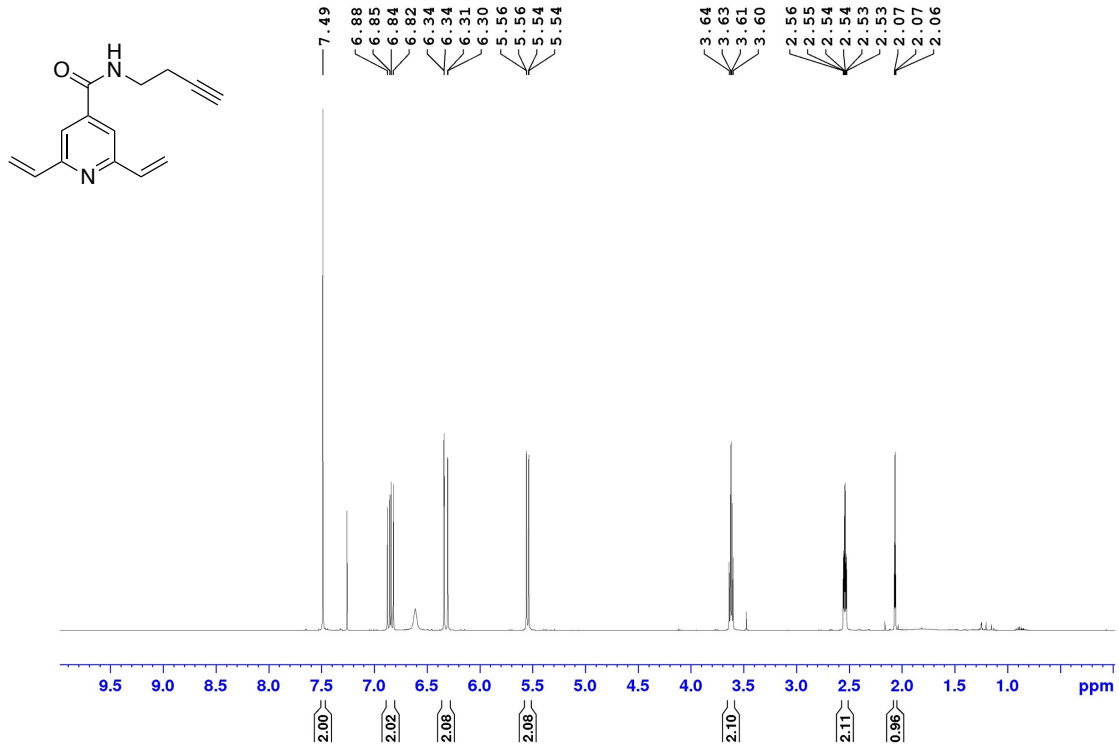

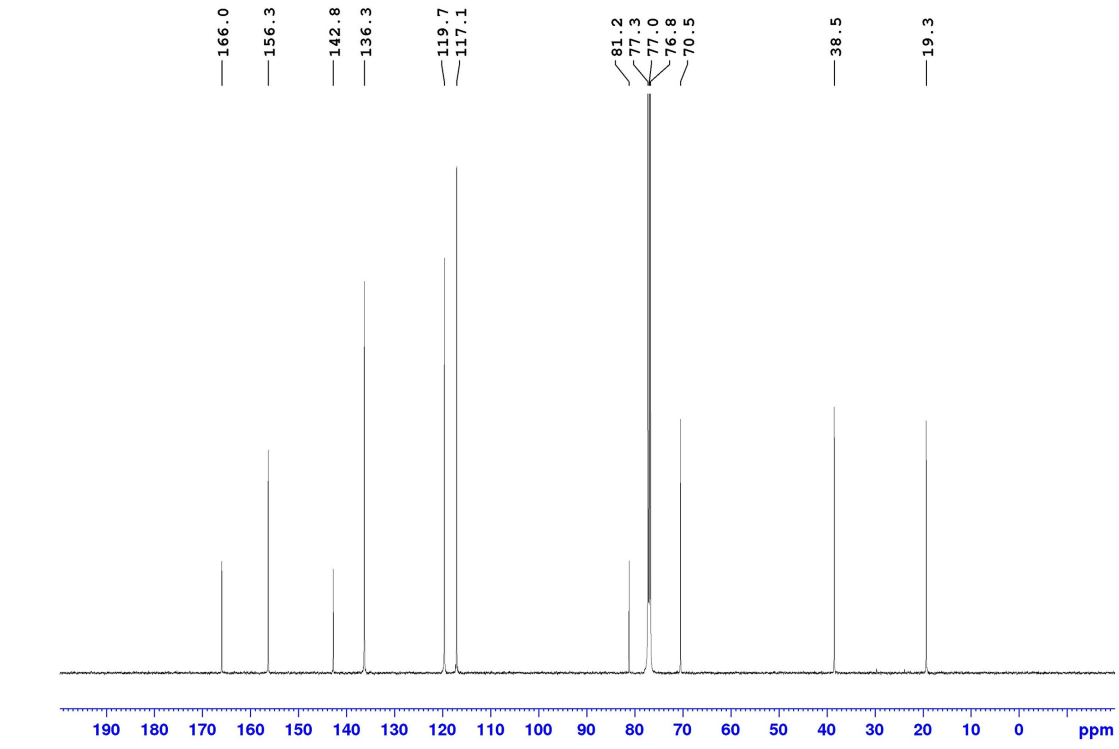

2,6-bis(2-(((*R*)-2-((*tert*-butoxycarbonyl)amino)-3-methoxy-3-oxopropyl)-thio)ethyl)isonicotinic acid (7)

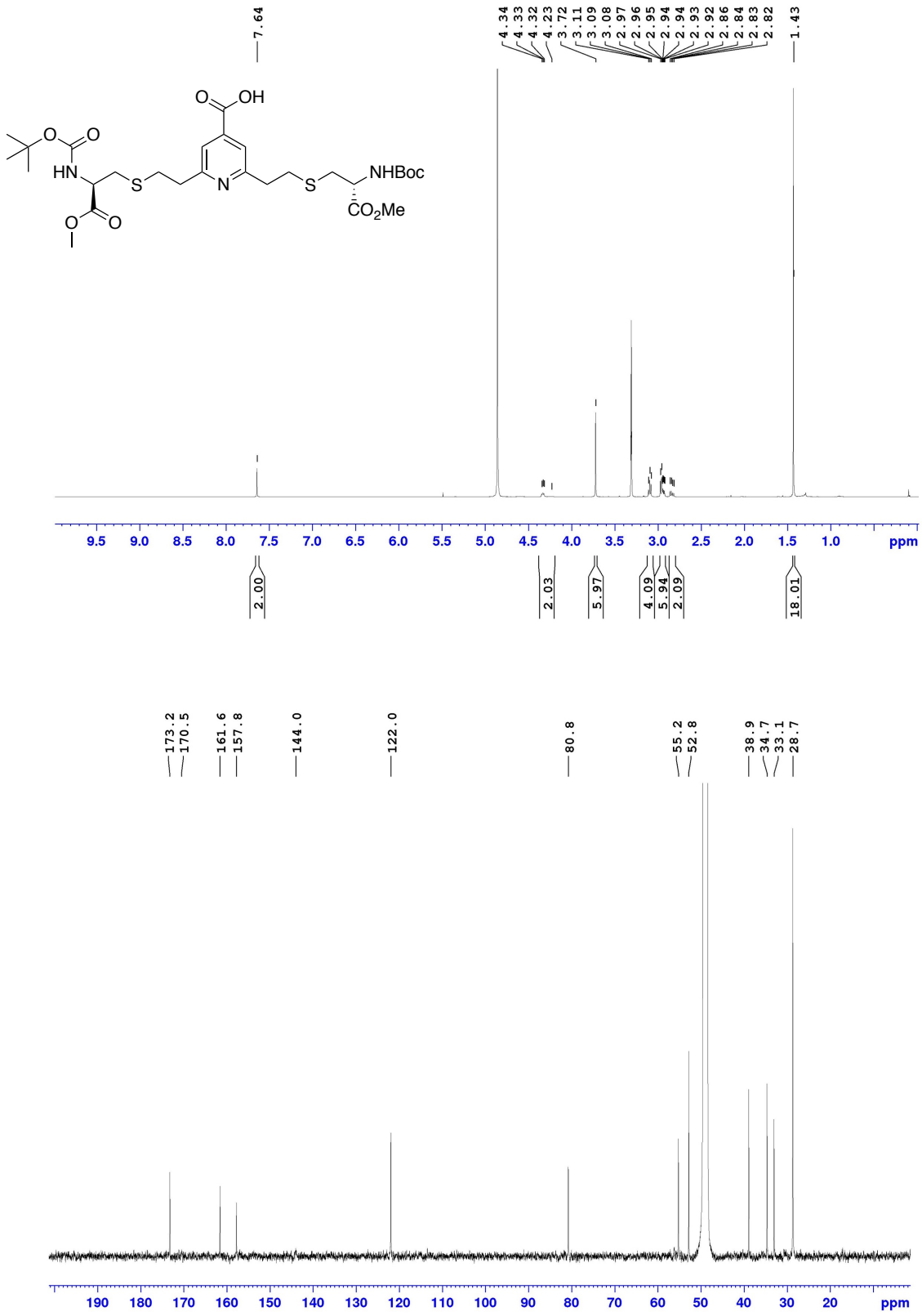

2-amino-4-vinylpyrimidine (11)

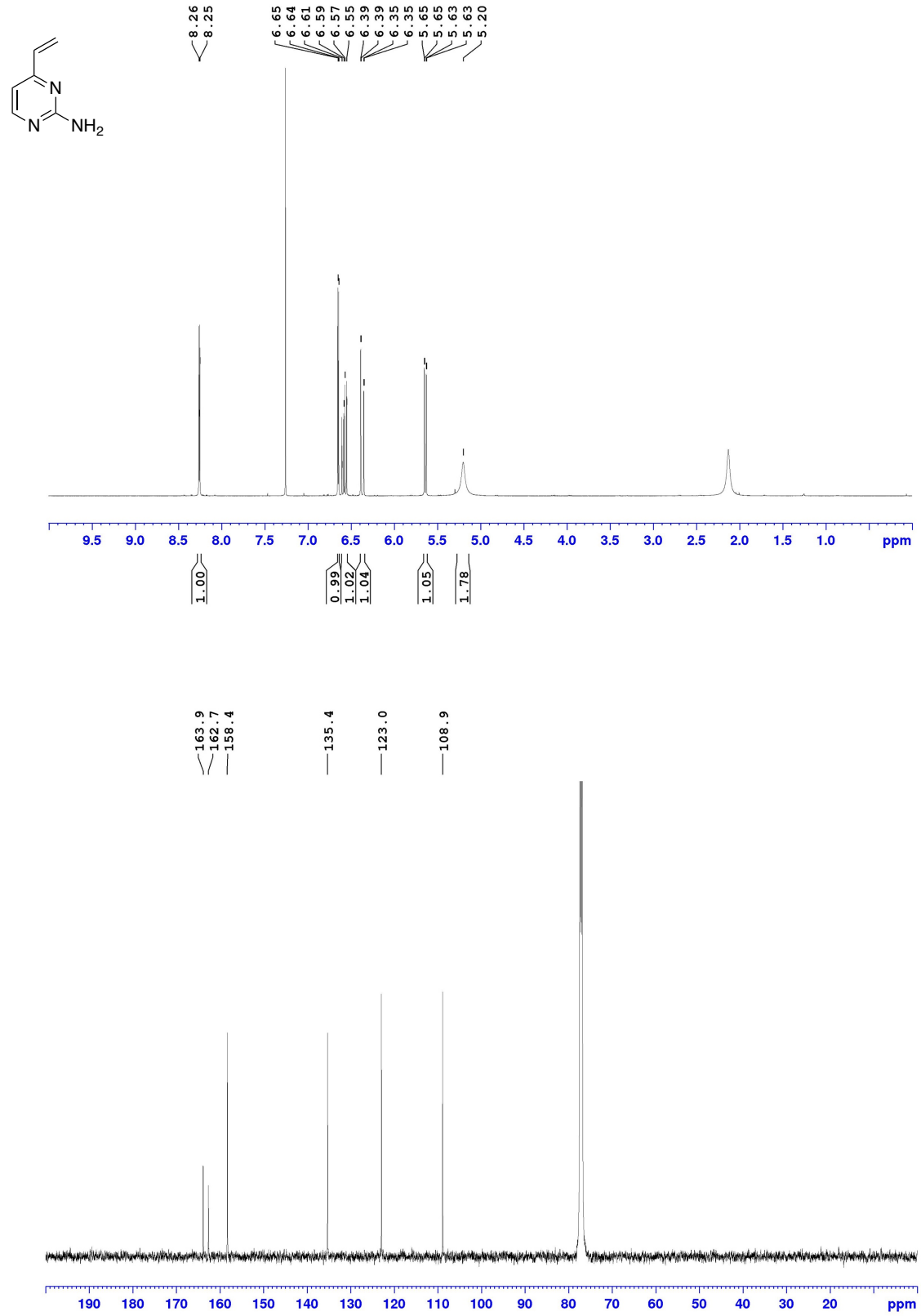

Methyl *S*-(2-(2-aminopyrimidin-4-yl)ethyl)-*N*-*tert*-butoxycarbonyl)-*L*-cysteinate (12)

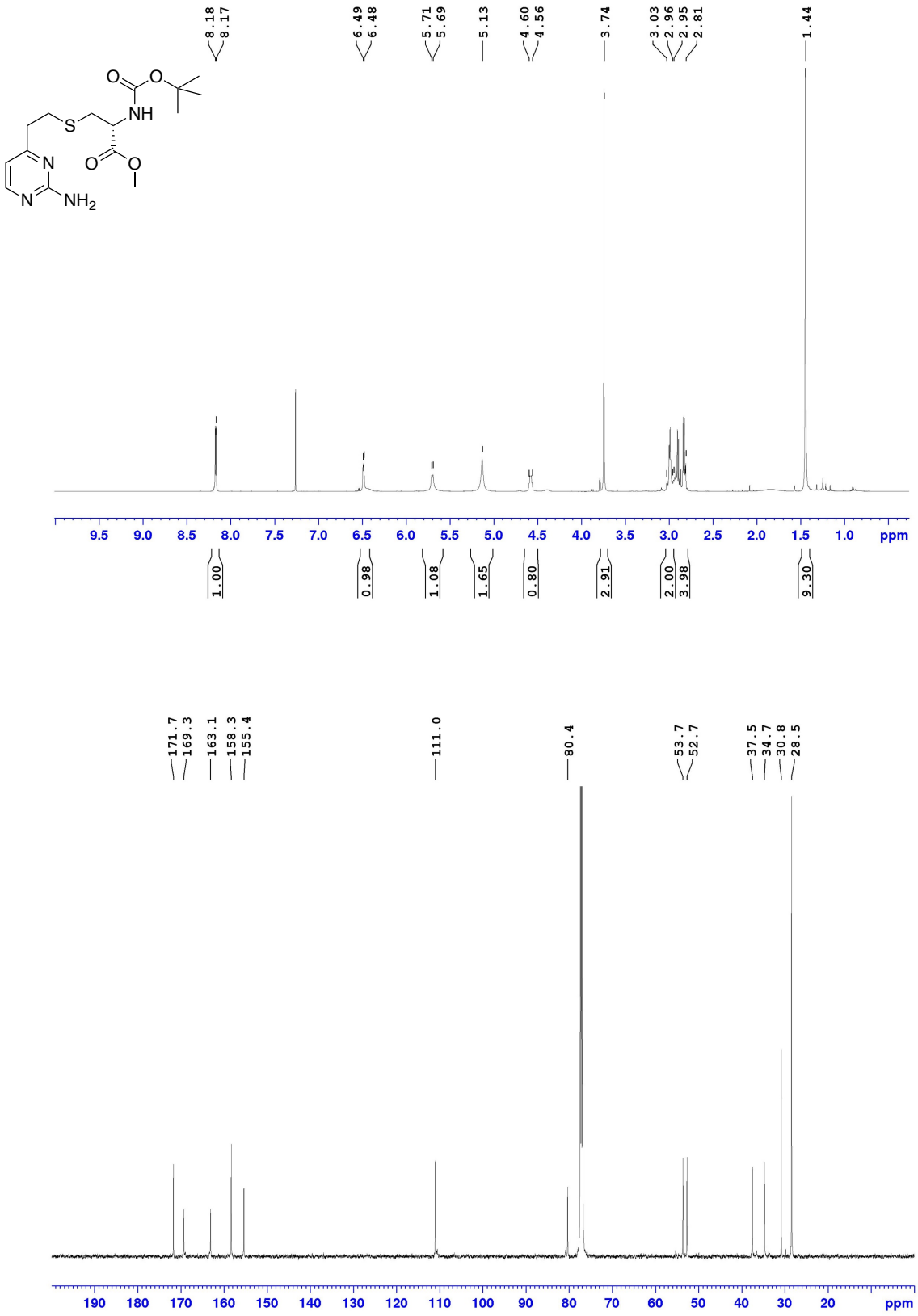

Methyl *S*-(1-benzyl-2,5-dioxopyrrolidin-3-yl)-*N*-(*tert*-butoxycarbonyl)-*L*-cysteinate (13)

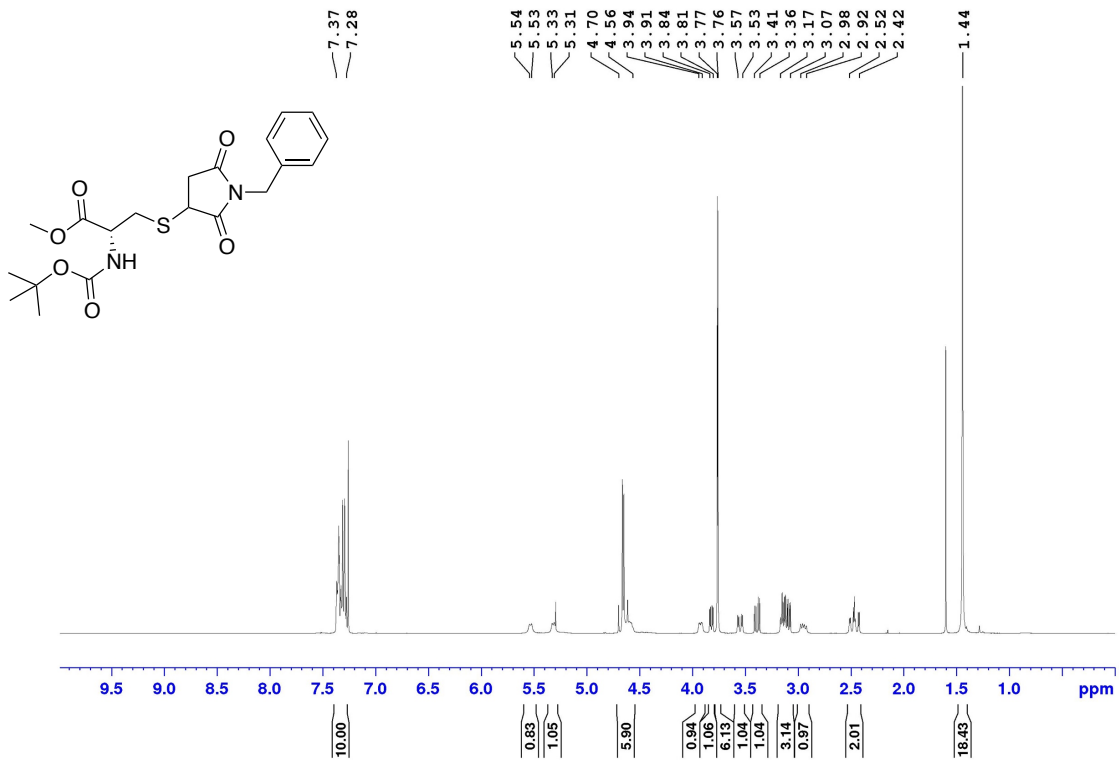

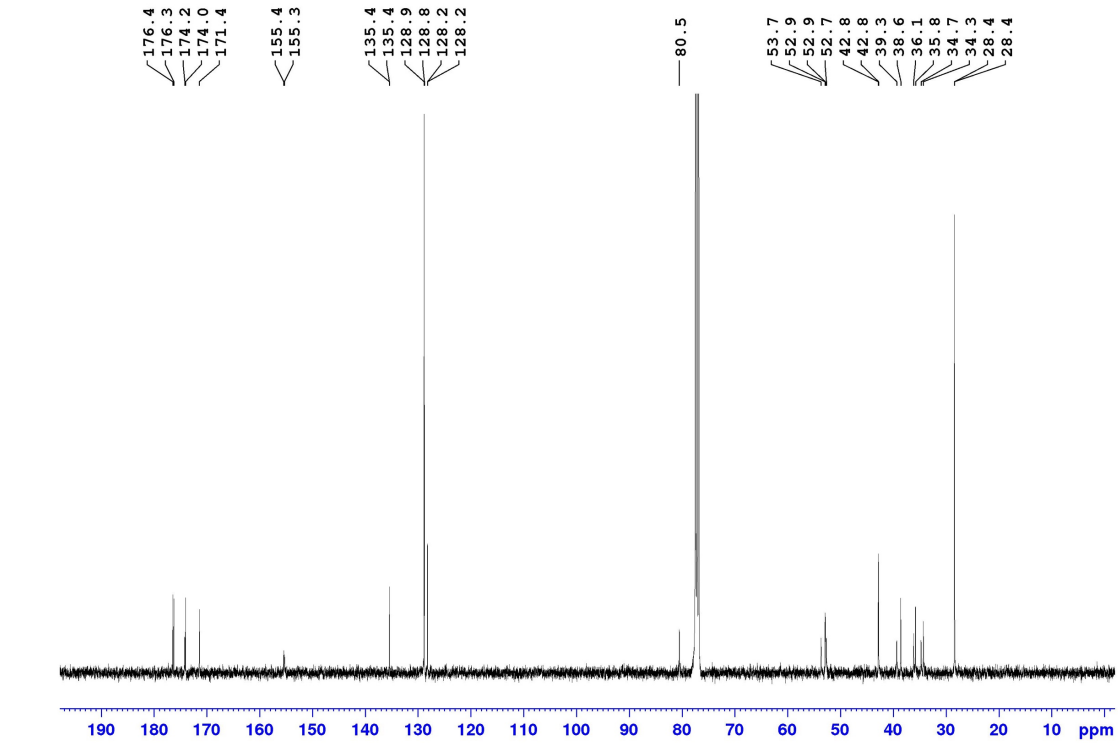

2-amino-4,6-divinylpyrimidine (15)

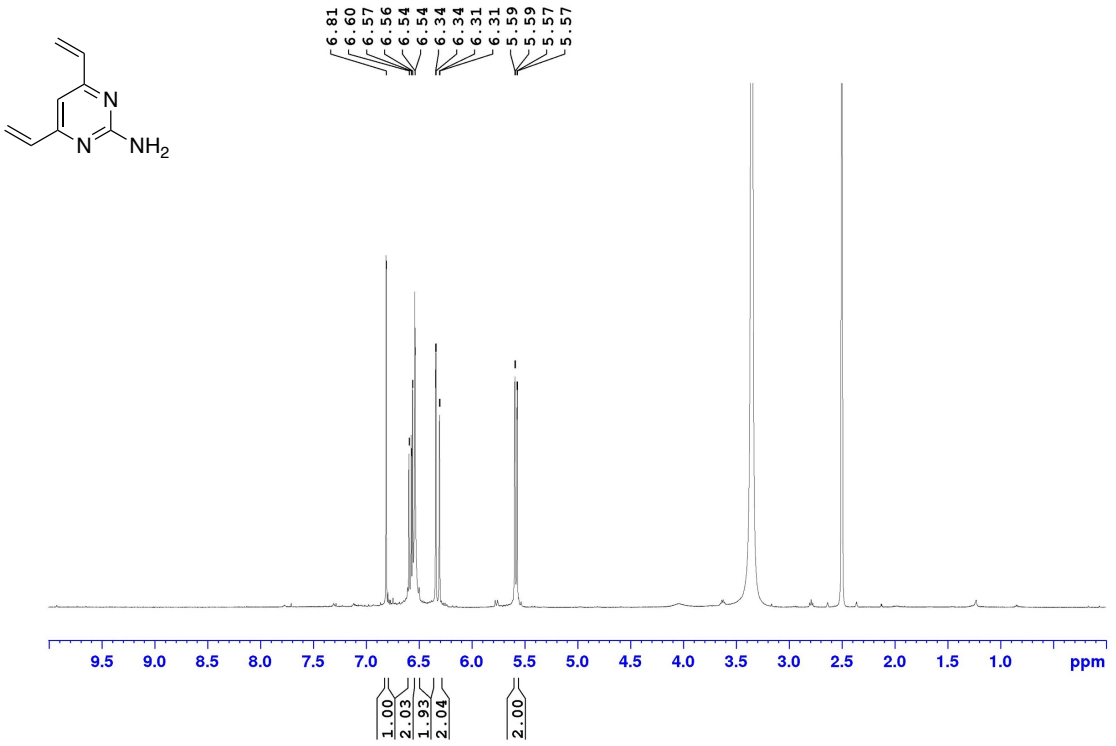

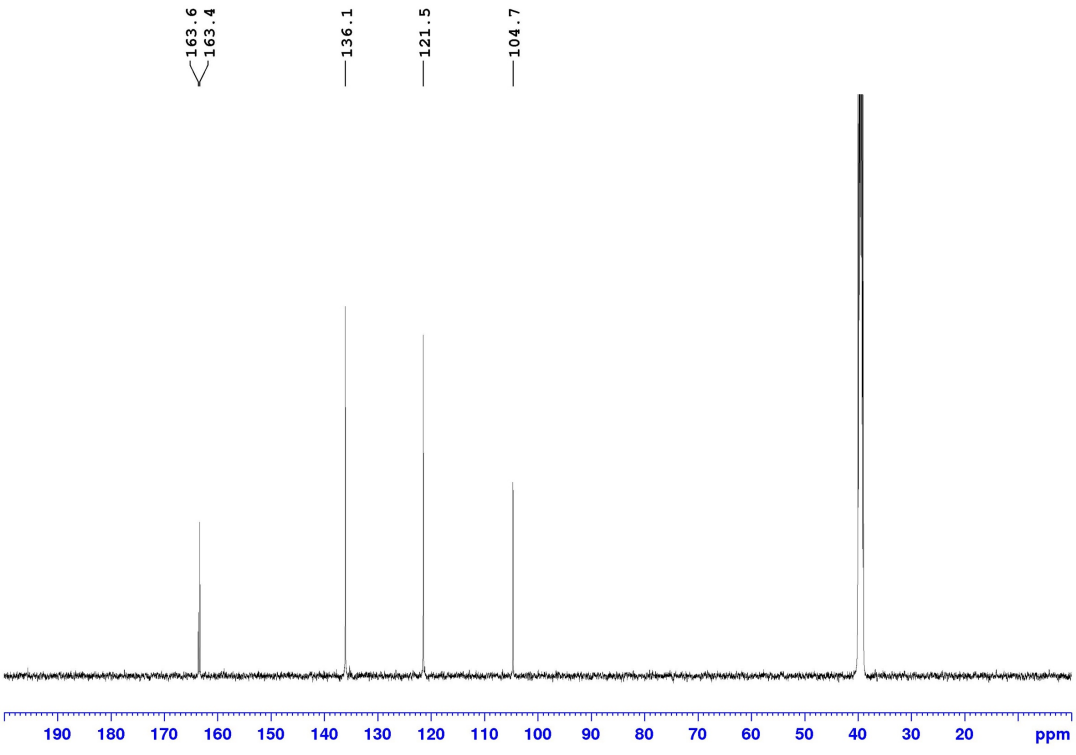

N-(hex-5-yn-1-yl)-4,6-divinylpyrimidin-2-amine (18)

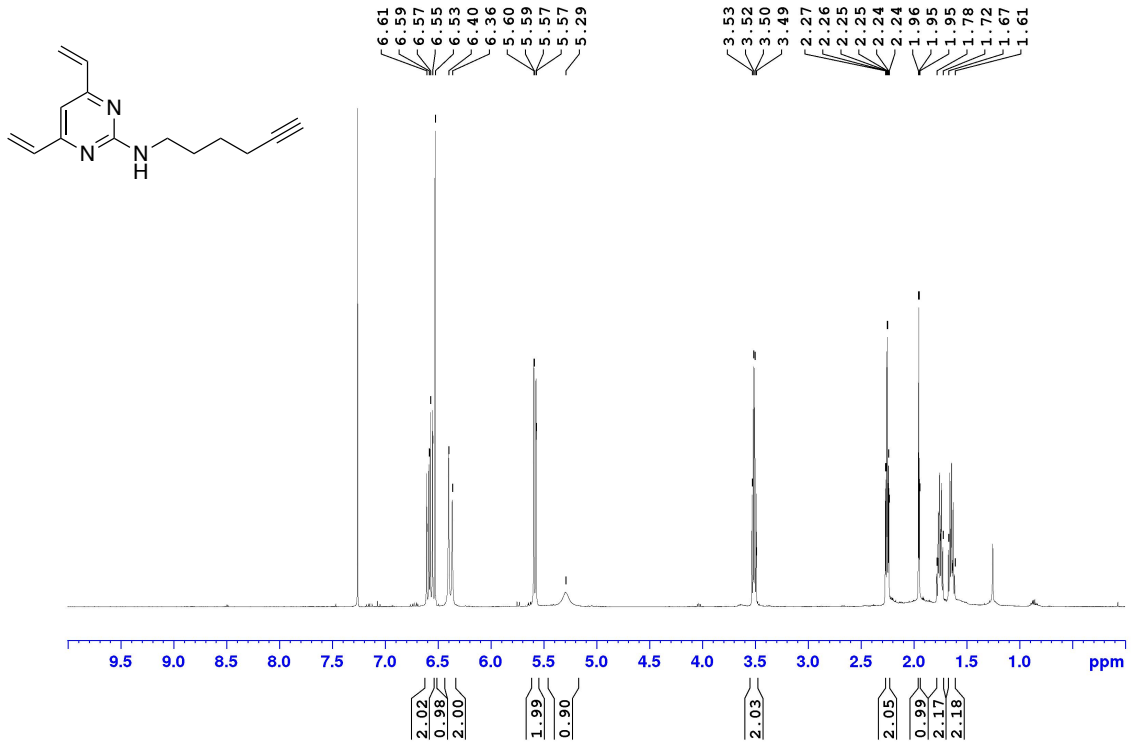

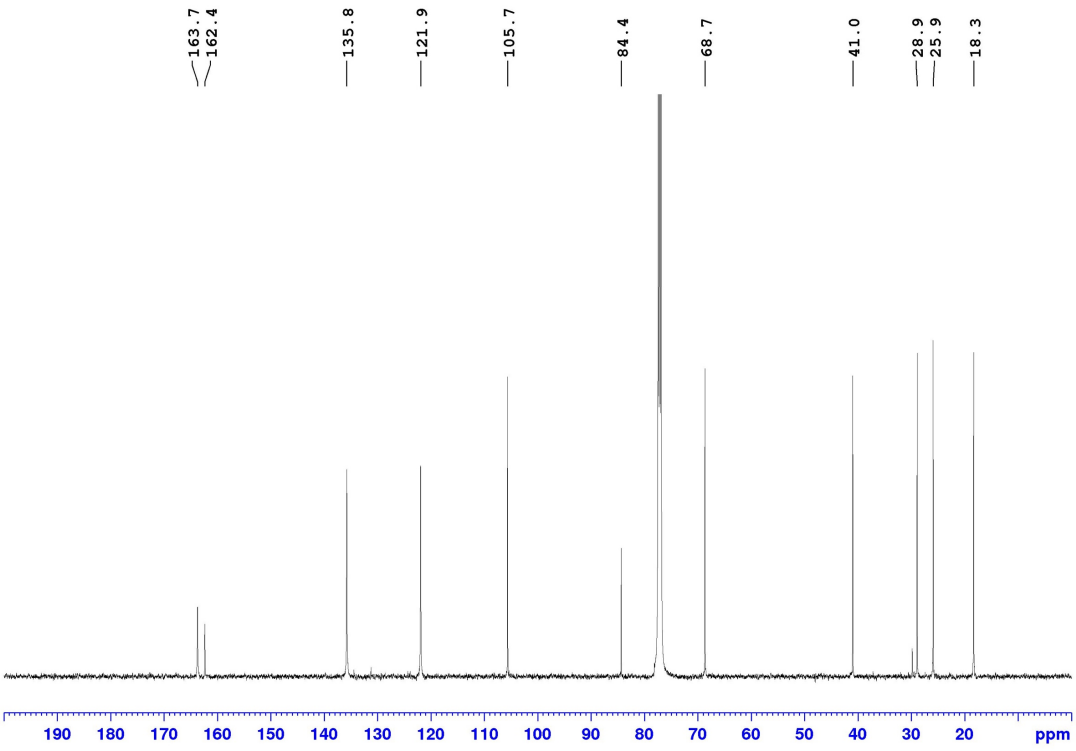

Ethyl *N*-(4,6-dichloropyrimidin-2-yl)-*N*-methylglycinate (21)

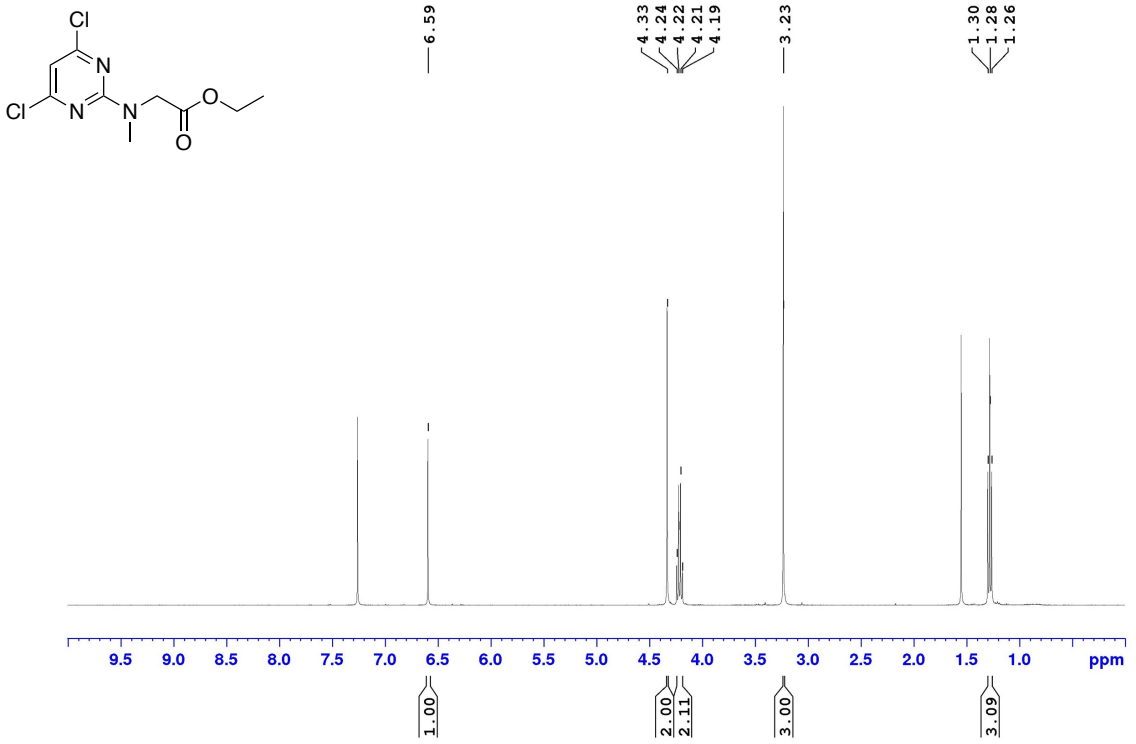

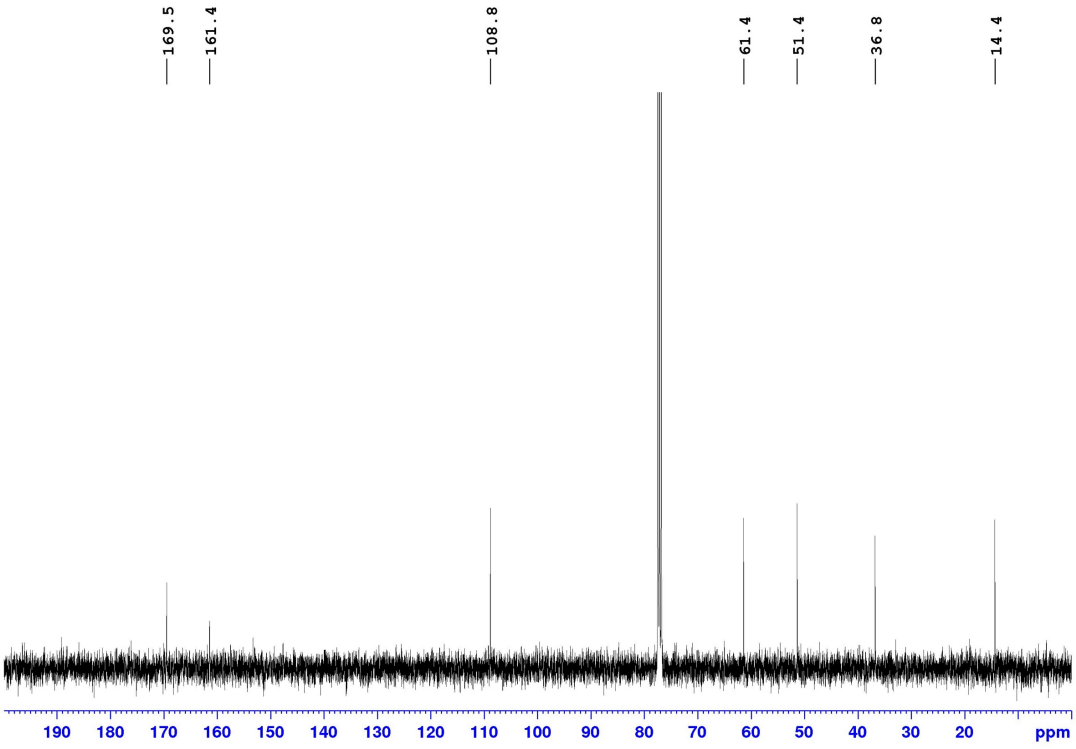

Ethyl *N*-(4,6-divinylpyrimidin-2-yl)-*N*-methylglycinate (23)

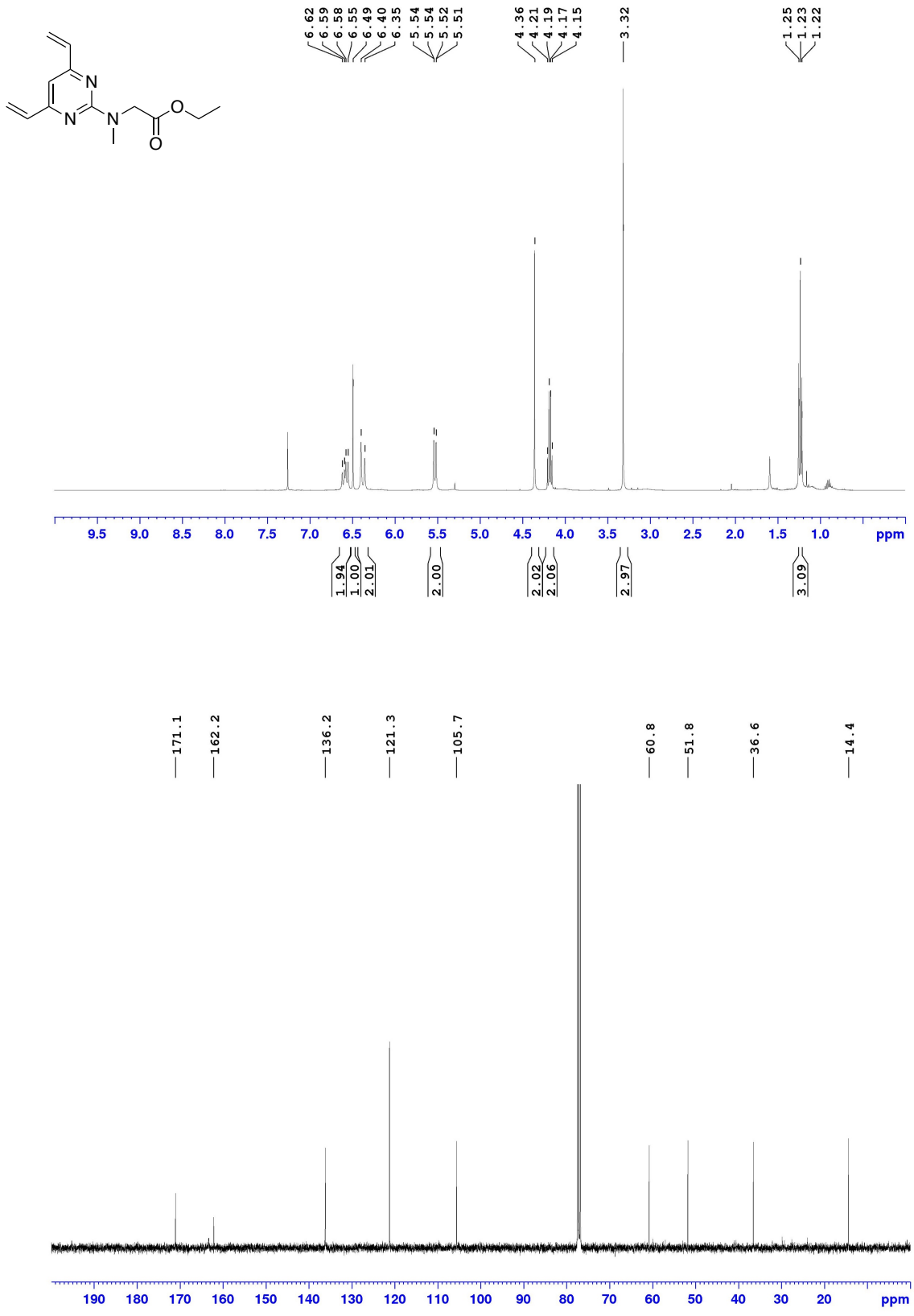

N-(4,6-divinylpyrimidin-2-yl)-*N*-methylglycine (24)

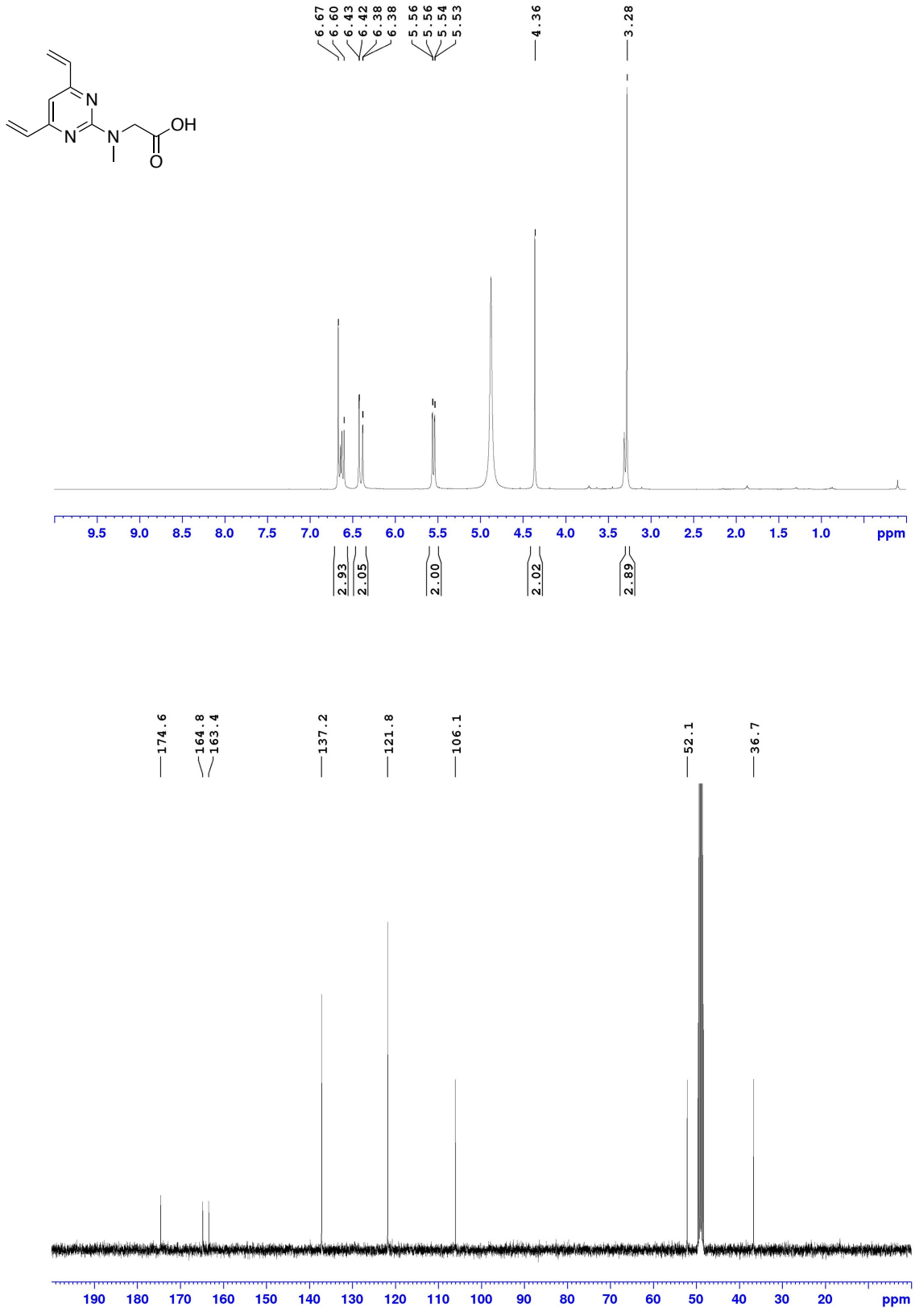

Dimethyl 3,3'-(((2-aminopyrimidine-4,6-diyl)bis(ethane-2,1-diyl))bis(sulfanediyl))(2*S*,2'*S*)bis(2-((*tert*-butoxycarbonyl)amino)propanoate) (25)

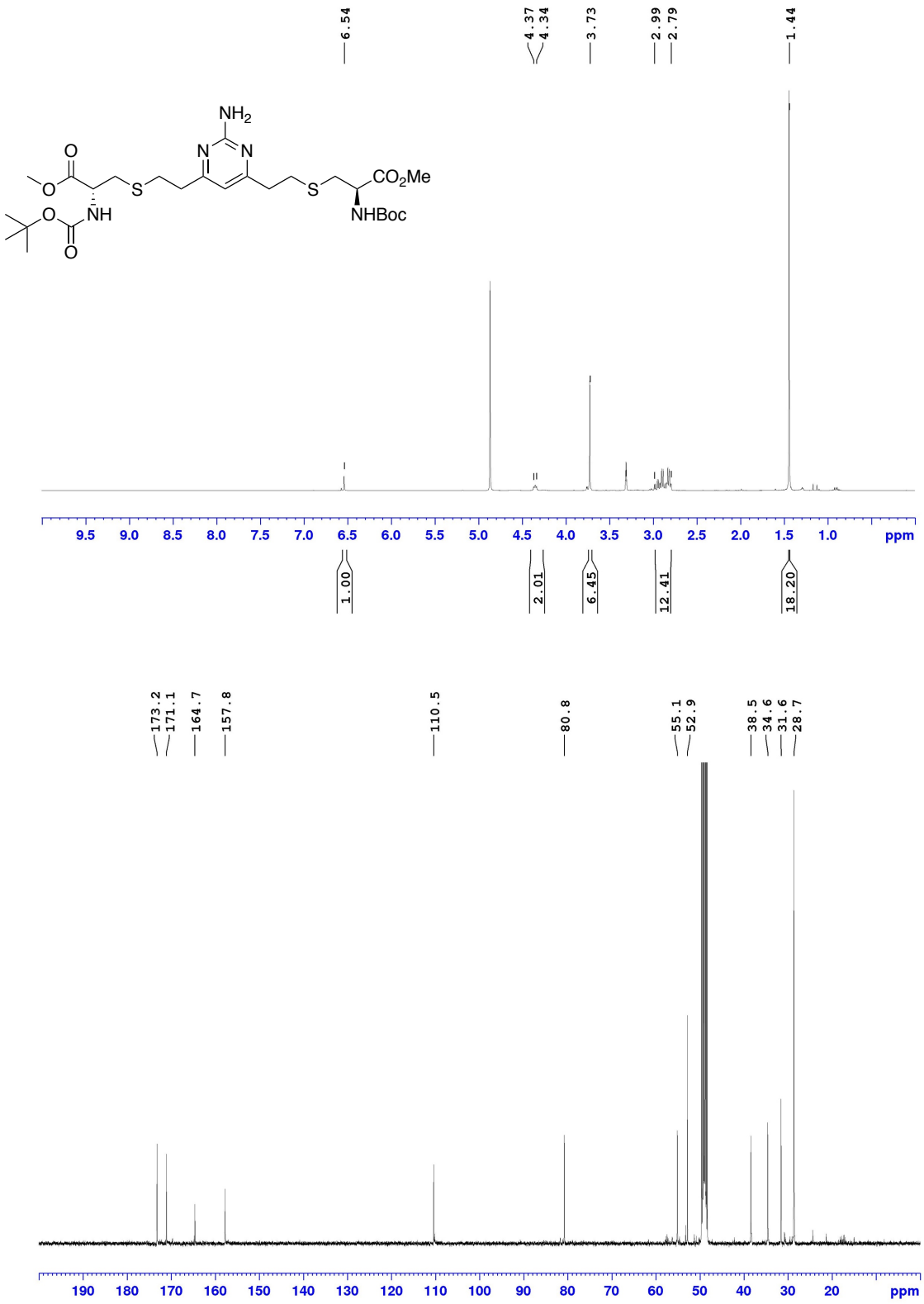

Dimethyl 3,3'-(((2-(hex-5-yn-1-ylamino)pyrimidine-4,6-diyl)bis(ethane-2,1-diyl))bis(sulfanediyl))(2*R*,2'*R*)-bis(2-((*tert*-butoxycarbonyl)amino)propanoate) (26)

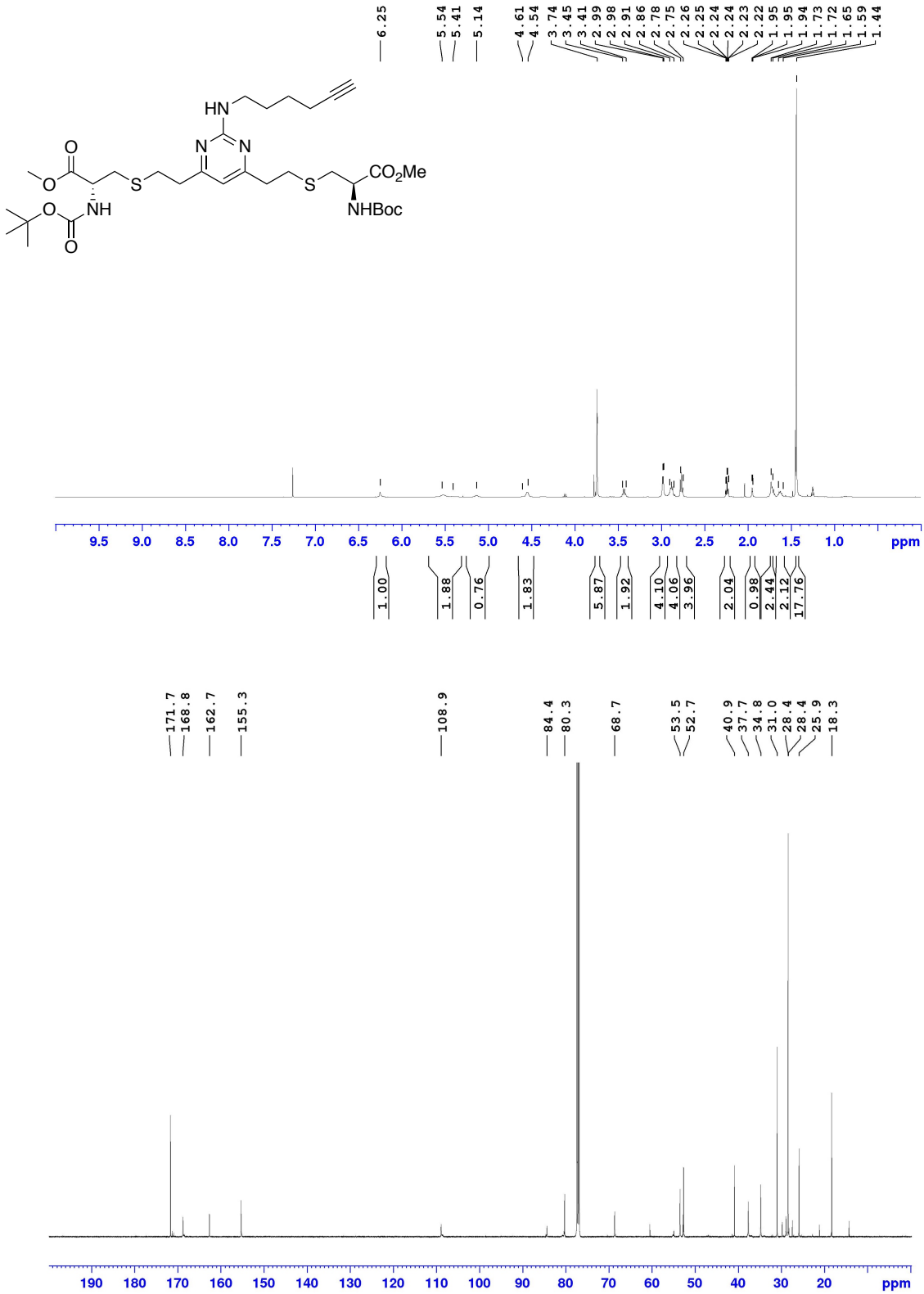

_N_-(4,6-bis(2-(((_R_)-2-((_tert_-butoxycarbonyl)amino)-3-methoxy-3-oxopropyl)thio)ethyl)pyrimidin-2-yl)-_N_-methylglycine (27)

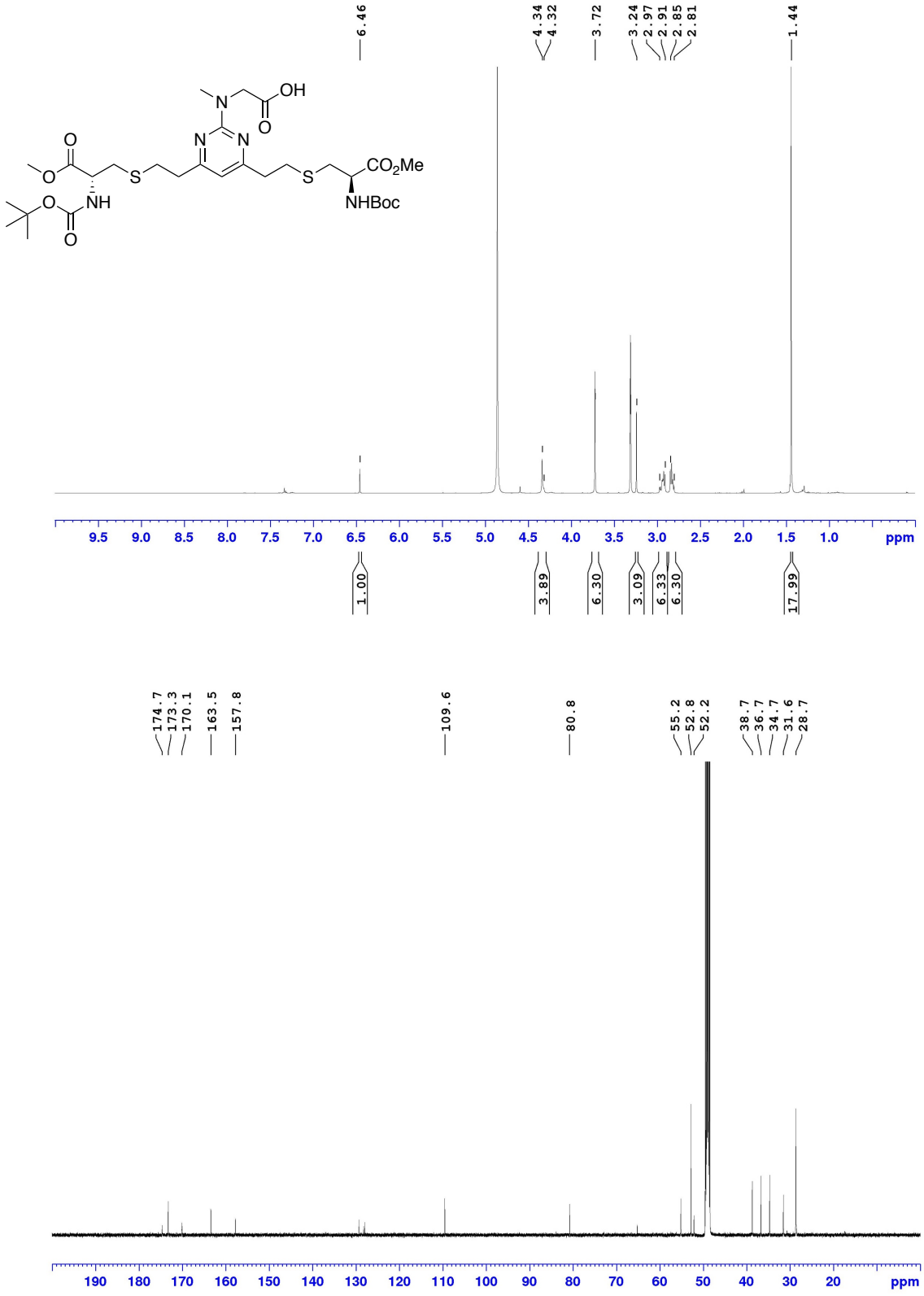

Dox-PEG$_4$-N$_3$ (37)

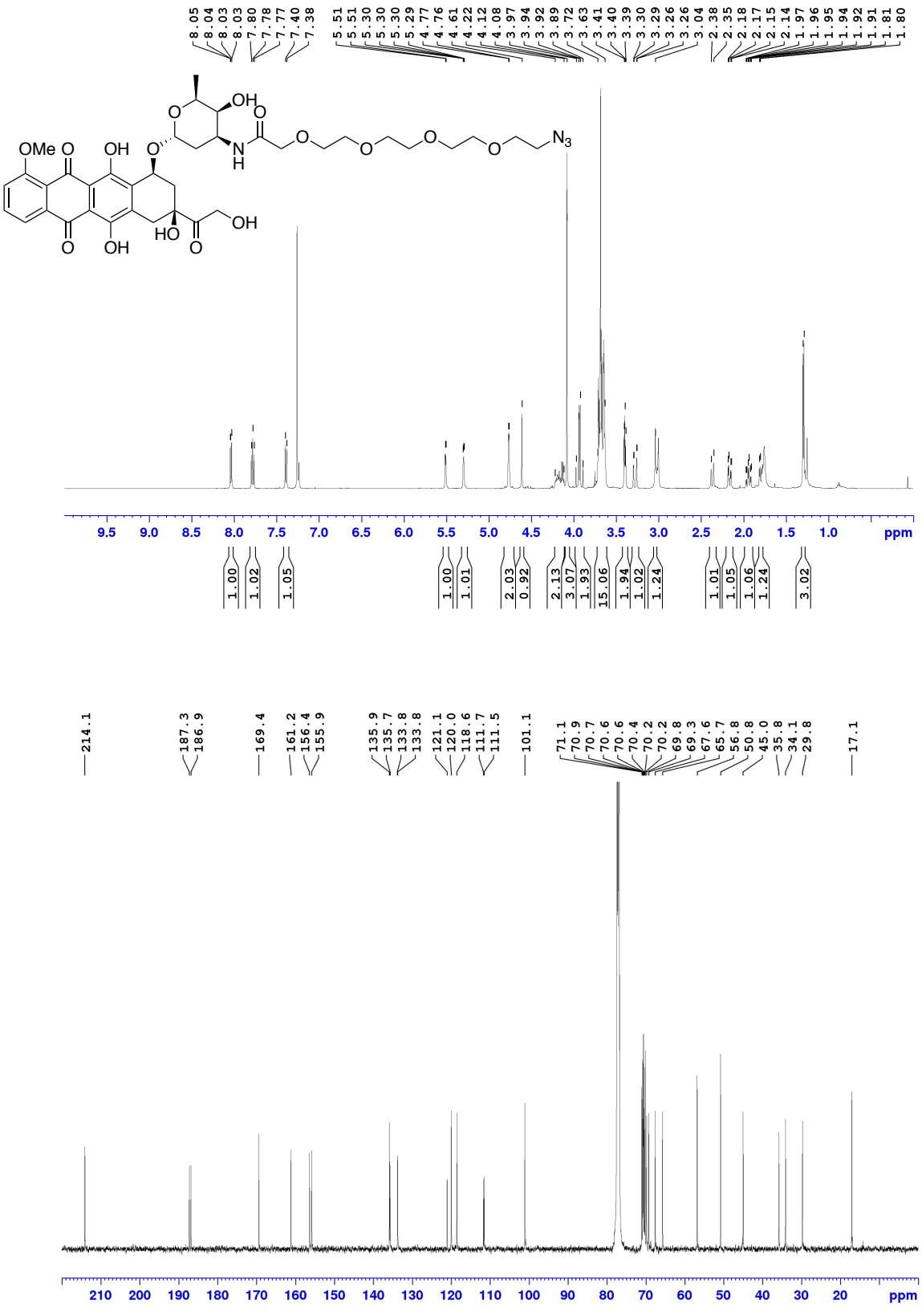

N_3-PEG$_4$-MMAE (40)

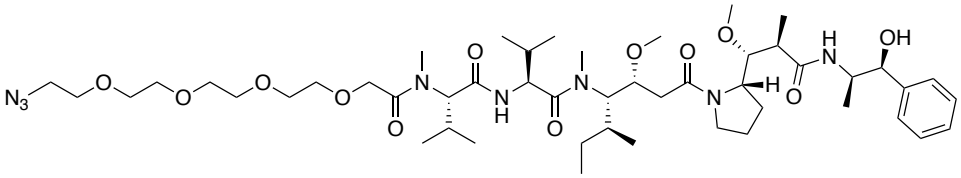

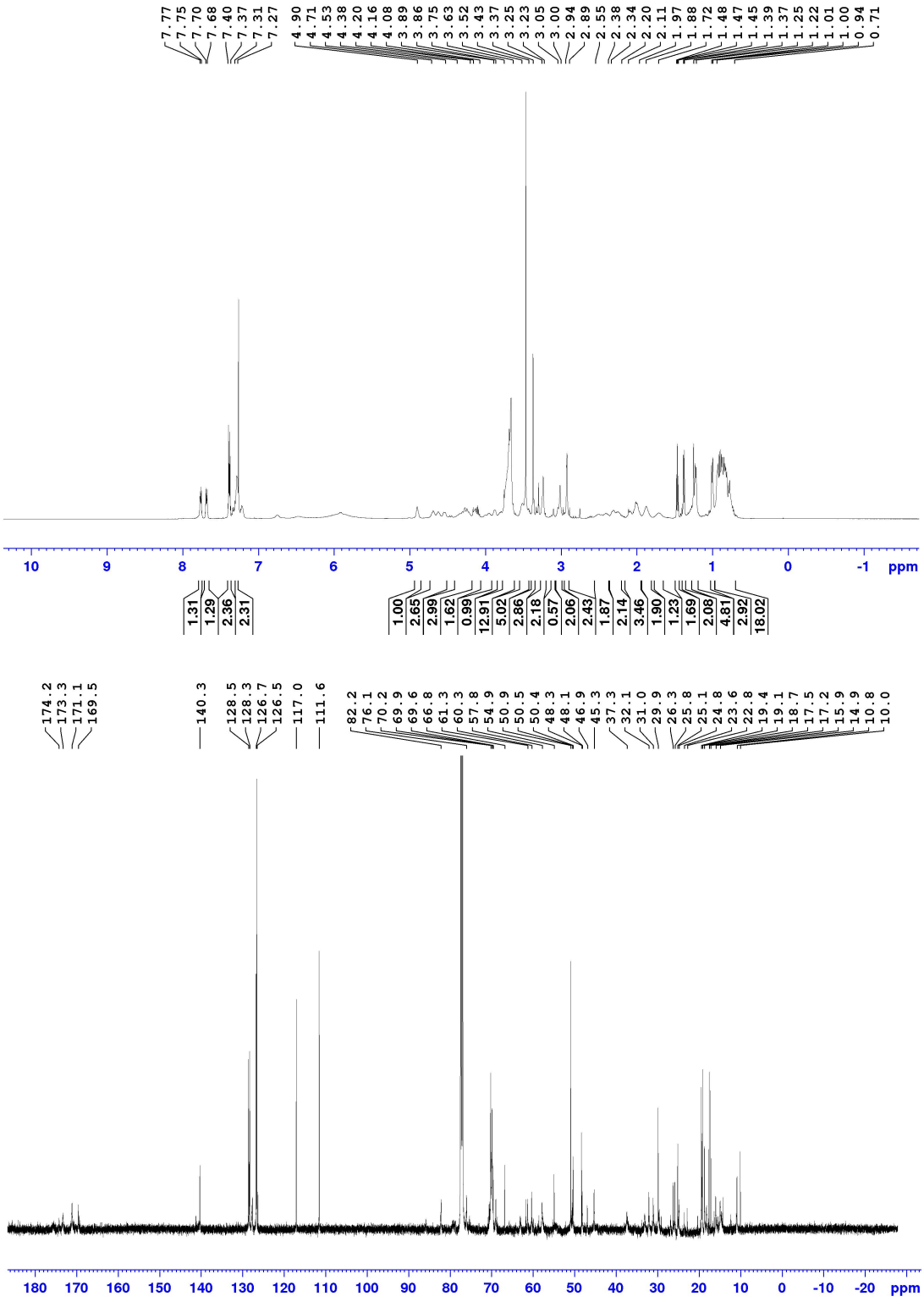

DVP-PEG$_4$-MMAE (41)

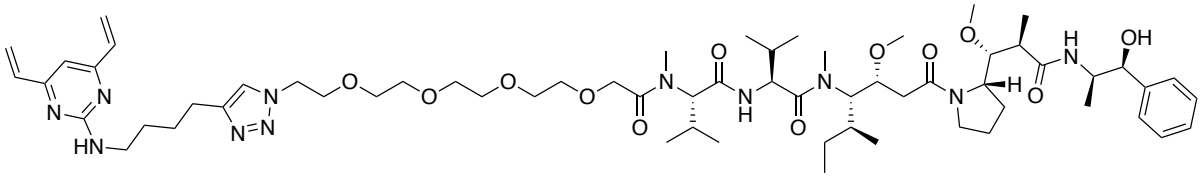

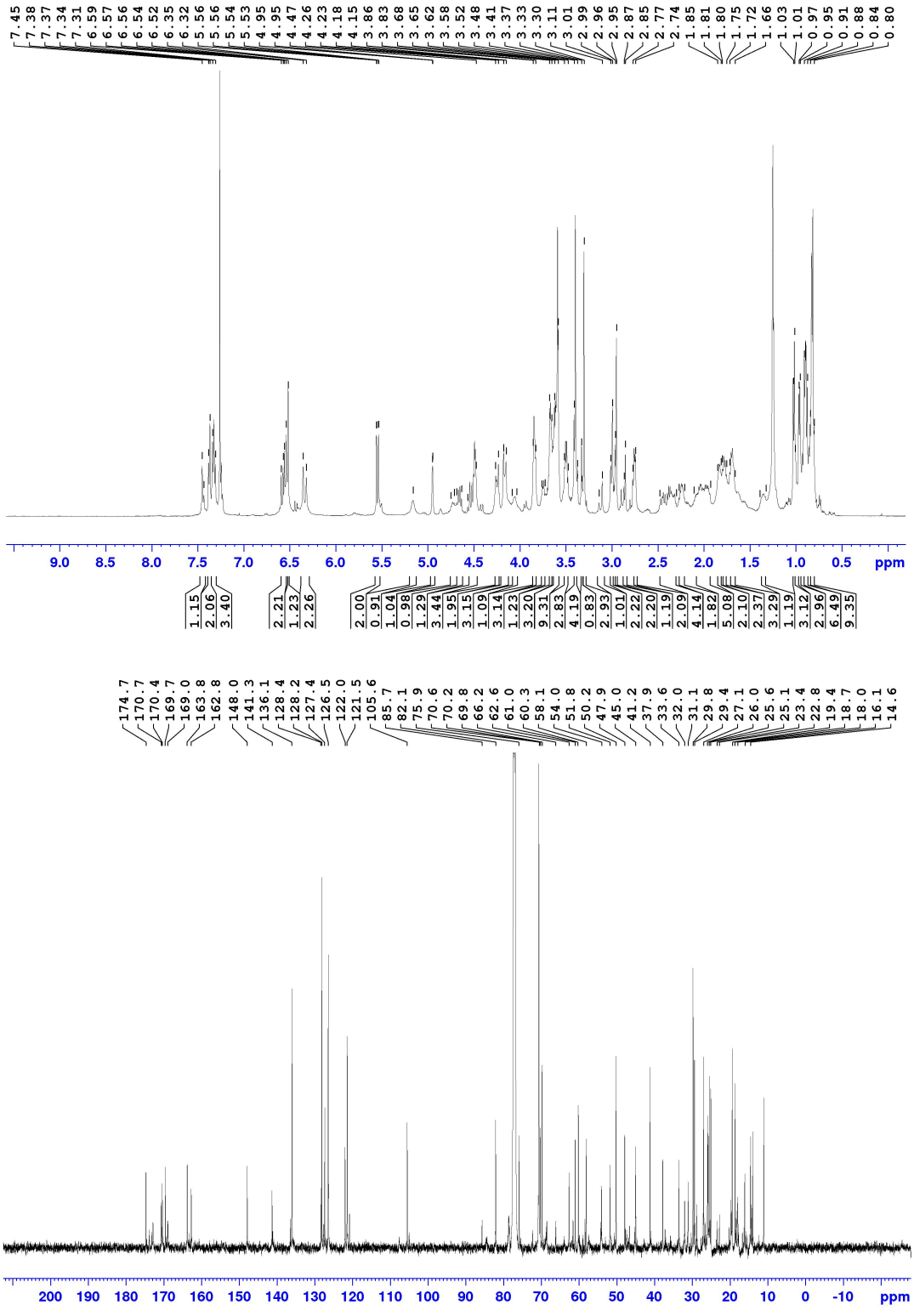

Alloc-Val-Ala-PABA-PNP (65)

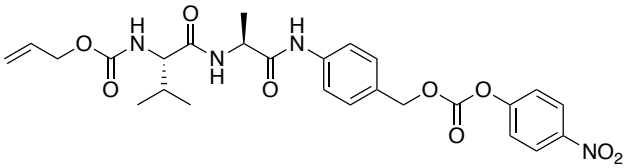

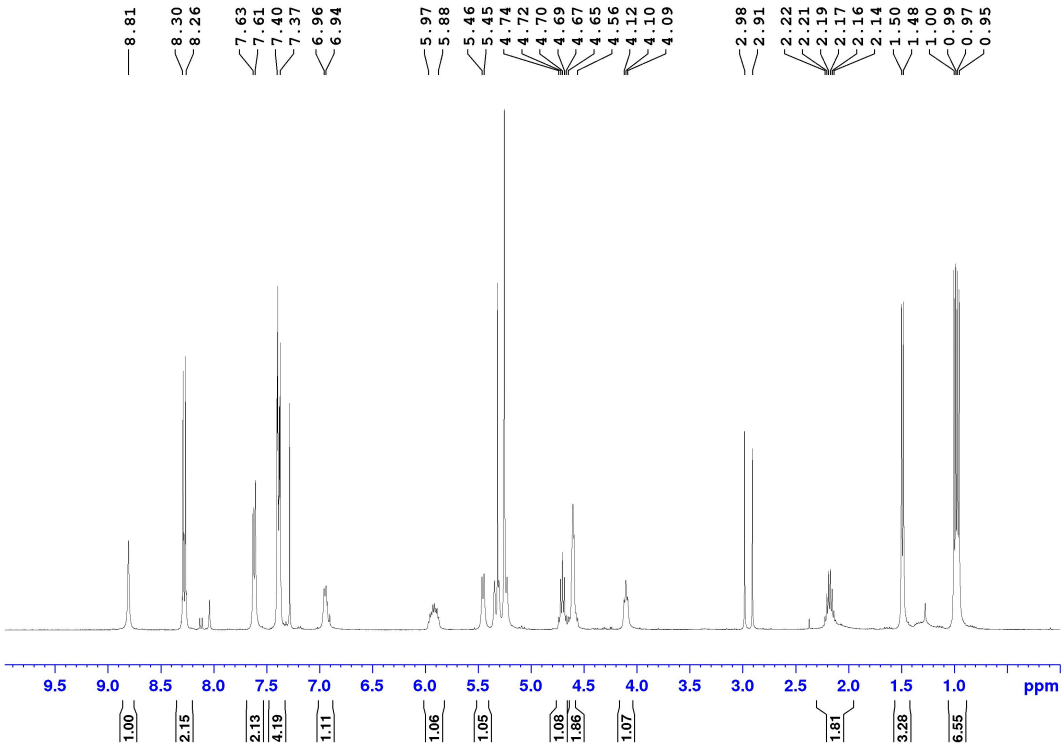

Ethyl 4-((4,6-dichloropyrimidin-2-yl)amino)butanoate (66)

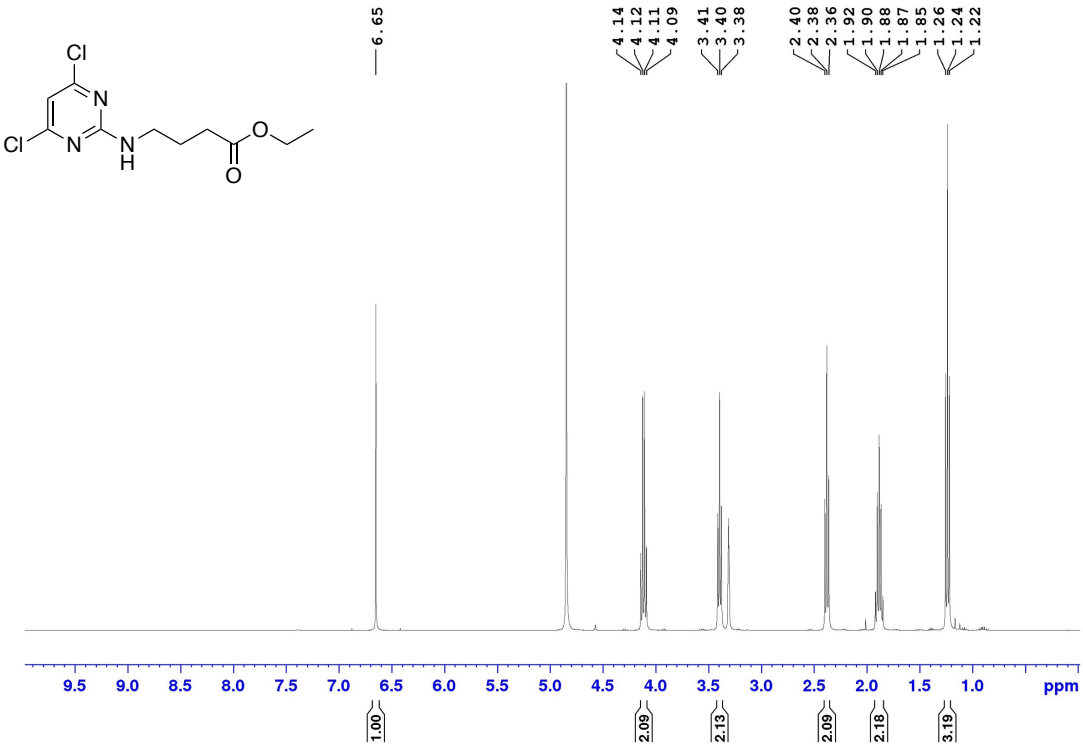

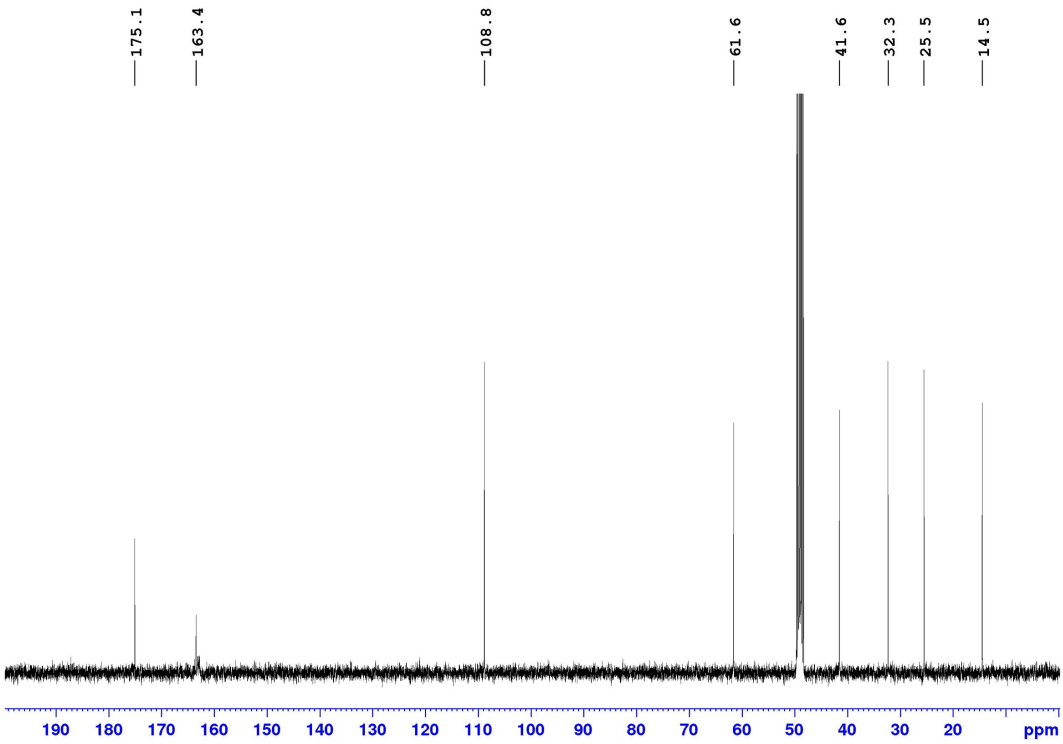

Ethyl 4-((4,6-divinylpyrimidin-2-yl)amino)butanoate (67)

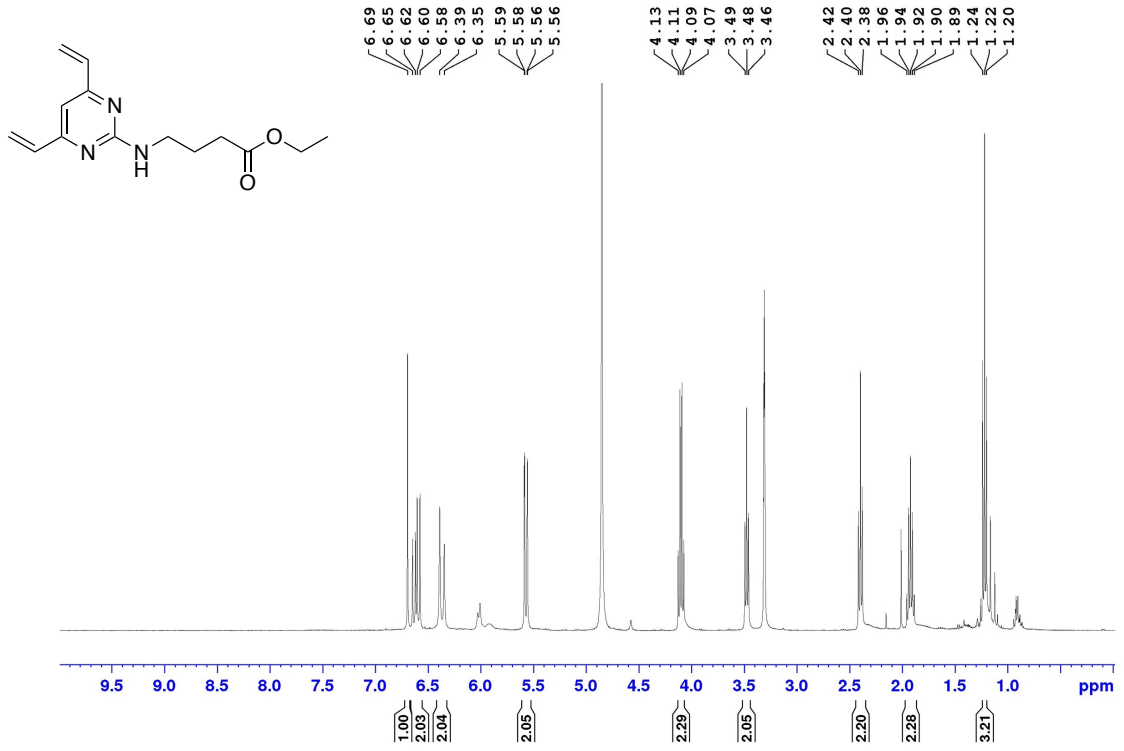

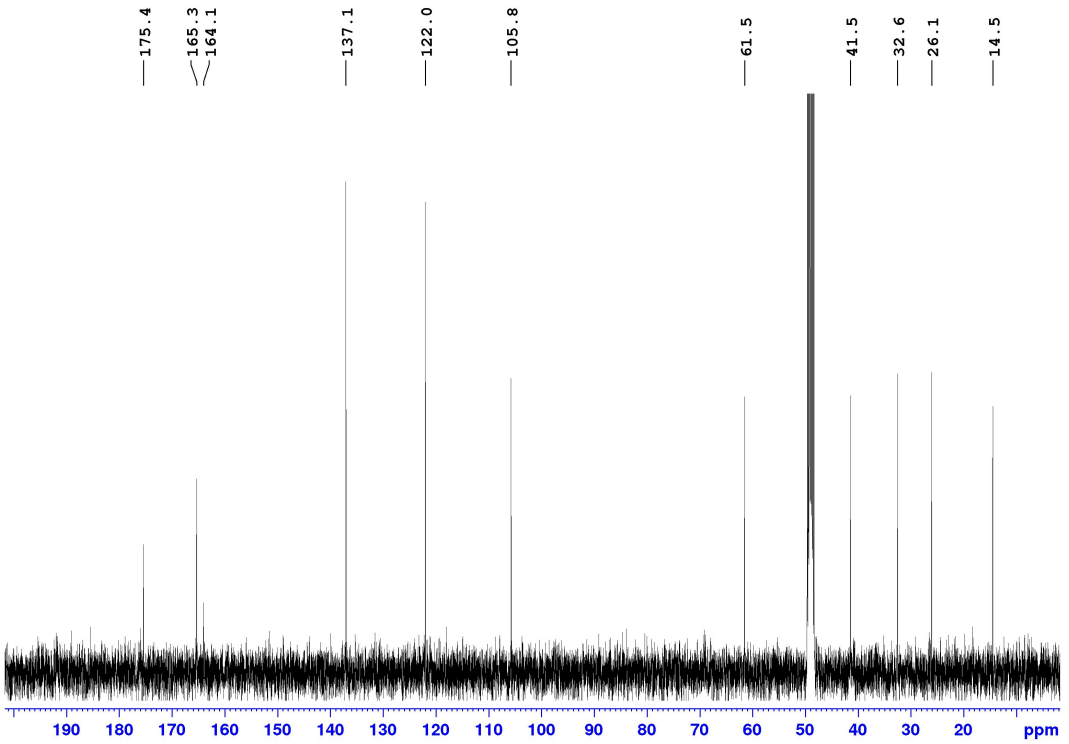

4-((4,6-divinylpyrimidin-2-yl)amino)butanoic acid (52)

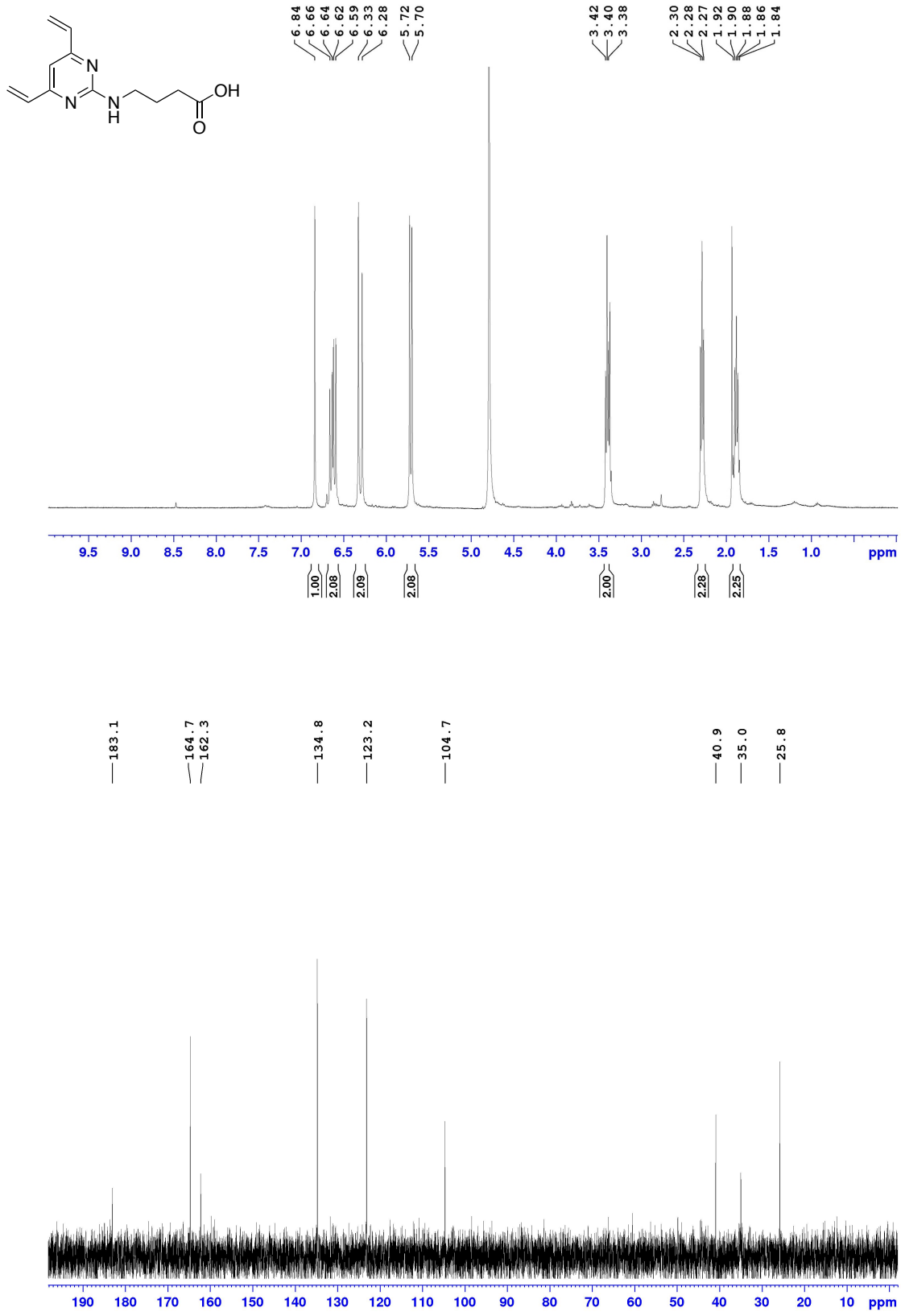

Fmoc-Val-Cit-OH (49)

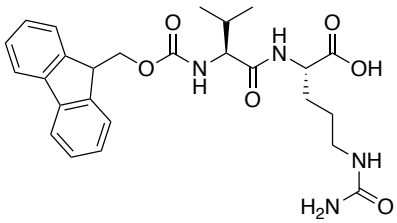

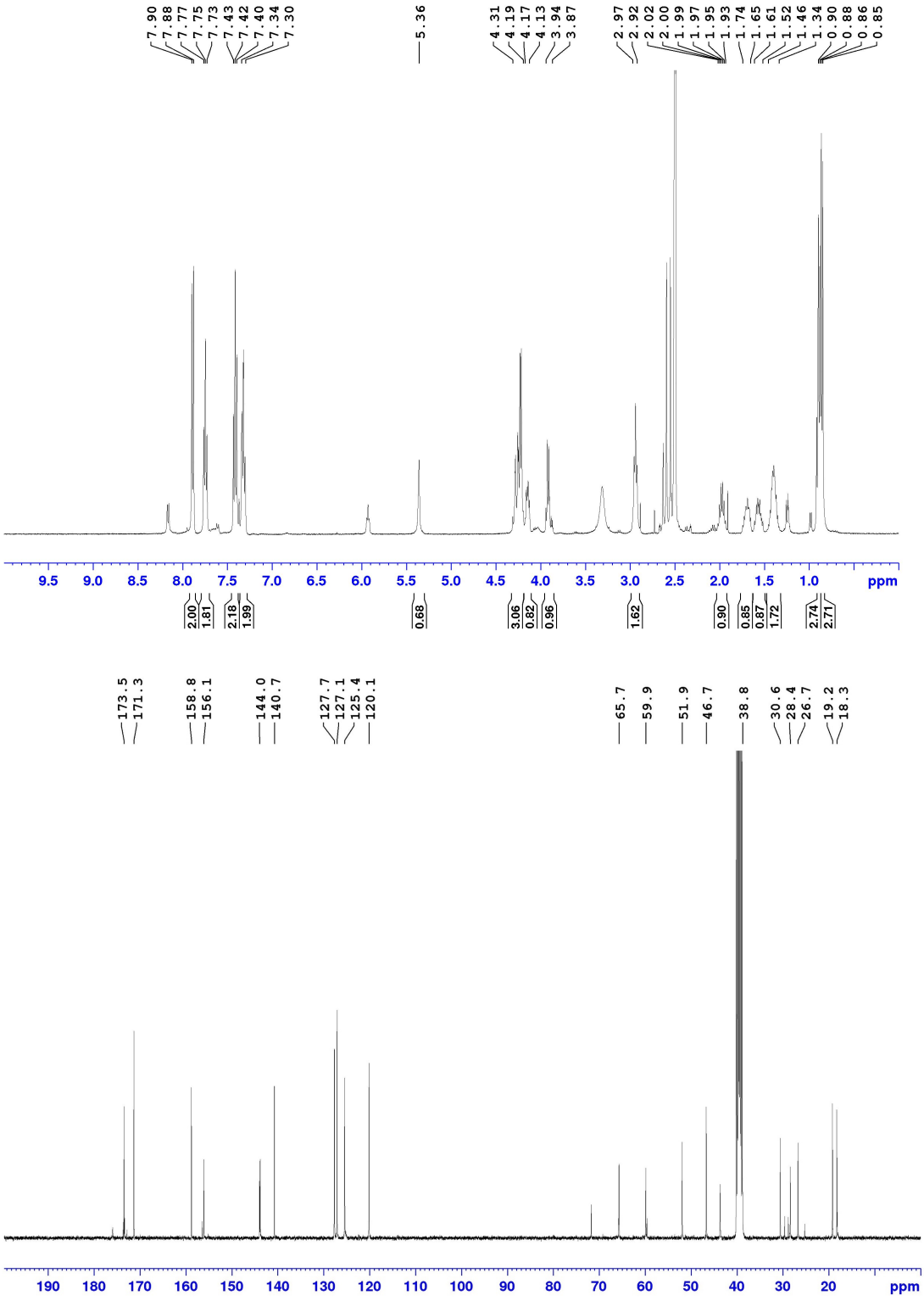

Fmoc-Val-Cit-PABA (50)

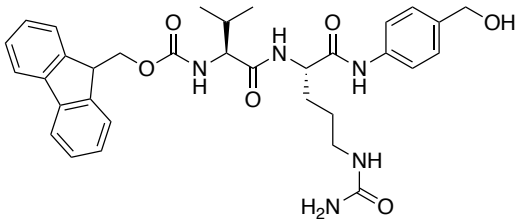

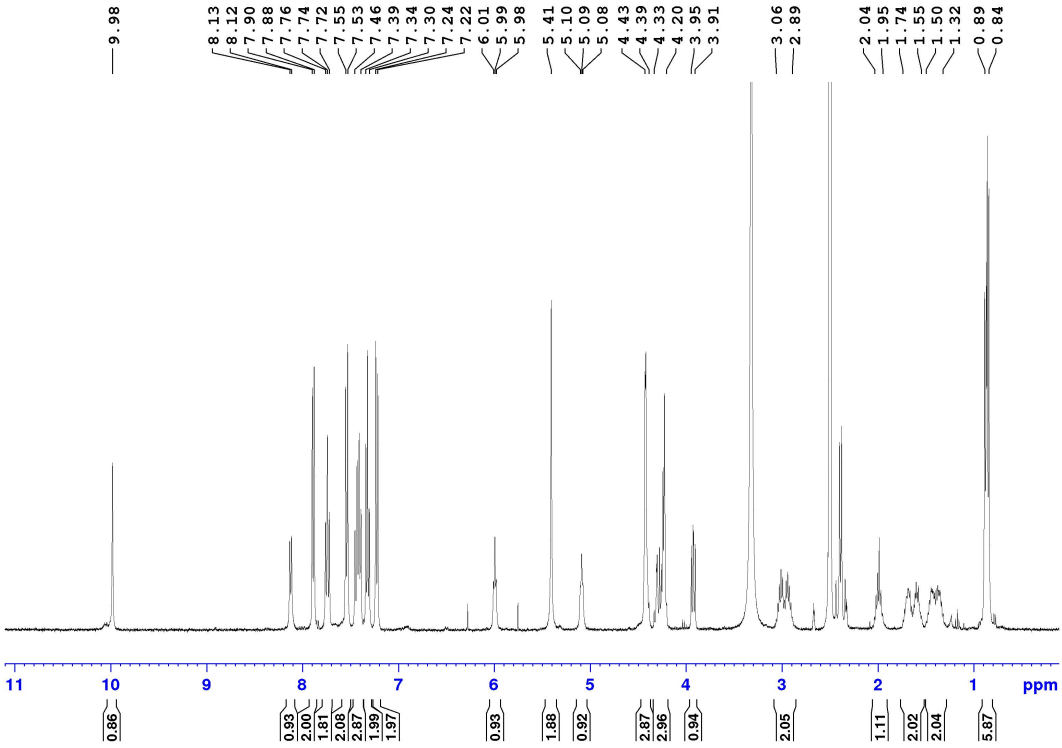

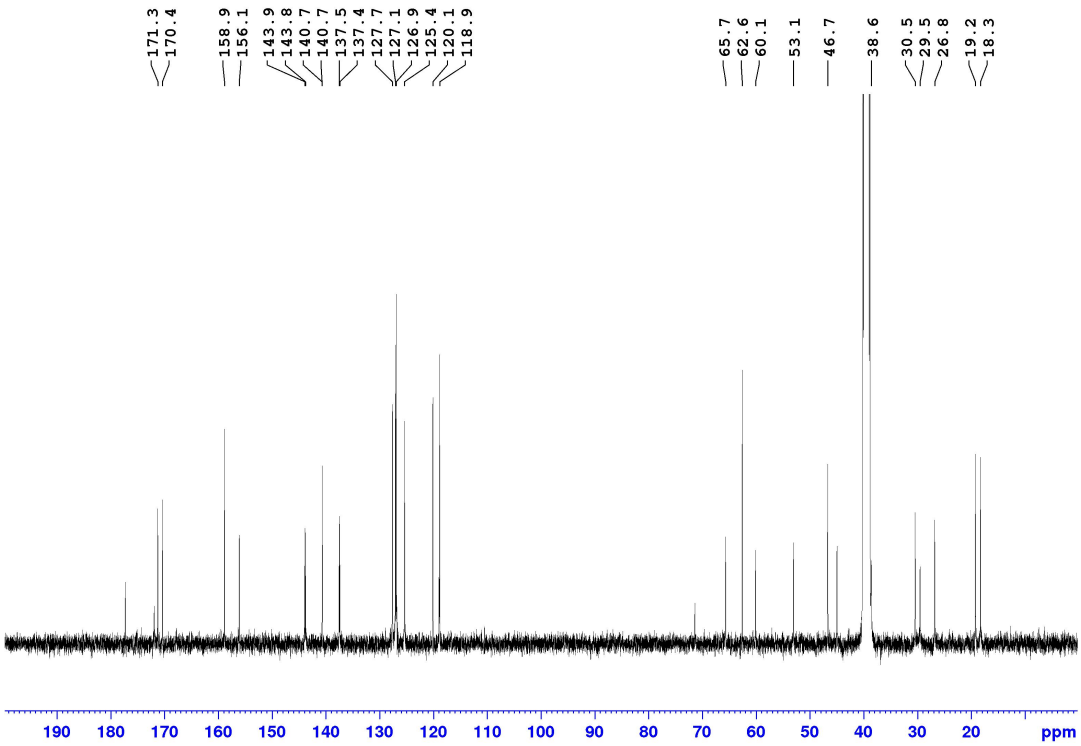

Ethyl 4-(hex-5-yn-1-ylamino)butanoate (69)

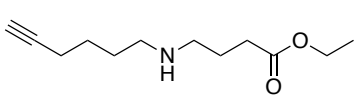

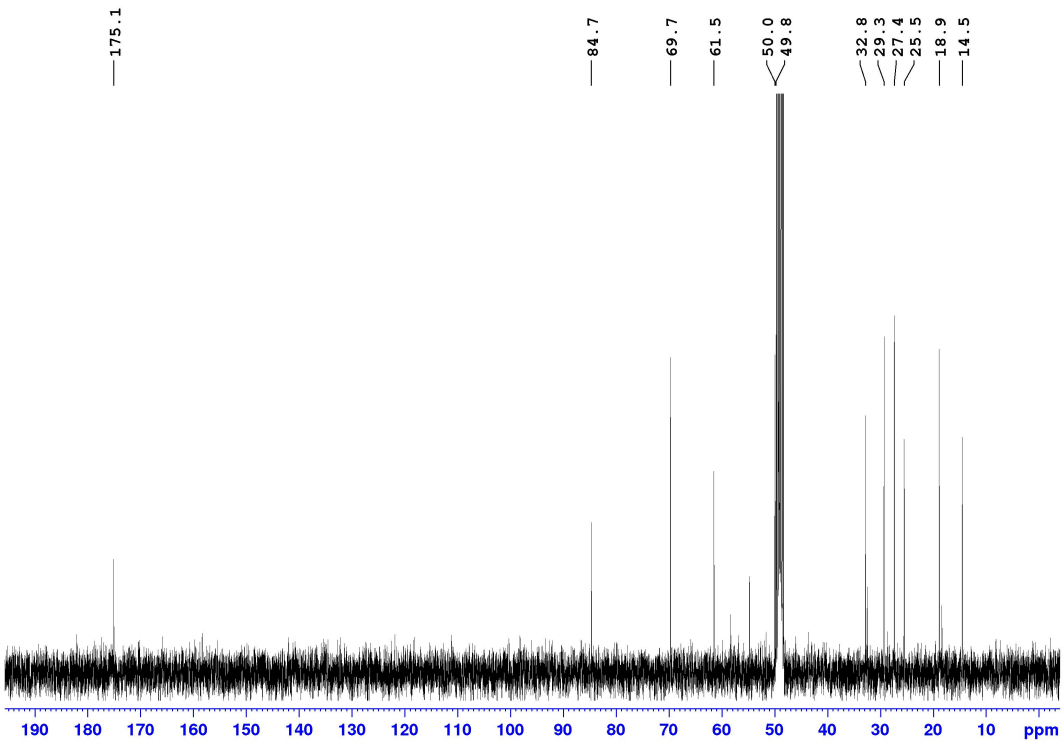

Ethyl 4-((4,6-dichloropyrimidin-2-yl)(hex-5-yn-1-yl)amino)butanoate (70)

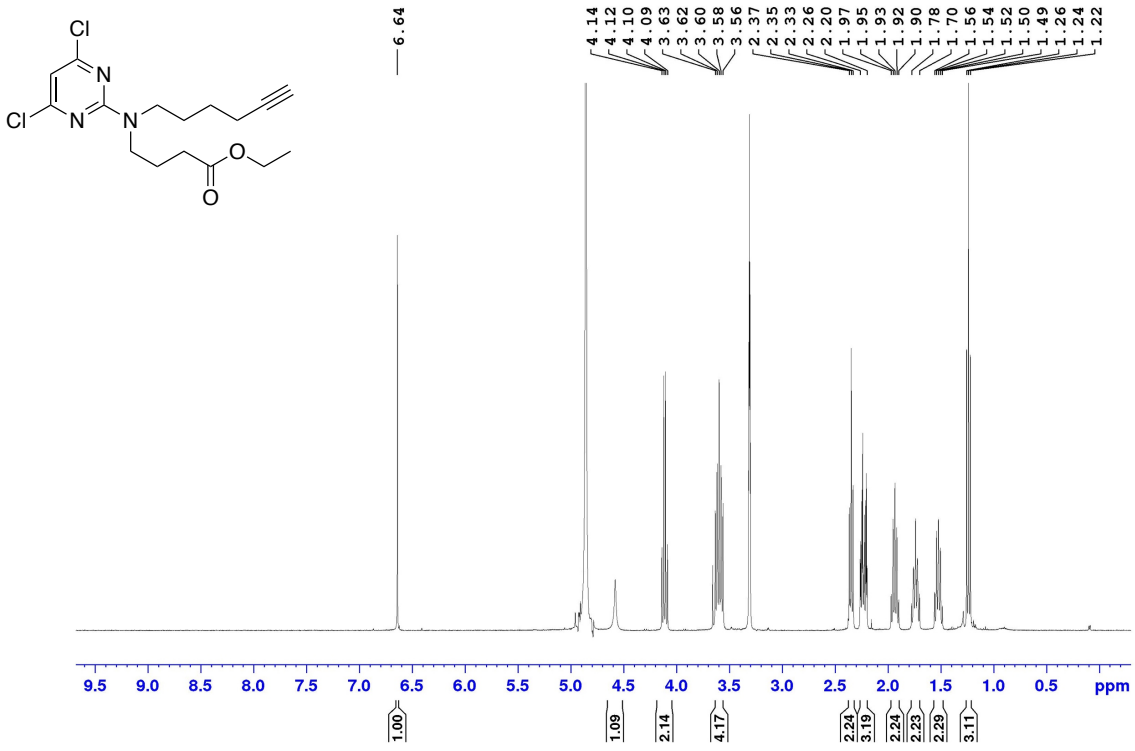

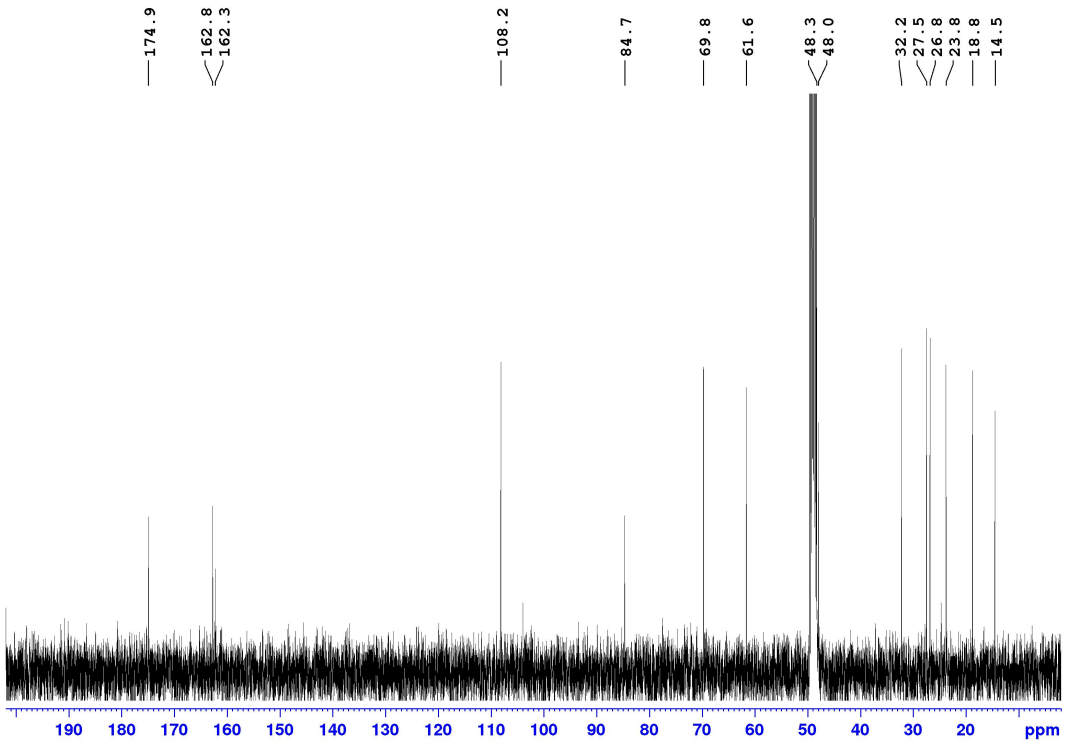

Ethyl 4-((4,6-divinylpyrimidin-2-yl)(hex-5-yn-1-yl)amino)butanoate (71)

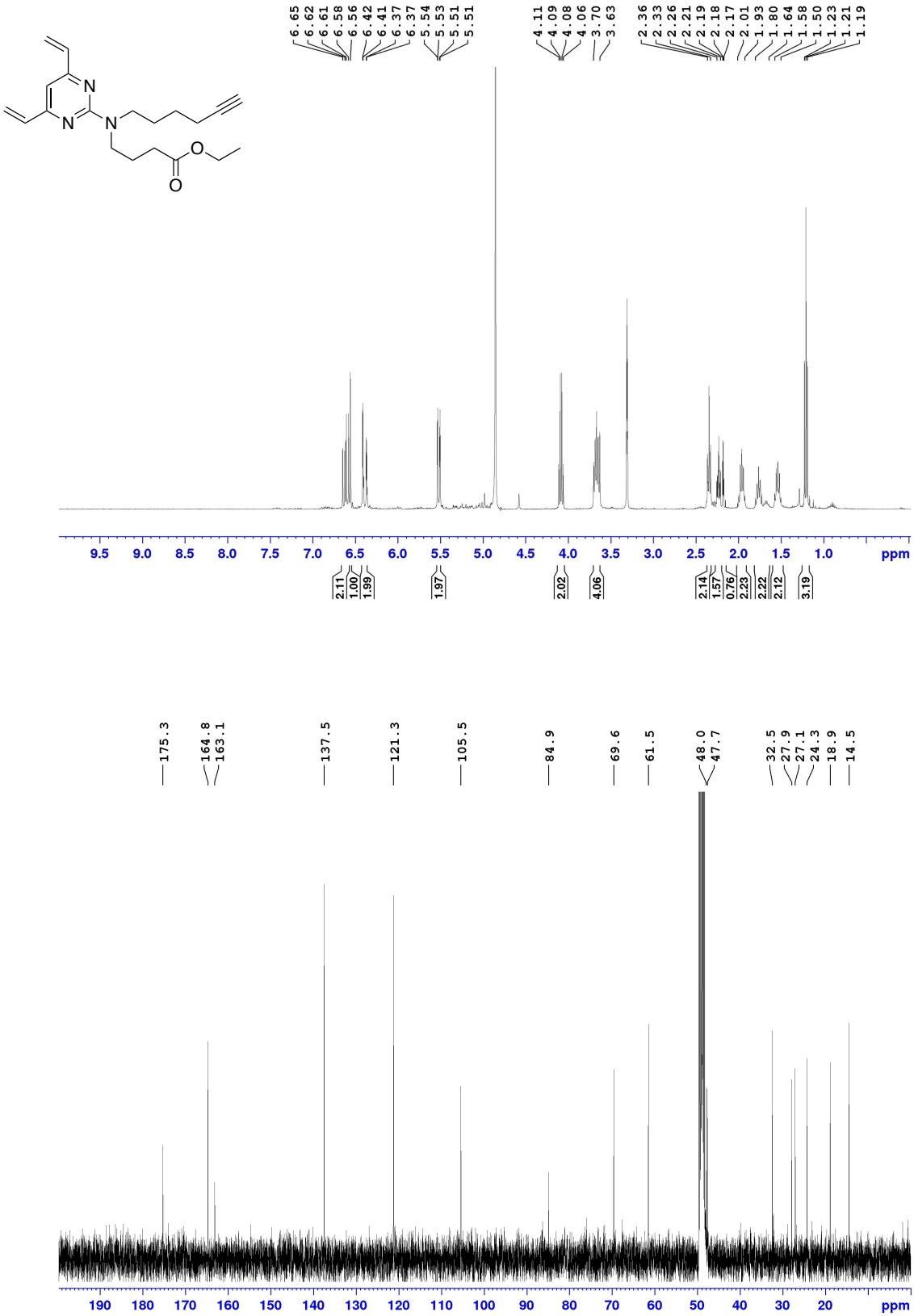

4-((4,6-divinylpyrimidin-2-yl)(hex-5-yn-1-yl)amino)butanoic acid (72)

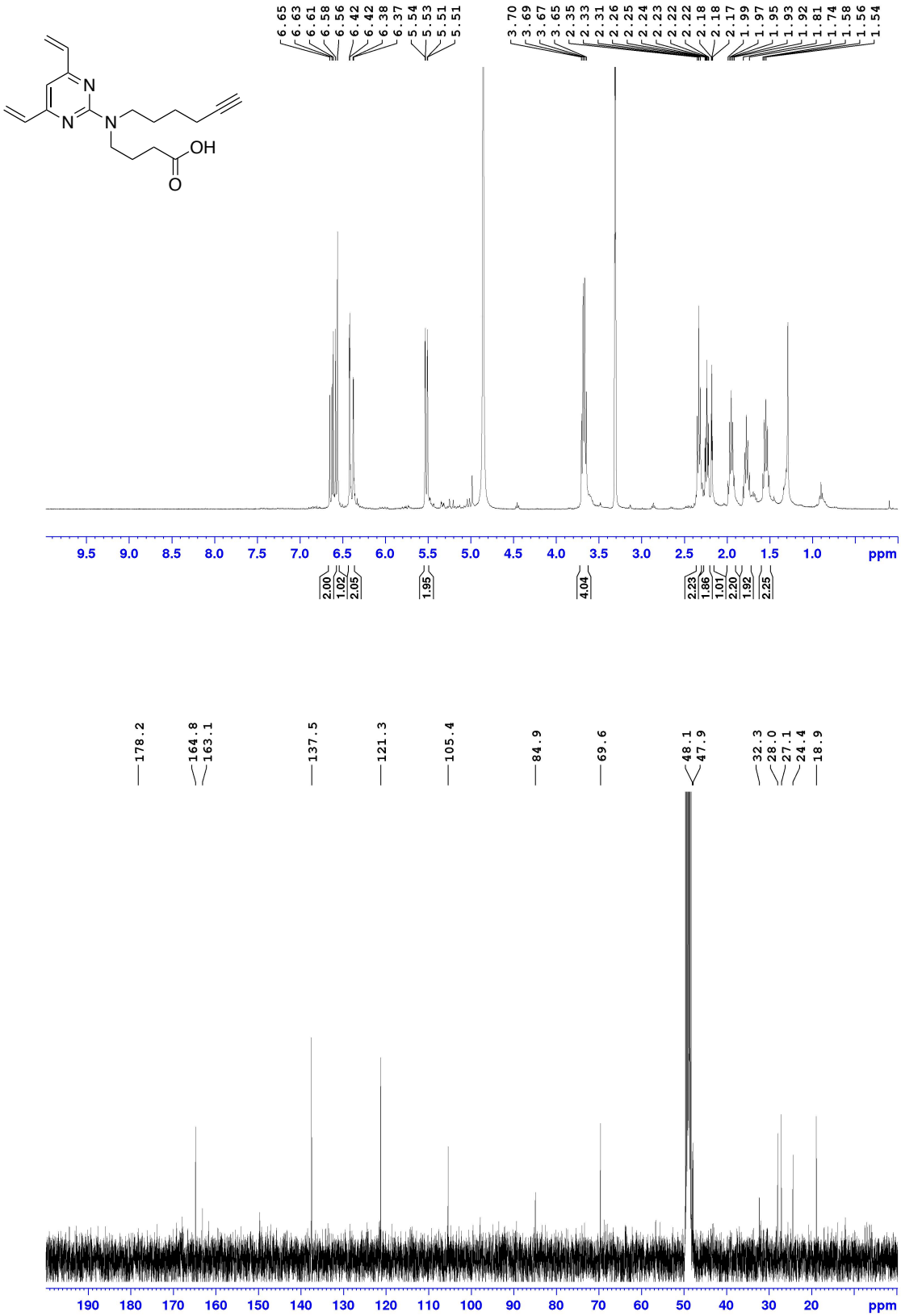

12 Stability

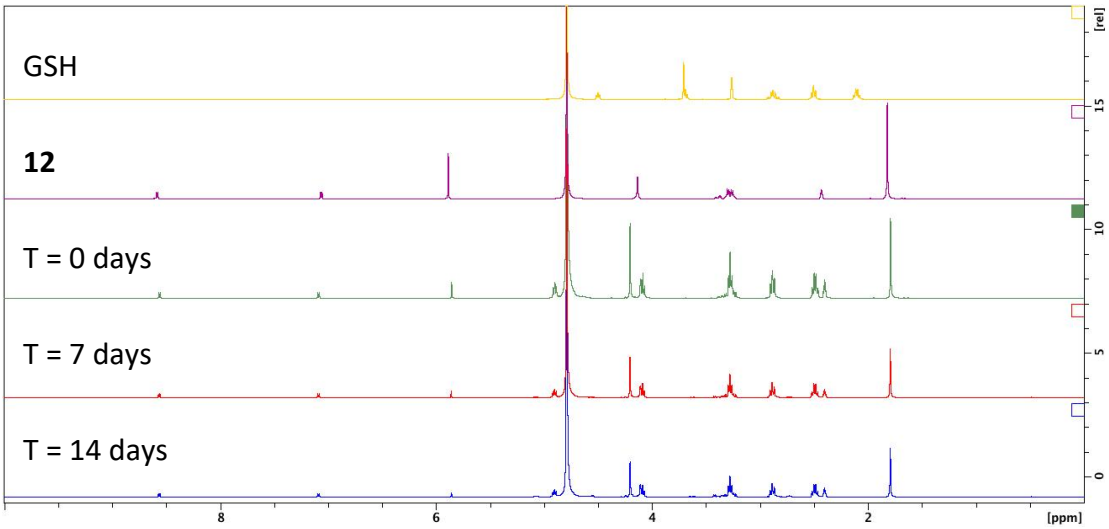

25 Stability

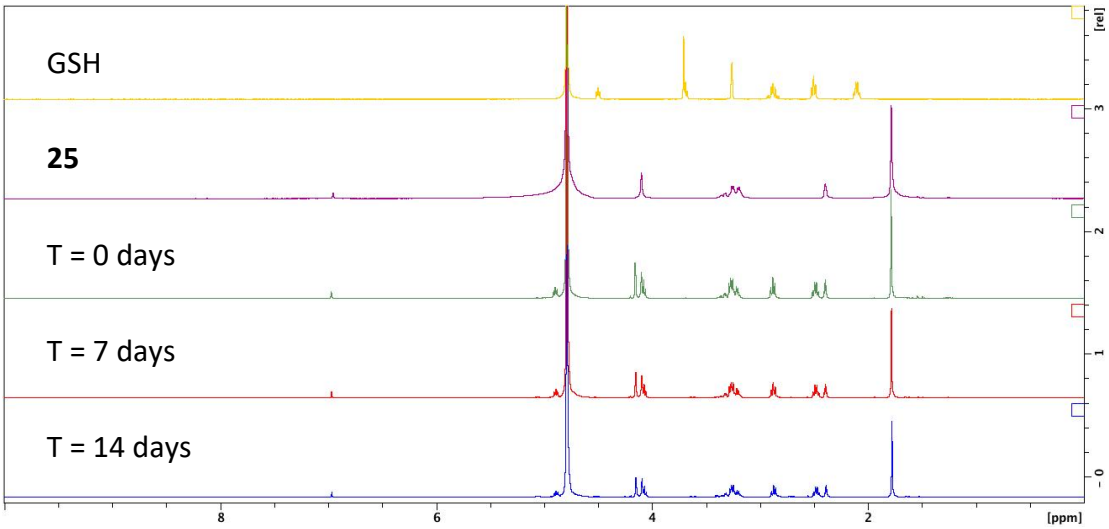

27 Stability

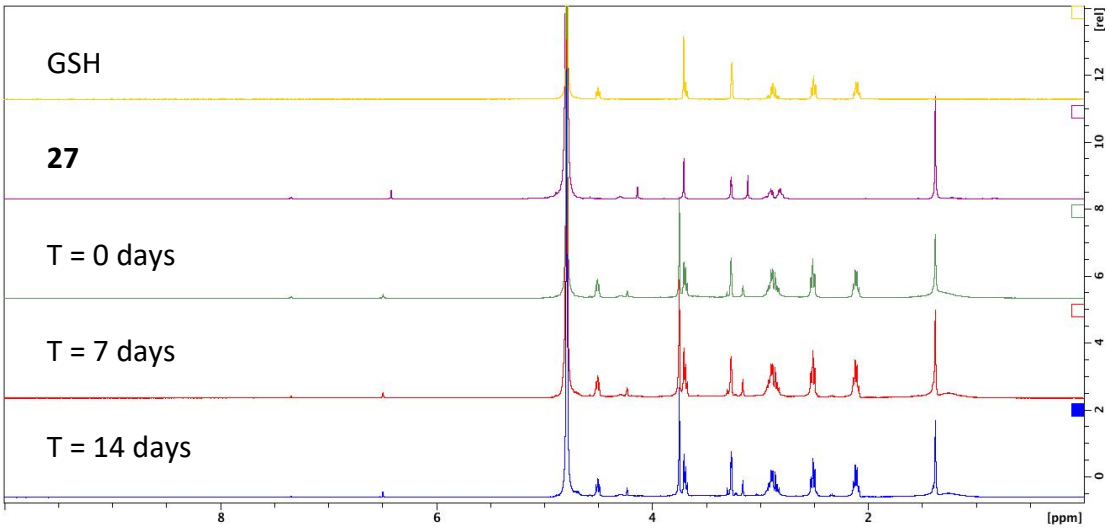

13 Stability

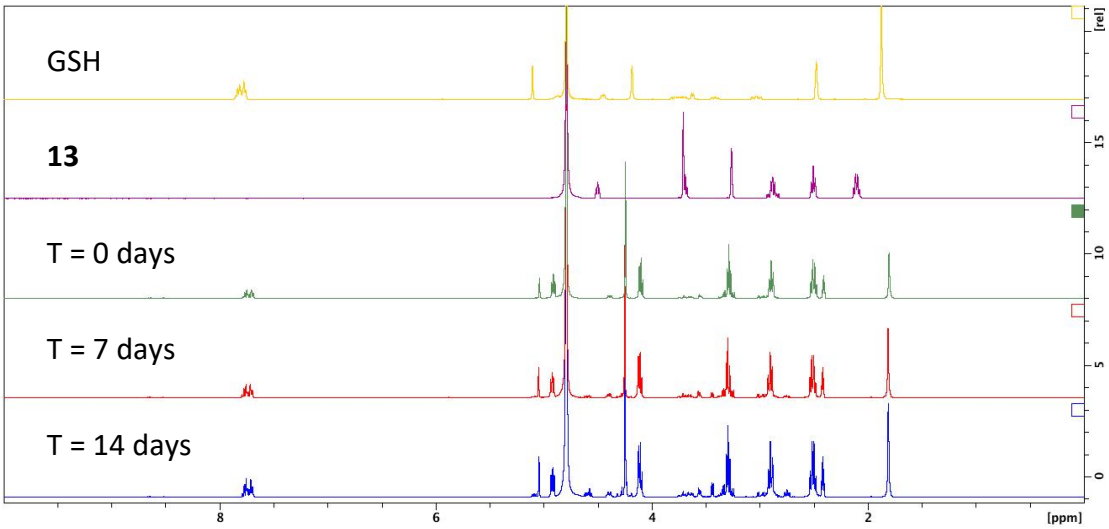

Appendix B – HPLC

N_3-PEG_4-MMAE (40)

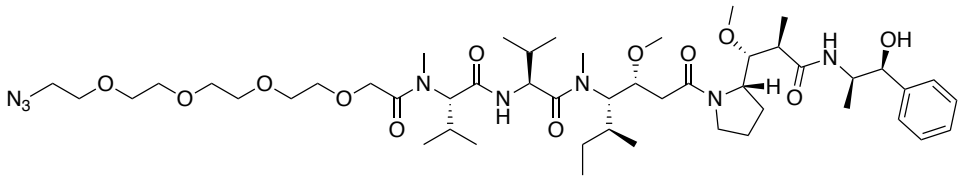

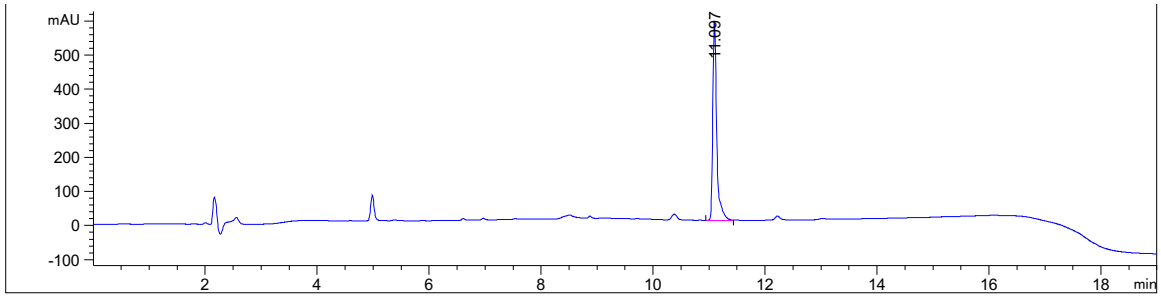

DVP-PEG_4-MMAE (41)

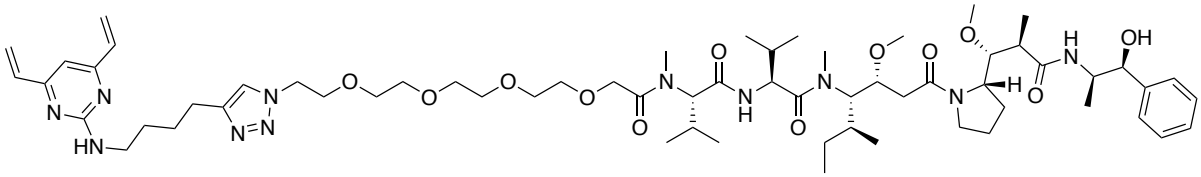

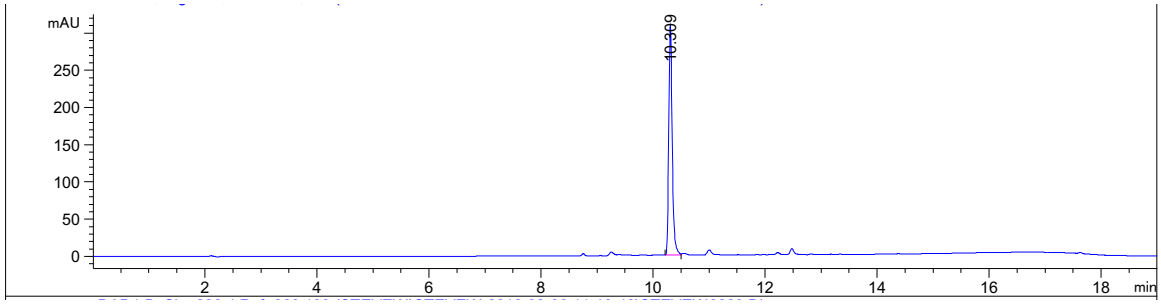

Alloc-Val-Ala-PABC-MMAE (44)

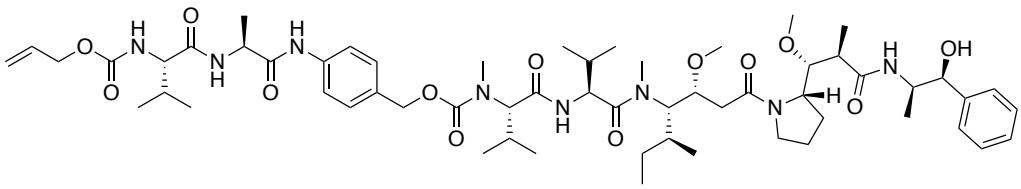

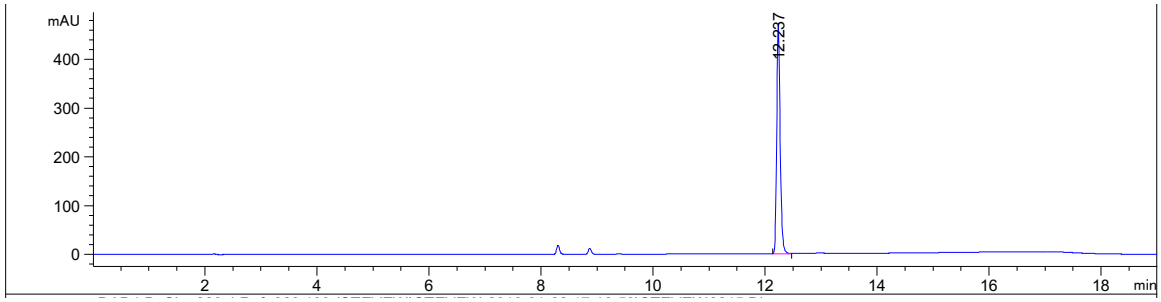

Amine-Val-Ala-PABC-MMAE (55)

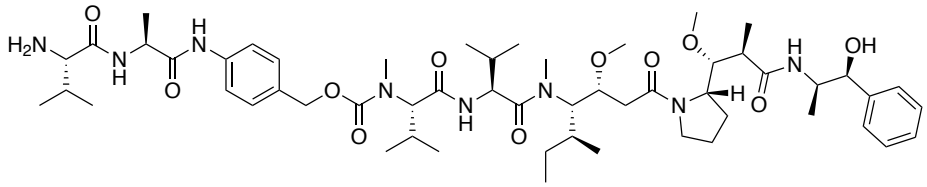

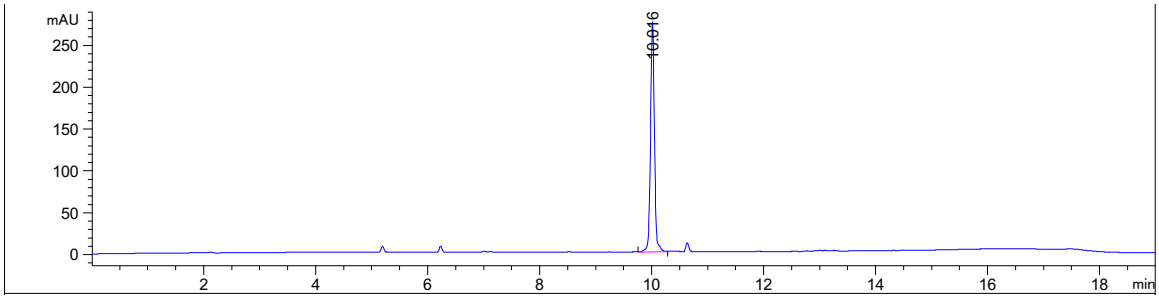

DVP(1C)-Val-Ala-PABC-MMAE (45)

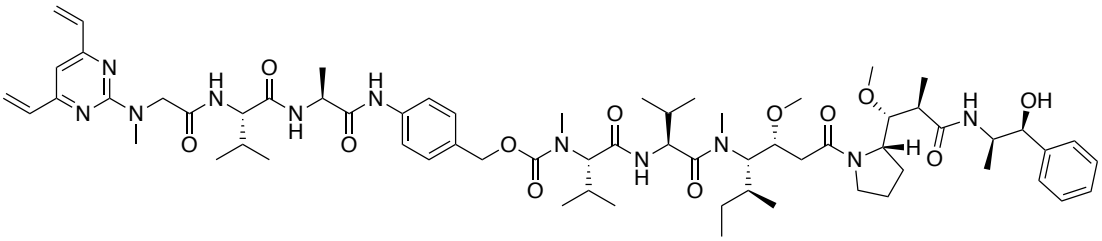

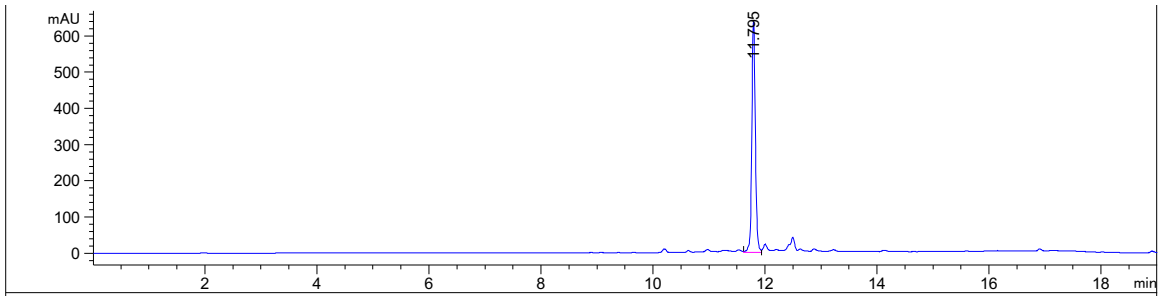

DVP(3C)-Val-Ala-PABC-MMAE (47)

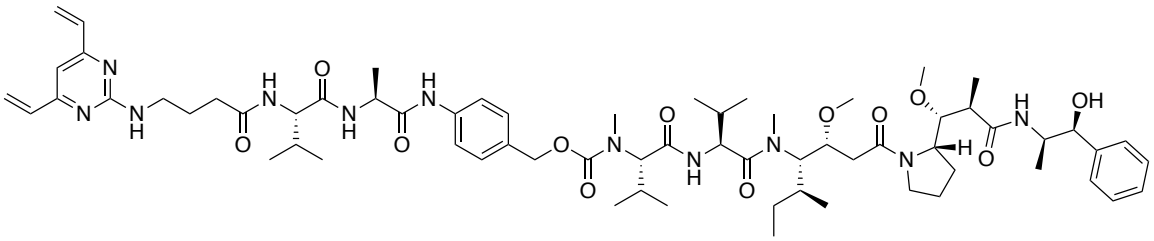

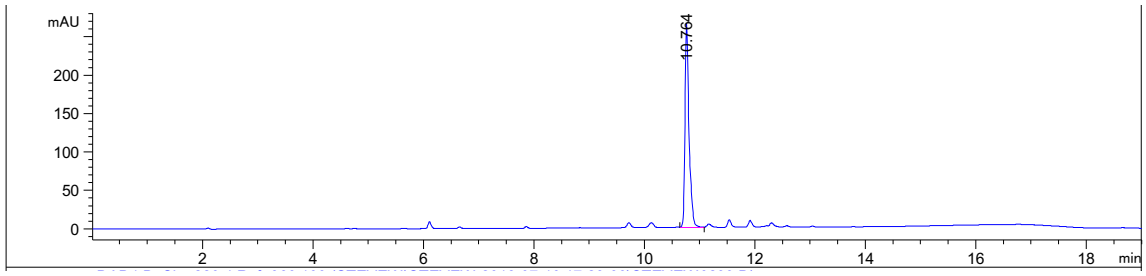

Fmoc-Val-Cit-PABC-MMAE (51)

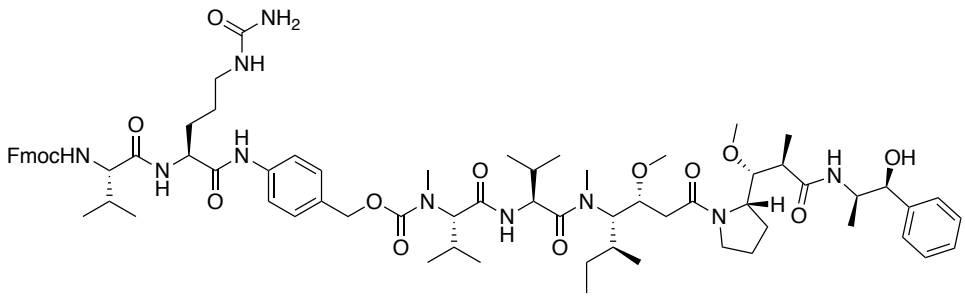

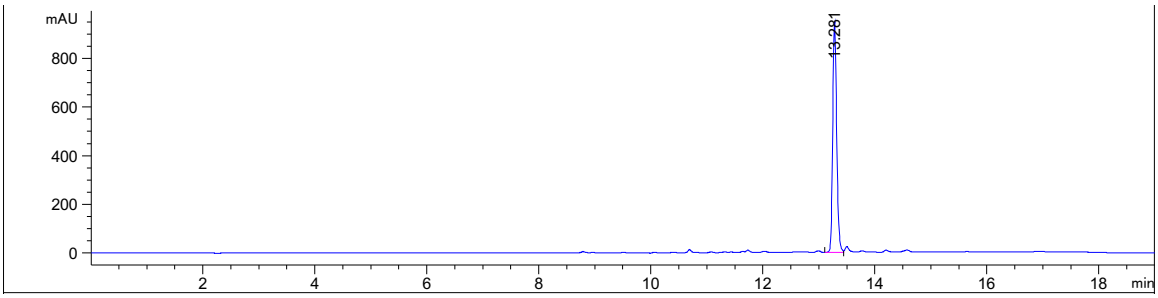

DVP(3C)-Val-Cit-PABC-MMAE (48)

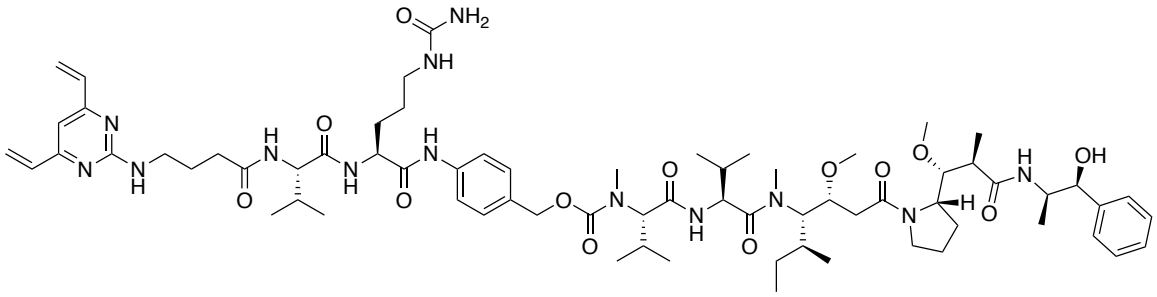

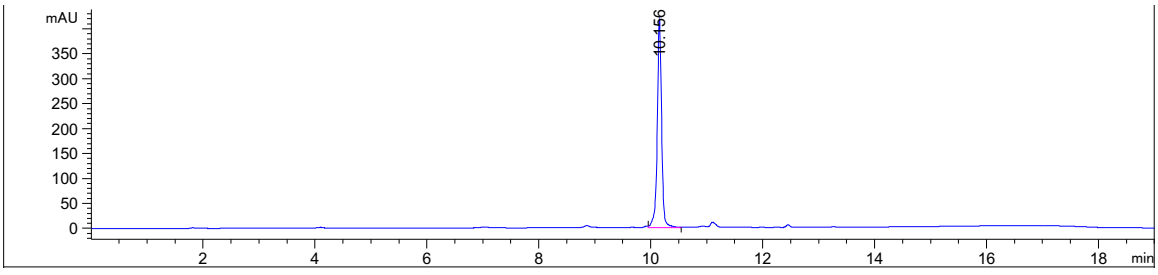

Fmoc-PEG$_5$-Val-Ala-PABC-MMAE (58)

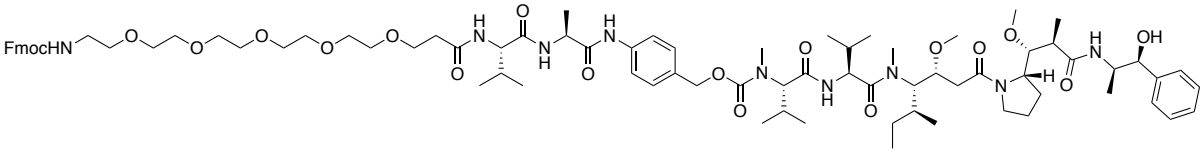

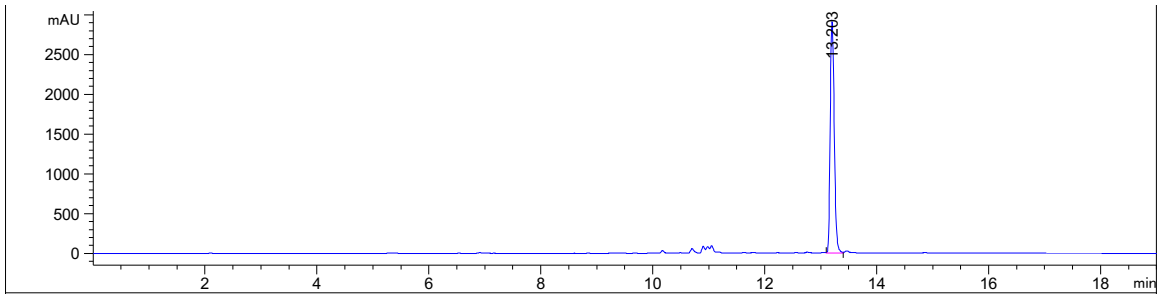

N$_3$-PEG$_9$-Val-Ala-PABC-MMAE (59)

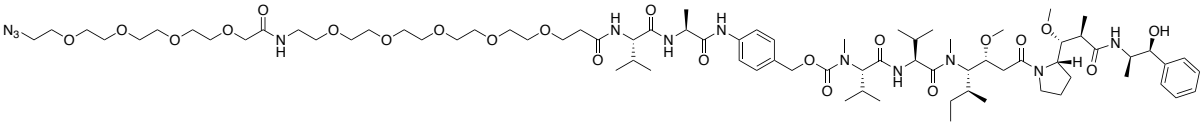

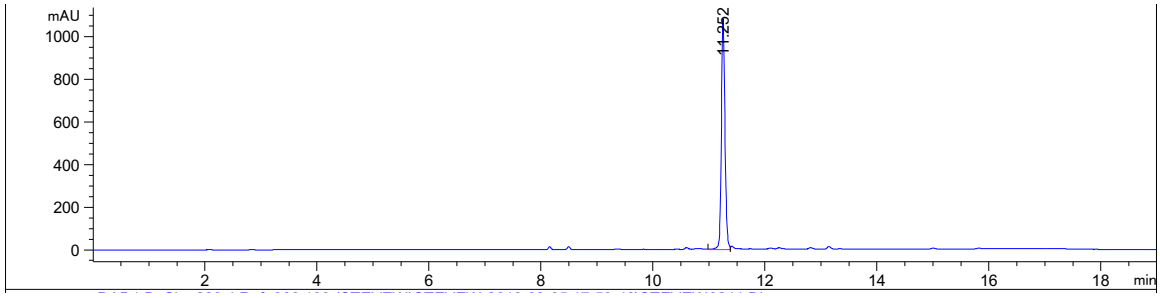

DVP-PEG$_9$-Val-Ala-PABC-MMAE (60)

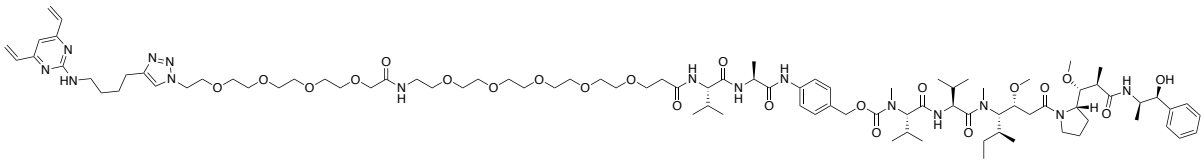

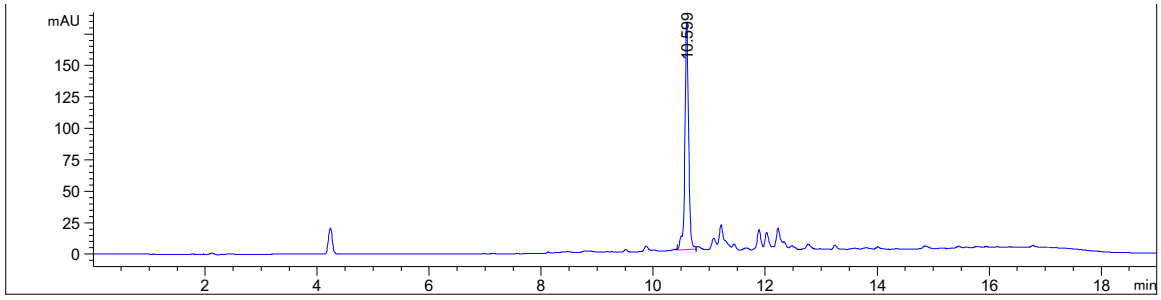

N_3-PEG$_4$-Val-Ala-PABC-MMAE (56)

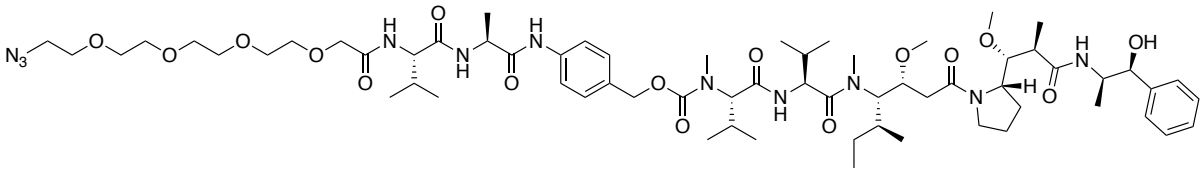

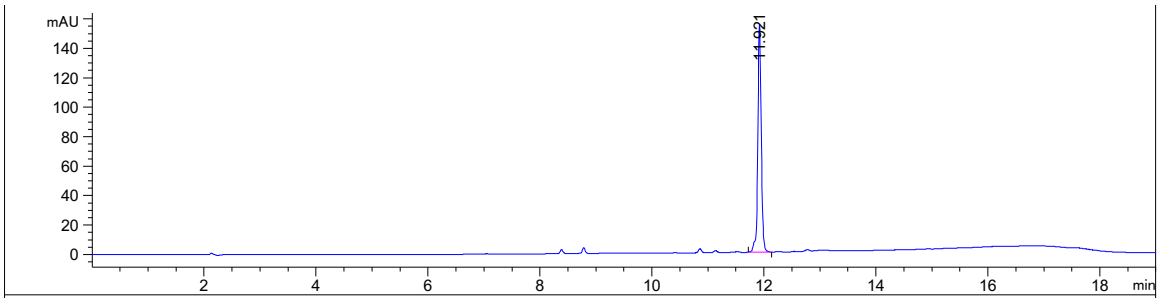

DVP-PEG$_4$-Val-Ala-PABC-MMAE (57)

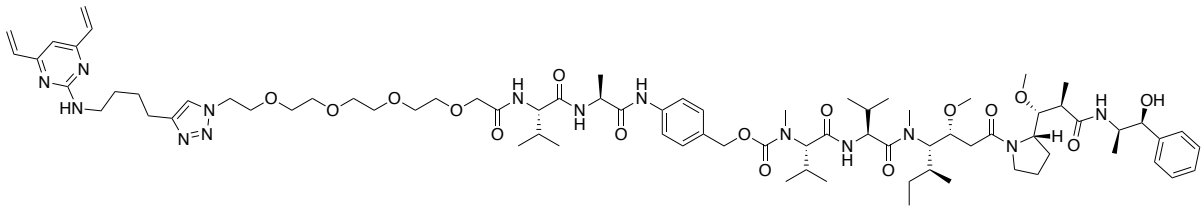

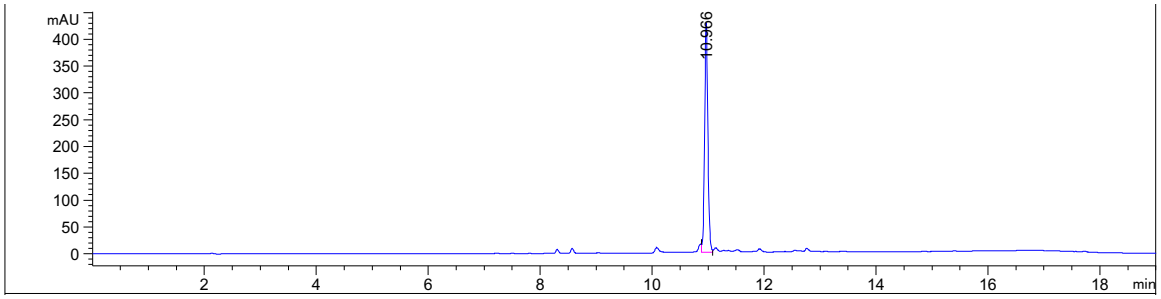

df-DVP-PEG$_5$-Val-Ala-PABC-MMAE (74)

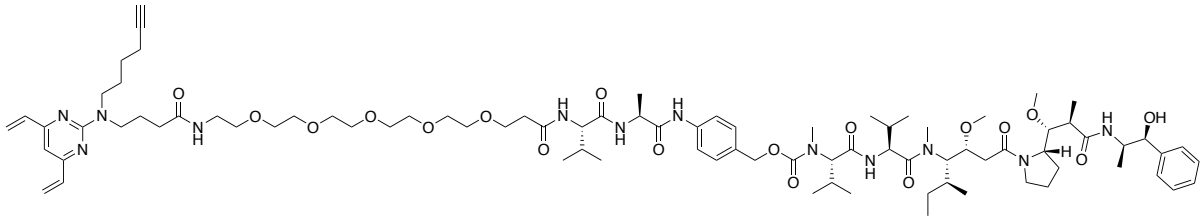

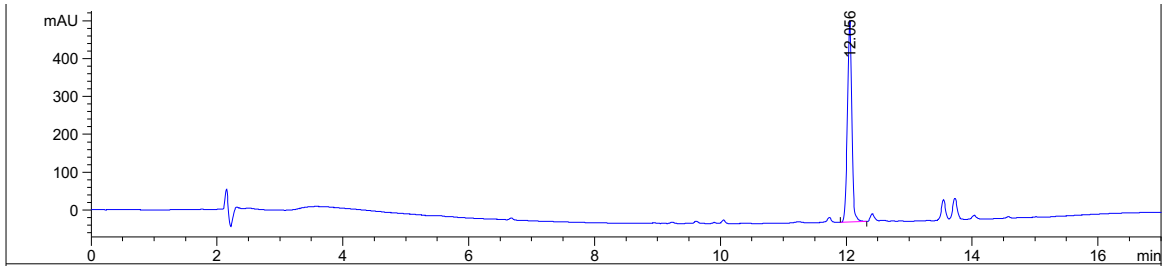

df-DVP-acid-PEG$_4$-Val-Ala-PABC-MMAE (76)

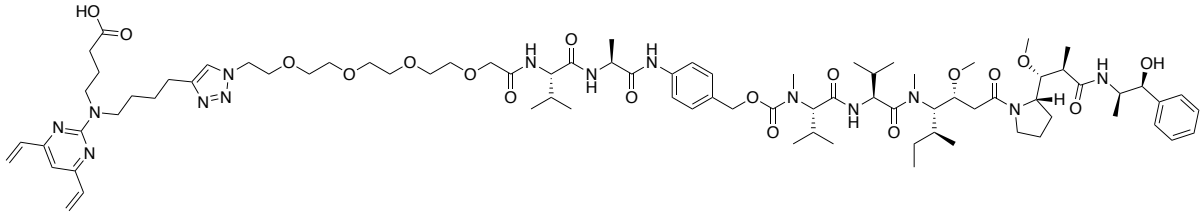

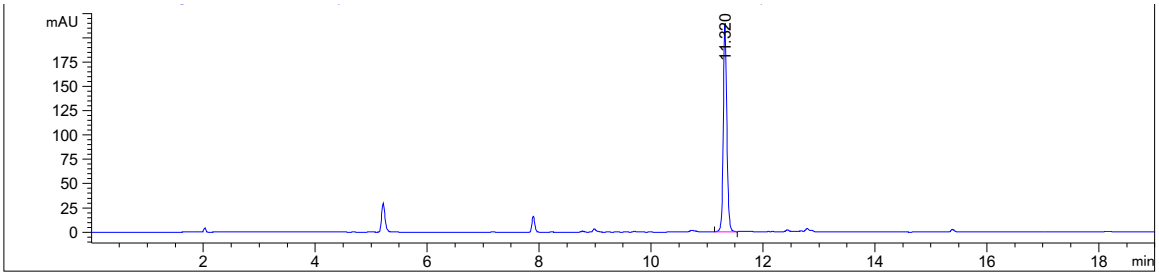

df-DVP-amide-alkyne-PEG$_4$-Val-Ala-PABC-MMAE (77)

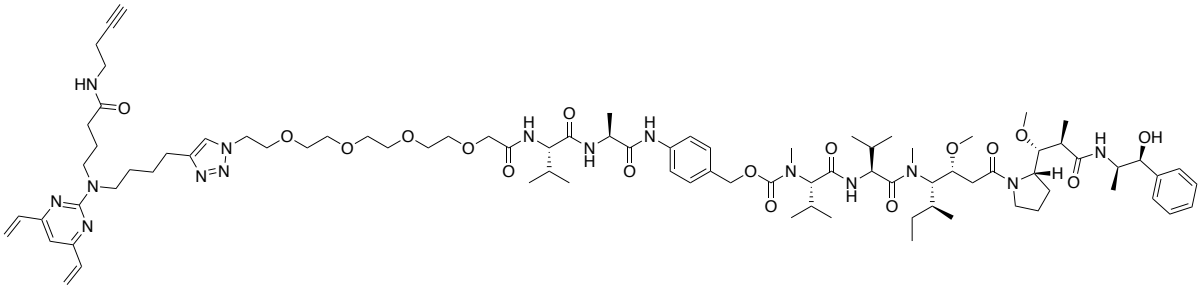

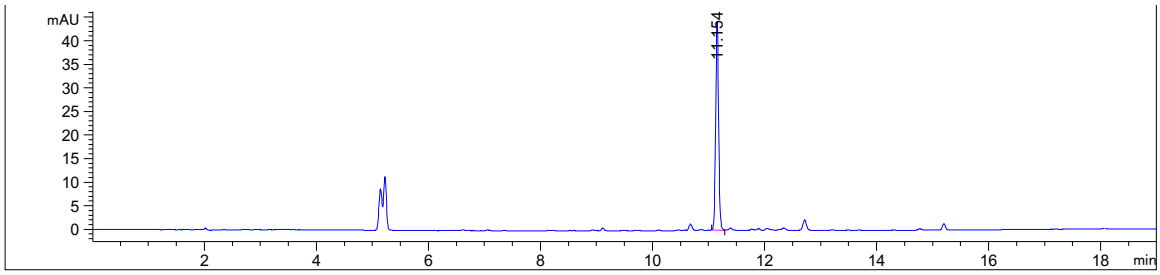

Divinylpyrimidine Chemoselectivity Studies

2-amino-4,6-divinylpyrimidine (15)

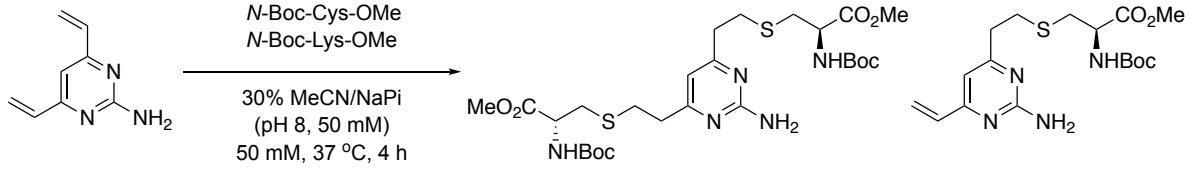

15 **25** **28**

MW = 617.78 **MW = 382.48**

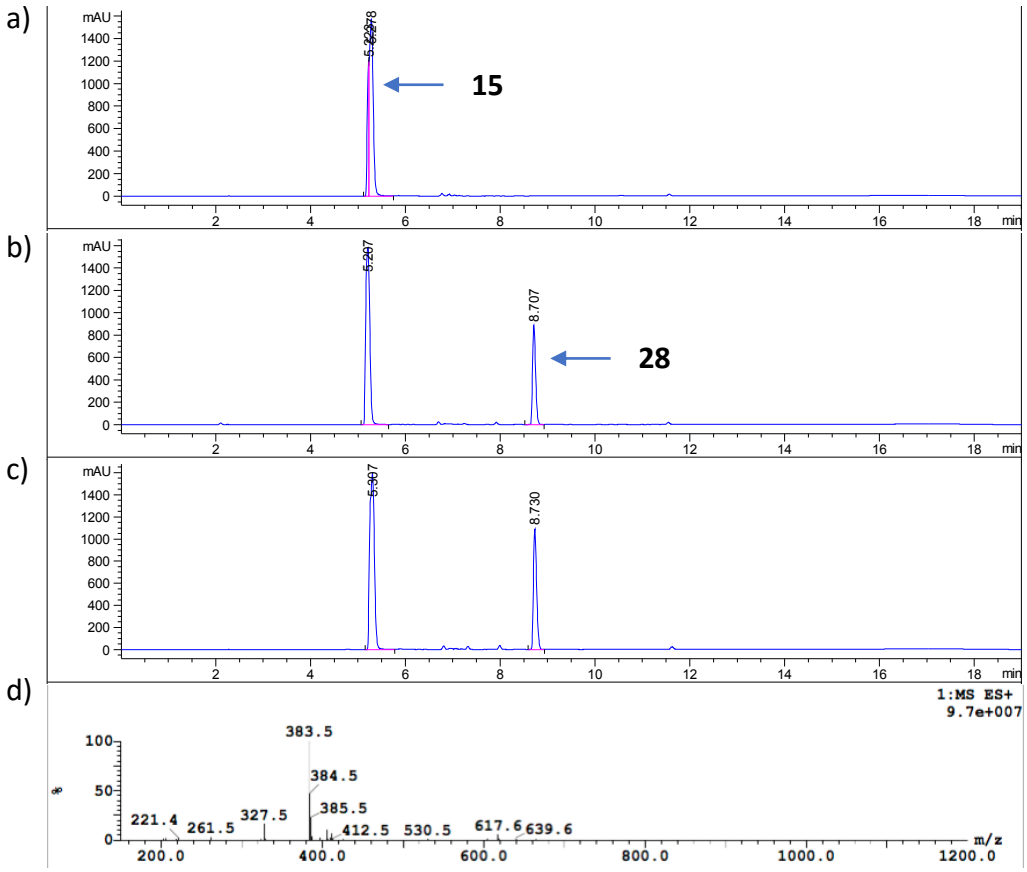

Figure A: HPLC trace of **a)** DVP **15**, **b)** the reaction of DVP **15** with *N*-Boc-Cys-OMe and *N*-Boc-Lys-OMe after two hours and **c)** after four hours, **d)** MS of the reaction after four hours.

N-(hex-5-yn-1-yl)-4,6-divinylpyrimidin-2-amine (18)

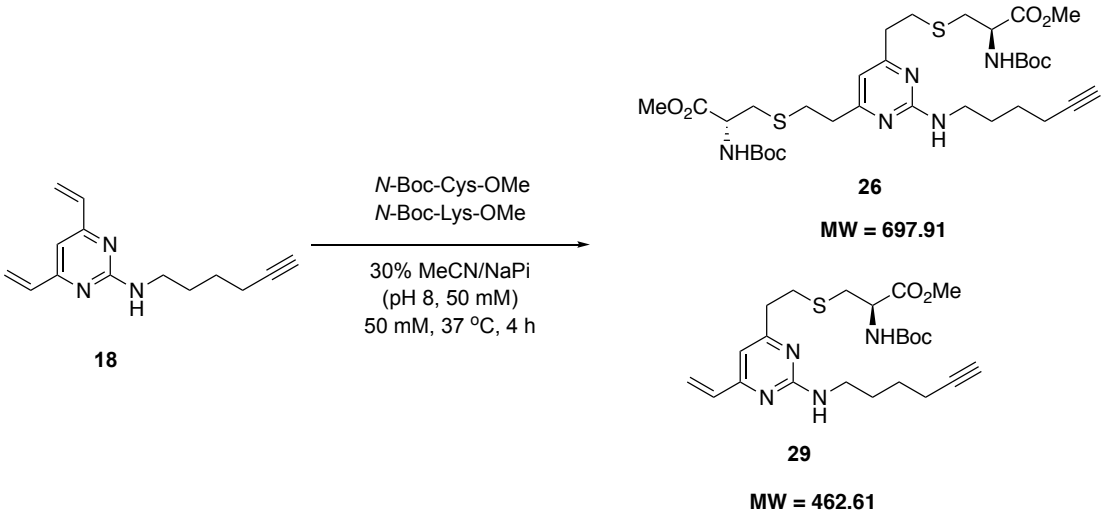

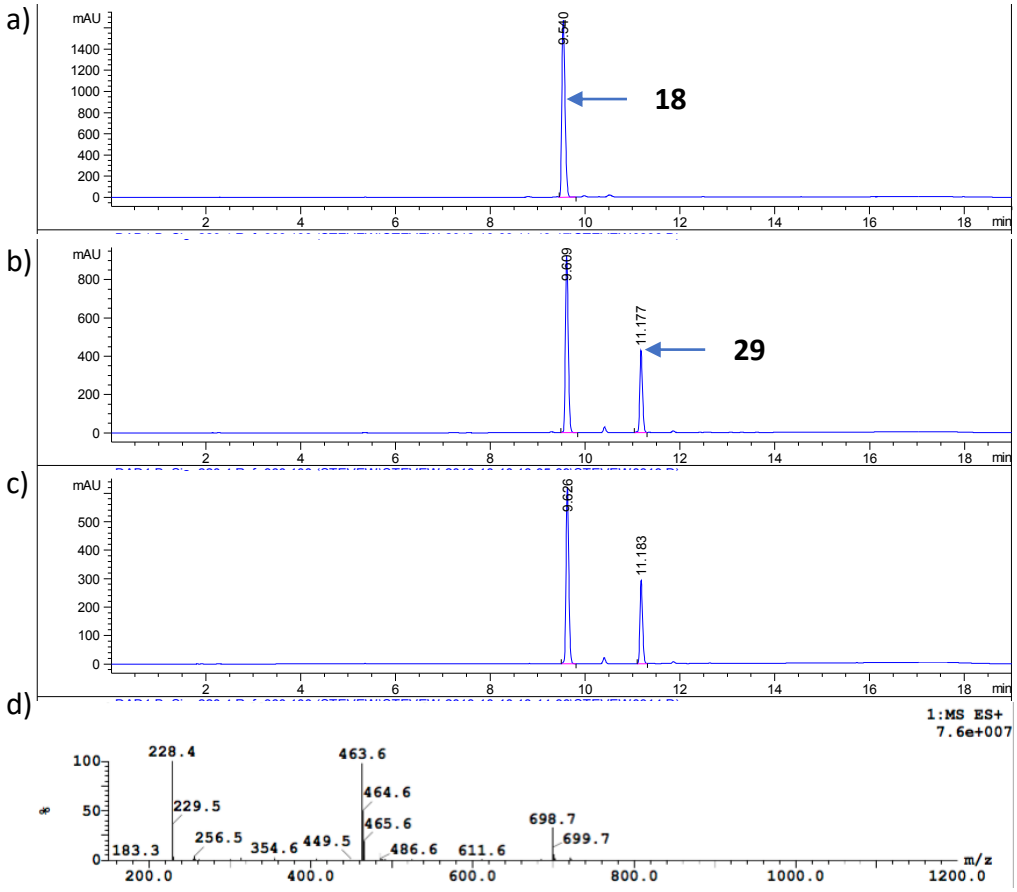

Figure B: HPLC trace of **a)** DVP **18**, **b)** the reaction of DVP **18** with *N*-Boc-Cys-OMe and *N*-Boc-Lys-OMe after two hours and **c)** after four hours, **d)** MS of the reaction after four hours.

N-(4,6-divinylpyrimidin-2-yl)-*N*-methylglycine (24)

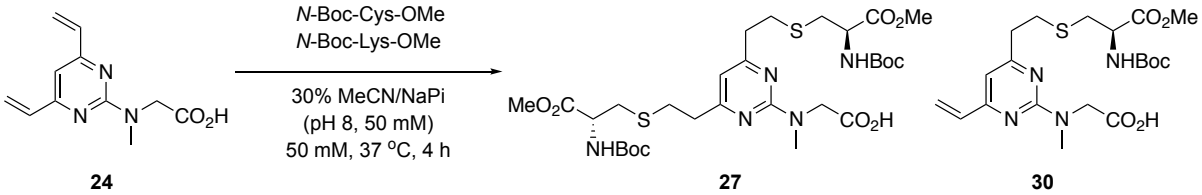

24 **27** **30**

MW = 689.84 **MW = 454.54**

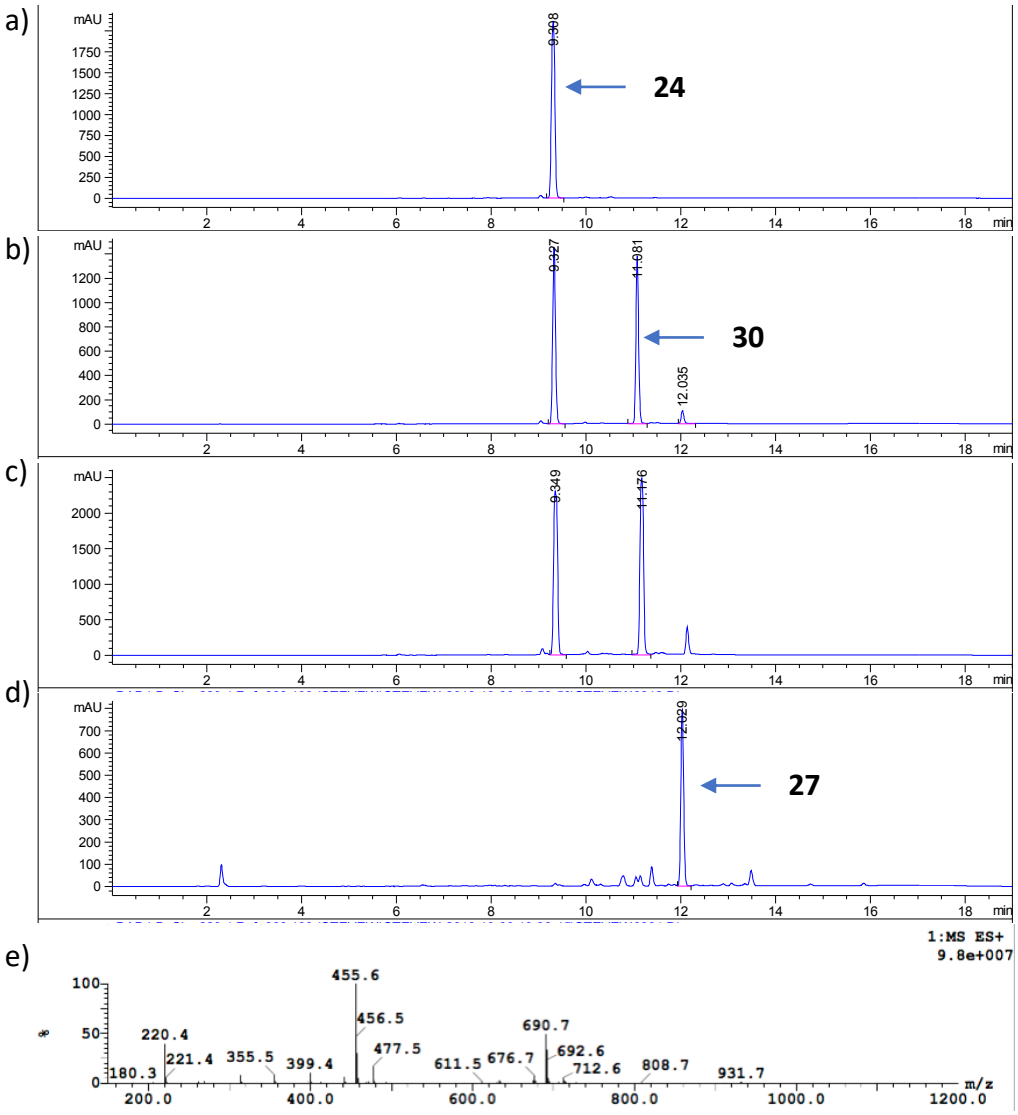

Figure C: HPLC trace of **a)** DVP **15**, **b)** the reaction of DVP **15** with *N*-Boc-Cys-OMe and *N*-Boc-Lys-OMe after two hours and **c)** after four hours, **d)** HPLC of carboxylic acid **27** and **e)** MS of the reaction after four hours.

Appendix C – Protein LCMS

Trastuzumab

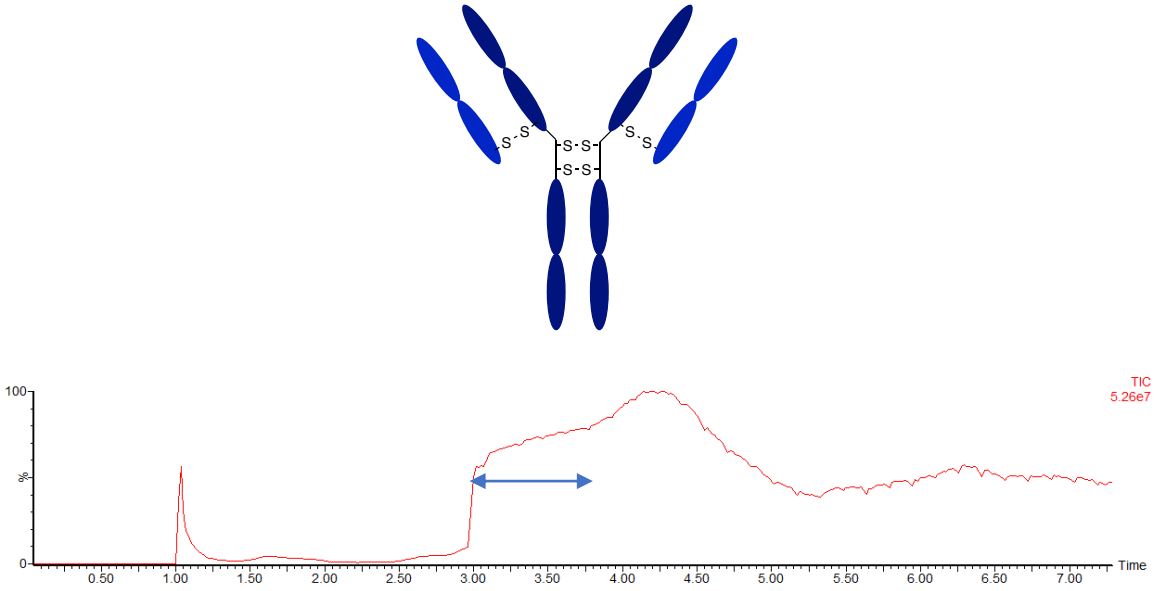

The arrow in TIC trace indicates area that was analysed. Peaks outside of this range did not contain proteinogenic signals and were excluded. Analysis was conducted in the same way for all protein LCMS traces.

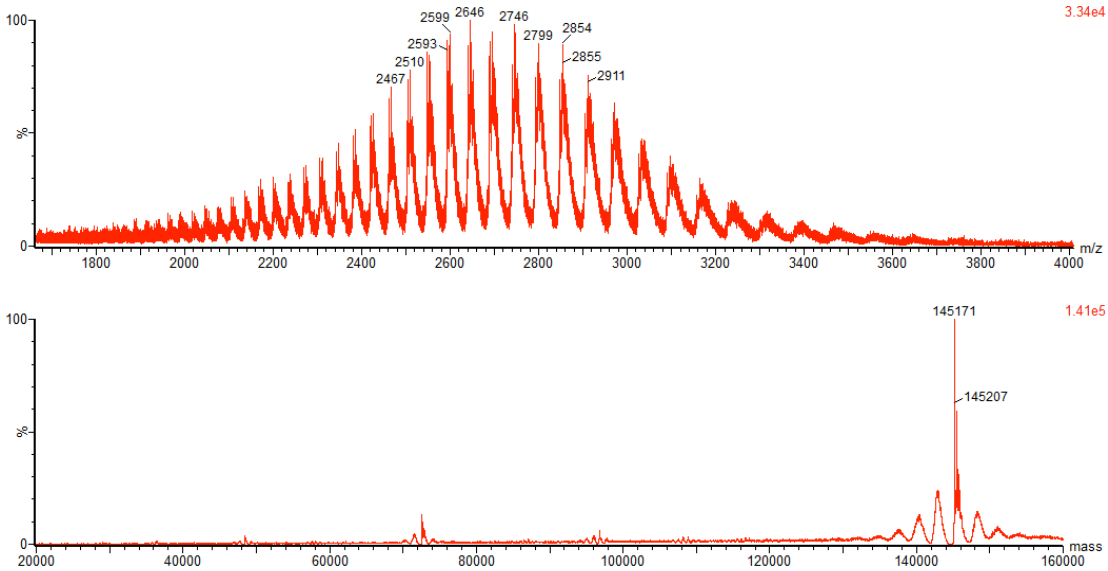

Reduced Trastuzumab

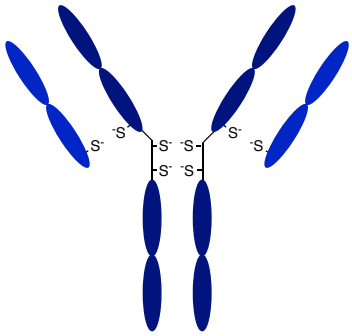

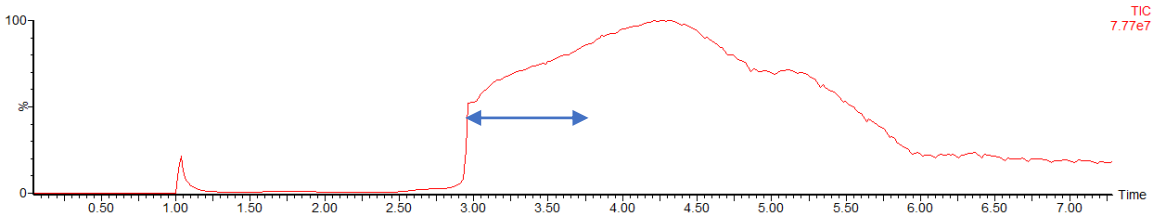

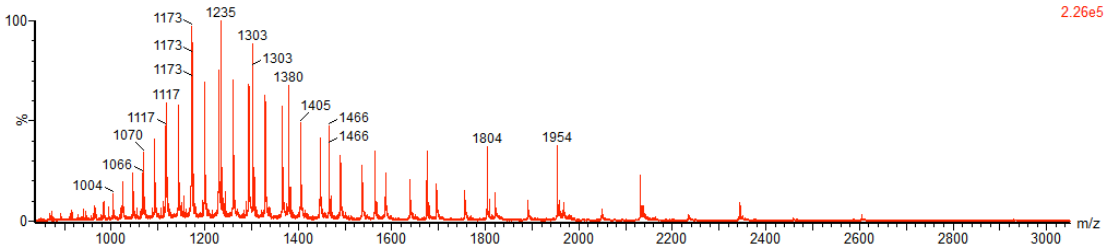

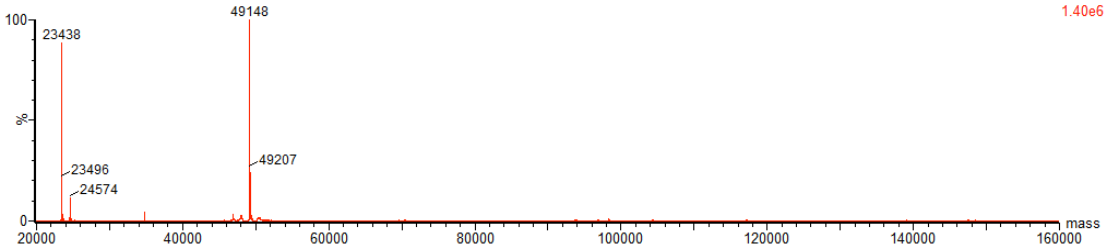

Reduced Trastuzumab pre-deglycosylation

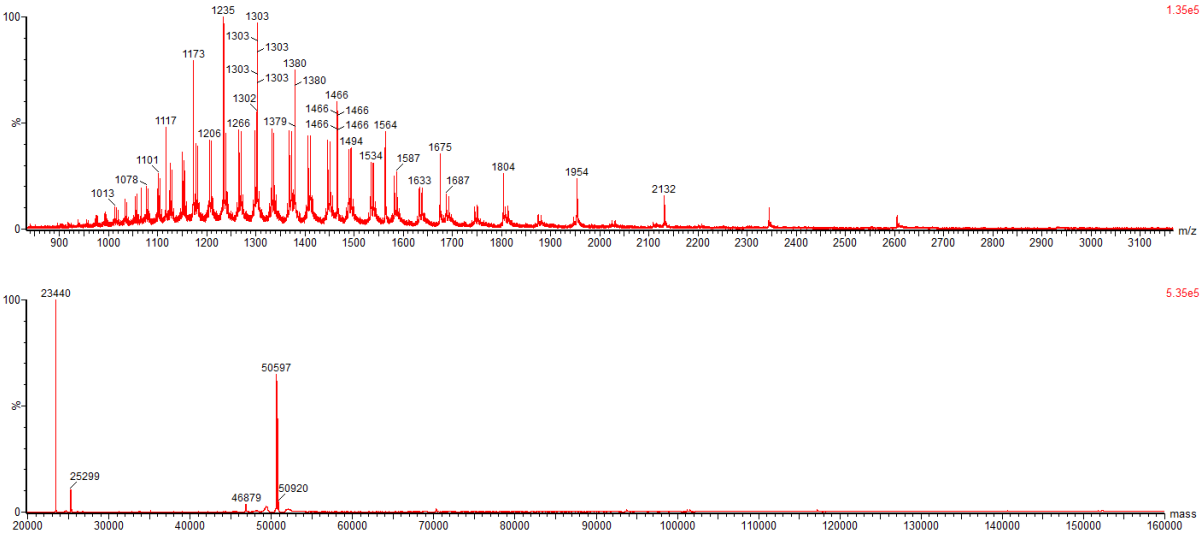

Trastuzumab Fab

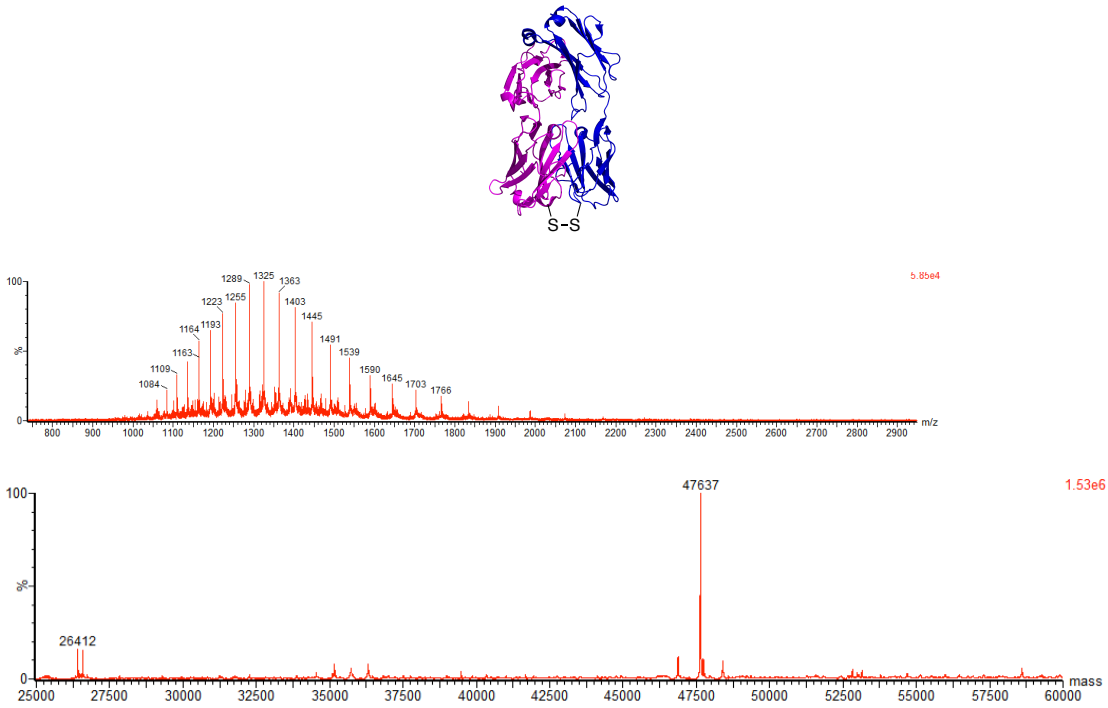

Trastuzumab reaction with divinylpyridine 10 mixture

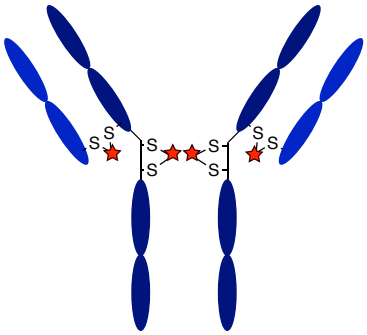

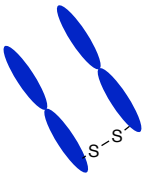

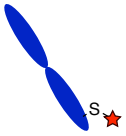

74,387 Da

Half antibody Heavy-Light

46,880 Da

Light chain dimer

23,615 Da

Light chain

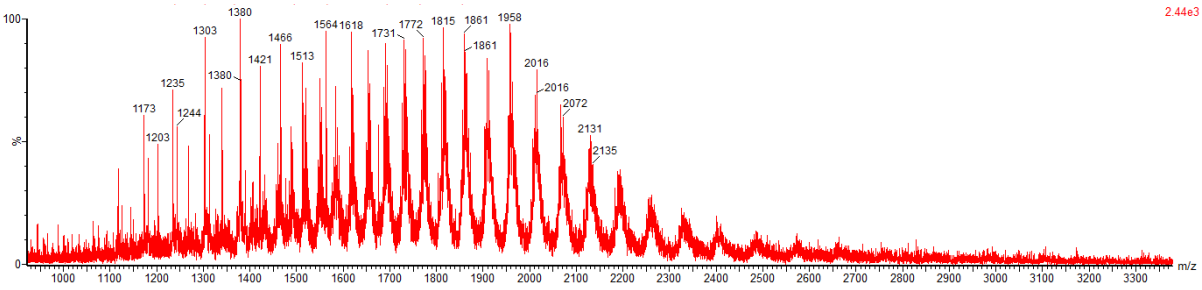

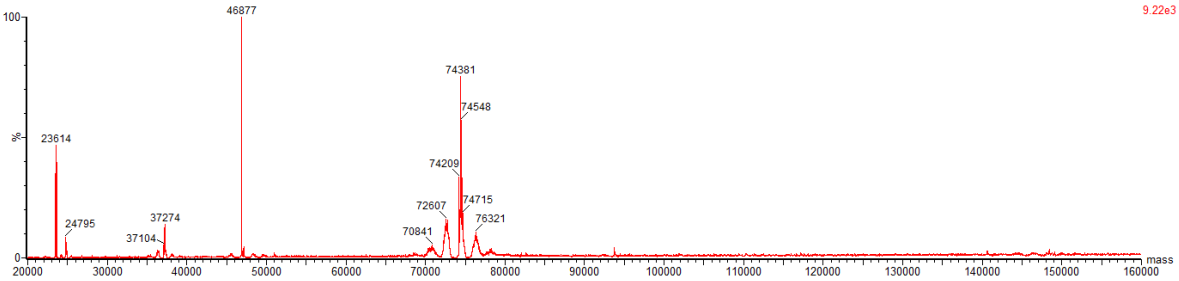

Trastuzumab Fab DVP (31)

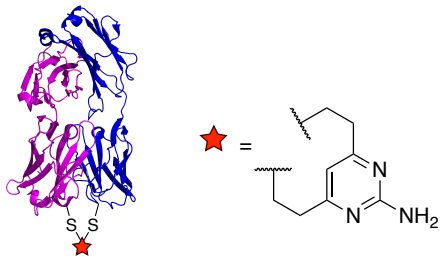

31

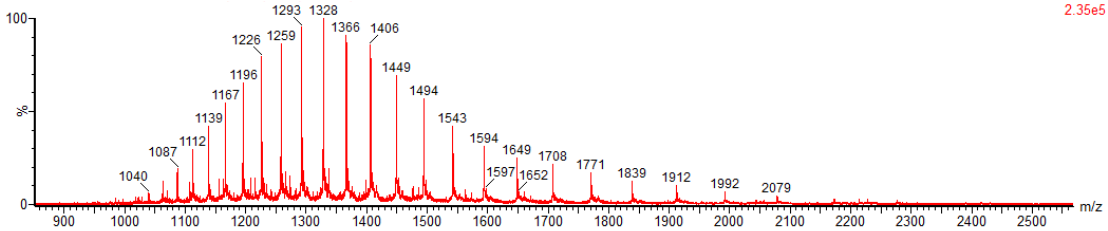

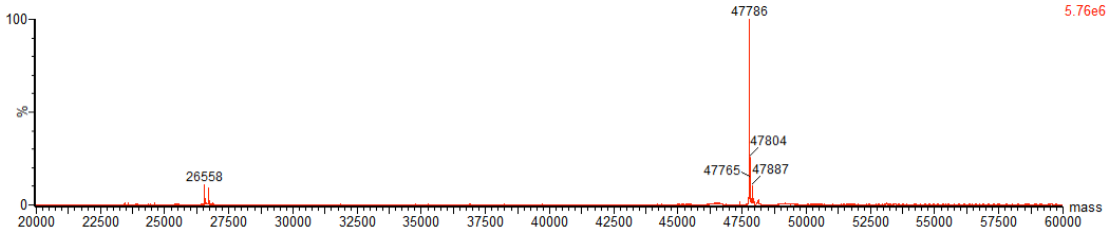

Trastuzumab Fab DVP (32)

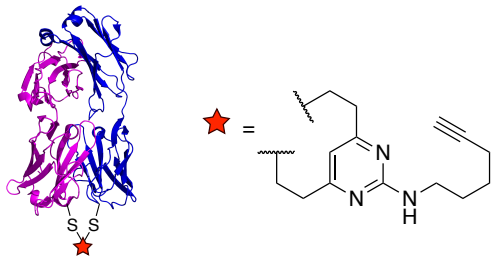

32

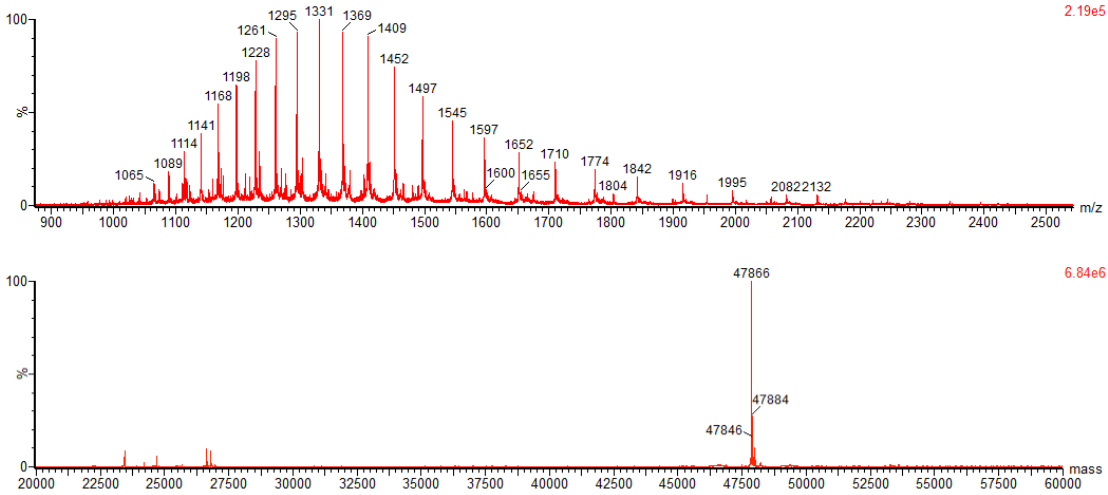

Trastuzumab Fab DVP (33)

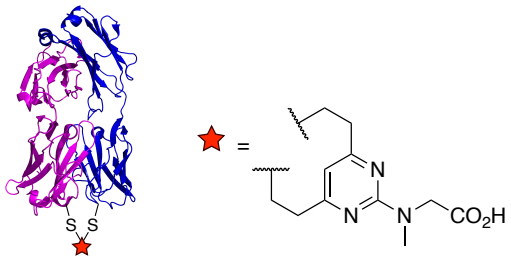

33

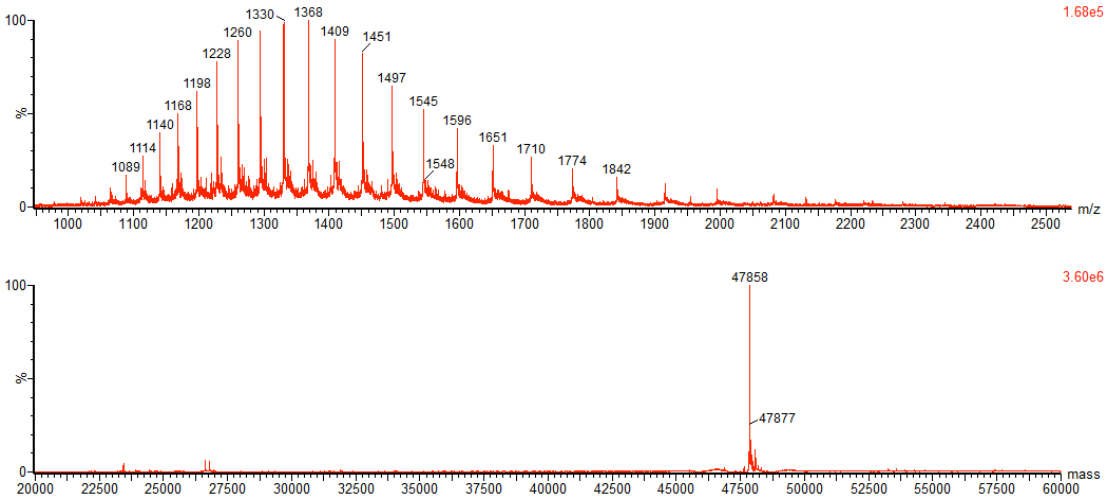

Trastuzumab DVP (34)

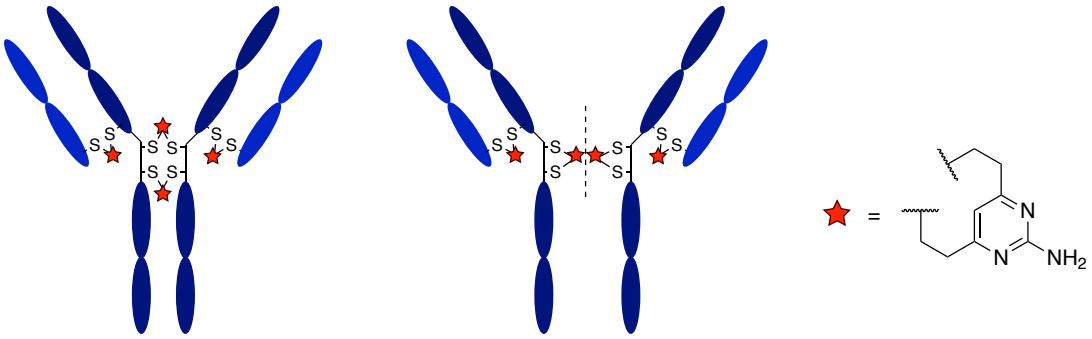

Full antibody **34** **Half antibody**

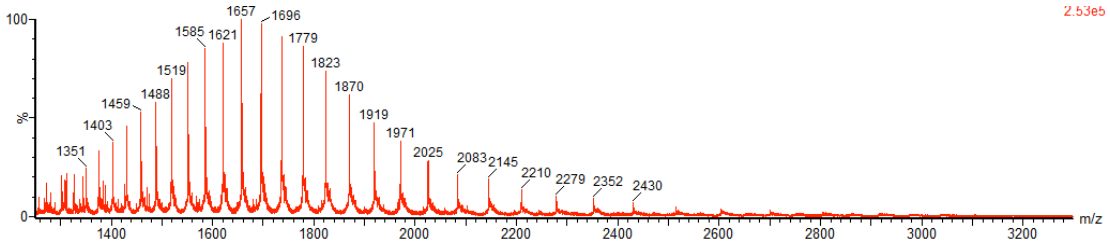

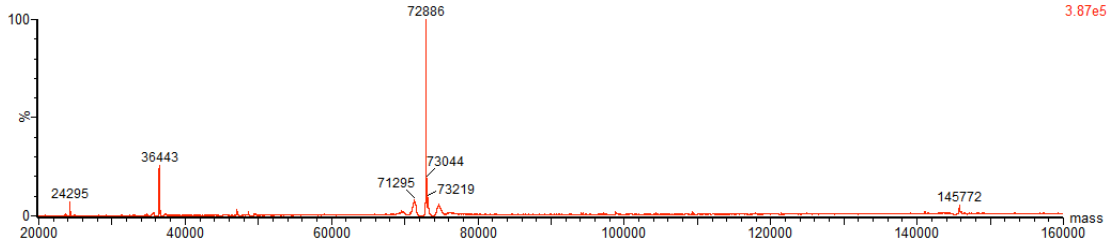

Trastuzumab DVP (35)

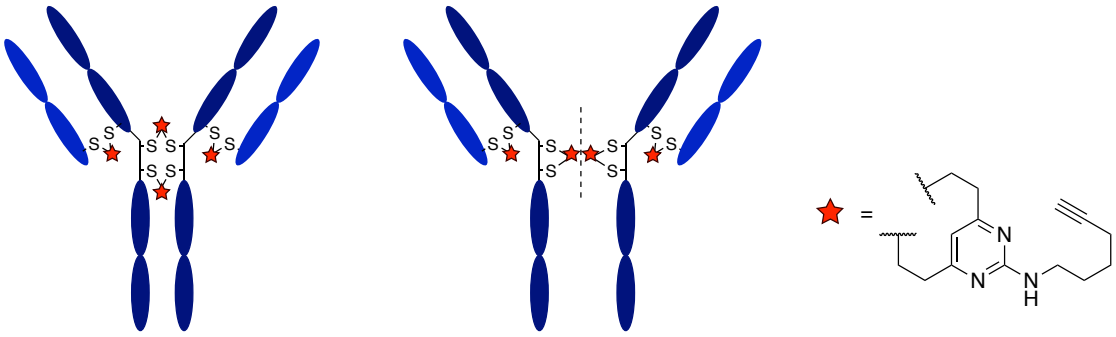

Full antibody **35** **Half antibody**

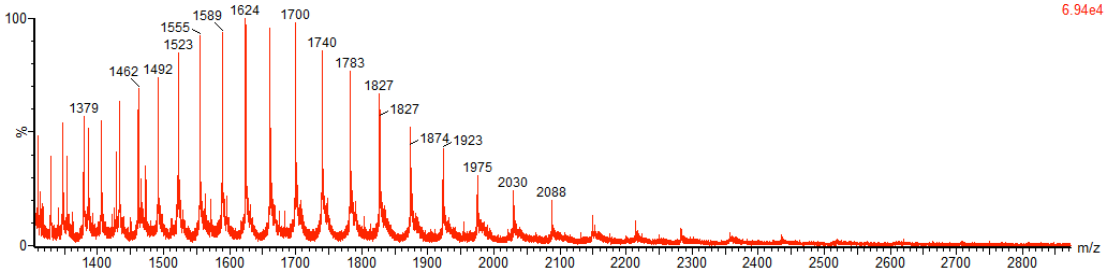

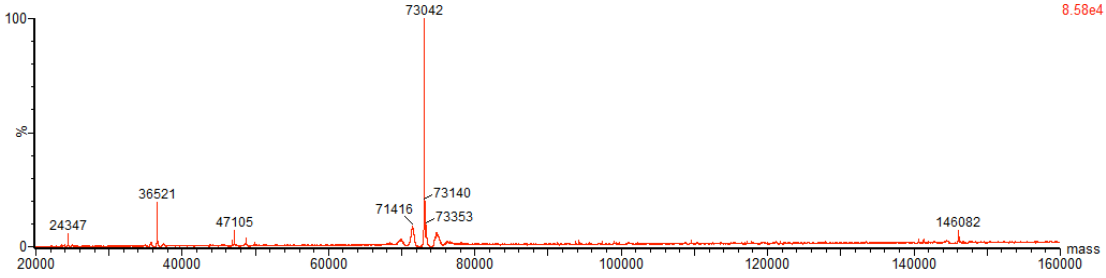

Trastuzumab DVP (36)

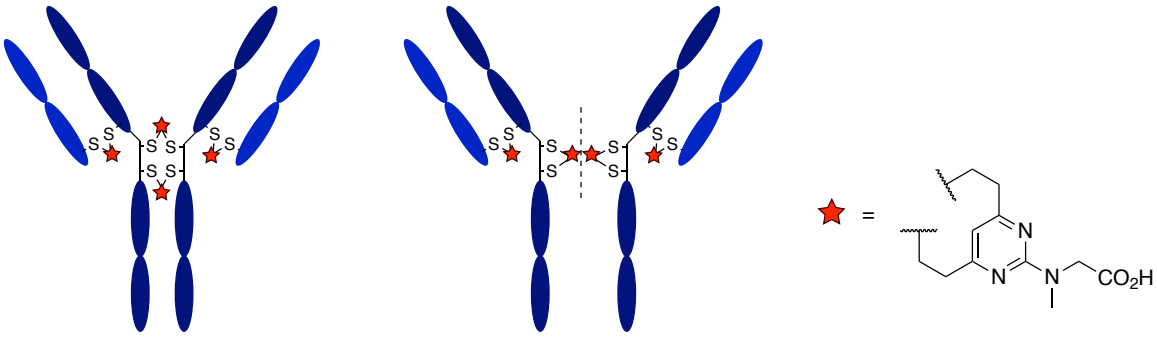

Full antibody **36** Half antibody

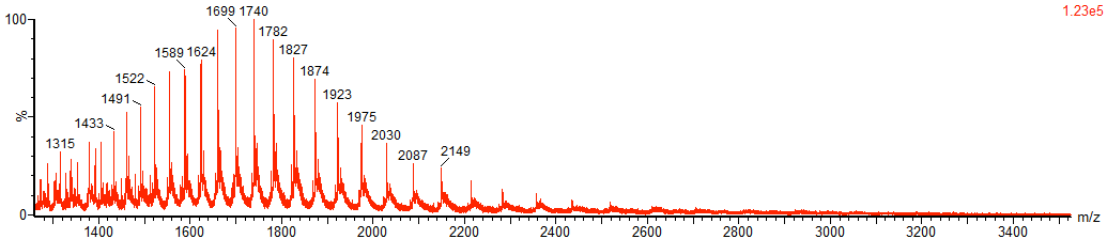

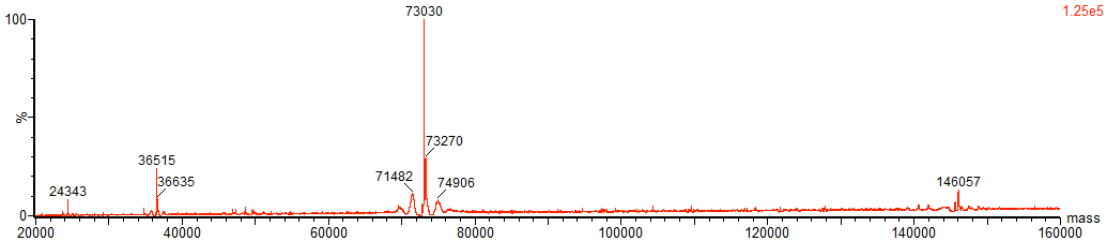

Trastuzumab-doxorubicin ADC (38)

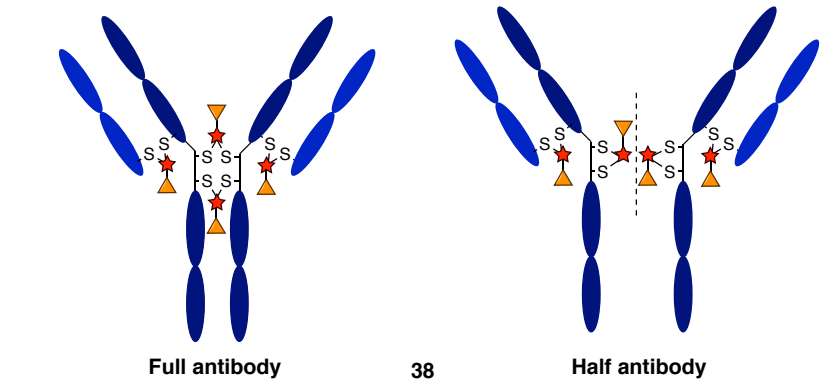

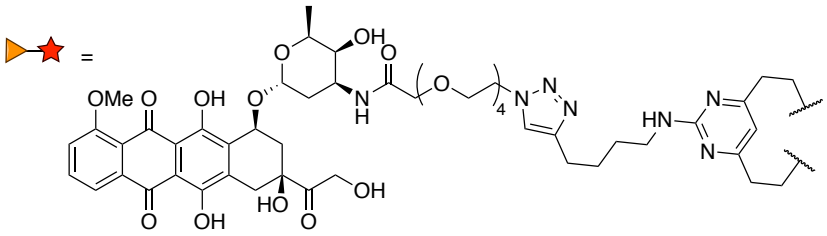

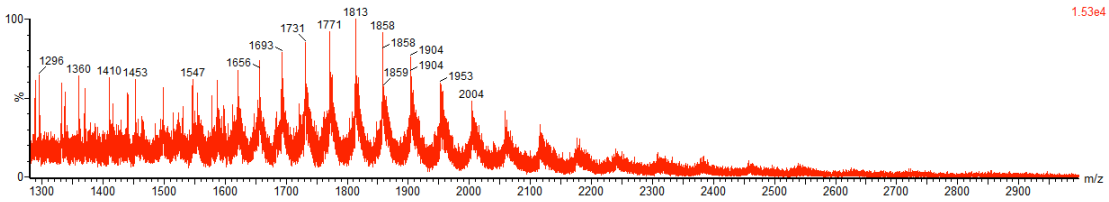

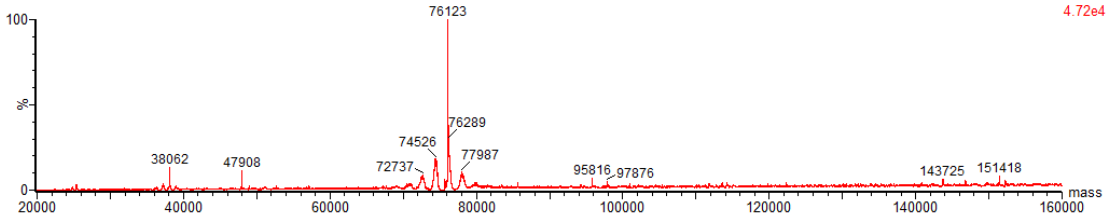

Non-cleavable Trastuzumab-MMAE ADC (42)

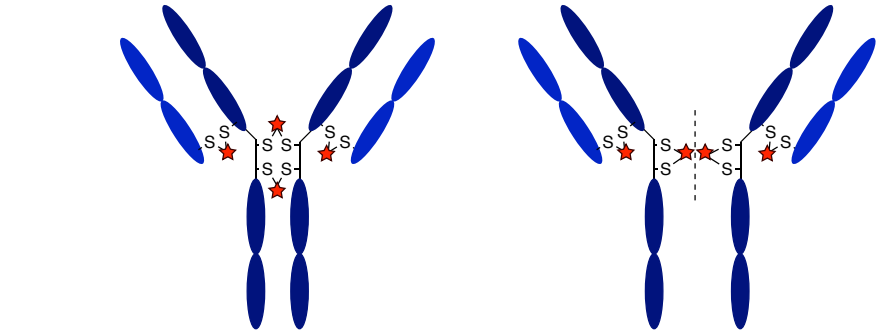

Full antibody 42 Half antibody

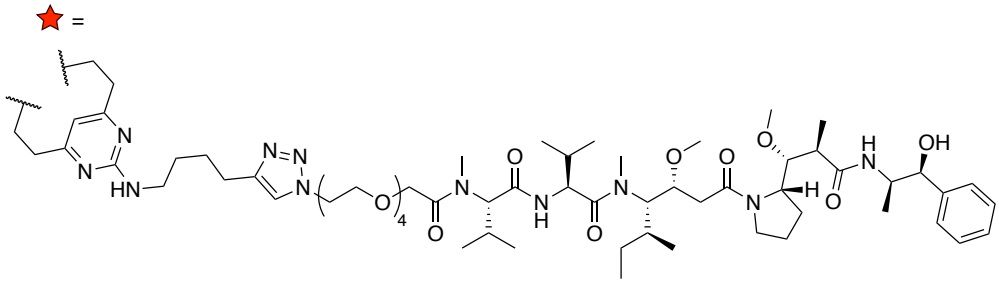

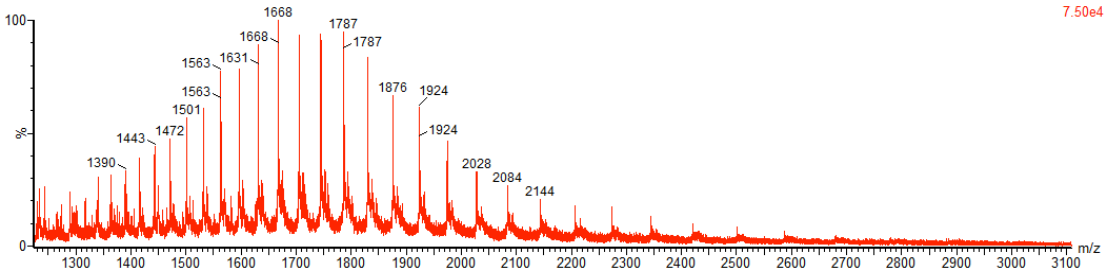

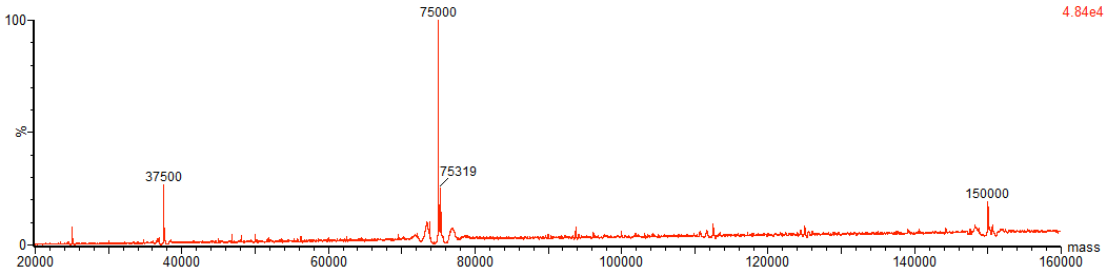

Trastuzumab DVP-PEG$_4$-Val-Ala-PABC-MMAE (62)

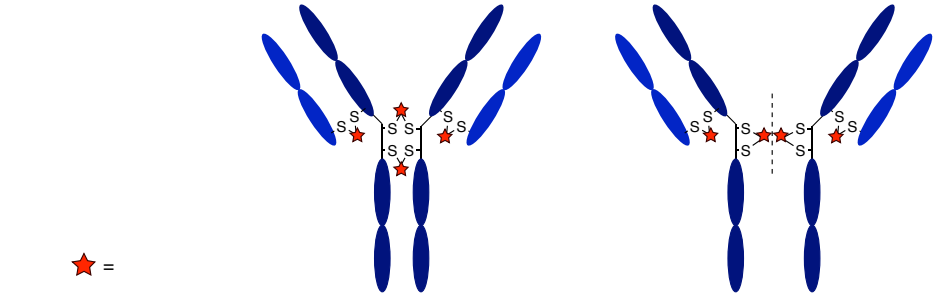

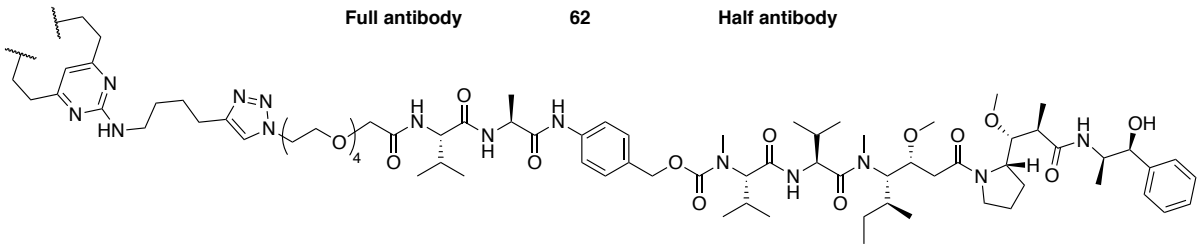

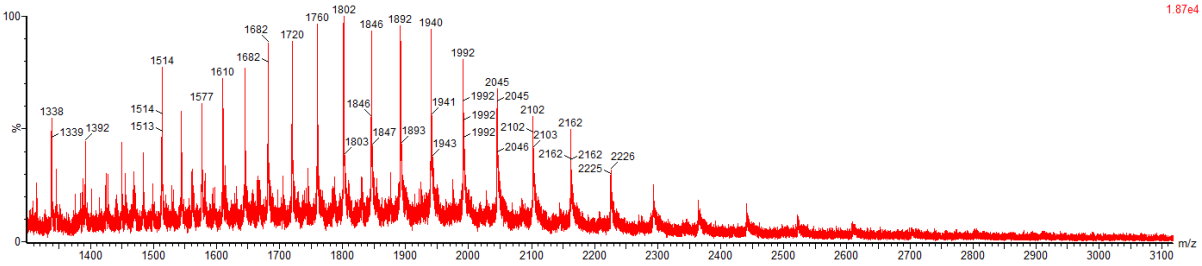

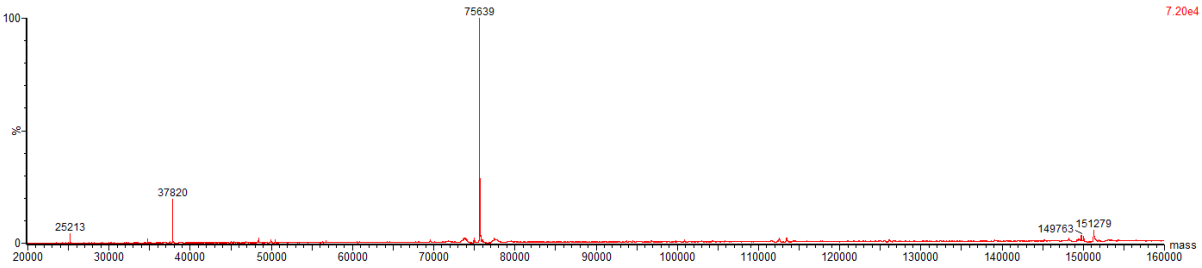

Trastuzumab df-DVP (73)

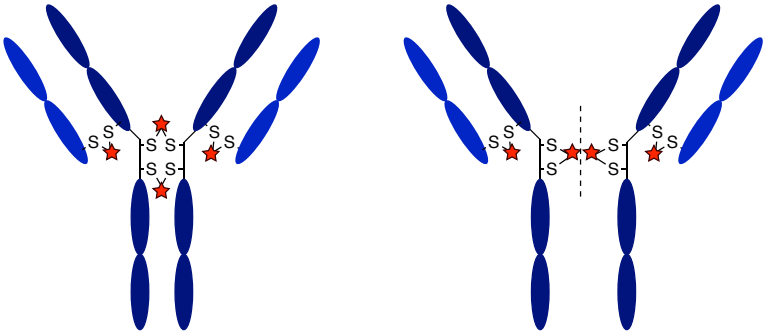

Full antibody **73** Half antibody

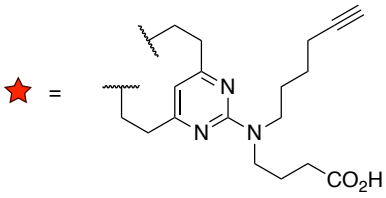

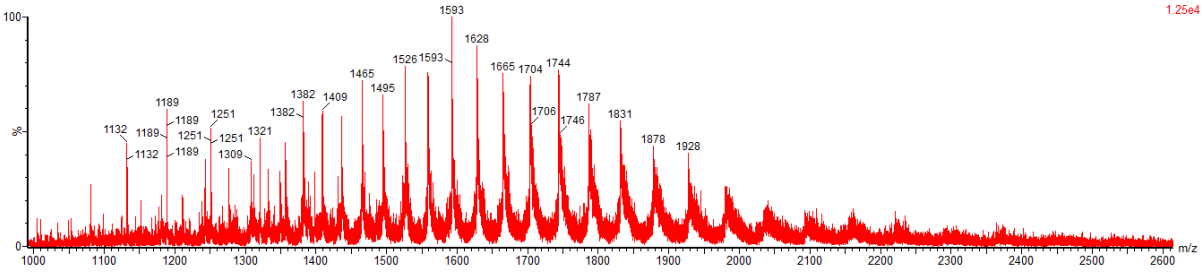

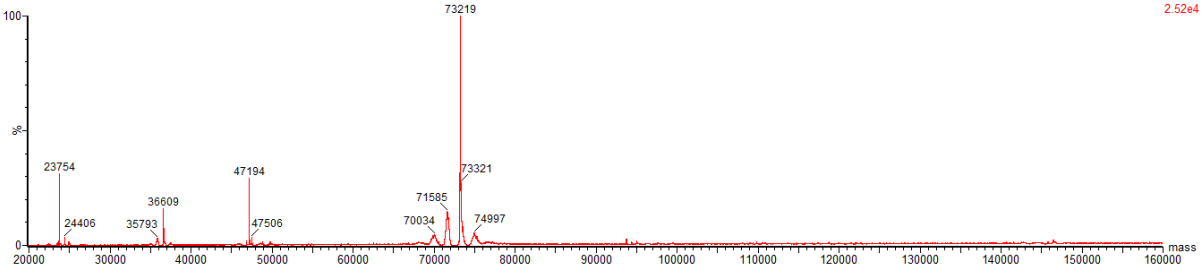

*Pf*RadA-dCys

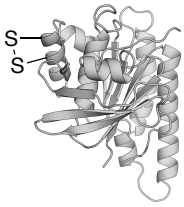

***Pf*RadA-dCys**

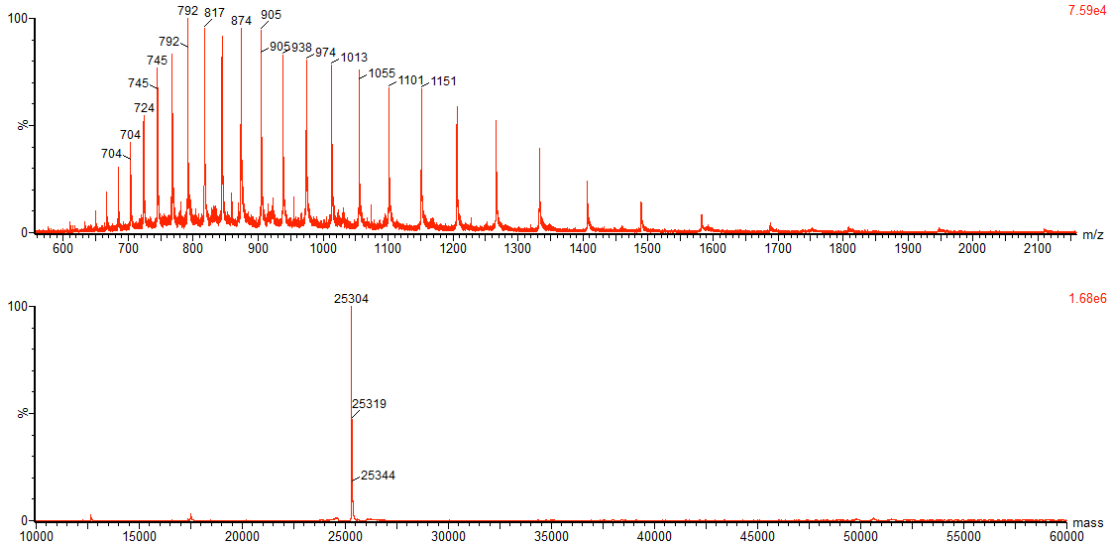

*Pf*RadA-dCys DVP (63)

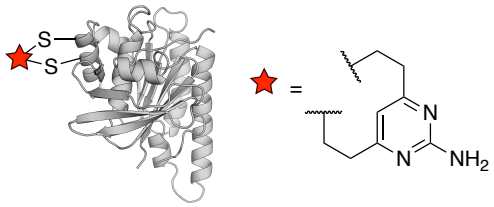

63

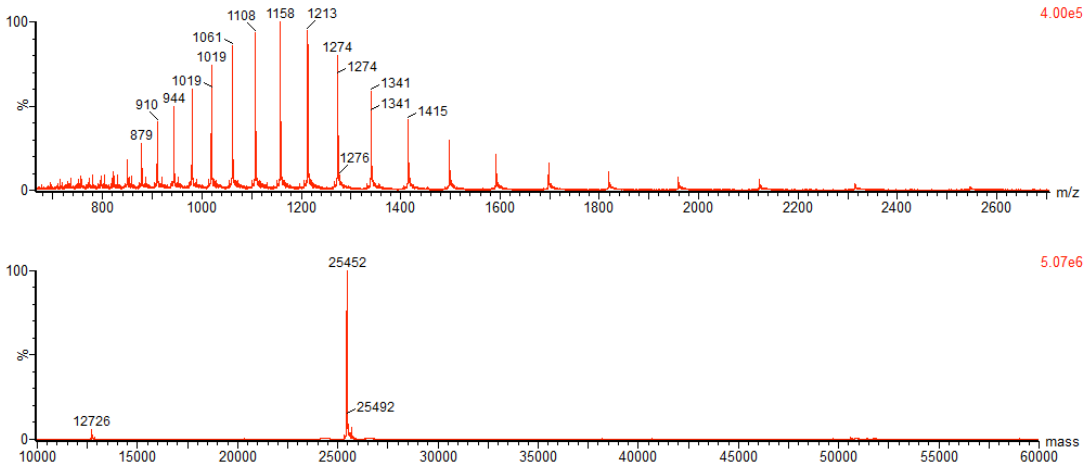

*Pf*RadA-dCys DVP (64)

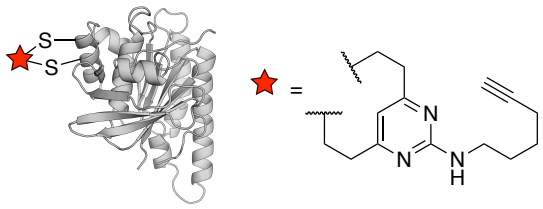

64

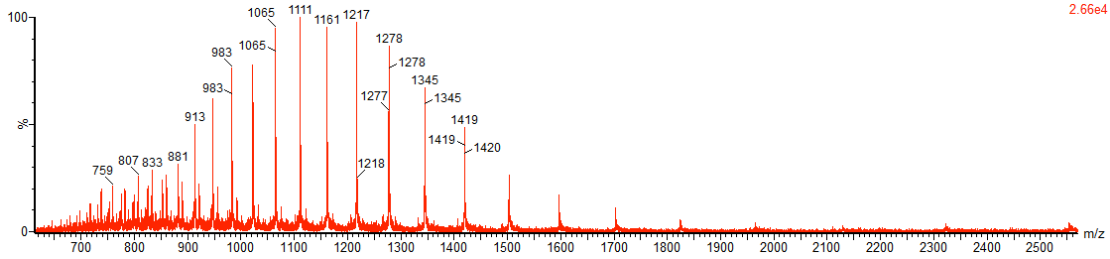

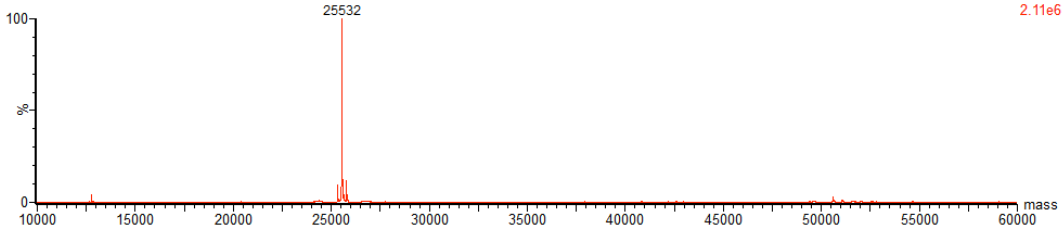

*Pf*RadA-dCys DVP (65)

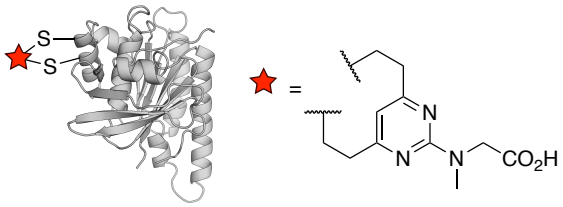

65

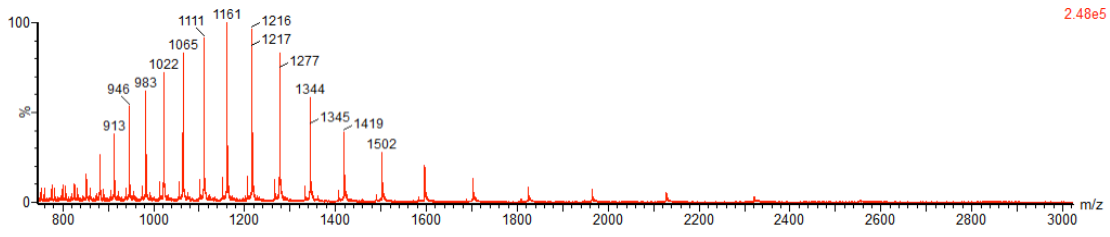

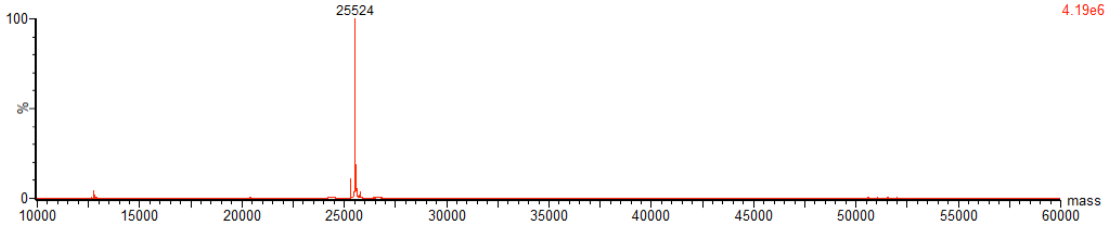

Appendix D – *Pf*RadA-dCys

pBAT4 Vector

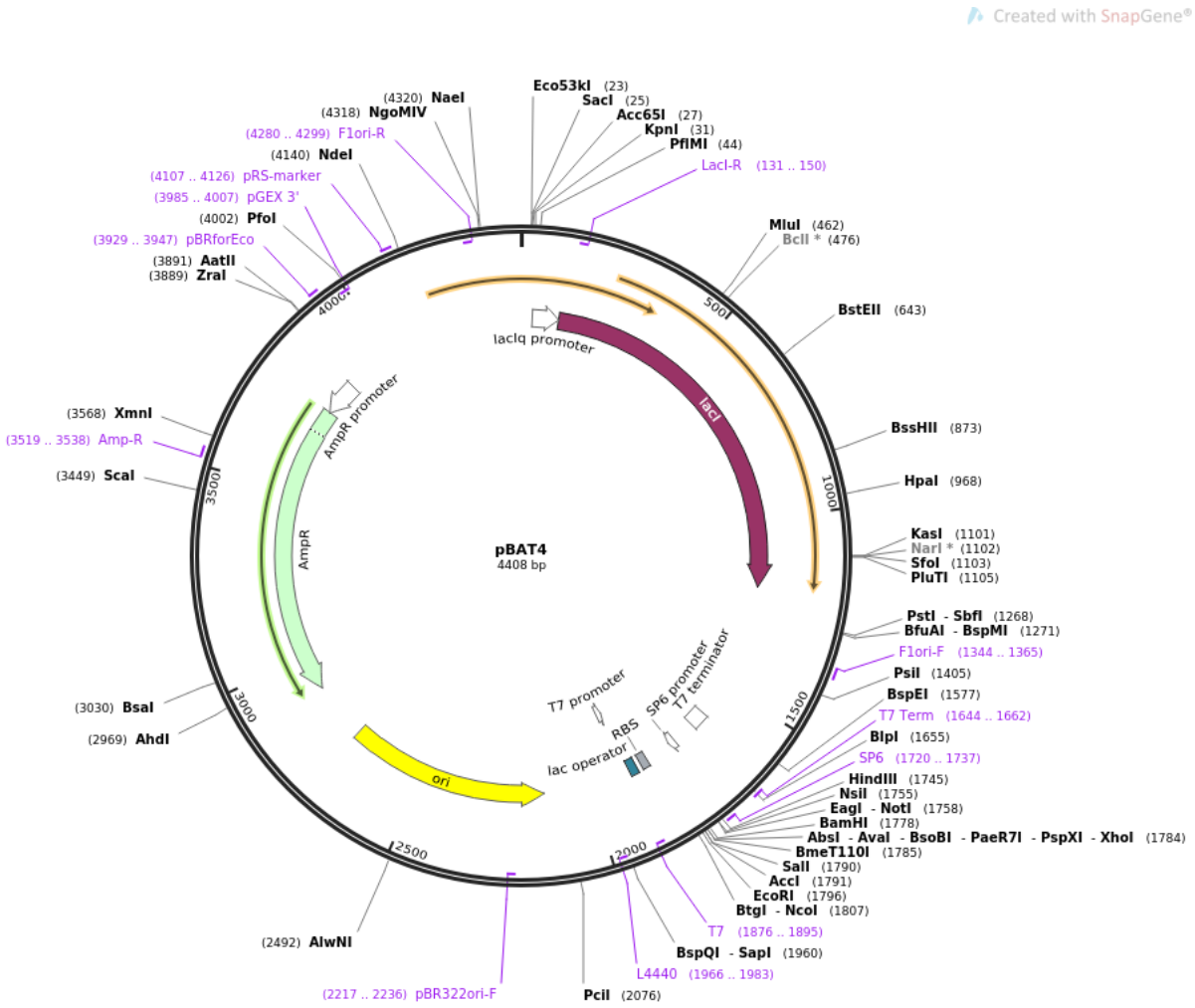

Obtained from Addgene website

*Pf*RadA-dCys Sequence

*ATIGRISTGSKSLDKLLGGGIETQAITEVFGEFGSGKTQLAHTLAVMVQLPPEEGGLNGSV
IWIDTENTFRPERIREIAQ**C**RGLDPDEVLKHIYVARAFNSNHQMLLVQQAEDKIKELLNTDR
PVKLLIVDSLTSHFRSEYIGRGALAERQQKLAKHLADLHRLANLYDIAVFVTNQVQANGGHI
LAHSATLRVYLRKGKGGKRIARLIDAPHLPEGEAVFSIT**C**KGIED

* *N*-terminus methionine cleaved

Appendix E – Publication

Chemical Science

EDGE ARTICLE

Cite this: *Chem. Sci.*, 2019, **10**, 694

All publication charges for this article have been paid for by the Royal Society of Chemistry

A general approach for the site-selective modification of native proteins, enabling the generation of stable and functional antibody–drug conjugates†‡

Stephen J. Walsh, [a] Soleilmane Omarjee,[b] Warren R. J. D. Galloway,[a] Terence T.-L. Kwan,[a] Hannah F. Sore, [a] Jeremy S. Parker, [c] Marko Hyvönen, [d] Jason S. Carroll *[b] and David R. Spring *[a]

Antibody–drug conjugates (ADCs) are a class of targeted therapeutics that utilize the specificity of antibodies to selectively deliver highly potent cytotoxins to target cells. Although recent years have witnessed significant interest in ADCs, problems remain with the standard linkage chemistries used for cytotoxin-antibody bioconjugation. These typically (1) generate unstable constructs, which may lead to premature cytotoxin release, (2) often give a wide variance in drug–antibody ratios (DAR) and (3) have poor control of attachment location on the antibody, resulting in a variable pharmacokinetic profile. Herein, we report a novel divinylpyrimidine (DVP) linker platform for selective bioconjugation *via* covalent re-bridging of reduced disulfide bonds on native antibodies. Model studies using the non-engineered trastuzumab antibody validate the utility of this linker platform for the generic generation of highly plasma-stable and functional antibody constructs that incorporate variable biologically relevant payloads (including cytotoxins) in an efficient and site-selective manner with precise control over DAR. DVP linkers were also used to efficiently re-bridge both monomeric and dimeric protein systems, demonstrating their potential utility for general protein modification, protein stabilisation or the development of other protein-conjugate therapeutics.

Received 18th October 2018
Accepted 6th November 2018

DOI: 10.1039/c8sc04645j

rsc.li/chemical-science

Introduction

The emergence of biotherapeutics in recent decades has opened up vast new areas of research for the treatment of a range of grievous diseases,[1,2] with antibody–drug conjugates (ADCs) demonstrating considerable promise as anticancer agents.[3,4] ADCs utilize the impeccable cell-targeting ability of an antibody in combination with the highly potent nature of a cytotoxic payload to achieve cell-selective cytotoxicity[5] while overcoming the dose-limiting toxicity of classical non-targeted small molecule chemotherapy.[6,7] There are currently four ADCs on the market[8–11] and over 60 other ADCs in clinical trials.[12] However, current approaches for ADC production still have numerous shortcomings. Stability, drug–antibody ratio (DAR) and drug distribution have all been shown to be crucial to the efficacy, safety and overall pharmacological profile of ADCs and are strongly influenced by the chemistry used to attach the linker to the antibody. Commonly employed nucleophilic bioconjugation at cysteine or lysine residues are pseudorandom: in theory, any of the targeted amino acids within the antibody can be modified. Consequently, there is a lack of selectivity, leading to the formation of ADCs which are heterogeneous in terms of the number of cytotoxin molecules incorporated (the DAR) and their locations on the antibody. Such constructs are associated with unreliable pharmacokinetic profiles and therefore, a reduced pharmacological effect.[13–17] Maleimide conjugation to reduced antibody cysteine thiols has been extensively used in ADC development (Fig. 1a). However, the formed succinimide thioether is inherently unstable in the body (due to a retro-Michael reaction) which leads to premature dissociation of the payload from the antibody.[18,19] The plasma stability of maleimide-based linkers has been increased by hydrolysis of the succinimide thioether ring through linker modifications or antibody engineering.[20,21] However, an inherently stable linker is preferential. The development of new ADC formats to enable site-selective antibody modification, including the

[a]*Department of Chemistry, University of Cambridge, Cambridge, CB2 1EW, UK. E-mail: spring@ch.cam.ac.uk*

[b]*Cancer Research UK Cambridge Institute, University of Cambridge, Cambridge, CB2 0RE, UK. E-mail: jason.carroll@cruk.cam.ac.uk*

[c]*Early Chemical Development, Pharmaceutical Development, IMED Biotech Unit, AstraZeneca, Macclesfield, UK*

[d]*Department of Biochemistry, University of Cambridge, Cambridge, CB2 1GA, UK*

† Dedicated to Professor Jack Baldwin on the occasion of his 80th birthday.

‡ Electronic supplementary information (ESI) available. See DOI: 10.1039/c8sc04645j

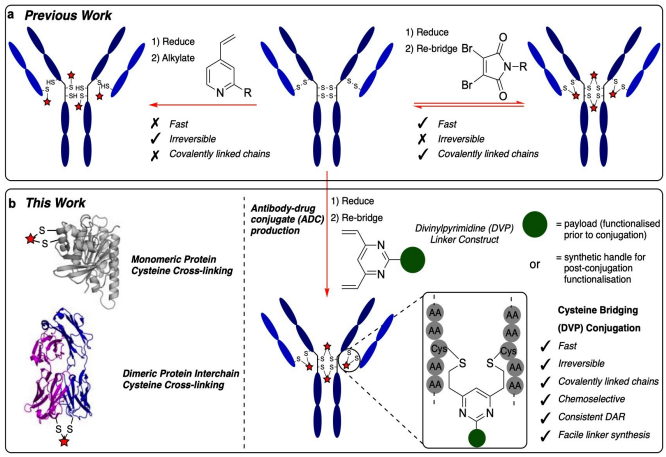

Fig. 1 (a) Previous work using monovinylpyridine or maleimide linkers for the generation of ADCs from native antibodies and (b) the divinylpyrimidine (DVP) linkers developed in this work generate homogeneous and stable ADCs *via* cysteine re-bridging (cross-linking).

incorporation of engineered cysteine residues[13] and unnatural amino acids[22,23] into the antibody sequence and the use of various enzymatic processes,[24–26] have produced ADCs with precise DAR and defined attachment points. While effective, these methods are complicated and generally inefficient.[27]

Recently, disulfide-bridging linkers have emerged for ADC production: a bis-reactive linker moiety undergoes reaction with both thiol residues derived from a reduced cysteine disulfide bond, leading to covalent re-bridging of the protein. Such linkers are capable of generating ADCs with more precise DAR and drug distribution as well as reforming covalent bonds between the antibody chains. Significant progress has been made in the field with this class of linker by Baker, Caddick and Chudasama and their co-workers, amongst others.[27–36] Despite these impressive advances, new methods are still required for the production of stable and homogeneous ADCs from non-engineered antibodies. We sought to develop a new disulfide bridging linker platform, which generated highly stable ADCs with precise DAR and drug distribution. Vinylpyridines have previously been used to modify proteins *via* cysteine conjugation.[37] Glythera has recently developed a monovinylpyridine-based linker platform for ADC construction with such conjugates demonstrating excellent stability (Fig. 1a). We envisaged that divinyl-functionalised hetero-aryl linkers could be used to achieve cysteine re-bridging, generating inherently stable constructs whilst also achieving precise control of DAR and site-of-attachment with native antibodies.

Herein, we report upon our investigations in this area and development of a novel divinylpyrimidine (DVP) linker platform for cysteine-bridging bioconjugation with a range of proteins (Fig. 1b). Model studies using the non-engineered trastuzumab antibody validate the utility of this linker platform for the generation of highly plasma-stable antibody constructs that incorporate different biologically relevant payloads in a robust and efficient manner. The utility of the DVP linker platform was also exemplified on other protein systems, exemplifying the

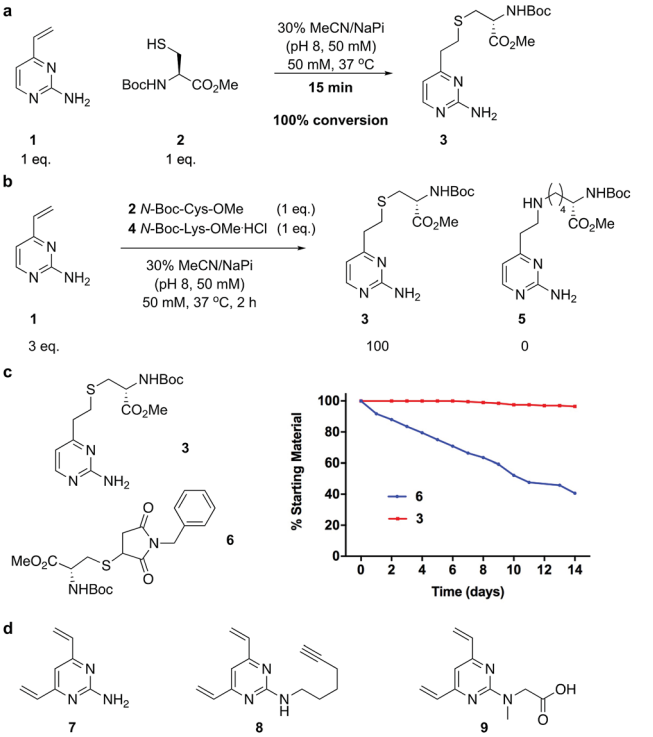

Fig. 2 Development and analysis of the DVP linkers. (a) conjugation of vinylpyrimidine **1** with *N*-Boc-Cys-OMe, (b) selectivity experiment by reaction of *N*-Boc-Cys-OMe and *N*-Boc-Lys-OMe with an excess of **1**, (c) stability comparison of vinylpyrimidine-conjugate **3** *versus* maleimide conjugate **6** in the presence of reduced GSH and (d) DVP linkers **7**, **8** and **9**.

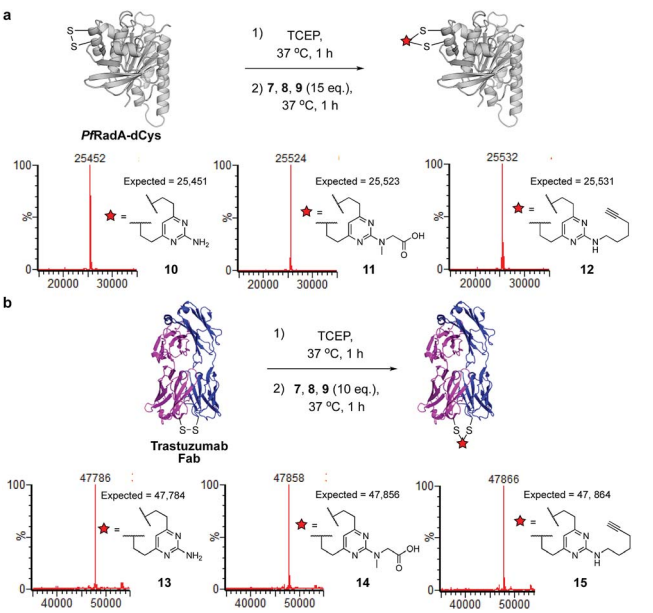

Fig. 3 Reaction conditions and subsequent LC-MS analysis for (a) modification of recombinant *Pf*RadA with DVP linkers **7**, **8** and **9** resulted in covalently re-bridged conjugates **10**, **11** and **12**, and (b) bridging of trastuzumab Fab with **7**, **8** and **9** resulted in the desired interchain bridged conjugates **13**, **14** and **15**.

capability of such linkers for a range of protein or peptide modification applications.

Results and discussion

We began our study by identifying the potential of a vinylheteroaryl scaffold for cysteine re-bridging. It was postulated that vinylpyridine bioconjugation would be too slow to enable efficient cross-linking but that replacement of the pyridine with a pyrimidine would enhance the reactivity to desirable levels by increasing the electron accepting capacity of the heteroaryl ring, without compromising the stability seen with vinylpyridine conjugates.[38] To test this hypothesis, vinylpyrimidine **1** (prepared by a Suzuki–Miyaura cross-coupling, see ESI‡) was reacted with Boc-Cys-OMe in a mixture of aqueous buffer and acetonitrile. Pleasingly, full conversion from **1** to conjugate **3** was achieved in 15 minutes, monitored by thin layer chromatography (TLC), under these bioconjugation compatible conditions (Fig. 2a). A competition experiment involving the reaction of **1** with Boc-Cys-OMe and Boc-Lys-OMe at alkaline pH showed full conversion to the cysteine conjugate **3**. No evidence of the lysine conjugate **5** was observed, even with an excess of vinylpyrimidine **1** present in the reaction (Fig. 2b and ESI Fig. S1‡). Similarly, **1** showed poor reactivity with tris(2-carboxyethyl) phosphine hydrochloride (TCEP), a commonly used reducing agent in cysteine bioconjugation (ESI Fig. S5‡), demonstrating the capability of this scaffold for chemoselective cysteine conjugation. The stability of conjugate **3** under physiological conditions was investigated by incubation with an excess of reduced L-glutathione (GSH) in pH 7.4 buffer at 37 °C. The stability was tracked *via* ^{1}H NMR and pleasingly, almost no degradation (<5%) was observed after two weeks. In comparison, the corresponding maleimide conjugate **6** showed >50% conversion to the glutathione-maleimide conjugate after two weeks under the same conditions (Fig. 2c and S6‡). This suggested that vinylpyrimidine bioconjugation could indeed be used to generate conjugates that are stable under physiological conditions. Efforts then turned to the synthesis of divinylpyrimidine (DVP) linkers which contained reactive synthetic handles suitable for attachment of other modalities, such as drugs or fluorophores. To this end, DVP linkers **7**, **8** and **9** were synthesised in one, two and three steps, respectively (Fig. 2d, see ESI‡ for synthetic details). The chemoselectivity of linkers **7**, **8** and **9** was then confirmed in an analogous way to monovinylpyrimidine **1** (ESI Fig. S1–S4‡). Subsequently, the stability of Boc-Cys-OMe modified **7**, **8** and **9** in the presence of GSH was also demonstrated *via* ^{1}H NMR (ESI Fig. S6‡).

We next sought to ascertain the reactivity of the DVP linkers in protein systems. RadA from *Pyrococcus furiosus* is a DNA recombinase enzyme that does not contain any cysteine residues. Through site-directed mutagenesis, a monomeric version was produced that contained two cysteine residues in close proximity in the tertiary structure (*Pf*RadA-dCys, ESI Fig. S25‡). Pleasingly, reduction of the mutant *Pf*RadA with TCEP followed by the addition of linkers **7**, **8** or **9** (15 equiv.) for 1 hour at 37 °C yielded excellent conversion to the desired covalently re-bridged conjugates **10**, **11** and **12**, as detected by LC-MS (Fig. 3a and ESI Fig. S7–S9‡). To evaluate the intended strategy further, the bridging reaction was appraised in a system where interchain bridging between two polypeptide chains would be required. Antibody Fabs (fragment, antigen binding) are heterodimeric proteins with the chains linked by a single disulfide. Evaluation of the DVP linker platform by reduction of trastuzumab Fab with TCEP, followed by reaction with **7**, **8** or **9** led to complete

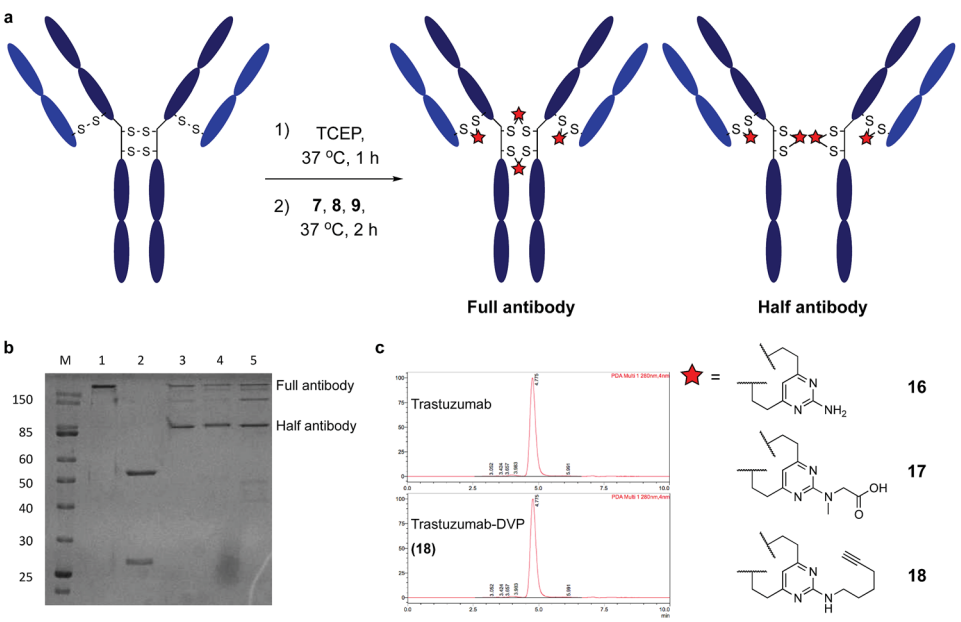

Fig. 4 Reaction of trastuzumab with the DVP linkers and subsequent analysis. (a) Cysteine bridging of trastuzumab with **7**, **8** or **9** resulted in re-bridged mAbs **16**, **17** and **18**, (b) analysis of conjugate **16**, **17** and **18** by SDS-PAGE; lane 1 is non-reducing, lanes 2–5 are reducing; lanes: (M) molecular weight marker, (1) trastuzumab, (2) reduced trastuzumab, (3) **16**, (4) **17**, (5) **18**, and (c) SEC analysis of **18**.

conversion to the desired interchain-bridged conjugates **13–15** in ~30 minutes using a slight excess of the linker (10 equiv.) (Fig. 3b and ESI Fig. S10–S13‡). Kinetic analysis of the bridging rate of **8** was conducted with 10 and 20 equivalents linker after TCEP reduction. Strikingly, >90% re-bridging of the Fab chains was observed for both stoichiometries after only 15 minutes (ESI Fig. S14‡). To confirm the selectivity of the DVP linker platform for cysteine residues, **8** was incubated with unreduced trastuzumab Fab and no reaction was observed after two hours at 37 °C (ESI Fig. S23‡). These results exemplify the potential for the DVP linker platform to serve as a general protein modification tool for monomeric and multimeric proteins.

Encouraged by earlier results, efforts shifted toward modification of an IgG antibody. DVP linkers potentially enable modification of all four interchain disulfides in an IgG_1, generating an ADC with definitive modification sites while giving a consistent DAR of four.[39] Trastuzumab mAb was reduced with TCEP, revealing eight free thiols as evidenced by LC-MS and Ellman's assay (ESI Fig. S15‡). Subsequently, the reduced antibody was treated with a slight excess of **7**, **8** or **9** (10 equiv. per disulfide) for two hours at 37 °C (Fig. 4a). Removal of small molecule reagents by dialysis was followed by LC-MS, SDS-PAGE and RP-HPLC analysis. The fully re-bridged mAbs **16**, **17** and **18** were evident by LC-MS, suggesting good conversion to the desired bioconjugates (ESI Fig. S15, S17 and S18‡). Analysis by SDS-PAGE and RP-HPLC confirmed the presence of the correctly bridged antibodies (Fig. 4b and ESI Fig. S17‡) along with the 'half-antibody' formed by intrachain bridging of the hinge region heavy chain cysteines, an issue seen with other re-bridging linkers.[35,40] A large number of conditions (reaction concentration, time, linker stoichiometry) were explored to avoid this 'half-antibody' formation, with little change observed (ESI Table S1 and Fig. S16‡). Through this process, it was found that the reaction worked efficiently (90–95% conversion to the bridged bioconjugates) at low concentrations (<10 μM) and with a slight excess of DVP (2.5 equiv. per disulfide). We postulate that the half-antibody conjugate remains useful as the modification site and DAR are still controlled and the stability of the

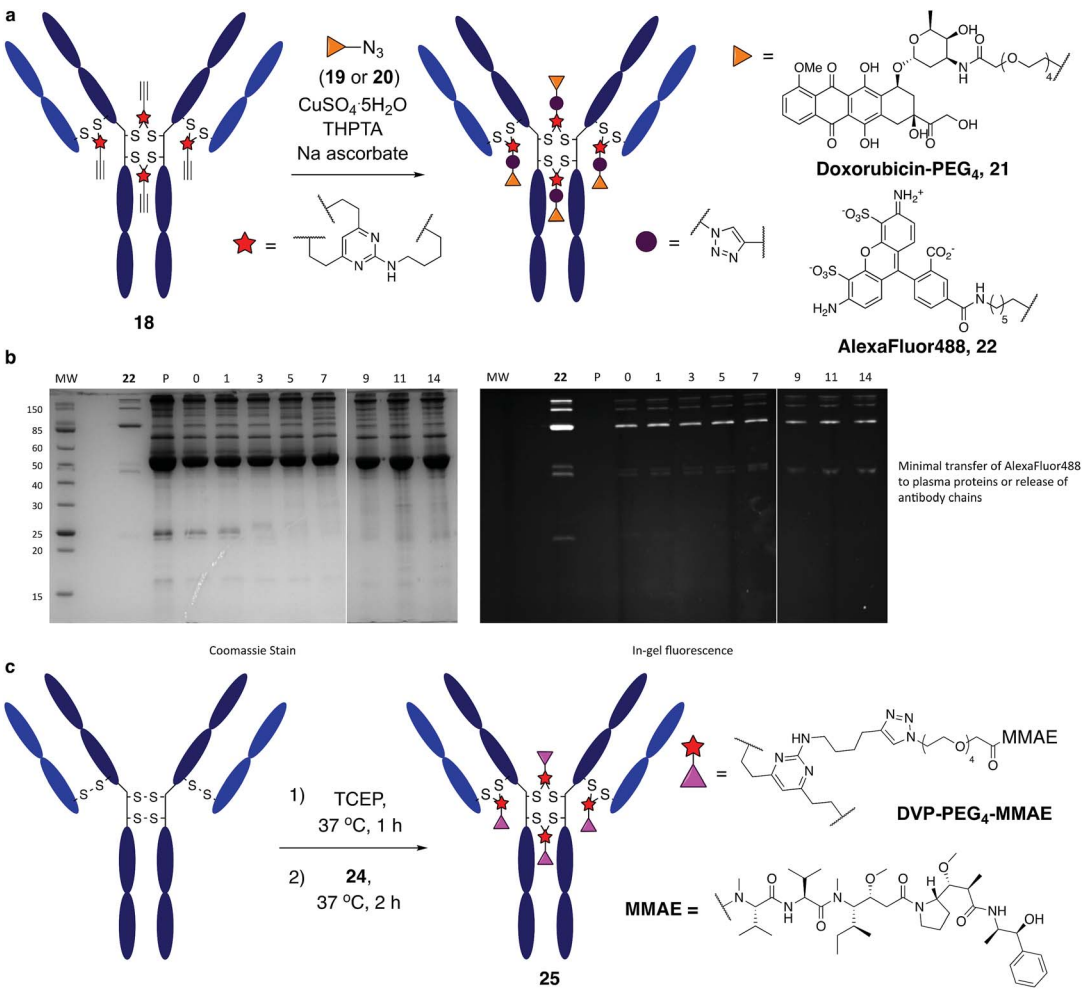

Fig. 5 Functional modification and stability analysis of DVP-modified trastuzumab. (a) On-antibody CuAAC reaction between modified trastuzumab, **18** forming a doxorubicin conjugate, **21** and an AlexaFluor™ 488 conjugate, **22**, (b) stability analysis by SDS-PAGE of conjugate **22** in human plasma supplemented with GSH; P = human plasma, MW = molecular weight marker, days of incubation indicated above the representative lane. Left gel is after coomassie staining, right gel is in-gel fluorescence measured before staining, and (c) DVP-mediated formation of an MMAE ADC, **25**.

conjugate conferred through the DVP linker remains. Crucially, the light and heavy chains are always re-bridged efficiently, ensuring that the Fab region (the region that confers receptor specificity to the antibody) is covalently linked. In order to determine the effect of bridging on mAb aggregation, antibody conjugate **18** was analysed by size-exclusion chromatography (SEC). This showed identical aggregation levels observed for **18** and the unmodified mAb (Fig. 4c).

It was anticipated that the synthetic handles present in DVP linkers would enable modular and divergent functionalisation, both before and after DVP antibody conjugation. Terminal alkyne-functionalised DVP **8** was identified as a suitable candidate for post-conjugation modification, as copper-catalysed azide-alkyne cycloaddition (CuAAC) chemistry offers a well-established method for diverse functionalisation under physiologically relevant conditions.[41] An azide-functionalised doxorubicin (**19**) was synthesised and reacted with **18** in the presence of $CuSO_4 \cdot 5H_2O$, tris(3-hydroxypropyltriazolylmethyl)amine (THPTA) and sodium ascorbate (Fig. 5a). Gratifyingly, excellent conversion to triazole product **21** was observed by LC-MS. DAR analysis by UV-vis spectroscopy also confirmed high conversion with a measured DAR of 4.0 (ESI Fig. S19‡). With the aim of creating a potentially valuable cellular imaging agent, conjugate **18** was reacted with AlexaFluor™ 488 azide **20** under CuAAC conditions (Fig. 5a). Similarly, excellent conversion was observed with a measured fluorophore-antibody ratio (FAR) of 3.9 (ESI Fig. S20‡).

Synthesis of **22** enabled assessment of the plasma stability of DVP bioconjugates. The fluorescent antibody conjugate was incubated in human plasma supplemented with GSH at 37 °C for two weeks. Pleasingly, in-gel fluorescence and coomassie staining revealed almost no transfer of the AlexaFluor™ 488 label onto plasma proteins, or release of individual heavy or light chains from the antibody (Fig. 5b and ESI Fig. 22‡). This analysis confirms the stability assessment made on the small molecule model system that DVP linkers enable the generation of highly stable bioconjugates.

Functionalisation before antibody conjugation was then examined using the highly potent dolastatin 10 analogue, monomethylauristatin E (MMAE) as a representative payload. A DVP–PEG_4–MMAE linker-warhead, **24** was prepared from **8** and azide-functionalised MMAE (**23**) (see ESI‡). Reaction of reduced trastuzumab with **24** (10 equiv. per disulfide) proceeded with excellent conversion to **25** *via* LC-MS (Fig. 5c and ESI Fig. S21‡).

The biological effects of DVP-bridging were then investigated. Firstly, trastuzumab conjugates, **16–18** all demonstrated comparable affinities to the native antibody for the HER2 receptor *via* enzyme-linked immunosorbent assay (ELISA) (Fig. 6a). Fluorescence-activated cell sorting (FACS) coupled with live individual cell imaging was next used to ensure that the DVP conjugation did not alter cellular recognition and selectivity. Fluorescent trastuzumab conjugate, **22** was incubated in both HER2-positive (SKBR3 and BT474) and HER2-negative (MCF7 and T47D) breast cancer cell lines. The cells were incubated at 37 °C for 1 hour to allow antigen binding and complex internalisation, followed by washing with PBS to remove any unbound antibody. Subsequent FACS analysis revealed full labelling of both HER2-positive cell lines while only minor labelling was observed with HER2-negative cell lines (Fig. 6b). Internalisation of the conjugate was observed in both HER2-positive cell types, with no internalisation visible in either HER2-negative cell line (Fig. 6c), confirming that DVP bridging does not affect receptor specificity, affinity or complex internalisation.

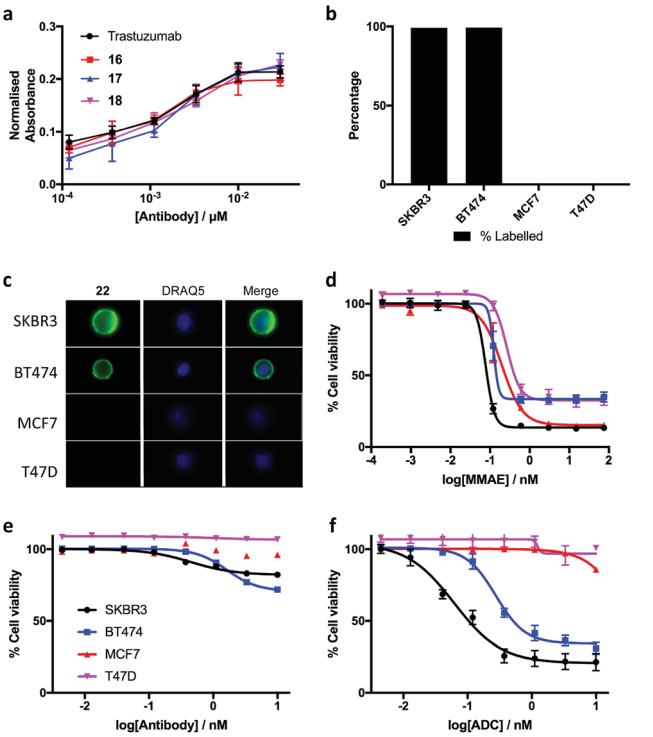

Fig. 6 Biological evaluation of the DVP linker platform. (a) Binding affinity comparison of trastuzumab, **16**, **17** and **18** *via* ELISA. Error bars represent the standard deviation of biological quadruplicates, (b) percentage labelling of HER2-positive and HER2-negative cells with **22**, (c) internalisation of **22** in HER2-positive cells without any observed internalisation in HER2-negative cells, and cytotoxicity in HER2-positive and HER2-negative cells with (d) MMAE, (e) trastuzumab and (f) DVP-MMAE ADC **25**. Viability data shows the mean of three independent experiments and error bars represent s.e.m.

Finally, evaluation of the *in vitro* cytotoxicity of a therapeutically relevant ADC was undertaken. DVP-MMAE ADC **25**, containing a non-cleavable linker was used to treat both HER2-positive (SKBR3 and BT474) and HER2-negative (MCF7 and T47D) cell lines. Cytotoxicity was only observed in the HER2-positive cell lines (Fig. 6f and ESI Fig. S24‡), demonstrating that DVP linkers do not affect the cell-killing ability of MMAE, enabling the use of these linkers for the delivery of auristatin payloads with non-cleavable linkers. In contrast to the specific cytotoxicity observed with our ADC, treatment of the same cell lines with free MMAE resulted in high levels of cytotoxicity in both HER2-positive and HER2-negative cell lines (Fig. 6d). Furthermore, incubation of unmodified trastuzumab with these cell lines did not cause significant cytotoxicity (Fig. 6e).

Conclusion

In conclusion, we have developed a novel DVP linker platform for bioconjugation through the covalent re-bridging of cysteine residues generated by the reduction of native disulfide bonds. Model studies using the trastuzumab antibody validate the utility of this linker platform for the efficient generation of highly plasma-stable antibody constructs from non-engineered antibodies. We have shown that this technology can be used to introduce different biologically relevant payloads, in an efficient and site-selective manner with control over DAR, either before or after bioconjugation, without recourse to any other additional processes. Furthermore, the conjugation platform utilizes a reaction that is orthogonal to other biocompatible reactions (such as the CuAAC), enabling their use in tandem with one another. The modified antibodies maintained their cellular specificity and receptor affinity, and a DVP-ADC demonstrated exquisite potency and selectivity for its target cells, while having little effect on the mechanism of action of its auristatin payload. In addition, the DVP linkers showed excellent cysteine re-bridging of monomeric and dimeric proteins, enabling their use for general protein modification,[42] protein stabilisation[43,44] or the development of other biotherapeutics such as stapled peptides.[45,46]

Conflicts of interest

There are no conflicts to declare.

Acknowledgements

We thank AstraZeneca for providing trastuzumab and MMAE for this research, Dr Philip Howard, Dr Luke Masterson and Dr Balakumar Vijayakrishnan at Spriogen for access to SEC and RP-HPLC, and Richard Grenfell and the Flow Cytometry Core at the CRUK Cambridge Institute for their help with FACS analysis. S. J. W. acknowledges a scholarship from AstraZeneca and the Cambridge Trusts. D. R. S. acknowledges support from the Engineering and Physical Sciences Research Council (EP/P020291/1) and Royal Society (Wolfson Research Merit Award). The Spring lab acknowledges general lab support from the EPSRC, BBSRC, MRC and Royal Society.

Notes and references

1 A. Beck, T. Wurch, C. Bailly and N. Corvaia, *Nat. Rev. Immunol.*, 2010, **10**, 345–352.
2 T. Ueda, *Biochim. Biophys. Acta, Proteins Proteomics*, 2014, **1844**, 2053–2057.
3 B. A. Teicher and J. H. Doroshow, *N. Engl. J. Med.*, 2012, **367**, 1847–1848.
4 A. Beck and J. M. Reichert, *mAbs*, 2014, **6**, 15–17.
5 L. Ducry and B. Stump, *Bioconjugate Chem.*, 2010, **21**, 5–13.
6 H. L. Perez, P. M. Cardarelli, S. Deshpande, S. Gangwar, G. M. Schroeder, G. D. Vite and R. M. Borzilleri, *Drug Discovery Today*, 2014, **19**, 869–881.
7 N. Diamantis and U. Banerji, *Br. J. Cancer*, 2016, **114**, 362–367.
8 P. D. Senter and E. L. Sievers, *Nat. Biotechnol.*, 2012, **30**, 631–637.
9 J. M. Lambert and R. V. J. Chari, *J. Med. Chem.*, 2014, **57**, 6949–6964.
10 C. D. Godwin, R. P. Gale and R. B. Walter, *Leukemia*, 2017, **31**, 1855–1868.
11 B. Shor, H.-P. Gerber and P. Sapra, *Mol. Immunol.*, 2015, **67**, 107–116.
12 A. Beck, L. Goetsch, C. Dumontet and N. Corvaïa, *Nat. Rev. Drug Discovery*, 2017, **16**, 315–337.
13 J. R. Junutula, H. Raab, S. Clark, S. Bhakta, D. D. Leipold, S. Weir, Y. Chen, M. Simpson, S. P. Tsai, M. S. Dennis, Y. Lu, Y. G. Meng, C. Ng, J. Yang, C. C. Lee, E. Duenas, J. Gorrell, V. Katta, A. Kim, K. McDorman, K. Flagella, R. Venook, S. Ross, S. D. Spencer, W. Lee Wong, H. B. Lowman, R. Vandlen, M. X. Sliwkowski, R. H. Scheller, P. Polakis and W. Mallet, *Nat. Biotechnol.*, 2008, **26**, 925–932.
14 P. Agarwal and C. R. Bertozzi, *Bioconjugate Chem.*, 2015, **26**, 176–192.
15 P. Strop, S.-H. Liu, M. Dorywalska, K. Delaria, R. G. Dushin, T.-T. Tran, W.-H. Ho, S. Farias, M. G. Casas, Y. Abdiche, D. Zhou, R. Chandrasekaran, C. Samain, C. Loo, A. Rossi, M. Rickert, S. Krimm, T. Wong, S. M. Chin, J. Yu, J. Dilley, J. Chaparro-Riggers, G. F. Filzen, C. J. O'Donnell, F. Wang, J. S. Myers, J. Pons, D. L. Shelton and A. Rajpal, *Chem. Biol.*, 2013, **20**, 161–167.
16 V. Chudasama, A. Maruani and S. Caddick, *Nat. Chem.*, 2016, **8**, 114–119.
17 K. J. Hamblett, P. D. Senter, D. F. Chace, M. M. C. Sun, J. Lenox, C. G. Cerveny, K. M. Kissler, S. X. Bernhardt, A. K. Kopcha, R. F. Zabinski, D. L. Meyer and J. A. Francisco, *Clin. Cancer Res.*, 2004, **10**, 7063–7070.
18 S. C. Alley, D. R. Benjamin, S. C. Jeffrey, N. M. Okeley, D. L. Meyer, R. J. Sanderson and P. D. Senter, *Bioconjugate Chem.*, 2008, **19**, 759–765.
19 A. D. Baldwin and K. L. Kiick, *Bioconjugate Chem.*, 2011, **22**, 1946–1953.
20 R. P. Lyon, J. R. Setter, T. D. Bovee, S. O. Doronina, J. H. Hunter, M. E. Anderson, C. L. Balasubramanian, S. M. Duniho, C. I. Leiske, F. Li and P. D. Senter, *Nat. Biotechnol.*, 2014, **32**, 1059–1062.
21 S. D. Fontaine, R. Reid, L. Robinson, G. W. Ashley and D. V. Santi, *Bioconjugate Chem.*, 2015, **26**, 145–152.
22 E. S. Zimmerman, T. H. Heibeck, A. Gill, X. Li, C. J. Murray, M. R. Madlansacay, C. Tran, N. T. Uter, G. Yin, P. J. Rivers, A. Y. Yam, W. D. Wang, A. R. Steiner, S. U. Bajad, K. Penta, W. Yang, T. J. Hallam, C. D. Thanos and A. K. Sato, *Bioconjugate Chem.*, 2014, **25**, 351–361.
23 J. Y. Axup, K. M. Bajjuri, M. Ritland, B. M. Hutchins, C. H. Kim, S. A. Kazane, R. Halder, J. S. Forsyth, A. F. Santidrian, K. Stafin, Y. Lu, H. Tran, A. J. Seller, S. L. Biroc, A. Szydlik, J. K. Pinkstaff, F. Tian, S. C. Sinha, B. Felding-Habermann, V. V Smider and P. G. Schultz, *Proc. Natl. Acad. Sci. U. S. A.*, 2012, **109**, 16101–16106.

24 P. Dennler, A. Chiotellis, E. Fischer, D. Brégeon, C. Belmant, L. Gauthier, F. Lhospice, F. Romagne and R. Schibli, *Bioconjugate Chem.*, 2014, **25**, 569–578.

25 Z. Zhu, B. Ramakrishnan, J. Li, Y. Wang, Y. Feng, P. Prabakaran, S. Colantonio, M. A. Dyba, P. K. Qasba and D. S. Dimitrov, *mAbs*, 2014, **6**, 1190–1200.

26 P. M. Drake, A. E. Albers, J. Baker, S. Banas, R. M. Barfield, A. S. Bhat, G. W. de Hart, A. W. Garofalo, P. Holder, L. C. Jones, R. Kudirka, J. McFarland, W. Zmolek and D. Rabuka, *Bioconjugate Chem.*, 2014, **25**, 1331–1341.

27 F. F. Schumacher, J. P. M. Nunes, A. Maruani, V. Chudasama, M. E. B. Smith, K. A. Chester, J. R. Baker and S. Caddick, *Org. Biomol. Chem.*, 2014, **12**, 7261–7269.

28 G. Badescu, P. Bryant, M. Bird, K. Henseleit, J. Swierkosz, V. Parekh, R. Tommasi, E. Pawlisz, K. Jurlewicz, M. Farys, N. Camper, X. Sheng, M. Fisher, R. Grygorash, A. Kyle, A. Abhilash, M. Frigerio, J. Edwards and A. Godwin, *Bioconjugate Chem.*, 2014, **25**, 1124–1136.

29 C. R. Behrens, E. H. Ha, L. L. Chinn, S. Bowers, G. Probst, M. Fitch-Bruhns, J. Monteon, A. Valdiosera, A. Bermudez, S. Liao-Chan, T. Wong, J. Melnick, J. W. Theunissen, M. R. Flory, D. Houser, K. Venstrom, Z. Levashova, P. Sauer, T. S. Migone, E. H. Van Der Horst, R. L. Halcomb and D. Y. Jackson, *Mol. Pharm.*, 2015, **12**, 3986–3998.

30 A. Maruani, M. E. B. Smith, E. Miranda, K. A. Chester, V. Chudasama and S. Caddick, *Nat. Commun.*, 2015, **6**, 6645.

31 J. P. M. Nunes, M. Morais, V. Vassileva, E. Robinson, V. S. Rajkumar, M. E. B. Smith, R. B. Pedley, S. Caddick, J. R. Baker and V. Chudasama, *Chem. Commun.*, 2015, **51**, 10624–10627.

32 M. E. B. Smith, F. F. Schumacher, C. P. Ryan, L. M. Tedaldi, D. Papaioannou, G. Waksman, S. Caddick and J. R. Baker, *J. Am. Chem. Soc.*, 2010, **132**, 1960–1965.

33 V. Chudasama, M. E. B. Smith, F. F. Schumacher, D. Papaioannou, G. Waksman, J. R. Baker and S. Caddick, *Chem. Commun.*, 2011, **47**, 8781.

34 M. T. W. Lee, A. Maruani, J. R. Baker, S. Caddick and V. Chudasama, *Chem. Sci.*, 2016, **7**, 799–802.

35 M. Morais, J. P. M. Nunes, K. Karu, N. Forte, I. Benni, M. E. B. Smith, S. Caddick, V. Chudasama and J. R. Baker, *Org. Biomol. Chem.*, 2017, **15**, 2947–2952.

36 P. Bryant, M. Pabst, G. Badescu, M. Bird, W. McDowell, E. Jamieson, J. Swierkosz, K. Jurlewicz, R. Tommasi, K. Henseleit, X. Sheng, N. Camper, A. Manin, K. Kozakowska, K. Peciak, E. Laurine, R. Grygorash, A. Kyle, D. Morris, V. Parekh, A. Abhilash, J. Choi, J. Edwards, M. Frigerio, M. P. Baker and A. Godwin, *Mol. Pharm.*, 2015, **12**, 1872–1879.

37 R. Sebastiano, A. Citterio, M. Lapadula and P. G. Righetti, *Rapid Commun. Mass Spectrom.*, 2003, **17**, 2380–2386.

38 J. R. Winther and C. Thorpe, *Biochim. Biophys. Acta, Gen. Subj.*, 2014, **1840**, 838–846.

39 L. Ducry, *Methods Mol. Biol.*, 2012, **899**, 489–497.

40 O. Koniev, I. Dovgan, B. Renoux, A. Ehkirch, J. Eberova, S. Cianférani, S. Kolodych, S. Papot and A. Wagner, *MedChemComm*, 2018, **9**, 827–830.

41 V. Hong, S. I. Presolski, C. Ma and M. G. Finn, *Angew. Chem., Int. Ed.*, 2009, **48**, 9879–9883.

42 R. E. Morgan, V. Chudasama, P. Moody, M. E. B. Smith and S. Caddick, *Org. Biomol. Chem.*, 2015, **13**, 4165–4168.

43 S. S. Wong and L. J. C. Wong, *Enzyme Microb. Technol.*, 1992, **14**, 866–874.

44 T. Schiffner, N. de Val, R. A. Russell, S. W. de Taeye, A. T. de la Peña, G. Ozorowski, H. J. Kim, T. Nieusma, F. Brod, A. Cupo, R. W. Sanders, J. P. Moore, A. B. Ward and Q. J. Sattentau, *J. Virol.*, 2016, **90**, 813–828.

45 Y. Wu, F. Villa, J. Maman, Y. H. Lau, L. Dobnikar, A. C. Simon, K. Labib, D. R. Spring and L. Pellegrini, *Angew. Chem., Int. Ed.*, 2017, **56**, 12866–12872.

46 A. M. Spokoyny, Y. Zou, J. J. Ling, H. Yu, Y. S. Lin and B. L. Pentelute, *J. Am. Chem. Soc.*, 2013, **135**, 5946–5949.